AFRL-VS-HA-TR-98-0104 (II)

INFRARED CELESTIAL BACKGROUNDS STUDIES
Volume 2: A Radiometric All-Sky Network of Absolutely Calibrated Stellar Spectra

Russell G. Walker
Martin Cohen

Vanguard Research, Inc.
5321 Scotts Valley Drive, Suite 204
Scotts Valley CA 95066

10 Sep 1998

FINAL REPORT

AIR FORCE RESEARCH LABORATORY
Space Vehicles Directorate
29 Randolph Rd
AIR FORCE MATERIEL COMMAND
Hanscom AFB, MA 01731-3010

" This technical report has been reviewed and is approved for publication."

MICHAEL P. EGAN
Contract Manager

STEPHAN D. PRICE, Chief
Background Characterization Branch

This report has been reviewed by the ESC Public Affairs Office (PA) and is releasable to the National Technical Information Service (NTIS).

Qualified requestors may obtain additional copies from the Defense Technical Information Center (DTIC). All others should apply to the National Technical Information Service (NTIS).

If your address has changed, if you wish to be removed from the mailing list, of if the addressee is no longer employed by your organization, please notify PL/IM, 29 Randolph Road, Hanscom AFB, MA. 01731-3010. This will assist us in maintaining a current mailing list.

Do not return copies of this report unless contractual obligations or notices on a specific document require that it be returned.

REPORT DOCUMENTATION PAGE

Form Approved
OMB No. 0704-0188

1. AGENCY USE ONLY *(Leave blank)*	2. REPORT DATE	3. REPORT TYPE AND DATES COVERED
	September 10, 1998	Final Report April 16, 1992 – July 15, 1998

4. TITLE AND SUBTITLE
Infrared Celestial Backgrounds Studies, ESD Contract No. F19628-92-C-0090
Volume 2. A Radiometric All-Sky Network of Absolutely Calibrated Stellar Spectra

5. FUNDING NUMBERS
C F19628-92-C-0090
PE 63215C
PR 3054
TA 01
WU AS

6. AUTHORS
Russell G. Walker and Martin Cohen

7. PERFORMING ORGANIZATION NAME(S) AND ADDRESS(ES)
Vanguard Research, Inc.
5321 Scotts Valley Drive, Suite 204
Scotts Valley, CA 95066

8. PERFORMING ORGANIZATION REPORT NUMBER
VRISV-98-01

9. SPONSORING/MONITORING AGENCY NAME(S) AND ADDRESS(ES)
Electronic Systems Division/PKR
Air Force Systems Command, USAF
Hanscom AFB, MA 01731-5320

10. SPONSORING/MONITORING AGENCY REPORT NUMBER
AFRL-VS-HA-TR-98-0104 (II)

11. SUPPLEMENTARY NOTES

12a. DISTRIBUTION/AVAILABILITY STATEMENT
Approved for public release; distribution unlimited

12b. DISTRIBUTION CODE

13. ABSTRACT *(Maximum 200 words)*

The purpose of this program was to extend and improve the present capability to predict celestial phenomenology pertinent to the design and successful operation of space based surveillance systems using the ultraviolet, optical, and infrared spectral regions. We pursued this goal through analysis and application of existing datasets and, in particular, by analysis of new satellite measurements that became available during the course of the project. Our work was concentrated in four major areas: 1) extension of an existing analytical model of the infrared point source sky (SKY), 2) development of a set of absolutely calibrated spectral stellar irradiance standards for the infrared, 3) analysis of new celestial data obtained by satellite, and 4) support of the infrared celestial measurements taken by the Midcourse Space Experiment (MSX) satellite.

Volume 1 summarizes the work performed under the contract, and includes reprints of the major papers published during the contractual period. Volume 2 presents the final release of an all-sky network of 422 stars with absolutely calibrated stellar spectra in the 1.2 to 35 μm region. Volume 2 also contains reprints of the complete series of published papers documenting the spectral calibration process and assumptions.

14. SUBJECT TERMS
Infrared calibration, celestial backgrounds, sky model

15. NUMBER OF PAGES
209 – Volume 2

16. PRICE CODE

17. SECURITY CLASSIFICATION OF REPORT	18. SECURITY CLASSIFICATION OF THIS PAGE	19. SECURITY CLASSIFICATION OF ABSTRACT	20. LIMITATION OF ABSTRACT
UNCLASSIFIED	UNCLASSIFIED	UNCLASSIFIED	UL

Table of Contents, Volume 2

List of Illustrations

List of Tables

A Self-Consistent Radiometric All-Sky Network of Absolutely Calibrated Stellar Spectra

1. Introduction

Several infrared (IR) satellites were launched in the period 1995-1996: the joint ISAS/NASA "IR Telescope in Space" (IRTS: Murakami et al. 1994,1996) that surveyed about 8% of the sky in 1995; the European Space Agency's "Infrared Space Observatory" (ISO: Kessler et al. 1996), with the involvement of the USA and Japan; and the US Midcourse Space Experiment (MSX: Mill et al. 1994), launched in spring 1996. NASA's WIRE ("Wide-field IR Explorer") mission is scheduled for a 1999 launch, and the stratospheric observatory project (SOFIA) is fast proceeding. There is an urgent need not only to rationalize IR calibration and place it in a common and well-defined context, but also to provide a network of calibrators well distributed across the sky, with a common traceable pedigree. This network should be sufficiently dense to have a member relatively close to an arbitrary direction because satellites and aircraft cannot afford major excursions in pointing to secure measurements of the few traditional calibration objects. Dynamic range, too, is an issue and such a network should include stars fainter than today's popular "standard" stars.

In the first paper of this series we described a self-consistent effort to provide absolutely calibrated broad and narrowband infrared photometry based upon a carefully selected, infrared-customized pair of stellar models for Vega and Sirius, created by Kurucz, and absolutely calibrated by Cohen et al. (1992a: hereafter Paper I). These hot stellar models have been employed as reference spectra to calibrate cool giants by methods detailed by Cohen, Walker & Witteborn (1992b: hereafter Paper II) and amplified by Cohen et al. (1995,1996a,1996b: hereafter Papers IV, VI, VII). This approach has yielded twelve infrared-bright secondary stellar standards with calibration pedigrees directly traceable to our primary radiometric standard, namely α CMa. These cool giant spectra are totally unlike any blackbody energy distribution, and are dominated by the fundamental absorption and overtones of CO and SiO. These molecular bands are common among cool giants and supergiants (Cohen et al. 1992c: hereafter Paper III). The issue of extrapolation of observed spectra to long wavelengths was also addressed in Papers IV (to 35 μm) and VII (to 300 μm). Paper V discusses the UKIRT CGS3 10/20-μm spectrometer's calibration characteristics because of its central role in the assembly of our composite spectra (Cohen & Davies 1995).

Papers II, IV and VII demonstrate the assembly of spectra for the popular infrared calibrators, β Gem (K0III), α Boo (K1.5III), α Hya (K3III), α Tau (K5III), and β And (M0III). In the present paper we demonstrate how any such observed spectrum, or "composite", can be used to create many calibrated stellar spectra. Our fundamental assumption is that the dereddened infrared spectrum of any observed K0-M0 giant accurately represents the intrinsic spectrum of any other giant with the identical type as the composite from which the "template" is created. Then, all that is needed to constrain the adopted template (spectral shape) for a specific star, spectroscopically unobserved in the infrared, is a measure of its individual interstellar reddening and its infrared photometry (with meaningful errors) in a "well-characterized" system of filters. By this we imply that we have digitized versions of their cold transmission profiles and actual, or at least generic, detector responses, and mean atmospheric transmission profiles. These combinations of filter, atmosphere (for ground-based data), and detector responses have been calibrated using our "zero magnitude" Vega spectrum (Paper I).

We emphasize "well-characterized" because too often the infrared literature abounds with "magnitudes" without: the definition of zero magnitude for each filter; any magnitudes adopted for a stipulated set of "standard stars"; a published accessible measurement of the filter transmission profile at its cold operating point; inclusion of the detector's radiance response curve; or any reference to a site-specific terrestrial atmospheric transmission profile. It is sometimes possible to establish "zero point offsets" (see subsection 4.2) for random published photometry but it is generally impossible to trace the separate influences on the magnitudes adopted for several different standards on the cited magnitudes for individual target stars of interest. Further, most infrared "calibration" has consisted of assuming that each distinct "calibrator" can be represented by a blackbody at its effective temperature. As illustrated in this series of papers, this is patently not the case. Worse, the extent of the errors made by the blackbody assumption differs from star to star, even at the same wavelength, rendering most published infrared photometry, and especially spectroscopy, untraceable and, therefore, not rectifiable *post facto* to any self-consistent calibration framework. It is these reasons that make a fresh approach to infrared stellar calibration desirable, and the needs of three recent infrared satellites during 1995-1998 that render our efforts timely.

It is our philosophy that spectrometers can provide accurate spectral shapes but not necessarily accurate spectrophotometric levels *cf.* Papers II,V). This is because one requires identical external conditions (seeing, atmospheric emission and transmission) both for target and reference stars (see Paper V); yet small apertures and narrow slits prevail. Therefore, we find it especially disturbing, in light of the plethora of different infrared photometric systems in the literature and in current usage, that many major observatories have decommissioned their photometers or are seriously contemplating this radical (economically-driven) action, in favor of infrared array cameras that not only perpetuate this infelicitous calibration legacy but suffer from their own particular calibration problems and limitations (*e.g.*, Glass 1993).

In October 1994 we built a prototype of the network of calibrators described in the current paper. The resulting 183 calibrated templates were provided to the IRTS, ISO, and MSX teams to address at least some of their calibration needs. The new network is more extensive, supported by a greater volume of more precise characterized photometry, and incorporates rigorous tracking of a greater number of sources of uncertainty. In Paper IX of the series, Cohen (1998) describes a pilot study and validation of the template technique applied to space-based (COBE/DIRBE) radiometry.

In Section 2 we describe the construction of a template from a "composite" observed spectrum, and its application to a star with characterized reliable photometry but lacking spectroscopy. The criteria used to select the 573 stars in our proposed radiometric network form the substance of Section 3. Section 4 describes the characterized photometry that we have used to create the calibrated templates. New photometry by Carter, Hammersley, Kidger and Noguchi, in direct support of this paper, appears in Appendices A-E. We also summarize the requisite attributes of these systems, and of all other traceable photometric systems that we have been able to calibrate, from archival cold scanned filter profiles and basis stars. Section 5 explains the logical flow of the template code. Section 6 tabulates the stars for which we have created calibrated templates, along with a discussion of their qualities and absolute uncertainties. Section 7 explains how to obtain our models, composites, and templates, and describes the information that accompanies each to provide traceability in the calibration, and to document the actual processes of composite assembly or template normalization. The complete series of papers documenting our spectral calibration process is reprinted in Appendix G of this volume.

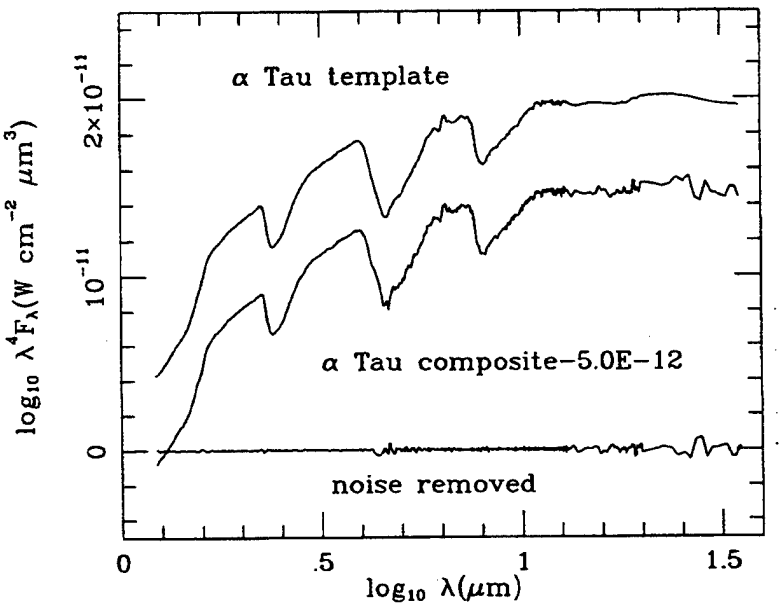

Fig. 1 The creation of a template from a composite (observed) spectrum. This example illustrates the result (upper curve) of lightly smoothing the observed absolute spectrum (middle curve, displaced vertically for easier display). Note that, for α Tau, the extinction is zero so no dereddening was applied to the composite. The high frequency "noise" that was filtered away is represented by the lowest curve.

2. Creating templates

One fully-observed K/M-giant spectrum can be used to create many calibrated stellar spectra if one makes the fundamental "template assumption", that the dereddened spectral shape of any observed K0-M0 giant accurately represents the intrinsic spectrum of any other giant with the same two-dimensional MK spectral type as the star from which the "template" is created. To customize the adopted template (*i.e.* the spectral shape) for a particular star requires photometry of it in a well-characterized system, together with pertinent uncertainties.

Every 1.2-35 μm K/M-giant spectrum is dereddened according to its own extinction (actually all the bright cool giants relevant to the present paper have zero reddening), and lightly smoothed in an information-preserving fashion (Jacobson 1990) that eliminates inappropriate high-frequency noise (*i.e.*, beyond the actual resolution of the spectrometers used for the original observations). Fig. 1 illustrates the result of this procedure for the K5III template derived from the α Tau composite, and shows the high-frequency noise that has been removed. The smoothed, intrinsic spectral shapes thereby provide calibrated "spectral templates" for giants of spectral types K0, 1.5, 3, 5, and M0. Specifically, the correspondence between spectral type, template, and the latest published absolute spectrum is as follows: K0, β Gem (Paper IV); K1.5, α Boo (Paper VII); K3, α Hya (Paper IV); K5, α Tau (Paper II); and M0, β And (Paper IV).

The procedure for templating a target star that is spectroscopically unobserved in the IR is to: select the appropriate intrinsic template shape; apply reddening according to the target star's extinction [determined from E(B-V)]; and normalize the resulting reddened template by

photometry specific to the star through fully characterized, absolutely calibrated, combinations of detector radiance response, filter passband, and site-specific mean terrestrial atmosphere (if ground-based data) or overall system response functions such as those provided by IRAS and DIRBE. The result is a scaled spectral template, with a mean scale factor determined from the set of comparisons of expected in-band fluxes to those actually observed, and an associated uncertainty, assessed from the inverse-variance-weighted set of multipliers for a star (one multiplier and associated uncertainty for each characterized passband used). Each template is as complete in its wavelength coverage as the pristine composite from which it was derived, namely 1.2-35 μm. No attempt has been made to regrid every composite to a common, or even an equally-spaced, wavelength scale, for such an interpolation would spawn yet another set of formal uncertainties. Note that the mean scale factor for a given template is relative to the appropriate composite stellar spectrum, so that two stars with the same scale factor, but made from different spectral templates, will not have the same angular diameter. The angular diameters that we use for each composite are those we derived in Paper VII, all of which agree well with direct observations.

The extinction determination merits discussion. We applied one of three methods for determining Av to each star templated. Extinctions for an appreciable number of K- and M-giants are given by McWilliam (1990), or are derivable from the E(B-V) presented by Feast, Whitelock & Carter (1990). Therefore, the first method was to consult these tabulations and to adopt these authors' estimates of Av or E(B-V), respectively. For stars not included their tables, we next estimated a distance to each star, assuming zero extinction, and using a recent set of tabulations for Mv (based on work by Gould & Flynn (1992) on K- and early-M giants). If a star was located within 75 pc of the Sun, we assigned zero extinction on the basis of its location within the local (dust-free) bubble (Fitzgerald 1968; Perry & Johnson 1982; Perry et al. 1982). Finally, the third method, for stars without tabulated Av and apparently beyond 75 pc if unreddened, was to compare the observed and intrinsic (B-V) colors of stars to be templated. If E(B-V) exceeded 0.075 then we formally reddened the template by R x E(B-V) (taking R, the ratio of total-to-selective extinction, as 3.10: *cf.* Barlow & Cohen 1977). The allowable range in (B-V) was obtained by halving Mermilliod's (1993, priv. comm.) estimate of the natural dispersion observed among unreddened stars of any given type (taken from his UBV archives: *e.g.*, Mermilliod 1994). For all stars found to have values of Av $\leq$0.044 by any of these three techniques, we applied no reddening because the effect of this would yield less than a 1% change in the template at 1.0 μm, and even less at our longer wavelengths. Our extinction law was taken to be that used in the SKY model (cf. Wainscoat et al. 1992).

3. The proposed radiometric network of stars

3.1. Requirements

We have assembled a list of candidate calibration objects based on their infrared brightness, degree of variability, complexity of spectrum, and isolation from nearby confusing sources. Our goal was to identify one such source per 50 square degrees of the sky, leading to a total of about 825 stars. The candidate calibration objects were selected from the IRAS Point Source Catalog (1988: hereafter PSC), and their nearby point, and extended-source, neighbors extracted, and the astronomical literature subsequently searched for additional associations, spectral types, luminosity classes, variability data, spectrometric, and photometric observations.

3.2. Selection criteria and procedure

Candidate calibration stars must conform to the following criteria (Walker & Cohen 1992), listed in the order that they were applied to our search of the IRAS database:

1. The candidate sources were required to have high quality IRAS flux measurements at 12 and 25 μm, and the limiting flux had to be consistent with achieving the desired source density (1 source per 50 deg^2) in the final list. The Infrared Point Source Sky Model "SKY" (Wainscoat et al. 1992; Cohen 1994) was used to estimate the density of K0-to-M0 giants at the galactic pole as a function of the limiting flux. It was found that inclusion of all stars with F25 > 1 Jy would satisfy the surface density requirement (where F25 is the IRAS PSC flux at 25 μm).

2. The sources had to be normal stars as defined by their location in the infrared color-color diagram. Walker & Cohen (1988) found that normal stars are confined to the [12]-[25]≤0.3, [25]-[60] ≤0.3 region of the IRAS 12, 25, 60 μm color plane so we required that the flux ratio F12/F25≥3.19 and, if the star had a high quality measurement at 60 μm (not required of all stars), the ratio F25/F60≥4.28.

A search of the PSC for sources that satisfied both criteria 1 and 2 produced 3331 stars. This subset of the PSC served as our database for further suitability tests.

3. As a further assurance of stellar "normality" we required that there be an IRAS association for the object, that the associated object be stellar, and not listed as a variable star, emission line object, or carbon star. We also demanded that the IRAS measurements indicate that the probability that the star is variable be less than 90%. Thirty seven sources were not stellar; 534 were optically-known variables, emission line objects, or carbon stars; and IRAS found 44 to be variable.

4. To insure precise photometry, each star must be isolated from other sources that might contribute flux within the field of view of a sensor. We required that the total flux from all known (*i.e.*, catalogued) sources within a radius of 6 arcmin of each network star be less than 5% of the flux at 12 and 25 μm from the potential calibrator. 662 sources failed this test, most of them located near the Galactic plane, or in the Magellanic Clouds, or along the line-of-sight to the Magellanic Clouds.

5. To further insure precise photometry, the star should not lie in a field of bright extended infrared emission. Here we demanded that the star not be associated by IRAS with a small extended source at either 12 or 25 μm, and that the emission at 12 μm due to infrared cirrus in the field (as determined by the PSC's CIRR3, 60-μm indicator) be less than 5% of the source's flux. The actual test applied is CIRR3<6.3xF12, based on our extrapolation of the mean cirrus emission spectrum from 60 to 12 μm, on consideration of the IRAS detectors' fields of view, and of the apertures and pixel sizes used by these recent infrared satellites. 244 sources failed the small extended source test, and 1451 failed to meet the infrared cirrus criterion. These rejected sources tend to be concentrated in a broad band about the Galactic plane; however, there is a significant high-latitude population.

6. Finally, we restricted our selection of calibration candidates to spectral types A0-M0 and luminosity classes II-IV (for K-M types) or III-V (for A-G), although stars were retained at this stage even if no luminosity class was available. This restriction was intended to limit the influence of molecular absorptions on the photospheric spectrum, and of excess emission due to either dust shells or free-free emission from stellar winds. (We emphasize this latter point in light of the fact that previous compendia of infrared "standard stars" have included a surprising number of supergiants. In our opinion, this risks including spectral energy distributions that are

wind-dominated, not photospheric, in the near- and mid-infrared, even among non-M-type supergiants.) Since IRAS detects late spectral types most efficiently, it is no surprise that 1742 stars failed these spectral constraints, including those stars for which no spectral type was found.

By cutting off our sample at type M0 we also greatly reduce the possibility of significant variability among the candidate stars. Eyer & Grenon (1997) have plotted the variability of stars across the Hertzsprung-Russell diagram. Their data demonstrate that one can select stars as late as M3III yet still not exceed 0.04 mag amplitude of variability in the Hipparcos band. K giants are usually not characterized by variability (Stebbins & Huffer 1930). In a recent study of 25% of the over 200 K giants named as known, or suspected, variables in the Yale Catalog of Bright Stars, Percy (1993) found only two stars to be clearly variable in B and/or V. Both are in our Atlas, and both showed visible amplitudes of 0.05^m on a time scale of order 1 month. In each case, all their precision near-infrared photometric points lie on the template curves, and their IRAS points are either on the template (31 Lyn = IRAS 08194+4320, K4.5III) or well within 2σ of it (AW CVn = IRAS 13495+3441); i.e., we can see no clear evidence in the infrared for problems of variability or non-contemporaneous photometry in these two stars.

3.3. Production of the Final List

Any star that met all of these criteria was the subject of an additional search of the literature to confirm the nature of the object, its spectral type and luminosity class, its inclusion in other star catalogs, and to annotate our list with the star's common name. Catalogs and databases searched include the Michigan Spectral Catalog, volumes 1 through 4 (Houk & Cowley 1975); the Fifth Yale Catalog of Bright Stars (Hoffleit & Warren 1991); Catalog of IRC Spectral Types (Bidelman 1980,1991); the Infrared Cross-Index (Schmitz *et al.* 1987); Catalog of Infrared Observations (Gezari *et al.* 1993); and SIMBAD. We deleted from the list all stars newly reclassified with unusual or composite spectral types, or listed as supergiants, or suspected to be variable. Composite types were retained among the binaries and doubles only when the combination of spatial separation and magnitude difference suggested negligible (<1%) contamination of the primary star by its companion.

3.4. Statistics of the Lists

Table 1 shows the distribution of those stars finally selected, according to their spectral type and luminosity class. The list is clearly dominated by K and M giants (482 out of the 573); only 87 stars have spectral type earlier than G9.5. This distribution is clearly the result of a compromise between the desire to use stars with relatively uncomplicated spectral energy distributions, and the necessity to have them bright enough to be observed in the infrared with at least low-resolution spectrographs.

The spatial distribution of the network of standards is shown in Fig. 2. The sky distribution of the current network of self-consistent low-resolution calibrators is shown in Fig. 2 which distinguishes; the 3 adopted calibrated Kurucz models (filled squares); the 9 observed low-resolution composites (open circles); and the 422 calibrated templates (crosses). The calibrators are well-distributed over the sky with the exception of several notable regions where the star density is low or zero. These are a region within about 15° of the Galactic Center, a 10° diameter region centered on the Large Magellanic Cloud, two regions near the north Galactic pole, and the IRAS 50° unsurveyed gap. There are another 123 stars that meet all our selection criteria but lack

Table 1. Spectral Types & Number of Stars & Number of Templates

Spectral Types	Number of Stars	Number of Templates
All A types	10	0
All F types	11	0
G0,1 all classes	4	0
G4 III	1	0
G5 II,III,IV	9	0
G6,6.5 II,III	4	0
G7,7.5 II,III	6	0
G8,8.5 II,III,IV	25	0
G9,9.5 III	21	4
K0,0.5 II,III,IV	47	46
K1,1.5 II,III	37	36
K2,2.5 II,III,IV	64	64
K3,3.5 II,III	72	71
K4,4.5 III	68	13
K5,5.5 II,III	103	101
K6 III	5	5
K7 III	4	4
K8 III	1	1
M0,0.5 II,III	79	77
M1.5,2.5 II,III	2	0
Total all types	573	422

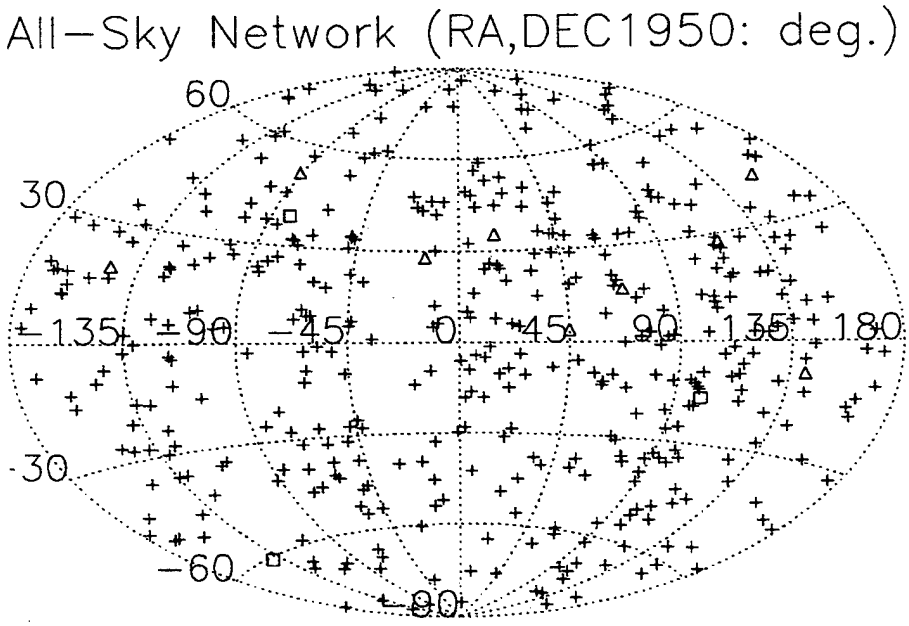

Fig. 2 The sky distribution of stars in the radiometric network. Squares denote spectra represented by adopted calibrated Kurucz models. Triangles are for low-resolution composites (bright K/M giants). Crosses are the 422 stars in the new fainter network.

a luminosity classification. These stars are all north of declination -20°, testifying to the need to extend the Michigan Classification project to the northern sky. The brightest star (α Boo) has 793 Jy at 12 μm. There are 14 stars brighter than 100 Jy at 12 μm, and 246 stars brighter than 10 Jy at 12 μm. The faintest stars have 5 Jy at 12 μm giving us over 2 orders of magnitude in mid-infrared dynamic range in the network.

4. Newly characterized filter systems

4.1. Absolute calibrations for zero magnitude

Table 2 indicates those systems and filters for which we have been able to secure full, cold, passband details and whose photometry we have been able to use in template normalization. We calculated terrestrial transmission curves specific to all the relevant observing sites, altitudes, and dates of observation using the PLEXUS code (Clark, 1996), and included a generic InSb radiance response curve when applicable. (Note that some authors, such as Alonso et al. (1994) already incorporate their detector's response in their published filter profiles, for example, for the broad passbands of the Tenerife 1.5m reflector (hereafter TCS = "Telescopio Carlos Sanchez"). The product of these three components for filter, atmosphere (when appropriate), and detector constitute our archived "system response curves". For every such curve, Table 2 presents our absolute calibrations in the form of the in-band irradiance for zero magnitude, its absolute uncertainty, the bandwidth, the associated isophotal flux density, $F\lambda$, and isophotal wavelength. These attributes were determined by integrating each system response curve over our calibrated Vega spectrum (Paper I) which we take as our definition of "zero magnitude" at all wavelengths. When we lacked the actual uncertainties in the measurement of a filter's transmission curve, we assigned a wavelength-independent fractional uncertainty of 5%. This component of error is in addition to the absolute uncertainty ("global bias": see Paper I) associated with the Vega spectrum (1.45%). Together, these components provide the error in the calculated in-band flux. The error associated with the isophotal flux density is strictly somewhat larger than that in the in-band irradiance because $F\lambda$ is derived from the in-band flux by dividing by the bandwidth, which has formal uncertainties of its own.

The narrowbands of Selby et al. (1988) are of particular value because their passbands sample the cleanest parts of the terrestrial transmission. One of us (PLH) has continued to make measurements with these filters. Any systematic differences between Hammersley's magnitudes and those of Selby et al. for stars in common are within the noise.

4.2. Zero point offsets

We also require the basis star(s) of any set of measurements. For many northern observers, Vega fills this niche. Consequently, if an observer publishes system magnitudes for Vega and these are not all zero, we can readily bring these magnitudes into our own context by forcing Vega to be zero. The algebraic quantities needed to achieve this are the "zero point offsets" (hereafter ZPO). Not every set of measurements includes Vega. Sirius can equally well provide us with the system offsets once we have calibrated it with respect to the zero magnitudes for the relevant system. Likewise, we can define the offsets if a set of measurements includes any cool giant stars for which we have created composite spectra.

Table 2. Calibration of the photometry systems supporting this work

System	Filter	In-band Flux W cm^{-2}	In-band Unc. W cm^{-2}	Bandwidth μm	F_λ(iso) W cm^{-2} μm^{-1}	λ_{iso} μm
Bessell-Brett	BBH	.3198E-13	.6190E-15	.2799E+00	.1143E-12	1.658
Bessell-Brett	BBK	.1432E-13	.2627E-15	.3613E+00	.3962E-13	2.204
Bessell-Brett	BBL	.3198E-14	.6208E-16	.4474E+00	.7148E-14	3.473
Bessell-Brett	BBL'	.2552E-14	.4950E-16	.5160E+00	.4945E-14	3.825
Bessell-Brett	BBM	.8579E-15	.1641E-16	.4057E+00	.2114E-14	4.764
DIRBE	Band2	.1419E-13	.2536E-15	.3640E+00	.3899E-13	2.214
DIRBE	Band3	.6256E-14	.1051E-15	.9086E+00	.6886E-14	3.507
DIRBE	Band4	.1267E-14	.2343E-16	.6561E+00	.1931E-14	4.877
DIRBE	Band5	.4240E-15	.6782E-17	.6560E+01	.6464E-16	11.58
DIRBE	Band6	.5105E-16	.9166E-18	.7238E+01	.7053E-17	20.22
ESO	ESOH	.2478E-13	.4271E-15	.2154E+00	.1150E-12	1.654
ESO	ESOK	.1366E-13	.2277E-15	.3393E+00	.4027E-13	2.195
ESO	ESOL	.3044E-14	.5163E-16	.5934E+00	.5130E-14	3.787
ESO	ESOM	.7378E-15	.1490E-16	.3388E+00	.2177E-14	4.728
ESO	ESON	.4422E-15	.7273E-17	.4036E+01	.1096E-15	10.14
ESO	ESON1	.1898E-15	.3856E-17	.8270E+00	.2295E-15	8.405
ESO	ESON2	.1390E-15	.2816E-17	.1087E+01	.1278E-15	9.750
ESO	ESON3	.5691E-16	.1252E-17	.1212E+01	.4696E-16	12.55
ESO	ESOQ	.1737E-16	.3717E-18	.1591E+01	.1092E-16	18.12
GBPP	ESOKPH	.2504E-13	.4195E-15	.2197E+00	.1140E-12	1.659
GBPP	ESOKPH0	.4211E-14	.8613E-16	.3307E-01	.1273E-12	1.605
GBPP	ESOKPK	.1311E-13	.2129E-15	.3294E+00	.3981E-13	2.202
GBPP	ESOKPK0	.1566E-14	.3046E-16	.4064E-01	.3853E-13	2.221
GBPP	ESOKPL'	.2943E-14	.4857E-16	.5774E+00	.5097E-14	3.794
GBPP	ESOKPL0	.2923E-15	.7230E-17	.5321E-01	.5494E-14	3.717
GBPP	ESOKPM	.6911E-15	.1218E-16	.3182E+00	.2172E-14	4.731
GBPP	ESOKPN1	.1457E-15	.2801E-17	.6163E+00	.2364E-15	8.41
GBPP	ESOKPN2	.1529E-15	.2805E-17	.1174E+01	.1302E-15	9.703
GBPP	ESOKPN3	.4068E-16	.8564E-18	.9467E+00	.4297E-16	12.84
IRAS	12	.5402E-15	.1124E-16	.6067E+01	.8905E-16	10.70
IRAS	25	.4583E-16	.8213E-18	.1002E+02	.4575E-17	22.54
IRC	BBK	.1432E-13	.1599E-15	.3613E+00	.3962E-13	2.204
IRTF(GBPP)	8.7	.1547E-15	.3037E-17	.8044E+00	.1924E-15	8.789
IRTF(GBPP)	9.8	.8895E-16	.1793E-17	.7242E+00	.1228E-15	9.847
IRTF(GBPP)	12.5	.5177E-16	.1119E-17	.1068E+01	.4847E-16	12.45
IRTF	N	.4199E-15	.6908E-17	.4360E+01	.9632E-16	10.47
IRTF	Q	.3580E-16	.7727E-18	.4985E+01	.7182E-17	20.13
KPNO	OTTO-H	.3133E-13	.5366E-15	.2735E+00	.1146E-12	1.656
KPNO	OTTO-K	.1266E-13	.2084E-15	.3274E+00	.3866E-13	2.219
KPNO	OTTO-L	.2845E-14	.4586E-16	.4044E+00	.7035E-14	3.488
KPNO	OTTO-M	.5140E-15	.9630E-17	.2256E+00	.2278E-14	4.672
McWilliam	2.17	.3846E-14	.6594E-16	.9239E-01	.4163E-13	2.175
McWilliam	2.40	.2103E-14	.3745E-16	.7397E-01	.2843E-13	2.409
Noguchi	Beijing-H	.2740E-13	.4170E-15	.2367E+00	.1158E-12	1.651
Noguchi	Beijing-K	.1271E-13	.1968E-15	.3187E+00	.3988E-13	2.200
Noguchi	Beijing-L	.2901E-14	.4626E-16	.5669E+00	.5116E-14	3.790
Noguchi	Tokyo-H	.2760E-13	.4202E-15	.2382E+00	.1159E-12	1.651
Noguchi	Tokyo-K	.1265E-13	.1959E-15	.3170E+00	.3991E-13	2.200

System	Filter	In-band Flux W cm^{-2}	In-band Unc. W cm^{-2}	Bandwidth μm	F_λ(iso) W cm^{-2} μm^{-1}	λ_{iso} μm
Noguchi	Tokyo-L	.2877E-14	.4587E-16	.5629E+00	.5110E-14	3.791
SAAO	SAH	.3319E-13	.6557E-15	.2893E+00	.1147E-12	1.655
SAAO	SAK	.1495E-13	.2910E-15	.3854E+00	.3878E-13	2.218
SAAO	SAL	.4096E-14	.7294E-16	.5480E+00	.7475E-14	3.433
Selby	Kn	.2155E-14	.4648E-16	.5471E-01	.3938E-13	2.208
Selby	Ln	.7324E-15	.1553E-16	.1416E+00	.5172E-14	3.779
Tenerife	TCSH	.2626E-13	.4359E-15	.2311E+00	.1137E-12	1.660
Tenerife	TCSK	.1347E-13	.2223E-15	.3208E+00	.4199E-13	2.170
Tenerife	TCSL'	.3074E-14	.5247E-16	.5298E+00	.5802E-14	3.668
UKIRT	H	.2950E-13	.4475E-15	.2563E+00	.1151E-12	1.654
UKIRT	K	.1412E-13	.2163E-15	.3413E+00	.4136E-13	2.179
UKIRT	L	.3290E-14	.5259E-16	.4976E+00	.6610E-14	3.544
UKIRT	L'	.2980E-14	.4768E-16	.5664E+00	.5261E-14	3.761
UKIRT	M	.7978E-15	.1377E-16	.3790E+00	.2105E-14	4.770
UKIRT	N	.4199E-15	.6908E-17	.4360E+01	.9632E-16	10.47
UKIRT	8.65	.2108E-15	.3891E-17	.1078E+01	.1955E-15	8.753
UKIRT	11.5	.7065E-16	.1448E-17	.1120E+01	.6308E-16	11.65
UKIRT	Q	.3580E-16	.7727E-18	.4985E+01	.7182E-17	20.13
WIRO	L	.4540E-14	.6959E-16	.6528E+00	.6955E-14	3.474
WIRO	M	.6424E-15	.1193E-16	.3644E+00	.1763E-14	4.990
WIRO	8.7	.1770E-15	.3412E-17	.8751E+00	.2023E-15	8.678
WIRO	N	.4280E-15	.7177E-17	.3155E+01	.1357E-15	9.603
WIRO	11.4	.1291E-15	.2391E-17	.1750E+01	.7376E-16	11.20
WIRO	12.6	.3512E-16	.8174E-18	.7648E+00	.4592E-16	12.62

Table 3 presents all the ZPOs for photometry data sets used to create templates. Note that a single system, such as the traditional ESO near-infrared filters, can have several sets of observers each of whose measurements may be subject to different ZPOs. Column 5 of Table 3 indicates observations of exactly which star(s) were used to define any ZPO for each observer. The final column in this table gives the full citation of the publication in which the relevant photometry appears.

Each of Appendices B, C, and D is organized so that measurements of Vega appear at the top, followed by data on any stars for which we have assembled and published a composite spectrum and, finally, data for typical stars of the network. Appendix A (Carter's SAAO measurements) have as basis an ensemble of B and A dwarfs. Vega itself is not observable from South Africa and the signal-to-noise obtained on the very bright Sirius does not reflect the real uncertainties in the system basis. The SAAO system, and its self-consistency, are described in detail by Carter (1990,1993) and by Glass (1991,1993), who also provide the relevant transformations between SAAO and the CTIO system, whose zero magnitude basis is Vega. Appendix E (Noguchi's work) was zero-pointed at *H K L* through his observations of β Gem and γ Dra. We cannot define an accurate zero point for *J* because our basis stars are these two K-giant composites. Further, after careful cross-checks between Noguchi's work and other characterized photometry from much higher sites, we decided not to use his *L*-band data for template scaling. This conservative approach is in keeping with the very low elevations of the Tokyo (sea level) and Xanglong (800m) sites.

Table 3. Zero point offsets for all photometry systems we have calibrated and used

Observer	System	Passband	ZPO(mag)	Definition	Citation
Allen	AAO	BBH	-.021±.01	HR 3314(A0V)	Allen \ Cragg 1983
Allen	AAO	BBK	-.012±.01	HR 3314(A0V)	Allen \ Cragg 1983
Allen	AAO	BBL'	-.029±.01	HR 3314(A0V)	Allen/ Cragg 1983
Alonso	Tenerife	TCSH	.017±.010	Vega	Alonso et al. 1994
Alonso	Tenerife	TCSK	.026±.010	Vega	Alonso et al. 1994
Alonso	Tenerife	TCSL'	-.027±.011	Vega	Alonso et al. 1994
Bouchet	ESO	ESOH	-.059±.01	Sirius	Bouchet et al. 1991
Bouchet	ESO	ESOK	-.031±.01	Sirius	Bouchet et al. 1991
Bouchet	ESO	ESOL	-.012±.01	Sirius	Bouchet et al. 1991
Bouchet	ESO	ESOM	-.017±.01	Sirius	Bouchet et al. 1991
Bouchet	ESO	ESOH	-.039±.009	Sirius	Bouchet et al. 1989
Bouchet	ESO	ESOK	-.014±.006	Sirius	Bouchet et al. 1989
Bouchet	ESO	ESOL	.014±.008	Sirius	Bouchet et al. 1989
Bouchet	ESO	ESOM	.007±.019	Sirius	Bouchet et al. 1989
Bouchet	ESO	ESON1	.111±.020	Sirius	Bouchet et al. 1989
Bouchet	ESO	ESON2	.014±.016	Sirius	Bouchet et al. 1989
Bouchet	ESO	ESON3	-.021±.021	Sirius	Bouchet et al. 1989
Carrasco	San Pedro Martir	BBH	.000±.003	Vega	Carrasco et al. 1991
Carrasco	San Pedro Martir	BBK	.000±.003	Vega	Carrasco et al. 1991
Carter	SAAO	SAH	.004±.005	A0V-ensemble	Appendix A
Carter	SAAO	SAK	-.002±.005	A0V-ensemble	Appendix A
Carter	SAAO	SAL	-.002±.010	A0V-ensemble	Appendix A
Castor	KPNO	OTTO-H	.00±.01	Vega	Castor \ Simon 1983
Castor	KPNO	OTTO-K	.00±.01	Vega	Castor \ Simon 1983
Castor	KPNO	OTTO-L	.00±.01	Vega	Castor \ Simon 1983
Castor	KPNO	OTTO-M	.00±.01	Vega	Castor \ Simon 1983
COBE	DIRBE	Band2	.00±.02	all composites	Paper IX
COBE	DIRBE	Band3	.00±.02	all composites	Paper IX
COBE	DIRBE	Band4	.00±.02	all composites	Paper IX
COBE	DIRBE	Band5	.00±.02	all composites	Paper IX
COBE	DIRBE	Band6	.00±.04	all composites	Paper IX
Engels	ESO	BBH	-.028±.02	Sirius	Engels 1981
Engels	ESO	BBK	-.011±.02	Sirius	Engels 1981
Engels	ESO	BBL	.039±.02	Sirius	Engels 1981
Engels	ESO	BBM	-.017±.02	Sirius	Engels 1981
Engels	ESO	BBM	-.017±.02	Sirius	Koornneef 1983b
Fluks	ESO	ESOH	-.059±.01	Sirius	Fluks et al. 1994
Fluks	ESO	ESOK	-.031±.01	Sirius	Fluks et al. 1994
Fluks	ESO	ESOL	-.012±.01	Sirius	Fluks et al. 1994
Fluks	ESO	ESOM	-.017±.01	Sirius	Fluks et al. 1994
Frogel	KPNO	BBH	.00±.01	Vega	Frogel et al. 1978
Frogel	KPNO	BBK	.00±.01	Vega	Frogel et al. 1978
Grasdalen	WIRO	BBK	.02±.02	Vega	Grasdalen et al. 1983
Grasdalen	WIRO	L	.03±.02	Vega	Grasdalen et al. 1983
Grasdalen	WIRO	M	.03±.02	Vega	Grasdalen et al. 1983

Observer	System	Passband	ZPO(mag)	Definition	Citation
Grasdalen	WIRO	8.7	.03±.02	Vega	Grasdalen et al. 1983
Grasdalen	WIRO	10.0	.03±.02	Vega	Grasdalen et al. 1983
Grasdalen	WIRO	11.4	.03±.02	Vega	Grasdalen et al. 1983
Grasdalen	WIRO	12.6	.03±.02	Vega	Grasdalen et al. 1983
Hammersley	Tenerife	Jn	-0.0±.010	Vega	Appendix C
Hammersley	Tenerife	Kn	0.000±.010	Vega	Appendix C
Hammersley	Tenerife	Ln	0.005±010	Vega	Appendix C
Hammersley	Tenerife	TCSJ	.001±.005	Vega	Appendix B
Hammersley	Tenerife	TCSH	.000±.005	Vega	Appendix B
Hammersley	Tenerife	TCSK	.000±.005	Vega	Appendix B
Hammersley	Tenerife	TCSL'	-.001±.007	Vega	Appendix B
IRC	IRC	BBK	-.022±0.050	prelim. Rel.2	Neugebauer & Leighton 1969
IRC(south)	IRC	BBK	-.04±0.050	prelim. Rel.2	Neugebauer & Leighton 1969
Johnson	LPL	V--BBK	-.04±.02	Rel.1 templates	Johnson et al. 1966
Johnson	LPL	V--BBL	025±.02	Rel.1 templates	Johnson et al. 1966
Kessler	IRTF	8.7	.005±.008	4 composites	Hammersley et al. 1998
Kessler	IRTF	9.8	.014±.008	4 composites	Hammersley et al. 1998
Kessler	IRTF	N	-.010±.010	4 composites	Hammersley et al. 1998
Kessler	IRTF	12.5	-.013±.010	4 composites	Hammersley et al. 1998
Kessler	IRTF	Q	-.003±.007	4 composites	Hammersley et al. 1998
Kidger	Tenerife	TCSJ	.001±.005	Vega	Appendix D
Kidger	Tenerife	TCSH	.000±.005	Vega	Appendix D
Kidger	Tenerife	TCSK	.000±.005	Vega	Appendix D
Kidger	Tenerife	TCSL'	-.001±.007	Vega	Appendix D
Koornneef	ESO	BBH	-.059±.01	Sirius	Koornneef 1983a
Koornneef	ESO	BBK	-.031±01	Sirius	Koornneef 1983a
Koornneef	ESO	BBL	-.012±.01	Sirius	Koornneef 1983a
Koornneef	ESO	BBM	-.017±01	Sirius	Koornneef 1983a
McWilliam	KPNO	2.17	-.002±006	Vega	McWilliam Lambert 1984
McWilliam	KPNO	2.40	-.007±.006	Vega	McWilliam Lambert 1984
McWilliam	KPNO	2.17	.028±.005	α Leo	McWilliam Lambert 1984
McWilliam	KPNO	2.40	.046±005	α Leo	McWilliam Lambert 1984
McWilliam	KPNO	2.17	.095±.009	HR 6092	McWilliam Lambert 1984
McWilliam	KPNO	2.40	.122±.009	HR 6092	McWilliam Lambert 1984
Noguchi	Beijing	Xanglong-H	.046±.020	β Gem, γ Dra	Appendix E
Noguchi	Beijing	Xanglong-K	.030±.020	β Gem, γ Dra	Appendix E
Noguchi	Beijing	Xanglong-L	-.059±.020	β Gem, γ Dra	Appendix E
Noguchi	Tokyo	ISAS-H	.046±.020	β Gem, γ Dra	Appendix E
Noguchi	Tokyo	ISAS-K	.030±.020	β Gem, γ Dra	Appendix E
Noguchi	Tokyo	ISAS-L	-.059±.020	β Gem, γ Dra	Appendix E
Selby	Tenerife	Kn	0.00±.01	Vega	Selby et al. 1988
Selby	Tenerife	Ln	0.00±01	Vega	Selby et al. 1988
Tapia	San Pedro	BBH	-.04±02	Vega	Tapia et al1986
Tapia	San Pedro	BBK	-.01±.02	Vega	Tapia et al 1986
Tapia	San Pedro	L	-.02±02	Vega	Tapia et al 1986
Tapia	San Pedro	M	.01±.02	Vega	Tapia et al 1986
Tokunaga	IRTF	UKIRT-N	.00±013	Sirius & Vega	Tokunaga et al 1986
Tokunaga	IRTF	UKIRT-Q	.0±.013	Sirius & Vega	Tokunaga et al 1986

Observer	System	Passband	ZPO(mag)	Definition	Citation
Van der Blieck	ESO	ESOKPH	-.013±.006	Sirius	van der Blieck et al 1996
Van der Blieck	ESO	ESOKPH0	-.038±.008	Sirius	van der Blieck et al 1996
Van der Blieck	ESO	ESOKPK	-.016±.006	Sirius	van der Blieck et al 1996
Van der Blieck	ESO	ESOKPK0	-.031±.001	Sirius	van der Blieck et al 1996
van der Blieck	ESO	ESOKPL'	-.017±.001	Sirius	van der Blieck et al 1996
van der Blieck	ESO	ESOKPL0	-.009±.010	Sirius	van der Blieck et al 1996
van der Blieck	ESO	ESOKPM	.003±.001	Sirius	van der Blieck et al 1996
van der Blieck	ESO	ESOKPN1	.034±.015	Sirius	van der Blieck et al 1996
van der Blieck	ESO	ESOKPN2	.063±.010	Sirius	van der Blieck et al 1996
van der Blieck	ESO	ESOKPN3	.003±.017	Sirius	van der Blieck et al 1996

Note: The "4 composites" used to zero-point the "Kessler IRTF" data were α Tau, β Gem, α Boo, and γ Dra.

4.3 Testing the new photometry for "closure"

We would like to assure that our well-characterized systems demonstrate "closure" in that their magnitudes for all our composites yield exactly what we would expect when integrating their passbands over these cool stellar spectra. To exemplify this closure we offer tests of Hammersley's photometry. First we treat his narrowband photometry in the Selby et al. (1988) bandpasses. The data set in Appendix C includes stars newly measured by Hammersley but without observations by Selby et al. (1988), and remeasurements to greater precision by Hammersley that were selected from Selby's archive. Appendix C incorporates data on all our composites so we have integrated combined filter, detector and atmosphere profiles over the composites to define our expected magnitudes. We have examined the ensemble average of differences in the sense (Appendix C-minus-expectation) for those bands we are able to integrate over our composite spectra. These yielded: *Kn*, 0.004±0.003; *Ln*, -0.007±0.005. After applying the zero point offsets (from Table 3) we found the final differences to be: 0.004±0.003; and –0.002±0.005, for the two relevant passbands. *Kn* and *Ln* are clearly consistent with zero, indicating a self-consistent set of magnitudes.

We have applied the identical analysis to Hammersley's broadband data (Appendix B) using Sirius and the seven cool composites. These yielded ensemble mean "observed-minus-expected" values of: *H*, -0.019±0.015; *K*, +0.002±0.013. After zero point corrections (Table 3) we found final mean differences of -0.019±0.015, and +0.003±0.013, for the *H K*, respectively. Again, *H* and *K* are clearly consistent with zero. So we likewise conclude that Hammersley's broadband measurements are self-consistent in the mean.

Both the *Jn* and *J* filters cut on slightly before our composites starting wavelengths so we cannot use these photometry points to scale any templates in the present paper. This implies that the magnitudes created from our set of composite spectra and presented in Table 3a of Paper IV for both *Jn* and *J* should be treated strictly as approximations. All *Jn* and *J* are potentially too faint by about 0.02^{m}. This effect does not affect any of the other magnitudes in Paper IV because all the other passbands are entirely contained within our 1.2-35 μm range, and in no way influences the scaling of templates because, again, *Jm* and *J* are never used for this purpose.

4.4. Other useful photometry archives

Table 2 summarizes all sets of photometry data that we have been able to utilize. The most abundant contributors (ranked in descending order of data directly useful to us for template scaling) have been: IRAS; "IRC" (subsection 4a); Carter (Appendix A); the "ISO Ground-Based

Preparatory Programme" (subsection 4c); Tenerife broadband programs (Appendices B and D); Johnson; the older ESO archives (Koornneef; Bouchet and colleagues); and Noguchi (Appendix E). Of course, both IRAS and IRC measurements suffer from appreciable formal uncertainties so that these data carry less weight in determining the mean scale factor of a template than do precision near-infrared (ground-based) data. Some usage of other photometry appears below.

a) The CalTech Two Micron Sky Survey

For many of our K- and M-giants, the CalTech Two Micron Sky Survey (Neugebauer & Leighton 1969: hereafter "IRC") provides K-band magnitudes, albeit measured with a PbS cell. An archival search at CalTech failed to produce a profile of the transmission of the actual *K* filter so we adopted Bessell & Brett's (1988) overall system response curve. In addition to the published IRC, we were able to utilize the unpublished southern extension (to declination –42°, thereby adding another 700+ stars to our IRC archive. Due to the rather large magnitude uncertainties in both the IRC data sets (typically 0.06^{m}), we felt it important to assess the actual zero point offset and its uncertainty from a large body of stars. Consequently, we created the new generation of calibrated templates firstly without using any IRC data. Then we integrated all these new templates over the IRC passband and compared our synthesized IRC-*K* magnitudes with those of the IRC and IRC/south separately. This provided us with separate zero point corrections for the IRC and IRC/south (see Table 3). The photometric uncertainties of the IRC/south were magnitude dependent, thus we adopted 0.05^{m} error for $K < 2.0$ and 0.06^{m} for $K > 2.0$, derived from the median uncertainty in each one-magnitude bin.

b) IRAS

For every star in the network, we have IRAS 12- and 25- μm data from both the PSC and the Faint Source Survey (Moshir et al. 1992: hereafter FSS). We translated both the PSC and FSS flux densities into our context (cf. Paper I) by multiplying by appropriate factors. For the PSC2 we used 0.976±0.007 and 0.936±0.022 at 12 and 25 μm, respectively (Table 3 of Paper I). To create the corresponding factors for the FSS we simply compared the ratio of FSS to PSC flux densities for 525 stars from the Walker-Cohen Atlas with spectral types late G to early M III. This gave FSS12/PSC12=0.994±0.003 and FSS25/PSC25=0.989±0.003, whence the associated scale factors to convert FSS Jy into our context are 1.006±0.003 and 1.011±0.004. We made use of both PSC and FSS flux densities because they represent independent methods of analyzing the original IRAS data.

c) "ISO Ground-Based Preparatory Programme: An ESO Key Programme"

In support of ISO, ESO organized a major ground-based photometry program of several hundred stars across the southern sky (van der Bliek *et al.* 1996), with extension to the north by Hammersley. The basic effort was directed toward securing near-infrared data in the common passbands of *J H K L*. The southern work also obtained data in five near-infrared narrowbands on many stars, supplemented occasionally by narrowbands in the 10-μm region. There was also a brief mid-infrared foray into the north, using the IRTF, that took 10 and 20-μm measurements on about 20 K- and M-giants. These observations took place in February/March of 1992; were analyzed with a multi-night reduction technique by Hammersley and delivered to ISO Calibration Liaison in November 1995 (hence their reference as IRTF_ISO 1995 in template headers); and will appear as Hammersley et al. (1998). All the relevant ESO passbands have been recharacterized and archived at Vilspa with the photometry, in support of ISO. For those

from the IRTF, we had already obtained copies of the original manufacturer's filter transmission curves. The original criteria for star selection by ESO were very different from those of our own network and resulted dominantly in warm dwarfs. However, a number of stars are in common with the Walker-Cohen network, particularly among the infrared-brighter stars covered at the longer wavelengths. The southern data furnish valuable photometry for an appreciable number of stars in our network.

d) Other useful characterized photometry

In addition to the above-mentioned photometry in characterized passbands, we located two other data sets that we were able to characterize adequately to the point where they provide valuable data to constrain the scaling of templates. The first is DIRBE, with flux densities drawn from the special subset of DIRBE's own calibrators (Hauser et al. 1997). Zero point offsets were established as essentially zero by Cohen (1998) and his associated zero-point uncertainties were used (Table 3).

The second is from McWilliam & Lambert (1984), who give filter profiles for two narrow bands near 2.17 and 2.40 μm, to which we added our mean atmospheric transmission curve for Kitt Peak, and the detector's spectral response function. The resulting system passbands were archived and integrated over our calibrated model for Vega (Paper I) to provide "zero magnitude" values of the in-band fluxes and isophotal flux densities (Table 2). McWilliam & Lambert (1984) observed over 100 late-K and M-giants through these two filters and in a broad *J* band, setting their color indices by Vega, which should have resulted in adequate zero points. However, two other "standard stars" were used for sky coverage. McWilliam (1996) has kindly provided us with full details so we know which of the three reference stars (Vega, α Leo, HR 6092) was used for each published program giant. From his detailed notes one can see that the *J* magnitudes adopted for the other two standards were discordant with the zero point for Vega by about 0.08^{m} (α Leo) and 0.06^{m} (HR 6092). These offsets in no way affect the measurements, or the conclusions, of McWilliam & Lambert (1984), who treated their stars solely in terms of color indices, adjusted to zero index for Vega. But, for our purposes, it is clearly essential to define separate zero point offsets for each cool giant, based on the actual standard star used.

A total of 34 McWilliam-Lambert program stars are in common with the set of 183 (first generation) templates that we created in October 1994 to test and establish the techniques described in the present paper. One star with a published absolute spectrum, γ Dra, was also measured. We integrated these two system passbands over the 34 calibrated templates and 1 composite spectrum to define our expected values for [2.17] and [2.40], along with formal uncertainties based on both the original composites and on the bias (Section 6) additionally associated with each of the individual calibrated templates.

These 35 stars fall into three groups; 13 stars were referred directly to Vega; 17 to α Leo; and 5 to HR 6092. We assigned individual errors to the McWilliam-Lambert observations using the typical uncertainties they specify, with slight reductions for stars measured more than once. Direct comparisons of our expected magnitudes with those observed by McWilliam & Lambert yielded the zero point offsets for this data set (Table 3). Our tabulated measurement errors also accommodate (in quadrature with the photometric measurement errors) the uncertainties with which we have been able to define these three pairs of zero point corrections. Once we defined the three sets of zero point offsets from the first generation templates for these 35 fiduciary stars, we were able to use McWilliam & Lambert photometry as part of the process for making new templates for these stars, and for 11 other stars in our network.

5. The template code

The creation of a calibrated spectral template for a star begins with selection of the star from the input list of stars to be templated. The input list is organized by IRAS name and also contains other designations for the star, such as, the HD, HR, and IRC numbers; a star common name; a spectral type and luminosity class; V, B-V, U-V; and the IRAS PSC and FCS 12 and 25 μm photometry. A smoothed composite is then selected that matches the spectral type and luminosity class of the star, and is corrected for extinction (see Section 2) along the line of sight to the star. Our photometry data base is then searched for observations of the star. The photometry data base is indexed by IRAS name and contains for each observation of the star the observed magnitude and its uncertainty; the name of the filter used; and a reference to the observer. These data are essential to recovering the proper relative system spectral response curve (filter), zero point offset (see Table 3), and zero magnitude flux calibration (see Table 2). A filter is selected. The observed magnitude in that filter is corrected for zero point offset, and then converted to an observed in-band flux using the zero magnitude flux calibration. Next the spectral irradiance of the extinction corrected, smoothed, composite is integrated over the spectral passband corresponding to the observed magnitude, producing an in-band flux for the composite. The ratio of the observed in-band flux to the composite in-band flux and its variance are then calculated. This process is repeated for each photometric measurement of the star. The inverse variance weighted mean ratio is then determined, and the new calibrated spectral template produced as the product of the mean ratio times the spectral irradiance of the extinction corrected, smoothed, composite. The errors of the new template are calculated from those of the original composite with the global bias component combined (root sum squared) with the error in the mean ratio (see Paper IV for a discussion of global and local biases).

We took stellar spectral classifications from a variety of sources, favoring the Perkins Revised types of Keenan & McNeil (1989) when available, or the Michigan Spectral Catalog, or the 5th Version of the Yale Catalog of Bright Stars (ranked in order of preference). These were applied over a range of ±0.5 of a spectral subclass so, for example, we applied the template derived from β Gem (K0IIIb) to any star between G9.5III and K0.5III. On the basis of analysis of the small differences between our composites for α Tau (K5+III) and β And (M0+IIIa), we additionally applied the K5 template to stars with types K5-M0, K6, K7, and K8III.

None of the stars for which we have already published low-resolution composite spectra was retained in the set of objects to be templated. Thus, αTra, a K3III for which Paper VI presents only a 3-35 μm high-resolution spectrum, is templated at low resolution in the present paper based on the 1.2-35 μm K3III spectrum of Paper IV.

We did not use Koornneef's (1983a) homogenized photometry when photometry from Bouchet et al. (1991) was available because these latter authors rereduced all the ESO data together, thereby subsuming Koornneef's work. We also found, after detailed comparisons between Appendix E and other *L*-band data on stars in common, that our own 3.5- μm measurements from low-altitude sites in China and Japan have rather large uncertainties compared with those in *J H K* and we preferred not use any of these *L*-band data.

Fig. 3 presents a montage of 8 calibrated stellar templates, offering a variety of different spectral types and available sets of photometry. All are shown in $\lambda^4 F_\lambda$ space, highlighting the essentially Rayleigh-Jeans character of the long-wavelength continua. All of the 422 calibrated templates are plotted in Appendix F of this volume.

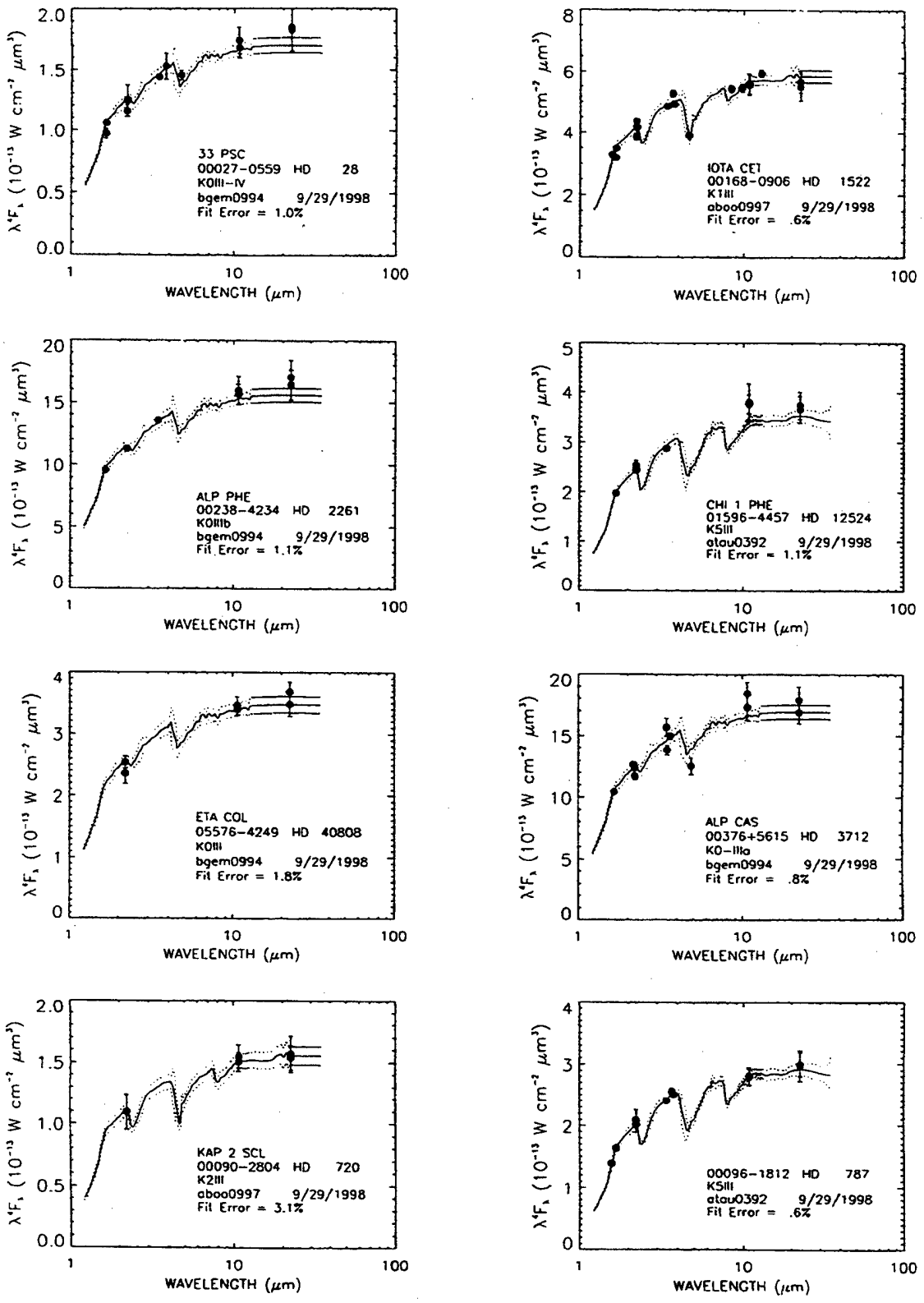

Fig. 3 Montage of 8 representative templates showing the individual characterized photometry used to normalize each template.

6. Statistics of the templates

Several distributions are of interest, namely those for the extinction values that we applied to the templates, the number of characterized photometry points available to normalize each template, the template biases, and the derived angular diameters.

Only 83 of the 422 calibrators were determined to have nonzero extinction and the distribution by Av appears in Fig. 4. At our current limiting flux density, most of these cool giants are within the local bubble.

The frequency of photometric observations (Fig. 5) clearly indicates the members of the network for which IRAS data alone provide the template normalization. These stars have only 4 photometric (PSC2 and FSS) measurements. Typical network calibrators have 5-10 measurements available for template scaling, reducing the resultant template bias by about a factor of 3 over that for an object with only IRAS data. Stars with 11-23 measurements have biases reduced by a further factor of 2.

Fig. 6 shows some evidence for a trimodal distribution in template biases. Stars in the sharper peak centered at about 1% represent 64% of the total. The 26% of the sample in the peak with bias centered at ~2.75% are stars for which we would like to secure more precise photometry in order to move them into the major peak associated with stars with the best available data. The peak centered at 4.75% arises from objects that entirely lack precision near-infrared photometry and were templated on the sole basis of their IRAS flux densities (perhaps augmented by an IRC or Johnson *K*-magnitude).

Fig. 7 illustrates the histogram of angular diameters for the new calibrators. This is sharply peaked, as expected from consideration of source counts, in the smallest bin between 1.5 and 2.5 mas. Diameters of this order have been measured recently by Van Belle and colleagues (Van Belle et al. 1998), using the Palomar Testbed Interferometer for visual intensity measurements in the K band. In Fig. 8 we compare the interferometric directly observed diameters with our own, labeled "radiometric diameters". The agreement is satisfactory and our method appears to lead to sensible diameters with formal errors significantly smaller than those associated with visual intensity measurements on stars at this brightness level (K±3.0).

Table 4 summarizes the 422 stars for which we have created templates. For brevity, the version of this table that appears in the printed paper lists just HD numbers (because these designate the file names of the calibrated spectral templates) and the derived angular diameters (with their uncertainties) in mas. The on-line file version (summary.dat) contains much more information on each star, and presents IRAS designations, common names, HR and HD numbers, the extinction we applied to the templates, the angular diameters with uncertainties, the template bias, and the number of photometry points used to normalize each individual template. To preserve the relationship between these two versions, note that Table 4 is ordered by implicit IRASNAME or, effectively, by B1950 Right Ascension.

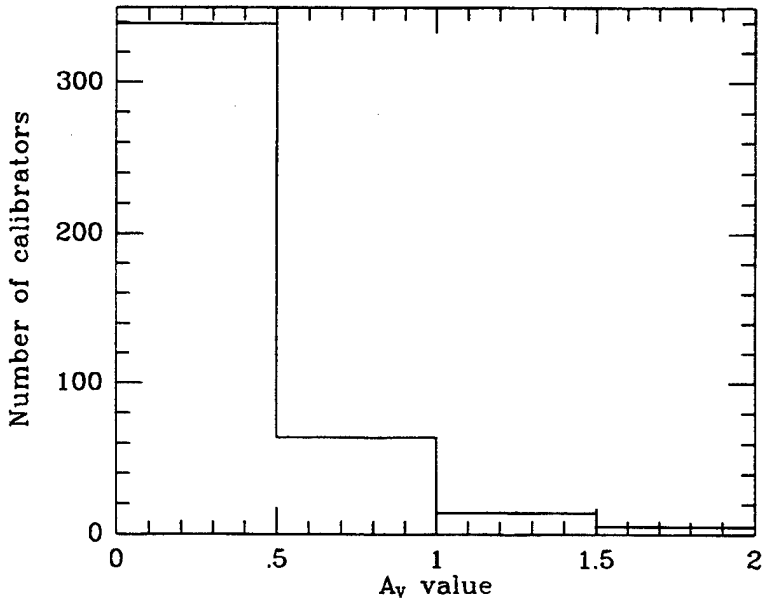

Fig. 4 The distribution of extinction values toward the 422 K/M giants.

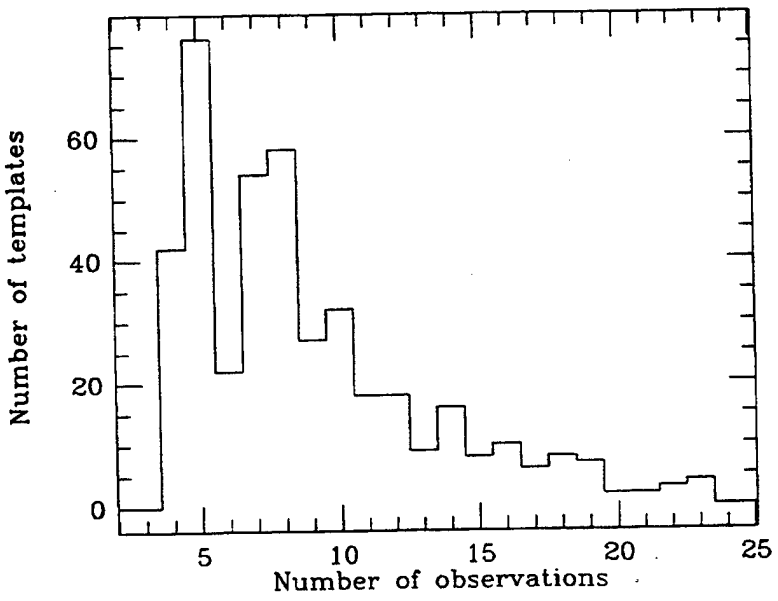

Fig. 5 The distribution of the number of available photometry points used to normalize each of the 422 calibrated spectral templates.

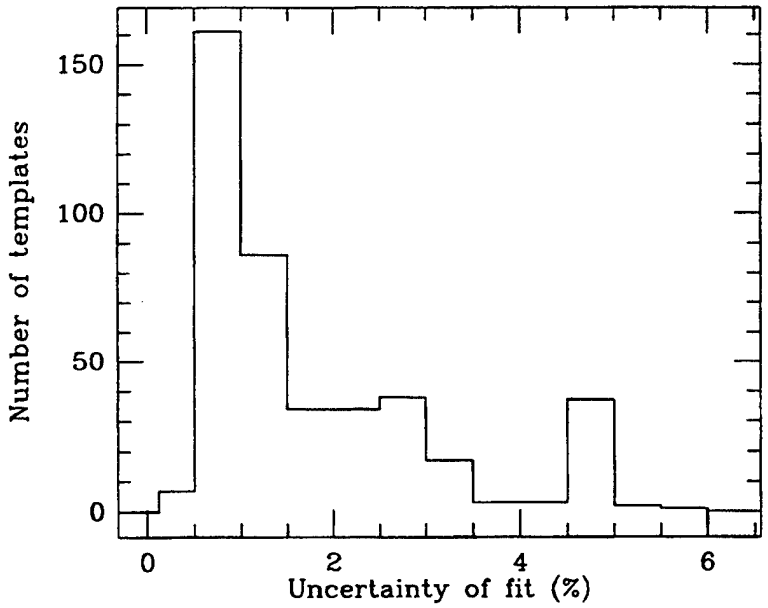

Fig. 6 The distribution of template biases among the 422 templates.

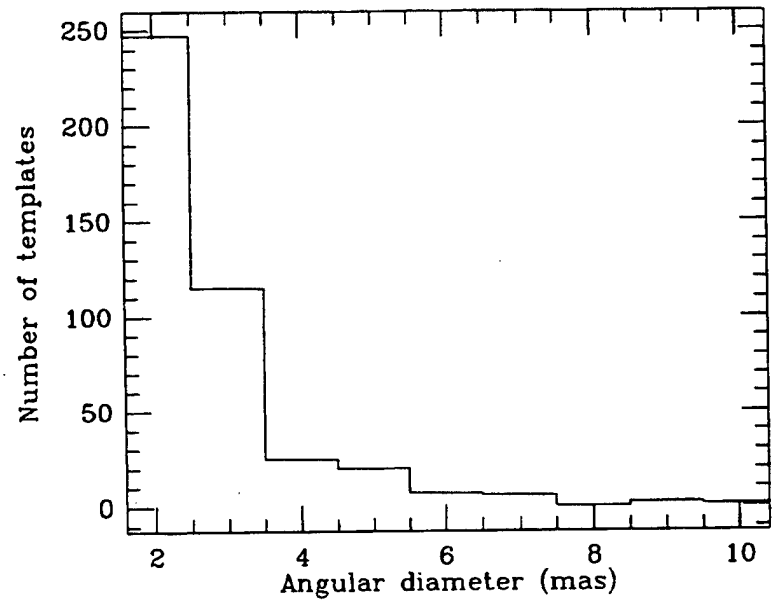

Fig. 7 The distribution of our derived angular diameters.

Table 4. Stars for which we have created calibrated templates

HD No.	Spectral Type	Diam. (mas)	Unc. (mas)	HD No.	Spectral Type	Diam. (mas)	Unc. (mas)
28	K0III-IV	1.73	.019	12524	K5III	2.77	.032
720	K2III	1.73	.032	12929	K2-IIIab	6.90	.074
787	K5III	2.50	.026	13520	K3.5III	2.94	.048
1032	M0.5III	3.07	.075	13596	M0III	2.44	.026
1255	M0III	3.06	.054	14146	M0III	1.99	.026
1240	M0III	2.58	.045	14641	K5III	2.20	.025
1522	K1III	3.37	.036	14890	K2III	1.91	.037
1635	K3-III	1.81	.020	14872	K4.5III	3.28	.056
1632	K5III	2.44	.027	15656	K5III	2.64	.029
1879	M0III	2.02	.023	16212	M0III	3.11	.032
2261	K0IIIb	5.25	.060	16815	K0.5IIIb	2.17	.023
2436	K5III	1.99	.022	17361	K1.5III	1.99	.030
2486	M0III	3.47	.089	17709	K5.5III	3.94	.059
2637	M0III	2.38	.025	18293	K3III	2.31	.057
3346	K6III	3.24	.053	18449	K2III	1.93	.030
3712	K0-IIIa	5.47	.058	19460	M0III	1.94	.020
4128	K0III	5.29	.054	19476	K0III	2.28	.025
4301	M0III	2.17	.024	19656	K1III	1.94	.022
4502	K1IIe	2.72	.036	20356	K5III	1.87	.021
4815	K5III	2.19	.025	20468	K2IIb	2.57	.035
5112	M0III	3.51	.037	20644	K3IIIa	3.61	.045
5234	K2III	1.97	.021	20893	K3III	1.85	.029
5462	M0III	2.36	.032	21552	K3III	3.13	.042
6112	M0III	2.51	.039	22663	K1III	1.95	.022
6186	K0III	1.94	.031	23249	K0+IV	2.48	.026
5848	K2II-III	2.51	.065	23319	K2.5III	2.12	.037
6805	K2-III	3.44	.036	23817	K2III	2.80	.075
6953	K7III	1.90	.036	25025	M0.5IIIb	8.74	.088
7318	K0III	1.66	.029	25165	K5III	2.04	.021
7647	K5III	2.09	.035	25477	K5III	2.01	.040
8388	K7III	2.58	.048	25274	K2III	2.02	.030
8498	M0III	2.52	.028	26311	K1II-III	1.78	.021
8512	K0IIIb	2.76	.030	26526	M0III	1.88	.031
8705	K2.5IIIb	2.06	.040	26846	K3III	1.86	.019
8810	K5III	2.13	.065	26967	K2III	2.76	.029
9138	K3III	2.57	.026	27442	K2IVa	1.95	.049
9362	K0IIIb	2.23	.023	27482	K5III	2.27	.031
9692	M0III	1.83	.021	27639	M0IIIab	3.08	.039
9927	K3-III	3.69	.046	27697	G9.5III	2.28	.024
10110	K5III	1.91	.021	28413	K4.5III	1.92	.050
10380	K3IIIb	2.93	.030	28305	G9.5III	2.61	.035
10550	K3II-III	2.11	.037	28749	K3II-III	2.15	.040
11353	K0III	2.73	.029	29085	K0+III	1.73	.018

Table 4 (cont.). Stars for which we have created calibrated templates

HD No.	Spectral Type	Diam. (mas)	Unc. (mas)	HD No.	Spectral Type	Diam. (mas)	Unc. (mas)
29503	K1.5IIIb	2.76	.031	47174	K2-III	1.97	.022
30080	K2III	1.78	.035	47536	K2III	1.74	.026
30338	K3III	2.03	.052	47667	K2IIIa	2.63	.043
31421	K2-III	2.74	.031	47914	K5III	2.73	.029
31398	K3II	7.38	.121	48217	M0III	2.73	.043
31767	K2-II	2.73	.044	48433	K0.5III	2.07	.027
31312	K5III	1.88	.025	49517	K3III	1.82	.046
32820	K3III	2.32	.030	49293	K0+IIIa	1.91	.023
32887	K5IIIv	6.08	.064	49877	K5III	2.27	.057
33554	K5III	2.69	.030	49520	K3III	1.96	.035
33872	K5III	1.93	.028	50310	K1III	4.46	.114
33856	K1III	2.19	.023	49968	K5III	1.93	.020
34334	K2.5III	2.68	.049	50235	K5III	2.25	.036
34450	M0.5III	2.25	.037	53501	K3III	2.08	.052
35536	K5III	2.25	.025	52960	K3III	2.11	.036
36167	K5III	3.66	.058	52976	K6III	1.96	.032
36678	M0III	2.64	.028	53287	M0III	2.14	.033
37160	K0IIIb	2.19	.023	53510	M0III	2.06	.021
37984	K1III	1.92	.021	54716	K3.5III	2.64	.039
38944	M0III	4.24	.047	55865	K0III	2.50	.060
39003	K0III	2.43	.031	55526	K2III	1.87	.048
39523	K1III	2.00	.052	55775	K5III	2.15	.056
39364	K0III	2.63	.041	57423	M0IIIab	2.94	.031
39425	K1.5III	3.99	.044	57646	K5III	2.26	.024
39400	K1.5IIb	2.46	.045	59311	K5III	2.10	.034
39853	K5III	2.38	.027	59381	K5III	2.26	.038
40091	K6III	2.58	.042	59294	K1III	2.31	.027
40035	K0-III	2.48	.026	59717	K5III	6.86	.100
40808	K0III	2.48	.034	60522	M0III-IIIb	5.00	.051
41047	K5III	2.47	.028	61248	K3III	2.44	.065
41312	K3III	2.42	.038	61338	K5III	3.28	.038
42540	K2.5III	1.95	.048	61294	M0III	2.52	.026
42633	K3III	1.82	.030	61603	K5III	1.96	.053
43785	K0.5IIIa	1.75	.025	62689	M0III	1.98	.056
44951	K3III	1.81	.031	61935	K0III	2.27	.023
45018	K5III	2.50	.041	62044	K1III	2.44	.029
45669	K5III	2.19	.053	62285	K4.5III	2.62	.053
46037	M0-1III	2.20	.038	63295	K0III	2.32	.057
46184	K3III	1.80	.027	62721	K5III	3.02	.034
46815	K3III	1.90	.029	62902	K5III	1.83	.031
45866	K5III	1.90	.025	63744	K0III	1.67	.025
47182	K4-5III	2.01	.036	63696	K5III	2.16	.039
47205	K1.5III-IV	2.43	.025	63697	K3III	1.88	.039

Table 4 (cont.). Stars for which we have created calibrated templates

HD No.	Spectral Type	Diam. (mas)	Unc. (mas)	HD No.	Spectral Type	Diam. (mas)	Unc. (mas)
64307	K3III	2.02	.033	90957	K3III	1.81	.036
65662	K3.5II-III	1.97	.053	91056	M0III	4.40	.112
65695	K2III	1.90	.032	92305	K5III	4.87	.051
66141	K2IIIb	2.69	.029	92682	K3II	2.19	.061
67582	K3III	2.39	.062	92523	K3III	2.43	.028
70272	K4.5III	4.30	.051	93813	K1.5IIIb	4.55	.047
70555	K2.5II-III	2.54	.037	94264	K0+III-IV	2.57	.032
71701	K2III	2.24	.057	94247	K3III	2.05	.023
71095	K5III	2.00	.022	94336	M0III	1.88	.025
71093	K5III	1.87	.019	95212	K5III	2.16	.025
71878	K1III	2.92	.073	95272	K0+III	2.28	.026
72094	K5III	2.88	.031	95314	K5III	1.92	.022
73108	K1+IIIb	2.17	.023	95578	M0III	3.87	.041
73471	K1III	2.25	.034	96833	K1III	4.24	.046
73603	K5III	2.24	.025	97576	K7III	2.60	.049
74442	K0IIIb	2.41	.031	98118	M0III	2.99	.031
74860	K5III	2.00	.023	98262	K3-III	4.60	.053
75691	K2.5III	3.17	.035	99167	K5III	3.58	.038
76110	M0III	2.52	.028	99998	K3.5III	3.03	.034
76351	K5III	1.94	.021	100029	M0III	6.08	.067
77996	K2II-III	1.83	.020	101666	K5III	2.45	.028
77800	K5III	2.67	.035	102224	K2III	3.35	.036
79354	K5III	2.67	.030	102461	K5III	3.03	.034
79554	K1III	1.81	.020	102964	K3III	2.60	.040
80493	K7IIIab	7.30	.078	105340	K2II-III	1.87	.049
81146	K2III	2.40	.036	105943	K5III	1.91	.026
81420	K5III	2.16	.023	106321	K3III	2.20	.025
81799	K2.5III	1.96	.032	107274	M0III	3.34	.038
82308	K4.5IIIb	4.12	.046	107328	K0.5IIIb	1.73	.018
82381	K2.5IIIb	2.16	.026	108381	K1III	2.15	.024
82668	K5III	7.13	.079	108985	K5III	1.79	.033
81817	K3IIIa	3.35	.087	109511	K2III	1.66	.035
82660	K5III	1.83	.021	109551	K2.5III	2.54	.039
83126	M0III	1.99	.028	110014	K2III	2.01	.023
83425	K3III	2.64	.027	110458	K0III	1.69	.018
83618	K2.5III	3.50	.048	111067	K3III	2.05	.022
83787	K6III	2.34	.028	111335	K5III	2.61	.034
85503	K2III	2.93	.043	111862	M0III	1.90	.021
86378	K5III	2.18	.023	111915	K3.5III	2.97	.034
87837	K3.5IIIb	3.31	.050	112213	M0III	3.24	.036
89388	K2.5II	5.23	.058	113092	K2III	1.79	.026
89682	K3II	3.17	.035	113996	K5-III	3.06	.032
89998	K1III	1.72	.020	114326	K5III	1.84	.021

Table 4 (cont.). Stars for which we have created calibrated templates

HD No.	Spectral Type	Diam. (mas)	Unc. (mas)	HD No.	Spectral Type	Diam. (mas)	Unc. (mas)
114780	M0III	2.32	.026	141992	K4.5III	3.40	.041
115046	M0III	2.29	.026	142574	K8IIIb	2.76	.029
115478	K3III	1.80	.020	142676	M0-1II	1.80	.047
116870	M0IIIv	2.70	.028	143107	K2IIIab	2.80	.030
116976	K0-IIIb	1.59	.018	143435	K5III	2.20	.024
119193	M0III	2.09	.023	144204	K5III	1.86	.020
120477	K5.5III	4.62	.050	145892	K5III	2.14	.023
120933	K5III	5.35	.059	145897	K3III	2.10	.023
121710	K3IIIb	2.43	.026	146051	M0.5III	10.03	.101
123123	K2-III	3.75	.039	146791	G9.5IIIb	3.00	.033
123139	K0-IIIb	5.46	.057	149009	K5III	2.37	.026
124547	K3-IIIb	2.62	.039	149447	K6III	4.68	.053
124294	K2.5III	3.29	.033	150798	K2II	8.98	.101
125560	K3III	1.96	.021	151217	K5III	2.84	.029
124882	K2III	2.87	.073	151249	K5III	5.58	.063
125932	K3III	2.28	.029	151680	K2.5III	5.96	.061
126927	K5III	2.31	.026	152326	K0.5IIIa	1.66	.027
127093	M0III	2.62	.034	152880	M0-1III	2.11	.035
127665	K3-III	3.92	.041	153210	K2III	3.85	.041
128000	K5III	2.09	.034	155410	K3III	1.96	.021
128068	K3III	2.07	.021	156283	K3II	5.29	.055
128902	K2III	1.99	.022	156652	M0III+	1.91	.024
129078	K3III	3.96	.099	156277	K2-III	2.05	.022
130157	K5III	2.10	.024	157325	M0III	2.60	.027
130694	K2.5IIIb	3.22	.035	158996	K5III	1.92	.024
132833	M0III	3.15	.034	157999	K2II	3.24	.035
133165	K0+IIIb	1.97	.032	158899	K3.5III	3.06	.032
133550	K5-III	2.07	.024	161096	K2III	4.63	.049
133774	K5III	2.86	.030	163588	K2III	3.13	.033
135758	K0-IIIa	1.91	.029	163376	M0III	4.09	.042
136028	K5III	1.87	.022	163770	K1IIa	3.15	.034
136422	K5III	5.69	.065	164646	M0IIIab	2.42	.027
137759	K2III	3.73	.040	168323	K5III	2.21	.031
137744	K4.5III	2.22	.025	168775	K2-IIIab	2.28	.025
138265	K5III	1.86	.022	168723	K0III-IV	2.98	.032
138481	K4.5IIIb	3.16	.034	168592	K4-5III	2.66	.047
138538	K1.5III	2.56	.067	169414	K2IIIab	3.03	.032
139669	K5-III	2.97	.035	169916	K1IIIb	4.24	.047
139063	K3.5III	4.27	.047	170693	K1.5III	2.03	.029
139127	K4.5III	3.39	.037	170951	M0III	1.76	.023
139663	K3-III	2.05	.021	171759	K0III	2.63	.065
140573	K2IIIb	4.94	.052	173780	K2III	1.95	.021
141477	M0.5IIIab	5.49	.056	174387	M0III	2.89	.032

Table 4 (cont.). Stars for which we have created calibrated templates

HD No.	Spectral Type	Diam. (mas)	Unc. (mas)	HD No.	Spectral Type	Diam. (mas)	Unc. (mas)
175775	K1III	3.37	.036	198134	K3III	2.11	.022
176524	K0III	1.69	.023	198048	K5III	3.06	.035
176670	K2.5III	2.41	.026	198357	K3II	1.78	.033
177808	M0III	2.40	.026	198542	M0III	5.16	.055
177716	K1.5IIIb	3.93	.043	199101	K5III	2.43	.026
178345	K0II	2.40	.025	199345	K5III	2.14	.024
179886	K3III	1.95	.033	199697	K3.5III	2.04	.022
180450	M0III	2.87	.032	199642	K5-M0III	1.89	.048
181109	M0III	1.97	.022	200644	K5III	2.47	.026
182709	K4-5III	2.32	.061	200914	M0.5III	4.43	.046
183439	M0.5IIIb	4.40	.046	201298	K5III	2.37	.031
184406	K3-IIIb	2.29	.023	201901	K3III	2.03	.040
184827	M0III	2.84	.044	203399	K5III	1.95	.032
184996	M0III	1.97	.051	203504	K1III	2.42	.030
186619	M0IIIab	2.27	.025	205478	K0III	2.42	.064
186791	K3II	7.06	.072	206445	K2III	1.81	.020
187150	K5III	1.94	.022	209688	K3III	2.71	.030
187660	K5III	1.83	.020	211416	K3III	5.99	.064
188056	K3III	1.90	.020	213310	M0II+B8V	5.43	.069
188154	K5III	2.52	.028	214868	K2.5III	2.69	.029
188310	G9.5IIIb	1.66	.021	216032	M0III	5.12	.053
188114	K0II-III	2.31	.024	216446	K3III	2.28	.059
188603	K2.5IIb	2.98	.034	216149	M0III	2.07	.021
189276	K4.5IIIa	3.06	.032	216397	M0III	3.38	.035
189319	M0-III	6.23	.064	217902	K5III	2.37	.027
189140	M0II-III	2.34	.046	218452	K5III	2.14	.024
189695	K5III	2.01	.023	218670	K1III	2.34	.027
189831	K5III	2.76	.029	219449	K1-III	2.24	.025
190056	K1III	2.00	.023	219784	K1III	2.13	.025
192107	K5III	2.44	.030	219981	M0III	2.01	.021
192781	K5III	1.88	.021	220009	K2III	1.99	.022
193002	M0-1III	2.01	.053	220088	M0III	2.35	.025
193579	K5III	1.98	.027	220363	K3III	1.99	.022
196171	K0III	3.27	.034	220440	M0III	2.38	.026
196321	K5II	3.27	.037	220954	K0.5III	1.99	.021
196917	M0III	2.53	.026	221588	M0III	2.48	.046
197912	K0IIIa	2.10	.029	222404	K1III-IV	3.38	.052
197989	K0III	4.58	.048	224630	K5III	2.49	.028
198149	K0IV	2.68	.029	224889	K3III	2.29	.061

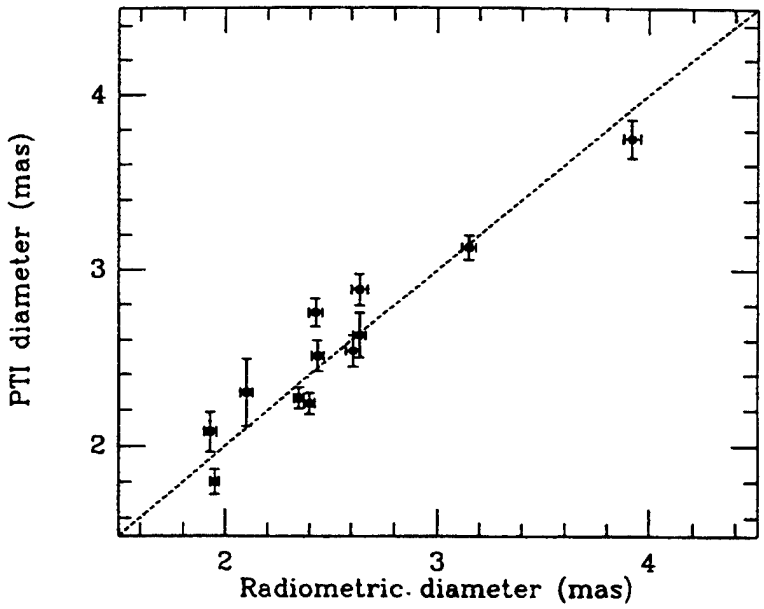

Fig. 8 Comparison of interferometrically measured stellar angular diameters with those we derive radiometrically. The dashed line passes through the origin with slope 1.

7. Template files and how to obtain them

A detailed header precedes every template created in this manner. This header is accompanied by: various names for each star (its IRASNAMEs, common name, HR and HD numbers); release version, date, and time of template creation; the template spectrum used; the extinctions of both the bright star that gave rise to the template shape and of the templated star; the angular diameter deduced for the stellar template (derived from the template scale factor and our published values of angular diameters for the bright composite spectra, in Paper VII); every piece of characterized photometry used to normalize the template, with abbreviated references; and full citations of the publication of this photometry. Table 5 illustrates the header for HD98118. Templates are always named for their HD designations, hence "HD98118.tem" will represent the file associated with this star.

Table 5. Template header information

```
IRAS PSC Name: 11147+0217
IRAS FSC Name: F11147+0217
75 LEO       HR 4371  HD 98118   M0III
IRC          203

Release 2.1
Date and time template processed:  9/29/1998   14: 4
Composite Spectrum Used:  band1093.tem
Av(composite) =  .00  Av(star) =  .00
Stellar Diameter (mas) =   2.99 +/-  .031
```

Table 5 (cont.) Template header Information

```
======================================================================
Photometry Used For Template Normalization:

Reference        Band      Mag   dMag  Iso_Wav  Iso_Flux  Flux_Unc
FLUKS 1994       H       1.599   .017    1.676  .279E-13  .565E-15
FLUKS 1994       K       1.400   .017    2.216  .114E-13  .226E-15
FLUKS 1994       L       1.253   .009    3.790  .164E-14  .248E-16
FLUKS 1994       M       1.534   .034    4.711  .539E-15  .189E-16
JOHNSON 1966     V-K     3.760   .030    2.231  .112E-13  .449E-15
MCWILLIAM 1984   2.17    1.328   .015    2.170  .123E-13  .213E-15
MCWILLIAM 1984   2.40    1.546   .015    2.406  .685E-14  .123E-15
NOGUCHI_T 1994   H       1.490   .030    1.674  .282E-13  .933E-15
NOGUCHI_T 1994   K       1.320   .030    2.220  .115E-13  .383E-15
IRAS FSC         12     12.890   .773   10.850  .281E-16  .170E-17
IRAS FSC         25      3.191   .255   22.530  .156E-17  .129E-18
IRAS PSC         12     12.800   .640   10.850  .278E-16  .140E-17
IRAS PSC         25      3.260   .293   22.530  .157E-17  .146E-18
IRC              K       1.398   .040    2.231  .111E-13  .632E-15

Notes: 1. IRAS PSC and FSC Mag and dMag are in Janskys.
       2. Iso_Wav is the isophotal wavelength in microns (um).
       3. Iso_Flux and Flux_Unc are the flux and flux uncertainty
          (1 sigma) at the isophotal wavelength in Watt/cm2/um.
       4. Johnson colors (e.g. V-K) are archived.  Thus MAG and dMag
          refer to a color index, but Iso_Wav, Iso_Flux, and Flux_Unc
          refer to the non-V filter.

======================================================================
References to the photometry used by the program to
normalize the spectral template:

IRAS Faint Source Catalog (FSC), Ver. 2, 1992, Moshir, et al.
IRAS Point Source Catalog (PSC), Ver. 2, 1988, Beichman, et al.
IRC - Neugebauer, G., and Leighton, R.B., 1969, California
   Institute of Technology, NASA SP-3047
Fluks, M.A., et al., 1994, Astron. & Astrophys. Supp. v105, p311
Johnson, H.L., et al. 1966, Comm. Lunar Plan. Lab. 63, p 99
McWilliam, A. and Lambert, D.L., 1984, PASP v 96, p882
Noguchi,K., 1994, ISAS Obs. in Cohen et al. 1999, Paper X, Table A5

======================================================================
Papers on "Spectral Irradiance Calibration in the Infrared:"

Cohen, M., Walker, R.G., Barlow, M.J., and Deacon, J.R.,1992,
   Paper I., Astron. J., v 104, p 1650.
Cohen, M., Walker, R.G., and Witteborn, F.C., 1992,
   Paper II, Astron. J., v 104, p 2030.
Cohen, M., Witteborn, F.C., Carbon, D.F., Augason, G.C.,
   Wooden, D., Bregman, J.D., and Goorvitch, D., 1992,
   Paper III., Astron. J., v 104, p 2045.
Cohen, M., Witteborn, F.C., Walker, R.G., Bregman, J.D., and
   Wooden, D.H., 1995, Paper IV., Astron. J., v 110, p 275
Cohen, M. and Davies, J.K., 1995, Paper V., Mon. Not. Roy.
        Astron. Soc., v 275, p 715
```

Table 5 (cont.) Template header Information

```
Cohen, M., Witteborn, F.C., Bregman, J.D., Wooden, D.H.,
        Salama, A., and Metcalfe, L., 1996, Paper VI.,
        Astron. J., v 112, p 241
Cohen, M., Witteborn, F.C., Carbon, D.F., Davies, J.K.,
        Wooden, D.H., and Bregman, J.D., 1996, Paper VII,
        Astron. J., v 112, p 2274
Cohen, M., Witteborn, F.C., Roush, T., Bregman, J.D., and
        Wooden, D.H., 1998, Paper VIII, Astron. J., v 115, p 1671
Cohen, M., 1998, Paper IX, Astron. J., v 115, p 2092
Cohen, M., Walker, R.G., Carter, B., Hammersley, P., Kidger, M.
   and Noguchi, K., 1999, Paper X., Astron.J. v 117, p 1864
================================================================

Notes:
1. Template spectra are NOT tabulated at equal intervals of
the wavelength, but rather at the wavelengths of the original
measurements.
2. In most cases "total uncertainty" is the appropriate error
term to use.  It is the standard deviation of the spectral
irradiance and includes the local and global uncertainties.
Local and global uncertainties are given as a percentage of the
irradiance.  Local uncertainties apply to a limited wavelength
range, while global uncertainties effect the entire spectrum.
Thus the global uncertainty does not contribute error to flux
ratios or color measurements, and may, in those cases, be
subtracted (in the RSS sense) from the total uncertainty.
```

The calibrated stellar spectra have a five-column format (as do the models and composites described in Papers IV-VII). We tabulate: wavelength (μm); monochromatic irradiance ($F\lambda$ in units of W cm^{-2} μm^{-1}; total uncertainty (also in units of W cm^{-2} μm^{-1}) associated with this value of $F\lambda$; local bias; and global bias. For most applications, "total uncertainty" is the error term most appropriate to use. It is the standard deviation of the spectral irradiance and incorporates the local and global biases. Local and global biases are given as percentages of the irradiance. The global bias does not contribute error to flux ratios or color measurements, and may be removed (in the root-sum-square sense) from the total error. Note that we prefer to provide pristine data, rather than to regrid each composite or template to an equally-spaced or common wavelength scale. Each composite has a different set of wavelengths. Consequently, template spectra are **not** tabulated at equal intervals of the wavelength, but rather at the wavelengths of the originally observed composite spectra.

The models and composites are now available on the CD-ROM series of The Astronomical Journal. All the templates described herein will likewise be eventually found in this same CD-ROM series. Currently, all the models, composites, and templates are available in the form of ASCII files from Dr. Michael P. Egan at AFRL/VSBC, 29 Randolph Road, Hanscom Air Force Base, MA, 01731-3010, (egan@pldac.plh.af.mil).

8. Conclusions

We have developed a self-consistent, all-sky network of over 430 infrared radiometric calibrators within a carefully constrained absolute framework following our definitions of "zero magnitude" for characterized photometric systems. Currently this network includes three types of calibrator: models; composites; and templates. Models connote the three calibrated Kurucz models for Sirius, Vega (Paper I), and α^1 Cen (Paper VI). Composites refer to the IR-bright K- and M-giants (and these are generally the brightest stars in the current network) as described in Papers II, and IV-VII. Templates form the substance of the present paper, represent the bulk of the network, and extend to irradiance levels about 150 times below that of the brightest composites.

The self-consistency arises because of the rigorous framework in which we have united both photometry and spectroscopy, and have constructed composites from their ratios to the modeled stars, primarily Sirius. Further, it has been possible to validate the self-consistency of the fainter members of this network through the Near-Infrared Spectrometer (NIRS: Noda et al. 1994), a 1.4-4.0 μm, low-resolution (≈0.11 μm), grating spectrometer carried aboard the IRTS. No IRTS scan passed over any of the model or composite stars. Therefore, the calibration was established through the use of calibrated templates. A set of four absolute calibrators was chosen (IRC+50276, θ Cnc, θ Her, and κ Gru). Using any of these calibrators to establish the conversion between raw signals and physical units, the resulting agreement between the observed spectra of the others and their independent, and unused, templates is remarkably good (*cf.* Matsumoto & Murakami 1996), ±2%. The templates for these four stars are based on three different composites (K1.5, K5, and M0III) and represent irradiance levels between 30 and 80 times fainter than their respective composites. This represents the first step in validating our fainter products and in demonstrating the self-consistency of the current network.

Such a network is entirely possible within an absolute radiometric tolerance of 5% between 1.2 and about 15 μm, and about 10% from 15-35 μm, figures of merit in keeping with external demands imposed on satellite programs. We advocate use of this network to support a wide range of astronomical observations, be they ground-based, airborne, or satellite sensors, because of the ongoing need to pursue a unified approach to infrared calibration **with a traceable pedigree**. Such a network of complete spectra is highly flexible and makes no assumptions whatsoever about any future filter profiles. It avoids the need for complex magnitude and color transformations between new and old photometric systems, at least as far as the assignment of in-band, or specific monochromatic absolute flux densities at isophotal wavelengths or frequencies are concerned. The network is capable of the accurate definition of real characteristics of new systems with arbitrary passbands, including non-standard passbands like the short K^1 of the DENIS and 2MASS projects, response curves notched to avoid deep terrestrial absorptions, and complex or divided bandpasses, such as result through the use of near-infrared "OH-suppressing" filters.

To enhance the quality of the current network would require new precision ground- or space-based photometry of stars with the spectral types for which we now have complete low-resolution templates. Such data would both carry more weight in the normalization of a template than older photometry with larger uncertainties (because of our inverse-variance-weighting scheme for template multipliers) and perhaps provide near-infrared "anchor" points for stars templated with IRAS data alone. We might also seek to make templates more specific to the very

late K-types (K6-8III), for example, based on Lyncis (K7III) rather than relying on our K5III template, but very few of these stars are to be found in the Walker-Cohen Atlas.

To augment the sample of 422 stars, we might choose different approaches. In the first, we might seek to construct new composites for the missing types, notably for K4III, and the mid- to late-G types (G7-8-9III). In the absence of the KAO, spectral fragments for these new composites might be available only from space-based spectrometers, e.g. the ISO SWS or PHOT-P and PHOT-S. Precision photometry might then be sought, or reliance again placed on IRAS measurements, so that the range from G6.5-G9III and all the K4IIIs could be templated. Such an extension would provide an additional maximum of 104 stars (49 late-G giants and 55 K4). We note, however, the worldwide flight from maintaining conventional (single-detector) infrared photometers at many major observatories. We commend those few institutions which have staunchly continued to offer bolometers and/or InSb systems, and sincerely hope that they will not be encouraged to dismiss these as redundant solely because of the plethora of infrared cameras available. "True photometry" will always have a role. It is yet to be demonstrated that cameras and their aasociated software are capable of the same stable, high-quality radiometry achieved by careful workers with single detectors and significant focal plane apertures.

MC and RGW gratefully acknowledge the support for these calibration efforts through Phillips Laboratory (now Air Force Research Laboratory) by Dr. Stephan Price on contract F19628-92-C-0900. It is a pleasure to thank our many colleagues who aided our efforts by supplying filter transmission profiles and pursuing questions of exactly which filters were in what photometers at specific times, notably Drs. Bob Gehrz, Terry Jones, Ian Glass, Chick Woodward, Dick Joyce, Harry Hyland, and Patrice Bouchet. We thank Dr. Andrew McWilliam for providing such detailed documentation for the McWilliam-Lambert narrow-band photometry. MC also thanks his colleagues on the ISO Calibration Working Group for their ongoing encouragement and support for this work, principally Drs. Andrea Moneti and Michel Breitfellner. This research has made use of the Simbad database, at CDS, Strasbourg, France.

References

Allen and Cragg, 1983, MNRAS 203, 777
Alonso, A. et al. 1994, A&A, 282, p684
Barlow, M. J. & Cohen, M. 1977, ApJ, 213, 737
Bessell, M. F. & Brett, J. M. 1988, PASP, 100, 1134
Bidelman, W. P. 1980, Publ. Warner & Swasey Obs., **2**, No. 6
Bidelman, W. P. 1991, priv. comm.
Bouchet, P. et al. 1989, A&AS, 80, 389
Bouchet, P. et al. 1991, A&AS, 91, 409
Carrasco, L. et al. 1991, PASP, 103, 987
Castor, J. I. & Simon, T. 1983, ApJ, 265, 304
Carter, B.S. 1990, MNRAS, 242, 1
Carter, B.S. 1993, in Proc. of "Precision Photometry", eds. Kilkenny, Lastovica & Menzies
Clark, F. O. 1996, "PLEXUS" Version 2.1a, CD-ROM, Phillips Laboratory, USAF
Cohen, M. 1994, AJ, 107, 582
Cohen, M. 1998, AJ, 115, 2092
Cohen, M. & Davies, J. K. 1995, MNRAS, 276, 715

Cohen, M., Walker, R. G., Barlow, M. J., & Deacon, J. R. 1992a, AJ, 104, 1650 [Paper I]
Cohen, M., Witteborn, F. C., Carbon, D. F., Augason, G. C., Wooden, D., Bregman, J., & Goorvitch, D. 1992b, AJ, 104, 2045 [Paper III]
Cohen, M., Walker, R. G., & Witteborn, F. C. 1992, AJ, 104, 2030 [Paper II]
Engels, D., et al. 1981, A&A,Supp. 45, 5
Eyer, L. & Grenon, M. 1997, in Proc. ESA Symp. "HIPPARCOS - Venice 1997"
Feast, M., Whitelock, P.A., & Carter, B. 1990, MNRAS, 247, 227
Fitzgerald, M. P. 1968, A&A, 4, 234
Fluks, M. A. et al. 1994, A&AS, 105, 311
Frogel, J. A. et al. 1978, ApJ, 220, 75
Gezari, D., Schmitz, M., Pitts, P. S., & Mead, J. 1993, Catalog of Infrared Observations: Third Edition, NASA RP-1294
Glass, I. S. 1991, Irish AJ, 17, 1
Glass, I. S. 1993, in Proc. IAU Colloquium 136, "Stellar Photometry - Current Techniques and Future Developments", eds. C. J. Butler & I. Elliott (Cambridge Univ. Press), p.10
Gould, A. & Flynn, C. 1992, A&A, 254, 105
Grasdalen, G.L., et al. 1983, ApJS, 53, p413
Hammersley, P. L. et al. 1998, A&AS, in press
Hauser, M.G., et al., 1997, COBE Ref. Pub. No. 97-A, Chap. 5.8.1
Hoffleit, D. & Warren Jr., W. H. 1991, 5th Revised Edition of the Bright Star Catalogue (available through the ADC)
Houk, N., & Cowley, A. P. 1975, The Michigan Spectral Catalogue: Vol. 1-4 (Lithocrafters Inc.: Michigan)
IRAS Point Source Catalog, version 2, 1988, IRAS Catalogs and Atlases. Volumes 2-6, NASA RP-1190 (GPO, Washington, DC) [PSC].
Johnson, H.L., et al. 1966, Comm. Lunar Plan. Lab. 63, 99
Keenan, P.C. & McNeil, R.C. 1989, ApJS, 71, 245
Koornneef, J., 1983a, A&AS 51, 489
Koornneef, J., 1983b, A&A,128, 84
McWilliam, A. 1990, ApJS, 74, 1075
McWilliam, A. & Lambert, D.L., 1984, PASP, 96, 882
Mermilliod, J.-C. 1994, Bull. Inf. CDS, 45, 3
Mill, J., O'Neil, R. R., Price, S. D., Romick, G. J., Uy, O. M., & Gaposchkin, E. M. 1994, AIAA, 31, 900
Noda, M. et al. 1994, ApJ, 428, 363
Percy, J. 1993, PASP, 105, 1422
Perry, C.L. & Johnson, L. 1982, A&AS 50, 451
Perry, C.L., Johnston, L. & Crawford, D.L.1982, AJ 87, 1751
Schmitz, M., Mead, J., & Gezari, D. 1987, Infrared Source Cross-Index NASA RP-1182
Selby, M. J., Hepburn, I., Blackwell, D. E., Booth, A. J., Haddock, D. J., Arribas, S., Leggett, S. K., & Mountain, C. M. 1988, A&AS, 74, 127
Tapia, M., Neri, L., & Roth, M., 1986, Rev. Mex., 13, 115
Tokunaga, A.T., et al., 1986, AJ, 92, 1183
van der Bliek, N.S., et al. 1996, A&AS, 119, 547
Wainscoat, R. J., Cohen, M., Volk, K., Walker, H. J., & Schwartz, D. E. 1992, ApJS, 83, 111
Walker, H. J. & Cohen, M. 1988, AJ, 95, 1801

Appendix A
Stellar Near-Infrared Photometry Acquired from SAAO - Brian Carter

NAME	J	H	K	L'	σ_J	σ_H	σ_K	$\sigma_{L'}$
HR 3	2.879	2.280	2.202	2.141	Carter	std.		
HR 37	2.695	1.866	1.724	1.585	5	2	8	3
HR 74	1.661	1.022	0.923	0.825	8	7	8	9
HD 1879	3.311	2.413	2.244	2.088	8	11	5	8
HR 98	1.733	1.376	1.334	1.322	Carter	std.		
HR 99	0.544	-0.107	-0.192	-0.293	4	3	4	8
HR 117	2.901	2.052	1.895	1.729	Carter	std.		
HR 188	0.401	-0.138	-0.224	-0.306	Carter	std.		
HR 201	3.179	2.256	2.092	1.948	4	9	10	1
HR 322	1.842	1.348	1.279	1.207	Carter	std.		
HR 334	1.622	0.985	0.886	0.779	Carter	std.		
HR 400	2.829	1.924	1.763	1.611	4	5	12	5
HR 402	1.870	1.271	1.189	1.113	10	6	8	4
HR 440	2.292	1.720	1.653	1.564	4	8	3	10
HD 9692	3.620	2.672	2.494	2.346	5	7	10	11
HR 539	1.933	1.314	1.224	1.129	Carter	std.		
HR 602	2.497	1.667	1.519	1.391	5	3	5	12
HR 688	3.040	2.171	2.019	1.880	7	2	8	4
HR 759	2.380	1.493	1.310	1.164	10	7	5	5
HD 20356	3.475	2.561	2.400	2.294	10	8	9	8
HR 1106	2.792	1.170	2.076	2.020	7	4	7	9
HR 1136	2.006	1.490	1.420	1.402	Carter	std.		
HR 1231	0.119	-0.780	-0.939	-1.052	8	3	7	6
HR 1318	2.998	2.354	2.266	2.172	Carter	std.		
HR 1326	2.058	1.434	1.349	1.281	Carter	std.		
HR 1393	1.462	0.642	0.506	0.403	6	4	4	9
HR 1453	2.842	2.279	2.202	2.161	Carter	std.		
HR 1481	2.057	1.431	1.344	1.281	4	3	7	12
HR 1654	0.736	-0.067	-0.204	-0.322	Carter	std.		
HR 2065	2.883	1.990	1.838	1.714	11	3	9	3
HR 2131	2.773	1.922	1.760	1.632	10	4	7	7
HR 2326	-1.179	-1.310	-1.333	-1.386	8	4	6	1
HR 2491	-1.385	-1.382	-1.367	-1.370	13	6	4	20
HR 2574	1.620	0.796	0.672	0.537	Carter	std.		
HR 3425	3.099	2.187	1.997	1.837	5	5	13	3
HR 3480	3.293	2.418	2.235	2.112	11	5	5	7
HR 3518	1.913	1.208	1.102	1.003	6	3	5	7
HR 3535	2.810	1.931	1.752	1.621	2	6	2	11
HR 3628	1.872	0.994	0.839	0.709	6	3	3	4
HR 3738	3.058	2.213	2.068	1.943	10	12	6	7
HR 3748	-0.319	-1.078	-1.221	-1.339	12	15	16	4
HR 3802	3.384	2.537	2.406	2.287	10	8	3	14
HR 3803	0.456	-0.407	-0.562	-0.687	7	3	7	4
HR 4050	0.932	0.170	0.026	-0.123	6	10	7	6
HR 4063	2.044	1.267	1.113	0.951	3	4	6	11
HR 4080	3.042	2.455	2.365	2.272	4	3	1	10
HR 4094	1.312	0.508	0.362	0.233	Carter	std.		

NAME	J	H	K	L'	σ_J	σ_H	σ_K	$\sigma_{L'}$
HR 4104	1.829	1.018	0.884	0.768	6	9	9	4
HR 4145	2.326	1.455	1.296	1.175	7	2	4	8
HR 4174	1.335	0.462	0.292	0.137	Carter	std.		
HR 4216	1.184	0.692	0.602	0.532	Carter	std.		
HR 4232	1.067	0.366	0.266	0.147	Carter	std.		
HR 4287	2.322	1.719	1.635	1.515	7	5	3	6
HR 4289	3.259	2.474	2.316	2.144	4	5	5	10
HR 4299	1.876	1.006	0.841	0.687	5	3	8	13
HR 4382	1.686	1.015	0.936	0.841	Carter	std.		
HR 4396	2.464	1.636	1.487	1.343	5	6	7	13
HR 4402	2.018	1.146	0.988	0.833	9	9	11	7
HR 4432	2.196	1.334	1.194	1.061	3	4	9	9
HR 4450	2.017	1.514	1.437	1.339	Carter	std.		
HR 4503	2.734	1.927	1.788	1.640	2	5	4	8
HR 4526	2.464	1.536	1.371	1.213	3	4	3	3
HR 4786	1.220	0.759	0.692	0.608	Carter	std.		
HR 4831	2.929	2.358	2.263	2.150	3	5	4	6
HR 4888	2.099	1.362	1.236	1.109	5	8	1	11
HR 4906	2.341	1.461	1.266	1.068	7	5	8	9
HR 5020	1.513	1.026	0.952	0.883	Carter	std.		
HR 5064	2.611	1.765	1.615	1.468	4	2	6	13
HR 5068	3.045	2.486	2.393	2.301	6	5	7	11
HR 5152	3.316	2.383	2.203	2.046	5	5	5	5
HR 5287	1.410	0.772	0.684	0.595	Carter	std.		
HR 5288	0.388	-0.178	-0.260	-0.361	Carter	std.		
HR 5315	1.913	1.118	1.004	0.885	Carter	std.		
HR 5410	2.893	2.055	1.916	1.772	8	5	6	8
HR 5513	3.199	2.328	2.156	2.000	2	3	6	1
HR 5526	2.015	1.188	1.068	0.951	7	5	3	13
HR 5590	2.440	1.489	1.311	1.156	9	8	6	9
HR 5615	3.262	2.369	2.187	2.028	3	6	8	7
HR 5622	2.479	1.631	1.472	1.325	5	5	8	8
HR 5705	0.948	0.097	-0.048	-0.181	11	8	10	11
HR 5743	2.986	2.135	1.983	1.852	3	5	4	6
HR 5794	1.335	0.577	0.455	0.337	6	8	6	5
HR 5797	1.974	1.206	1.073	0.955	6	1	7	5
HR 6056	-0.177	-1.061	-1.228	-1.345	6	7	7	6
HR 6075	1.635	1.090	1.012	0.971	6	11	10	10
HR 6166	1.388	0.528	0.368	0.247	9	12	16	2
HR 6217	-0.339	-1.077	-1.206	-1.336	11	5	8	8
HR 6229	1.022	0.145	-0.009	-0.123	7	5	4	5
HR 6241	0.440	-0.183	-0.273	-0.363	Carter	std.		
HR 6417	2.758	2.072	1.972	1.889	4	2	4	10
HR 6553	1.050	0.809	0.765	0.734	8	11	14	2
HR 6682	1.818	0.904	0.728	0.599	7	10	10	4
HR 6855	1.855	1.012	0.871	0.773	6	8	3	8
HR 6869	1.652	1.094	1.024	0.989	8	13	10	5
HR 6913	1.082	0.482	0.396	0.340	5	10	10	7
HR 7092	2.560	1.649	1.482	1.352	5	7	8	3
HR 7150	1.640	1.014	0.915	0.827	Carter	std.		

NAME	J	H	K	L'	σ_J	σ_H	σ_K	$\sigma_{L'}$
HR 7234	1.358	0.686	0.588	0.497	Carter	std.		
HR 7259	2.201	1.588	1.485	1.369	5	3	3	8
HR 7323	3.436	2.505	2.325	2.181	4	3	8	7
HD 187150	3.423	2.494	2.316	2.183	4	6	7	6
HR 7559	3.404	2.570	2.413	2.300	6	4	6	7
HR 7584	2.832	1.928	1.760	1.624	8	7	7	6
HR 7604	2.168	1.418	1.284	1.157	5	2	5	11
HR 7652	2.424	1.646	1.519	1.407	5	6	6	3
HR 7659	2.875	2.130	2.030	1.939	5	4	2	3
HR 7754	2.030	1.520	1.447	1.397	Carter	std.		
HR 7869	1.464	0.904	0.823	0.746	Carter	std.		
HR 7873	2.180	1.294	1.149	1.028	7	7	2	1
HR 7909	2.768	1.933	1.757	1.608	3	4	5	10
HR 7952	2.280	1.434	1.290	1.176	4	5	9	5
HR 7980	1.249	0.365	0.202	0.057	Carter	std.		
HR 8015	3.006	2.210	2.065	1.942	2	7	6	10
HR 8080	1.583	0.712	0.540	0.399	5	6	2	7
HR 8411	2.270	1.559	1.437	1.324	3	7	9	3
HR 8502	0.600	-0.162	-0.289	-0.399	5	5	3	5
HR 8679	1.239	0.384	0.222	0.096	6	2	2	4
HR 8685	3.082	2.308	2.183	2.068	10	8	5	8
HR 8774	2.809	1.989	1.840	1.736	3	5	6	10
HR 8820	2.301	1.777	1.692	1.623	6	5	4	2
HR 8841	2.480	1.877	1.794	1.720	6	2	5	6
HR 8863	2.611	1.994	1.908	1.816	3	4	3	10
HR 8898	2.913	2.048	1.880	1.739	9	4	2	3
HR 9073	2.795	1.927	1.765	1.631	7	5	6	7

Note: Individual standard deviations (in millimags.) follow the magnitudes

Appendix B
Stellar Broadband Near-Infrared Photometry Acquired from Tenerife
Peter Hammersley

NAME	J	σ_J	H	σ_H	K	σ_K	L'	$\sigma_{L'}$
HR 7001	-0.001	0.005	0.000	0.005	-0.001	0.005	.001	.007
HR 337	-.962	.006	-1.756	.006	-1.942	.005	-2.009	.001
HR 1457	-1.938	.015	-2.649	.005	-2.854	.008	-2.986	.003
HR 2491	-1.411	.005	-1.385	.005	-1.388	.010		
HR 2990	-.576	.007	-1.024	.007	-1.116	.007		
HR 5340	-2.249	.007	-2.878	.005	-2.992	.011	-3.124	.006
HR 6705	-.433	.005	-1.148	.005	-1.309	.005	-1.442	.008
HR 8775	-1.255	.007	-2.112	.013	-2.333	.008	-2.414	.004
HR 80	3.092	.009	2.423	.010	2.285	.010	2.190	.014
HR 168	.316	.011	-.208	.005	-.327	.005		
HR 253	2.788	.026	2.165	.005	2.059	.005	1.981	.006
HR 434	2.376	.022	1.676	.013	1.530	.012		
HR 464	1.571	.010					.653	.002
HR 489	2.148	.005	1.492	.034	1.297	.007	1.144	.010
HR 500							1.868	.006
HR 617							-.743	.006
HR 648	2.758	.008	1.998	.007	1.810	.007	2.015	.026
HR 940	3.253	.007	2.484	.007	2.299	.008	2.184	.016
HR 941	2.138	.007	1.695	.007	1.596	.007		
HR 947	2.711	.007	2.197	.007	2.093	.007	1.423	.011
HR 999							.717	.009
HR 1015							2.165	.006
HR 1373	2.124	.007	1.702	.007	1.596	.007		
HR 1866	2.645	.007	1.865	.007	1.671	.007		
HR 1907	2.285	.007	1.780	.007	1.692	.007		
HR 2077	1.994	.007	1.520	.007	1.428	.007		
HR 2427	2.734	.007	2.178	.007	2.060	.007		
HR 2491	-1.411	.005	-1.385	.005	-1.388	.010		
HR 2663	3.072	.008	2.348	.007	2.186	.006		
HR 2795	2.294	.007	1.581	.007	1.399	.007		
HR 2905	1.172	.007	.442	.007	.265	.006		
HR 2935	2.730	.007	1.963	.006	1.785	.006		
HR 3669	3.096	.006	2.445	.008	2.320	.010		
HR 4246	2.811	.015	2.162	.010	2.042	.009		
HR 4377	1.096	.024	.411	.017	.282	.020		
HR 4518	1.602	.010	1.010	.005	.908	.005	.818	.008
HR 4737	2.470	.008	1.977	.005	1.881	.005		
HR 4813	2.669	.016	2.139	.013	2.024	.011		
HR 4851	2.805	.005	2.146	.005	2.023	.005		
HR 5013	3.053	.013	2.436	.009	2.310	.006	.236	.004
HR 5219							-.089	.003
HR 5247	2.503	.005	1.800	.005	1.653	.005		
HR 5370	2.782	.012	2.246	.009	2.131	.005		
HR 5429	1.363	.011	.736	.005	.618	.005	.520	.004
HR 5464	3.089	.007	2.310	.011	2.170	.005		
HR 5744	1.322	.005	.776	.005	.675	.005	.584	.010

NAME	J	σ_J	H	σ_H	K	σ_K	L'	$\sigma_{L'}$
HR 5763	2.132	.009	1.369	.006	1.197	.005		
HR 5854	.696	.005	.183	.006	.080	.010		
HR 5879	1.045	.005	.242	.010	.064	.017		
HR 5924	2.469	.010	1.700	.011	1.529	.005		
HR 5947	2.012	.005	1.405	.005	1.293	.005	1.218	.004
HR 5957	2.887	.005	2.135	.005	1.980	.005		
HR 5981	3.264	.008	2.520	.005	2.371	.014		
HR 6047	2.884	.005	2.187	.005	2.037	.009		
HR 6048	2.817	.007	2.153	.005	2.022	.007		
HR 6132	1.236	.029	.746	.024	.651	.022	1.864	.008
HR 6154	2.781	.008	2.033	.005	1.853	.006		
HR 6228	2.342	.005	1.624	.008	1.443	.007		
HR 6299	1.259	.005	0.730	.005	0.528	.005	0.554	.003
HR 6388	2.877	.020	2.248	.008	2.129	.006	2.010	.013
HR 6418	.776	.006	.114	.005	-.024	.005	-.148	.005
HR 6464	2.625	.007	1.845	.006	1.702	.013		
HR 6498	1.781	.005	1.130	.005	.975	.005	.854	.008
HR 6526	1.967	.009	1.293	.006	1.153	.005	1.056	.011
HR 6556	1.728	.005	1.654	.005	1.639	.005		
HR 6603	.825	.009	.311	.007	.192	.008	.115	.008
HR 6623	2.125	.005	1.812	.005	1.746	.008		
HR 6688	1.738	.011	1.172	.008	1.056	.005	.968	.004
HR 6695	1.735	.008	1.169	.006	1.040	.005		
HR 6872	2.379	.005	1.847	.005	1.739	.005	1.646	.010
HR 6895	1.801	.005	1.226	.005	1.115	.008	1.044	.010
HR 7064	2.770	.005	2.187	.005	2.073	.005	1.991	.006
HR 7192	2.520	.005	1.859	.005	1.711	.005	1.592	.010
HR 7328	2.141	.020	1.707	.017	1.624	.016		
HR 7429	2.430	.005	1.875	.005	1.759	.005	1.677	.017
HR 7525	.217	.006	-.466	.005	-.631	.005	-.750	.006
HR 7557	.316	.006	.210	.005	.191	.008	.184	.008
HR 7576	2.882	.008	2.331	.005	2.194	.005		
HR 7633	2.259	.005	1.496	.013	1.337	.005	1.170	.009
HR 7635	.668	.005	-.063	.008	-.230	.014	-.353	.005
HR 7742	3.211	.020	2.486	.009	2.339	.023		
HR 7949	.673	.009	.160	.005	.065	.009	.021	.004
HR 7956	2.700	.005	2.086	.005	1.956	.005	1.875	.008
HR 7957	1.785	.007	1.344	.005	1.245	.005		
HR 8005	2.709	.007	1.943	.007	1.785	.009		
HR 8032	2.848	.005	2.173	.005	2.025	.006	1.925	.016
HR 8066	2.740	.006	2.011	.014	1.829	.013	1.636	.016
HR 8287	3.195	.016	2.489	.008	2.340	.014	2.221	.009
HR 8632	2.240	.008	1.596	.008	1.471	.009	1.375	.018
HR 8699	2.023	.008	1.277	.007	1.094	.007	.994	.004
HR 8804	2.860	.007	2.206	.007	2.047	.008		
HR 8876	3.095	.007	2.382	.007	2.218	.007	2.119	.011
HR 8878	2.814	.015	2.150	.009	2.025	.009	1.952	.014
HR 8882	2.790	.010	2.052	.010	1.879	.010	1.776	.017
HR 8893	2.856	.005	2.226	.009	2.088	.008	2.004	.023
HR 8916	2.477	.022	1.977	.013	1.877	.012		

Appendix C
Stellar Near-Infrared Narrowband Photometry Acquired from Tenerife
Peter Hammersley

NAME	Jn	σ_{Jn}	Kn	σ_{Kn}	Ln	σ_{Ln}
HR 7001	.007	.010	.000	.010	-.005	.010
HR 337	-.910	.020	-1.930	.010	-2.060	.010
HR 1457	-1.950	.020	-2.940	.010	-3.050	.010
HR 2990	-.590	.005	-1.140	.005	-1.210	.005
HR 5340	-2.233	.010	-3.075	.010	-3.150	.010
HR 6705	-.414	.020	-1.370	.010	-1.460	.030
HR 8775	-1.210	.005	-2.330	.005	-2.490	.
HR 1963	2.840	.010	2.090	.005	2.010	.005
HR 4954	2.180	.005	1.260	.005	1.130	.005
HR 5602			1.330	.005		
HR 5755	3.240	.030	2.330	.020	2.220	.020
HR 5763	2.173	.010	1.160	.010	.990	.020
HR 5826	2.222	.010	1.290	.010	1.170	.050
HR 5924	2.553	.005	1.510	.005	1.410	.005
HR 5957	2.901	.010	1.970	.010	1.930	.030
HR 5981	3.261	.010	2.340	.005	2.190	.005
HR 6047	2.970	.005	2.020	.005	1.930	.005
HR 6056			-1.330	.005		
HR 6075			.980	.005		
HR 6132			.620	.005		
HR 6136	2.899	.040	1.980	.020	1.880	.050
HR 6154	2.773	.005	1.880	.005		
HR 6228	2.402	.010	1.400	.010	1.310	.030
HR 6464	2.653	.005	1.650	.005	1.480	.005
HR 6529	3.120	.010	2.240	.020	2.120	.040
HR 6603	.862	.005	.190	.005	.060	.005
HR 6623			1.740	.005		
HR 6688			1.020	.005		
HR 6695	1.733	.030	1.025	.010	.960	.020
HR 6703			1.570	.005		
HR 6895			1.100	.005		
HR 7180	2.841	.010	2.220	.005		
HR 7237	2.802	.030	1.840	.030	1.700	.030
HR 7310	1.338	.010	.740	.010	.690	.060
HR 7405	1.503	.010	.460	.005	.380	.005
HR 7525	.250	.020	-.650	.010	-.735	.030
HR 7557	.367	.030	.250	.030	.270	.030
HR 7595	2.849	.005	2.250	.005	2.220	.005
HR 7633	2.212	.010	1.240	.010	1.120	.030
HR 7742	3.180	.010	2.290	.010	2.210	.040
HR 7754	1.970	.005	1.390	.005		
HR 8499	2.573	.010	2.025	.010	1.945	.020
HR 8684	1.928	.020	1.345	.020	1.265	.030
HR 8916	2.484	.030	1.860	.020	1.780	.100

Appendix D
Stellar Broadband Near-Infrared Photometry Acquired from Tenerife
Mark Kidger

NAME	J	σ_J	H	σ_H	K	σ_K	L'	$\sigma_{L'}$
HR 7001	-.001	.005	.000	.005	-.001	.005	.002	.005
HR 0079	2.762	.022	1.982	.010	1.798	.011	1.674	.044
HR 0106	3.096	.010	2.351	.012	2.182	.013	2.084	.044
HR 0215	1.917	.026	1.403	.028	1.322	.031		
HR 0470	3.286	.010	2.511	.012	2.337	.013	2.239	.044
HR 0736	2.459	.008	1.761	.009	1.604	.010	1.510	.031
HR 1286	3.173	.014	2.534	.015	2.390	.021		
HR 1684	2.406	.010	1.706	.012	1.542	.013	1.419	.044
HR 1963	2.828	.021	2.222	.017	2.103	.022		
HR 2459	2.367	.005	1.699	.005	1.537	.006	1.409	.044
HR 2533	3.109	.011	2.444	.012	2.298	.011	2.169	.036
HR 2560	2.826	.005	2.418	.005	2.327	.005	2.281	.008
HR 2804	2.916	.005	2.180	.014	1.989	.008	1.834	.044
HR 2864	2.457	.026	1.883	.028	1.735	.028	1.638	.027
HR 2938	2.022	.037	1.260	.036	1.100	.015	.979	.036
HR 2973	2.216	.037	1.712	.031	1.586	.028	1.553	.027
HR 3003	2.196	.010	1.471	.012	1.302	.013	1.189	.044
HR 3304	3.138	.005	2.487	.005	2.347	.005	2.255	.005
HR 3305	3.056	.010	2.366	.012	2.212	.013	2.054	.044
HR 3357	2.336	.010	1.621	.012	1.422	.015	1.259	.044
HR 3403	2.520	.006	1.948	.006	1.855	.005	1.796	.023
HR 3550	3.045	.010	2.424	.005	2.271	.006	2.129	.044
HR 3660	2.501	.011	1.766	.012	1.602	.013	1.464	.044
HR 3773	1.526	.010	.816	.012	.647	.013	.479	.044
HR 3939	2.892	.005	2.202	.013	2.038	.011	1.899	.044
HR 4280	2.922	.011	2.212	.022	2.049	.018	1.924	.044
HR 4335	1.118	.027	.518	.028	.405	.028	.363	.027
HR 4608	2.438	.005	1.970	.005	1.888	.005	1.771	.012
HR 4954	2.131	.011	1.468	.013	1.318	.015	1.200	.028
HR 4962	3.236	.011	2.543	.013	2.393	.014	2.260	.028
HR 5200	1.256	.013	.548	.013	.398	.015	.260	.028
HR 5219	1.131	.011	.328	.013	.123	.014	-.064	.028
HR 6136	2.840	.005	2.175	.005	2.013	.005	1.891	.010
HR 6220	1.876	.005	1.431	.005	1.350	.005	1.257	.011

Appendix E
Stellar Near-Infrared Photometry Acquired from Japan & China
Kunio Noguchi

NAME	SITE	J	H	K	L
HR 2990	T	-0.54	-1.06	-1.16	-1.17
HR 6705	B	-0.41	-1.22	-1.34	-1.39
HR 79	B	2.83	1.92	1.72	1.57
HR 106	B	3.27	2.39	2.23	2.00
HD 5462	B	3.14	2.17	1.91	1.78
HR 470	B	3.30	2.46	2.31	2.09
HR 648	B	2.75	1.93	1.75	1.68
HD 14146	B	3.41	2.48	2.25	2.13
HR 736	B	2.48	1.66	1.53	1.48
HR 940	B	3.29	2.45	2.29	2.22
HR 1286	B	3.27	2.50	2.37	2.18
HD 27482	B	3.31	2.31	2.05	1.91
HR 1370	B	2.43	1.51	1.29	1.12
HR 1373	T	2.17	1.63	1.56	1.51
HR 1572	T	3.41	2.51	2.35	2.22
HR 1684	B	2.64	1.75	1.56	1.43
HR 1866	B	2.75	1.78	1.62	1.53
HR 1907	T	2.19	1.65	1.57	1.56
HR 1963	B	2.91	2.20	2.10	2.08
HR 2011	B	1.67	0.80	0.61	0.40
HR 2012	T	2.13	1.52	1.40	1.31
HR 2077	T	2.02	1.48	1.40	1.35
HR 2363	T	3.30	2.45	2.28	2.08
HR 2459	T	2.51	1.74	1.58	1.42
HR 2478	T	2.52	1.88	1.78	1.66
HR 2506	T	2.63	2.03	1.95	1.82
HR 2533	B	3.25	2.44	2.28	2.19
HR 2663	T	3.14	2.27	2.13	1.99
HR 2795	T	2.32	1.53	1.34	1.23
HR 2804	T	3.00	2.09	1.93	1.70
HR 2864	T	2.48	1.77	1.64	1. 51
HR 2905	T	1.26	0.44	0.27	0.09
HR 2938	T	2.11	1.32	1.16	0.97
HR 2935	T	2.83	1.92	1.73	1.56
HR 2973	T	2.27	1.67	1.56	1.50
HR 3003	T	2.23	1.42	1.27	1.21
HR 3305	T	3.19	2.30	2.16	2.05
HR 3304	T	3.23	2.43	2.29	2.16
HR 3357	T	2.38	1.55	1.36	1.26
HR 3403	T	2.62	1.93	1.79	1.65
HR 3461	T	2.09	1.53	1.44	1.39
HR 3550	T	3.20	2.41	2.22	2.03
HR 3609	T	2.50	1.72	1.57	1.47
HR 3660	T	2.45	1.61	1.46	1.38
HR 3669	T	3.13	2.37	2.26	2.14
HR 3773	T	1.51	0.75	0.60	0.40

NAME	SITE	J	H	K	L
HR 3939	T	2.91	2.09	1.95	1.84
HR 4069	T	0.06	-0.77	-0.92	-1.06
HR 4247	T	1.95	1.38	1.30	1.23
HD 94336	T	3.44	2.54	2.32	2.19
HR 4280	T	2.99	2.11	1.97	1.74
HR 4335	T	1.12	0.53	0.42	0.27
HR 4371	T	2.25	1.49	1.32	1.19
HR 4434	T	0.91	-0.02	-0.21	-0.32
HR 4639	T	3.33	2.47	2.32	2.17
HR 4690	T	2.21	1.39	1.18	0.91
HR 4863	T	2.58	1.77	1.61	1.53
HR 4884	T	3.36	2.47	2.31	2.33
HR 4954	T	2.16	1.35	1.20	1.04
HR 4962	T	3.32	2.48	2.34	2.14
HR 4986	T	2.98	2.07	1.89	1.73
HR 4998	T	2.87	2.03	1.89	1.72
HR 5200	T	1.35	0.53	0.36	0.20
HR 5219	T	1.19	0.28	0.08	-0.09
HD 127093	T	2.80	1.84	1.61	1.48
HR 5755	T	3.35	2.48	2.33	2.19
HR 5763	T	2.20	1.40	1.22	0.98
HR 5826	T	2.35	1.55	1.34	1.21
HR 5924	T	2.49	1.66	1.50	1.41
HR 5957	T	3.03	2.14	1.97	1.92
HR 5981	T	3.38	2.50	2.35	2.21
HR 6047	T	3.03	2.21	2.07	2.02
HR 6154	T	2.94	2.05	1.85	1.
HR 6228	T	2.45	1.62	1.44	1.23
HD 156652	B	3.54	2.55	2.38	2.11
HR 6464	B	2.68	1.81	1.63	1.49
HR 6695	B	1.80	1.12	1.00	0.85
HR 6728	B	2.80	1.91	1.79	1.66
HD 170951	B	3.63	2.72	2.51	2.41
HR 7237	B	2.88	1.97	1.81	1.65
HR 7302	B	2.62	1.65	1.44	1.27
HR 7405	B	1.55	0.70	0.56	0.47
HR 7514	B	3.16	2.16	1.94	1.86
HR 7633	B	2.30	1.41	1.24	1.21
HR 7635	B	0.74	-0.05	-0.22	-0.33
HR 7648	B	3.15	2.33	2.19	2.12
HR 7780	B	3.19	2.36	2.21	2.09
HR 8005	B	2.79	1.87	1.69	1.59
HR 8066	B	2.87	1.91	1.72	1.55
HR 8090	B	3.00	2.04	1.84	1.75
HR 8572	B	1.16	0.27	0.06	-0.13
HR 8699	B	2.00	1.19	1.03	0.92
HR 8804	B	3.01	2.18	2.02	1.96
HR 8882	B	2.86	2.01	1.86	1.

Individual errors are not given but typical values are: J: ± 0.03; H : ±0.04; K : ±0.05; L : ±0.06. Site: "T", ISAS, Tokyo, Japan; "B", Xanglong, Beijing, China.

Appendix F
Spectra of the 422 Stars of the Calibration Network

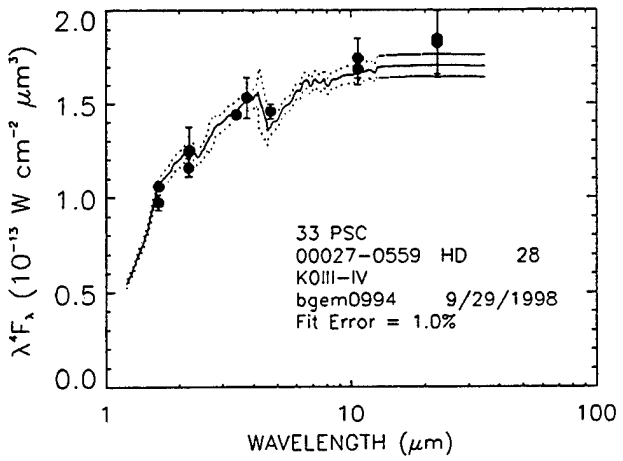
33 PSC
00027-0559 HD 28
K0III-IV
bgem0994 9/29/1998
Fit Error = 1.0%
$\lambda^4 F_\lambda$ (10^{-13} W cm^{-2} μm^3)
WAVELENGTH (μm)

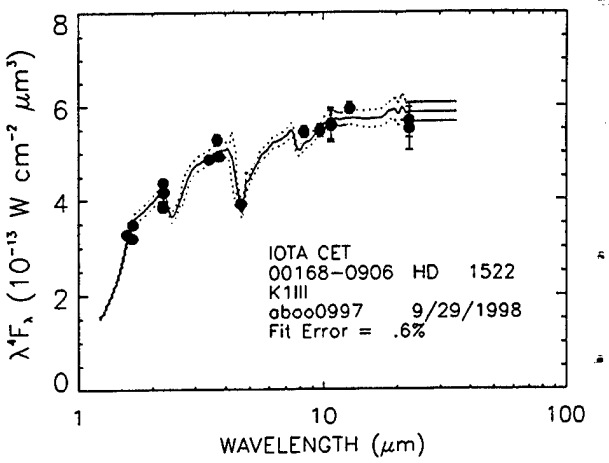
IOTA CET
00168-0906 HD 1522
K1III
aboo0997 9/29/1998
Fit Error = .6%
$\lambda^4 F_\lambda$ (10^{-13} W cm^{-2} μm^3)
WAVELENGTH (μm)

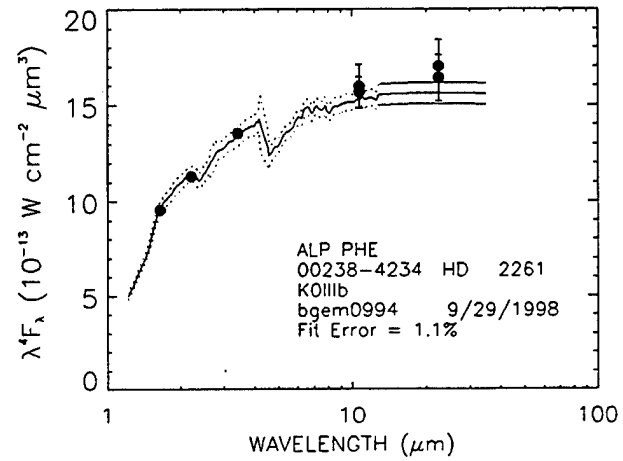
ALP PHE
00238-4234 HD 2261
K0IIIb
bgem0994 9/29/1998
Fit Error = 1.1%
$\lambda^4 F_\lambda$ (10^{-13} W cm^{-2} μm^3)
WAVELENGTH (μm)

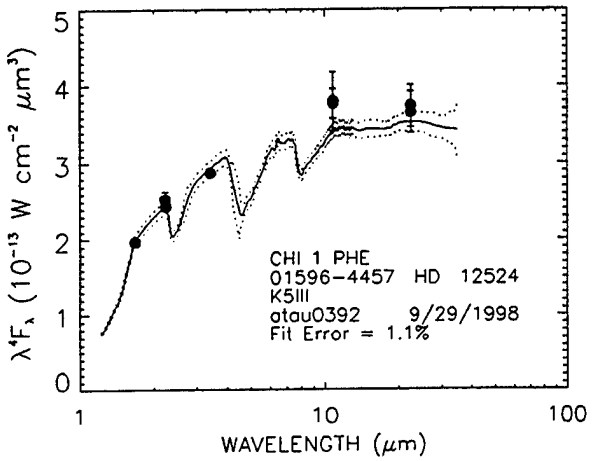
CHI 1 PHE
01596-4457 HD 12524
K5III
atau0392 9/29/1998
Fit Error = 1.1%
$\lambda^4 F_\lambda$ (10^{-13} W cm^{-2} μm^3)
WAVELENGTH (μm)

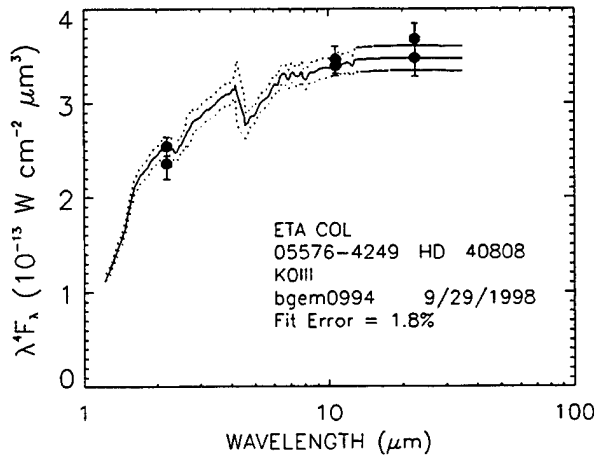
ETA COL
05576-4249 HD 40808
K0III
bgem0994 9/29/1998
Fit Error = 1.8%
$\lambda^4 F_\lambda$ (10^{-13} W cm^{-2} μm^3)
WAVELENGTH (μm)

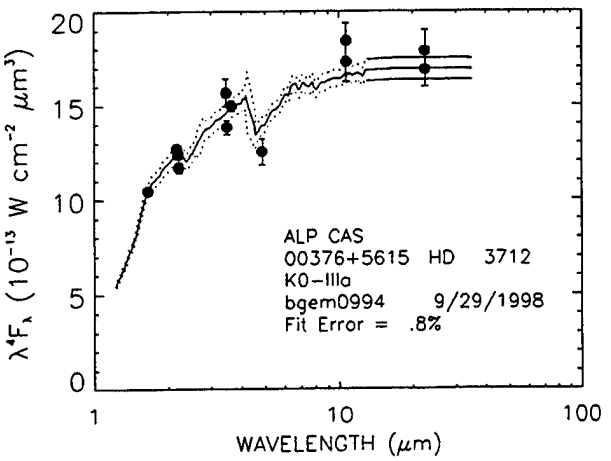
ALP CAS
00376+5615 HD 3712
K0-IIIa
bgem0994 9/29/1998
Fit Error = .8%
$\lambda^4 F_\lambda$ (10^{-13} W cm^{-2} μm^3)
WAVELENGTH (μm)

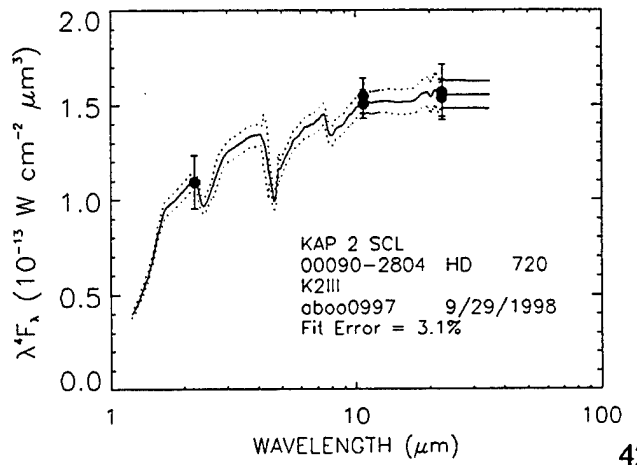
KAP 2 SCL
00090-2804 HD 720
K2III
aboo0997 9/29/1998
Fit Error = 3.1%
$\lambda^4 F_\lambda$ (10^{-13} W cm^{-2} μm^3)
WAVELENGTH (μm)

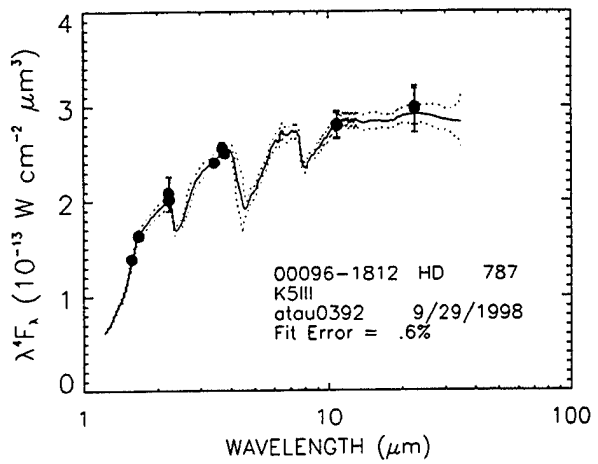
00096-1812 HD 787
K5III
atau0392 9/29/1998
Fit Error = .6%
$\lambda^4 F_\lambda$ (10^{-13} W cm^{-2} μm^3)
WAVELENGTH (μm)

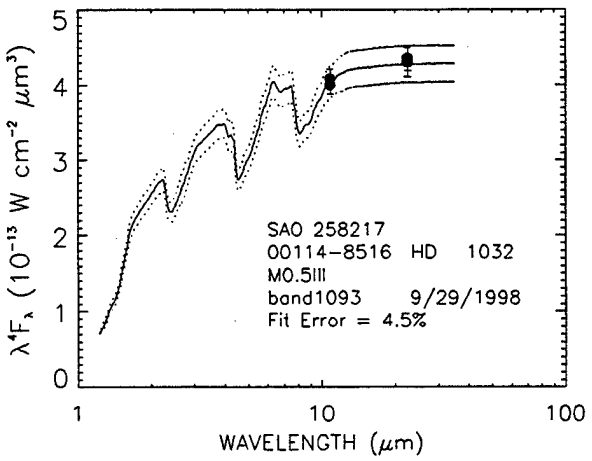
SAO 258217
00114-8516 HD 1032
M0.5III
band1093 9/29/1998
Fit Error = 4.5%
WAVELENGTH (μm)

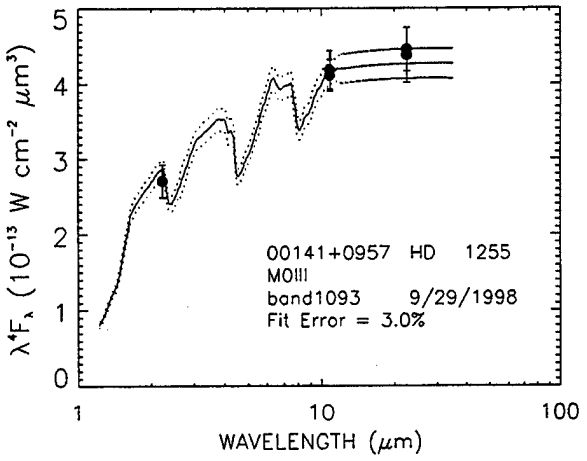
00141+0957 HD 1255
M0III
band1093 9/29/1998
Fit Error = 3.0%
WAVELENGTH (μm)

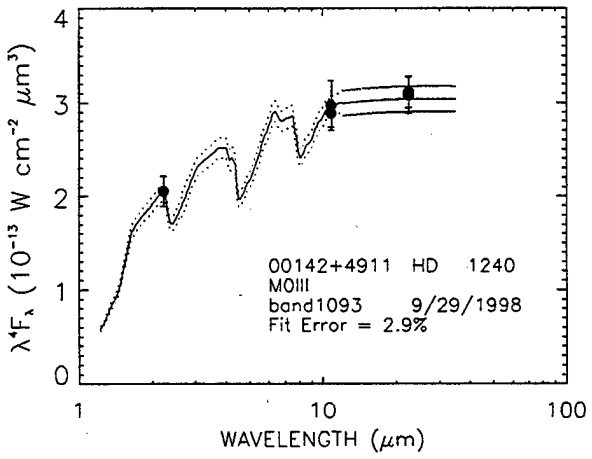
00142+4911 HD 1240
M0III
band1093 9/29/1998
Fit Error = 2.9%
WAVELENGTH (μm)

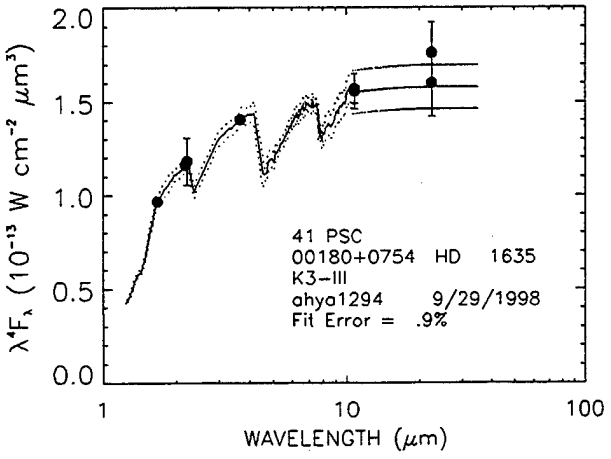
41 PSC
00180+0754 HD 1635
K3-III
ahya1294 9/29/1998
Fit Error = .9%
WAVELENGTH (μm)

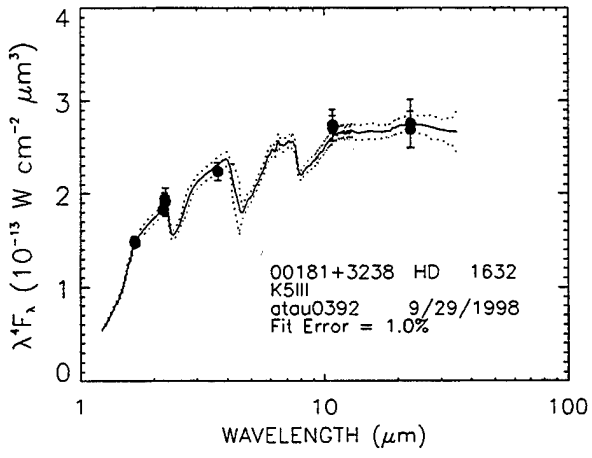
00181+3238 HD 1632
K5III
atau0392 9/29/1998
Fit Error = 1.0%
WAVELENGTH (μm)

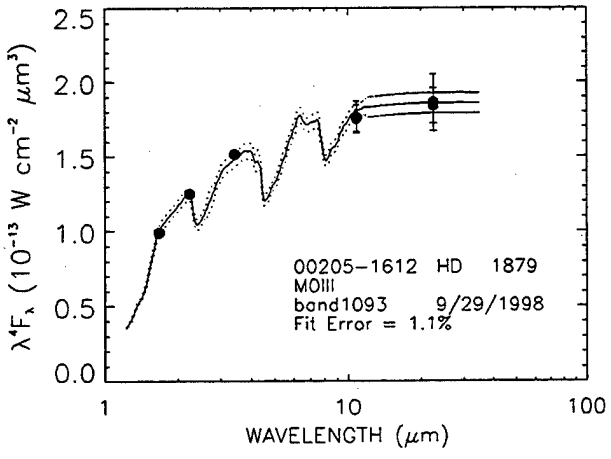
00205-1612 HD 1879
M0III
band1093 9/29/1998
Fit Error = 1.1%
WAVELENGTH (μm)

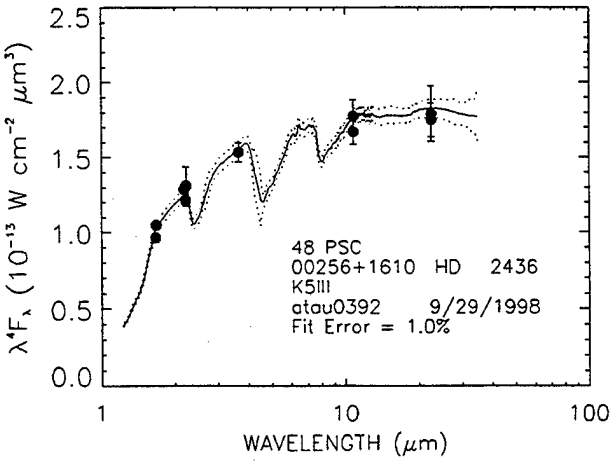
48 PSC
00256+1610 HD 2436
K5III
atau0392 9/29/1998
Fit Error = 1.0%
WAVELENGTH (μm)

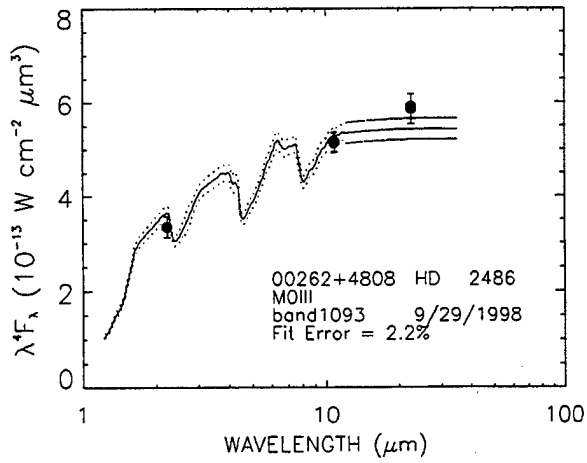
00262+4808 HD 2486
M0III
band1093 9/29/1998
Fit Error = 2.2%
WAVELENGTH (μm)

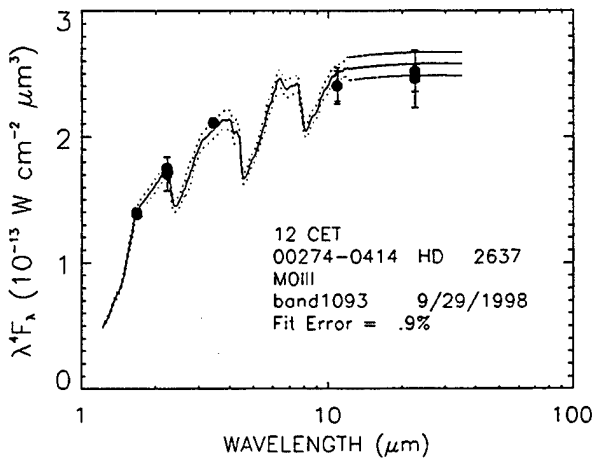
12 CET
00274-0414 HD 2637
M0III
band1093 9/29/1998
Fit Error = .9%
WAVELENGTH (μm)

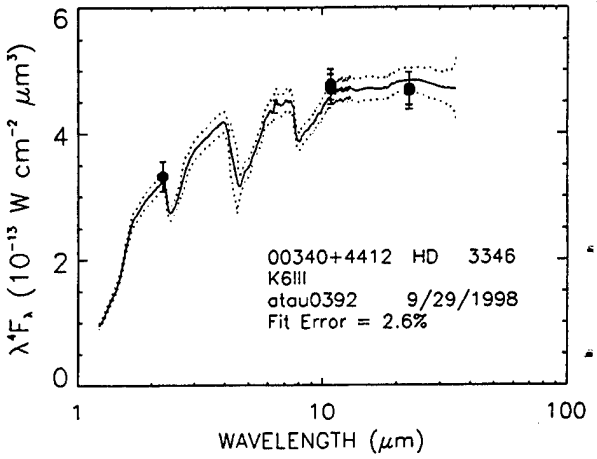
00340+4412 HD 3346
K6III
atau0392 9/29/1998
Fit Error = 2.6%
WAVELENGTH (μm)

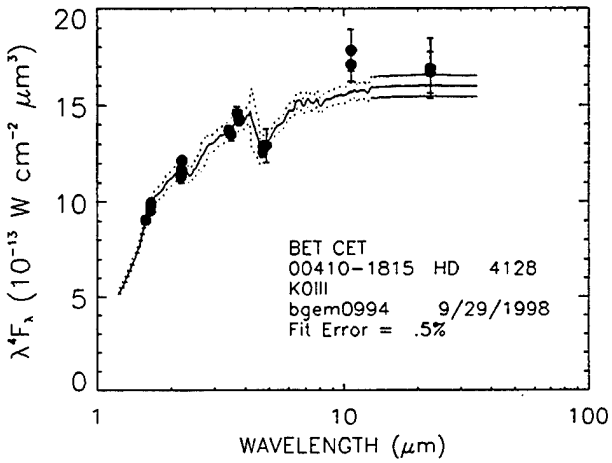
BET CET
00410-1815 HD 4128
K0III
bgem0994 9/29/1998
Fit Error = .5%
WAVELENGTH (μm)

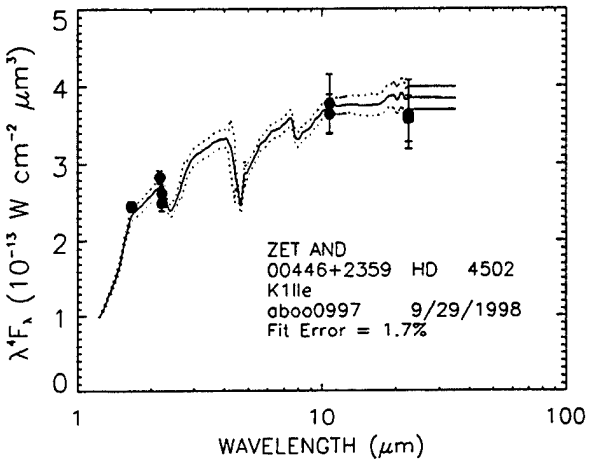
ZET AND
00446+2359 HD 4502
K1IIe
aboo0997 9/29/1998
Fit Error = 1.7%
WAVELENGTH (μm)

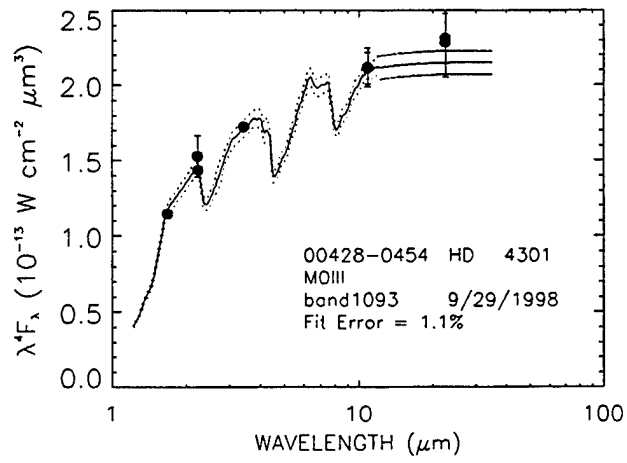
00428-0454 HD 4301
M0III
band1093 9/29/1998
Fit Error = 1.1%
WAVELENGTH (μm)

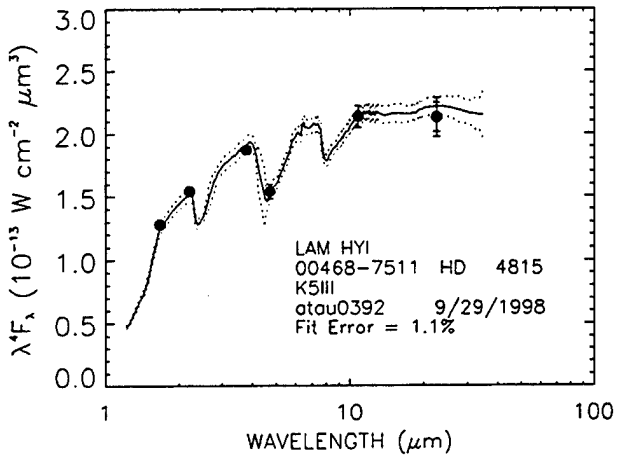
LAM HYI
00468-7511 HD 4815
K5III
atau0392 9/29/1998
Fit Error = 1.1%
WAVELENGTH (μm)

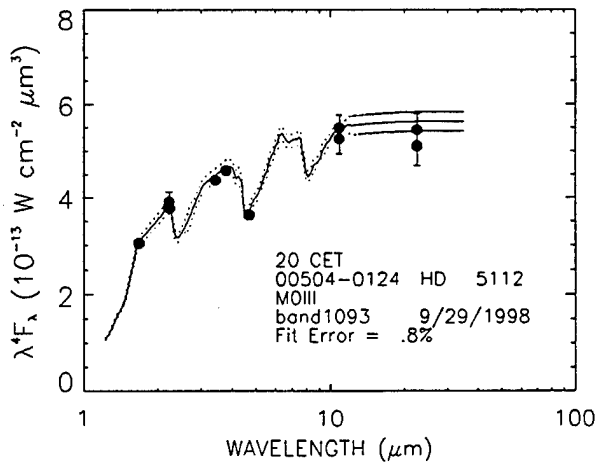
20 CET
00504-0124 HD 5112
M0III
band1093 9/29/1998
Fit Error = .8%
WAVELENGTH (μm)

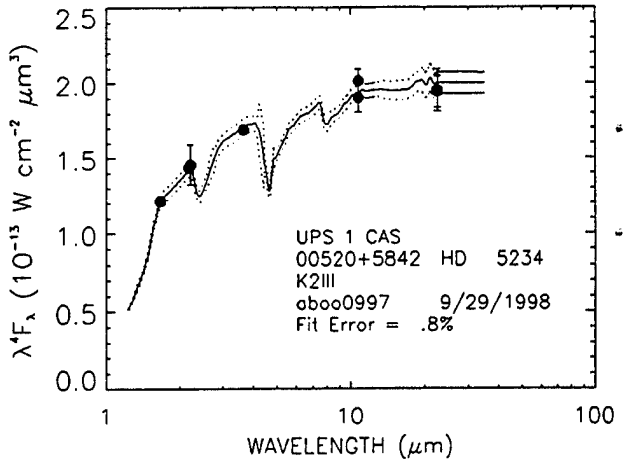
UPS 1 CAS
00520+5842 HD 5234
K2III
aboo0997 9/29/1998
Fit Error = .8%
WAVELENGTH (μm)

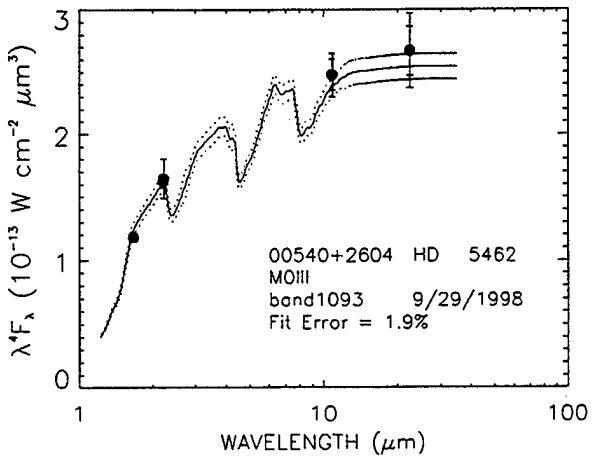
00540+2604 HD 5462
M0III
band1093 9/29/1998
Fit Error = 1.9%
WAVELENGTH (μm)

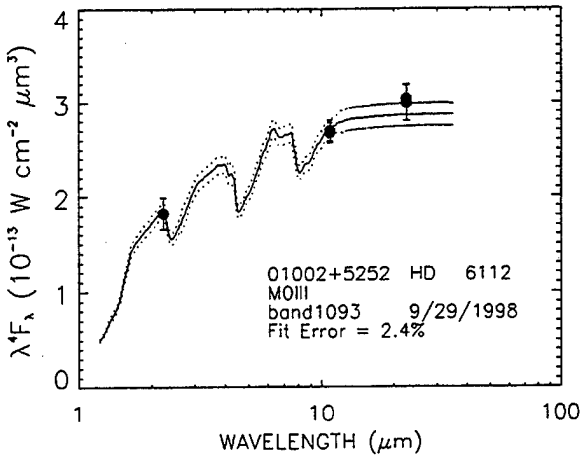
01002+5252 HD 6112
M0III
band1093 9/29/1998
Fit Error = 2.4%
WAVELENGTH (μm)

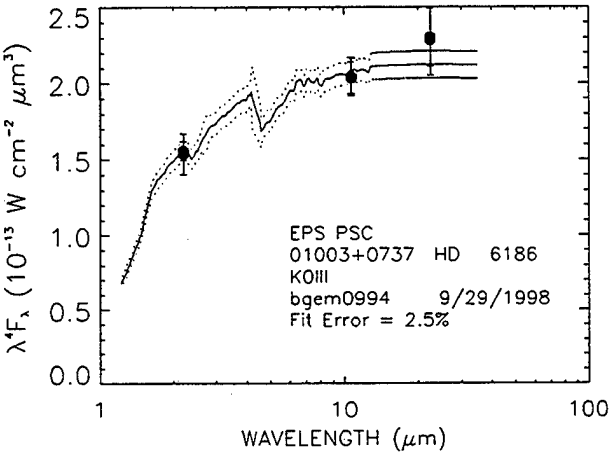
EPS PSC
01003+0737 HD 6186
K0III
bgem0994 9/29/1998
Fit Error = 2.5%
WAVELENGTH (μm)

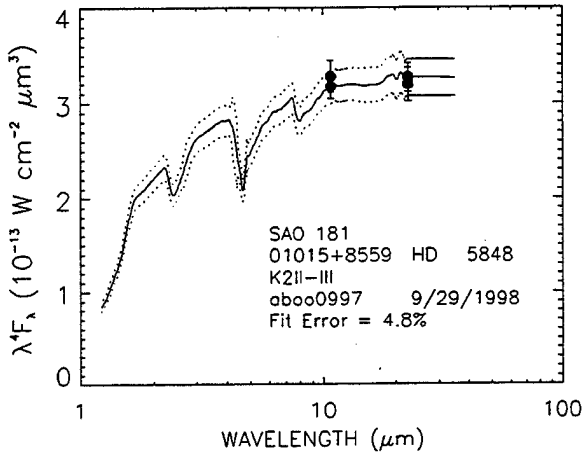
SAO 181
01015+8559 HD 5848
K2II-III
aboo0997 9/29/1998
Fit Error = 4.8%
WAVELENGTH (μm)

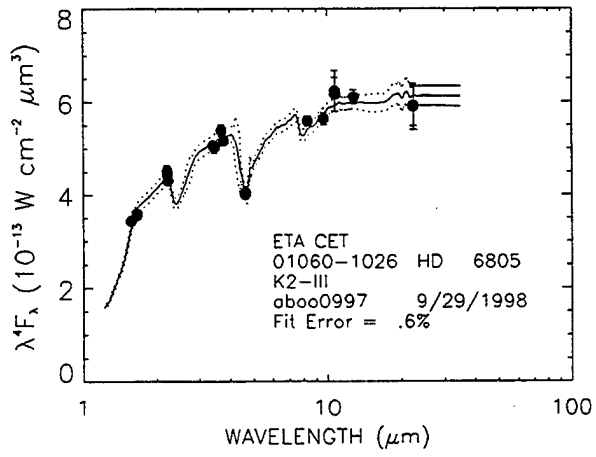
ETA CET
01060-1026 HD 6805
K2-III
aboo0997 9/29/1998
Fit Error = .6%
WAVELENGTH (μm)

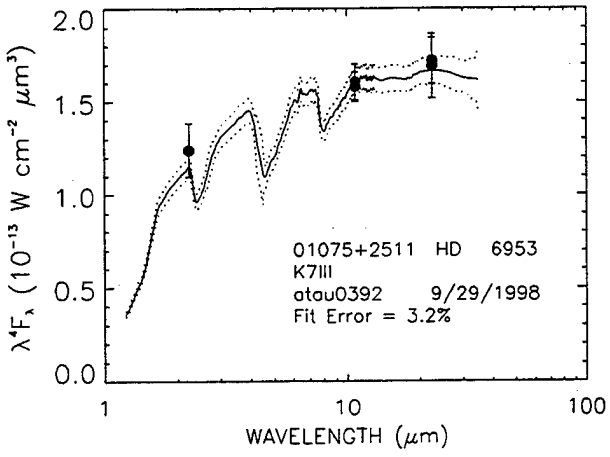
01075+2511 HD 6953
K7III
atau0392 9/29/1998
Fit Error = 3.2%
WAVELENGTH (μm)

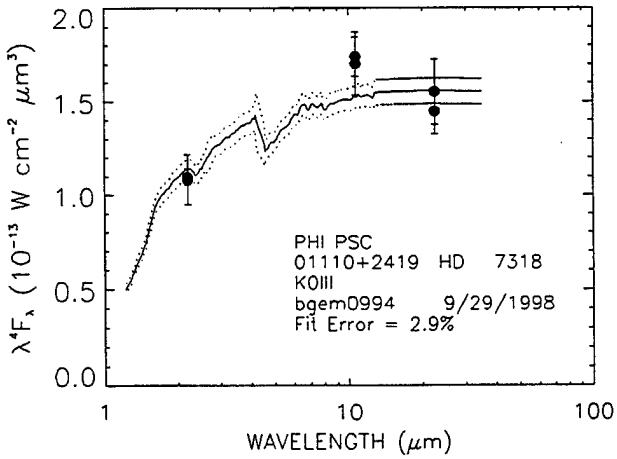
PHI PSC
01110+2419 HD 7318
K0III
bgem0994 9/29/1998
Fit Error = 2.9%
WAVELENGTH (μm)

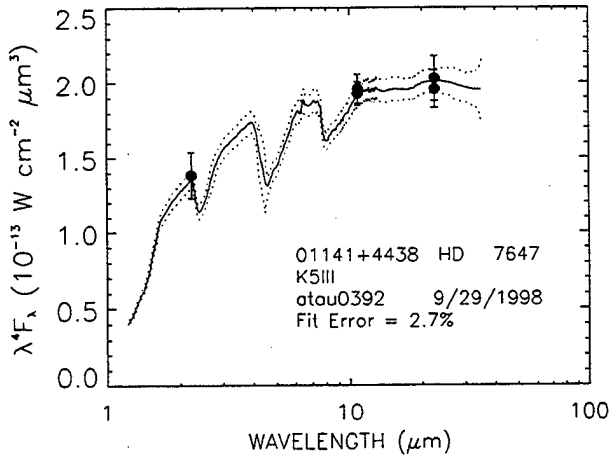
01141+4438 HD 7647
K5III
atau0392 9/29/1998
Fit Error = 2.7%
WAVELENGTH (μm)

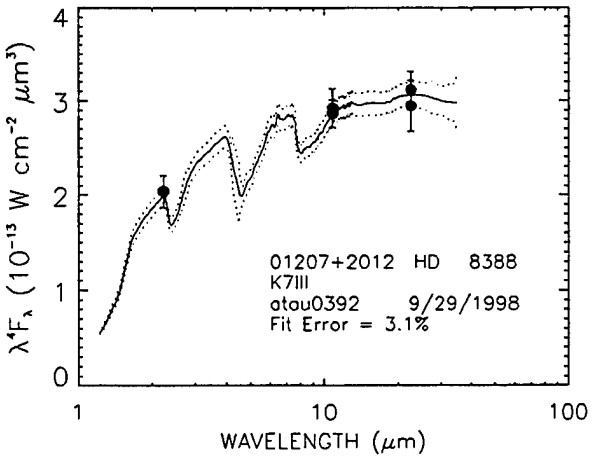
01207+2012 HD 8388
K7III
atau0392 9/29/1998
Fit Error = 3.1%
WAVELENGTH (μm)
λ⁴Fλ (10⁻¹³ W cm⁻² μm³)

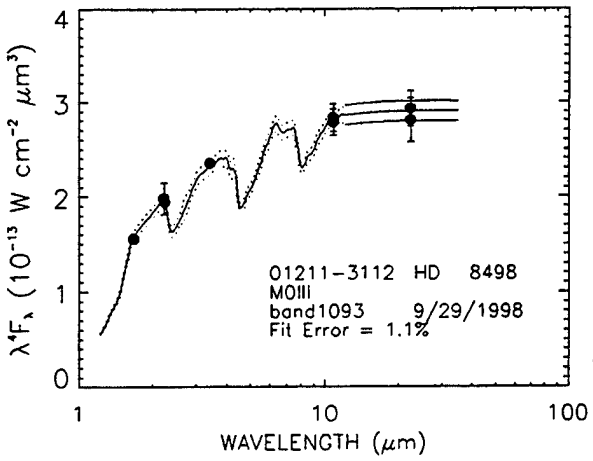
01211−3112 HD 8498
MOIII
band1093 9/29/1998
Fit Error = 1.1%
WAVELENGTH (μm)
λ⁴Fλ (10⁻¹³ W cm⁻² μm³)

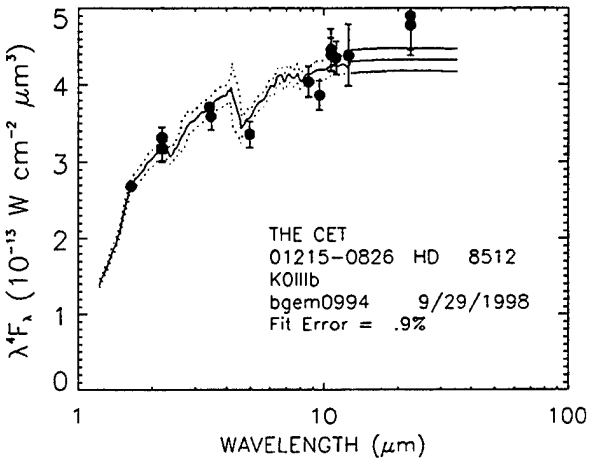
THE CET
01215−0826 HD 8512
KOIIIb
bgem0994 9/29/1998
Fit Error = .9%
WAVELENGTH (μm)
λ⁴Fλ (10⁻¹³ W cm⁻² μm³)

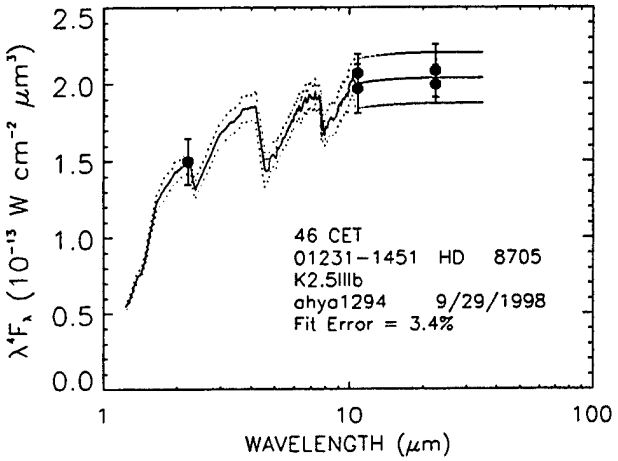
46 CET
01231−1451 HD 8705
K2.5IIIb
ahya1294 9/29/1998
Fit Error = 3.4%
WAVELENGTH (μm)
λ⁴Fλ (10⁻¹³ W cm⁻² μm³)

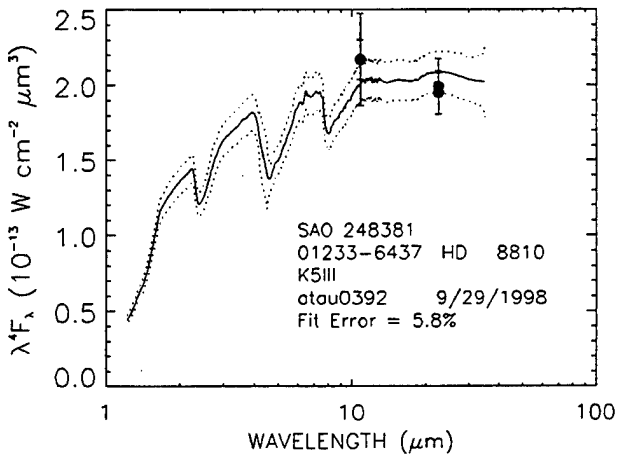
SAO 248381
01233−6437 HD 8810
K5III
atau0392 9/29/1998
Fit Error = 5.8%
WAVELENGTH (μm)
λ⁴Fλ (10⁻¹³ W cm⁻² μm³)

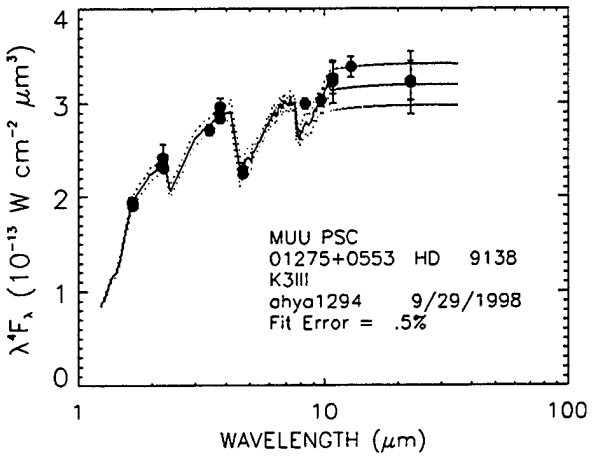
MUU PSC
01275+0553 HD 9138
K3III
ahya1294 9/29/1998
Fit Error = .5%
WAVELENGTH (μm)
λ⁴Fλ (10⁻¹³ W cm⁻² μm³)

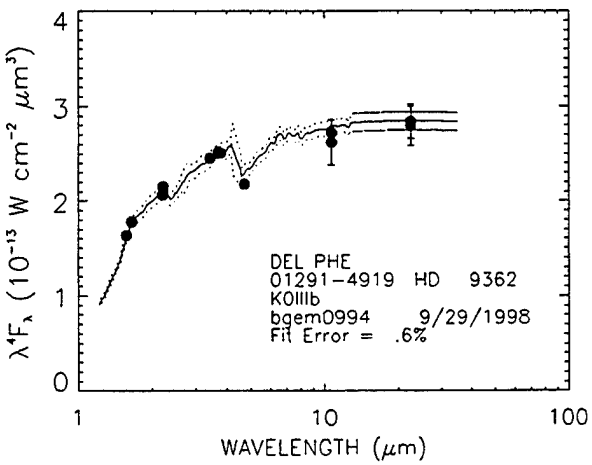
DEL PHE
01291−4919 HD 9362
KOIIIb
bgem0994 9/29/1998
Fit Error = .6%
WAVELENGTH (μm)
λ⁴Fλ (10⁻¹³ W cm⁻² μm³)

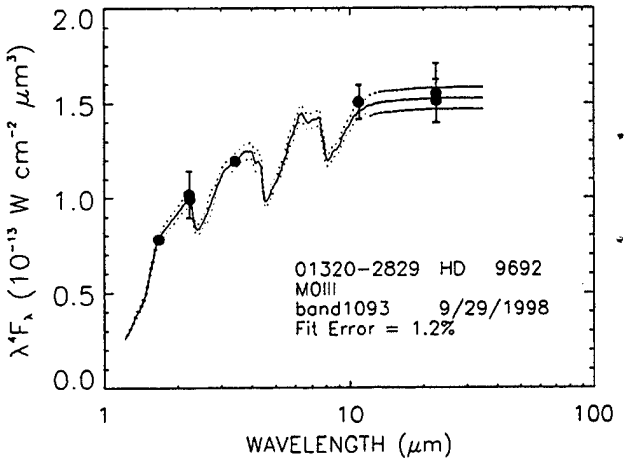
01320−2829 HD 9692
MOIII
band1093 9/29/1998
Fit Error = 1.2%
WAVELENGTH (μm)
λ⁴Fλ (10⁻¹³ W cm⁻² μm³)

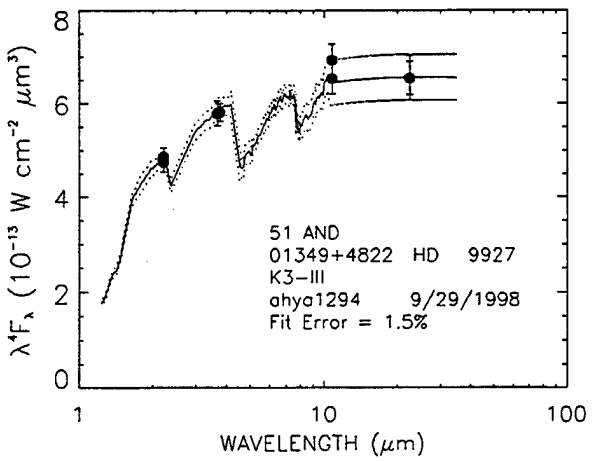
51 AND
01349+4822 HD 9927
K3-III
ahya1294 9/29/1998
Fit Error = 1.5%
WAVELENGTH (μm)

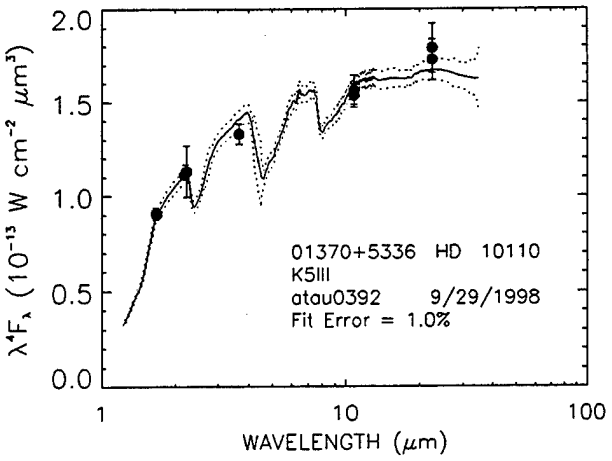
01370+5336 HD 10110
K5III
atau0392 9/29/1998
Fit Error = 1.0%
WAVELENGTH (μm)

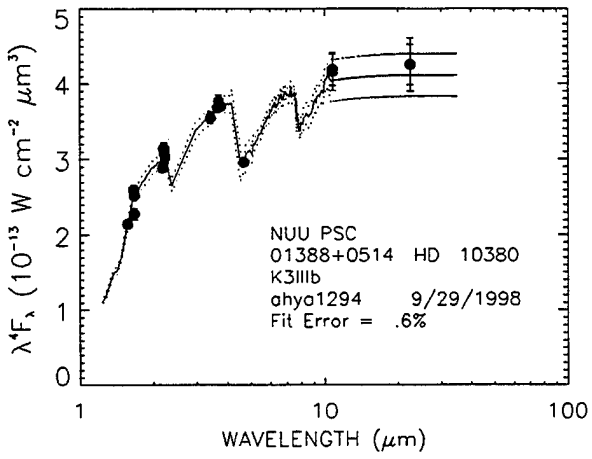
NUU PSC
01388+0514 HD 10380
K3IIIb
ahya1294 9/29/1998
Fit Error = .6%
WAVELENGTH (μm)

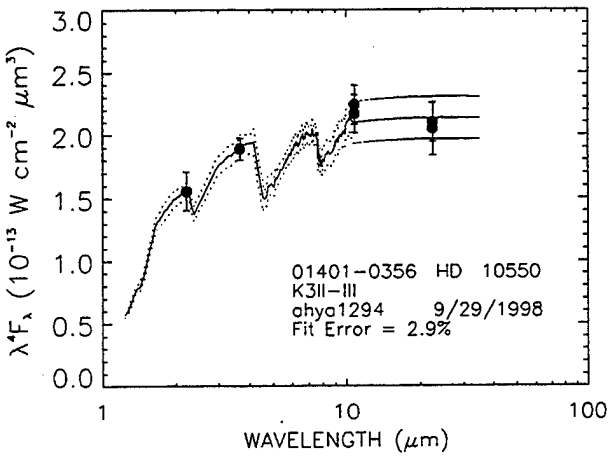
01401-0356 HD 10550
K3II-III
ahya1294 9/29/1998
Fit Error = 2.9%
WAVELENGTH (μm)

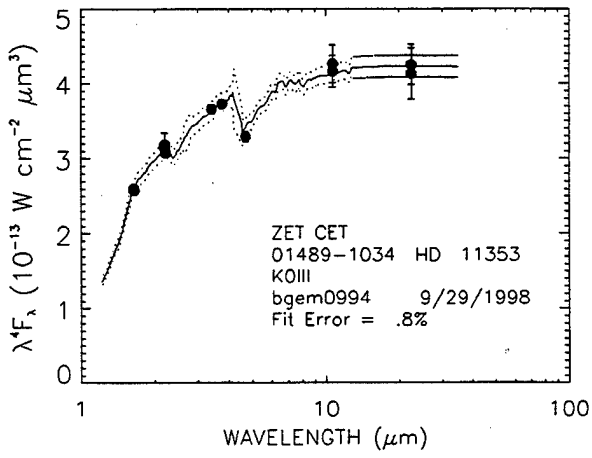
ZET CET
01489-1034 HD 11353
KOIII
bgem0994 9/29/1998
Fit Error = .8%
WAVELENGTH (μm)

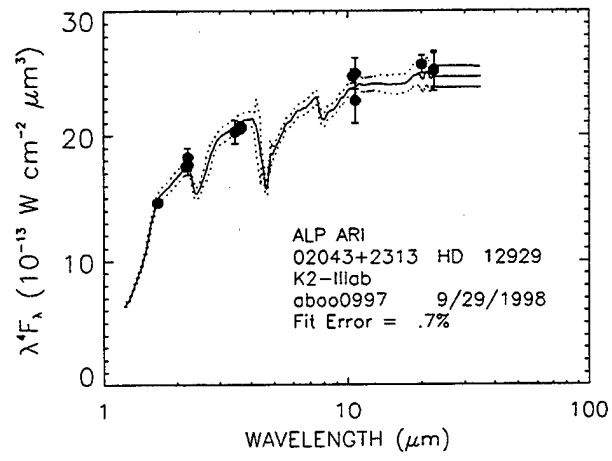
ALP ARI
02043+2313 HD 12929
K2-IIIab
aboo0997 9/29/1998
Fit Error = .7%
WAVELENGTH (μm)

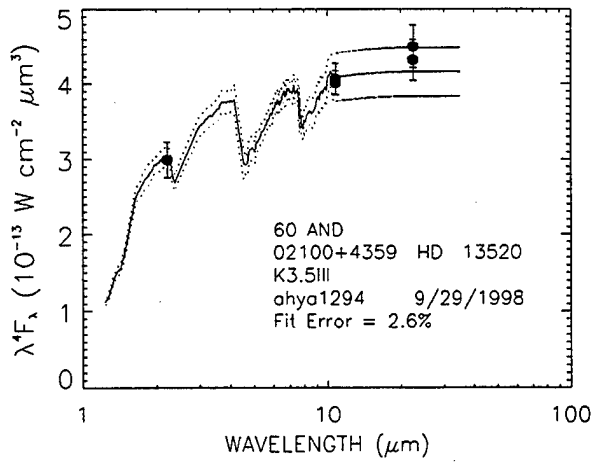
60 AND
02100+4359 HD 13520
K3.5III
ahya1294 9/29/1998
Fit Error = 2.6%
WAVELENGTH (μm)

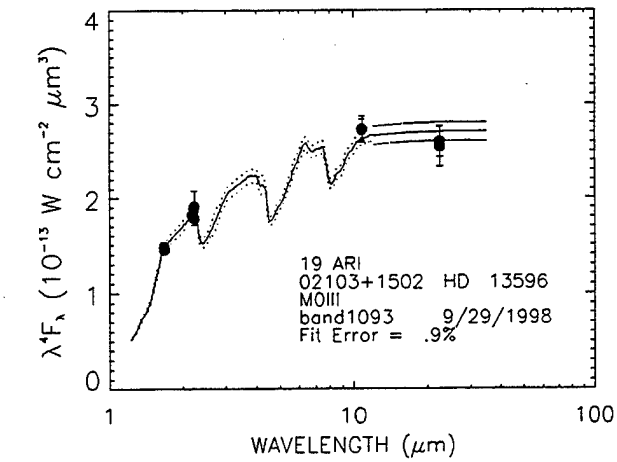
19 ARI
02103+1502 HD 13596
MOIII
band1093 9/29/1998
Fit Error = .9%
WAVELENGTH (μm)

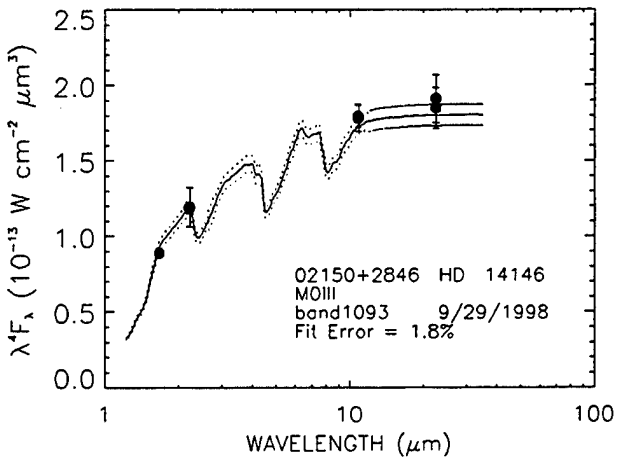
02150+2846 HD 14146
M0III
band1093 9/29/1998
Fit Error = 1.8%
WAVELENGTH (μm)

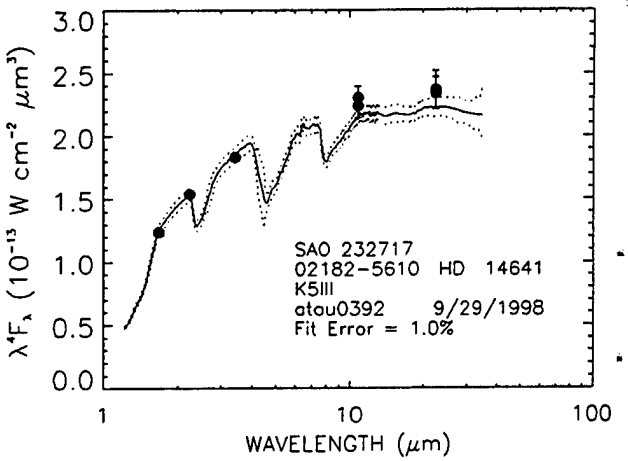
SAO 232717
02182-5610 HD 14641
K5III
atau0392 9/29/1998
Fit Error = 1.0%
WAVELENGTH (μm)

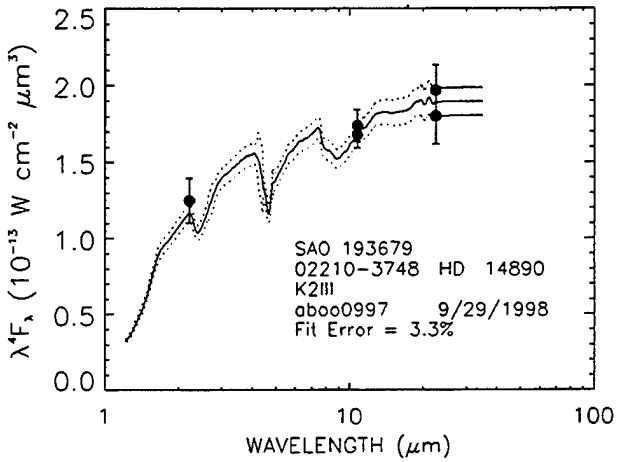
SAO 193679
02210-3748 HD 14890
K2III
aboo0997 9/29/1998
Fit Error = 3.3%
WAVELENGTH (μm)

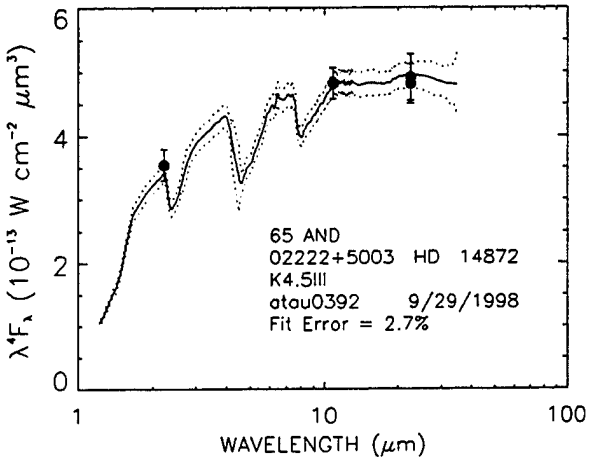
65 AND
02222+5003 HD 14872
K4.5III
atau0392 9/29/1998
Fit Error = 2.7%
WAVELENGTH (μm)

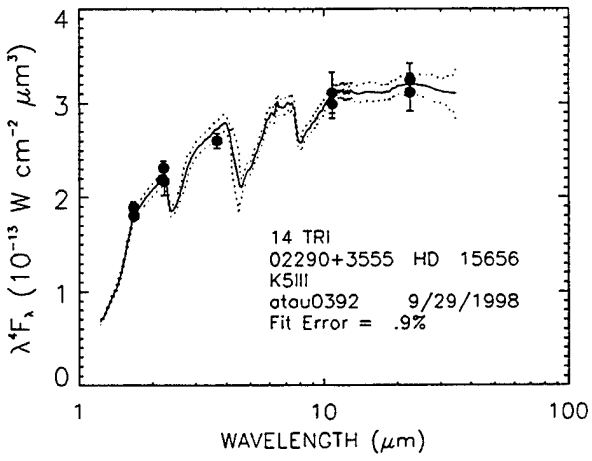
14 TRI
02290+3555 HD 15656
K5III
atau0392 9/29/1998
Fit Error = .9%
WAVELENGTH (μm)

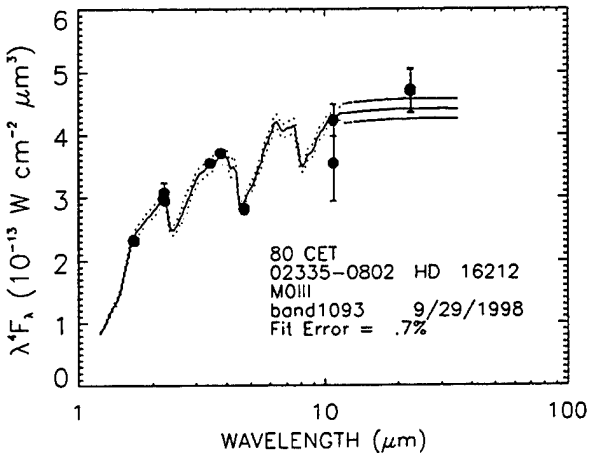
80 CET
02335-0802 HD 16212
M0III
band1093 9/29/1998
Fit Error = .7%
WAVELENGTH (μm)

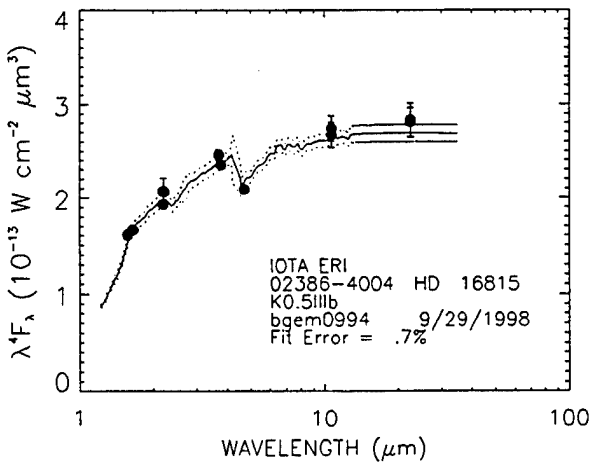
IOTA ERI
02386-4004 HD 16815
K0.5IIIb
bgem0994 9/29/1998
Fit Error = .7%
WAVELENGTH (μm)

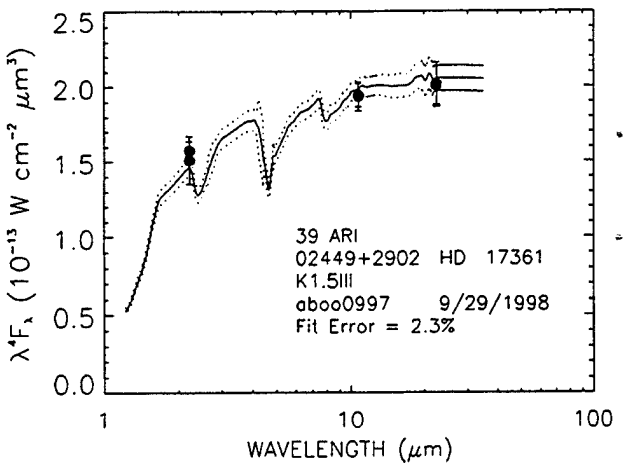
39 ARI
02449+2902 HD 17361
K1.5III
aboo0997 9/29/1998
Fit Error = 2.3%
WAVELENGTH (μm)

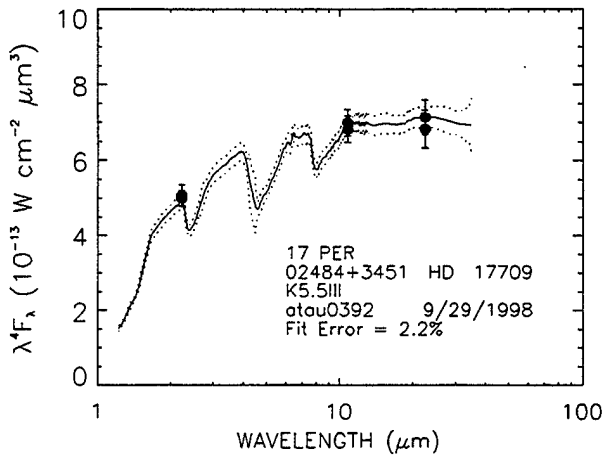
17 PER
02484+3451 HD 17709
K5.5III
atau0392 9/29/1998
Fit Error = 2.2%
λ^4F_λ (10^{-13} W cm^{-2} μm^3)
WAVELENGTH (μm)

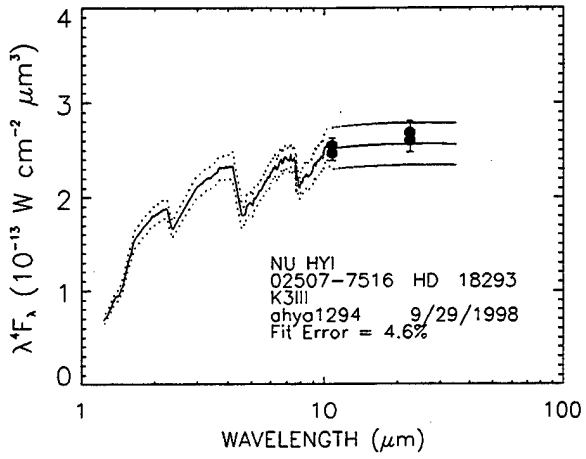
NU HYI
02507−7516 HD 18293
K3III
ahya1294 9/29/1998
Fit Error = 4.6%
λ^4F_λ (10^{-13} W cm^{-2} μm^3)
WAVELENGTH (μm)

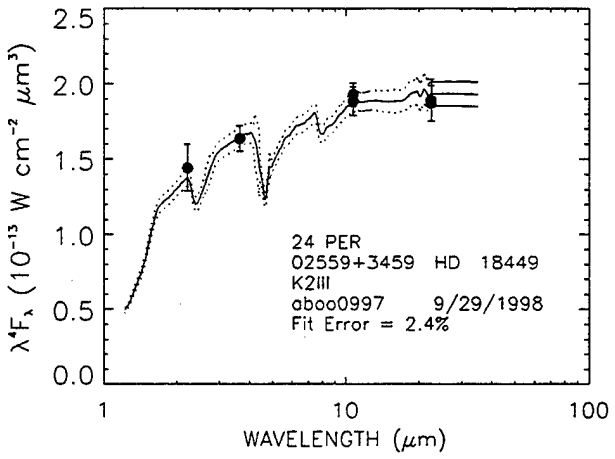
24 PER
02559+3459 HD 18449
K2III
aboo0997 9/29/1998
Fit Error = 2.4%
λ^4F_λ (10^{-13} W cm^{-2} μm^3)
WAVELENGTH (μm)

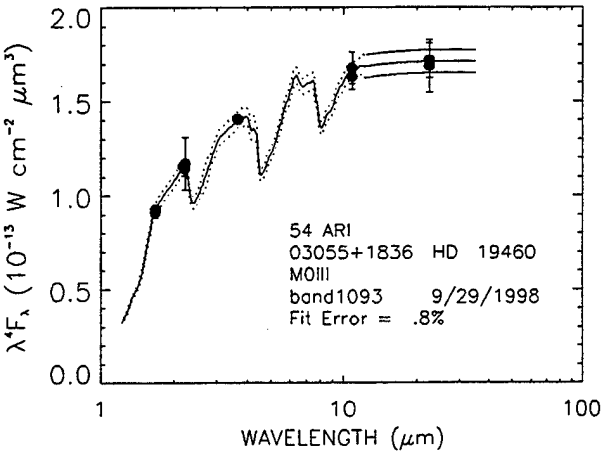
54 ARI
03055+1836 HD 19460
M0III
band1093 9/29/1998
Fit Error = .8%
λ^4F_λ (10^{-13} W cm^{-2} μm^3)
WAVELENGTH (μm)

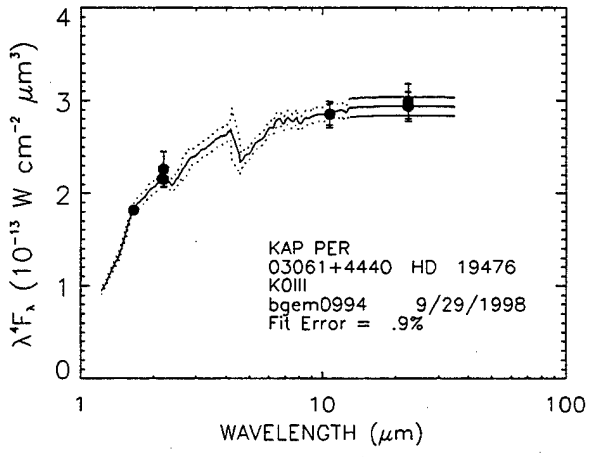
KAP PER
03061+4440 HD 19476
K0III
bgem0994 9/29/1998
Fit Error = .9%
λ^4F_λ (10^{-13} W cm^{-2} μm^3)
WAVELENGTH (μm)

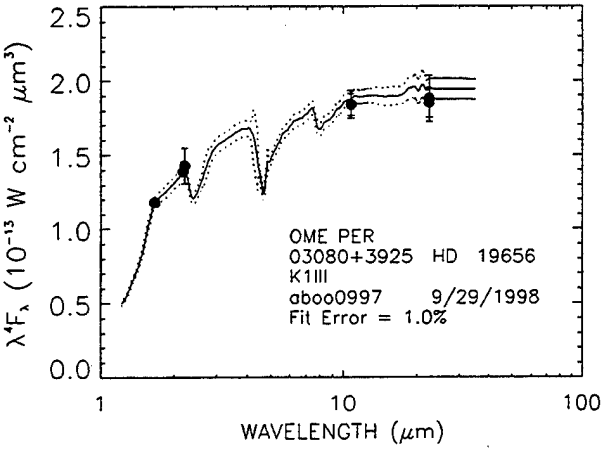
OME PER
03080+3925 HD 19656
K1III
aboo0997 9/29/1998
Fit Error = 1.0%
λ^4F_λ (10^{-13} W cm^{-2} μm^3)
WAVELENGTH (μm)

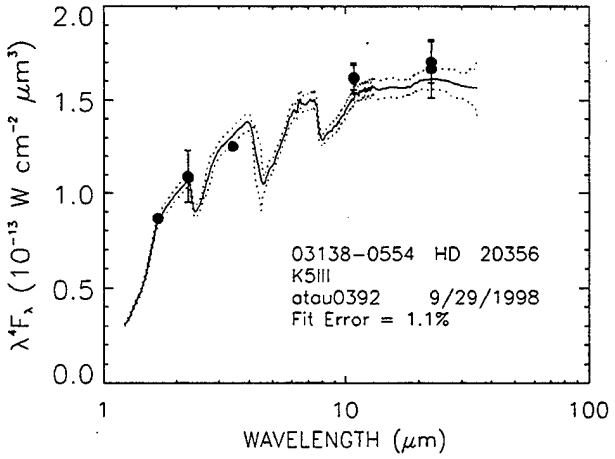
03138−0554 HD 20356
K5III
atau0392 9/29/1998
Fit Error = 1.1%
λ^4F_λ (10^{-13} W cm^{-2} μm^3)
WAVELENGTH (μm)

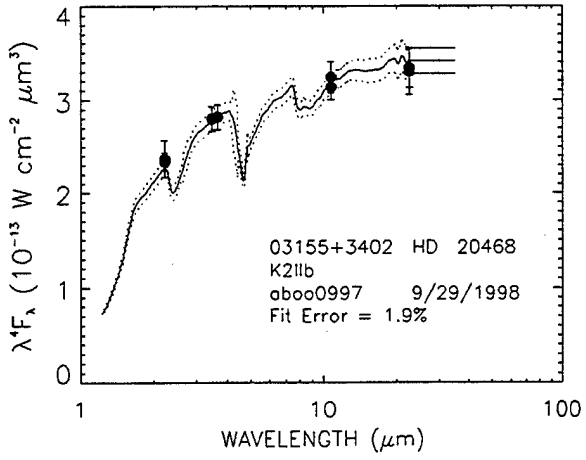
03155+3402 HD 20468
K2IIb
aboo0997 9/29/1998
Fit Error = 1.9%
λ^4F_λ (10^{-13} W cm^{-2} μm^3)
WAVELENGTH (μm)

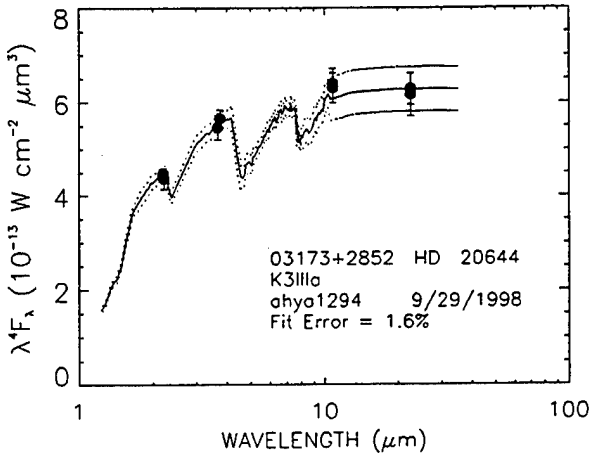
03173+2852 HD 20644
K3IIIa
ahya1294 9/29/1998
Fit Error = 1.6%
WAVELENGTH (μm)

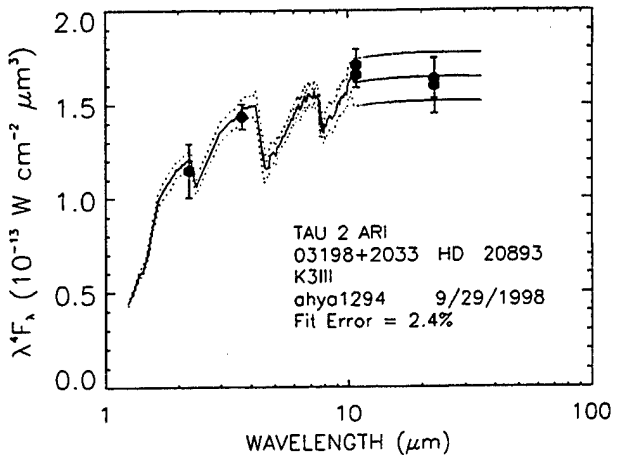
TAU 2 ARI
03198+2033 HD 20893
K3III
ahya1294 9/29/1998
Fit Error = 2.4%
WAVELENGTH (μm)

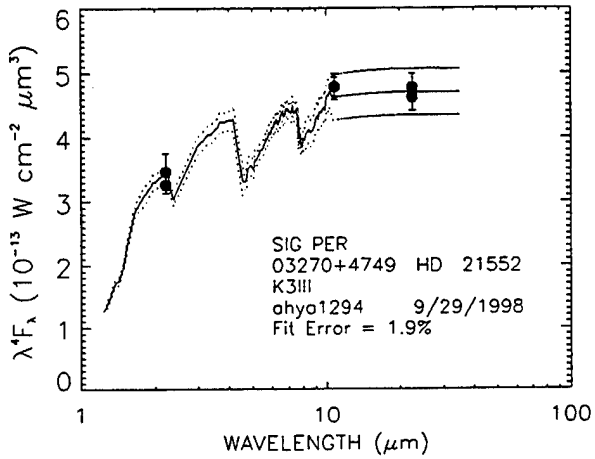
SIG PER
03270+4749 HD 21552
K3III
ahya1294 9/29/1998
Fit Error = 1.9%
WAVELENGTH (μm)

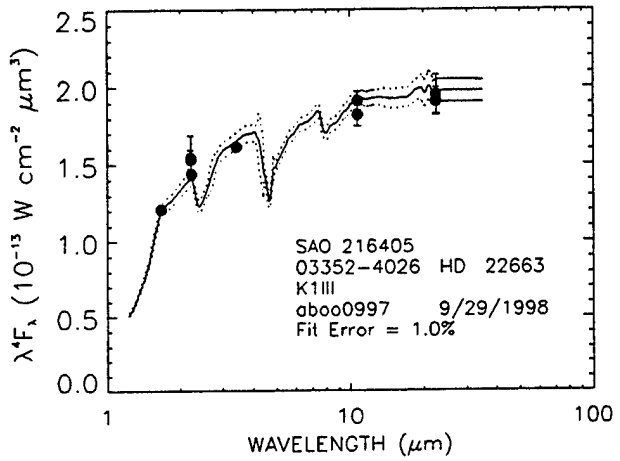
SAO 216405
03352-4026 HD 22663
K1III
aboo0997 9/29/1998
Fit Error = 1.0%
WAVELENGTH (μm)

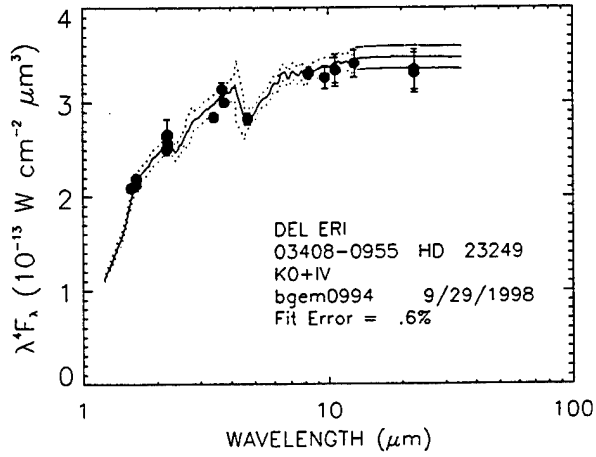
DEL ERI
03408-0955 HD 23249
K0+IV
bgem0994 9/29/1998
Fit Error = .6%
WAVELENGTH (μm)

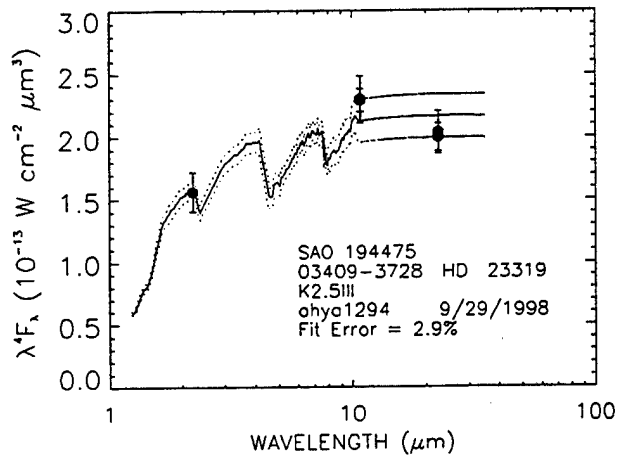
SAO 194475
03409-3728 HD 23319
K2.5III
ahya1294 9/29/1998
Fit Error = 2.9%
WAVELENGTH (μm)

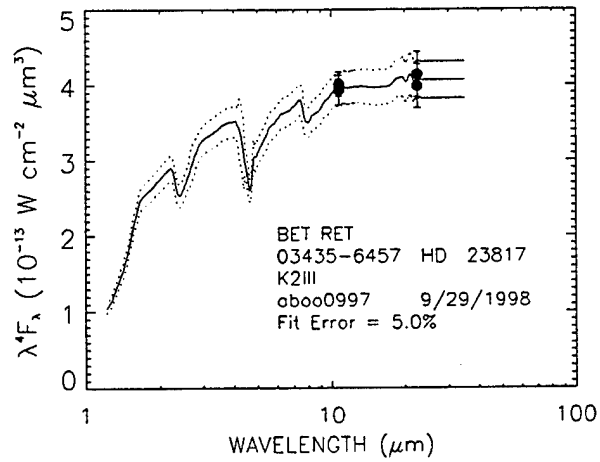
BET RET
03435-6457 HD 23817
K2III
aboo0997 9/29/1998
Fit Error = 5.0%
WAVELENGTH (μm)

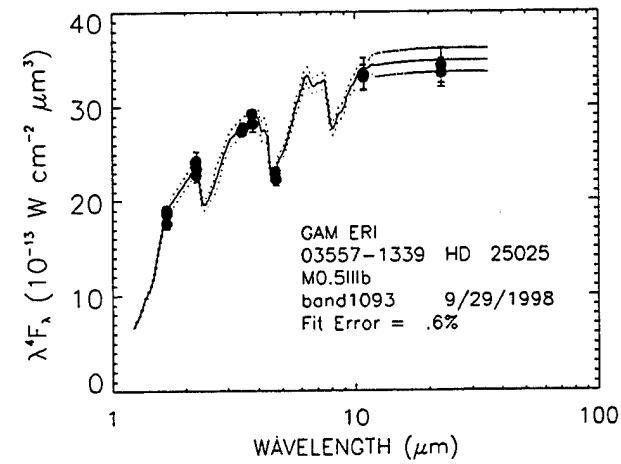
GAM ERI
03557-1339 HD 25025
M0.5IIIb
band1093 9/29/1998
Fit Error = .6%
WAVELENGTH (μm)

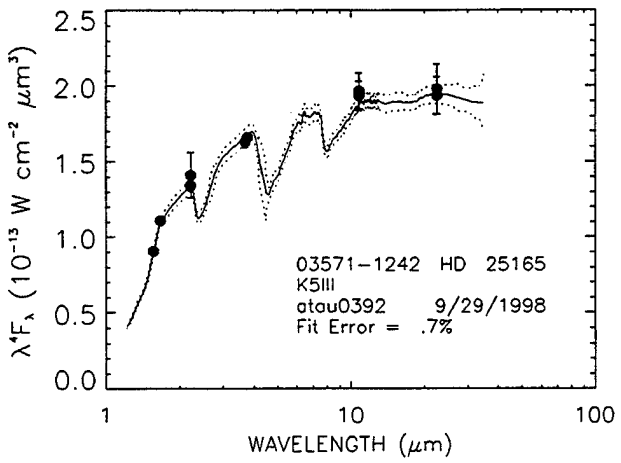
03571−1242 HD 25165
K5III
atau0392 9/29/1998
Fit Error = .7%
WAVELENGTH (μm)

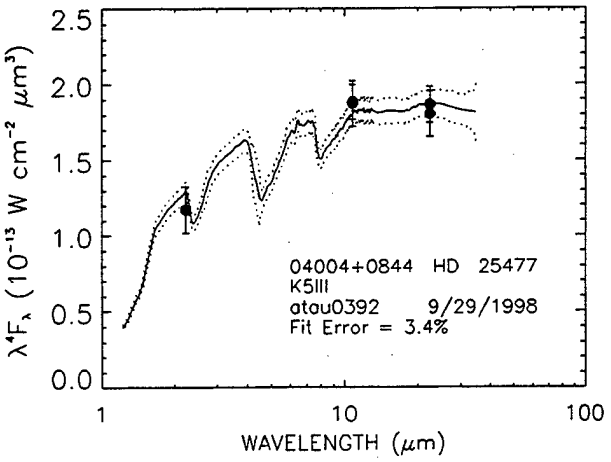
04004+0844 HD 25477
K5III
atau0392 9/29/1998
Fit Error = 3.4%
WAVELENGTH (μm)

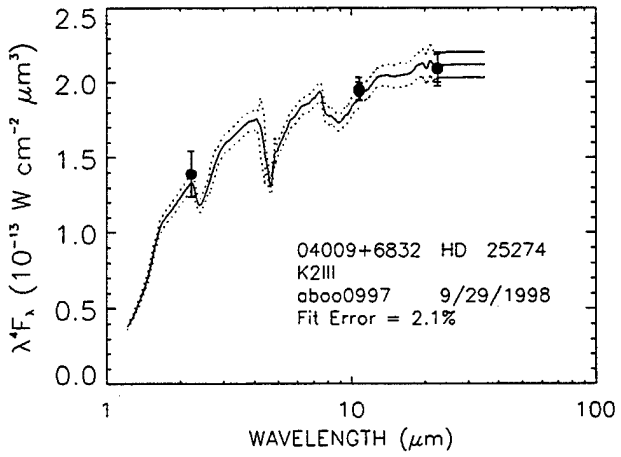
04009+6832 HD 25274
K2III
aboo0997 9/29/1998
Fit Error = 2.1%
WAVELENGTH (μm)

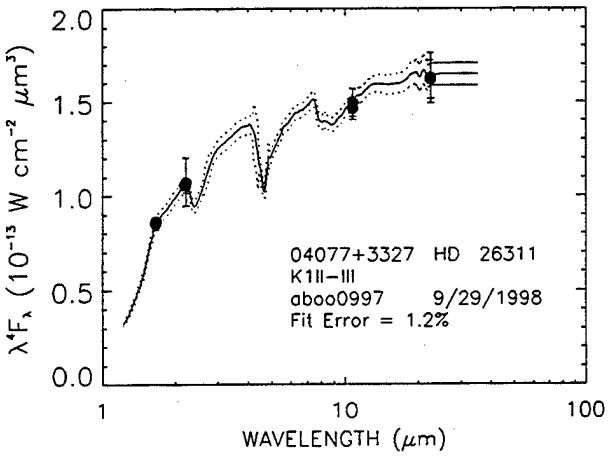
04077+3327 HD 26311
K1II−III
aboo0997 9/29/1998
Fit Error = 1.2%
WAVELENGTH (μm)

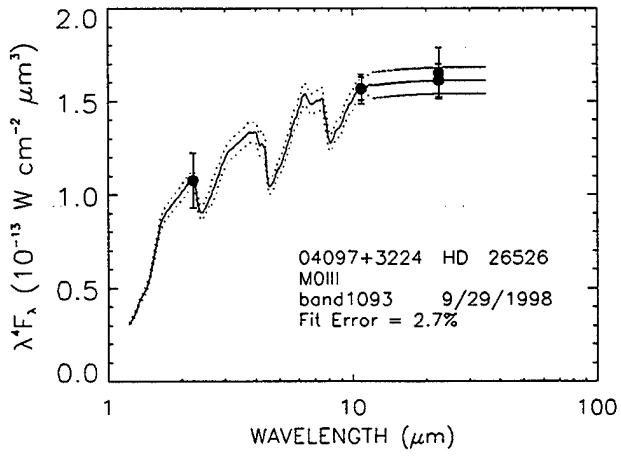
04097+3224 HD 26526
MOIII
band1093 9/29/1998
Fit Error = 2.7%
WAVELENGTH (μm)

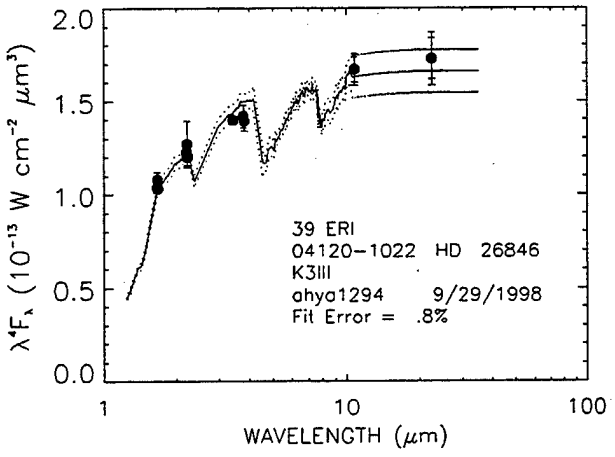
39 ERI
04120−1022 HD 26846
K3III
ahya1294 9/29/1998
Fit Error = .8%
WAVELENGTH (μm)

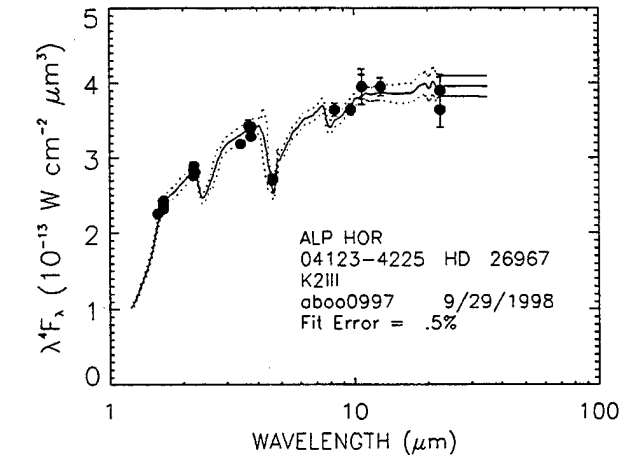
ALP HOR
04123−4225 HD 26967
K2III
aboo0997 9/29/1998
Fit Error = .5%
WAVELENGTH (μm)

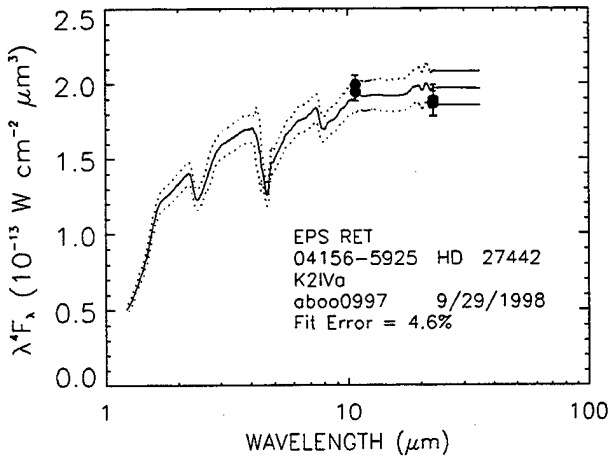
EPS RET
04156−5925 HD 27442
K2IVa
aboo0997 9/29/1998
Fit Error = 4.6%
WAVELENGTH (μm)

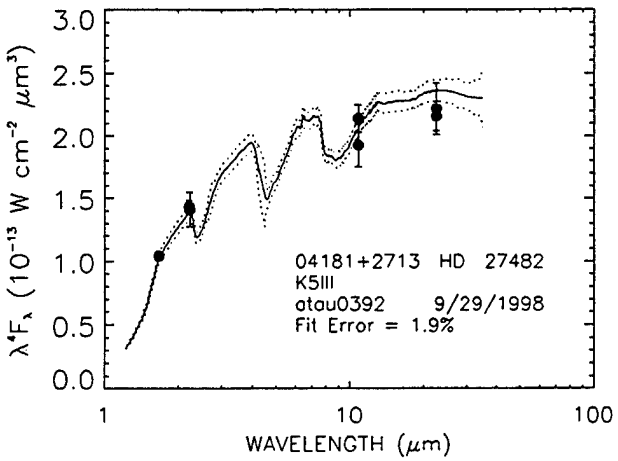
04181+2713 HD 27482
K5III
atau0392 9/29/1998
Fit Error = 1.9%
WAVELENGTH (μm)

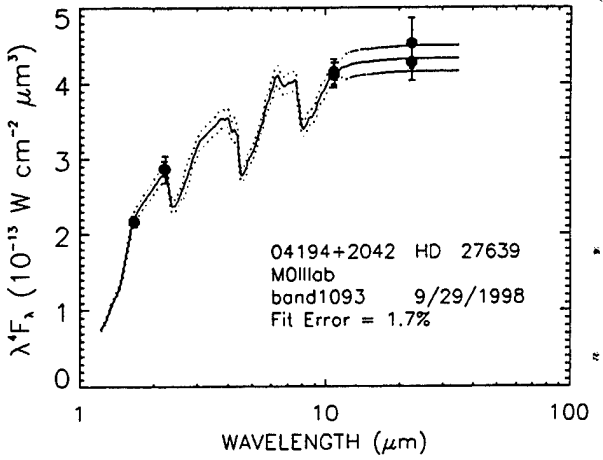
04194+2042 HD 27639
M0IIIab
band1093 9/29/1998
Fit Error = 1.7%
WAVELENGTH (μm)

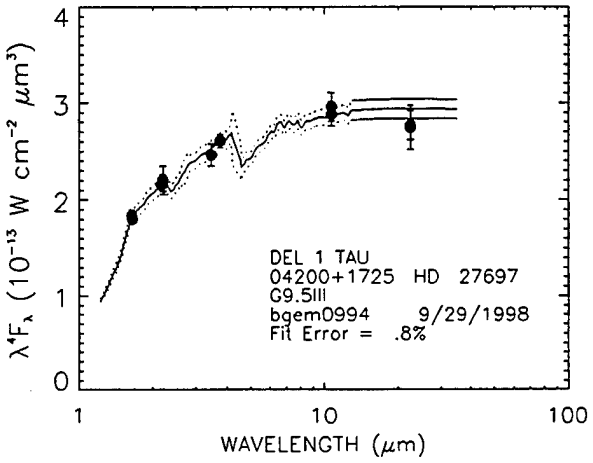
DEL 1 TAU
04200+1725 HD 27697
G9.5III
bgem0994 9/29/1998
Fit Error = .8%
WAVELENGTH (μm)

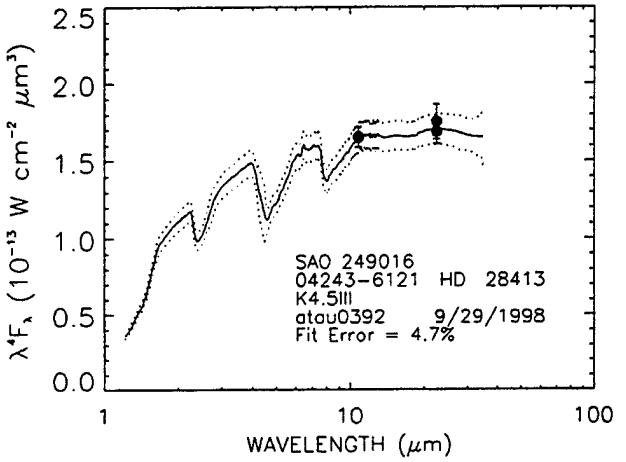
SAO 249016
04243-6121 HD 28413
K4.5III
atau0392 9/29/1998
Fit Error = 4.7%
WAVELENGTH (μm)

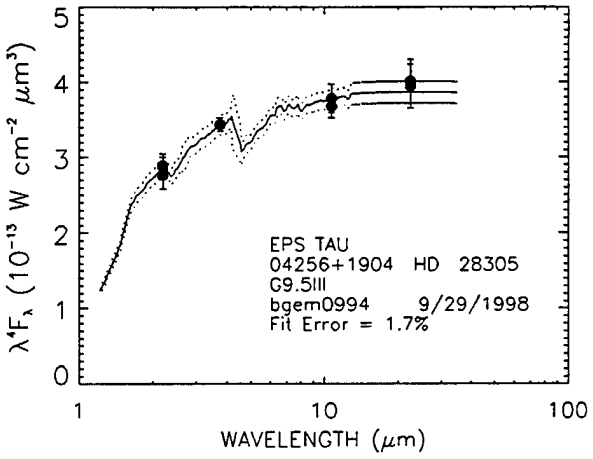
EPS TAU
04256+1904 HD 28305
G9.5III
bgem0994 9/29/1998
Fit Error = 1.7%
WAVELENGTH (μm)

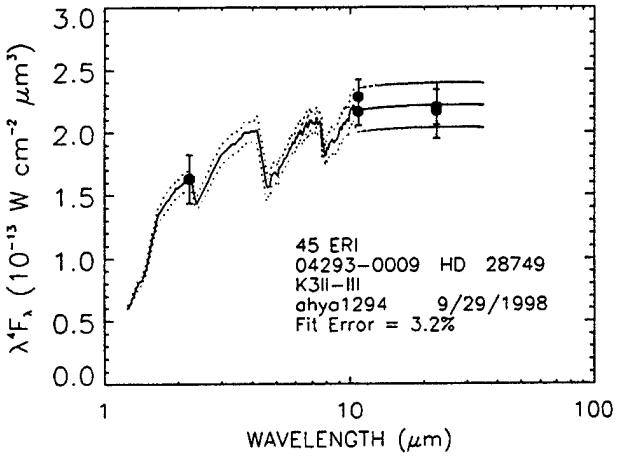
45 ERI
04293-0009 HD 28749
K3II-III
ahya1294 9/29/1998
Fit Error = 3.2%
WAVELENGTH (μm)

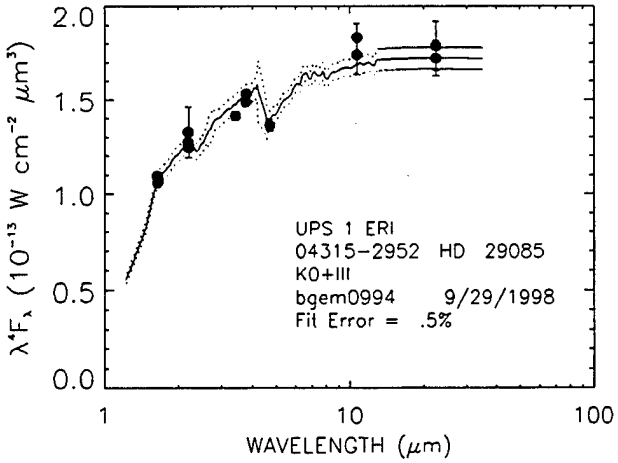
UPS 1 ERI
04315-2952 HD 29085
K0+III
bgem0994 9/29/1998
Fit Error = .5%
WAVELENGTH (μm)

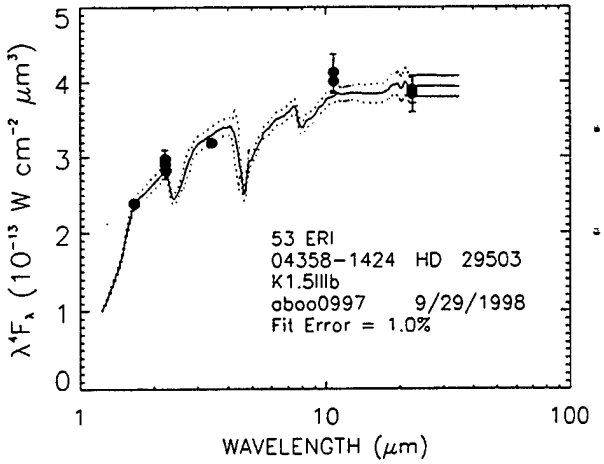
53 ERI
04358-1424 HD 29503
K1.5IIIb
aboo0997 9/29/1998
Fit Error = 1.0%
WAVELENGTH (μm)

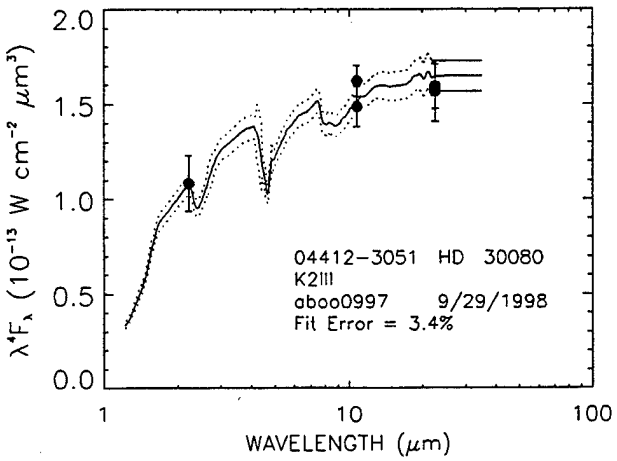
04412−3051 HD 30080
K2III
aboo0997 9/29/1998
Fit Error = 3.4%
WAVELENGTH (μm)

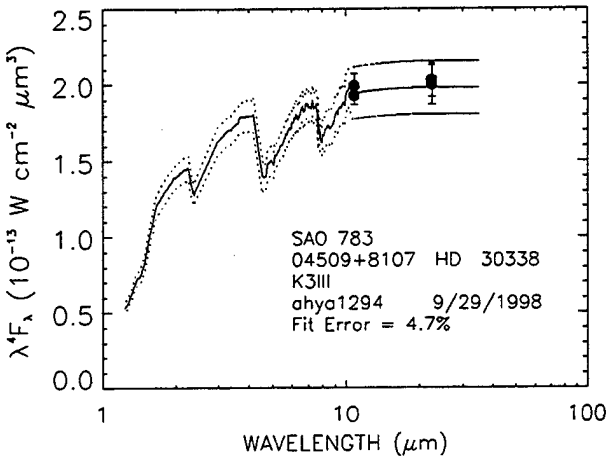
SAO 783
04509+8107 HD 30338
K3III
ahya1294 9/29/1998
Fit Error = 4.7%
WAVELENGTH (μm)

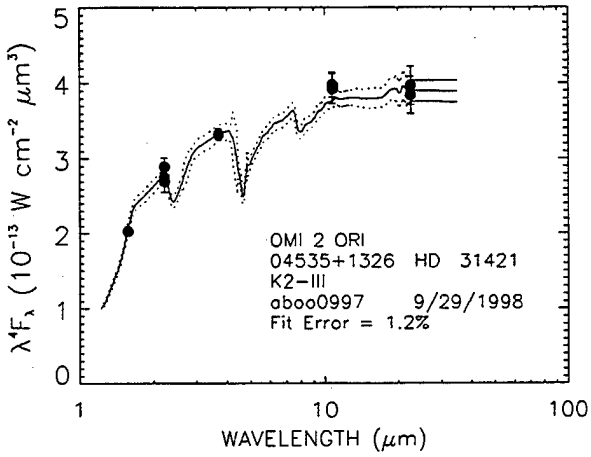
OMI 2 ORI
04535+1326 HD 31421
K2−III
aboo0997 9/29/1998
Fit Error = 1.2%
WAVELENGTH (μm)

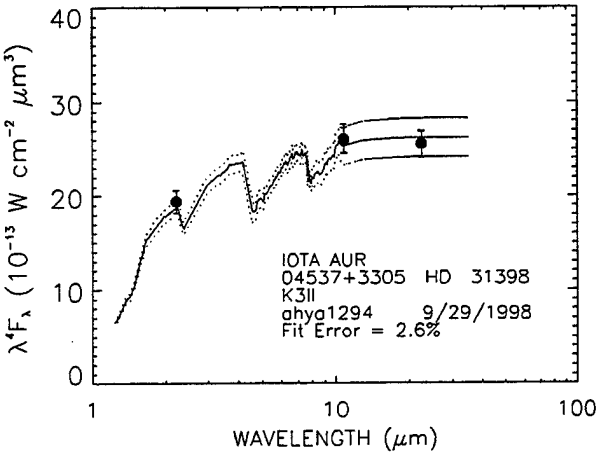
IOTA AUR
04537+3305 HD 31398
K3II
ahya1294 9/29/1998
Fit Error = 2.6%
WAVELENGTH (μm)

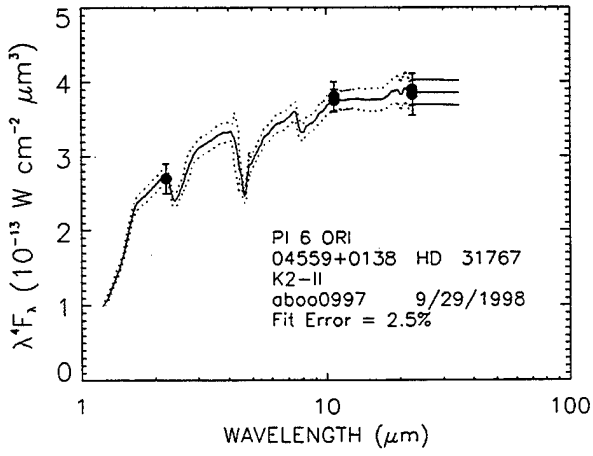
PI 6 ORI
04559+0138 HD 31767
K2−II
aboo0997 9/29/1998
Fit Error = 2.5%
WAVELENGTH (μm)

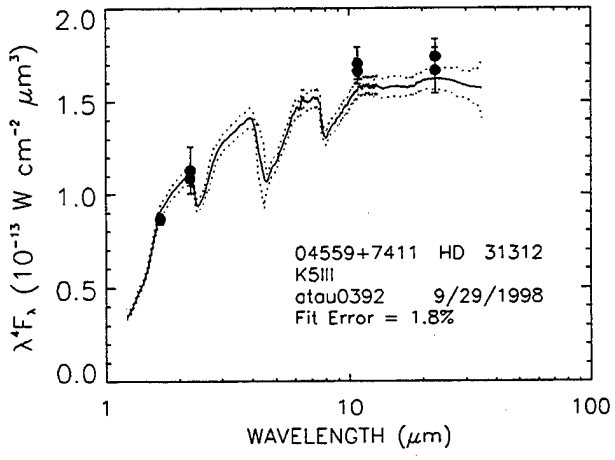
04559+7411 HD 31312
K5III
atau0392 9/29/1998
Fit Error = 1.8%
WAVELENGTH (μm)

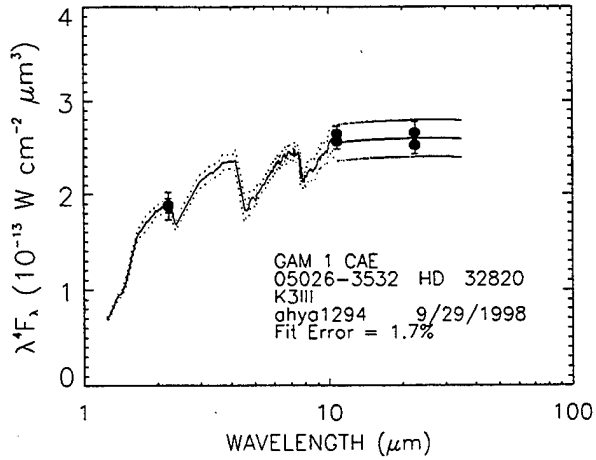
GAM 1 CAE
05026−3532 HD 32820
K3III
ahya1294 9/29/1998
Fit Error = 1.7%
WAVELENGTH (μm)

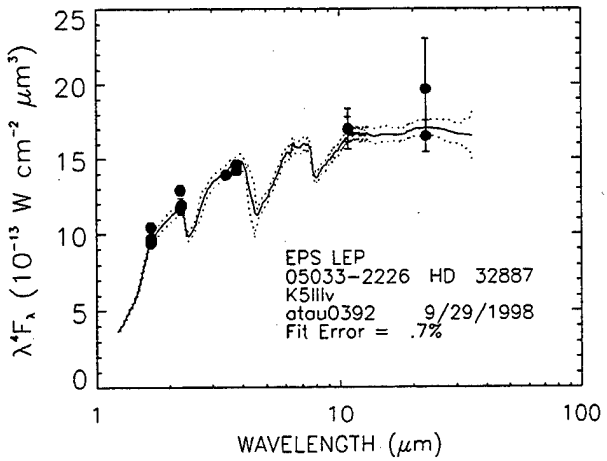
EPS LEP
05033−2226 HD 32887
K5IIIv
atau0392 9/29/1998
Fit Error = .7%
WAVELENGTH (μm)

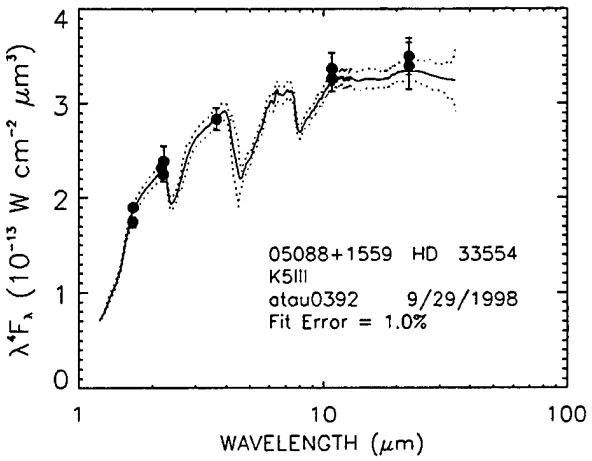
05088+1559 HD 33554
K5III
atau0392 9/29/1998
Fit Error = 1.0%
WAVELENGTH (μm)
λ⁴Fλ (10⁻¹³ W cm⁻² μm³)

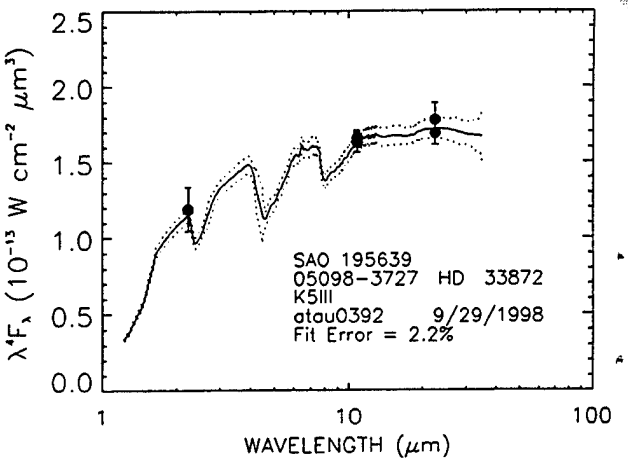
SAO 195639
05098-3727 HD 33872
K5III
atau0392 9/29/1998
Fit Error = 2.2%
WAVELENGTH (μm)
λ⁴Fλ (10⁻¹³ W cm⁻² μm³)

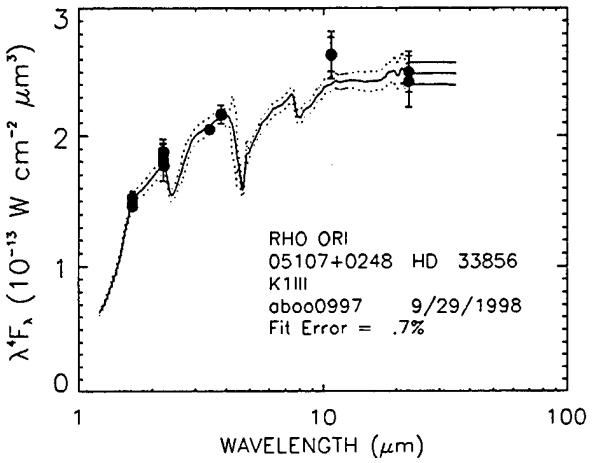
RHO ORI
05107+0248 HD 33856
K1III
aboo0997 9/29/1998
Fit Error = .7%
WAVELENGTH (μm)
λ⁴Fλ (10⁻¹³ W cm⁻² μm³)

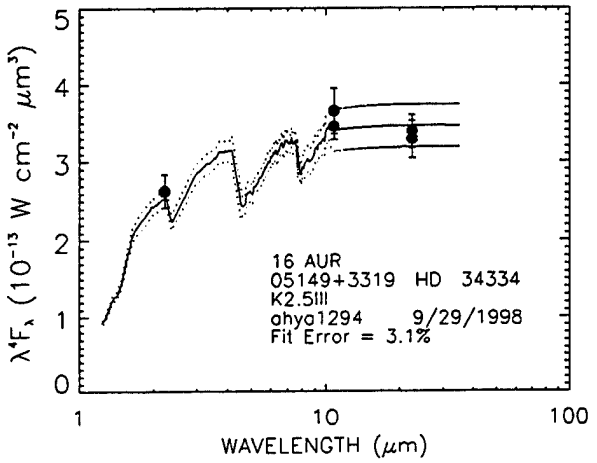
16 AUR
05149+3319 HD 34334
K2.5III
ahyg1294 9/29/1998
Fit Error = 3.1%
WAVELENGTH (μm)
λ⁴Fλ (10⁻¹³ W cm⁻² μm³)

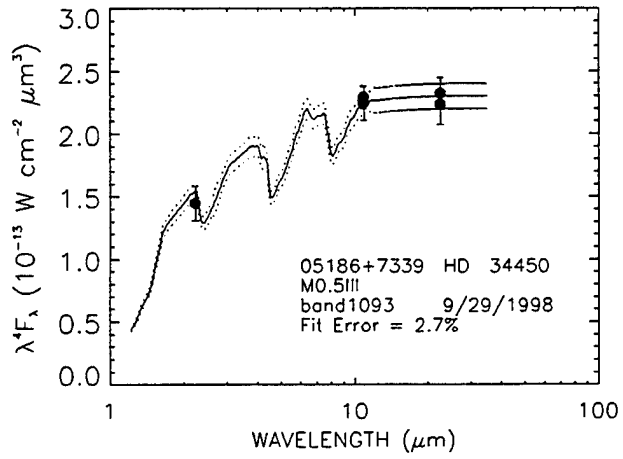
05186+7339 HD 34450
M0.5III
band1093 9/29/1998
Fit Error = 2.7%
WAVELENGTH (μm)
λ⁴Fλ (10⁻¹³ W cm⁻² μm³)

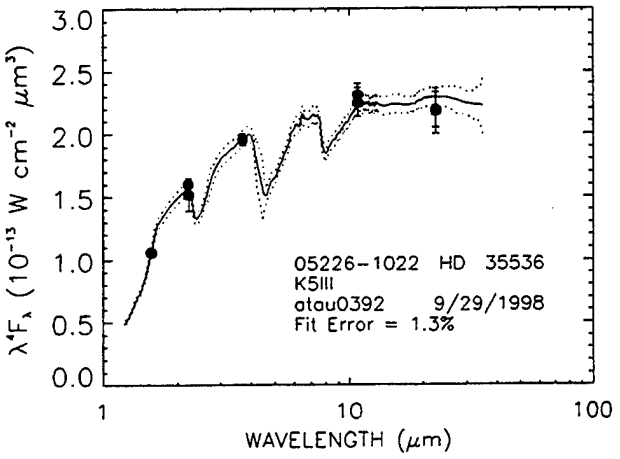
05226-1022 HD 35536
K5III
atau0392 9/29/1998
Fit Error = 1.3%
WAVELENGTH (μm)
λ⁴Fλ (10⁻¹³ W cm⁻² μm³)

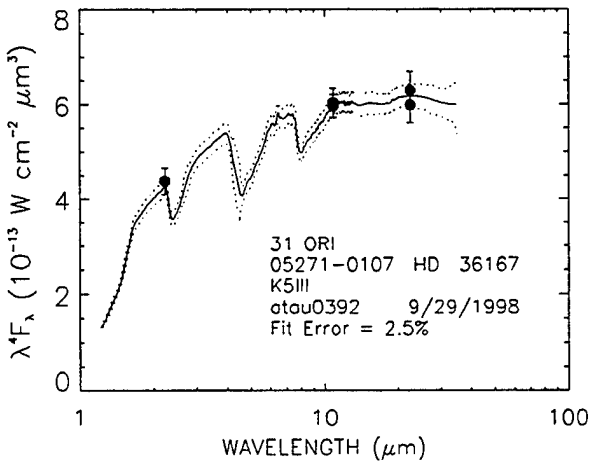
31 ORI
05271-0107 HD 36167
K5III
atau0392 9/29/1998
Fit Error = 2.5%
WAVELENGTH (μm)
λ⁴Fλ (10⁻¹³ W cm⁻² μm³)

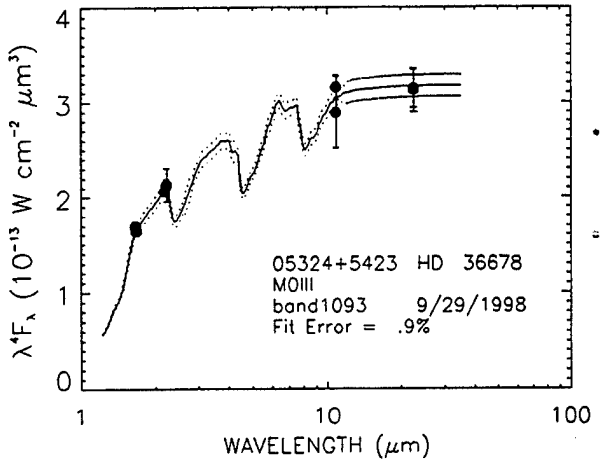
05324+5423 HD 36678
M0III
band1093 9/29/1998
Fit Error = .9%
WAVELENGTH (μm)
λ⁴Fλ (10⁻¹³ W cm⁻² μm³)

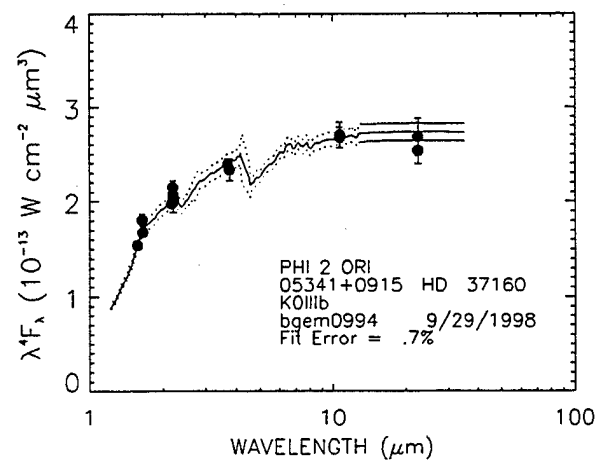
PHI 2 ORI
05341+0915 HD 37160
K0IIIb
bgem0994 9/29/1998
Fit Error = .7%
WAVELENGTH (μm)

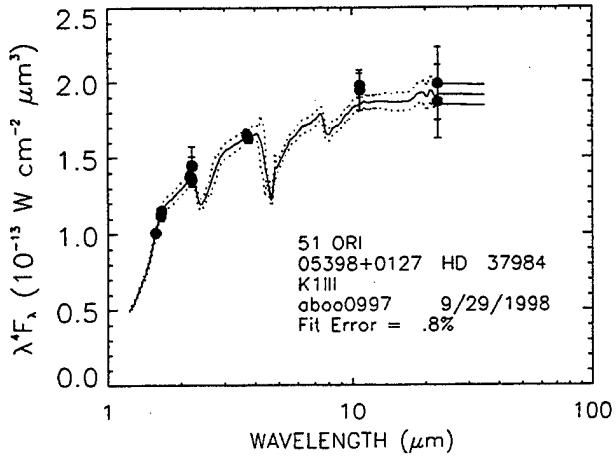
51 ORI
05398+0127 HD 37984
K1III
aboo0997 9/29/1998
Fit Error = .8%
WAVELENGTH (μm)

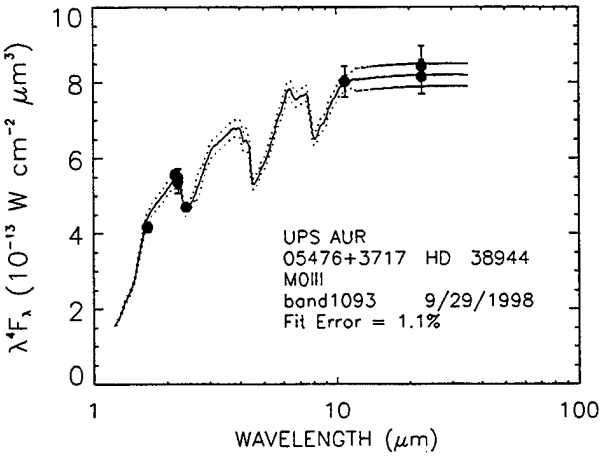
UPS AUR
05476+3717 HD 38944
M0III
band1093 9/29/1998
Fit Error = 1.1%
WAVELENGTH (μm)

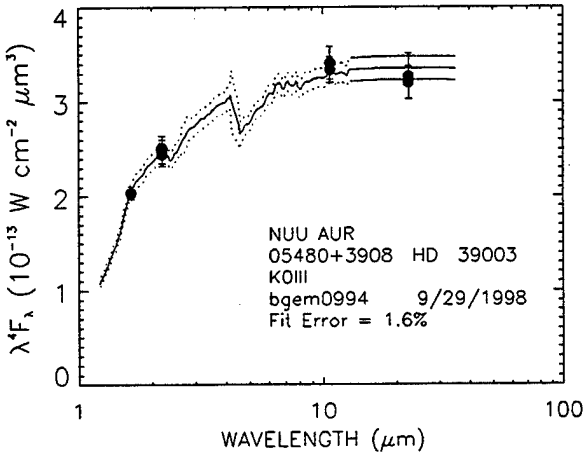
NUU AUR
05480+3908 HD 39003
K0III
bgem0994 9/29/1998
Fit Error = 1.6%
WAVELENGTH (μm)

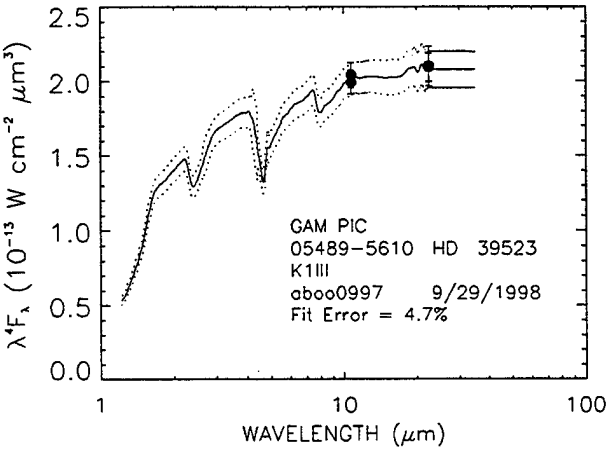
GAM PIC
05489-5610 HD 39523
K1III
aboo0997 9/29/1998
Fit Error = 4.7%
WAVELENGTH (μm)

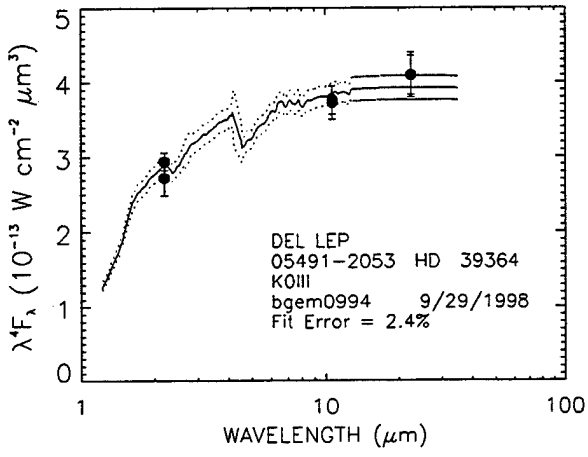
DEL LEP
05491-2053 HD 39364
K0III
bgem0994 9/29/1998
Fit Error = 2.4%
WAVELENGTH (μm)

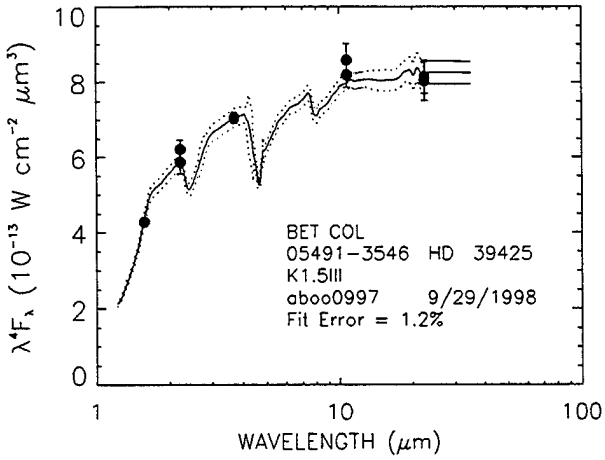
BET COL
05491-3546 HD 39425
K1.5III
aboo0997 9/29/1998
Fit Error = 1.2%
WAVELENGTH (μm)

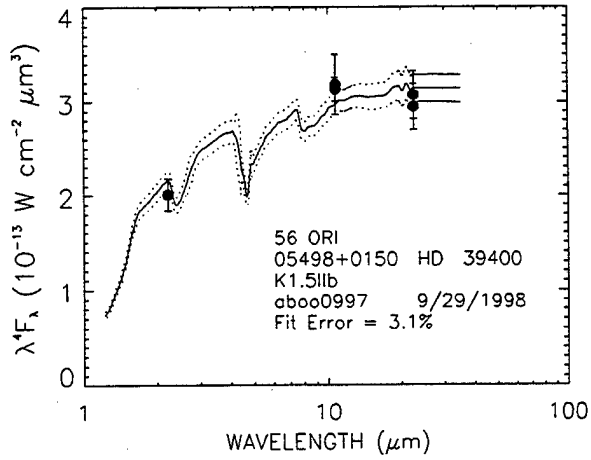
56 ORI
05498+0150 HD 39400
K1.5IIb
aboo0997 9/29/1998
Fit Error = 3.1%
WAVELENGTH (μm)

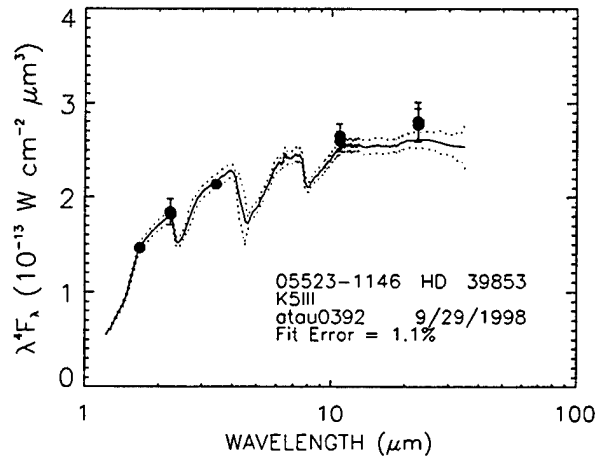
05523−1146 HD 39853
K5III
atau0392 9/29/1998
Fit Error = 1.1%
WAVELENGTH (μm)

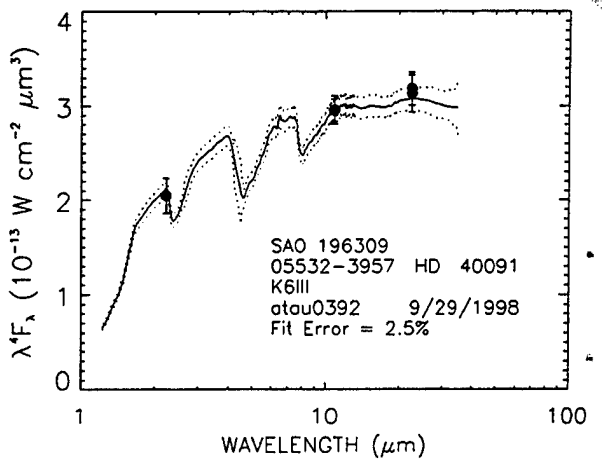
SAO 196309
05532−3957 HD 40091
K6III
atau0392 9/29/1998
Fit Error = 2.5%
WAVELENGTH (μm)

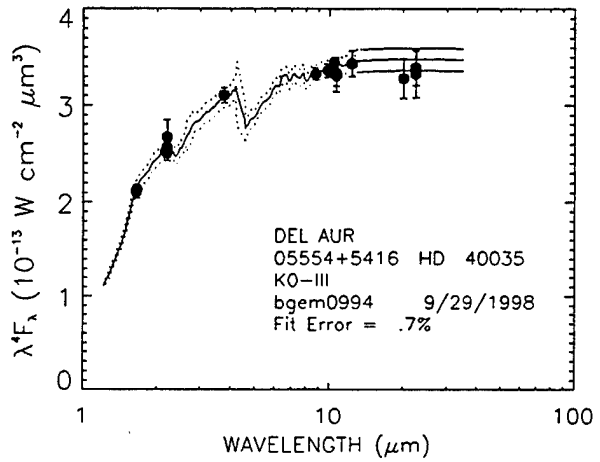
DEL AUR
05554+5416 HD 40035
K0−III
bgem0994 9/29/1998
Fit Error = .7%
WAVELENGTH (μm)

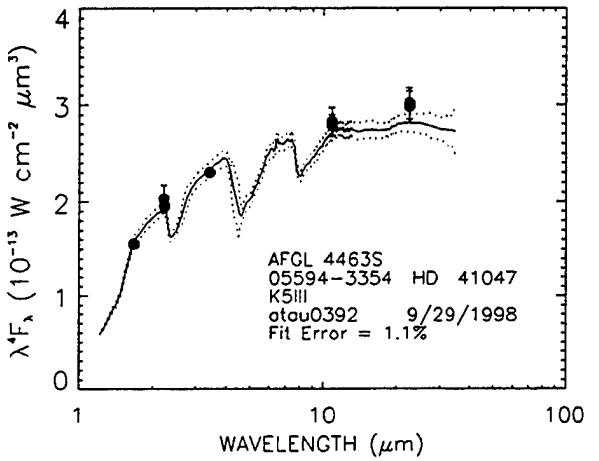
AFGL 4463S
05594−3354 HD 41047
K5III
atau0392 9/29/1998
Fit Error = 1.1%
WAVELENGTH (μm)

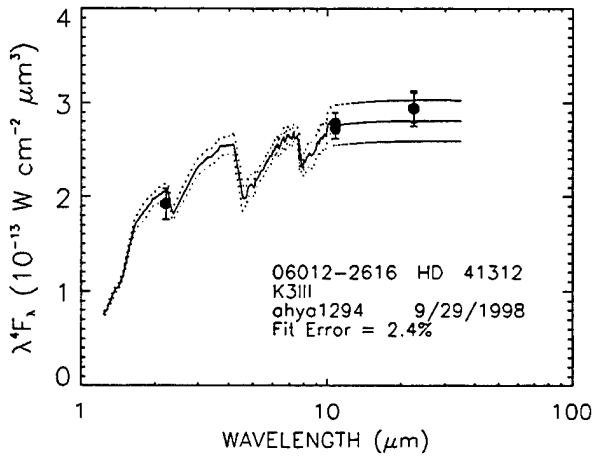
06012−2616 HD 41312
K3III
ahya1294 9/29/1998
Fit Error = 2.4%
WAVELENGTH (μm)

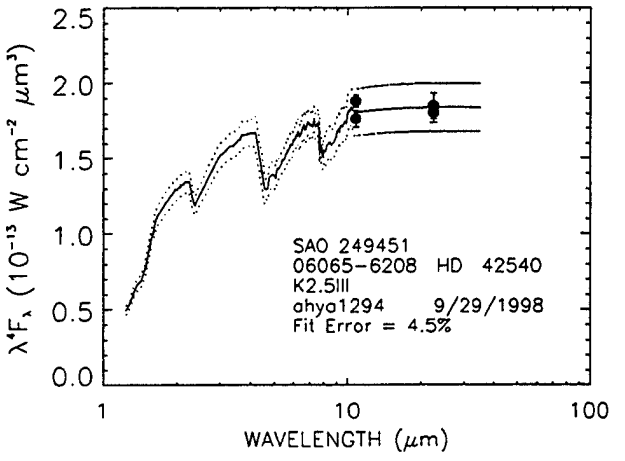
SAO 249451
06065−6208 HD 42540
K2.5III
ahya1294 9/29/1998
Fit Error = 4.5%
WAVELENGTH (μm)

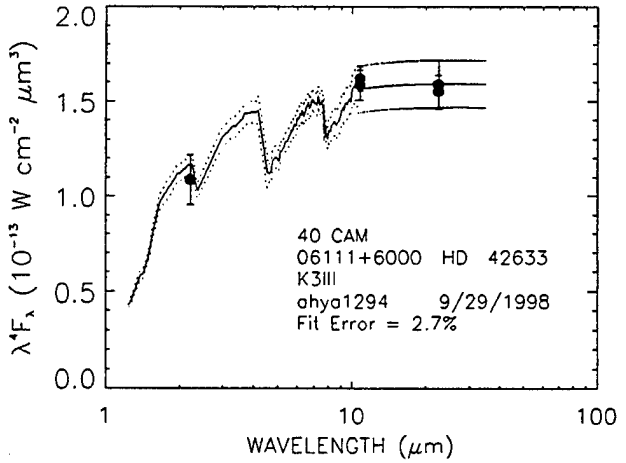
40 CAM
06111+6000 HD 42633
K3III
ahya1294 9/29/1998
Fit Error = 2.7%
WAVELENGTH (μm)

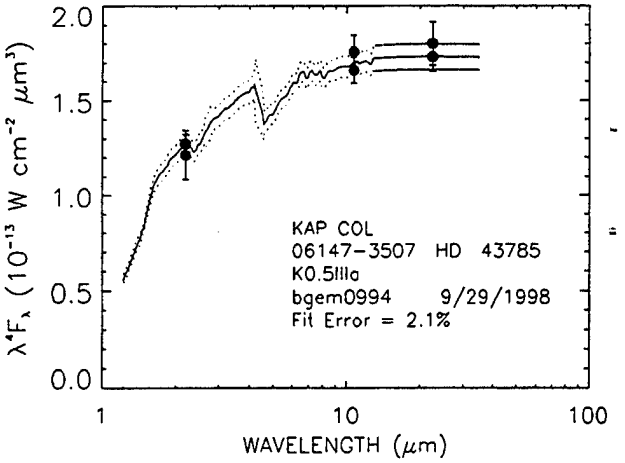
KAP COL
06147−3507 HD 43785
K0.5IIIa
bgem0994 9/29/1998
Fit Error = 2.1%
WAVELENGTH (μm)

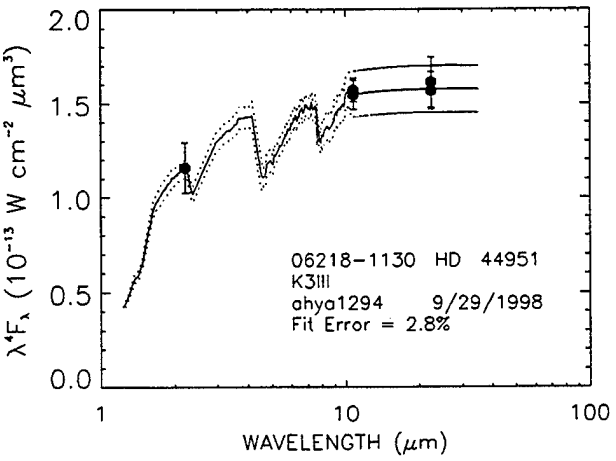
06218−1130 HD 44951
K3III
ahya1294 9/29/1998
Fit Error = 2.8%
WAVELENGTH (μm)

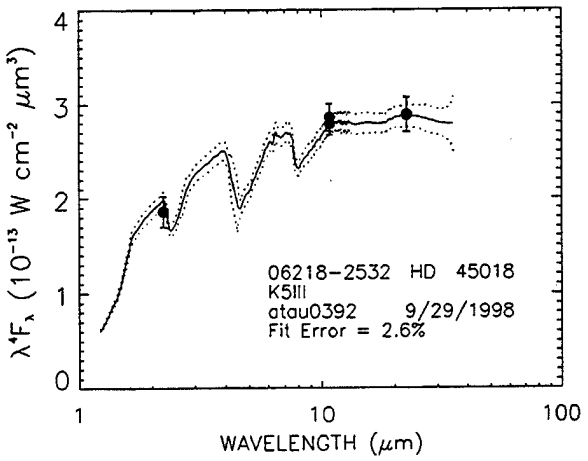
06218−2532 HD 45018
K5III
atau0392 9/29/1998
Fit Error = 2.6%
WAVELENGTH (μm)

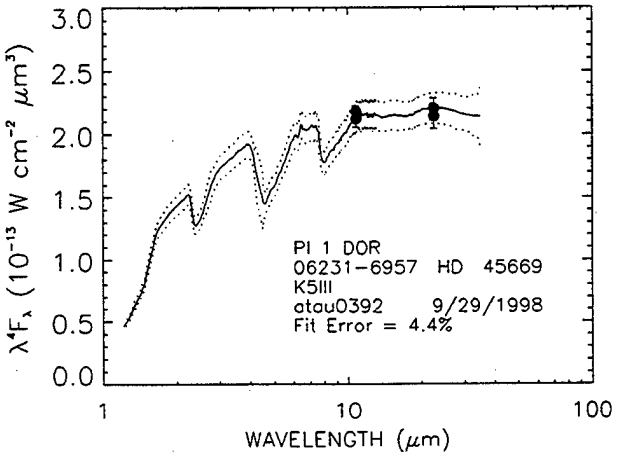
PI 1 DOR
06231−6957 HD 45669
K5III
atau0392 9/29/1998
Fit Error = 4.4%
WAVELENGTH (μm)

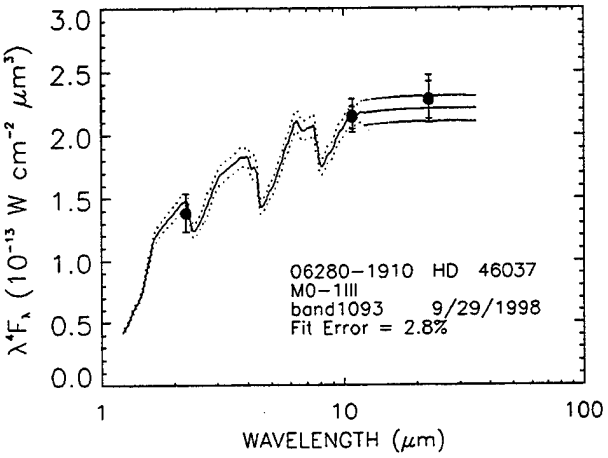
06280−1910 HD 46037
M0−1III
band1093 9/29/1998
Fit Error = 2.8%
WAVELENGTH (μm)

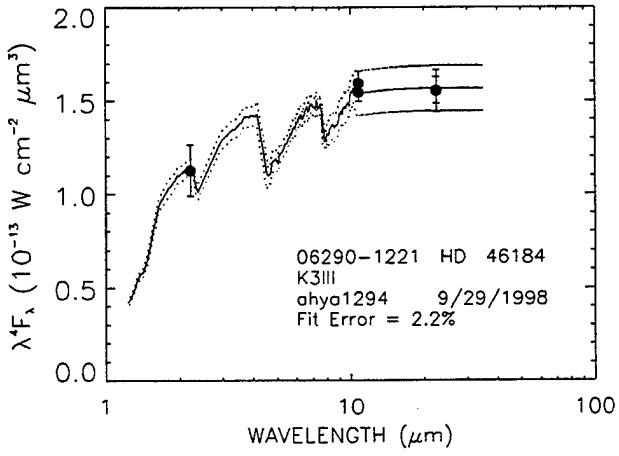
06290−1221 HD 46184
K3III
ahya1294 9/29/1998
Fit Error = 2.2%
WAVELENGTH (μm)

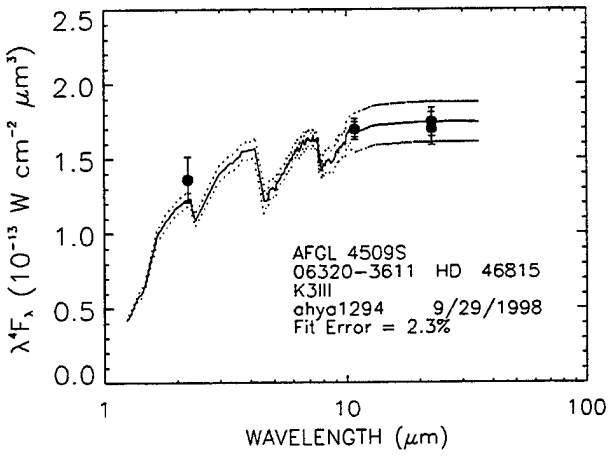
AFGL 4509S
06320−3611 HD 46815
K3III
ahya1294 9/29/1998
Fit Error = 2.3%
WAVELENGTH (μm)

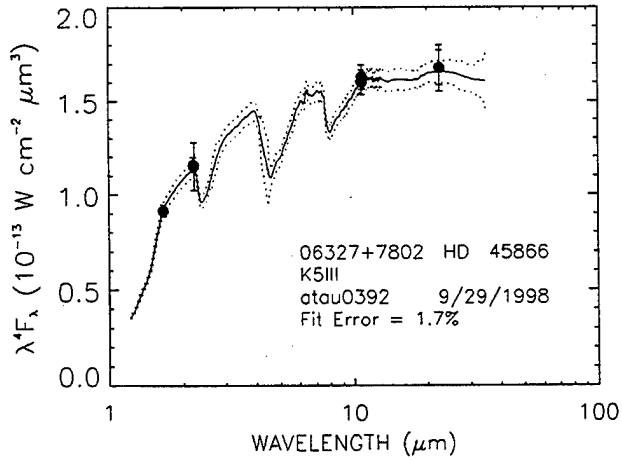
06327+7802 HD 45866
K5III
atau0392 9/29/1998
Fit Error = 1.7%
WAVELENGTH (μm)

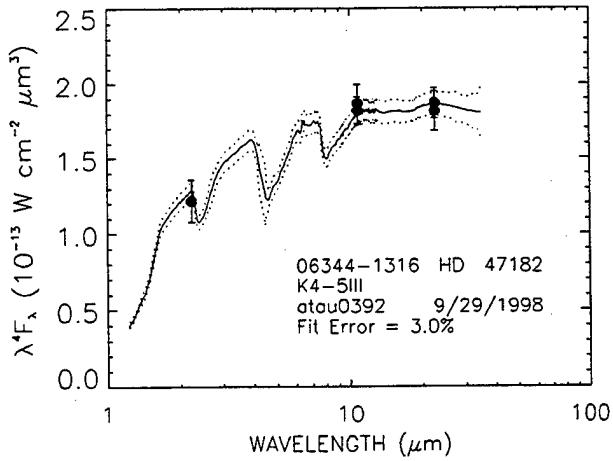
06344−1316 HD 47182
K4−5III
atau0392 9/29/1998
Fit Error = 3.0%
WAVELENGTH (μm)

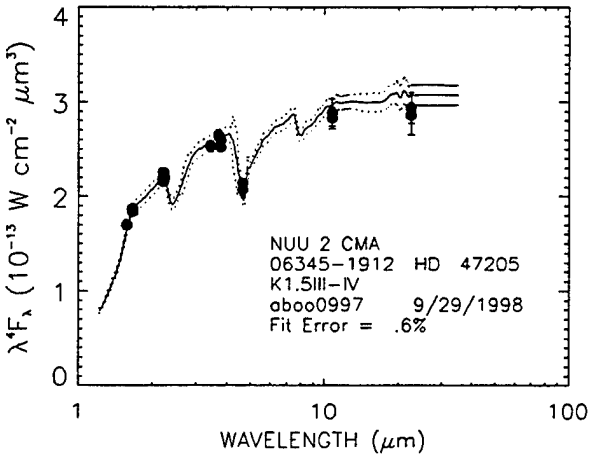
NUU 2 CMA
06345-1912 HD 47205
K1.5III-IV
aboo0997 9/29/1998
Fit Error = .6%
WAVELENGTH (μm)

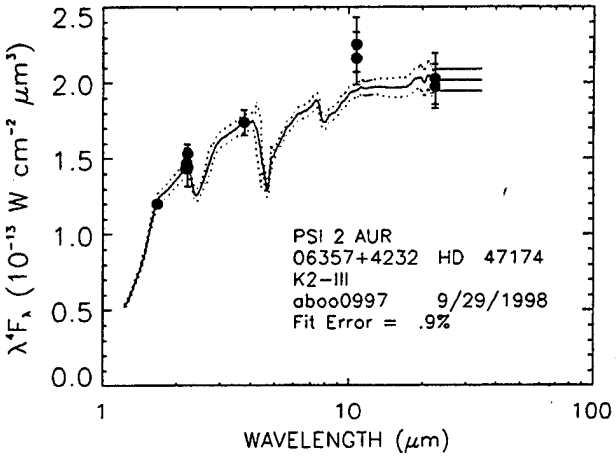
PSI 2 AUR
06357+4232 HD 47174
K2-III
aboo0997 9/29/1998
Fit Error = .9%
WAVELENGTH (μm)

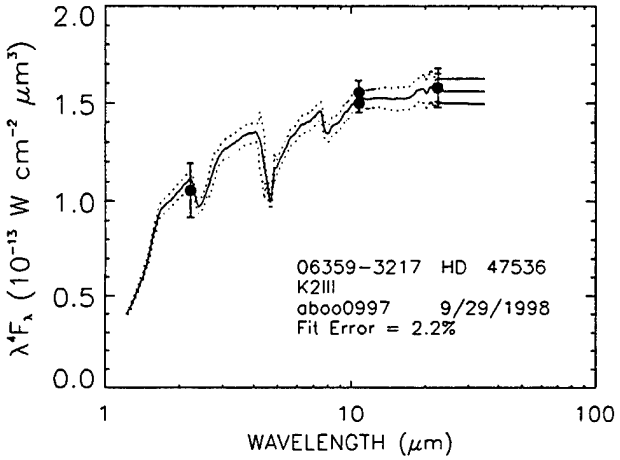
06359-3217 HD 47536
K2III
aboo0997 9/29/1998
Fit Error = 2.2%
WAVELENGTH (μm)

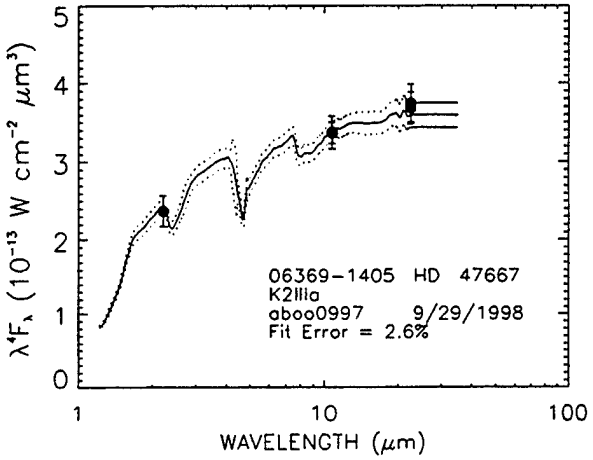
06369-1405 HD 47667
K2IIIa
aboo0997 9/29/1998
Fit Error = 2.6%
WAVELENGTH (μm)

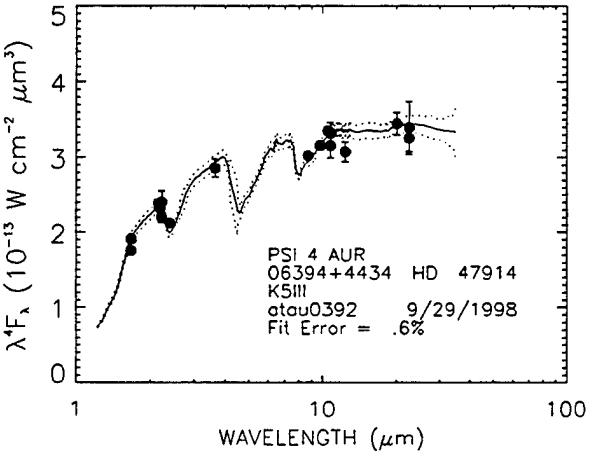
PSI 4 AUR
06394+4434 HD 47914
K5III
atau0392 9/29/1998
Fit Error = .6%
WAVELENGTH (μm)

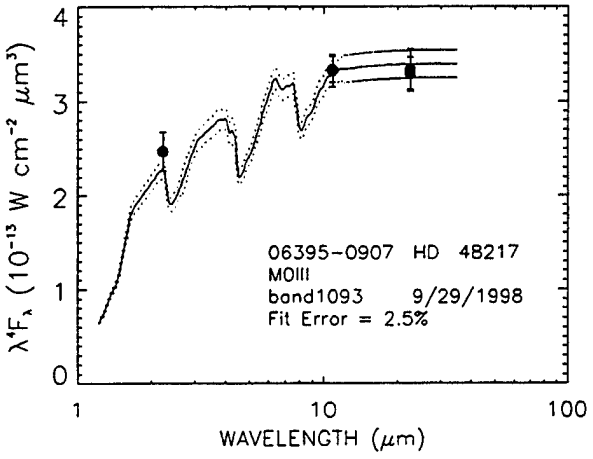
06395-0907 HD 48217
M0III
band1093 9/29/1998
Fit Error = 2.5%
WAVELENGTH (μm)

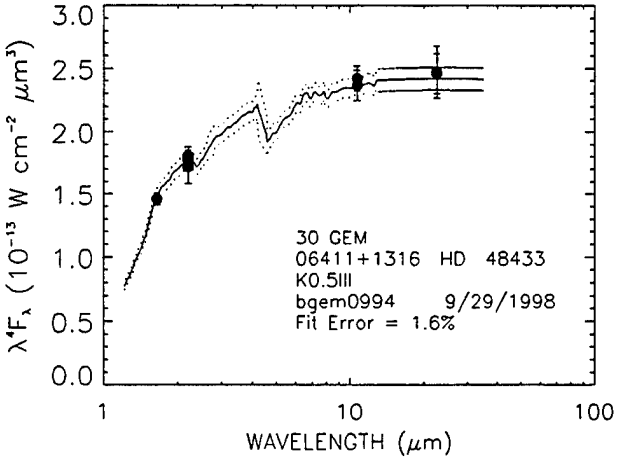
30 GEM
06411+1316 HD 48433
K0.5III
bgem0994 9/29/1998
Fit Error = 1.6%
WAVELENGTH (μm)

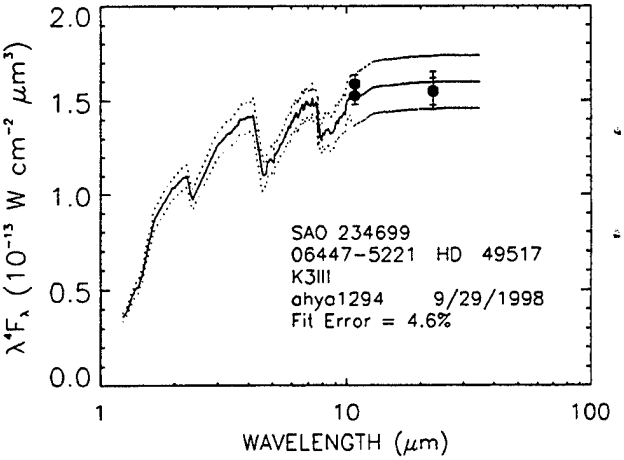
SAO 234699
06447-5221 HD 49517
K3III
ahya1294 9/29/1998
Fit Error = 4.6%
WAVELENGTH (μm)

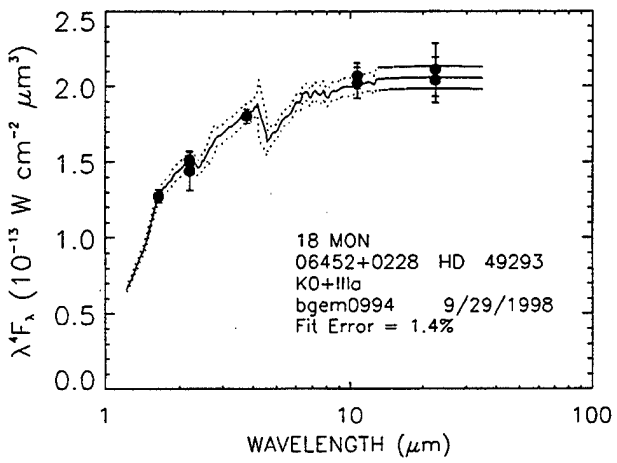
18 MON
06452+0228 HD 49293
K0+IIIa
bgem0994 9/29/1998
Fit Error = 1.4%
WAVELENGTH (μm)

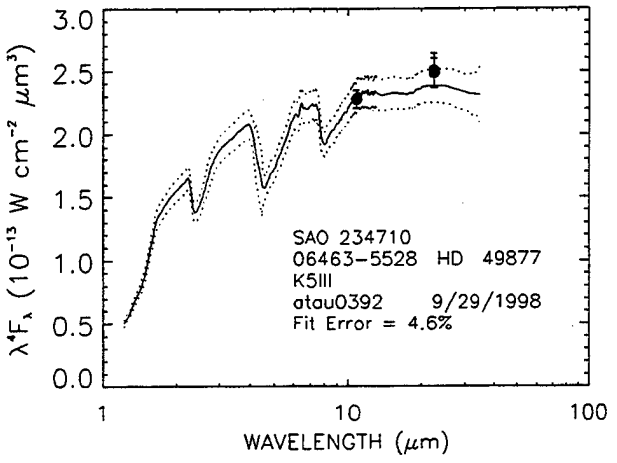
SAO 234710
06463-5528 HD 49877
K5III
atau0392 9/29/1998
Fit Error = 4.6%
WAVELENGTH (μm)

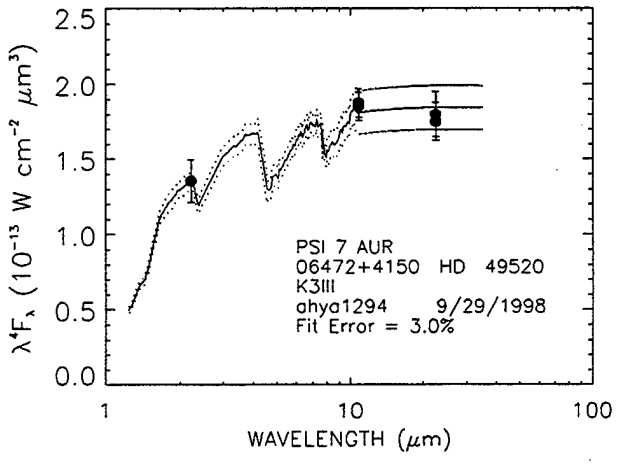
PSI 7 AUR
06472+4150 HD 49520
K3III
ahya1294 9/29/1998
Fit Error = 3.0%
WAVELENGTH (μm)

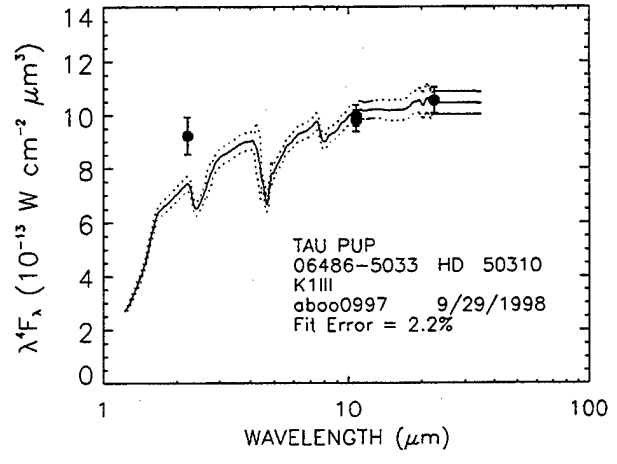
TAU PUP
06486-5033 HD 50310
K1III
aboo0997 9/29/1998
Fit Error = 2.2%
WAVELENGTH (μm)

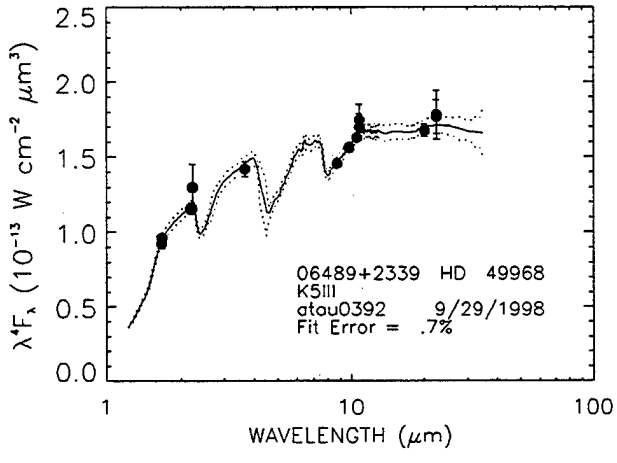
06489+2339 HD 49968
K5III
atau0392 9/29/1998
Fit Error = .7%
WAVELENGTH (μm)

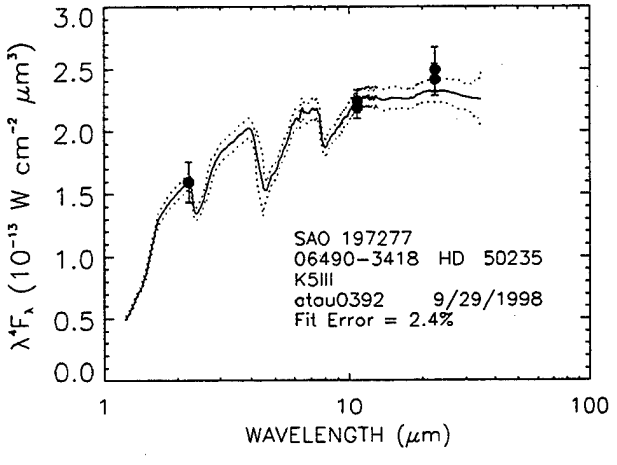
SAO 197277
06490-3418 HD 50235
K5III
atau0392 9/29/1998
Fit Error = 2.4%
WAVELENGTH (μm)

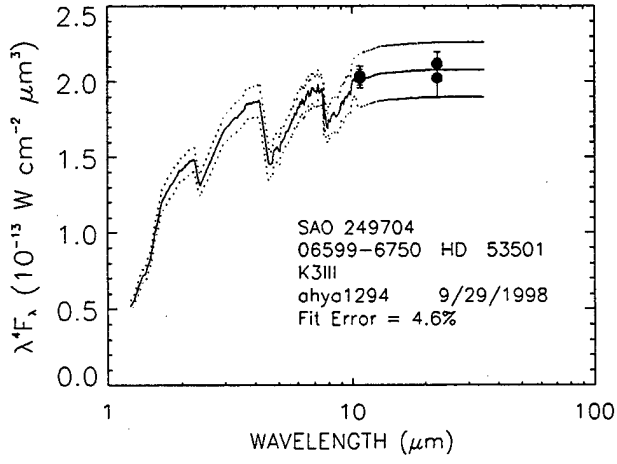
SAO 249704
06599-6750 HD 53501
K3III
ahya1294 9/29/1998
Fit Error = 4.6%
WAVELENGTH (μm)

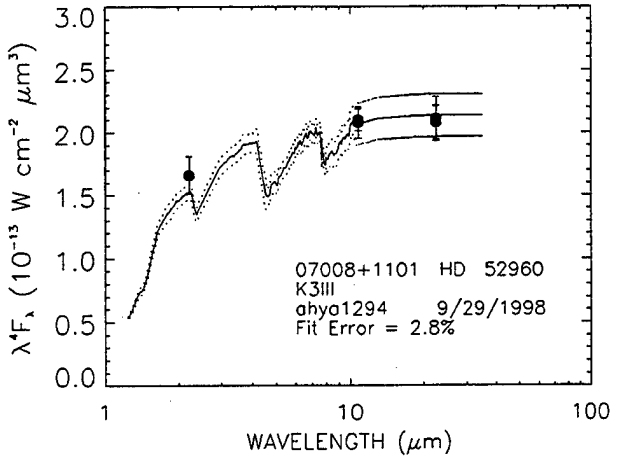
07008+1101 HD 52960
K3III
ahya1294 9/29/1998
Fit Error = 2.8%
WAVELENGTH (μm)

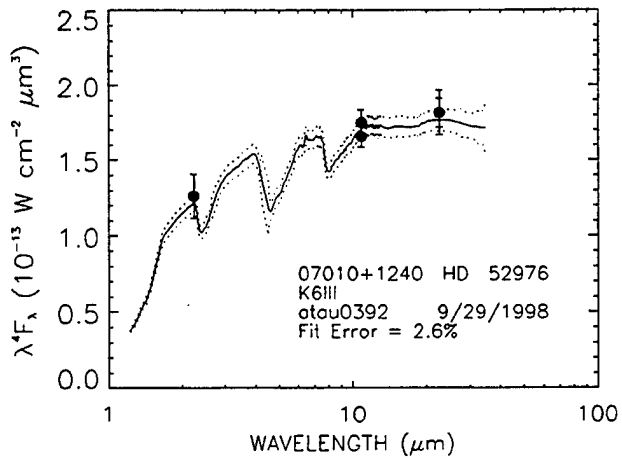
07010+1240 HD 52976
K6III
atau0392 9/29/1998
Fit Error = 2.6%
WAVELENGTH (μm)

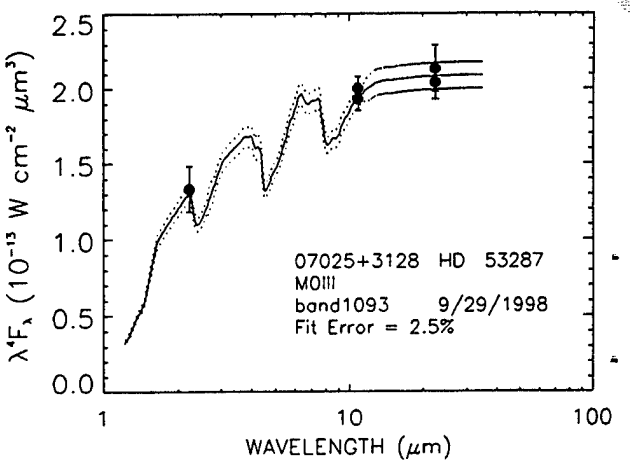
07025+3128 HD 53287
MOIII
band1093 9/29/1998
Fit Error = 2.5%
WAVELENGTH (μm)

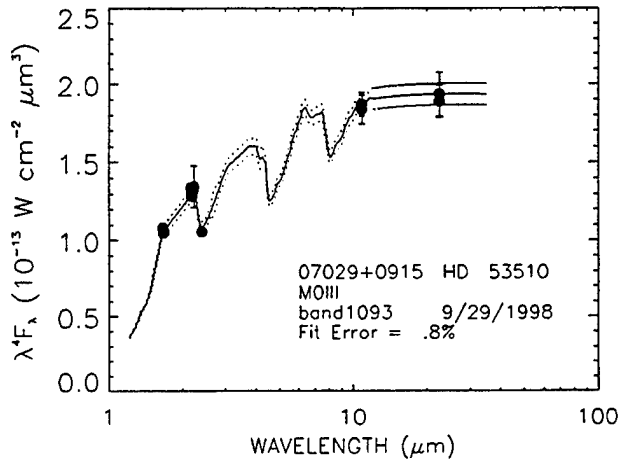
07029+0915 HD 53510
MOIII
band1093 9/29/1998
Fit Error = .8%
WAVELENGTH (μm)

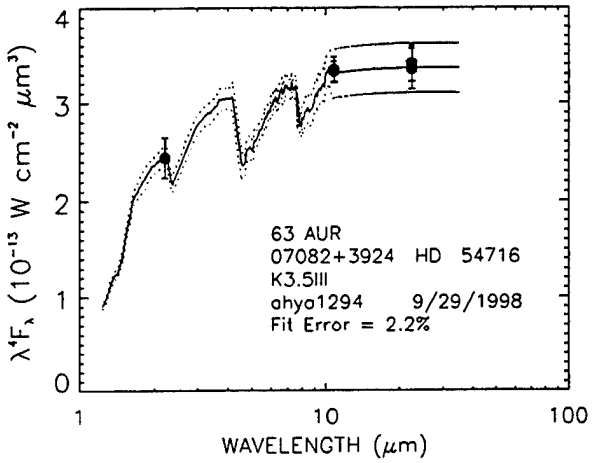
63 AUR
07082+3924 HD 54716
K3.5III
ahya1294 9/29/1998
Fit Error = 2.2%
WAVELENGTH (μm)

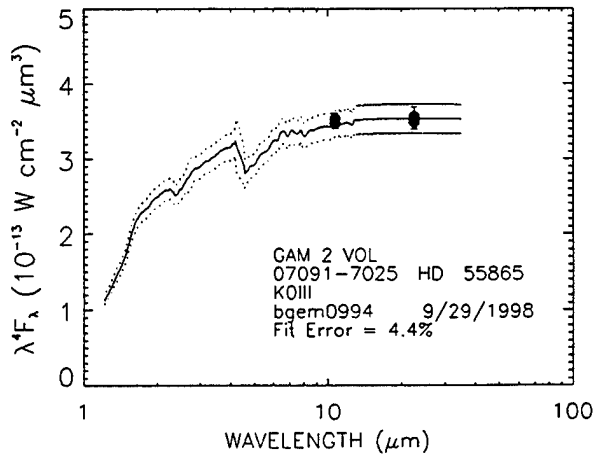
GAM 2 VOL
07091-7025 HD 55865
KOIII
bgem0994 9/29/1998
Fit Error = 4.4%
WAVELENGTH (μm)

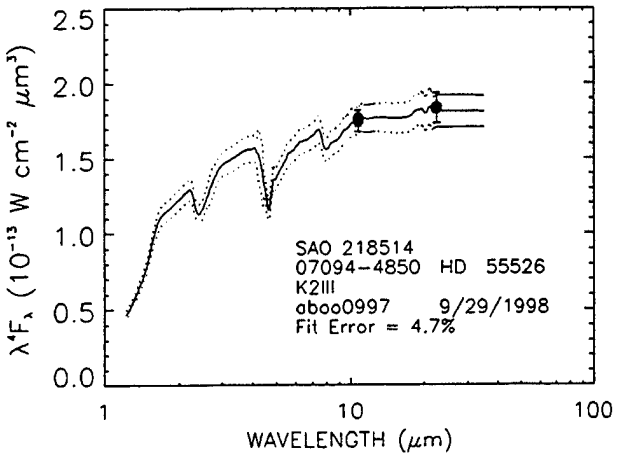
SAO 218514
07094-4850 HD 55526
K2III
aboo0997 9/29/1998
Fit Error = 4.7%
WAVELENGTH (μm)

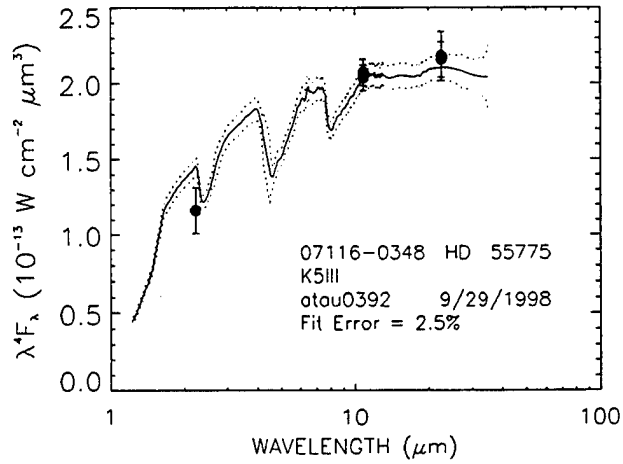
07116-0348 HD 55775
K5III
atau0392 9/29/1998
Fit Error = 2.5%
WAVELENGTH (μm)

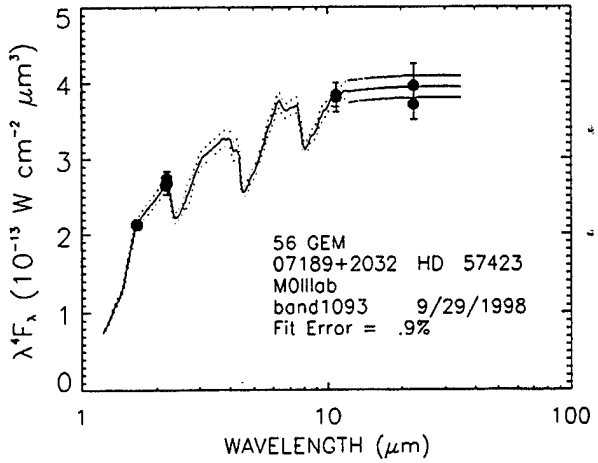
56 GEM
07189+2032 HD 57423
MOIIIab
band1093 9/29/1998
Fit Error = .9%
WAVELENGTH (μm)

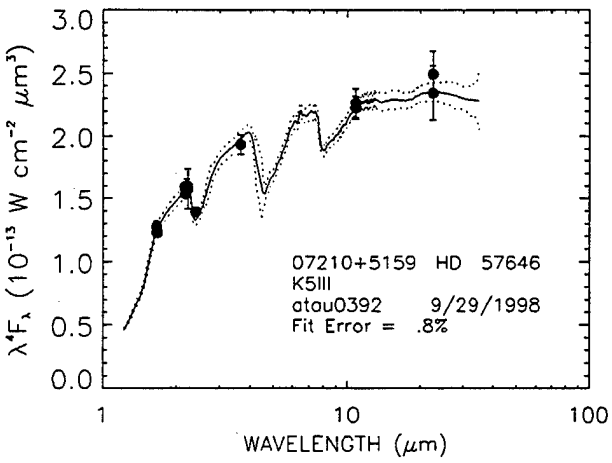
07210+5159 HD 57646
K5III
atau0392 9/29/1998
Fit Error = .8%
λ^4F_λ (10^{-13} W cm^{-2} μm^3)
WAVELENGTH (μm)

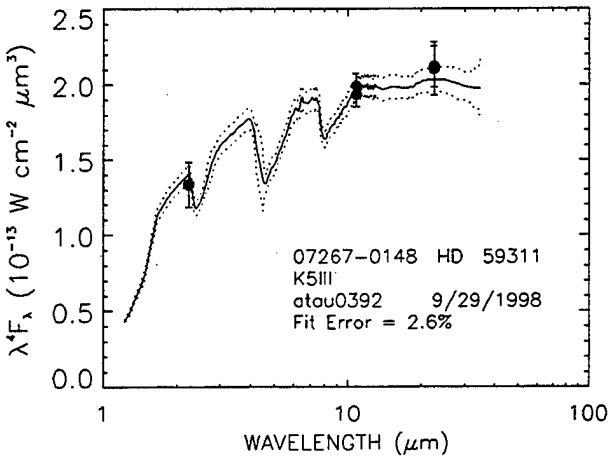
07267−0148 HD 59311
K5III
atau0392 9/29/1998
Fit Error = 2.6%
λ^4F_λ (10^{-13} W cm^{-2} μm^3)
WAVELENGTH (μm)

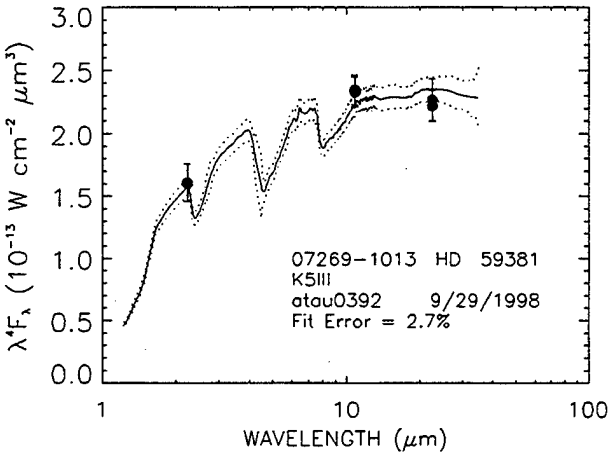
07269−1013 HD 59381
K5III
atau0392 9/29/1998
Fit Error = 2.7%
λ^4F_λ (10^{-13} W cm^{-2} μm^3)
WAVELENGTH (μm)

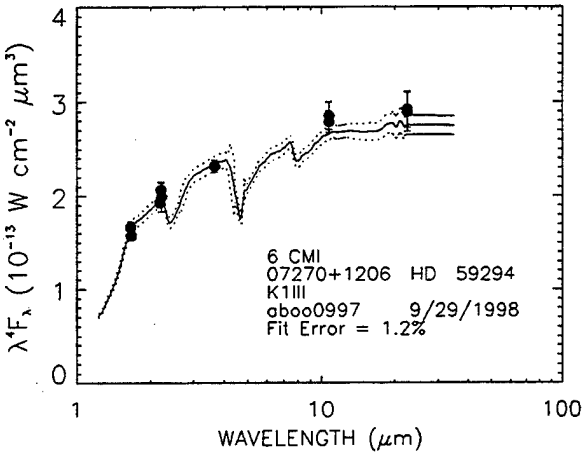
6 CMI
07270+1206 HD 59294
K1III
aboo0997 9/29/1998
Fit Error = 1.2%
λ^4F_λ (10^{-13} W cm^{-2} μm^3)
WAVELENGTH (μm)

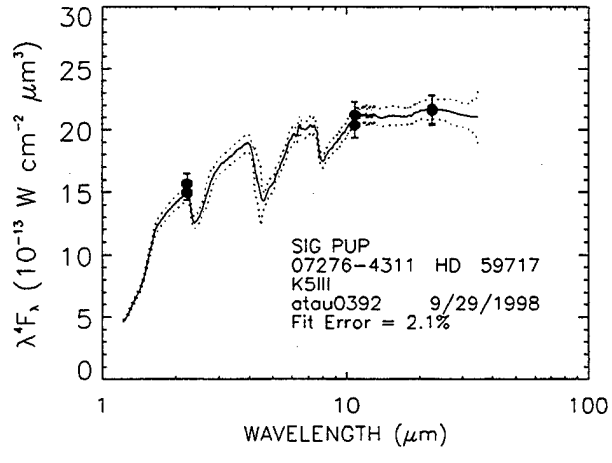
SIG PUP
07276−4311 HD 59717
K5III
atau0392 9/29/1998
Fit Error = 2.1%
λ^4F_λ (10^{-13} W cm^{-2} μm^3)
WAVELENGTH (μm)

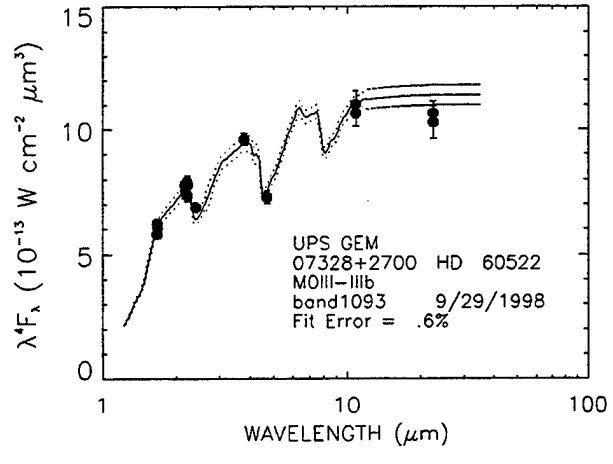
UPS GEM
07328+2700 HD 60522
MOIII−IIIb
band1093 9/29/1998
Fit Error = .6%
λ^4F_λ (10^{-13} W cm^{-2} μm^3)
WAVELENGTH (μm)

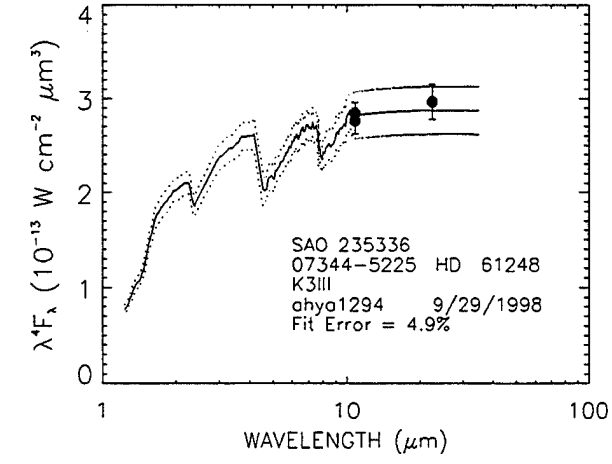
SAO 235336
07344−5225 HD 61248
K3III
ahya1294 9/29/1998
Fit Error = 4.9%
λ^4F_λ (10^{-13} W cm^{-2} μm^3)
WAVELENGTH (μm)

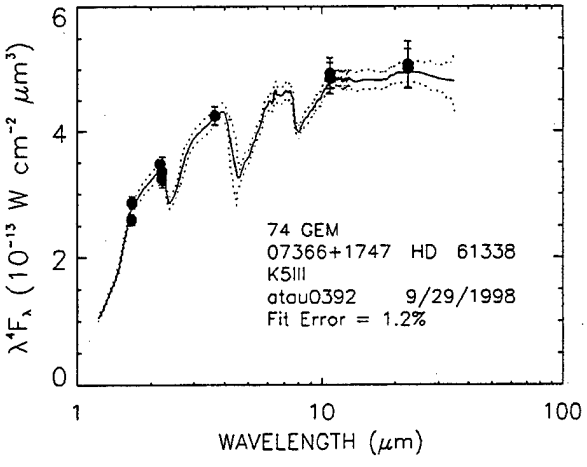
74 GEM
07366+1747 HD 61338
K5III
atau0392 9/29/1998
Fit Error = 1.2%
λ^4F_λ (10^{-13} W cm^{-2} μm^3)
WAVELENGTH (μm)

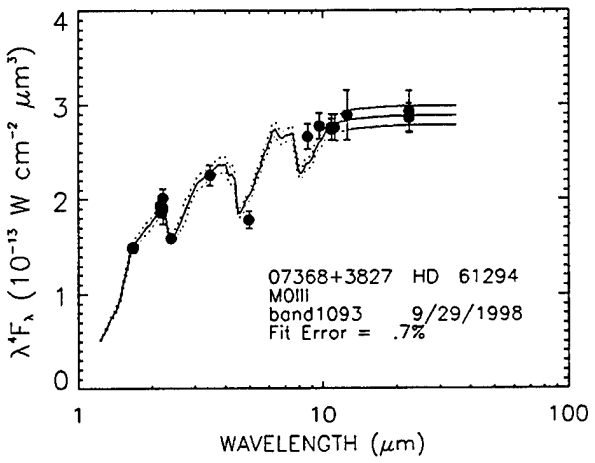
07368+3827 HD 61294
M0III
band1093 9/29/1998
Fit Error = .7%
λ^4F_λ (10^{-13} W cm^{-2} μm^3)
WAVELENGTH (μm)

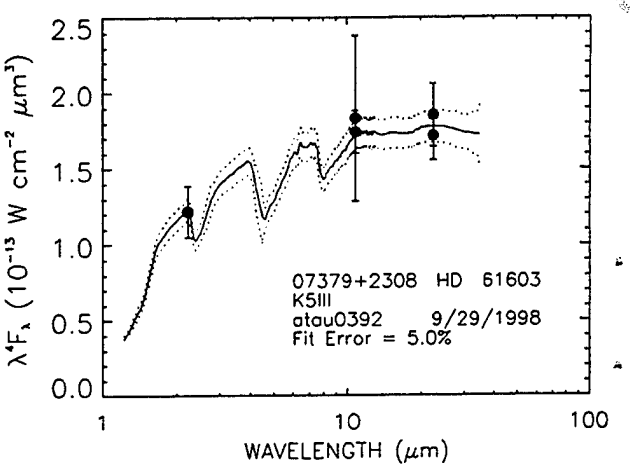
07379+2308 HD 61603
K5III
atau0392 9/29/1998
Fit Error = 5.0%
λ^4F_λ (10^{-13} W cm^{-2} μm^3)
WAVELENGTH (μm)

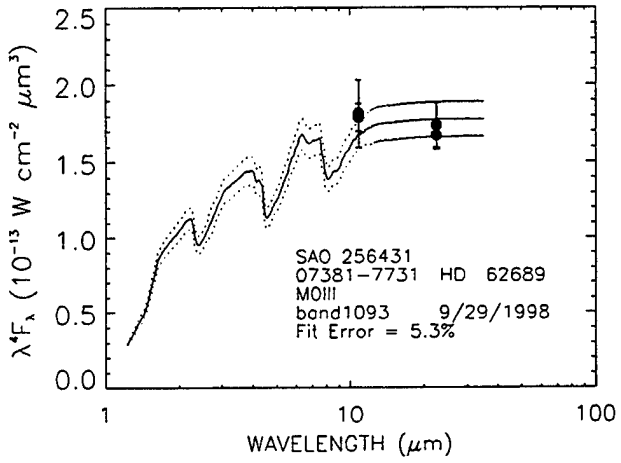
SAO 256431
07381-7731 HD 62689
M0III
band1093 9/29/1998
Fit Error = 5.3%
λ^4F_λ (10^{-13} W cm^{-2} μm^3)
WAVELENGTH (μm)

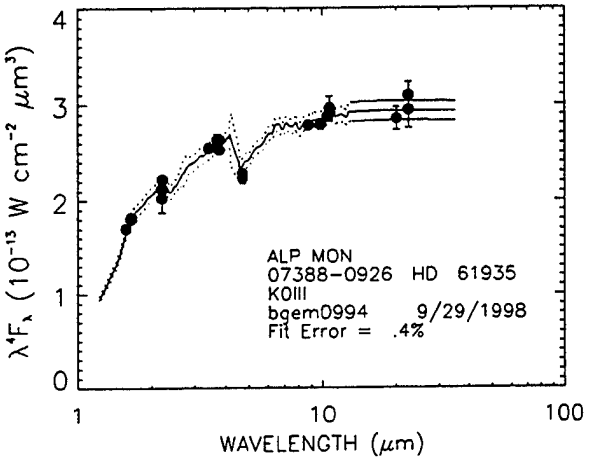
ALP MON
07388-0926 HD 61935
K0III
bgem0994 9/29/1998
Fit Error = .4%
λ^4F_λ (10^{-13} W cm^{-2} μm^3)
WAVELENGTH (μm)

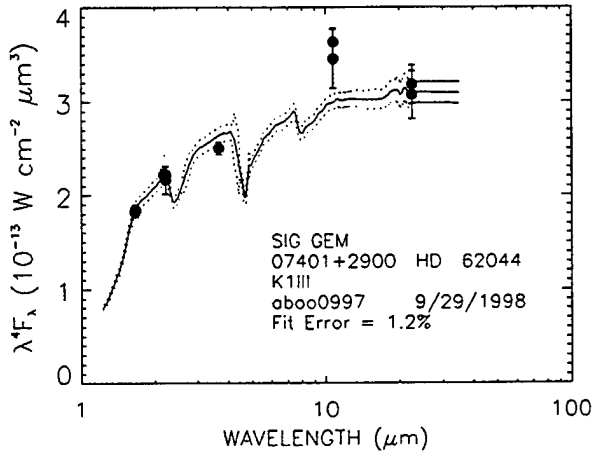
SIG GEM
07401+2900 HD 62044
K1III
aboo0997 9/29/1998
Fit Error = 1.2%
λ^4F_λ (10^{-13} W cm^{-2} μm^3)
WAVELENGTH (μm)

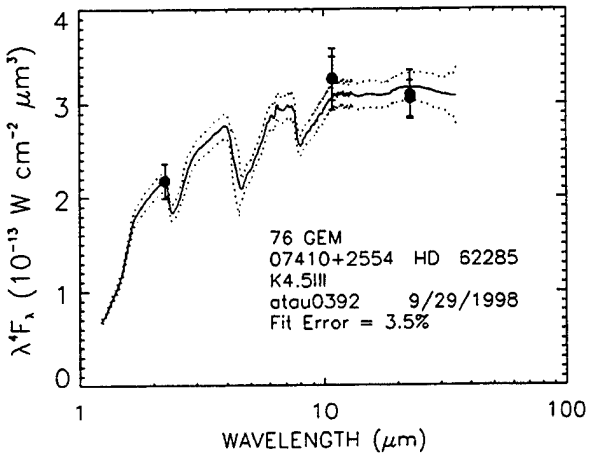
76 GEM
07410+2554 HD 62285
K4.5III
atau0392 9/29/1998
Fit Error = 3.5%
λ^4F_λ (10^{-13} W cm^{-2} μm^3)
WAVELENGTH (μm)

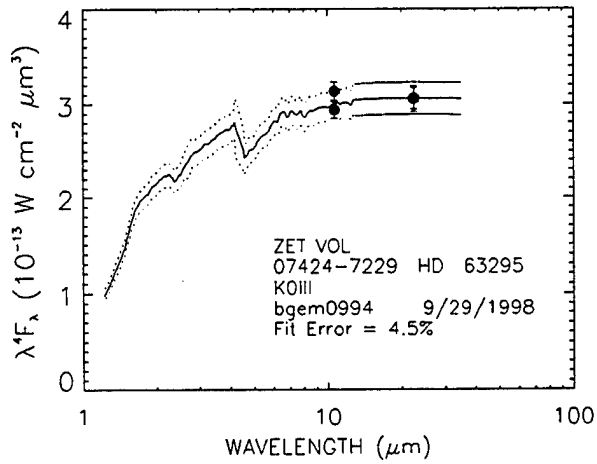
ZET VOL
07424-7229 HD 63295
K0III
bgem0994 9/29/1998
Fit Error = 4.5%
λ^4F_λ (10^{-13} W cm^{-2} μm^3)
WAVELENGTH (μm)

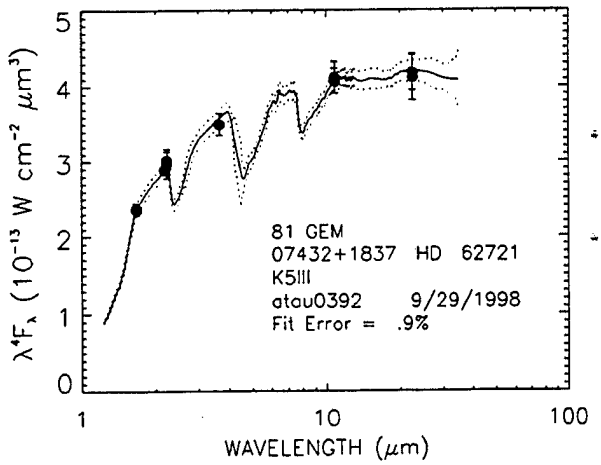
81 GEM
07432+1837 HD 62721
K5III
atau0392 9/29/1998
Fit Error = .9%
λ^4F_λ (10^{-13} W cm^{-2} μm^3)
WAVELENGTH (μm)

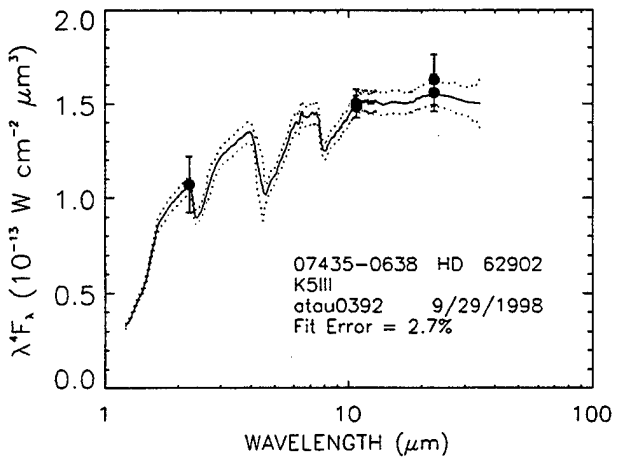
07435−0638 HD 62902
K5III
atau0392 9/29/1998
Fit Error = 2.7%
λ^4F_λ (10^{-13} W cm^{-2} μm^3)
WAVELENGTH (μm)

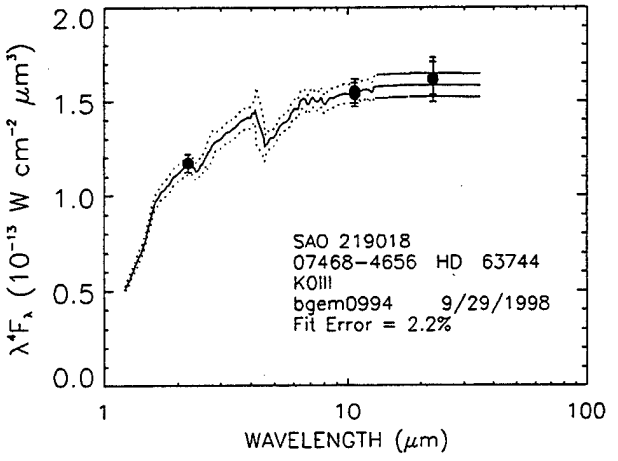
SAO 219018
07468−4656 HD 63744
K0III
bgem0994 9/29/1998
Fit Error = 2.2%
λ^4F_λ (10^{-13} W cm^{-2} μm^3)
WAVELENGTH (μm)

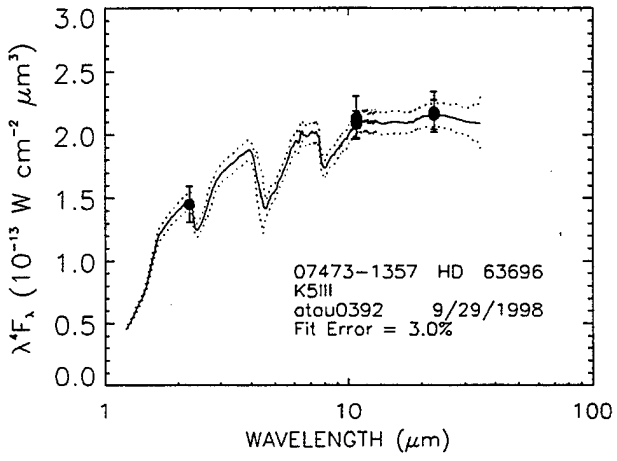
07473−1357 HD 63696
K5III
atau0392 9/29/1998
Fit Error = 3.0%
λ^4F_λ (10^{-13} W cm^{-2} μm^3)
WAVELENGTH (μm)

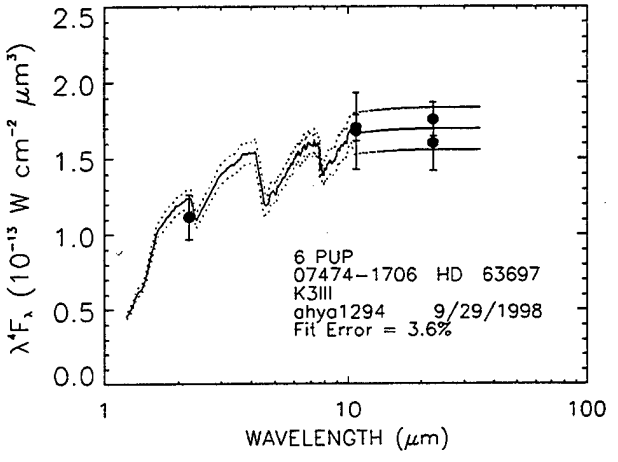
6 PUP
07474−1706 HD 63697
K3III
ahya1294 9/29/1998
Fit Error = 3.6%
λ^4F_λ (10^{-13} W cm^{-2} μm^3)
WAVELENGTH (μm)

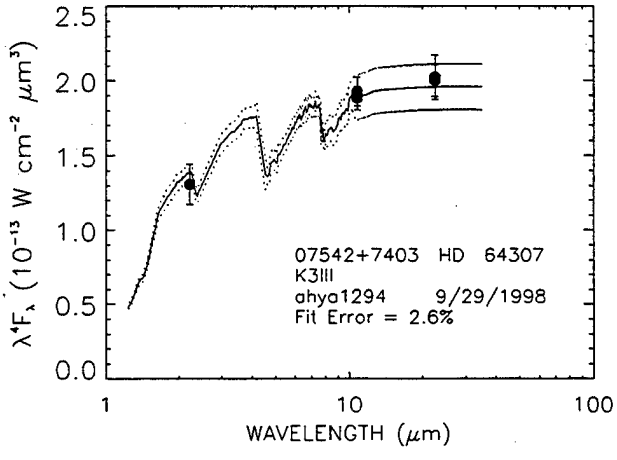
07542+7403 HD 64307
K3III
ahya1294 9/29/1998
Fit Error = 2.6%
λ^4F_λ (10^{-13} W cm^{-2} μm^3)
WAVELENGTH (μm)

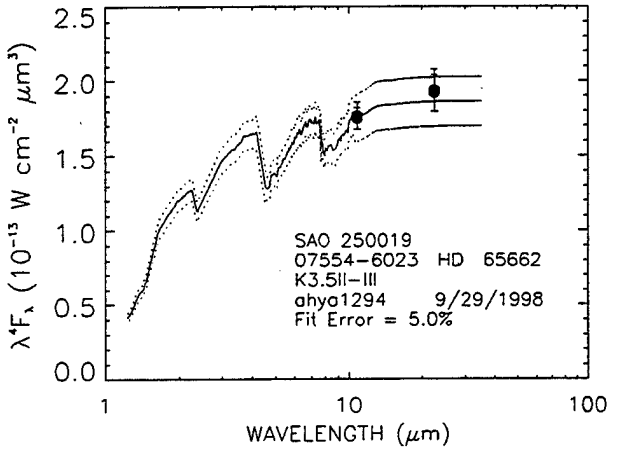
SAO 250019
07554−6023 HD 65662
K3.5II−III
ahya1294 9/29/1998
Fit Error = 5.0%
λ^4F_λ (10^{-13} W cm^{-2} μm^3)
WAVELENGTH (μm)

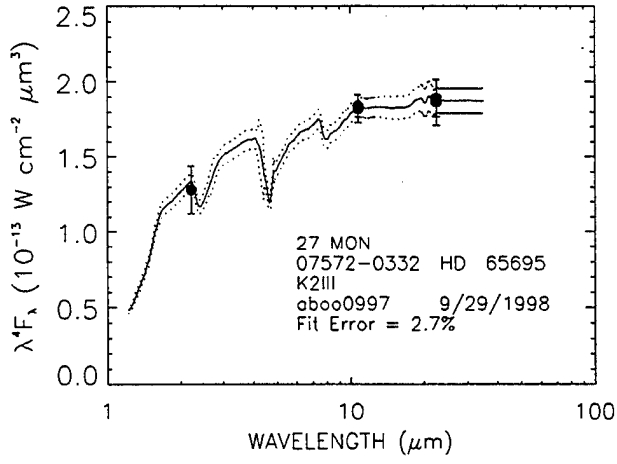
27 MON
07572−0332 HD 65695
K2III
aboo0997 9/29/1998
Fit Error = 2.7%
λ^4F_λ (10^{-13} W cm^{-2} μm^3)
WAVELENGTH (μm)

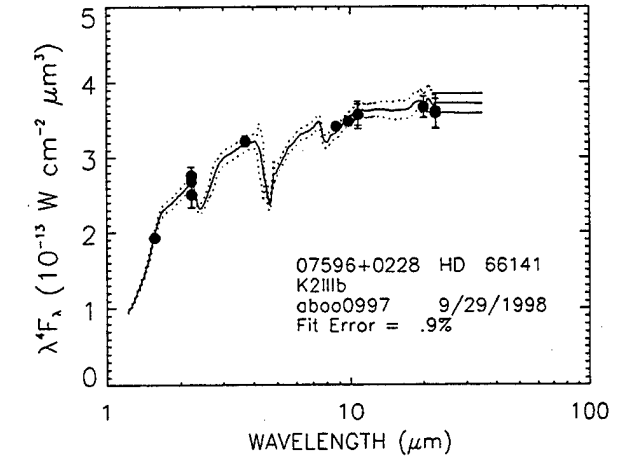
07596+0228 HD 66141
K2IIIb
aboo0997 9/29/1998
Fit Error = .9%
λ^4F_λ (10^{-13} W cm^{-2} μm^3)
WAVELENGTH (μm)

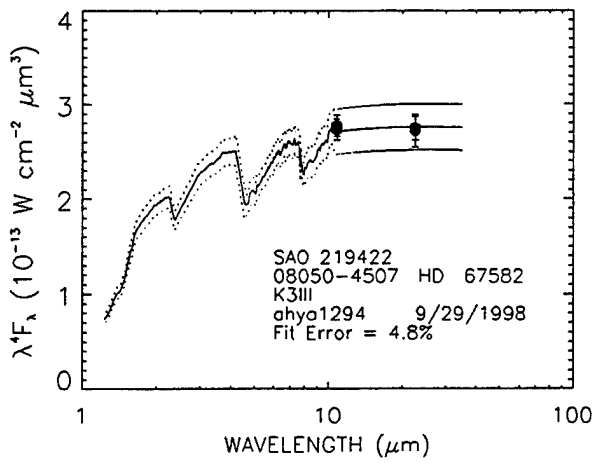
SAO 219422
08050-4507 HD 67582
K3III
ahya1294 9/29/1998
Fit Error = 4.8%
WAVELENGTH (μm)

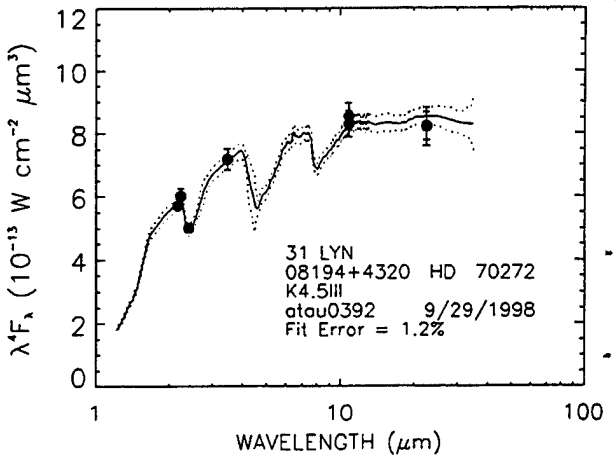
31 LYN
08194+4320 HD 70272
K4.5III
atau0392 9/29/1998
Fit Error = 1.2%
WAVELENGTH (μm)

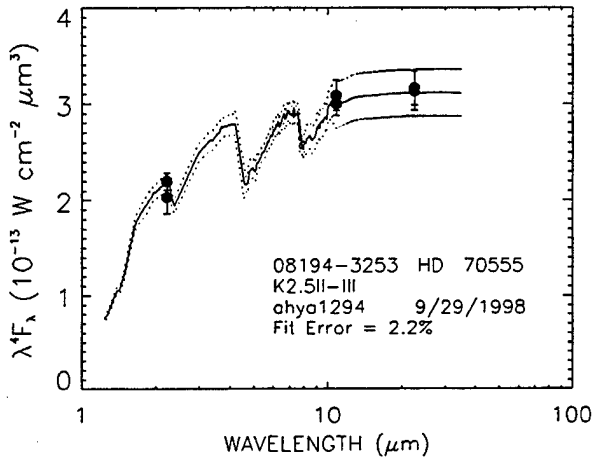
08194-3253 HD 70555
K2.5II-III
ahya1294 9/29/1998
Fit Error = 2.2%
WAVELENGTH (μm)

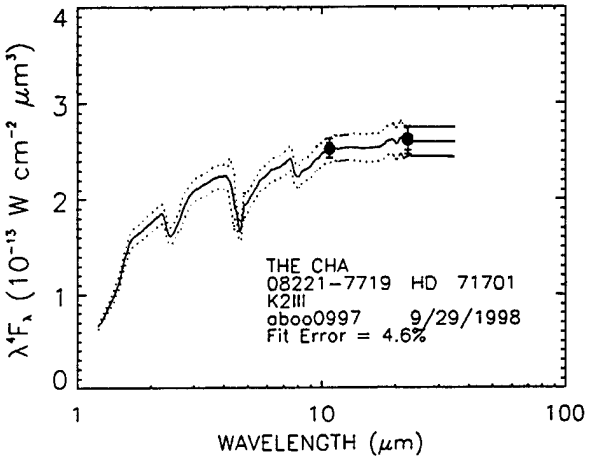
THE CHA
08221-7719 HD 71701
K2III
aboo0997 9/29/1998
Fit Error = 4.6%
WAVELENGTH (μm)

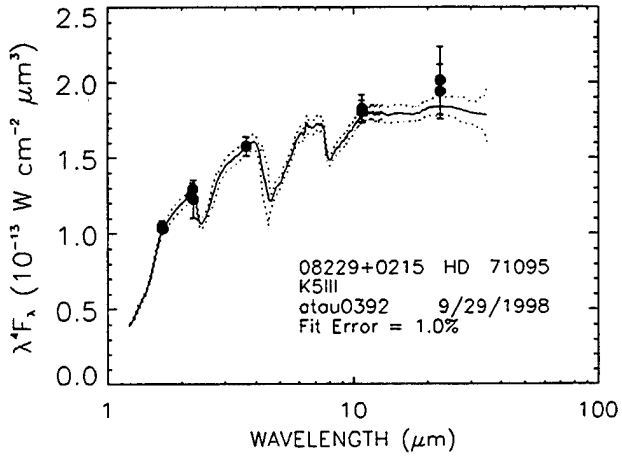
08229+0215 HD 71095
K5III
atau0392 9/29/1998
Fit Error = 1.0%
WAVELENGTH (μm)

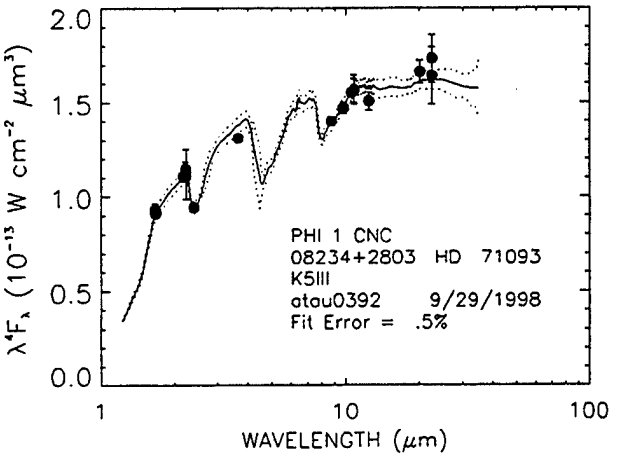
PHI 1 CNC
08234+2803 HD 71093
K5III
atau0392 9/29/1998
Fit Error = .5%
WAVELENGTH (μm)

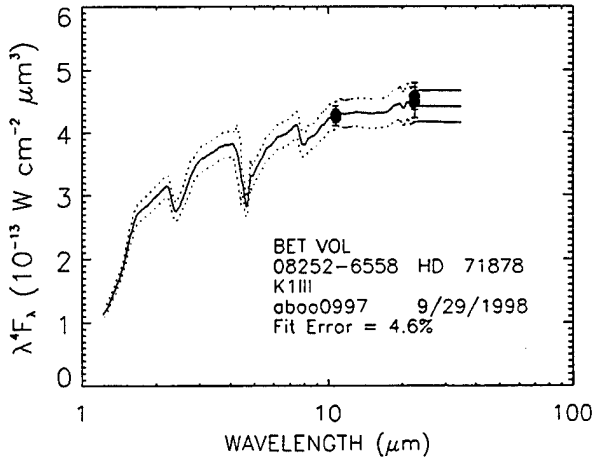
BET VOL
08252-6558 HD 71878
K1III
aboo0997 9/29/1998
Fit Error = 4.6%
WAVELENGTH (μm)

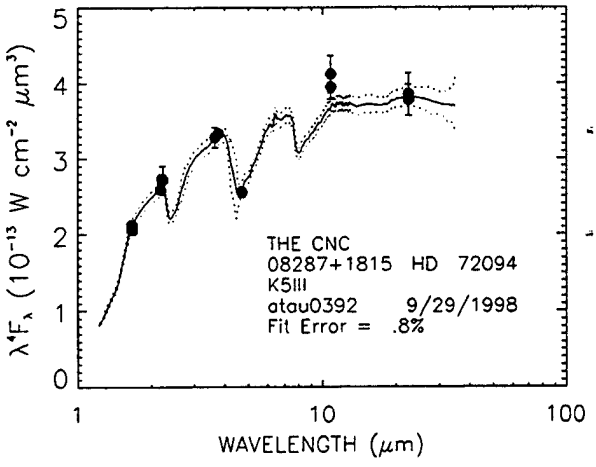
THE CNC
08287+1815 HD 72094
K5III
atau0392 9/29/1998
Fit Error = .8%
WAVELENGTH (μm)

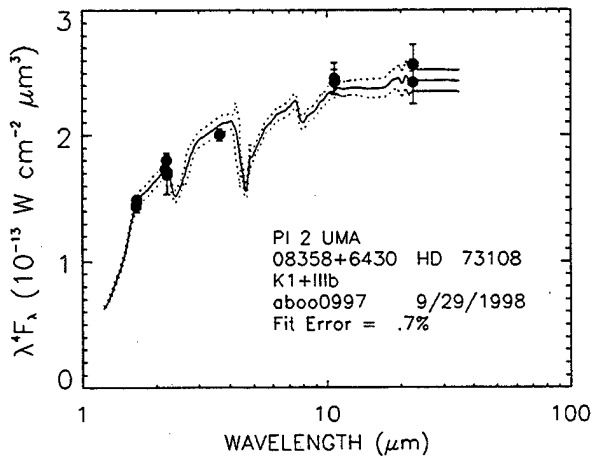
PI 2 UMA
08358+6430 HD 73108
K1+IIIb
aboo0997 9/29/1998
Fit Error = .7%
λ^4F_λ (10^{-13} W cm^{-2} μm^3)
WAVELENGTH (μm)

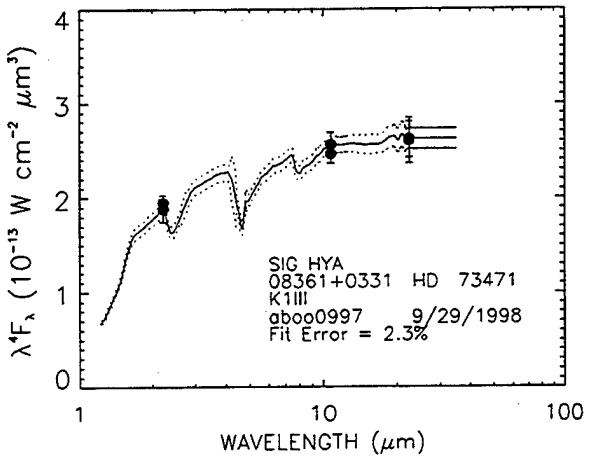
SIG HYA
08361+0331 HD 73471
K1III
aboo0997 9/29/1998
Fit Error = 2.3%
λ^4F_λ (10^{-13} W cm^{-2} μm^3)
WAVELENGTH (μm)

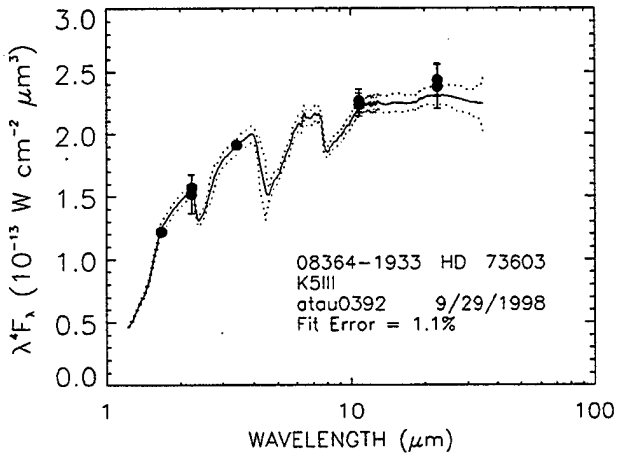
08364-1933 HD 73603
K5III
atau0392 9/29/1998
Fit Error = 1.1%
λ^4F_λ (10^{-13} W cm^{-2} μm^3)
WAVELENGTH (μm)

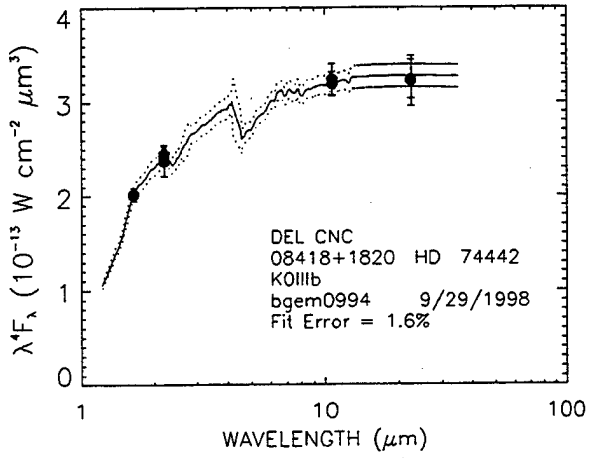
DEL CNC
08418+1820 HD 74442
K0IIIb
bgem0994 9/29/1998
Fit Error = 1.6%
λ^4F_λ (10^{-13} W cm^{-2} μm^3)
WAVELENGTH (μm)

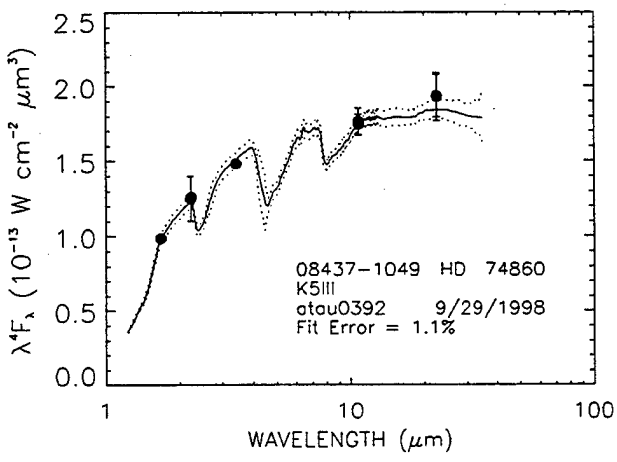
08437-1049 HD 74860
K5III
atau0392 9/29/1998
Fit Error = 1.1%
λ^4F_λ (10^{-13} W cm^{-2} μm^3)
WAVELENGTH (μm)

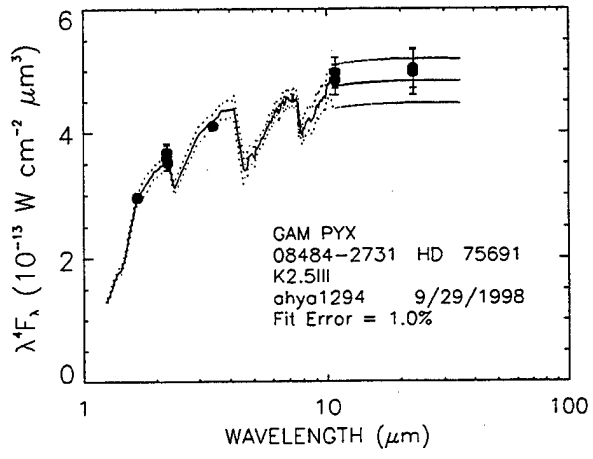
GAM PYX
08484-2731 HD 75691
K2.5III
ahya1294 9/29/1998
Fit Error = 1.0%
λ^4F_λ (10^{-13} W cm^{-2} μm^3)
WAVELENGTH (μm)

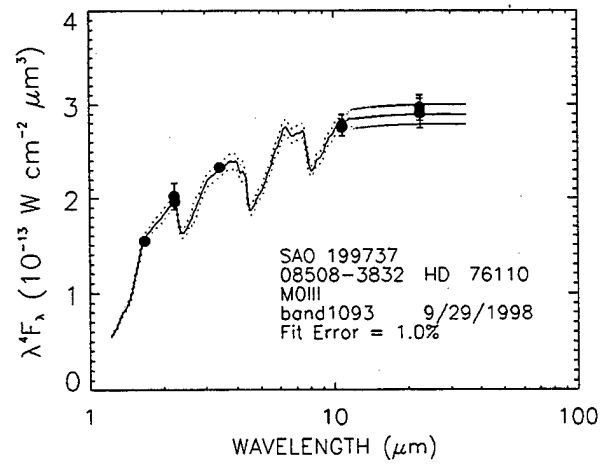
SAO 199737
08508-3832 HD 76110
MOIII
band1093 9/29/1998
Fit Error = 1.0%
λ^4F_λ (10^{-13} W cm^{-2} μm^3)
WAVELENGTH (μm)

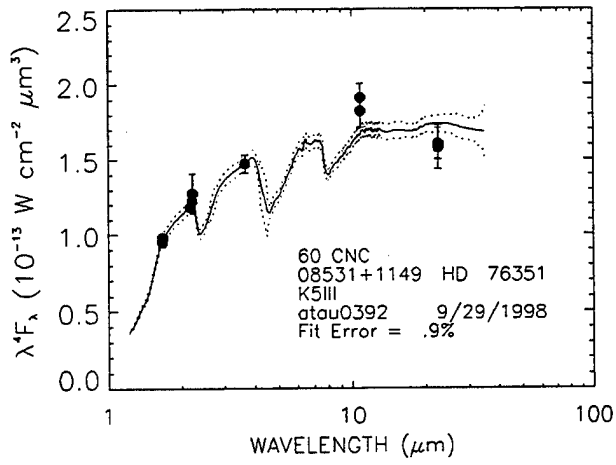
60 CNC
08531+1149 HD 76351
K5III
atau0392 9/29/1998
Fit Error = .9%
λ^4F_λ (10^{-13} W cm^{-2} μm^3)
WAVELENGTH (μm)

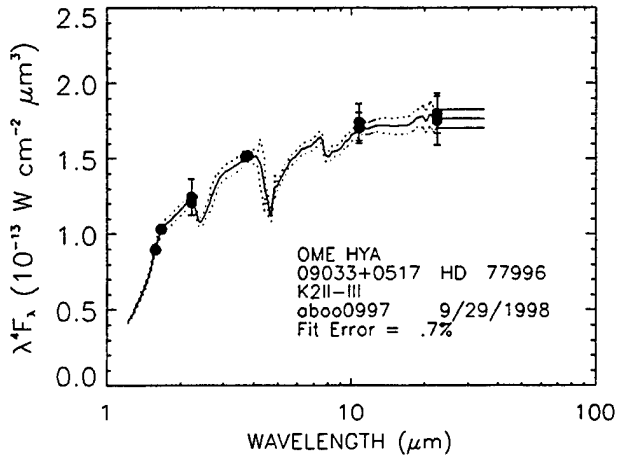
OME HYA
09033+0517 HD 77996
K2II-III
aboo0997 9/29/1998
Fit Error = .7%
WAVELENGTH (μm)

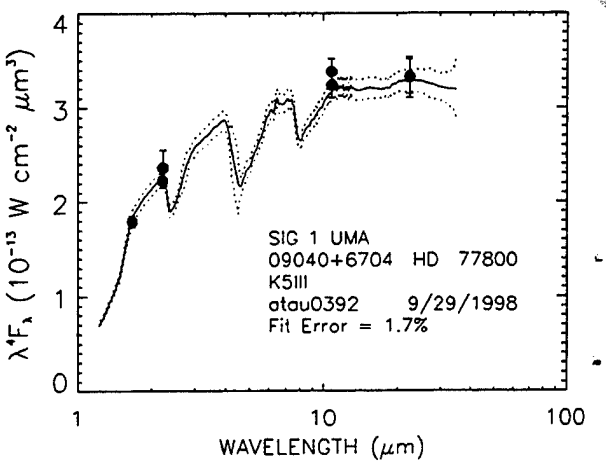
SIG 1 UMA
09040+6704 HD 77800
K5III
atau0392 9/29/1998
Fit Error = 1.7%
WAVELENGTH (μm)

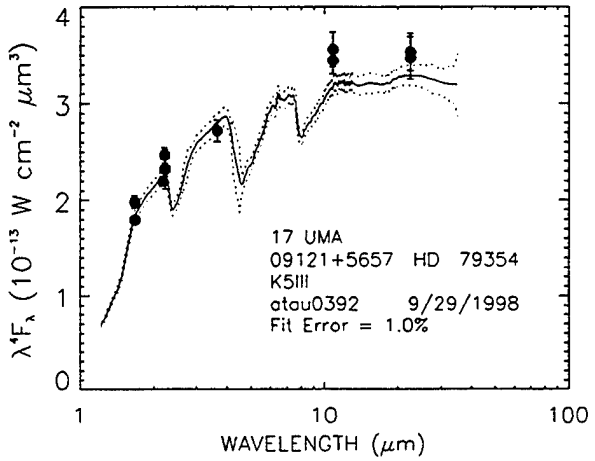
17 UMA
09121+5657 HD 79354
K5III
atau0392 9/29/1998
Fit Error = 1.0%
WAVELENGTH (μm)

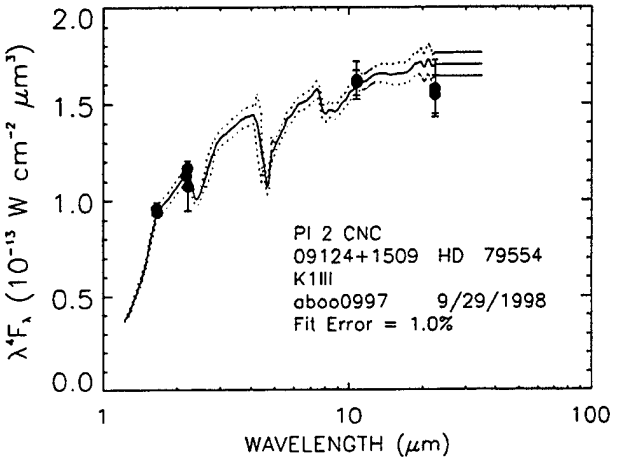
PI 2 CNC
09124+1509 HD 79554
K1III
aboo0997 9/29/1998
Fit Error = 1.0%
WAVELENGTH (μm)

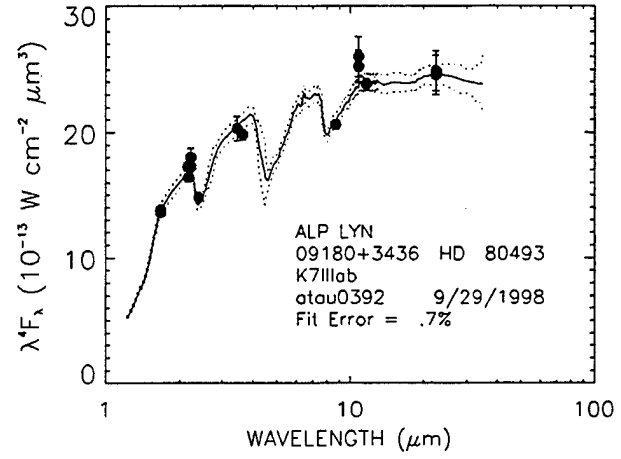
ALP LYN
09180+3436 HD 80493
K7IIIab
atau0392 9/29/1998
Fit Error = .7%
WAVELENGTH (μm)

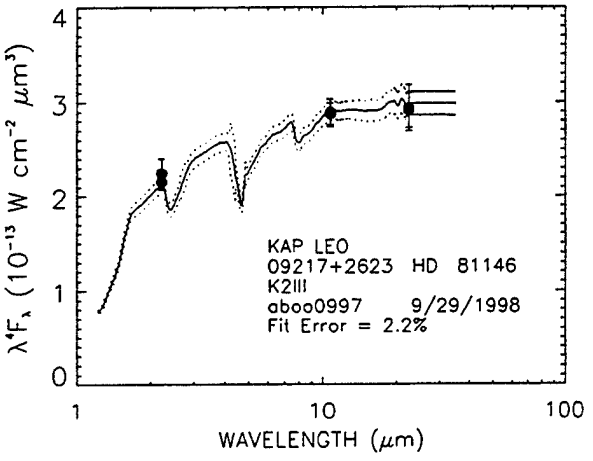
KAP LEO
09217+2623 HD 81146
K2III
aboo0997 9/29/1998
Fit Error = 2.2%
WAVELENGTH (μm)

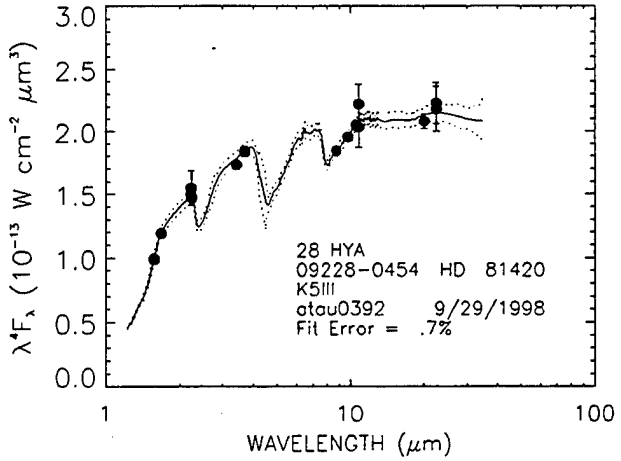
28 HYA
09228-0454 HD 81420
K5III
atau0392 9/29/1998
Fit Error = .7%
WAVELENGTH (μm)

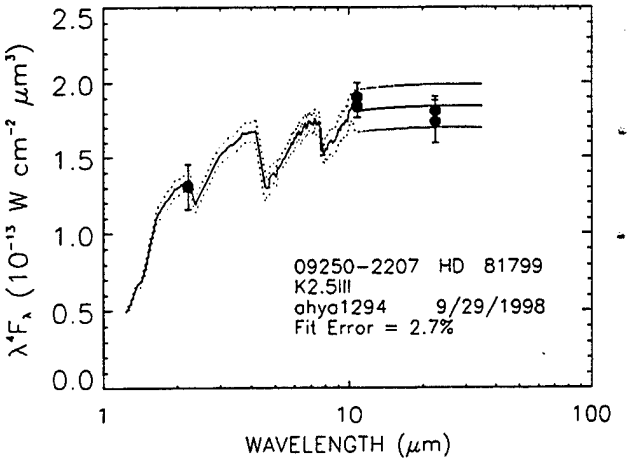
09250-2207 HD 81799
K2.5III
ahya1294 9/29/1998
Fit Error = 2.7%
WAVELENGTH (μm)

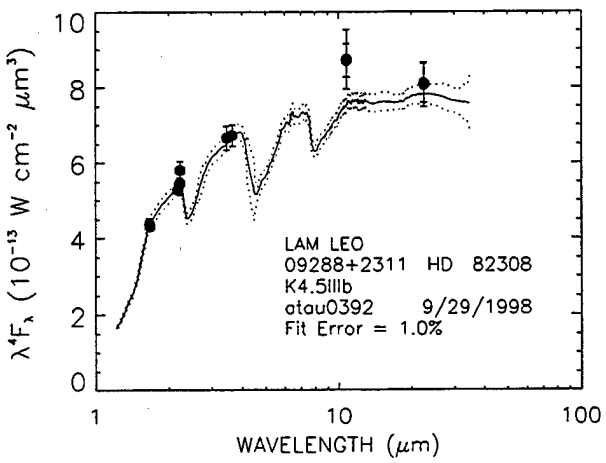
LAM LEO
09288+2311 HD 82308
K4.5IIIb
atau0392 9/29/1998
Fit Error = 1.0%
λ^4F_λ (10^{-13} W cm^{-2} μm^3)
WAVELENGTH (μm)

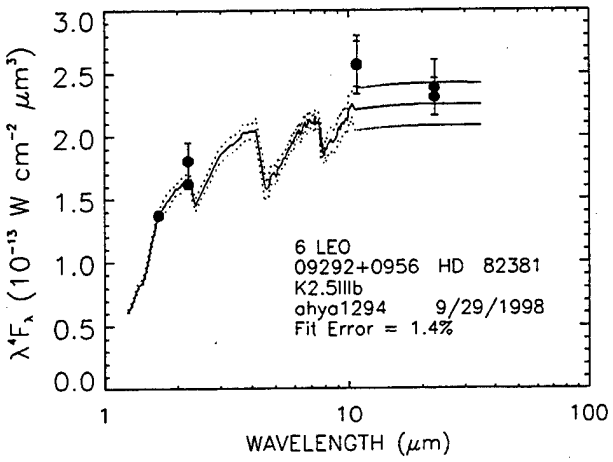
6 LEO
09292+0956 HD 82381
K2.5IIIb
ahya1294 9/29/1998
Fit Error = 1.4%
λ^4F_λ (10^{-13} W cm^{-2} μm^3)
WAVELENGTH (μm)

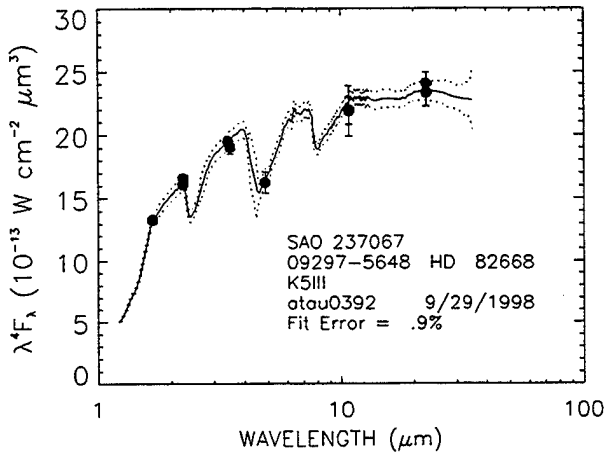
SAO 237067
09297−5648 HD 82668
K5III
atau0392 9/29/1998
Fit Error = .9%
λ^4F_λ (10^{-13} W cm^{-2} μm^3)
WAVELENGTH (μm)

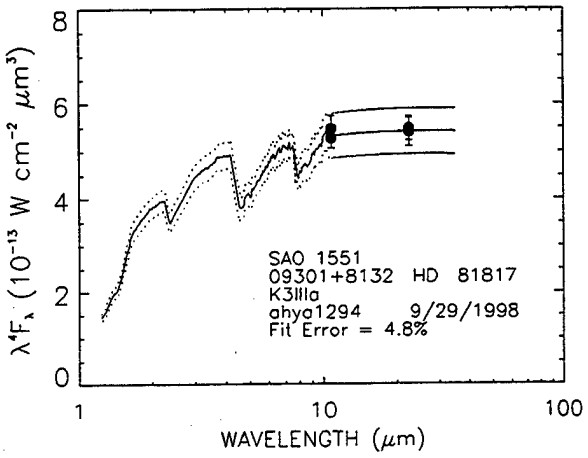
SAO 1551
09301+8132 HD 81817
K3IIIa
ahya1294 9/29/1998
Fit Error = 4.8%
λ^4F_λ (10^{-13} W cm^{-2} μm^3)
WAVELENGTH (μm)

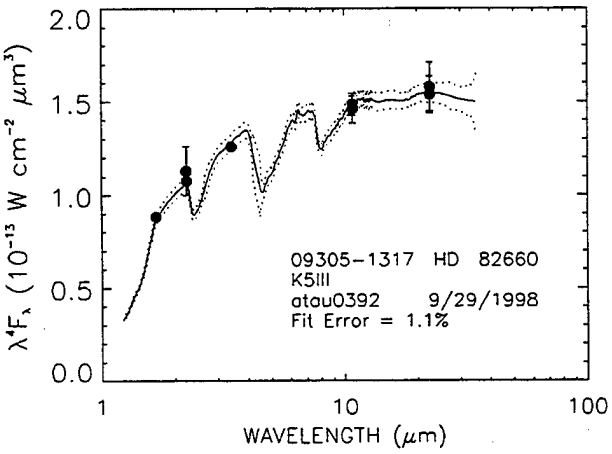
09305−1317 HD 82660
K5III
atau0392 9/29/1998
Fit Error = 1.1%
λ^4F_λ (10^{-13} W cm^{-2} μm^3)
WAVELENGTH (μm)

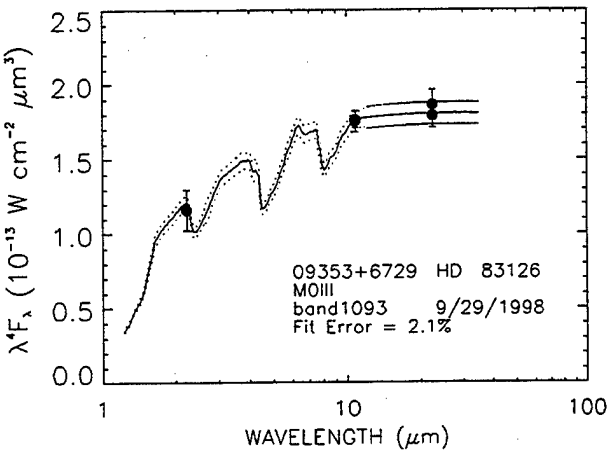
09353+6729 HD 83126
M0III
band1093 9/29/1998
Fit Error = 2.1%
λ^4F_λ (10^{-13} W cm^{-2} μm^3)
WAVELENGTH (μm)

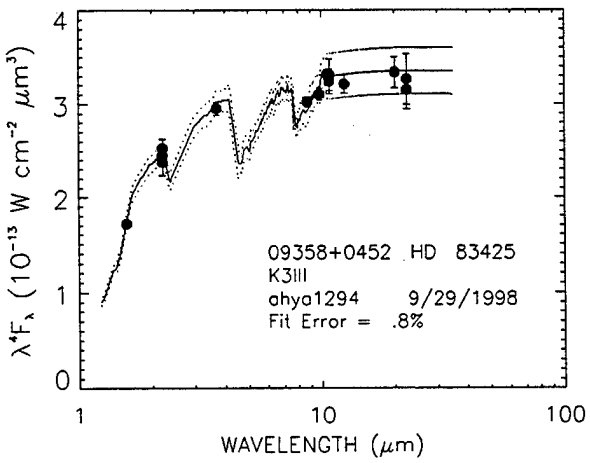
09358+0452 HD 83425
K3III
ahya1294 9/29/1998
Fit Error = .8%
λ^4F_λ (10^{-13} W cm^{-2} μm^3)
WAVELENGTH (μm)

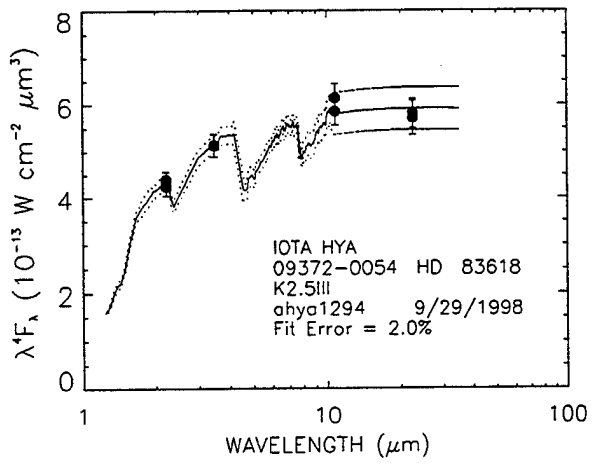
IOTA HYA
09372−0054 HD 83618
K2.5III
ahya1294 9/29/1998
Fit Error = 2.0%
λ^4F_λ (10^{-13} W cm^{-2} μm^3)
WAVELENGTH (μm)

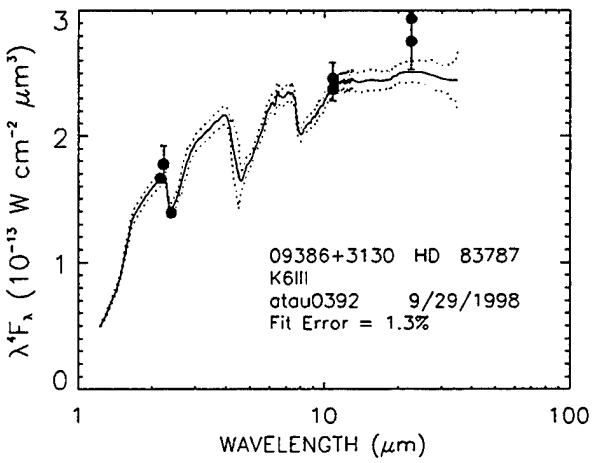
09386+3130 HD 83787
K6III
atau0392 9/29/1998
Fit Error = 1.3%
WAVELENGTH (μm)

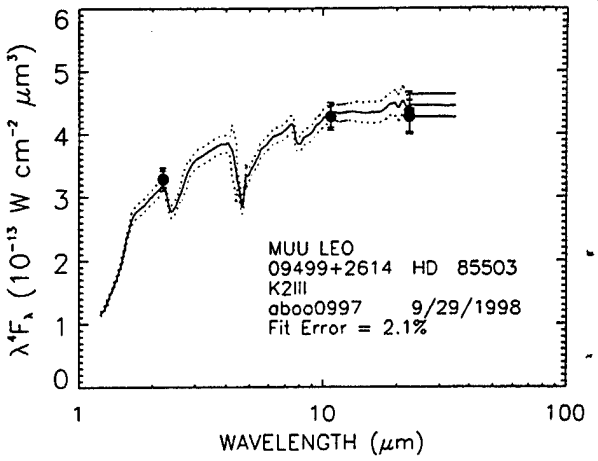
MUU LEO
09499+2614 HD 85503
K2III
aboo0997 9/29/1998
Fit Error = 2.1%
WAVELENGTH (μm)

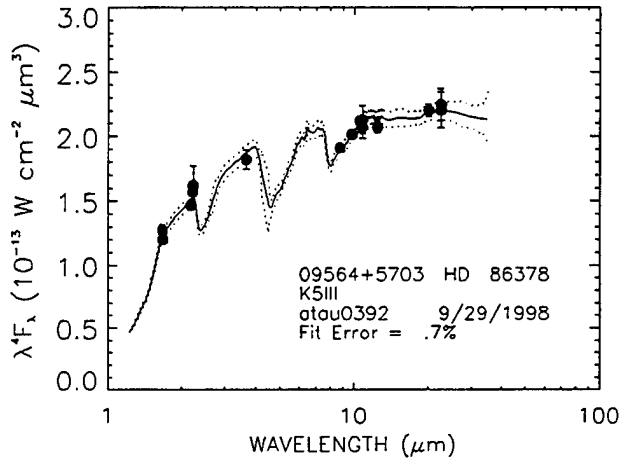
09564+5703 HD 86378
K5III
atau0392 9/29/1998
Fit Error = .7%
WAVELENGTH (μm)

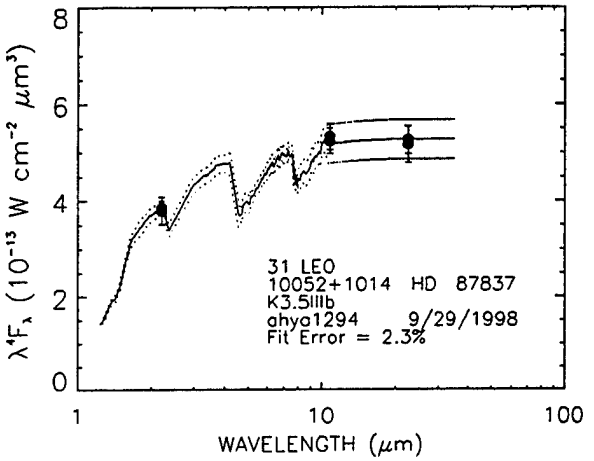
31 LEO
10052+1014 HD 87837
K3.5IIIb
ahya1294 9/29/1998
Fit Error = 2.3%
WAVELENGTH (μm)

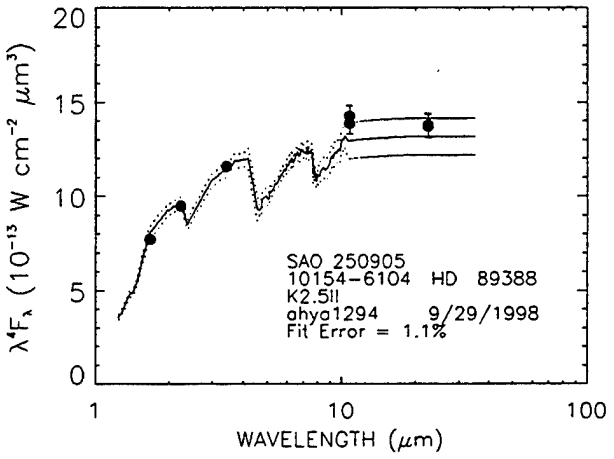
SAO 250905
10154-6104 HD 89388
K2.5II
ahya1294 9/29/1998
Fit Error = 1.1%
WAVELENGTH (μm)

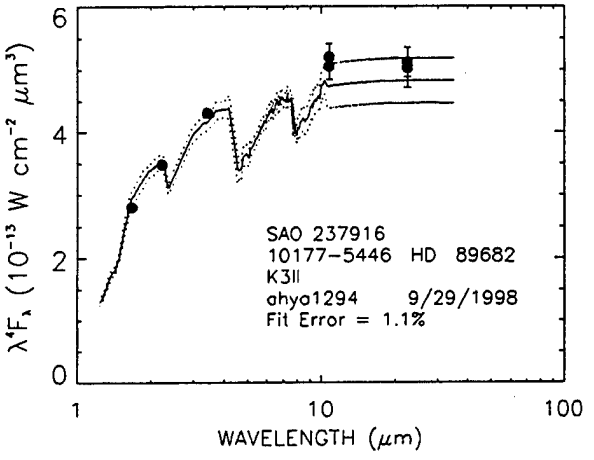
SAO 237916
10177-5446 HD 89682
K3II
ahya1294 9/29/1998
Fit Error = 1.1%
WAVELENGTH (μm)

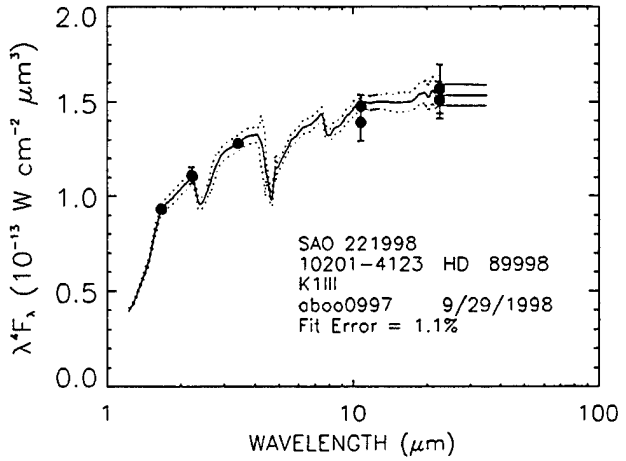
SAO 221998
10201-4123 HD 89998
K1III
aboo0997 9/29/1998
Fit Error = 1.1%
WAVELENGTH (μm)

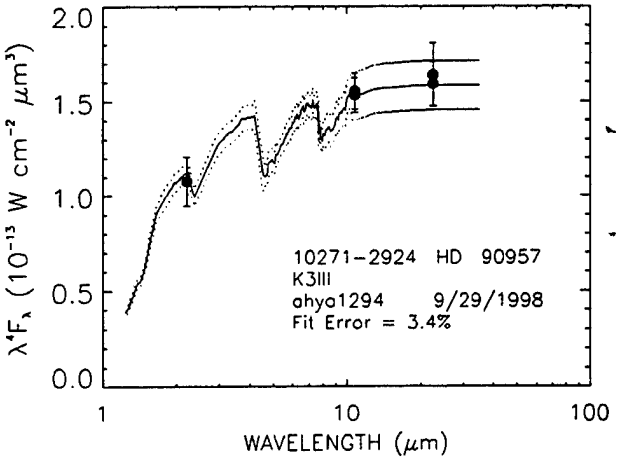
10271-2924 HD 90957
K3III
ahya1294 9/29/1998
Fit Error = 3.4%
WAVELENGTH (μm)

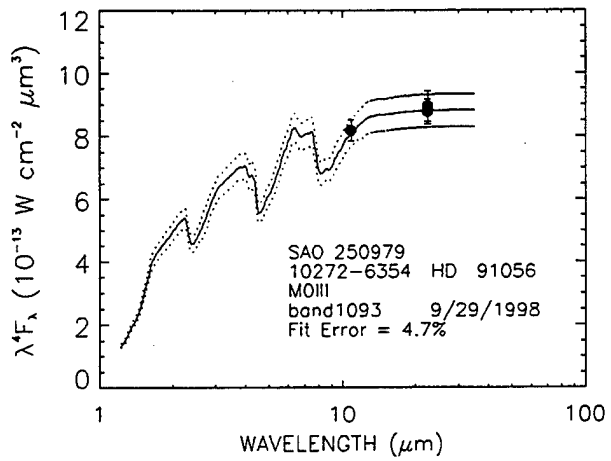
SAO 250979
10272-6354 HD 91056
MOIII
band1093 9/29/1998
Fit Error = 4.7%
WAVELENGTH (μm)

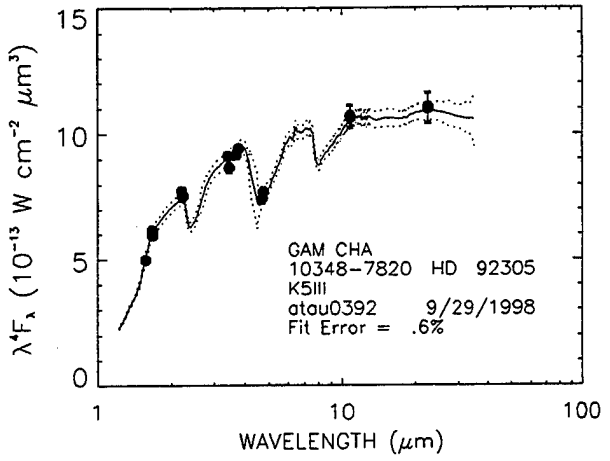
GAM CHA
10348-7820 HD 92305
K5III
atau0392 9/29/1998
Fit Error = .6%
WAVELENGTH (μm)

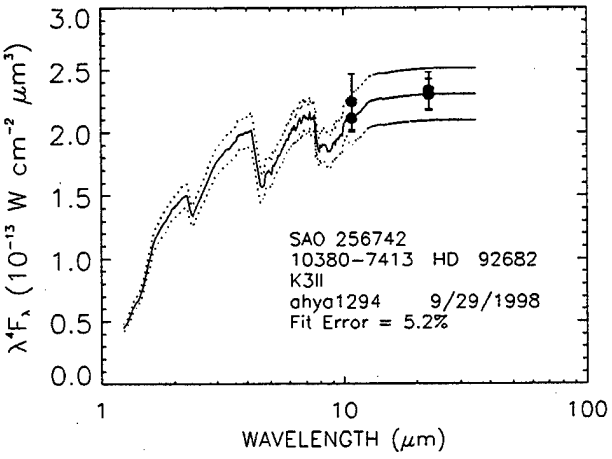
SAO 256742
10380-7413 HD 92682
K3II
ahya1294 9/29/1998
Fit Error = 5.2%
WAVELENGTH (μm)

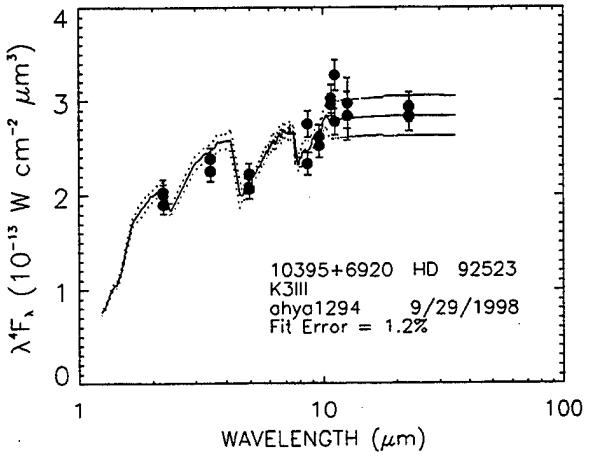
10395+6920 HD 92523
K3III
ahya1294 9/29/1998
Fit Error = 1.2%
WAVELENGTH (μm)

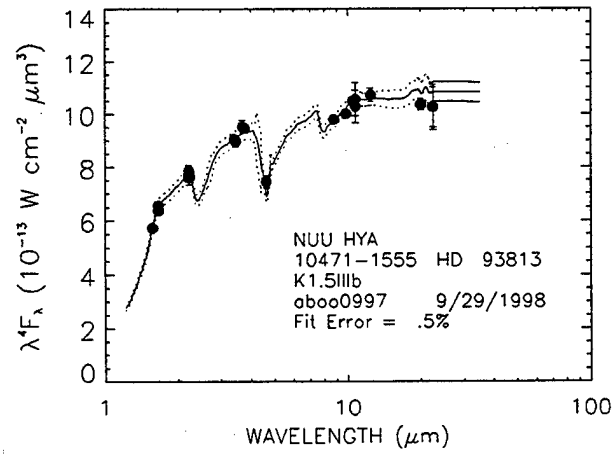
NUU HYA
10471-1555 HD 93813
K1.5IIIb
aboo0997 9/29/1998
Fit Error = .5%
WAVELENGTH (μm)

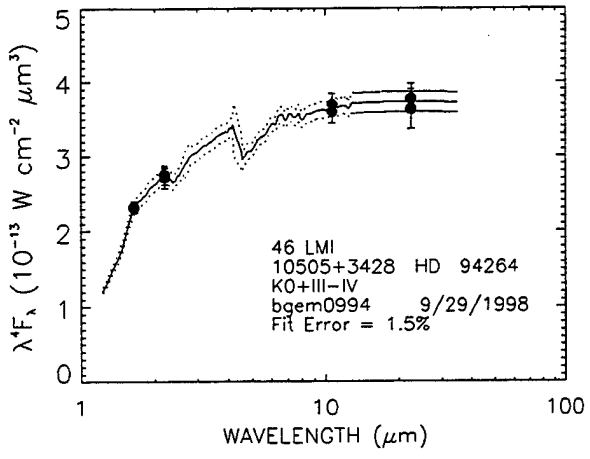
46 LMI
10505+3428 HD 94264
K0+III-IV
bgem0994 9/29/1998
Fit Error = 1.5%
WAVELENGTH (μm)

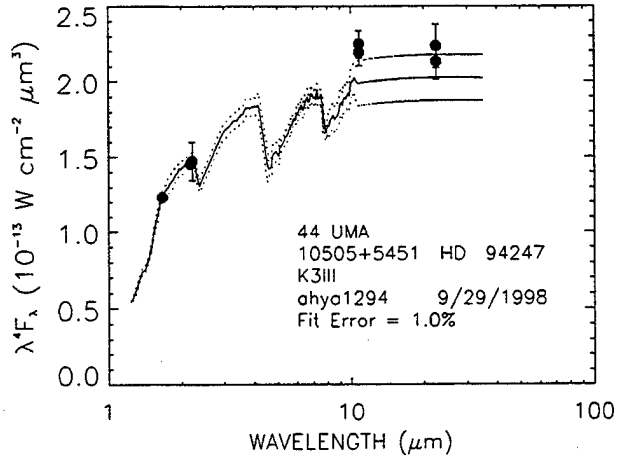
44 UMA
10505+5451 HD 94247
K3III
ahya1294 9/29/1998
Fit Error = 1.0%
WAVELENGTH (μm)

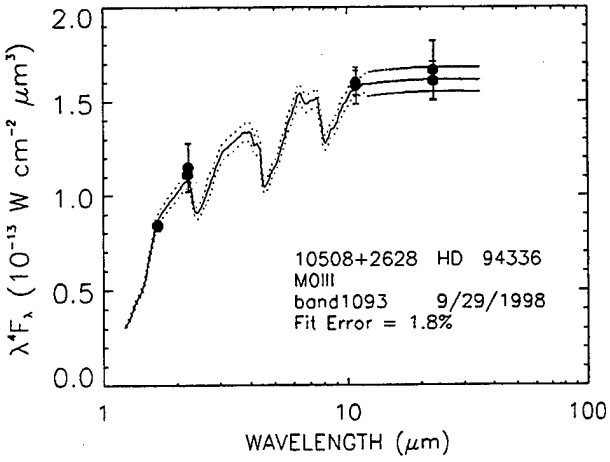
10508+2628 HD 94336
MOIII
band1093 9/29/1998
Fit Error = 1.8%
WAVELENGTH (μm)

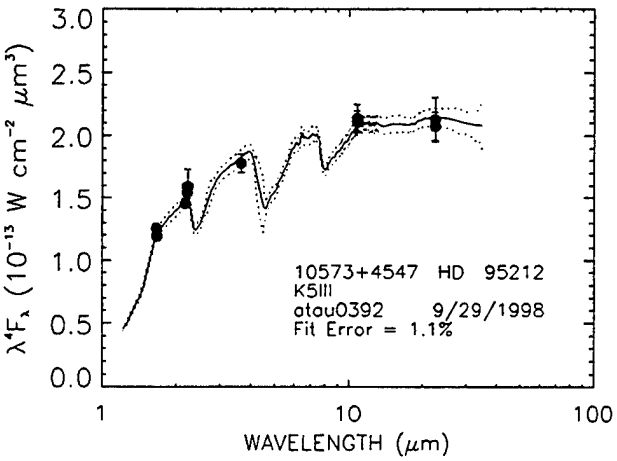
10573+4547 HD 95212
K5III
atau0392 9/29/1998
Fit Error = 1.1%
WAVELENGTH (μm)

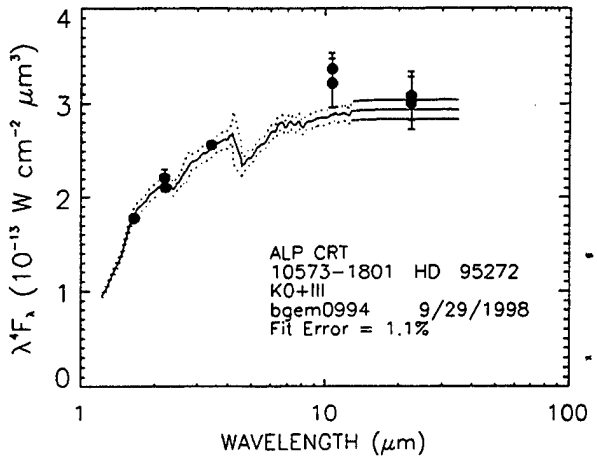
ALP CRT
10573−1801 HD 95272
K0+III
bgem0994 9/29/1998
Fit Error = 1.1%
WAVELENGTH (μm)

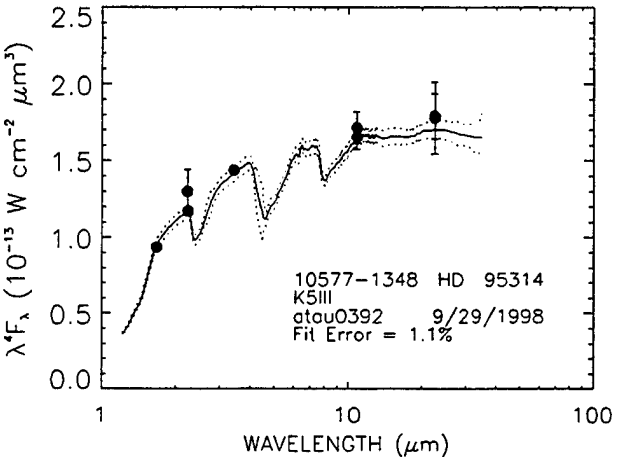
10577−1348 HD 95314
K5III
atau0392 9/29/1998
Fit Error = 1.1%
WAVELENGTH (μm)

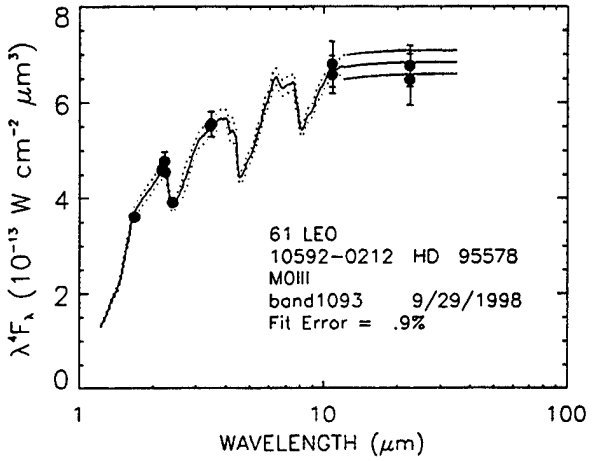
61 LEO
10592−0212 HD 95578
M0III
band1093 9/29/1998
Fit Error = .9%
WAVELENGTH (μm)

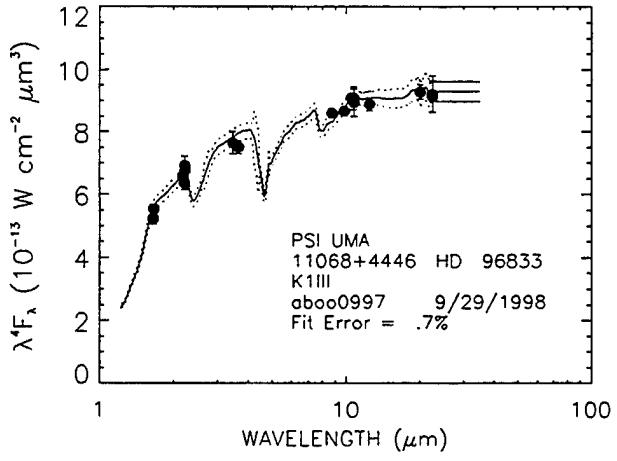
PSI UMA
11068+4446 HD 96833
K1III
aboo0997 9/29/1998
Fit Error = .7%
WAVELENGTH (μm)

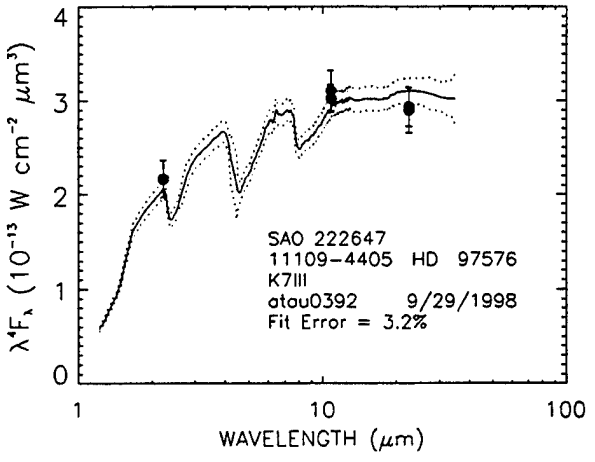
SAO 222647
11109−4405 HD 97576
K7III
atau0392 9/29/1998
Fit Error = 3.2%
WAVELENGTH (μm)

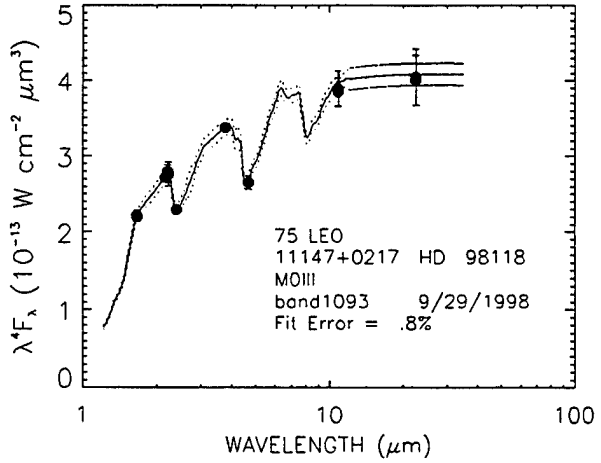
75 LEO
11147+0217 HD 98118
M0III
band1093 9/29/1998
Fit Error = .8%
WAVELENGTH (μm)

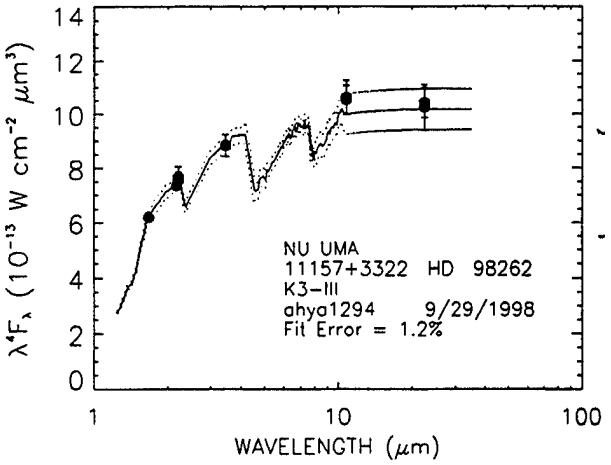
NU UMA
11157+3322 HD 98262
K3−III
ahya1294 9/29/1998
Fit Error = 1.2%
WAVELENGTH (μm)

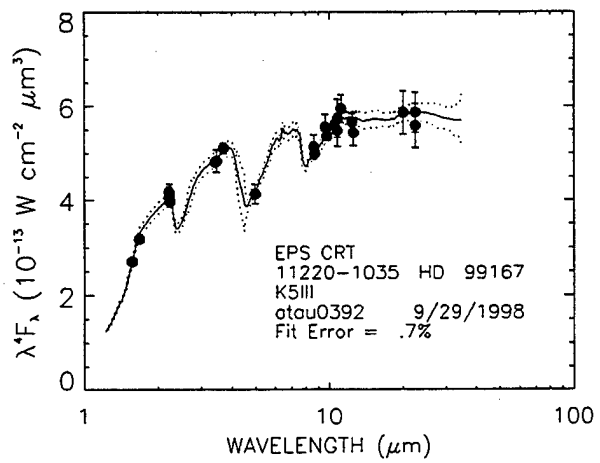
EPS CRT
11220-1035 HD 99167
K5III
atau0392 9/29/1998
Fit Error = .7%
λ^4F_λ (10^{-13} W cm^{-2} μm^3)
WAVELENGTH (μm)

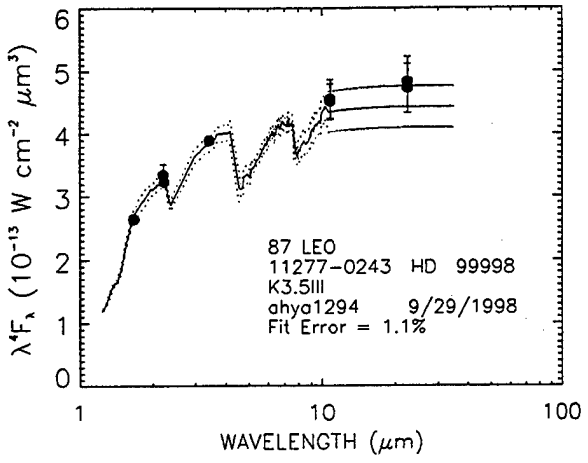
87 LEO
11277-0243 HD 99998
K3.5III
ahya1294 9/29/1998
Fit Error = 1.1%
λ^4F_λ (10^{-13} W cm^{-2} μm^3)
WAVELENGTH (μm)

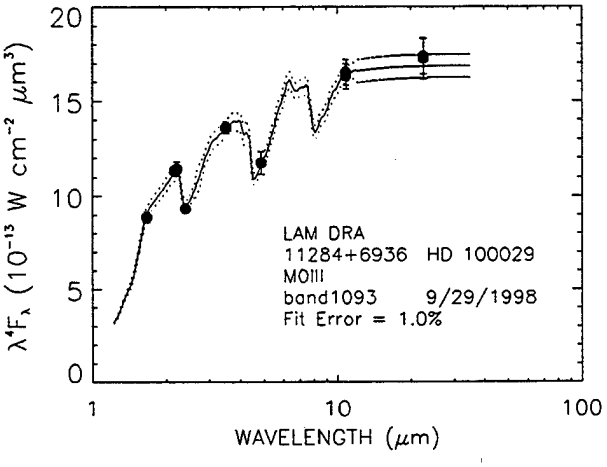
LAM DRA
11284+6936 HD 100029
M0III
band1093 9/29/1998
Fit Error = 1.0%
λ^4F_λ (10^{-13} W cm^{-2} μm^3)
WAVELENGTH (μm)

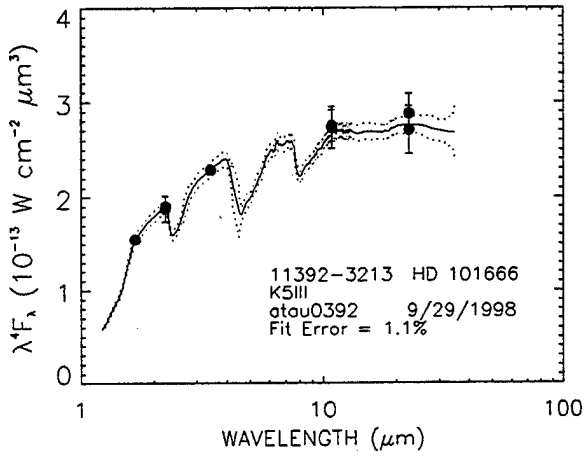
11392-3213 HD 101666
K5III
atau0392 9/29/1998
Fit Error = 1.1%
λ^4F_λ (10^{-13} W cm^{-2} μm^3)
WAVELENGTH (μm)

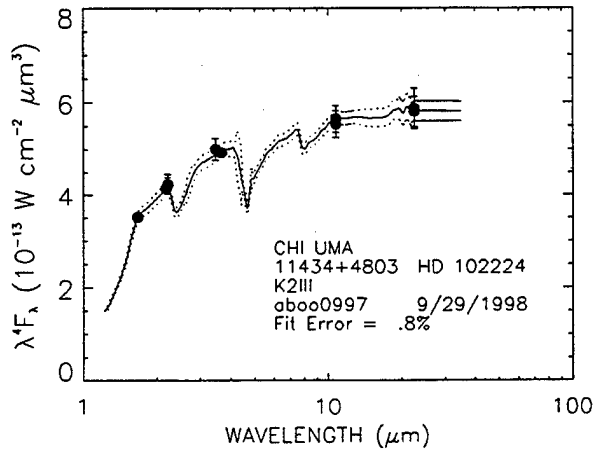
CHI UMA
11434+4803 HD 102224
K2III
aboo0997 9/29/1998
Fit Error = .8%
λ^4F_λ (10^{-13} W cm^{-2} μm^3)
WAVELENGTH (μm)

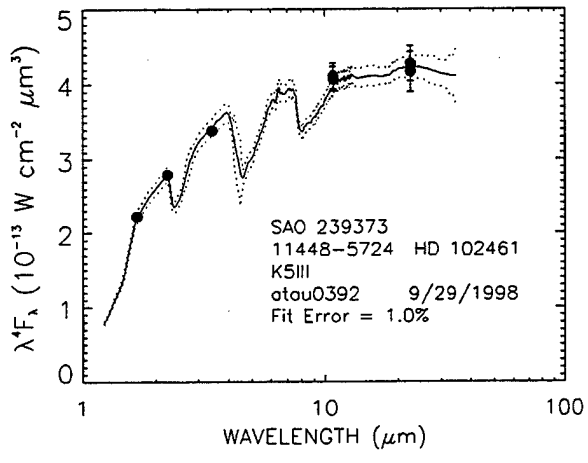
SAO 239373
11448-5724 HD 102461
K5III
atau0392 9/29/1998
Fit Error = 1.0%
λ^4F_λ (10^{-13} W cm^{-2} μm^3)
WAVELENGTH (μm)

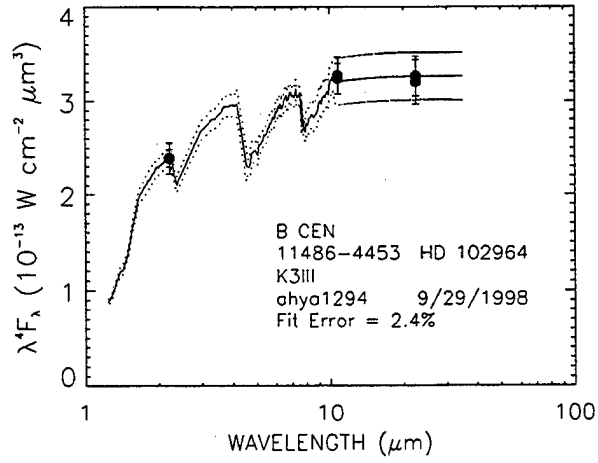
B CEN
11486-4453 HD 102964
K3III
ahya1294 9/29/1998
Fit Error = 2.4%
λ^4F_λ (10^{-13} W cm^{-2} μm^3)
WAVELENGTH (μm)

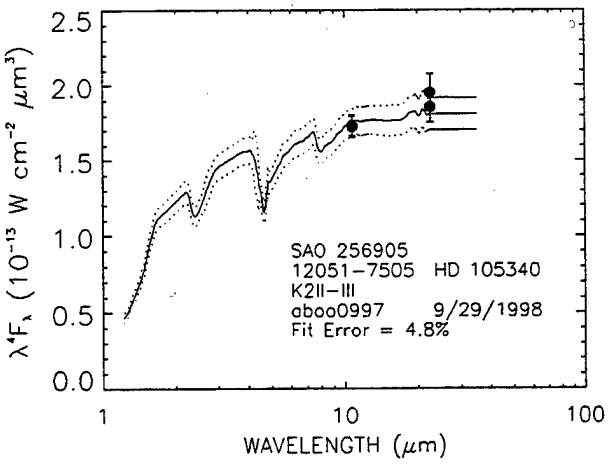
SAO 256905
12051-7505 HD 105340
K2II-III
aboo0997 9/29/1998
Fit Error = 4.8%
λ^4F_λ (10^{-13} W cm^{-2} μm^3)
WAVELENGTH (μm)

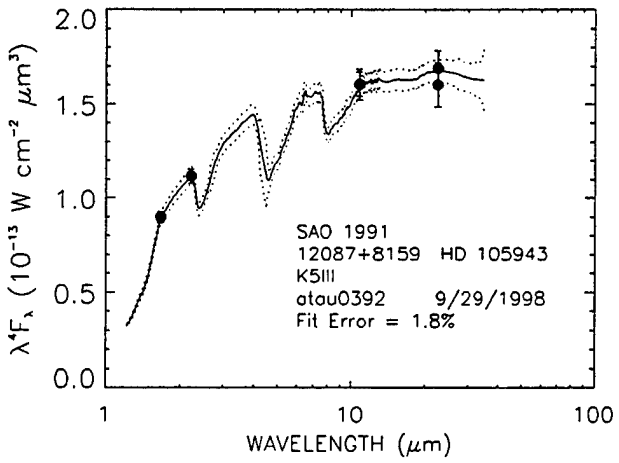
SAO 1991
12087+8159 HD 105943
K5III
atau0392 9/29/1998
Fit Error = 1.8%
WAVELENGTH (μm)

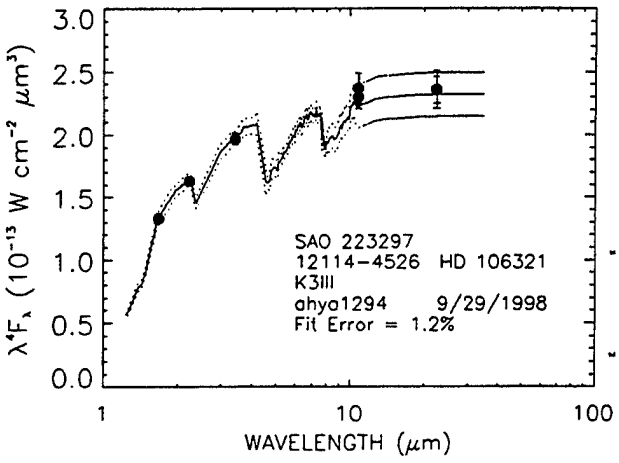
SAO 223297
12114-4526 HD 106321
K3III
ahya1294 9/29/1998
Fit Error = 1.2%
WAVELENGTH (μm)

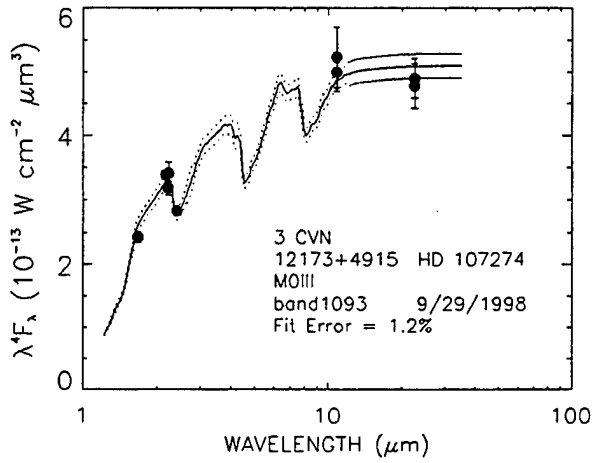
3 CVN
12173+4915 HD 107274
M0III
band1093 9/29/1998
Fit Error = 1.2%
WAVELENGTH (μm)

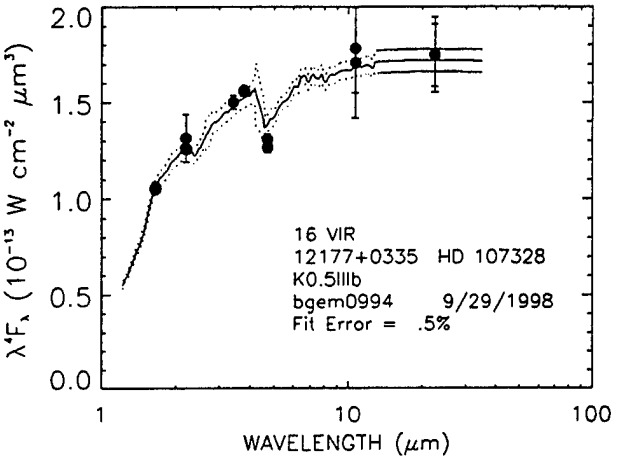
16 VIR
12177+0335 HD 107328
K0.5IIIb
bgem0994 9/29/1998
Fit Error = .5%
WAVELENGTH (μm)

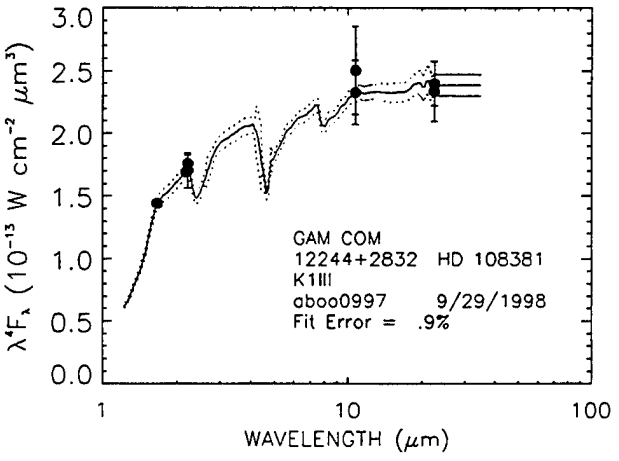
GAM COM
12244+2832 HD 108381
K1III
aboo0997 9/29/1998
Fit Error = .9%
WAVELENGTH (μm)

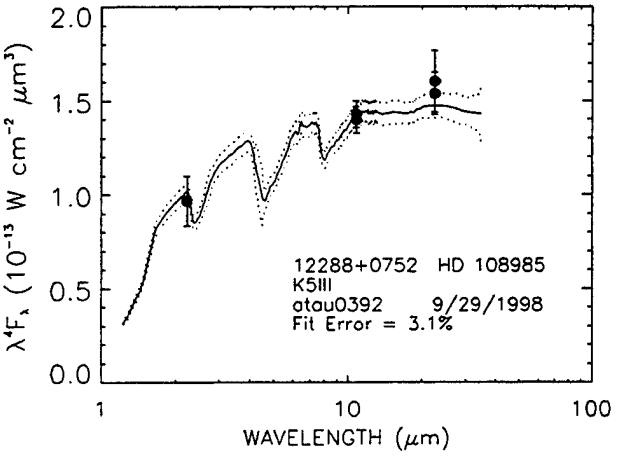
12288+0752 HD 108985
K5III
atau0392 9/29/1998
Fit Error = 3.1%
WAVELENGTH (μm)

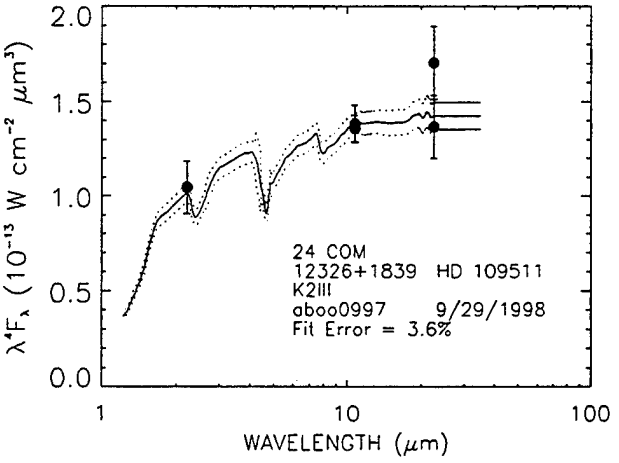
24 COM
12326+1839 HD 109511
K2III
aboo0997 9/29/1998
Fit Error = 3.6%
WAVELENGTH (μm)

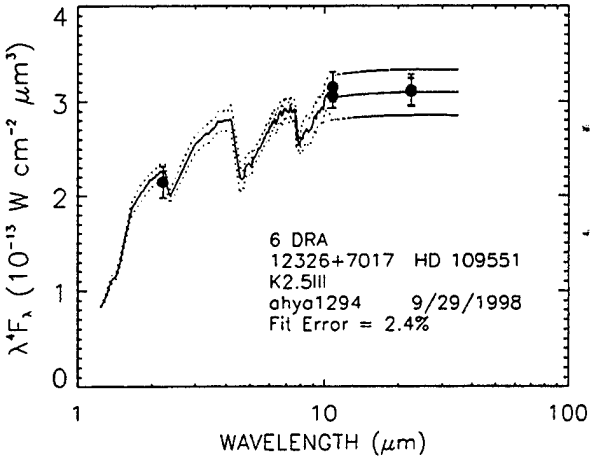
6 DRA
12326+7017 HD 109551
K2.5III
ahya1294 9/29/1998
Fit Error = 2.4%
WAVELENGTH (μm)

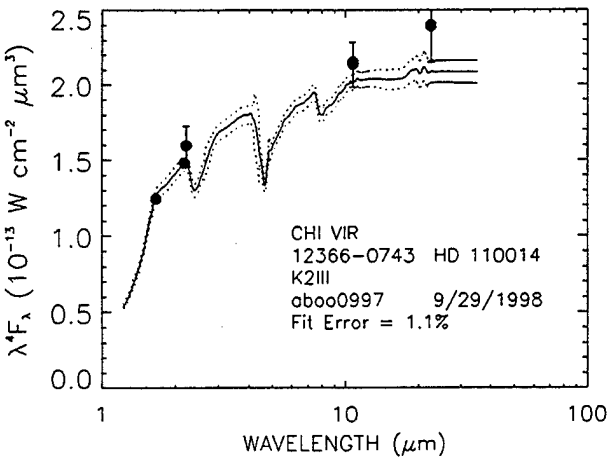
CHI VIR
12366-0743 HD 110014
K2III
aboo0997 9/29/1998
Fit Error = 1.1%
λ^4F_λ (10^{-13} W cm^{-2} μm^3)
WAVELENGTH (μm)

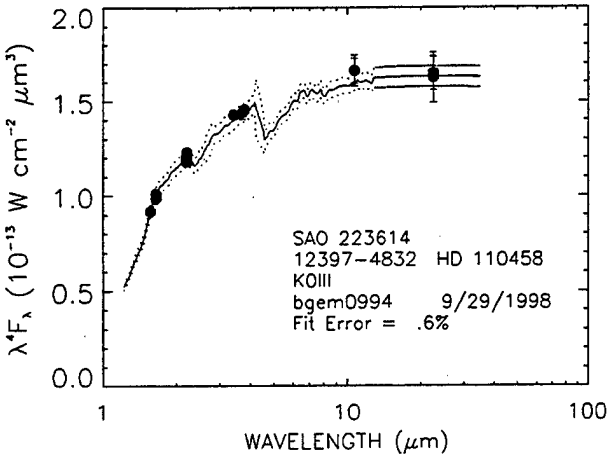
SAO 223614
12397-4832 HD 110458
KOIII
bgem0994 9/29/1998
Fit Error = .6%
λ^4F_λ (10^{-13} W cm^{-2} μm^3)
WAVELENGTH (μm)

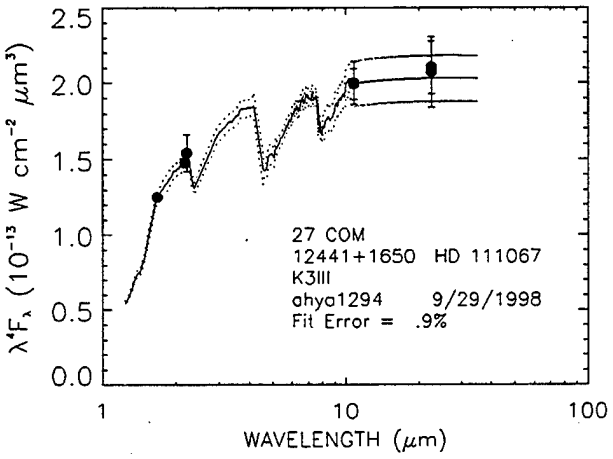
27 COM
12441+1650 HD 111067
K3III
ahya1294 9/29/1998
Fit Error = .9%
λ^4F_λ (10^{-13} W cm^{-2} μm^3)
WAVELENGTH (μm)

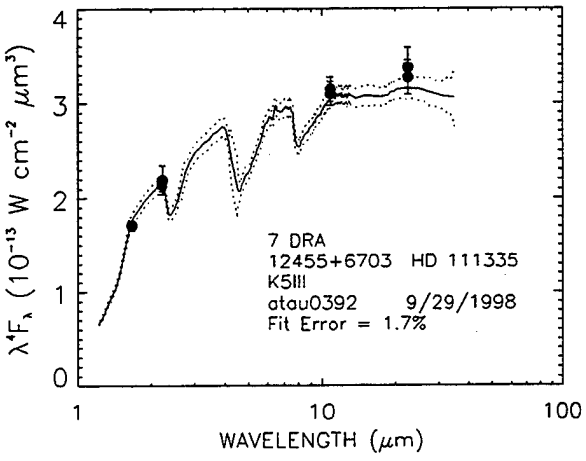
7 DRA
12455+6703 HD 111335
K5III
atau0392 9/29/1998
Fit Error = 1.7%
λ^4F_λ (10^{-13} W cm^{-2} μm^3)
WAVELENGTH (μm)

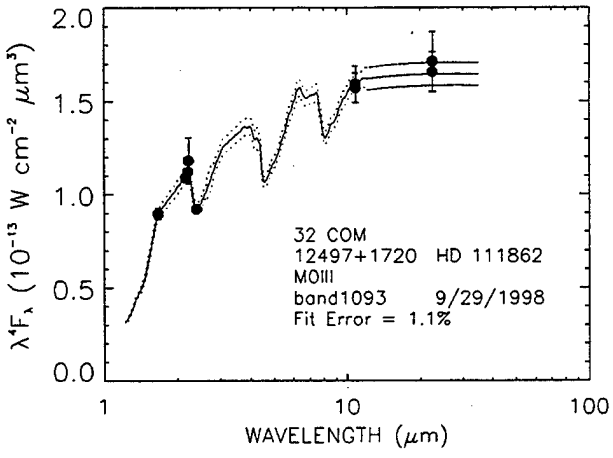
32 COM
12497+1720 HD 111862
MOIII
band1093 9/29/1998
Fit Error = 1.1%
λ^4F_λ (10^{-13} W cm^{-2} μm^3)
WAVELENGTH (μm)

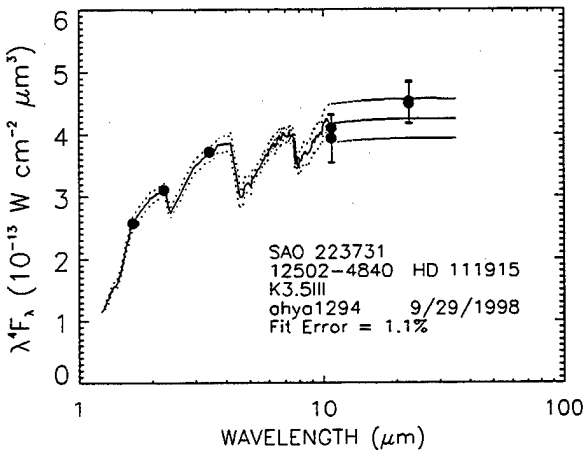
SAO 223731
12502-4840 HD 111915
K3.5III
ahya1294 9/29/1998
Fit Error = 1.1%
λ^4F_λ (10^{-13} W cm^{-2} μm^3)
WAVELENGTH (μm)

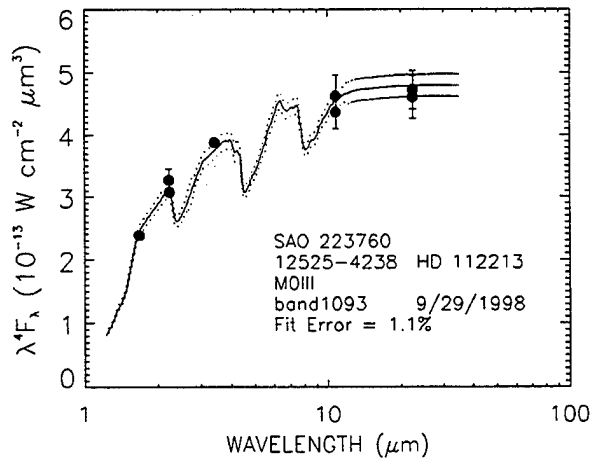
SAO 223760
12525-4238 HD 112213
MOIII
band1093 9/29/1998
Fit Error = 1.1%
λ^4F_λ (10^{-13} W cm^{-2} μm^3)
WAVELENGTH (μm)

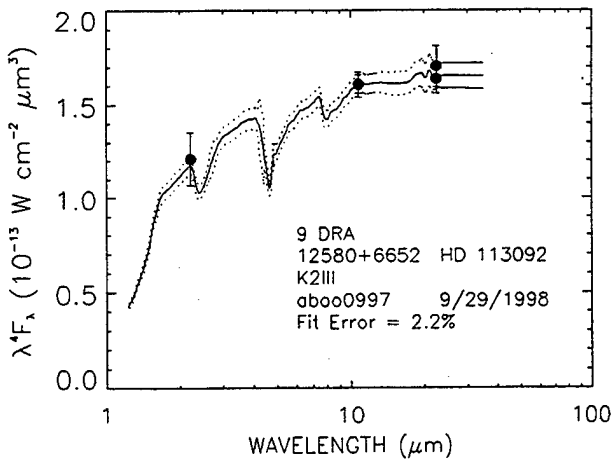
9 DRA
12580+6652 HD 113092
K2III
aboo0997 9/29/1998
Fit Error = 2.2%
λ^4F_λ (10^{-13} W cm^{-2} μm^3)
WAVELENGTH (μm)

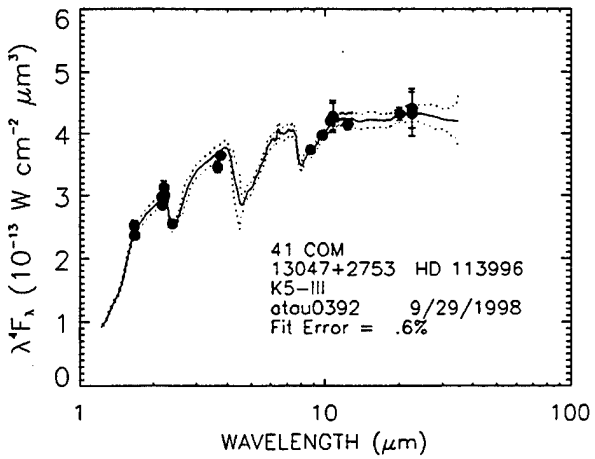
41 COM
13047+2753 HD 113996
K5-III
atau0392 9/29/1998
Fit Error = .6%
WAVELENGTH (μm)
λ⁴Fλ (10⁻¹³ W cm⁻² μm³)

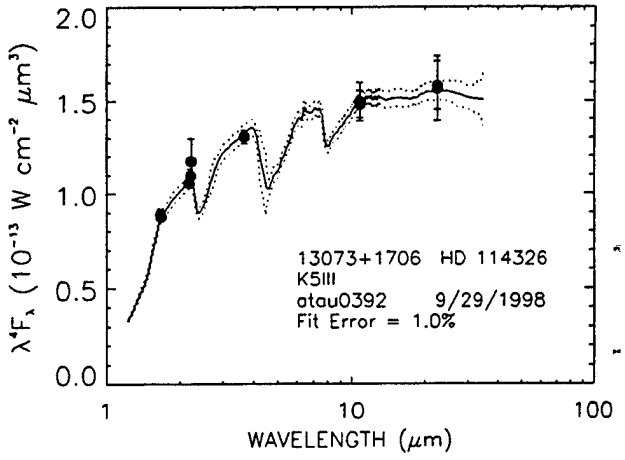
13073+1706 HD 114326
K5III
atau0392 9/29/1998
Fit Error = 1.0%
WAVELENGTH (μm)
λ⁴Fλ (10⁻¹³ W cm⁻² μm³)

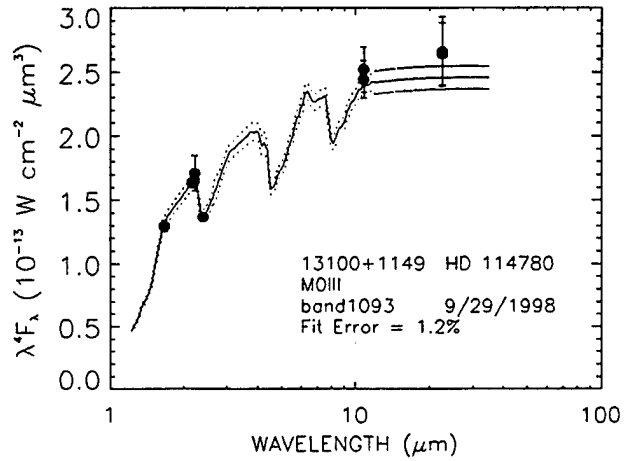
13100+1149 HD 114780
MOIII
band1093 9/29/1998
Fit Error = 1.2%
WAVELENGTH (μm)
λ⁴Fλ (10⁻¹³ W cm⁻² μm³)

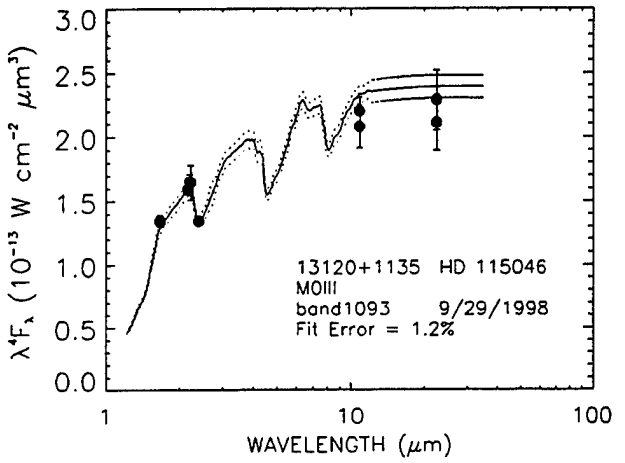
13120+1135 HD 115046
MOIII
band1093 9/29/1998
Fit Error = 1.2%
WAVELENGTH (μm)
λ⁴Fλ (10⁻¹³ W cm⁻² μm³)

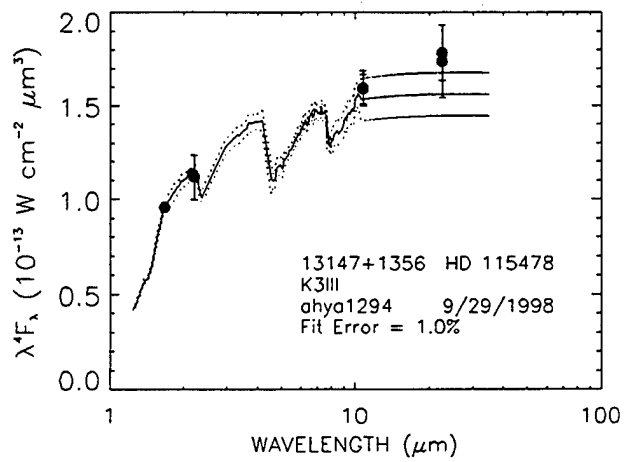
13147+1356 HD 115478
K3III
ahya1294 9/29/1998
Fit Error = 1.0%
WAVELENGTH (μm)
λ⁴Fλ (10⁻¹³ W cm⁻² μm³)

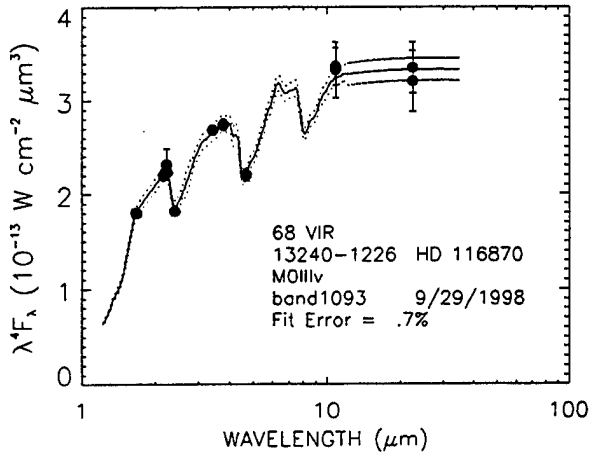
68 VIR
13240-1226 HD 116870
MOIIIv
band1093 9/29/1998
Fit Error = .7%
WAVELENGTH (μm)
λ⁴Fλ (10⁻¹³ W cm⁻² μm³)

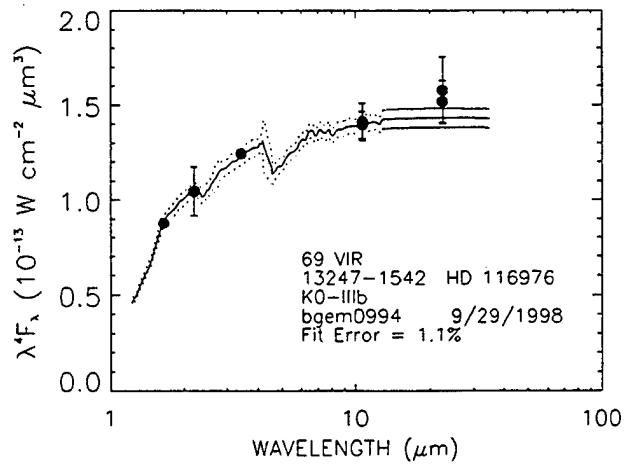
69 VIR
13247-1542 HD 116976
K0-IIIb
bgem0994 9/29/1998
Fit Error = 1.1%
WAVELENGTH (μm)
λ⁴Fλ (10⁻¹³ W cm⁻² μm³)

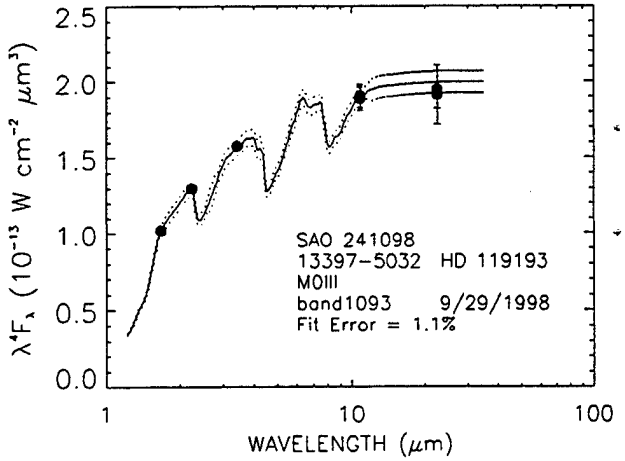
SAO 241098
13397-5032 HD 119193
MOIII
band1093 9/29/1998
Fit Error = 1.1%
WAVELENGTH (μm)
λ⁴Fλ (10⁻¹³ W cm⁻² μm³)

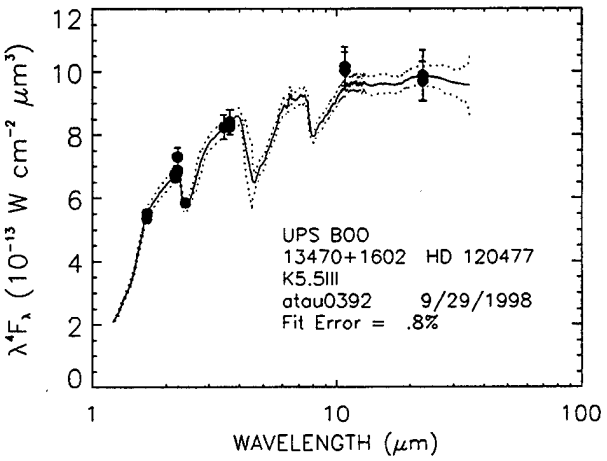
UPS BOO
13470+1602 HD 120477
K5.5III
atau0392 9/29/1998
Fit Error = .8%
λ^4F_λ (10^{-13} W cm^{-2} μm^3)
WAVELENGTH (μm)

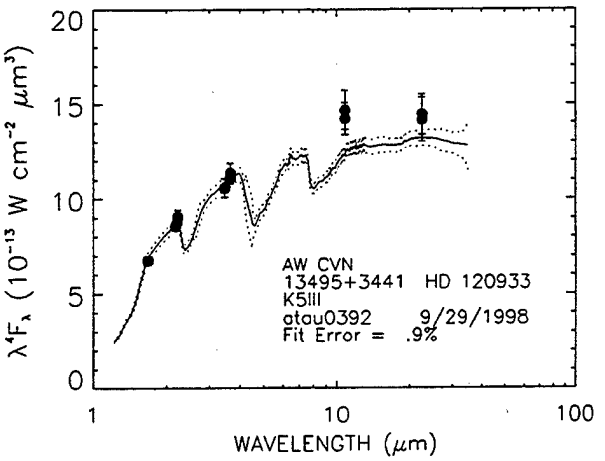
AW CVN
13495+3441 HD 120933
K5III
atau0392 9/29/1998
Fit Error = .9%
λ^4F_λ (10^{-13} W cm^{-2} μm^3)
WAVELENGTH (μm)

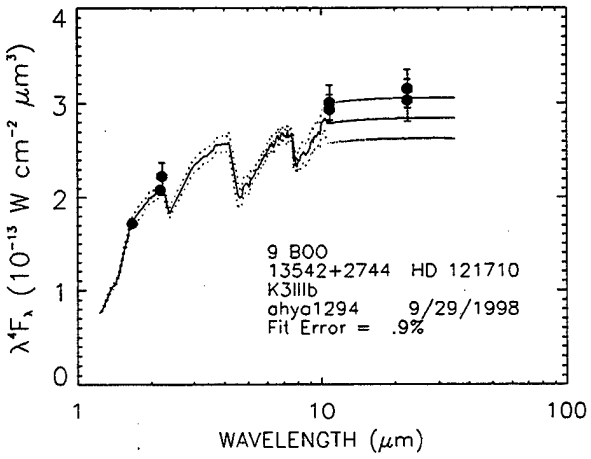
9 BOO
13542+2744 HD 121710
K3IIIb
ahya1294 9/29/1998
Fit Error = .9%
λ^4F_λ (10^{-13} W cm^{-2} μm^3)
WAVELENGTH (μm)

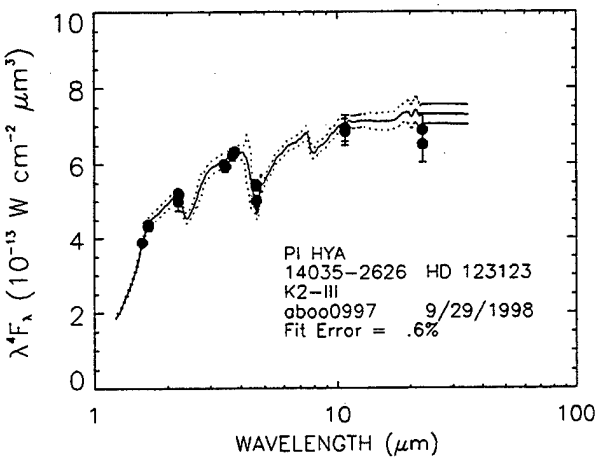
PI HYA
14035−2626 HD 123123
K2−III
aboo0997 9/29/1998
Fit Error = .6%
λ^4F_λ (10^{-13} W cm^{-2} μm^3)
WAVELENGTH (μm)

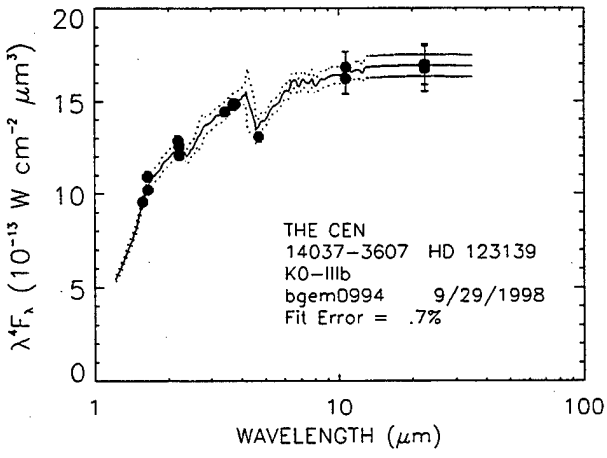
THE CEN
14037−3607 HD 123139
K0−IIIb
bgem0994 9/29/1998
Fit Error = .7%
λ^4F_λ (10^{-13} W cm^{-2} μm^3)
WAVELENGTH (μm)

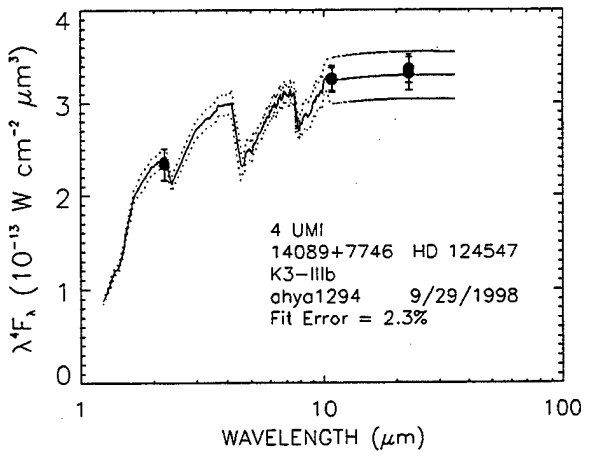
4 UMI
14089+7746 HD 124547
K3−IIIb
ahya1294 9/29/1998
Fit Error = 2.3%
λ^4F_λ (10^{-13} W cm^{-2} μm^3)
WAVELENGTH (μm)

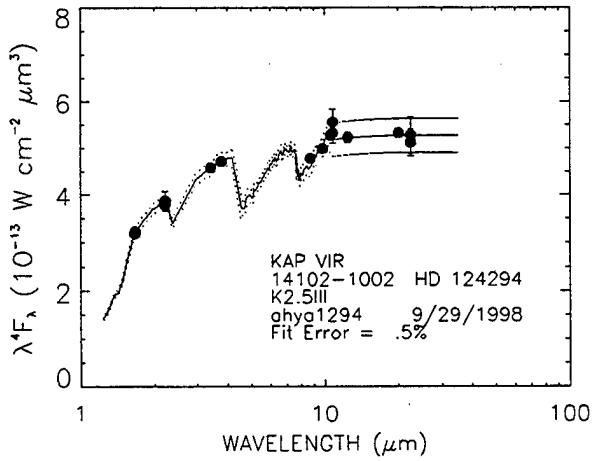
KAP VIR
14102−1002 HD 124294
K2.5III
ahya1294 9/29/1998
Fit Error = .5%
λ^4F_λ (10^{-13} W cm^{-2} μm^3)
WAVELENGTH (μm)

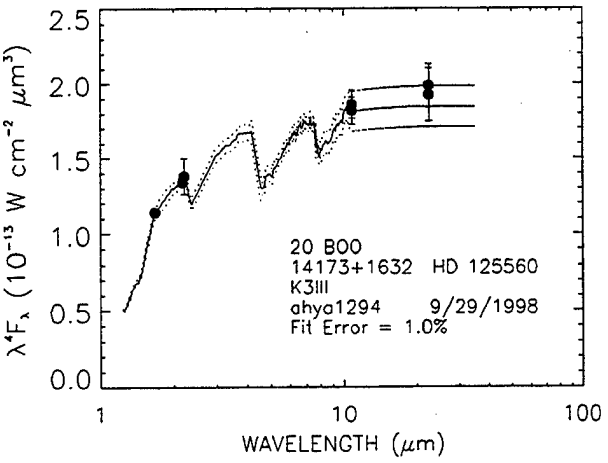
20 BOO
14173+1632 HD 125560
K3III
ahya1294 9/29/1998
Fit Error = 1.0%
λ^4F_λ (10^{-13} W cm^{-2} μm^3)
WAVELENGTH (μm)

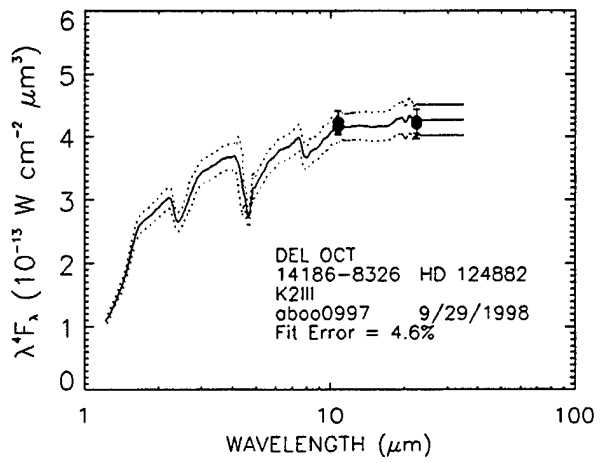
DEL OCT
14186-8326 HD 124882
K2III
aboo0997 9/29/1998
Fit Error = 4.6%
λ^4F_λ (10^{-13} W cm^{-2} μm^3)
WAVELENGTH (μm)

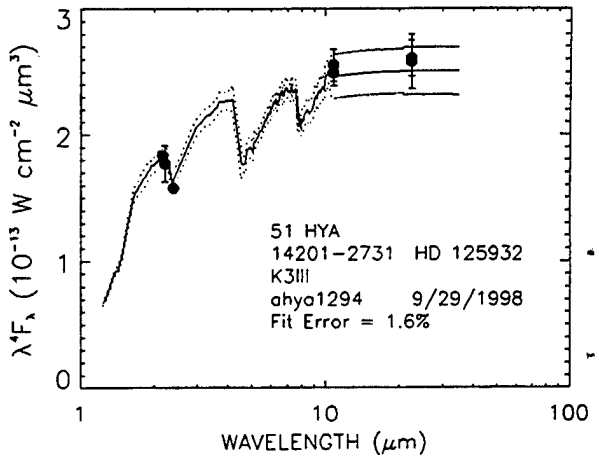
51 HYA
14201-2731 HD 125932
K3III
ahya1294 9/29/1998
Fit Error = 1.6%
λ^4F_λ (10^{-13} W cm^{-2} μm^3)
WAVELENGTH (μm)

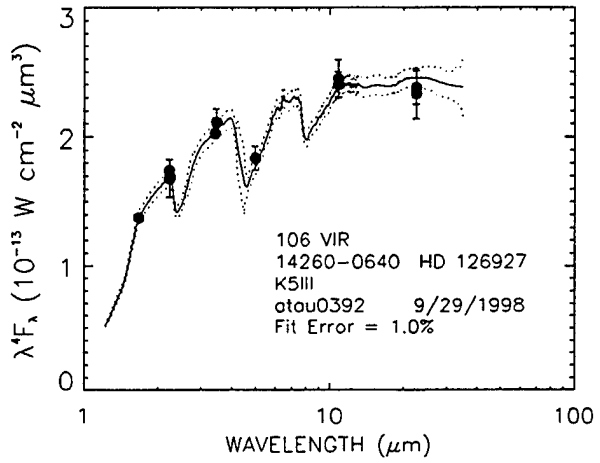
106 VIR
14260-0640 HD 126927
K5III
atau0392 9/29/1998
Fit Error = 1.0%
λ^4F_λ (10^{-13} W cm^{-2} μm^3)
WAVELENGTH (μm)

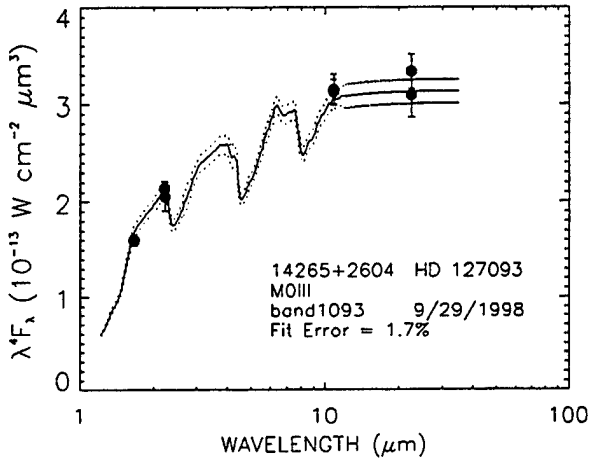
14265+2604 HD 127093
M0III
band1093 9/29/1998
Fit Error = 1.7%
λ^4F_λ (10^{-13} W cm^{-2} μm^3)
WAVELENGTH (μm)

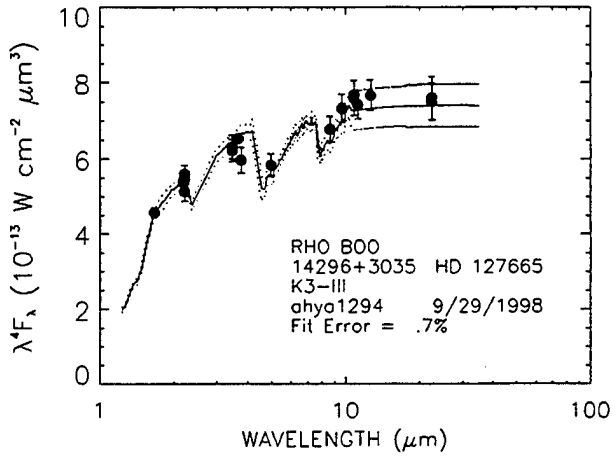
RHO BOO
14296+3035 HD 127665
K3-III
ahya1294 9/29/1998
Fit Error = .7%
λ^4F_λ (10^{-13} W cm^{-2} μm^3)
WAVELENGTH (μm)

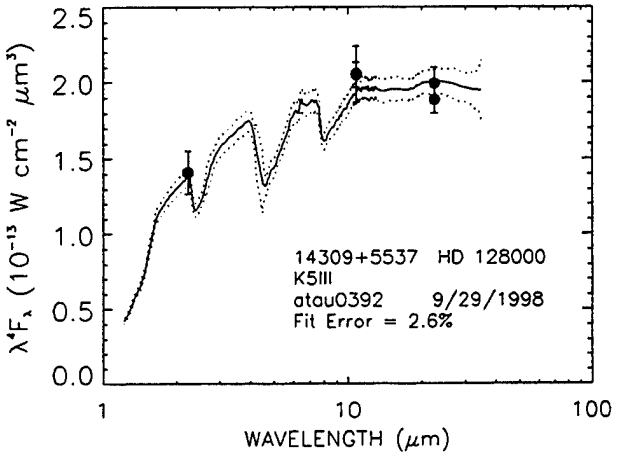
14309+5537 HD 128000
K5III
atau0392 9/29/1998
Fit Error = 2.6%
λ^4F_λ (10^{-13} W cm^{-2} μm^3)
WAVELENGTH (μm)

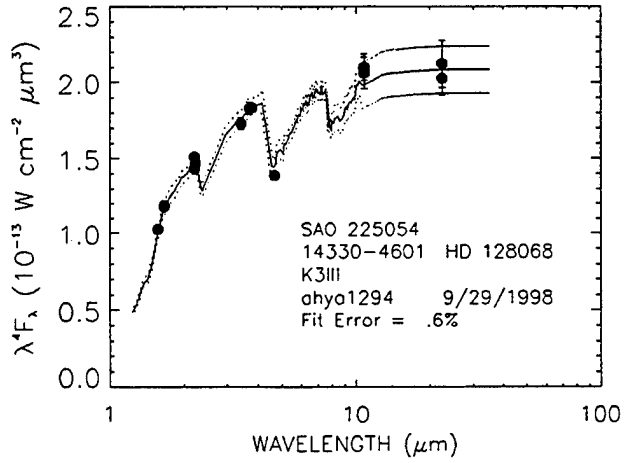
SAO 225054
14330-4601 HD 128068
K3III
ahya1294 9/29/1998
Fit Error = .6%
λ^4F_λ (10^{-13} W cm^{-2} μm^3)
WAVELENGTH (μm)

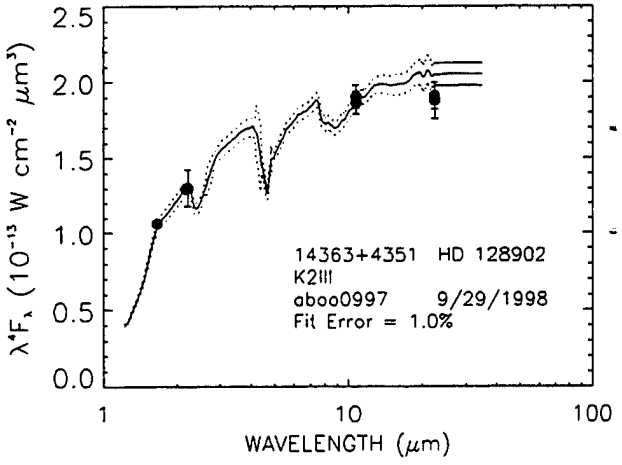
14363+4351 HD 128902
K2III
aboo0997 9/29/1998
Fit Error = 1.0%
λ^4F_λ (10^{-13} W cm^{-2} μm^3)
WAVELENGTH (μm)

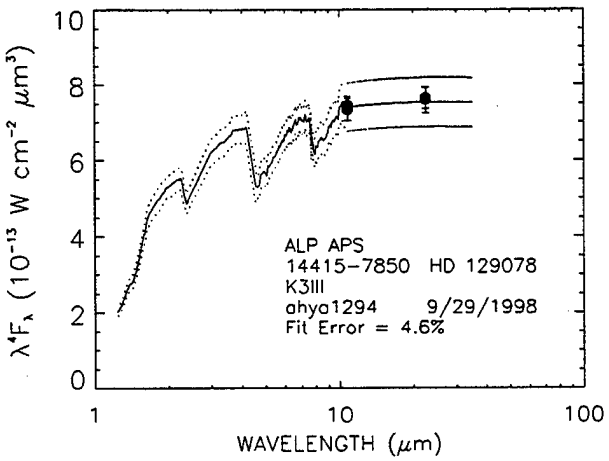
ALP APS
14415−7850 HD 129078
K3III
ahya1294 9/29/1998
Fit Error = 4.6%
WAVELENGTH (μm)

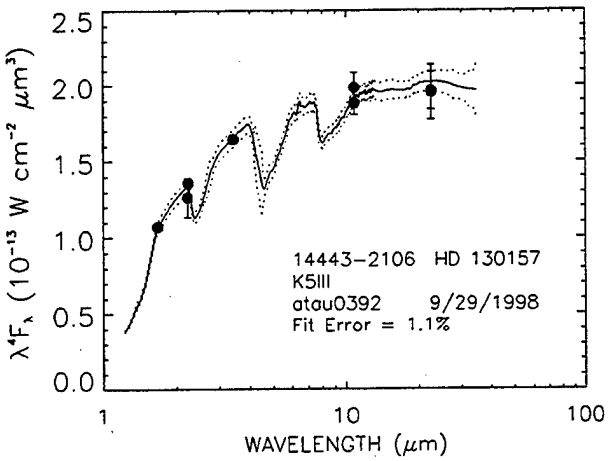
14443−2106 HD 130157
K5III
atau0392 9/29/1998
Fit Error = 1.1%
WAVELENGTH (μm)

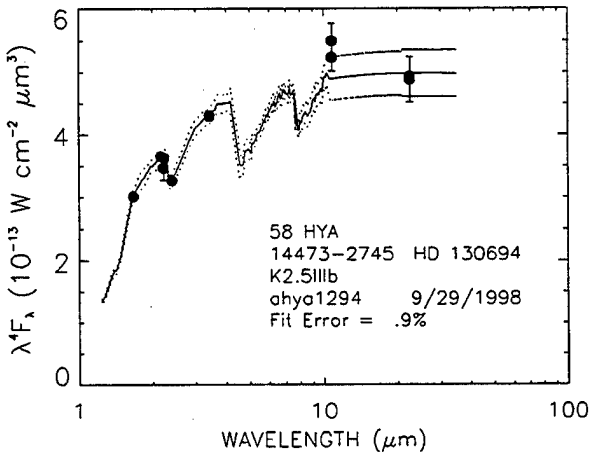
58 HYA
14473−2745 HD 130694
K2.5IIIb
ahya1294 9/29/1998
Fit Error = .9%
WAVELENGTH (μm)

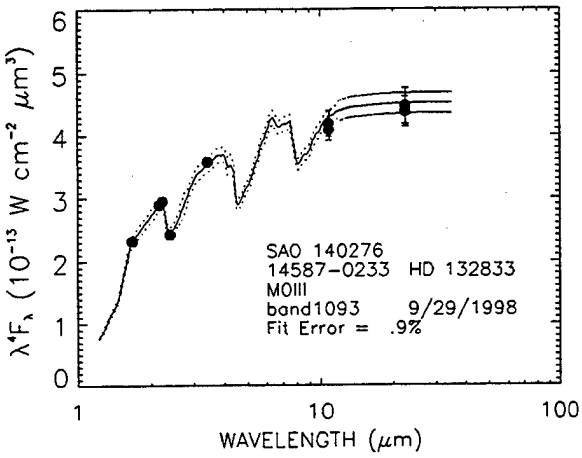
SAO 140276
14587−0233 HD 132833
MOIII
band1093 9/29/1998
Fit Error = .9%
WAVELENGTH (μm)

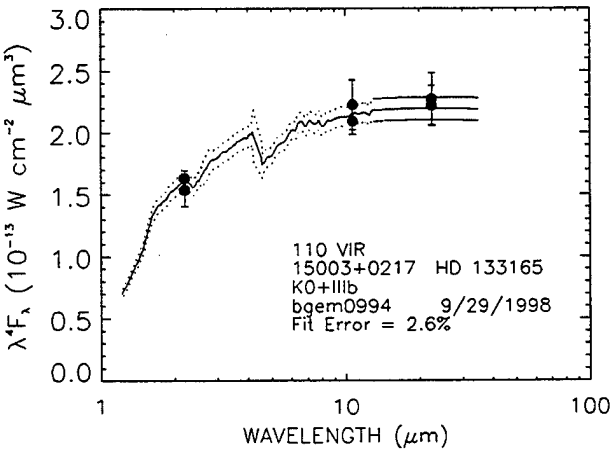
110 VIR
15003+0217 HD 133165
K0+IIIb
bgem0994 9/29/1998
Fit Error = 2.6%
WAVELENGTH (μm)

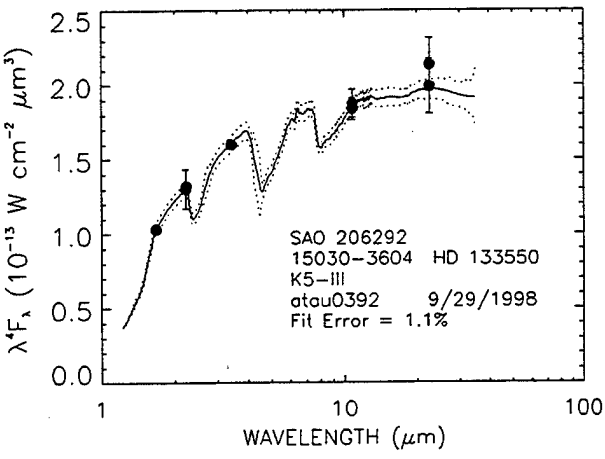
SAO 206292
15030−3604 HD 133550
K5−III
atau0392 9/29/1998
Fit Error = 1.1%
WAVELENGTH (μm)

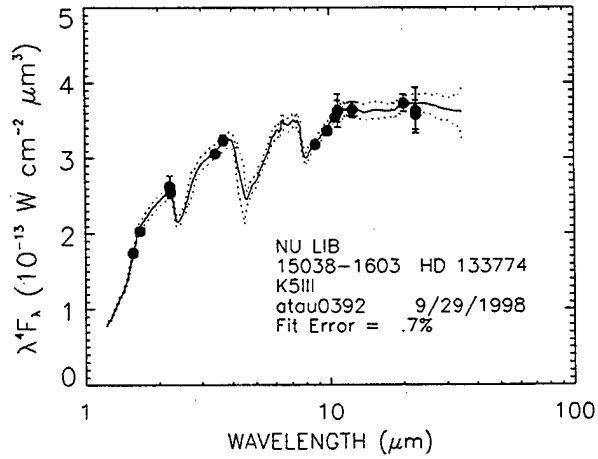
NU LIB
15038−1603 HD 133774
K5III
atau0392 9/29/1998
Fit Error = .7%
WAVELENGTH (μm)

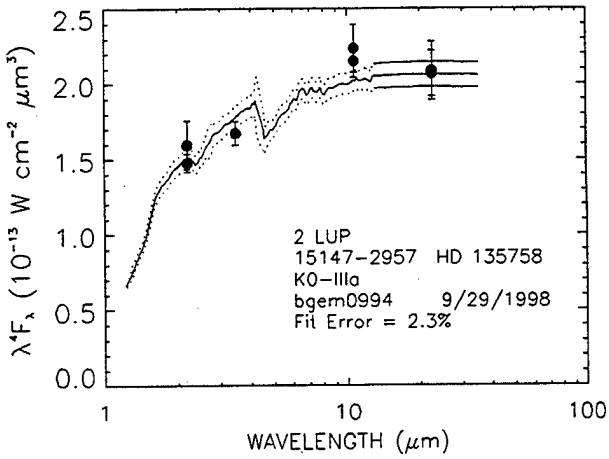
2 LUP
15147−2957 HD 135758
K0−IIIa
bgem0994 9/29/1998
Fit Error = 2.3%
WAVELENGTH (μm)

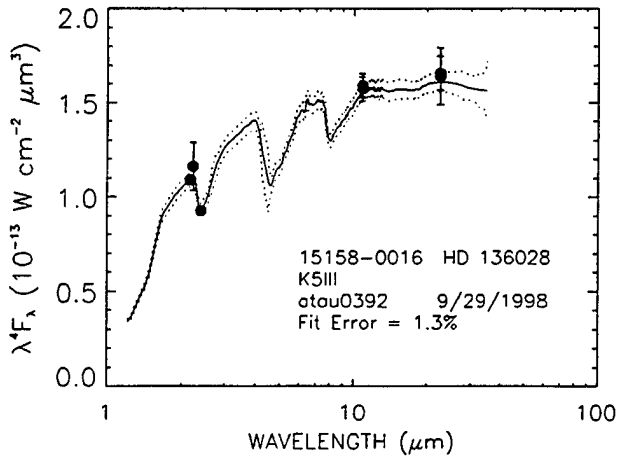
15158−0016 HD 136028
K5III
atau0392 9/29/1998
Fit Error = 1.3%
WAVELENGTH (μm)

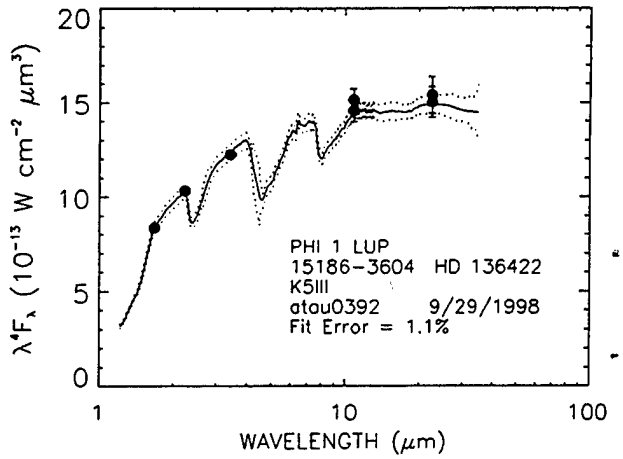
PHI 1 LUP
15186−3604 HD 136422
K5III
atau0392 9/29/1998
Fit Error = 1.1%
WAVELENGTH (μm)

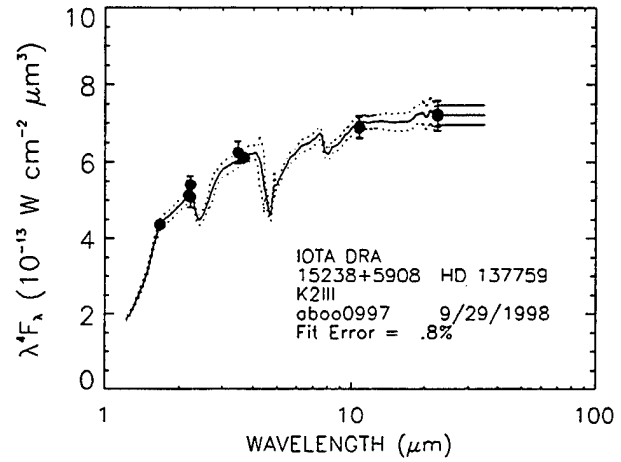
IOTA DRA
15238+5908 HD 137759
K2III
aboo0997 9/29/1998
Fit Error = .8%
WAVELENGTH (μm)

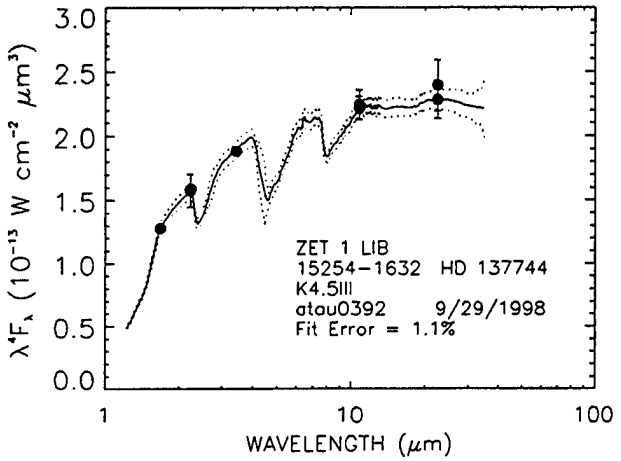
ZET 1 LIB
15254−1632 HD 137744
K4.5III
atau0392 9/29/1998
Fit Error = 1.1%
WAVELENGTH (μm)

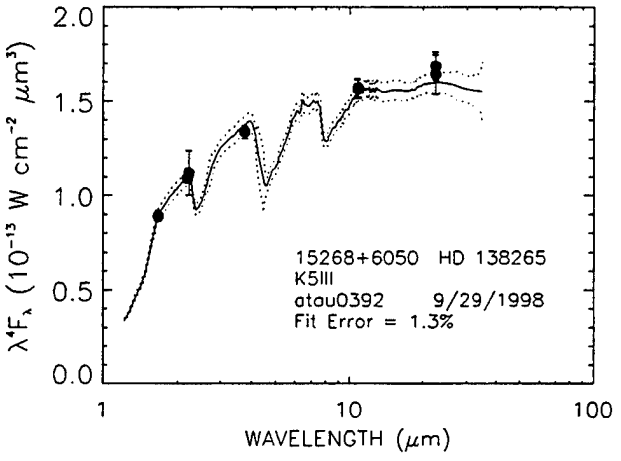
15268+6050 HD 138265
K5III
atau0392 9/29/1998
Fit Error = 1.3%
WAVELENGTH (μm)

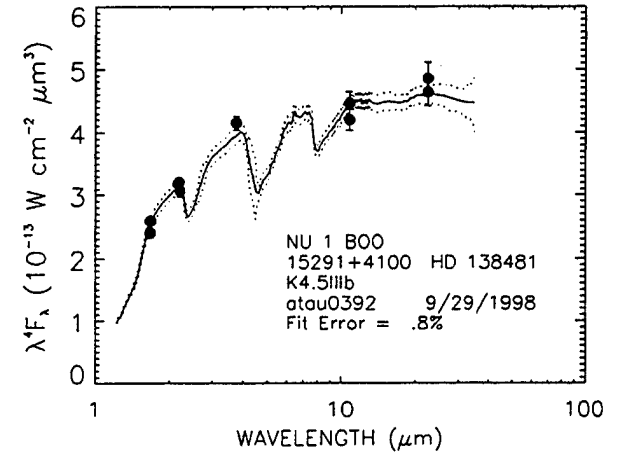
NU 1 BOO
15291+4100 HD 138481
K4.5IIIb
atau0392 9/29/1998
Fit Error = .8%
WAVELENGTH (μm)

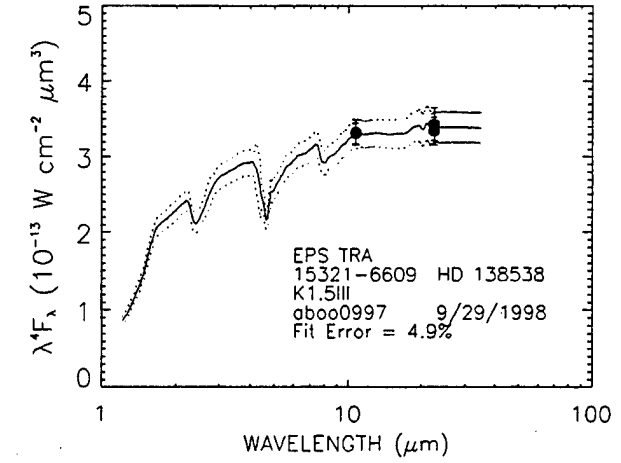
EPS TRA
15321−6609 HD 138538
K1.5III
aboo0997 9/29/1998
Fit Error = 4.9%
WAVELENGTH (μm)

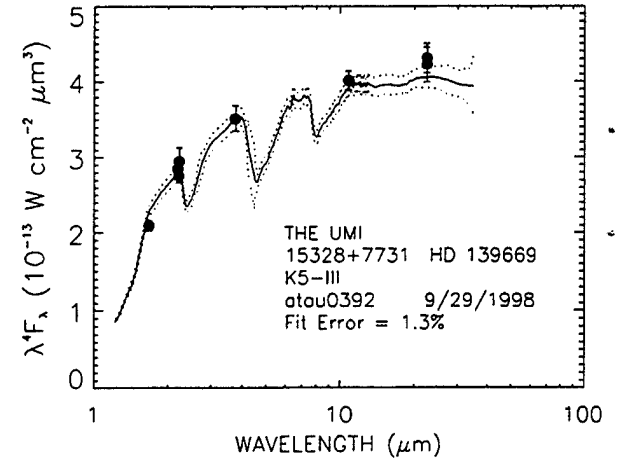
THE UMI
15328+7731 HD 139669
K5−III
atau0392 9/29/1998
Fit Error = 1.3%
WAVELENGTH (μm)

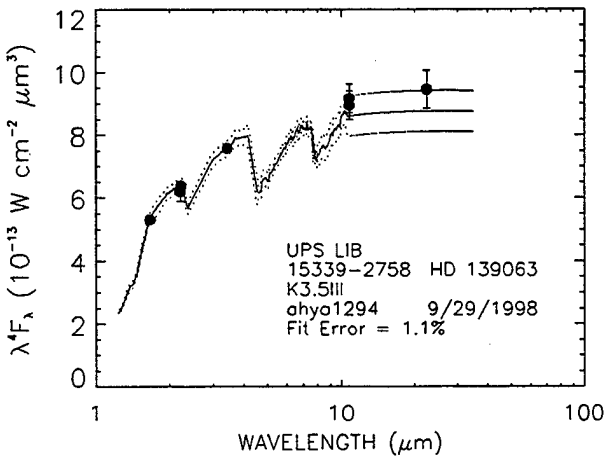
UPS LIB
15339-2758 HD 139063
K3.5III
ahya1294 9/29/1998
Fit Error = 1.1%
λ^4F_λ (10^{-13} W cm^{-2} μm^3)
WAVELENGTH (μm)

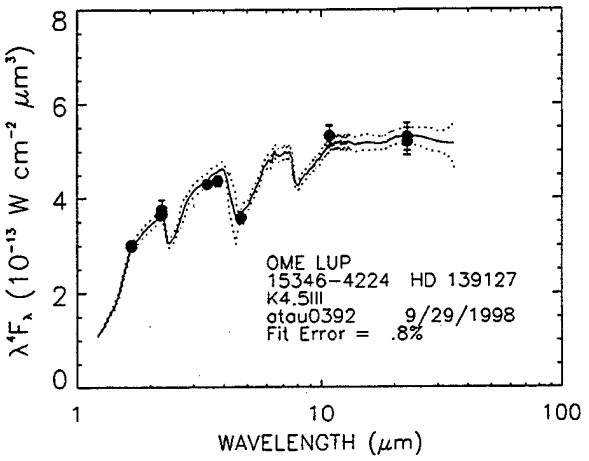
OME LUP
15346-4224 HD 139127
K4.5III
atau0392 9/29/1998
Fit Error = .8%
λ^4F_λ (10^{-13} W cm^{-2} μm^3)
WAVELENGTH (μm)

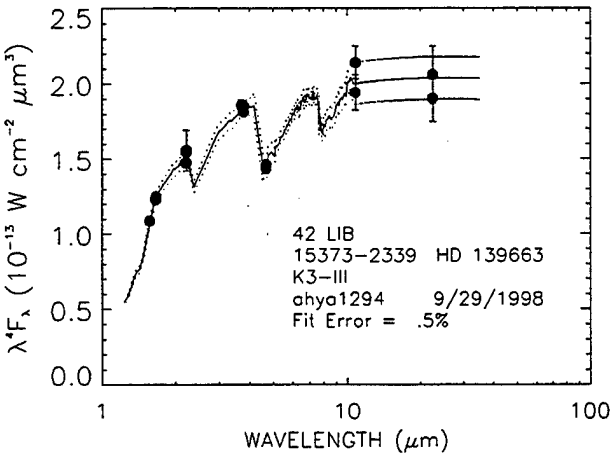
42 LIB
15373-2339 HD 139663
K3-III
ahya1294 9/29/1998
Fit Error = .5%
λ^4F_λ (10^{-13} W cm^{-2} μm^3)
WAVELENGTH (μm)

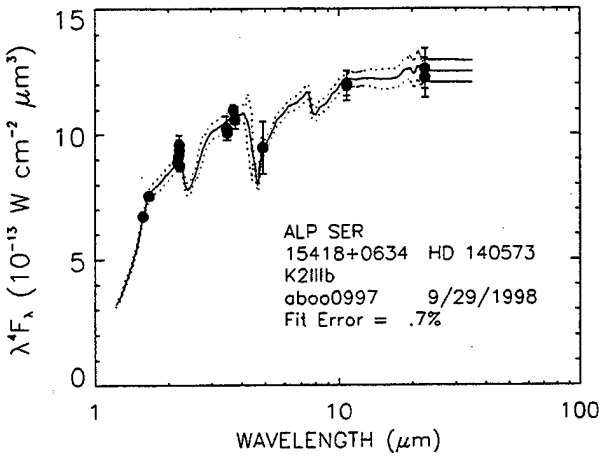
ALP SER
15418+0634 HD 140573
K2IIIb
aboo0997 9/29/1998
Fit Error = .7%
λ^4F_λ (10^{-13} W cm^{-2} μm^3)
WAVELENGTH (μm)

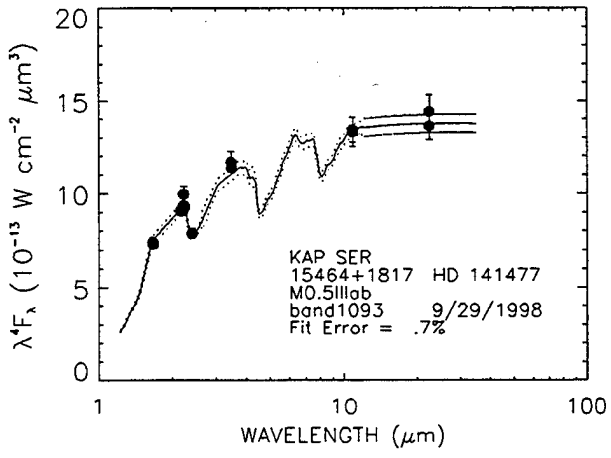
KAP SER
15464+1817 HD 141477
M0.5IIIab
band1093 9/29/1998
Fit Error = .7%
λ^4F_λ (10^{-13} W cm^{-2} μm^3)
WAVELENGTH (μm)

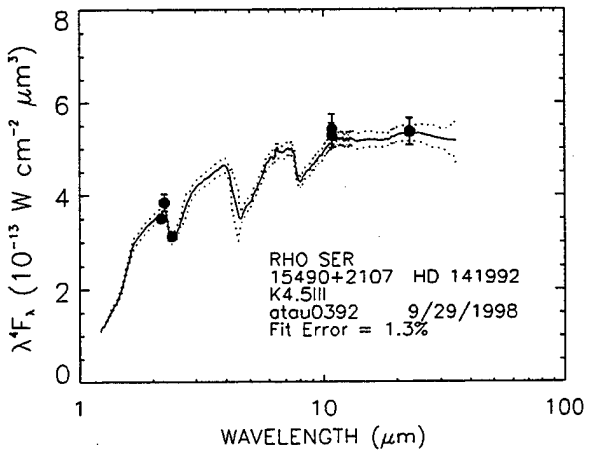
RHO SER
15490+2107 HD 141992
K4.5III
atau0392 9/29/1998
Fit Error = 1.3%
λ^4F_λ (10^{-13} W cm^{-2} μm^3)
WAVELENGTH (μm)

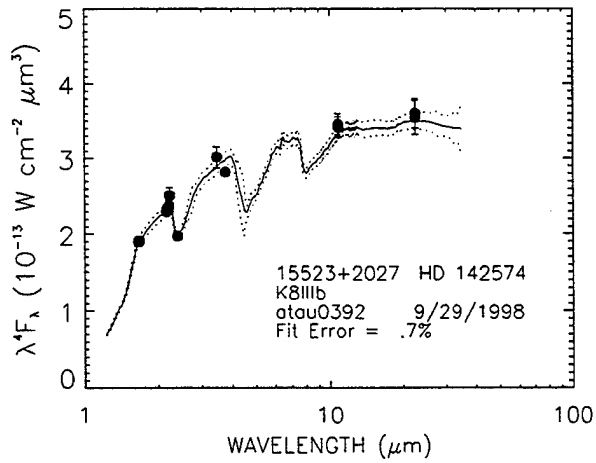
15523+2027 HD 142574
K8IIIb
atau0392 9/29/1998
Fit Error = .7%
λ^4F_λ (10^{-13} W cm^{-2} μm^3)
WAVELENGTH (μm)

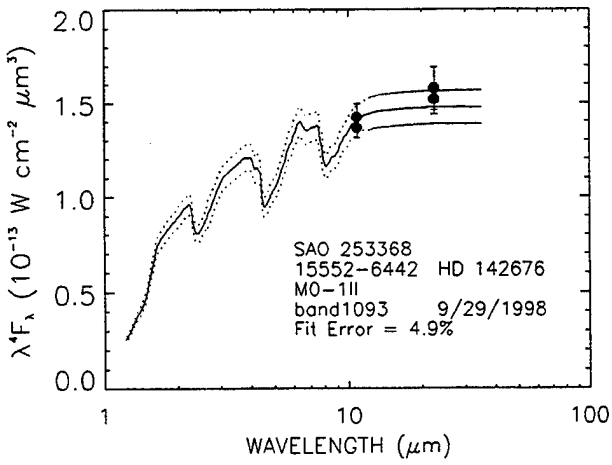
SAO 253368
15552-6442 HD 142676
M0-1II
band1093 9/29/1998
Fit Error = 4.9%
λ^4F_λ (10^{-13} W cm^{-2} μm^3)
WAVELENGTH (μm)

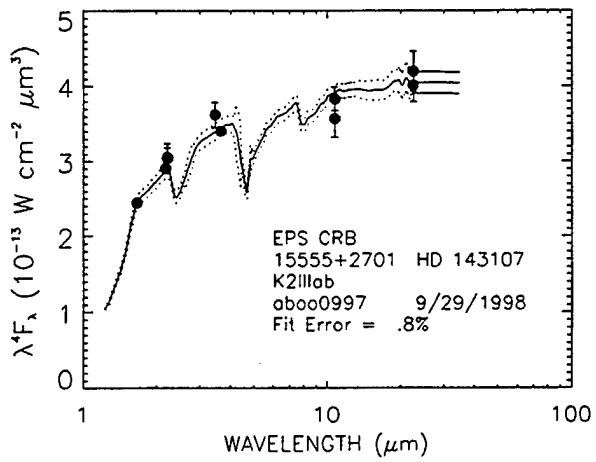
EPS CRB
15555+2701 HD 143107
K2IIIab
aboo0997 9/29/1998
Fit Error = .8%
WAVELENGTH (μm)

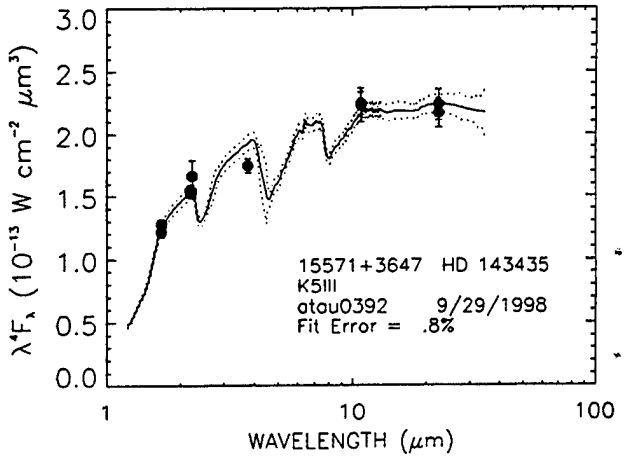
15571+3647 HD 143435
K5III
atau0392 9/29/1998
Fit Error = .8%
WAVELENGTH (μm)

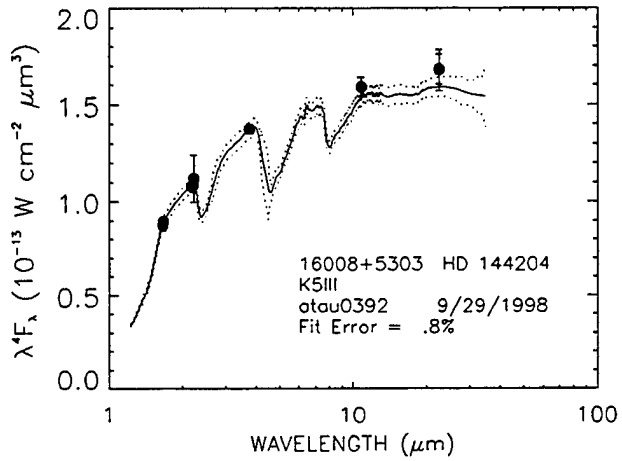
16008+5303 HD 144204
K5III
atau0392 9/29/1998
Fit Error = .8%
WAVELENGTH (μm)

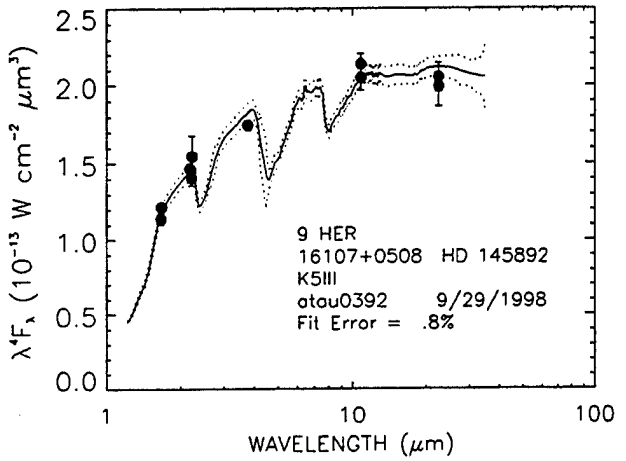
9 HER
16107+0508 HD 145892
K5III
atau0392 9/29/1998
Fit Error = .8%
WAVELENGTH (μm)

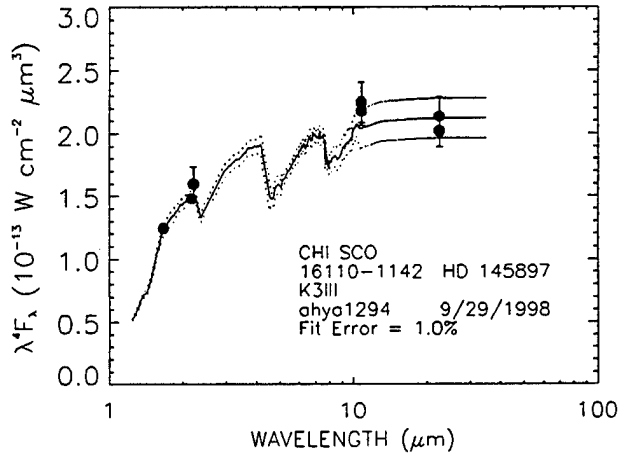
CHI SCO
16110-1142 HD 145897
K3III
ahya1294 9/29/1998
Fit Error = 1.0%
WAVELENGTH (μm)

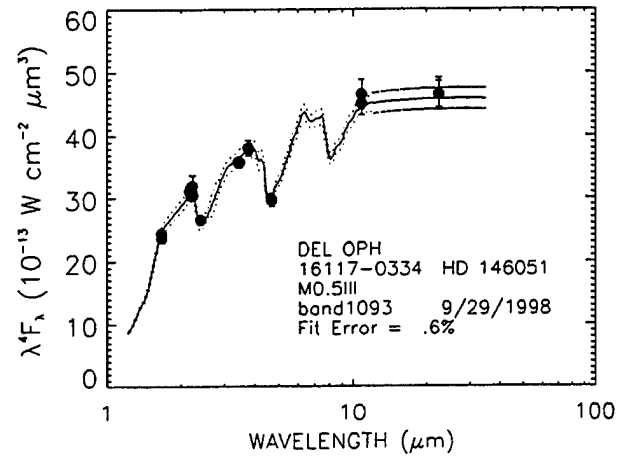
DEL OPH
16117-0334 HD 146051
M0.5III
band1093 9/29/1998
Fit Error = .6%
WAVELENGTH (μm)

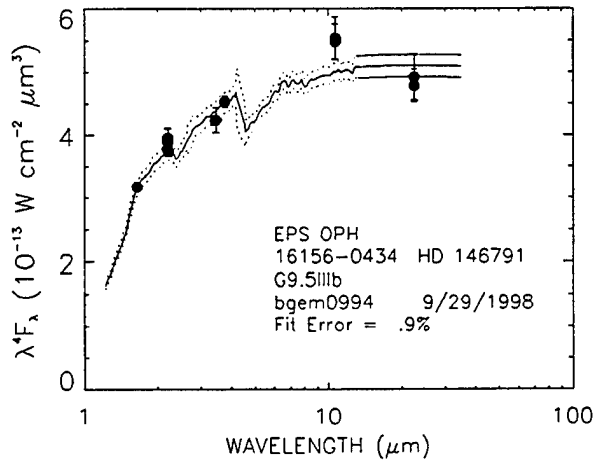
EPS OPH
16156-0434 HD 146791
G9.5IIIb
bgem0994 9/29/1998
Fit Error = .9%
WAVELENGTH (μm)

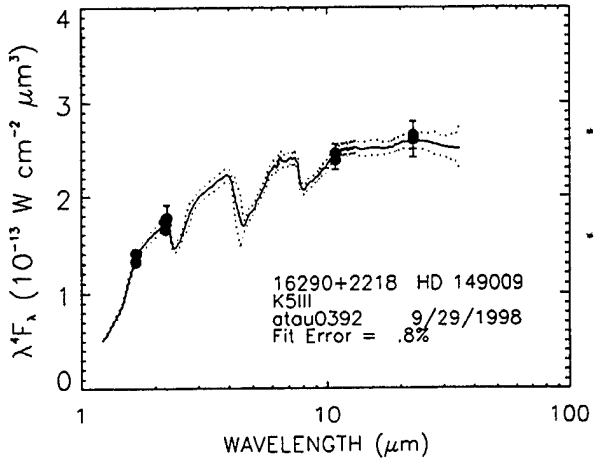
16290+2218 HD 149009
K5III
atau0392 9/29/1998
Fit Error = .8%
WAVELENGTH (μm)

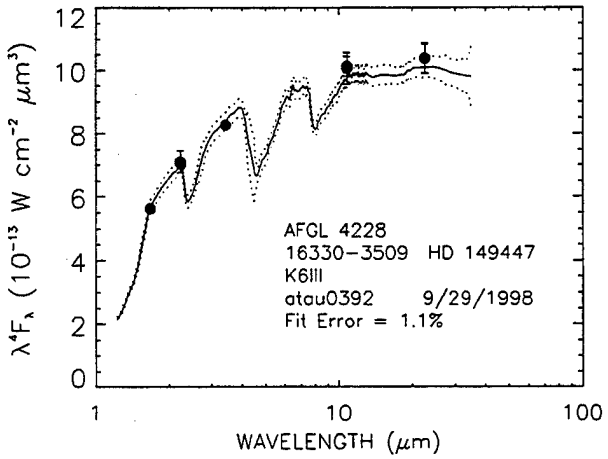
AFGL 4228
16330−3509 HD 149447
K6III
atau0392 9/29/1998
Fit Error = 1.1%
λ^4F_λ (10^{-13} W cm^{-2} μm^3)
WAVELENGTH (μm)

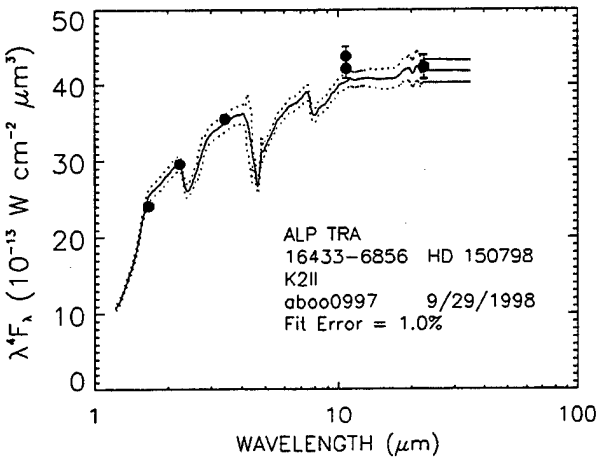
ALP TRA
16433−6856 HD 150798
K2II
aboo0997 9/29/1998
Fit Error = 1.0%
λ^4F_λ (10^{-13} W cm^{-2} μm^3)
WAVELENGTH (μm)

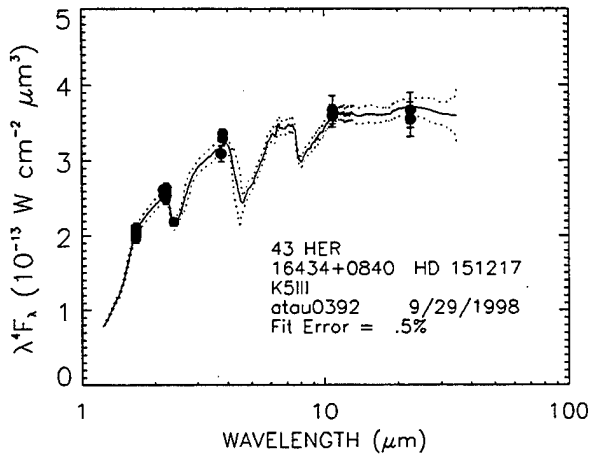
43 HER
16434+0840 HD 151217
K5III
atau0392 9/29/1998
Fit Error = .5%
λ^4F_λ (10^{-13} W cm^{-2} μm^3)
WAVELENGTH (μm)

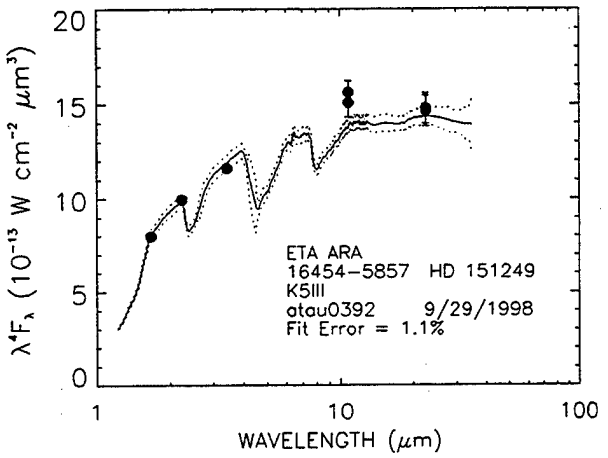
ETA ARA
16454−5857 HD 151249
K5III
atau0392 9/29/1998
Fit Error = 1.1%
λ^4F_λ (10^{-13} W cm^{-2} μm^3)
WAVELENGTH (μm)

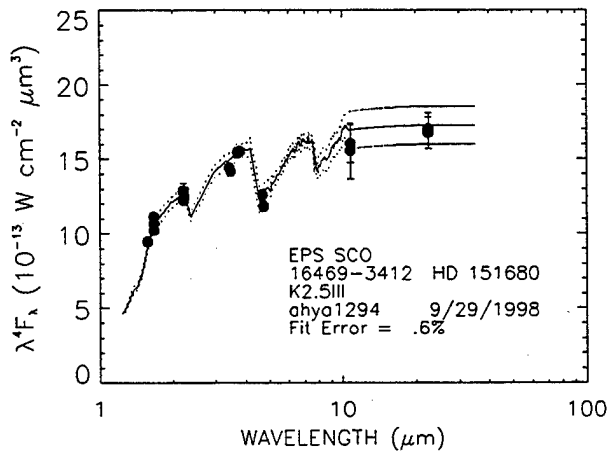
EPS SCO
16469−3412 HD 151680
K2.5III
ahya1294 9/29/1998
Fit Error = .6%
λ^4F_λ (10^{-13} W cm^{-2} μm^3)
WAVELENGTH (μm)

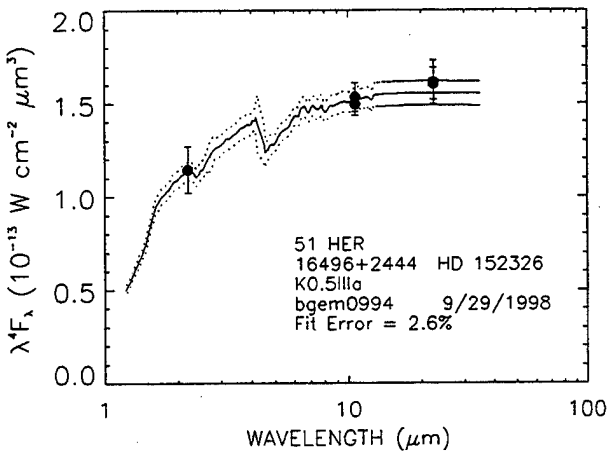
51 HER
16496+2444 HD 152326
K0.5IIIa
bgem0994 9/29/1998
Fit Error = 2.6%
λ^4F_λ (10^{-13} W cm^{-2} μm^3)
WAVELENGTH (μm)

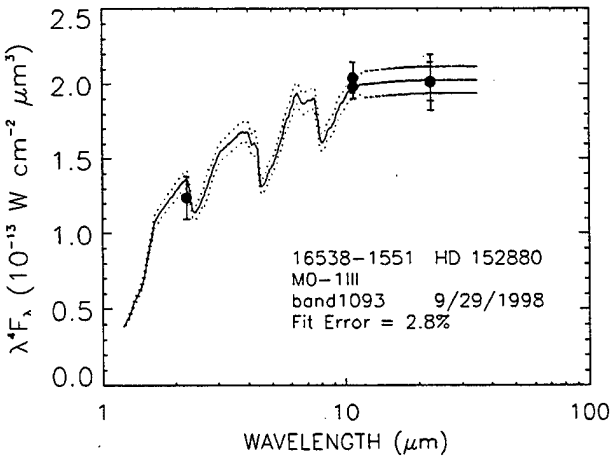
16538−1551 HD 152880
M0−1III
band1093 9/29/1998
Fit Error = 2.8%
λ^4F_λ (10^{-13} W cm^{-2} μm^3)
WAVELENGTH (μm)

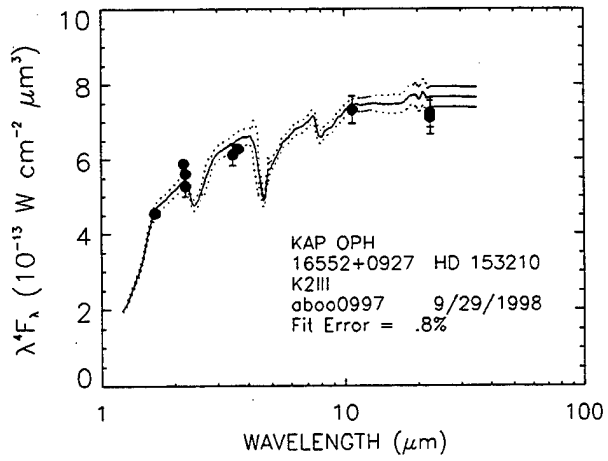
KAP OPH
16552+0927 HD 153210
K2III
aboo0997 9/29/1998
Fit Error = .8%
λ^4F_λ (10^{-13} W cm^{-2} μm^3)
WAVELENGTH (μm)

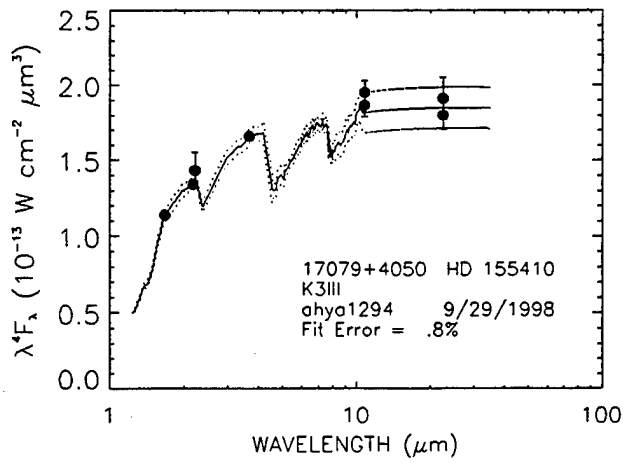
17079+4050 HD 155410
K3III
ahya1294 9/29/1998
Fit Error = .8%
WAVELENGTH (μm)

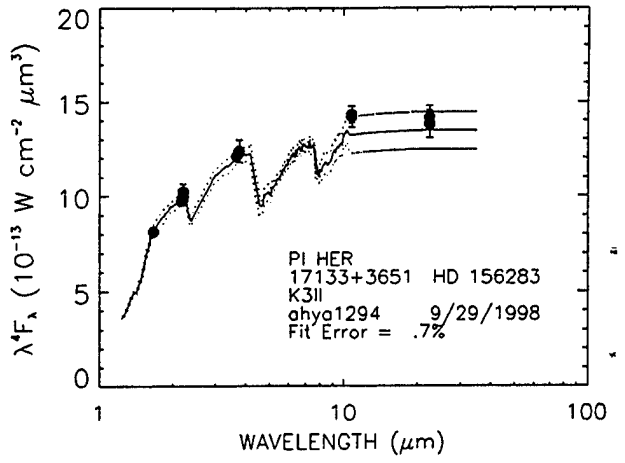
PI HER
17133+3651 HD 156283
K3II
ahya1294 9/29/1998
Fit Error = .7%
WAVELENGTH (μm)

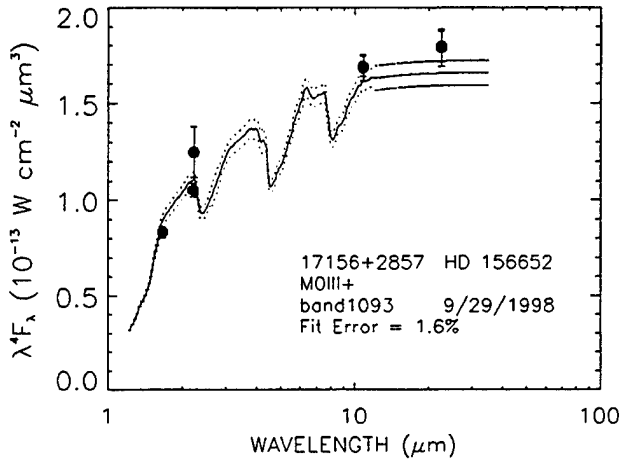
17156+2857 HD 156652
M0III+
band1093 9/29/1998
Fit Error = 1.6%
WAVELENGTH (μm)

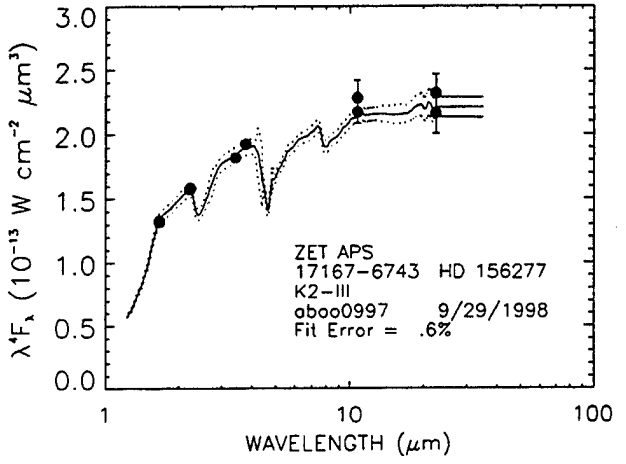
ZET APS
17167-6743 HD 156277
K2-III
aboo0997 9/29/1998
Fit Error = .6%
WAVELENGTH (μm)

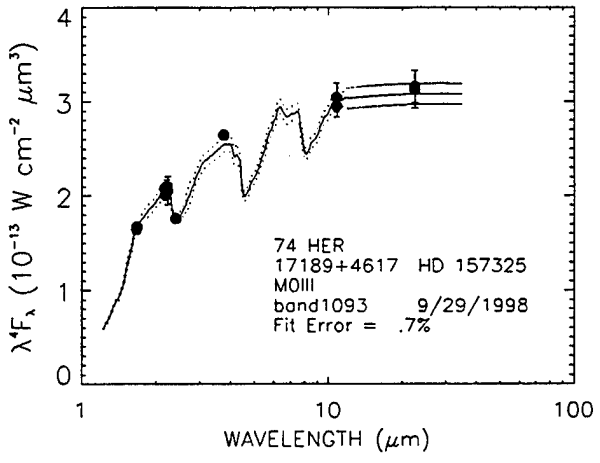
74 HER
17189+4617 HD 157325
M0III
band1093 9/29/1998
Fit Error = .7%
WAVELENGTH (μm)

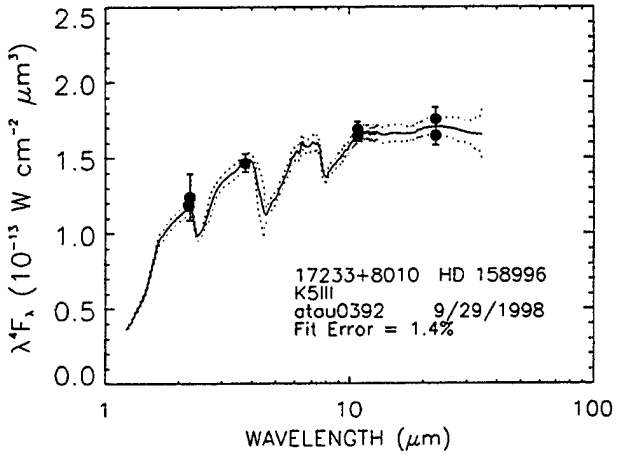
17233+8010 HD 158996
K5III
atau0392 9/29/1998
Fit Error = 1.4%
WAVELENGTH (μm)

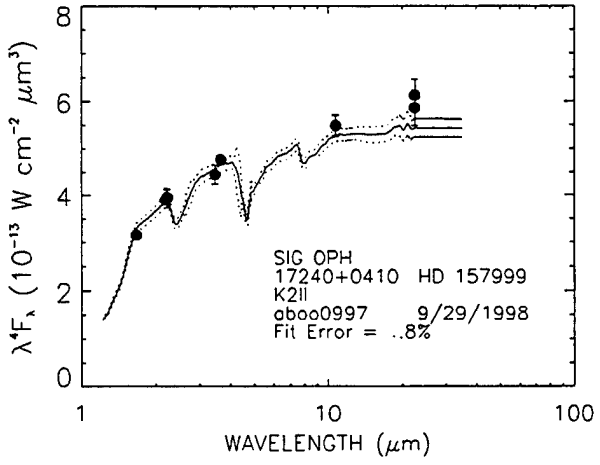
SIG OPH
17240+0410 HD 157999
K2II
aboo0997 9/29/1998
Fit Error = .8%
WAVELENGTH (μm)

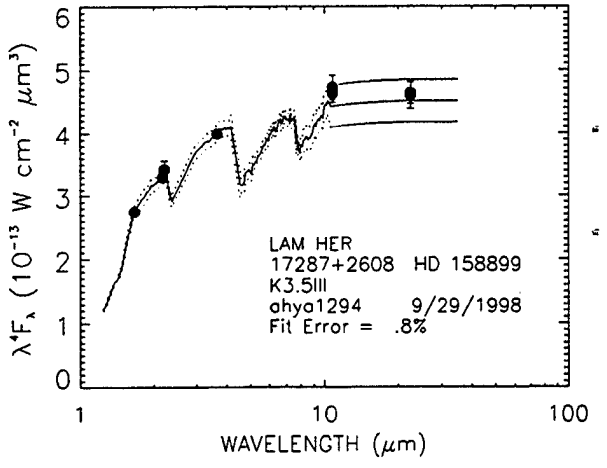
LAM HER
17287+2608 HD 158899
K3.5III
ahya1294 9/29/1998
Fit Error = .8%
WAVELENGTH (μm)

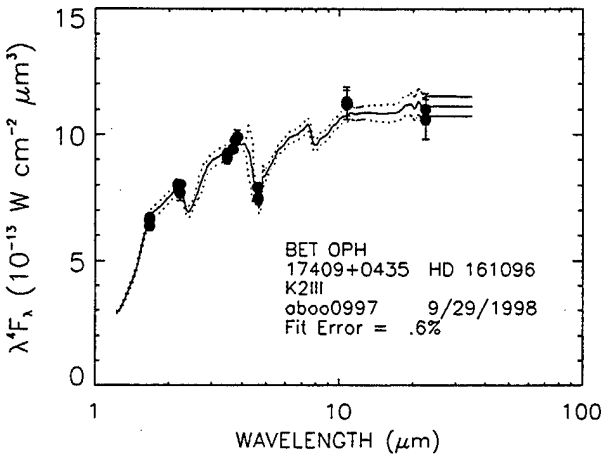
BET OPH
17409+0435 HD 161096
K2III
aboo0997 9/29/1998
Fit Error = .6%
λ^4F_λ (10^{-13} W cm^{-2} μm^3)
WAVELENGTH (μm)

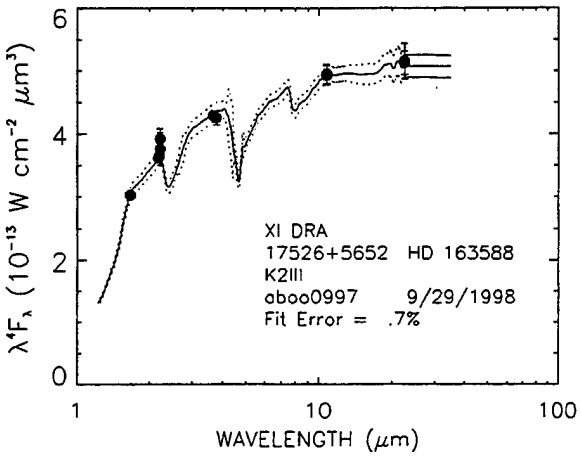
XI DRA
17526+5652 HD 163588
K2III
aboo0997 9/29/1998
Fit Error = .7%
λ^4F_λ (10^{-13} W cm^{-2} μm^3)
WAVELENGTH (μm)

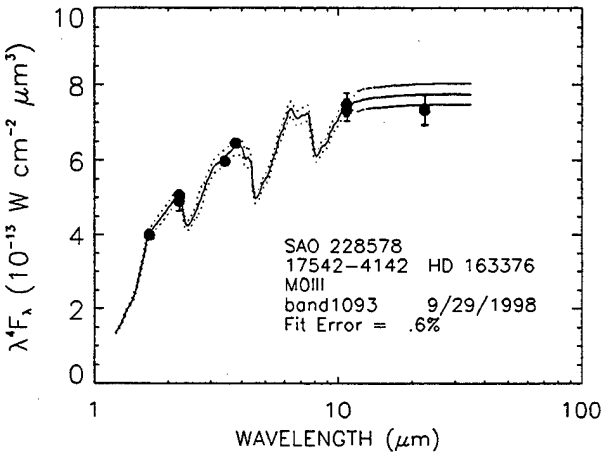
SAO 228578
17542−4142 HD 163376
MOIII
band1093 9/29/1998
Fit Error = .6%
λ^4F_λ (10^{-13} W cm^{-2} μm^3)
WAVELENGTH (μm)

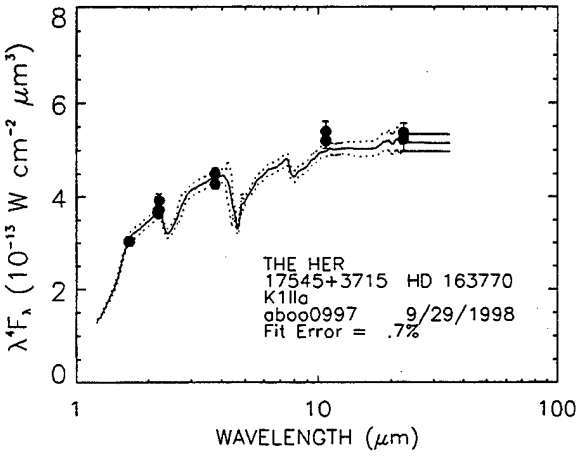
THE HER
17545+3715 HD 163770
K1IIa
aboo0997 9/29/1998
Fit Error = .7%
λ^4F_λ (10^{-13} W cm^{-2} μm^3)
WAVELENGTH (μm)

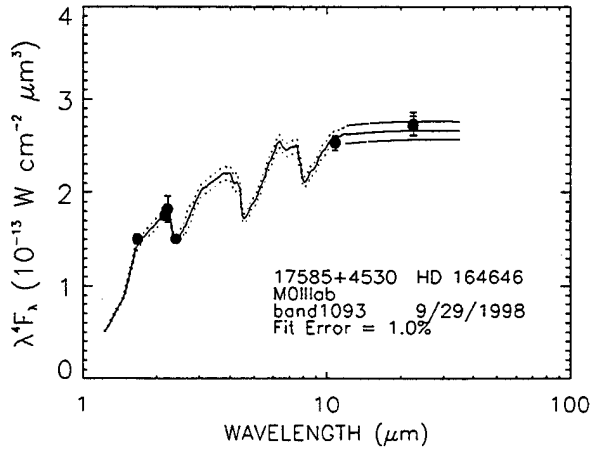
17585+4530 HD 164646
MOIIIab
band1093 9/29/1998
Fit Error = 1.0%
λ^4F_λ (10^{-13} W cm^{-2} μm^3)
WAVELENGTH (μm)

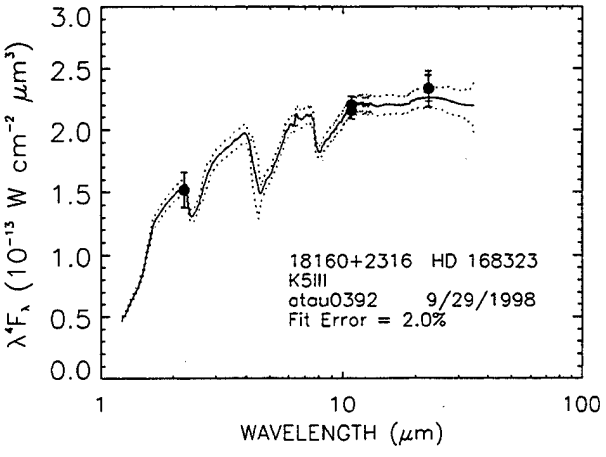
18160+2316 HD 168323
K5III
atau0392 9/29/1998
Fit Error = 2.0%
λ^4F_λ (10^{-13} W cm^{-2} μm^3)
WAVELENGTH (μm)

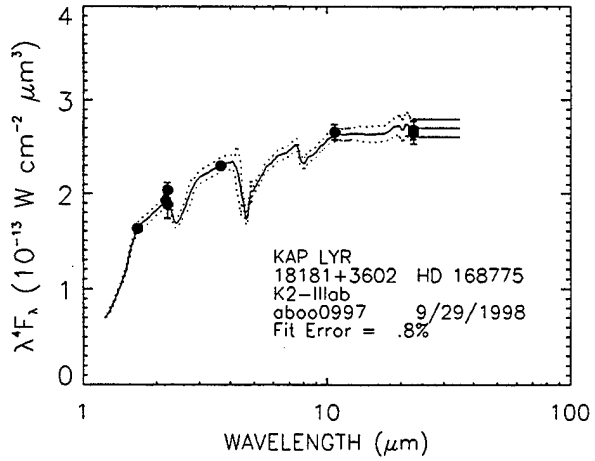
KAP LYR
18181+3602 HD 168775
K2−IIIab
aboo0997 9/29/1998
Fit Error = .8%
λ^4F_λ (10^{-13} W cm^{-2} μm^3)
WAVELENGTH (μm)

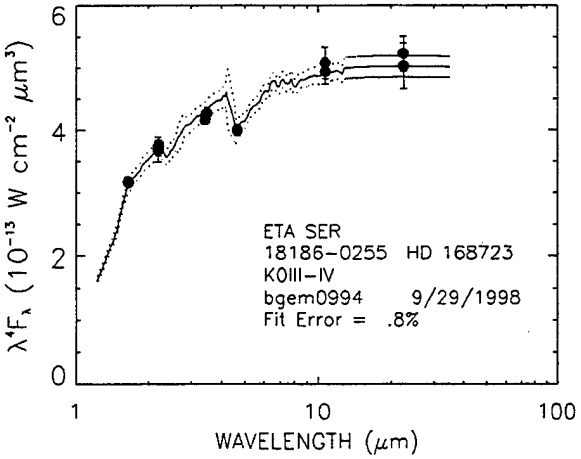
ETA SER
18186−0255 HD 168723
KOIII−IV
bgem0994 9/29/1998
Fit Error = .8%
λ^4F_λ (10^{-13} W cm^{-2} μm^3)
WAVELENGTH (μm)

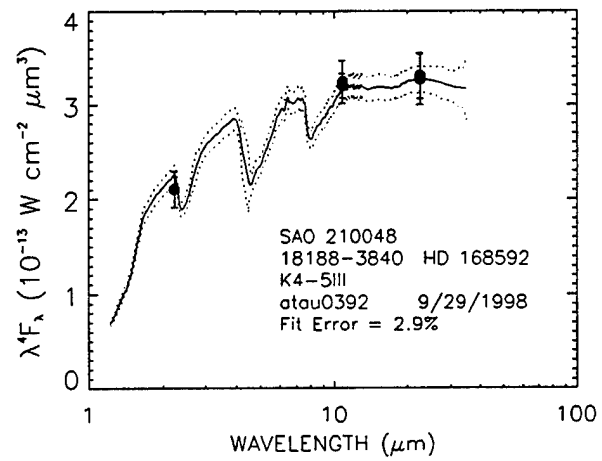
SAO 210048
18188-3840 HD 168592
K4-5III
atau0392 9/29/1998
Fit Error = 2.9%
WAVELENGTH (μm)

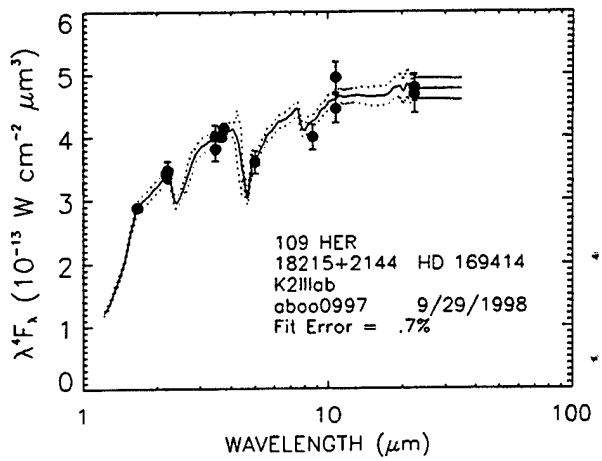
109 HER
18215+2144 HD 169414
K2IIIab
aboo0997 9/29/1998
Fit Error = .7%
WAVELENGTH (μm)

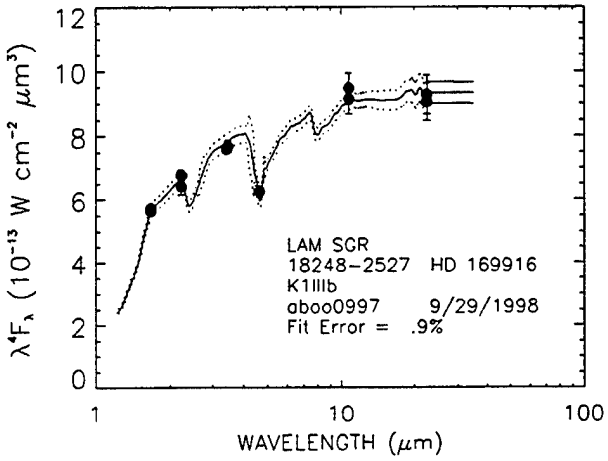
LAM SGR
18248-2527 HD 169916
K1IIIb
aboo0997 9/29/1998
Fit Error = .9%
WAVELENGTH (μm)

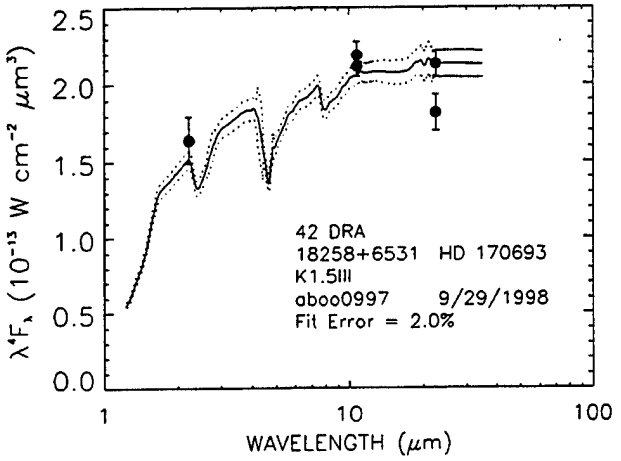
42 DRA
18258+6531 HD 170693
K1.5III
aboo0997 9/29/1998
Fit Error = 2.0%
WAVELENGTH (μm)

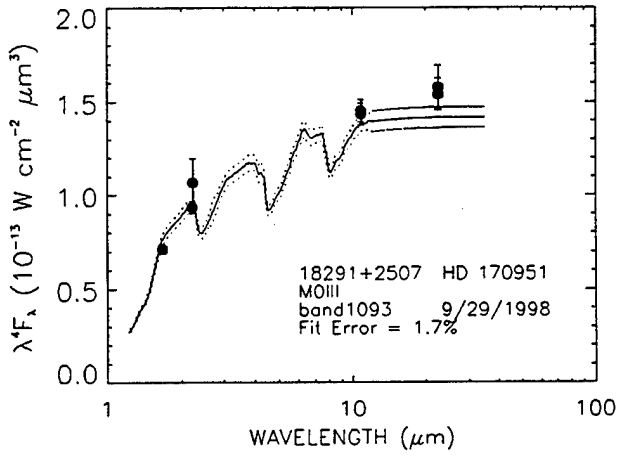
18291+2507 HD 170951
M0III
band1093 9/29/1998
Fit Error = 1.7%
WAVELENGTH (μm)

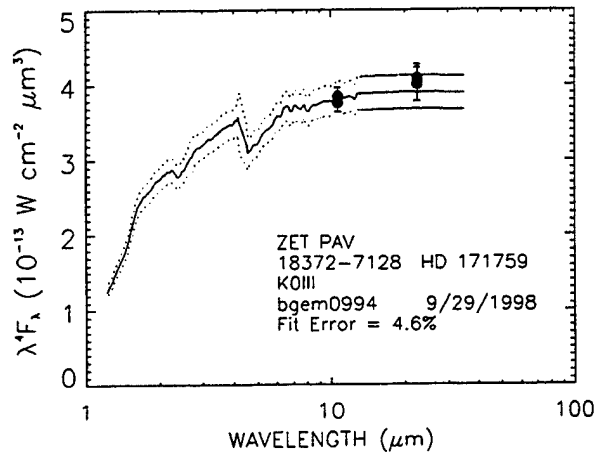
ZET PAV
18372-7128 HD 171759
K0III
bgem0994 9/29/1998
Fit Error = 4.6%
WAVELENGTH (μm)

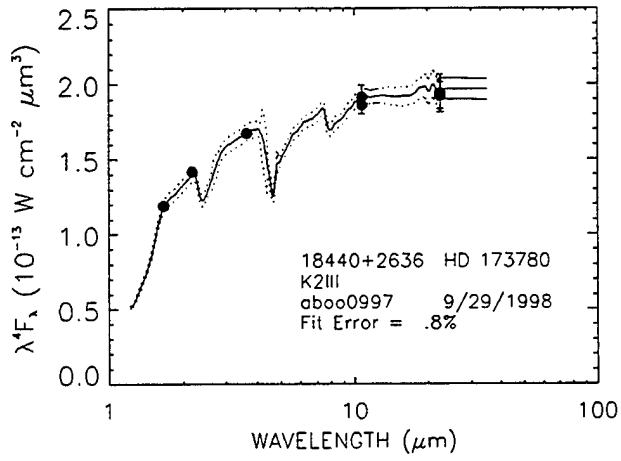
18440+2636 HD 173780
K2III
aboo0997 9/29/1998
Fit Error = .8%
WAVELENGTH (μm)

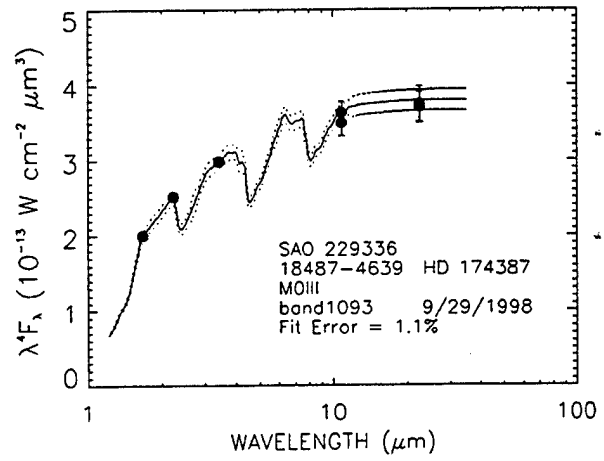
SAO 229336
18487-4639 HD 174387
M0III
band1093 9/29/1998
Fit Error = 1.1%
WAVELENGTH (μm)

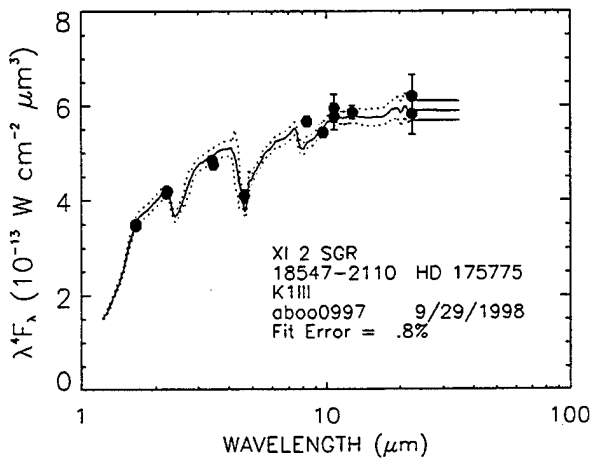
XI 2 SGR
18547-2110 HD 175775
K1III
aboo0997 9/29/1998
Fit Error = .8%
λ^4F_λ (10^{-13} W cm^{-2} μm^3)
WAVELENGTH (μm)

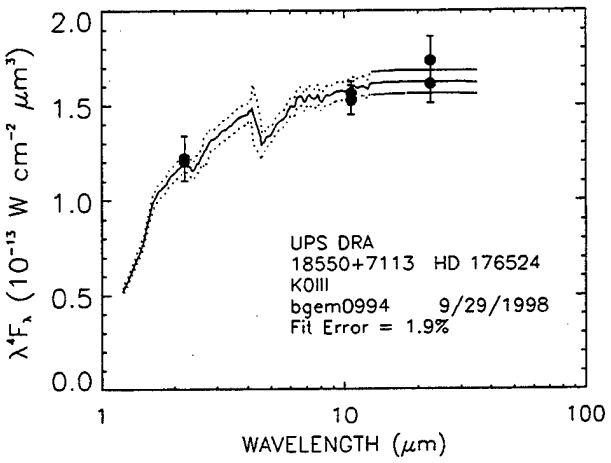
UPS DRA
18550+7113 HD 176524
KOIII
bgem0994 9/29/1998
Fit Error = 1.9%
λ^4F_λ (10^{-13} W cm^{-2} μm^3)
WAVELENGTH (μm)

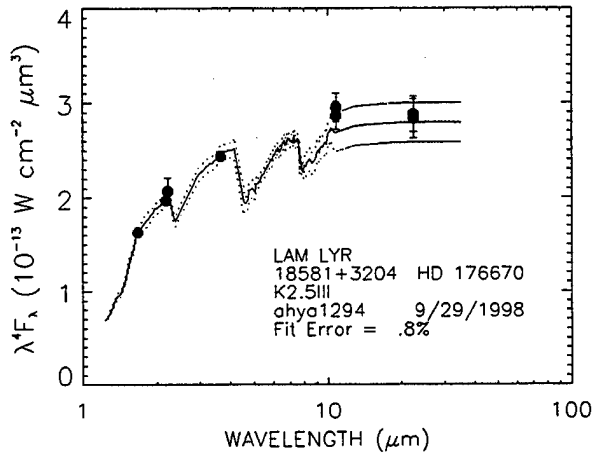
LAM LYR
18581+3204 HD 176670
K2.5III
ahya1294 9/29/1998
Fit Error = .8%
λ^4F_λ (10^{-13} W cm^{-2} μm^3)
WAVELENGTH (μm)

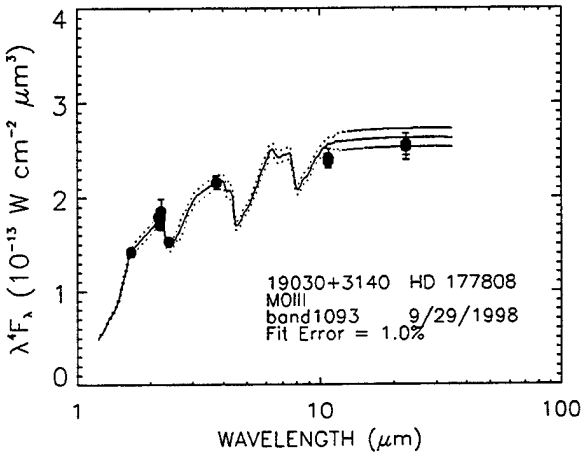
19030+3140 HD 177808
MOIII
band1093 9/29/1998
Fit Error = 1.0%
λ^4F_λ (10^{-13} W cm^{-2} μm^3)
WAVELENGTH (μm)

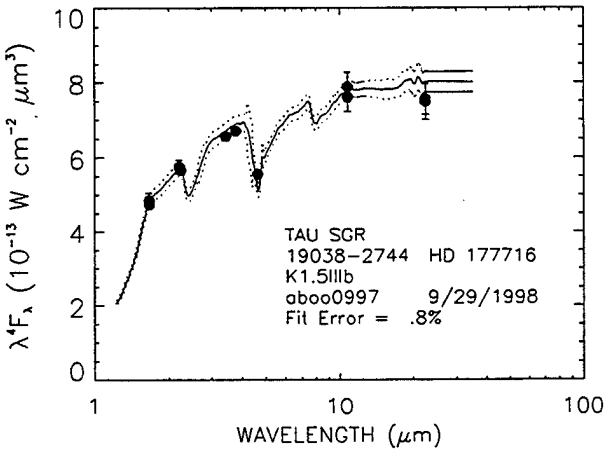
TAU SGR
19038-2744 HD 177716
K1.5IIIb
aboo0997 9/29/1998
Fit Error = .8%
λ^4F_λ (10^{-13} W cm^{-2} μm^3)
WAVELENGTH (μm)

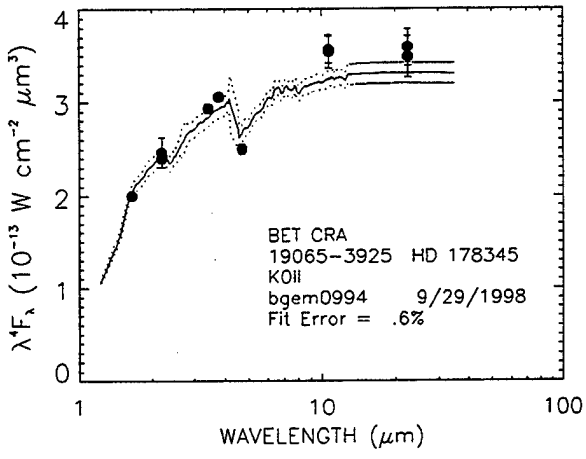
BET CRA
19065-3925 HD 178345
KOII
bgem0994 9/29/1998
Fit Error = .6%
λ^4F_λ (10^{-13} W cm^{-2} μm^3)
WAVELENGTH (μm)

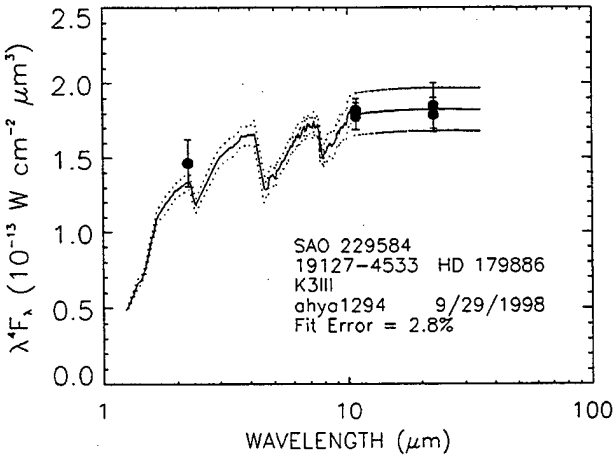
SAO 229584
19127-4533 HD 179886
K3III
ahya1294 9/29/1998
Fit Error = 2.8%
λ^4F_λ (10^{-13} W cm^{-2} μm^3)
WAVELENGTH (μm)

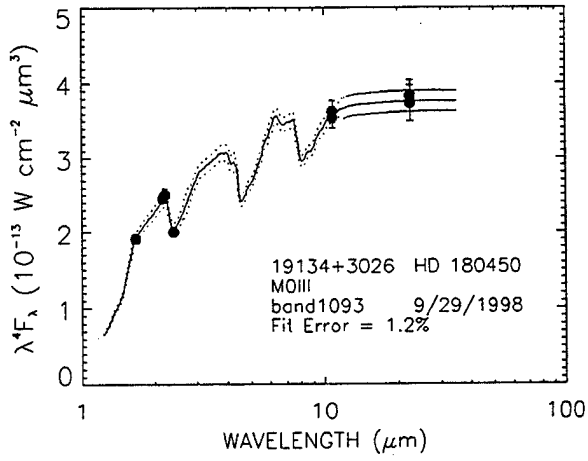
19134+3026 HD 180450
MOIII
band1093 9/29/1998
Fit Error = 1.2%
λ^4F_λ (10^{-13} W cm^{-2} μm^3)
WAVELENGTH (μm)

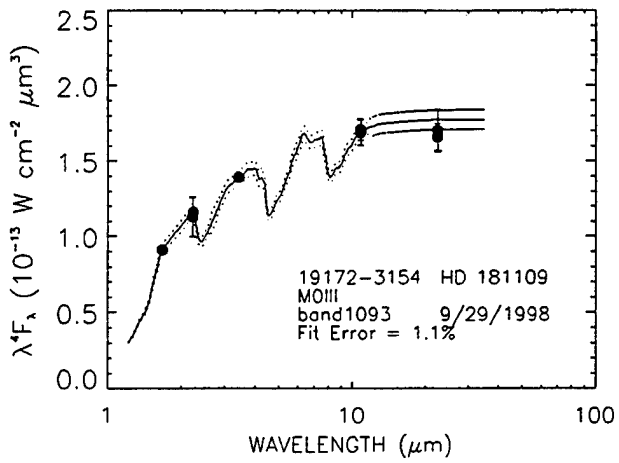
19172-3154 HD 181109
M0III
band1093 9/29/1998
Fit Error = 1.1%
WAVELENGTH (μm)

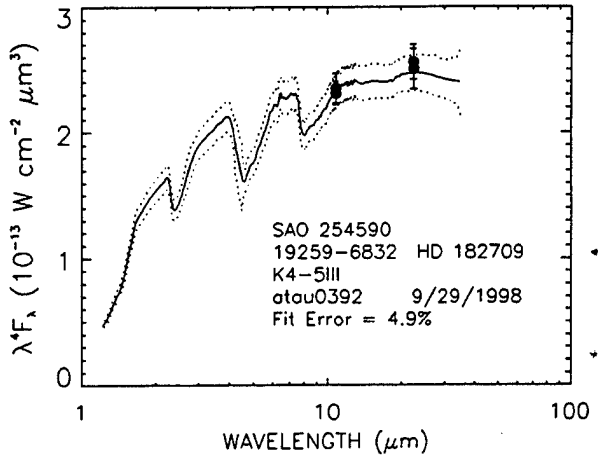
SAO 254590
19259-6832 HD 182709
K4-5III
atau0392 9/29/1998
Fit Error = 4.9%
WAVELENGTH (μm)

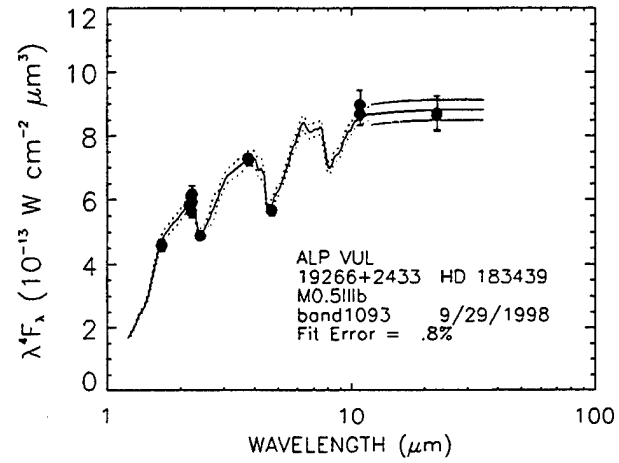
ALP VUL
19266+2433 HD 183439
M0.5IIIb
band1093 9/29/1998
Fit Error = .8%
WAVELENGTH (μm)

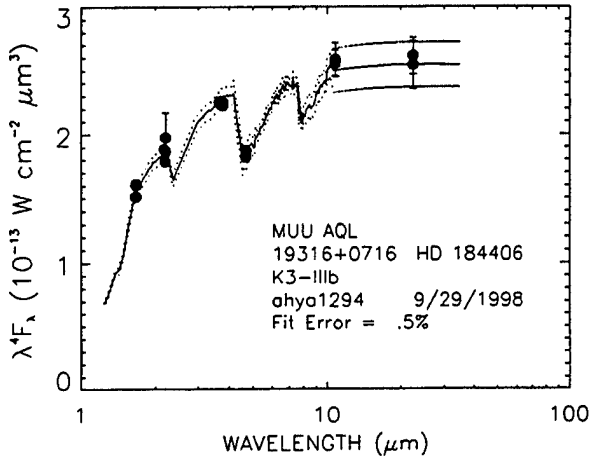
MUU AQL
19316+0716 HD 184406
K3-IIIb
ahya1294 9/29/1998
Fit Error = .5%
WAVELENGTH (μm)

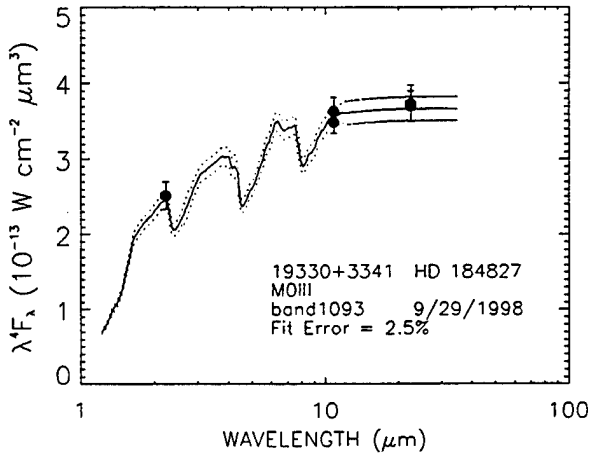
19330+3341 HD 184827
M0III
band1093 9/29/1998
Fit Error = 2.5%
WAVELENGTH (μm)

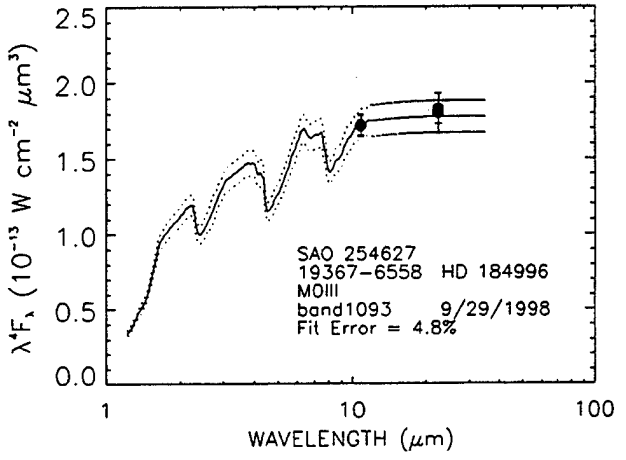
SAO 254627
19367-6558 HD 184996
M0III
band1093 9/29/1998
Fit Error = 4.8%
WAVELENGTH (μm)

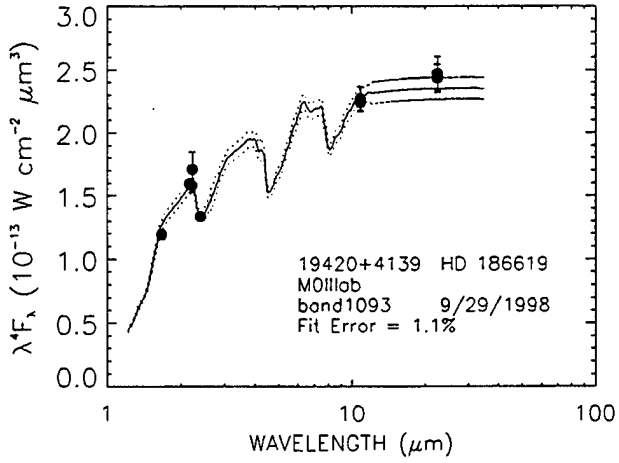
19420+4139 HD 186619
M0IIIab
band1093 9/29/1998
Fit Error = 1.1%
WAVELENGTH (μm)

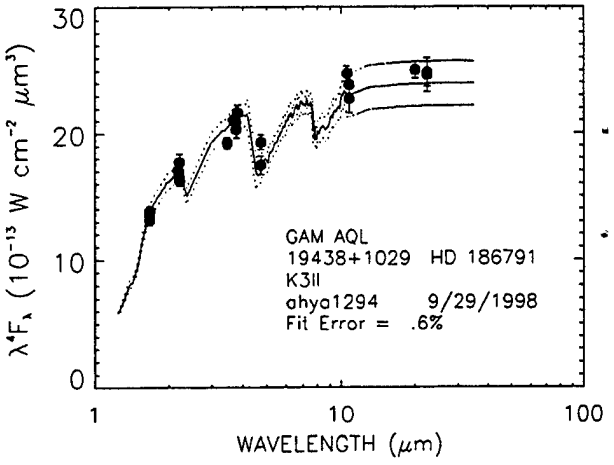
GAM AQL
19438+1029 HD 186791
K3II
ahya1294 9/29/1998
Fit Error = .6%
WAVELENGTH (μm)

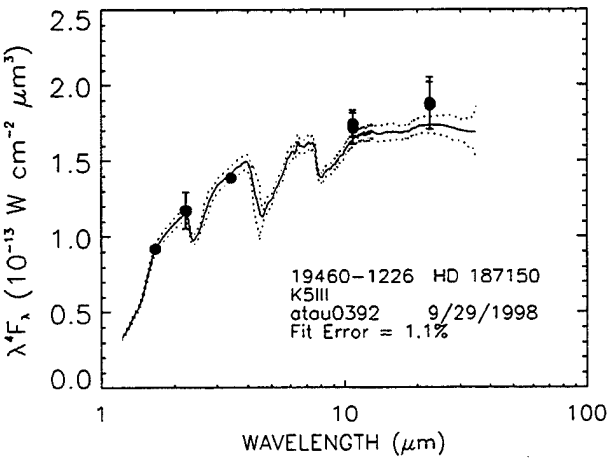
19460−1226 HD 187150
K5III
atau0392 9/29/1998
Fit Error = 1.1%
λ^4F_λ (10^{-13} W cm^{-2} μm^3)
WAVELENGTH (μm)

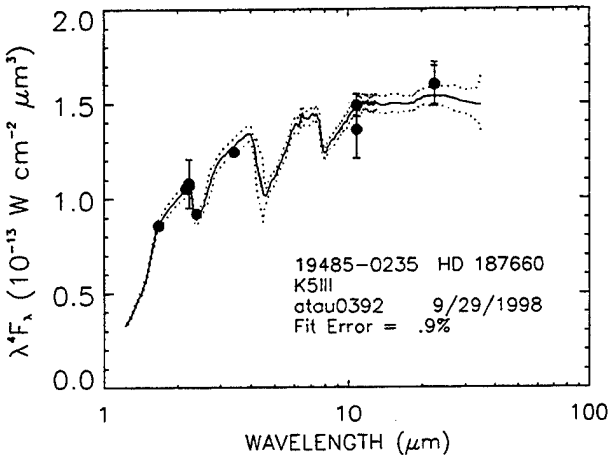
19485−0235 HD 187660
K5III
atau0392 9/29/1998
Fit Error = .9%
λ^4F_λ (10^{-13} W cm^{-2} μm^3)
WAVELENGTH (μm)

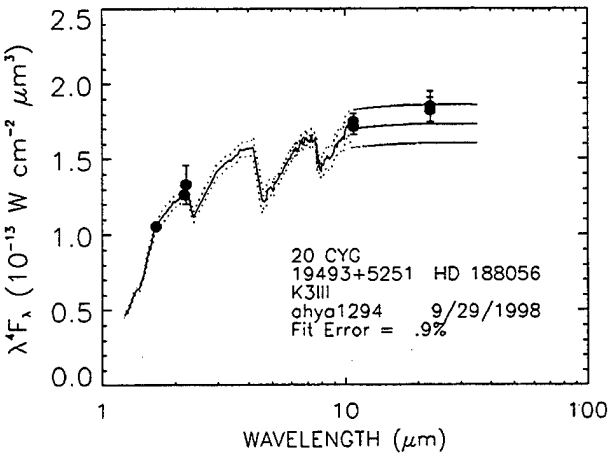
20 CYG
19493+5251 HD 188056
K3III
ahya1294 9/29/1998
Fit Error = .9%
λ^4F_λ (10^{-13} W cm^{-2} μm^3)
WAVELENGTH (μm)

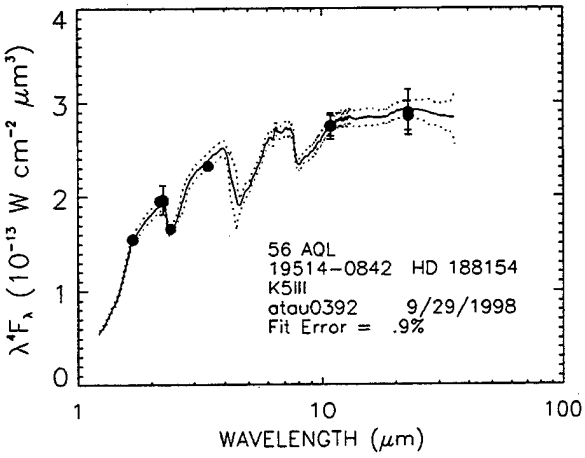
56 AQL
19514−0842 HD 188154
K5III
atau0392 9/29/1998
Fit Error = .9%
λ^4F_λ (10^{-13} W cm^{-2} μm^3)
WAVELENGTH (μm)

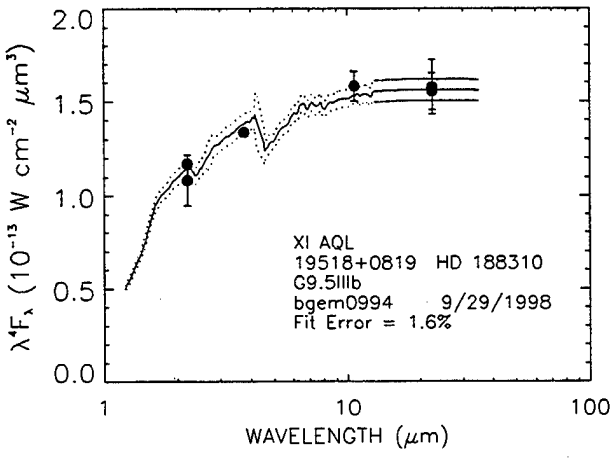
XI AQL
19518+0819 HD 188310
G9.5IIIb
bgem0994 9/29/1998
Fit Error = 1.6%
λ^4F_λ (10^{-13} W cm^{-2} μm^3)
WAVELENGTH (μm)

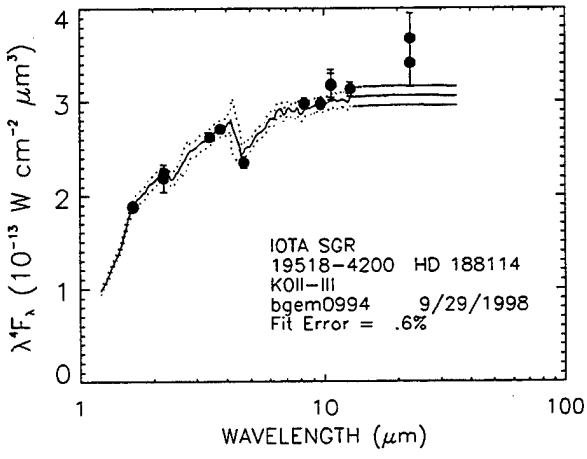
IOTA SGR
19518−4200 HD 188114
KOII−III
bgem0994 9/29/1998
Fit Error = .6%
λ^4F_λ (10^{-13} W cm^{-2} μm^3)
WAVELENGTH (μm)

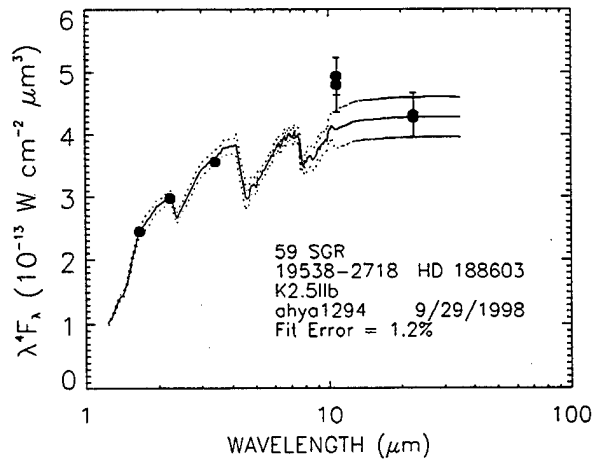
59 SGR
19538−2718 HD 188603
K2.5IIb
ahya1294 9/29/1998
Fit Error = 1.2%
λ^4F_λ (10^{-13} W cm^{-2} μm^3)
WAVELENGTH (μm)

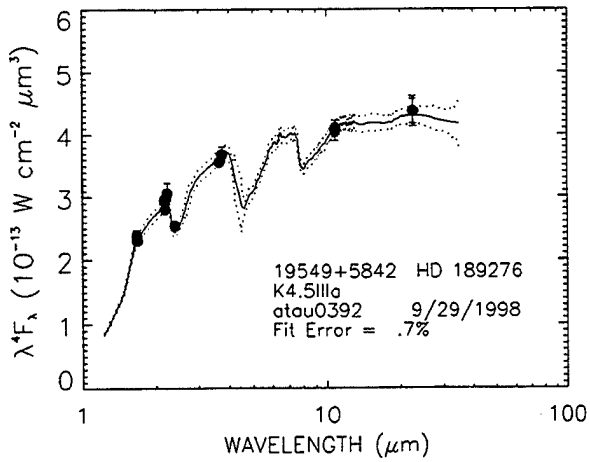
19549+5842 HD 189276
K4.5IIIa
atau0392 9/29/1998
Fit Error = .7%
λ^4F_λ (10^{-13} W cm^{-2} μm^3)
WAVELENGTH (μm)

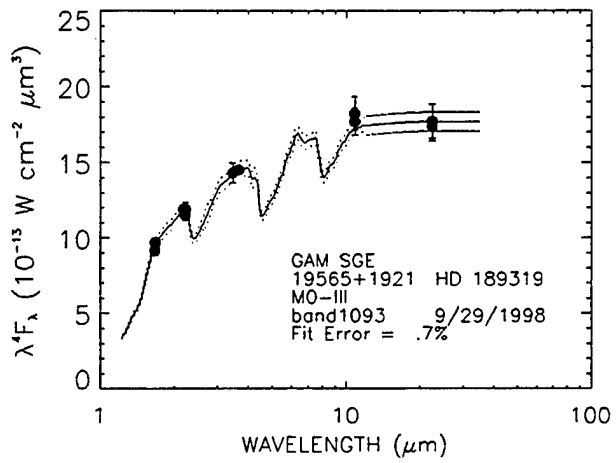
GAM SGE
19565+1921 HD 189319
M0-III
band1093 9/29/1998
Fit Error = .7%
WAVELENGTH (μm)

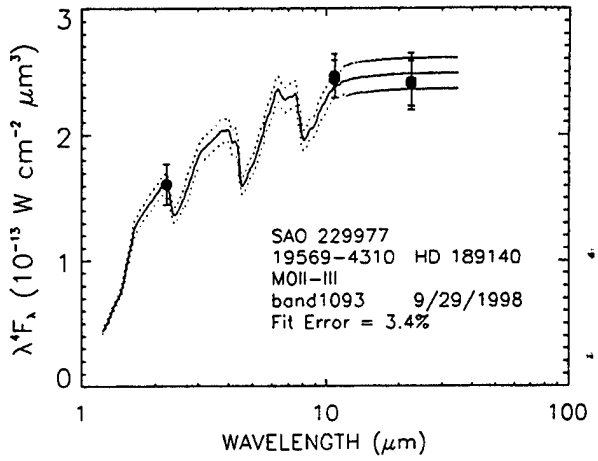
SAO 229977
19569-4310 HD 189140
M0II-III
band1093 9/29/1998
Fit Error = 3.4%
WAVELENGTH (μm)

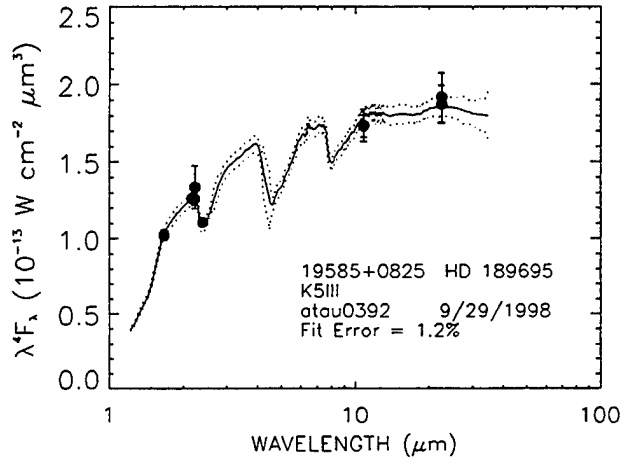
19585+0825 HD 189695
K5III
atau0392 9/29/1998
Fit Error = 1.2%
WAVELENGTH (μm)

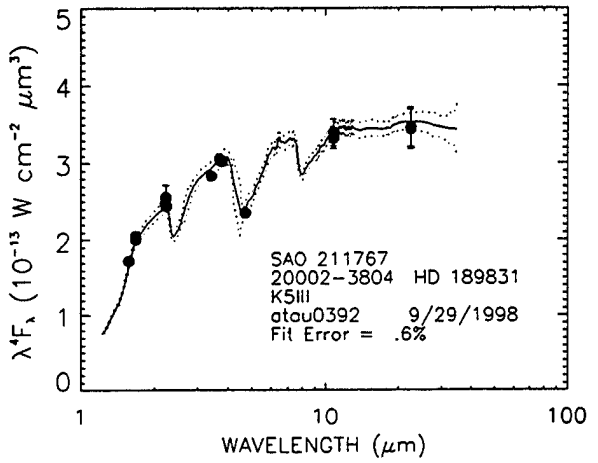
SAO 211767
20002-3804 HD 189831
K5III
atau0392 9/29/1998
Fit Error = .6%
WAVELENGTH (μm)

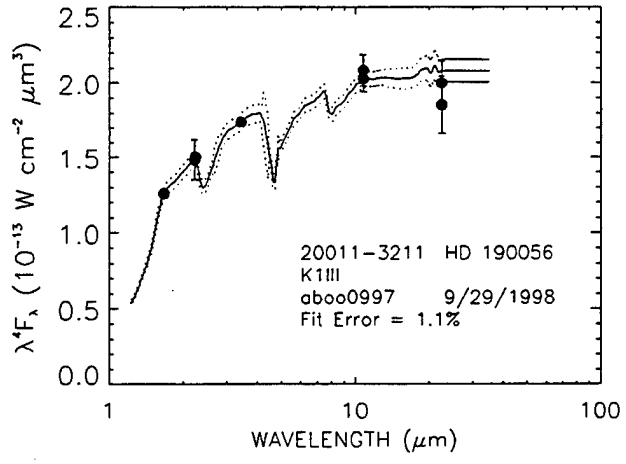
20011-3211 HD 190056
K1III
aboo0997 9/29/1998
Fit Error = 1.1%
WAVELENGTH (μm)

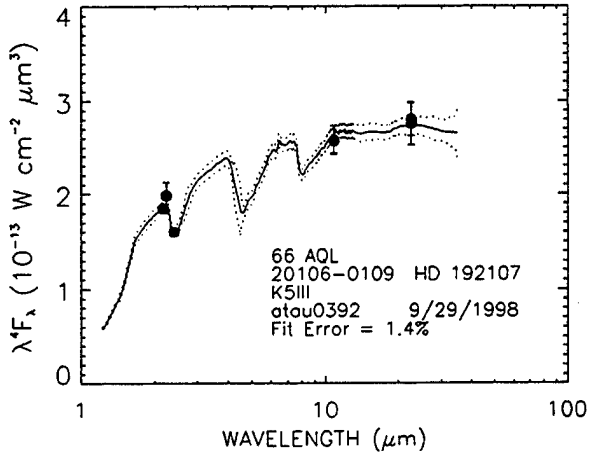
66 AQL
20106-0109 HD 192107
K5III
atau0392 9/29/1998
Fit Error = 1.4%
WAVELENGTH (μm)

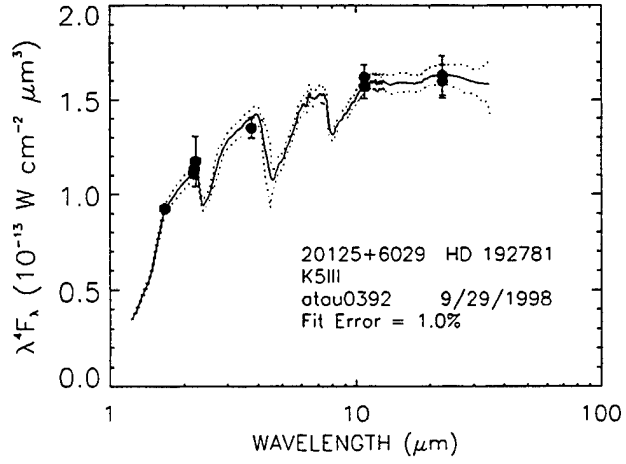
20125+6029 HD 192781
K5III
atau0392 9/29/1998
Fit Error = 1.0%
WAVELENGTH (μm)

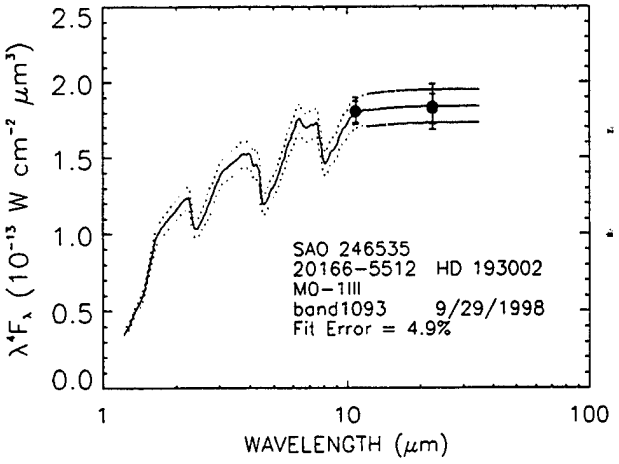
SAO 246535
20166-5512 HD 193002
M0-1III
band1093 9/29/1998
Fit Error = 4.9%
WAVELENGTH (μm)

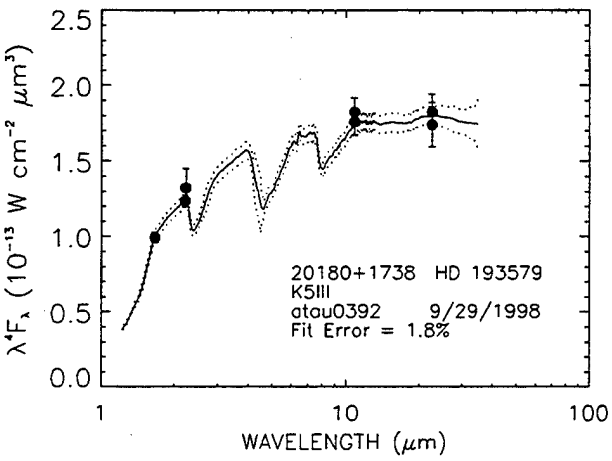
20180+1738 HD 193579
K5III
atau0392 9/29/1998
Fit Error = 1.8%
λ^4F_λ (10^{-13} W cm^{-2} μm^3)
WAVELENGTH (μm)

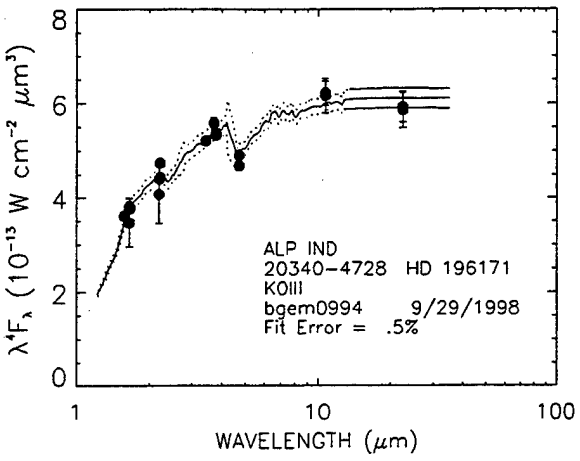
ALP IND
20340−4728 HD 196171
KOIII
bgem0994 9/29/1998
Fit Error = .5%
λ^4F_λ (10^{-13} W cm^{-2} μm^3)
WAVELENGTH (μm)

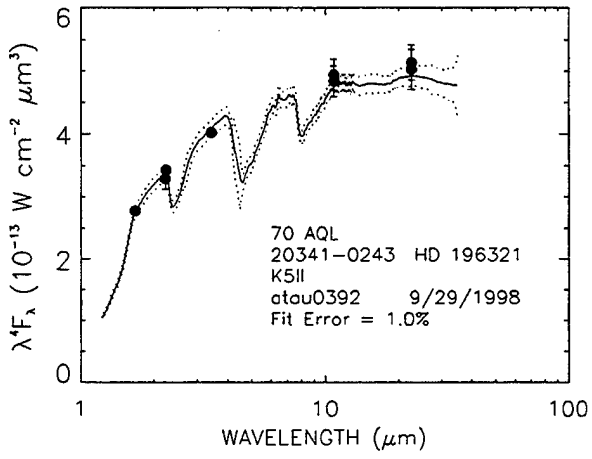
70 AQL
20341−0243 HD 196321
K5II
atau0392 9/29/1998
Fit Error = 1.0%
λ^4F_λ (10^{-13} W cm^{-2} μm^3)
WAVELENGTH (μm)

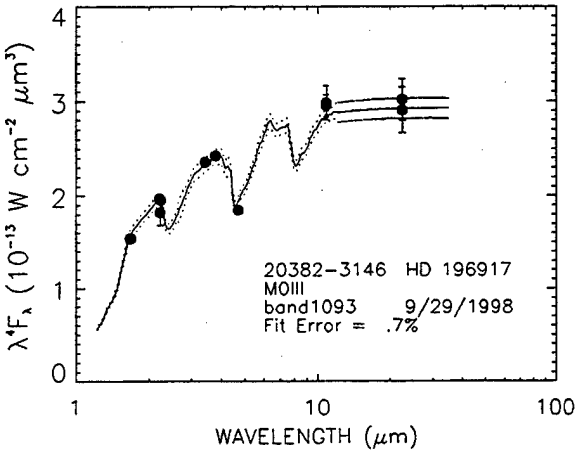
20382−3146 HD 196917
MOIII
band1093 9/29/1998
Fit Error = .7%
λ^4F_λ (10^{-13} W cm^{-2} μm^3)
WAVELENGTH (μm)

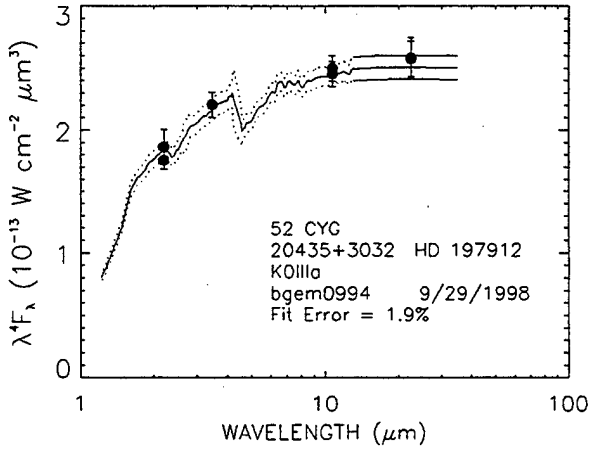
52 CYG
20435+3032 HD 197912
KOIIIa
bgem0994 9/29/1998
Fit Error = 1.9%
λ^4F_λ (10^{-13} W cm^{-2} μm^3)
WAVELENGTH (μm)

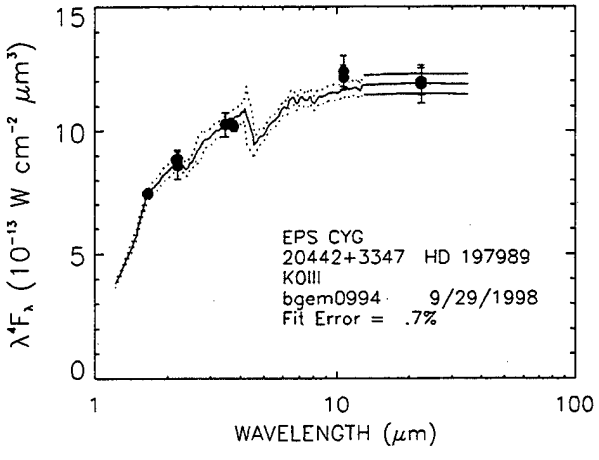
EPS CYG
20442+3347 HD 197989
KOIII
bgem0994 9/29/1998
Fit Error = .7%
λ^4F_λ (10^{-13} W cm^{-2} μm^3)
WAVELENGTH (μm)

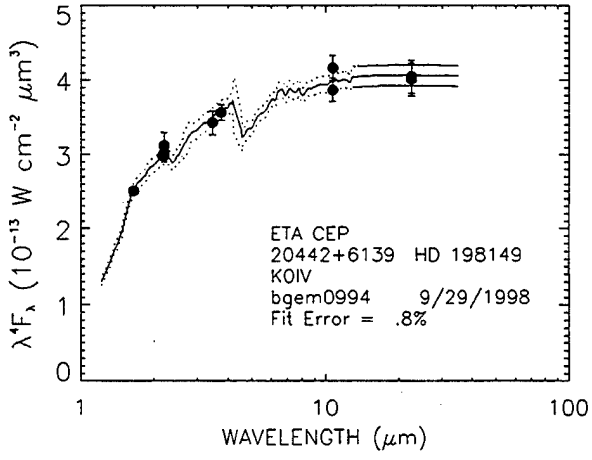
ETA CEP
20442+6139 HD 198149
KOIV
bgem0994 9/29/1998
Fit Error = .8%
λ^4F_λ (10^{-13} W cm^{-2} μm^3)
WAVELENGTH (μm)

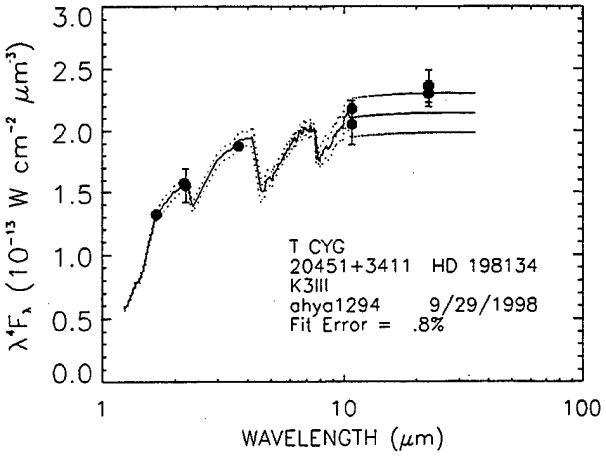
T CYG
20451+3411 HD 198134
K3III
ahya1294 9/29/1998
Fit Error = .8%
λ^4F_λ (10^{-13} W cm^{-2} μm^3)
WAVELENGTH (μm)

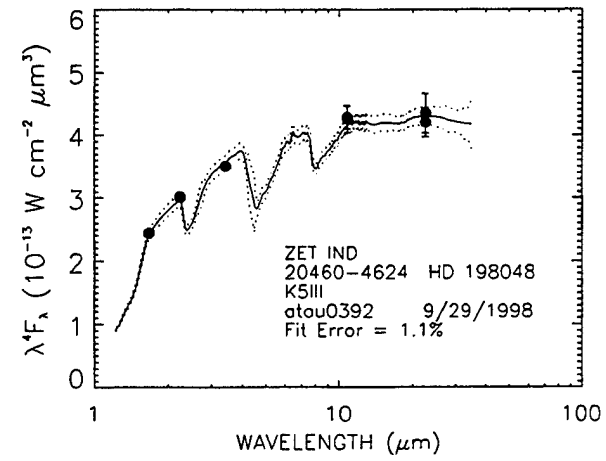
ZET IND
20460−4624 HD 198048
K5III
atau0392 9/29/1998
Fit Error = 1.1%
WAVELENGTH (μm)

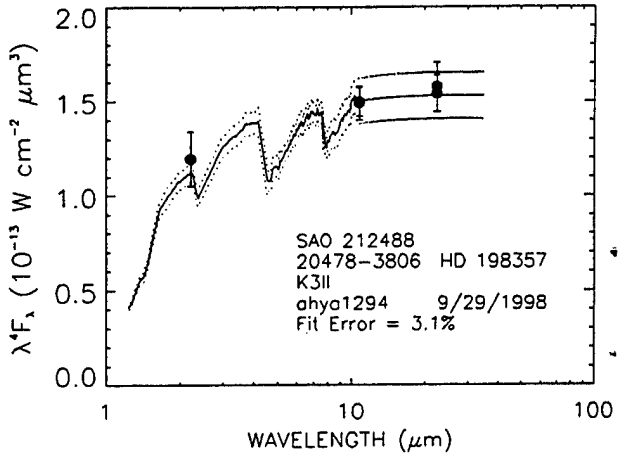
SAO 212488
20478−3806 HD 198357
K3II
ahya1294 9/29/1998
Fit Error = 3.1%
WAVELENGTH (μm)

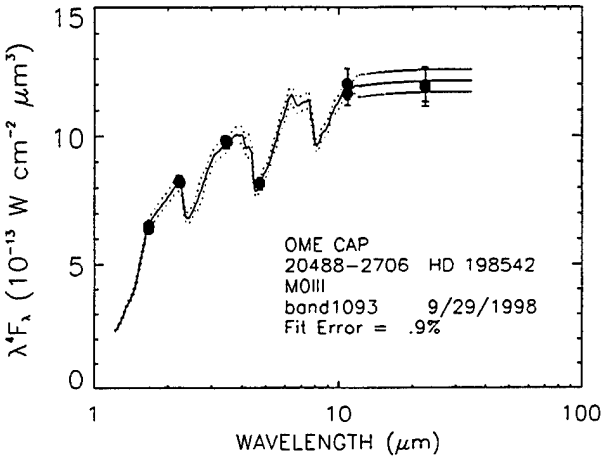
OME CAP
20488−2706 HD 198542
M0III
band1093 9/29/1998
Fit Error = .9%
WAVELENGTH (μm)

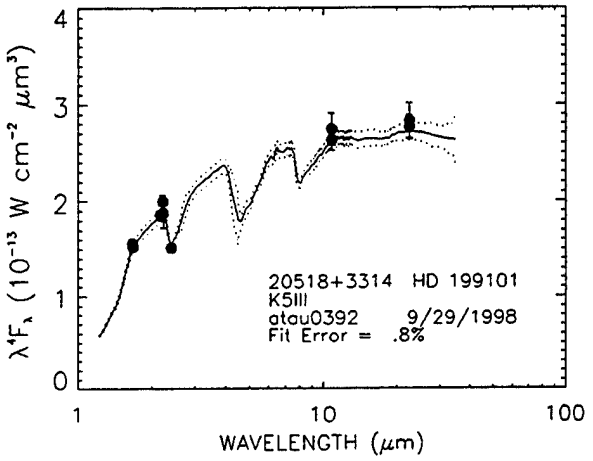
20518+3314 HD 199101
K5III
atau0392 9/29/1998
Fit Error = .8%
WAVELENGTH (μm)

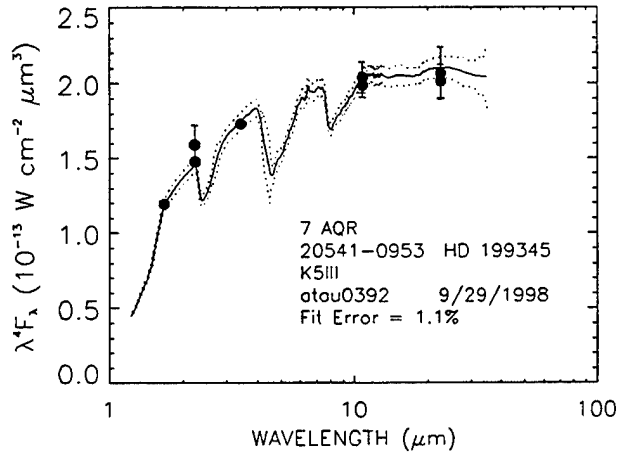
7 AQR
20541−0953 HD 199345
K5III
atau0392 9/29/1998
Fit Error = 1.1%
WAVELENGTH (μm)

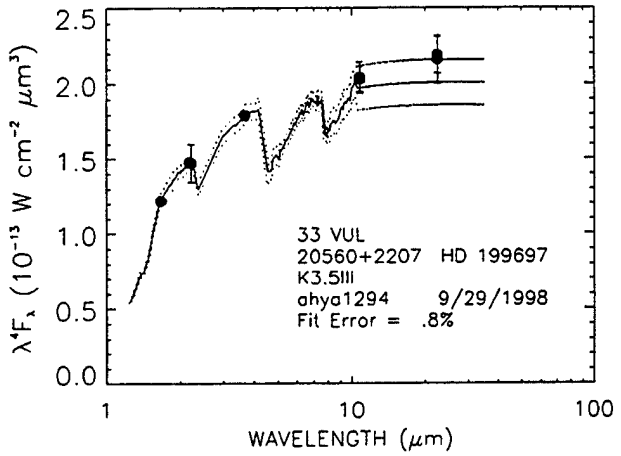
33 VUL
20560+2207 HD 199697
K3.5III
ahya1294 9/29/1998
Fit Error = .8%
WAVELENGTH (μm)

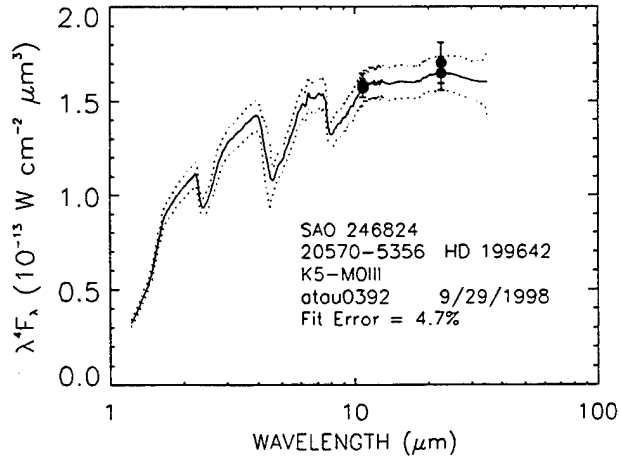
SAO 246824
20570−5356 HD 199642
K5−M0III
atau0392 9/29/1998
Fit Error = 4.7%
WAVELENGTH (μm)

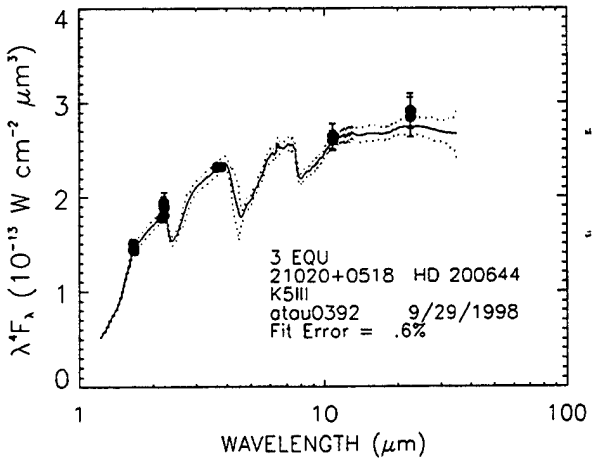
3 EQU
21020+0518 HD 200644
K5III
atau0392 9/29/1998
Fit Error = .6%
WAVELENGTH (μm)

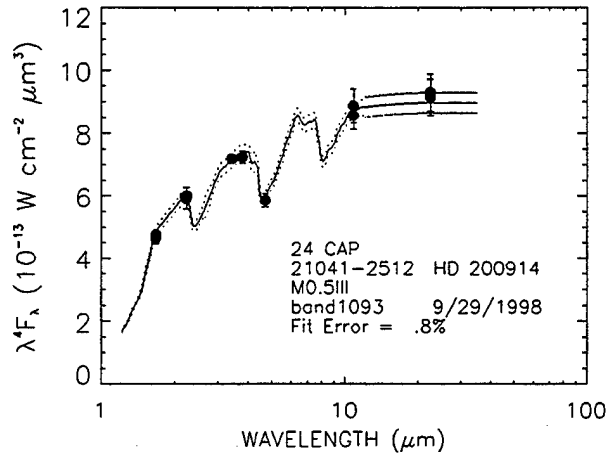
24 CAP
21041−2512 HD 200914
M0.5III
band1093 9/29/1998
Fit Error = .8%
λ^4F_λ (10^{-13} W cm^{-2} μm^3)
WAVELENGTH (μm)

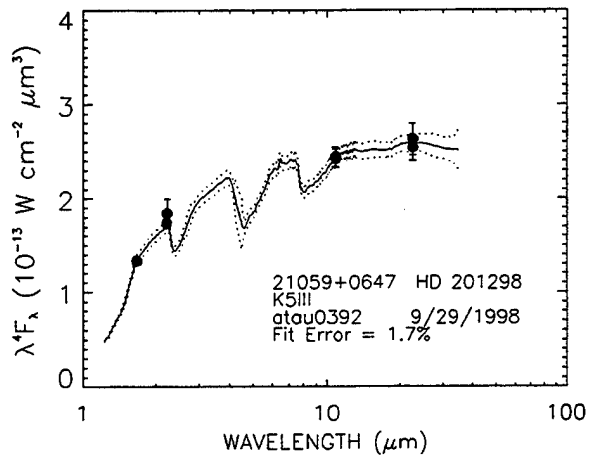
21059+0647 HD 201298
K5III
atau0392 9/29/1998
Fit Error = 1.7%
λ^4F_λ (10^{-13} W cm^{-2} μm^3)
WAVELENGTH (μm)

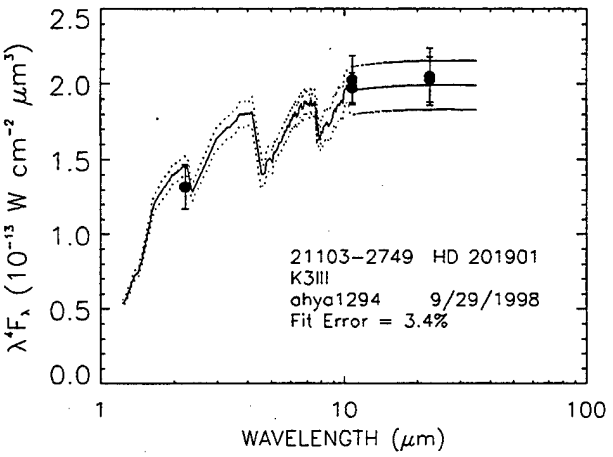
21103−2749 HD 201901
K3III
ahya1294 9/29/1998
Fit Error = 3.4%
λ^4F_λ (10^{-13} W cm^{-2} μm^3)
WAVELENGTH (μm)

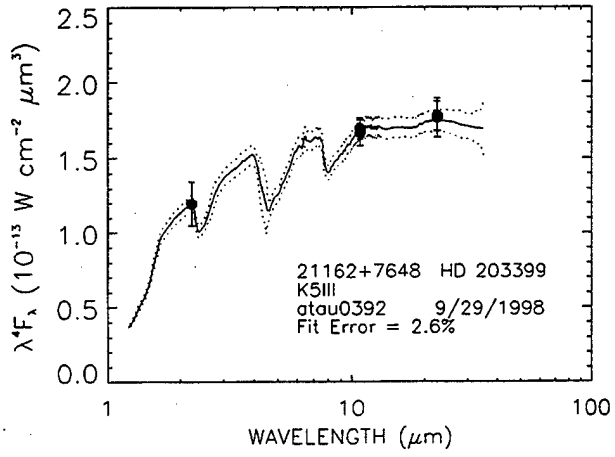
21162+7648 HD 203399
K5III
atau0392 9/29/1998
Fit Error = 2.6%
λ^4F_λ (10^{-13} W cm^{-2} μm^3)
WAVELENGTH (μm)

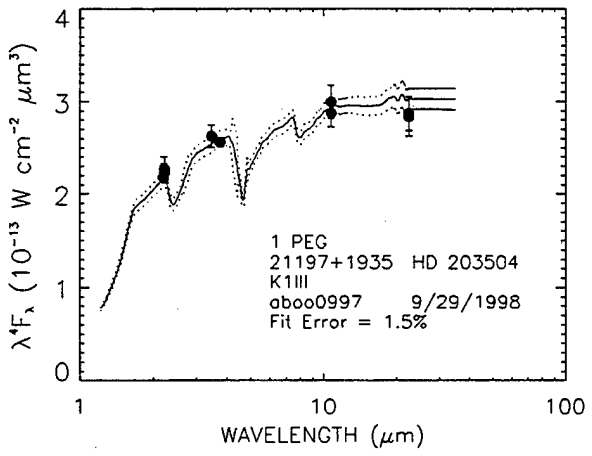
1 PEG
21197+1935 HD 203504
K1III
aboo0997 9/29/1998
Fit Error = 1.5%
λ^4F_λ (10^{-13} W cm^{-2} μm^3)
WAVELENGTH (μm)

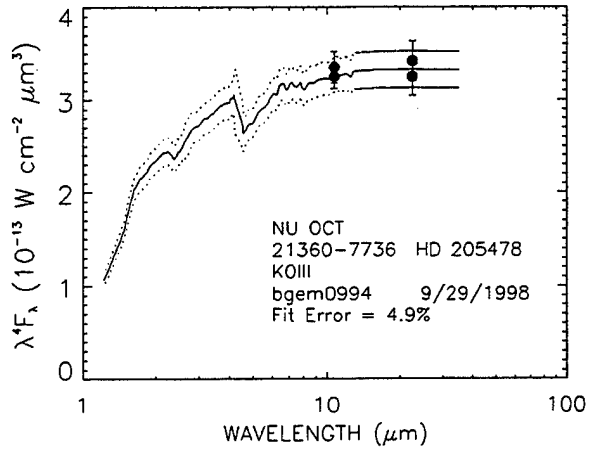
NU OCT
21360−7736 HD 205478
KOIII
bgem0994 9/29/1998
Fit Error = 4.9%
λ^4F_λ (10^{-13} W cm^{-2} μm^3)
WAVELENGTH (μm)

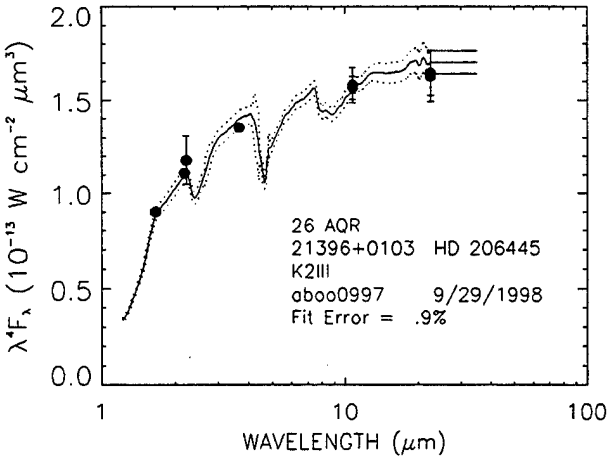
26 AQR
21396+0103 HD 206445
K2III
aboo0997 9/29/1998
Fit Error = .9%
λ^4F_λ (10^{-13} W cm^{-2} μm^3)
WAVELENGTH (μm)

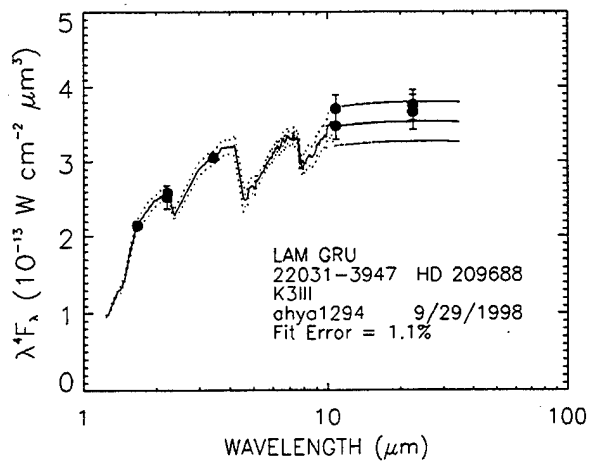
LAM GRU
22031−3947 HD 209688
K3III
ahya1294 9/29/1998
Fit Error = 1.1%
λ^4F_λ (10^{-13} W cm^{-2} μm^3)
WAVELENGTH (μm)

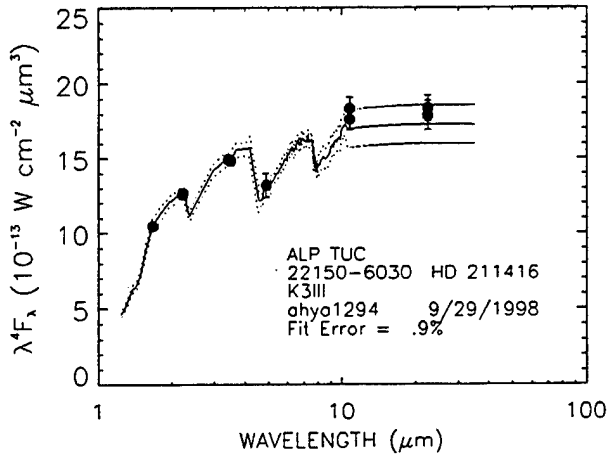
ALP TUC
22150-6030 HD 211416
K3III
ahya1294 9/29/1998
Fit Error = .9%
$\lambda^4 F_\lambda$ (10^{-13} W cm^{-2} μm^3)
WAVELENGTH (μm)

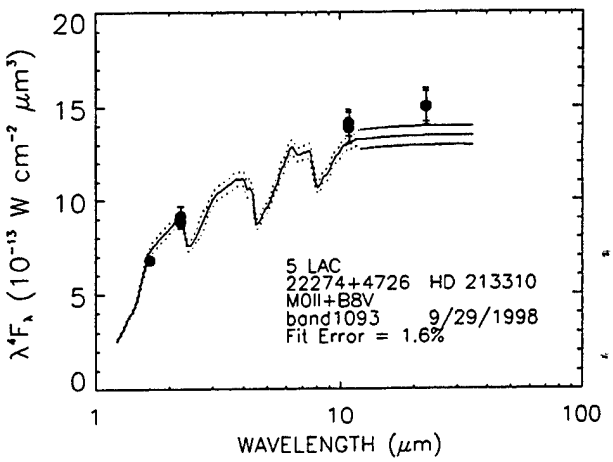
5 LAC
22274+4726 HD 213310
M0II+B8V
band1093 9/29/1998
Fit Error = 1.6%
$\lambda^4 F_\lambda$ (10^{-13} W cm^{-2} μm^3)
WAVELENGTH (μm)

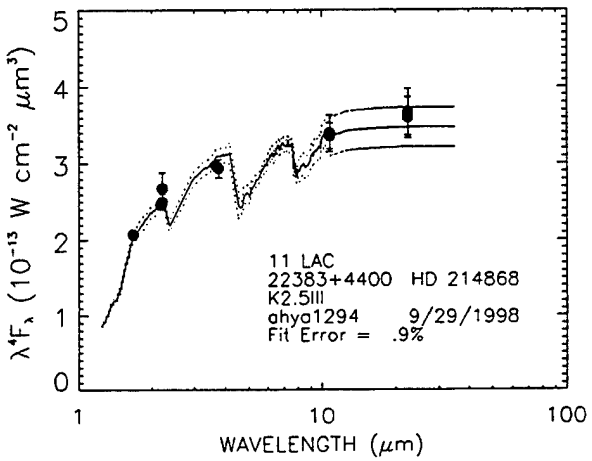
11 LAC
22383+4400 HD 214868
K2.5III
ahya1294 9/29/1998
Fit Error = .9%
$\lambda^4 F_\lambda$ (10^{-13} W cm^{-2} μm^3)
WAVELENGTH (μm)

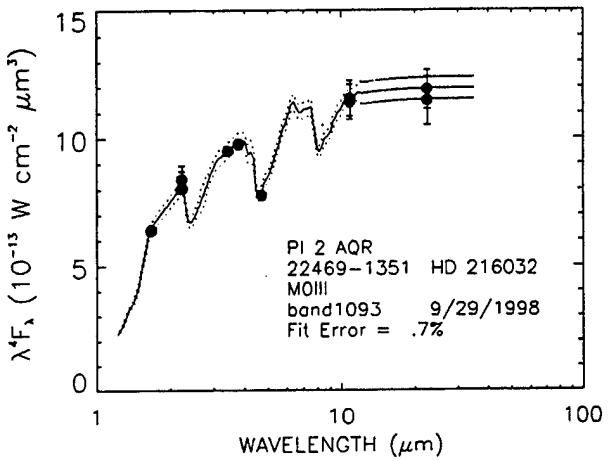
PI 2 AQR
22469-1351 HD 216032
M0III
band1093 9/29/1998
Fit Error = .7%
$\lambda^4 F_\lambda$ (10^{-13} W cm^{-2} μm^3)
WAVELENGTH (μm)

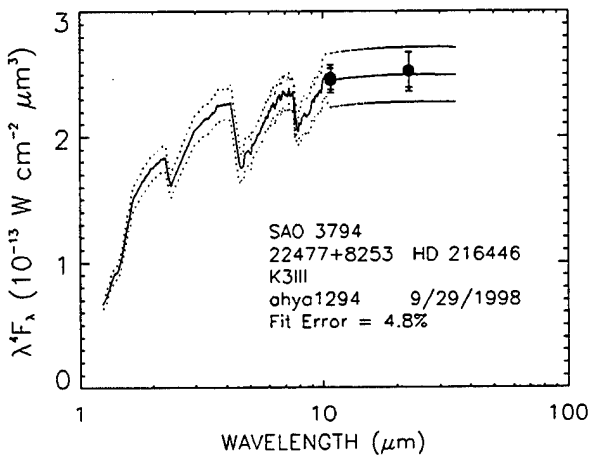
SAO 3794
22477+8253 HD 216446
K3III
ahya1294 9/29/1998
Fit Error = 4.8%
$\lambda^4 F_\lambda$ (10^{-13} W cm^{-2} μm^3)
WAVELENGTH (μm)

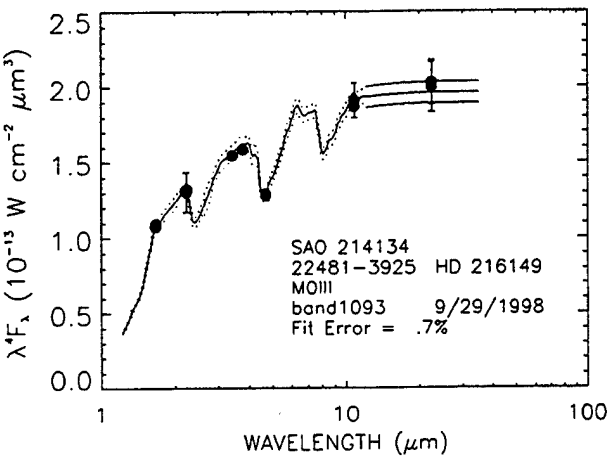
SAO 214134
22481-3925 HD 216149
M0III
band1093 9/29/1998
Fit Error = .7%
$\lambda^4 F_\lambda$ (10^{-13} W cm^{-2} μm^3)
WAVELENGTH (μm)

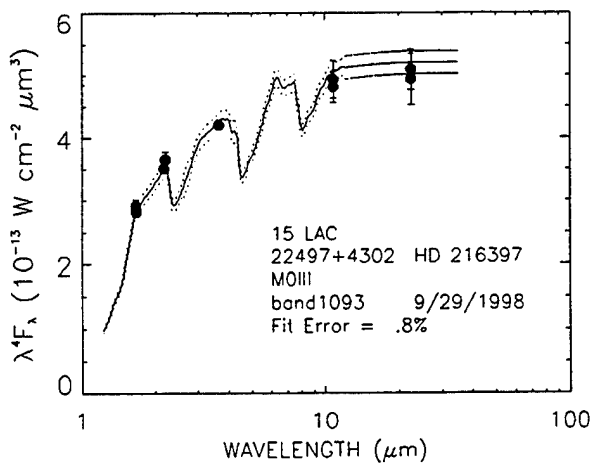
15 LAC
22497+4302 HD 216397
M0III
band1093 9/29/1998
Fit Error = .8%
$\lambda^4 F_\lambda$ (10^{-13} W cm^{-2} μm^3)
WAVELENGTH (μm)

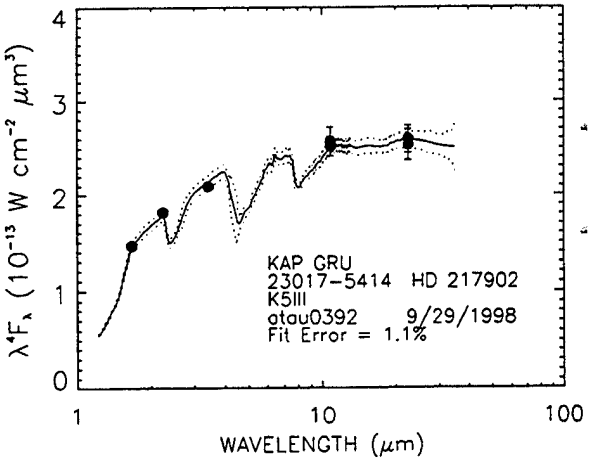
KAP GRU
23017-5414 HD 217902
K5III
qtau0392 9/29/1998
Fit Error = 1.1%
$\lambda^4 F_\lambda$ (10^{-13} W cm^{-2} μm^3)
WAVELENGTH (μm)

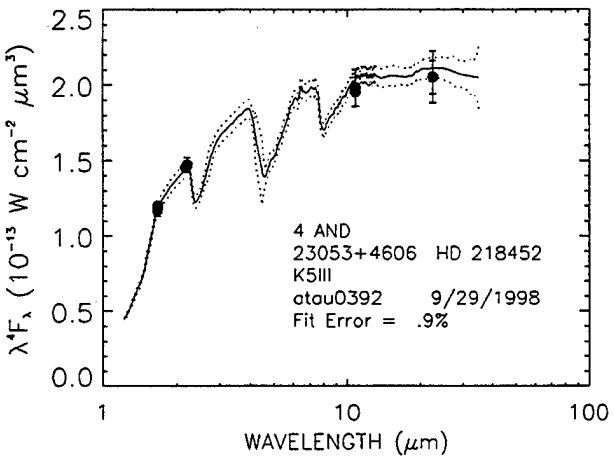
4 AND
23053+4606 HD 218452
K5III
atau0392 9/29/1998
Fit Error = .9%
λ^4F_λ (10^{-13} W cm^{-2} μm^3)
WAVELENGTH (μm)

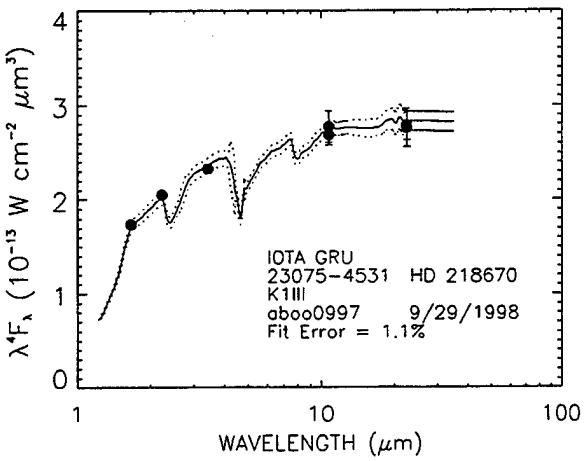
IOTA GRU
23075−4531 HD 218670
K1III
aboo0997 9/29/1998
Fit Error = 1.1%
λ^4F_λ (10^{-13} W cm^{-2} μm^3)
WAVELENGTH (μm)

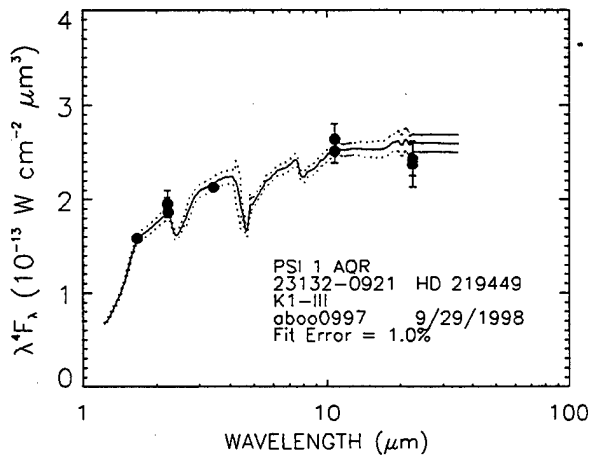
PSI 1 AQR
23132−0921 HD 219449
K1−III
aboo0997 9/29/1998
Fit Error = 1.0%
λ^4F_λ (10^{-13} W cm^{-2} μm^3)
WAVELENGTH (μm)

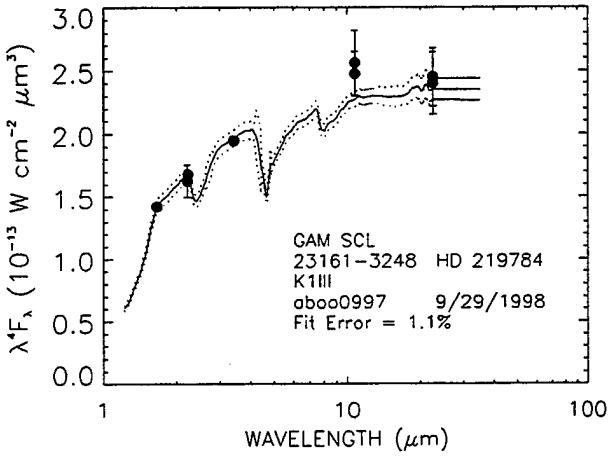
GAM SCL
23161−3248 HD 219784
K1III
aboo0997 9/29/1998
Fit Error = 1.1%
λ^4F_λ (10^{-13} W cm^{-2} μm^3)
WAVELENGTH (μm)

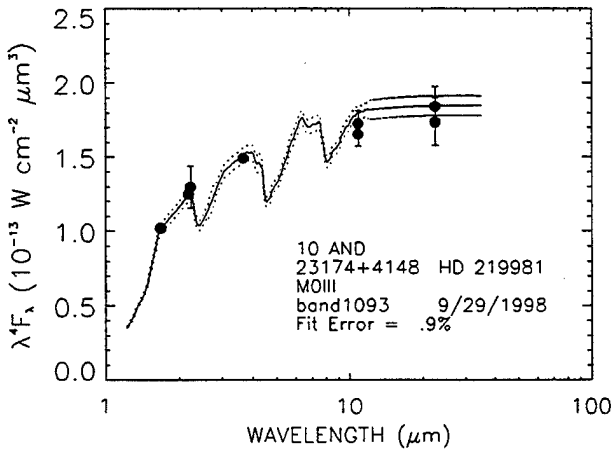
10 AND
23174+4148 HD 219981
MOIII
band1093 9/29/1998
Fit Error = .9%
λ^4F_λ (10^{-13} W cm^{-2} μm^3)
WAVELENGTH (μm)

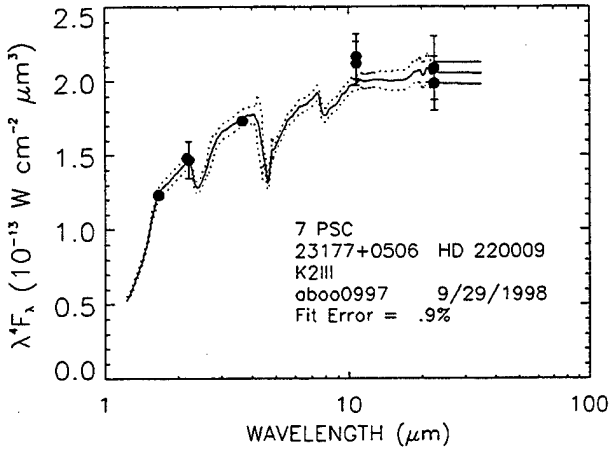
7 PSC
23177+0506 HD 220009
K2III
aboo0997 9/29/1998
Fit Error = .9%
λ^4F_λ (10^{-13} W cm^{-2} μm^3)
WAVELENGTH (μm)

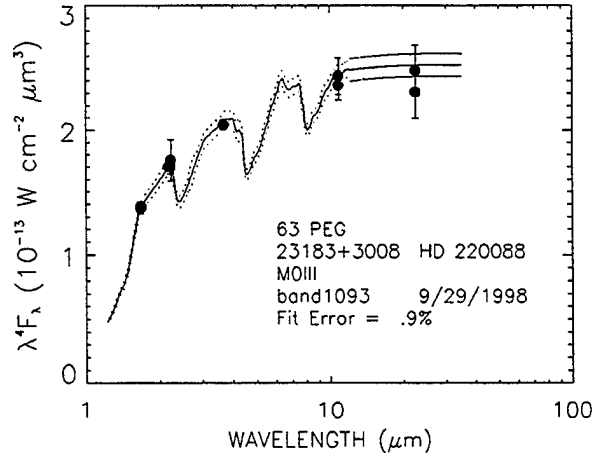
63 PEG
23183+3008 HD 220088
MOIII
band1093 9/29/1998
Fit Error = .9%
λ^4F_λ (10^{-13} W cm^{-2} μm^3)
WAVELENGTH (μm)

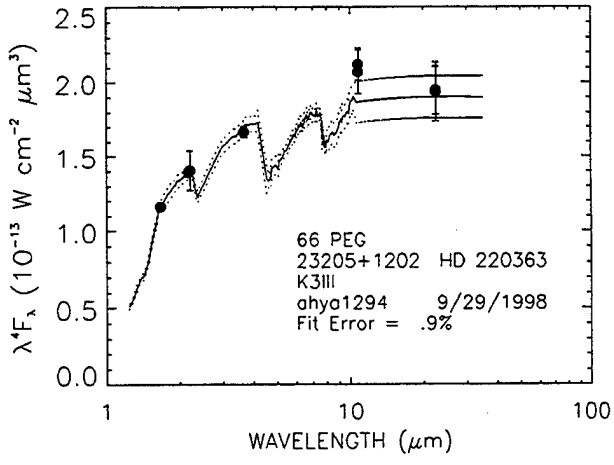
66 PEG
23205+1202 HD 220363
K3III
ahya1294 9/29/1998
Fit Error = .9%
λ^4F_λ (10^{-13} W cm^{-2} μm^3)
WAVELENGTH (μm)

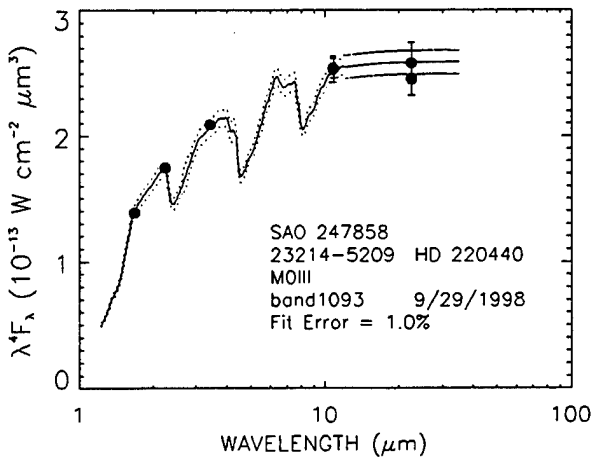
SAO 247858
23214-5209 HD 220440
M0III
band1093 9/29/1998
Fit Error = 1.0%
λ^4F_λ (10^{-13} W cm^{-2} μm^3)
WAVELENGTH (μm)

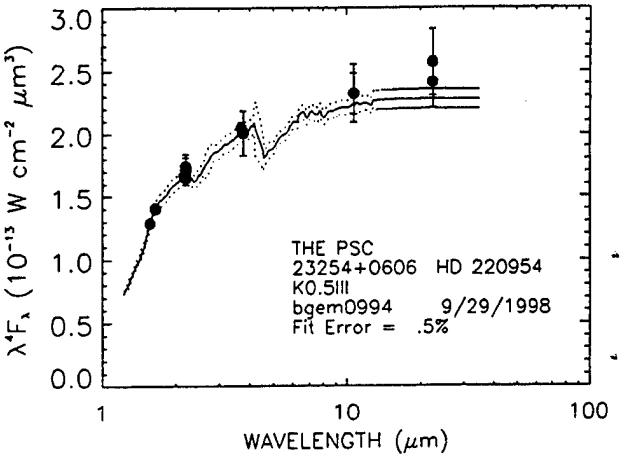
THE PSC
23254+0606 HD 220954
K0.5III
bgem0994 9/29/1998
Fit Error = .5%
λ^4F_λ (10^{-13} W cm^{-2} μm^3)
WAVELENGTH (μm)

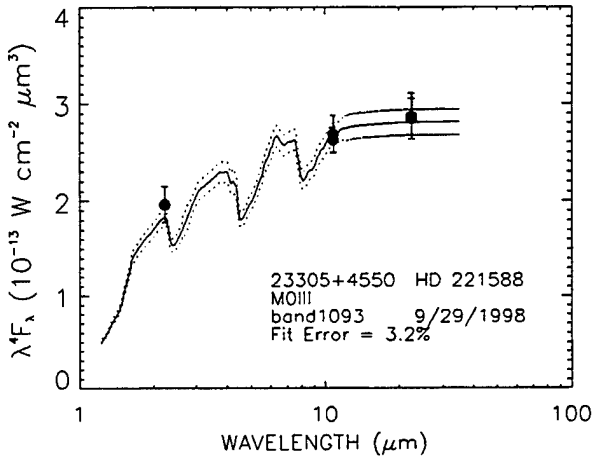
23305+4550 HD 221588
M0III
band1093 9/29/1998
Fit Error = 3.2%
λ^4F_λ (10^{-13} W cm^{-2} μm^3)
WAVELENGTH (μm)

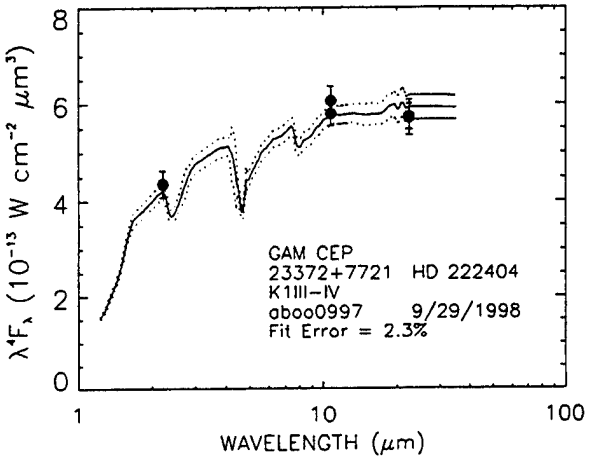
GAM CEP
23372+7721 HD 222404
K1III-IV
aboo0997 9/29/1998
Fit Error = 2.3%
λ^4F_λ (10^{-13} W cm^{-2} μm^3)
WAVELENGTH (μm)

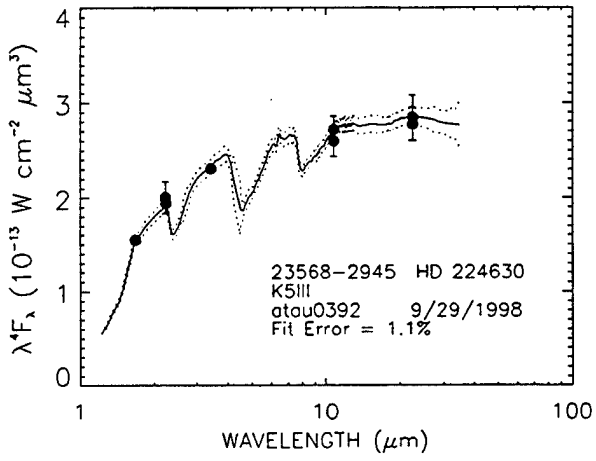
23568-2945 HD 224630
K5III
atau0392 9/29/1998
Fit Error = 1.1%
λ^4F_λ (10^{-13} W cm^{-2} μm^3)
WAVELENGTH (μm)

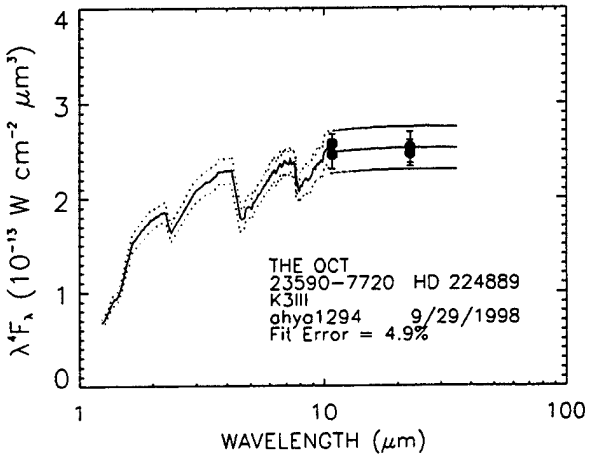
THE OCT
23590-7720 HD 224889
K3III
ahya1294 9/29/1998
Fit Error = 4.9%
λ^4F_λ (10^{-13} W cm^{-2} μm^3)
WAVELENGTH (μm)

Appendix G
Spectral Irradiance Calibration Papers

SPECTRAL IRRADIANCE CALIBRATION IN THE INFRARED. I. GROUND-BASED AND *IRAS* BROADBAND CALIBRATIONS

MARTIN COHEN

Radio Astronomy Laboratory, University of California, Berkeley, California 94720, Jamieson Science & Engineering, Inc., 5321 Scotts Valley Drive, Suite 204, Scotts Valley, California 95066

RUSSELL G. WALKER

Jamieson Science & Engineering, Inc., 5321 Scotts Valley Drive, Suite 204, Scotts Valley, California 95066

MICHAEL J. BARLOW AND JOHN R. DEACON

Department of Physics & Astronomy, University College London, Gower Street, London WC1E 6BT, United Kingdom

Received 19 March 1992; revised 12 June 1992

ABSTRACT

We describe an approach to absolute stellar calibration of broad and narrowband infrared filters based upon new models of Vega and Sirius due to Kurucz [private communication (1991)] and calculated by him, for the first time, with realistic stellar metallicities and a finely-gridded wavelength scale in the infrared. After normalizing the Vega model so that it matches Hayes' [*Calibration of Fundamental Stellar Quantities*, Proc. IAU Symposium No. 111 (1985)] weighted average of six monochromatic 5556A measurements we integrate the model through a variety of infrared filters using determinations of filter transmission profiles obtained at their actual operating temperature, and detailed model calculations for terrestrial atmospheric transmission. This provides in-band fluxes for Vega, which we define to be zero magnitude at all wavelengths shortward of 20 μm. We use existing infrared photometry differentially to establish an absolute scale for the new Sirius model. This yields an angular diameter within 1σ of the mean determined interferometrically by Hanbury Brown *et al.* [MNRAS, 167, 121 (1974)]. For practical purposes, Sirius provides the absolute calibration beyond the 20 μm region because of Vega's dust shell. Isophotal wavelengths and monochromatic flux densities for both Vega and Sirius are tabulated. We attempt a comparison of our calibration figures for the *IRAS* wavebands with the process used to generate the original *IRAS* absolute calibration. A complete duplication of that process is not currently possible. Preliminary indications are that *IRAS* is too high by 2%, 6%, 3%, and 12% at 12, 25, 60, and 100 μm, respectively.

1. INTRODUCTION

In his critical review of the optical absolute calibration of Vega, Hayes (1985) states of the corresponding situation in the infrared: "The calibration of the IR, and the availability of secondary standard stars in the IR, is yet immature, and I recommend more effort... ." Unfortunately, infrared astronomical calibration has been developed from the completely erroneous assumption that normal stars can be represented by Planck functions at their effective temperatures (although local fits to some blackbody in a restricted region may be an adequate approximation for some purposes). Recently, Cohen *et al.* (1992) have demonstrated from ratios of cool stellar spectra to that of Sirius that even early K-type stars such as α Boo are far from featureless blackbodies. In order to develop spectrally continuous absolute standards in the infrared, Cohen *et al.* (1992: hereafter CWW) have devised a technique for splicing together absolutely calibrated versions of existing spectral fragments and have demonstrated the method by producing a complete 1.2–35 μm absolutely calibrated spectrum of α Tau. Their method depends in part upon correct normalization of spectral fragments in accordance with infrared stellar photometry. In the present paper we describe the independent effort at broadband infrared calibration that supports this spectral calibration scheme.

Blackwell and colleagues have for some years applied the Infrared Flux Method to photometry of bright stars and derived effective temperatures and angular diameters by use of the MARCS model atmosphere code, and adoption of a calibration between infrared magnitudes and flux densities. In their early work these authors used the absolute mountaintop measurements of Vega (e.g., Blackwell *et al.* 1983; Selby *et al.* 1983; Mountain *et al.* 1985; Leggett *et al.* 1986; Blackwell *et al.* 1986; Blackwell *et al.* 1990). However, in their most recent paper (Blackwell *et al.* 1991), they have abandoned these ground-based measurements and have instead adopted the Vega model by Dreiling & Bell (1980). They justify this change in philosophy on the basis of the substantially tighter run of effective temperature with wavelength, for the many stars that they analyze, when using Dreiling and Bell in order to calibrate their infrared narrowband photometry, as opposed to the absolute measurements. They attribute this difference essentially to the intrinsic difficulties of the ground-based measurements. We follow the philosophy of Blackwell *et al.* (1991) in the use of a model atmosphere to provide cali-

 0004-6256/92/101650-08$00.90

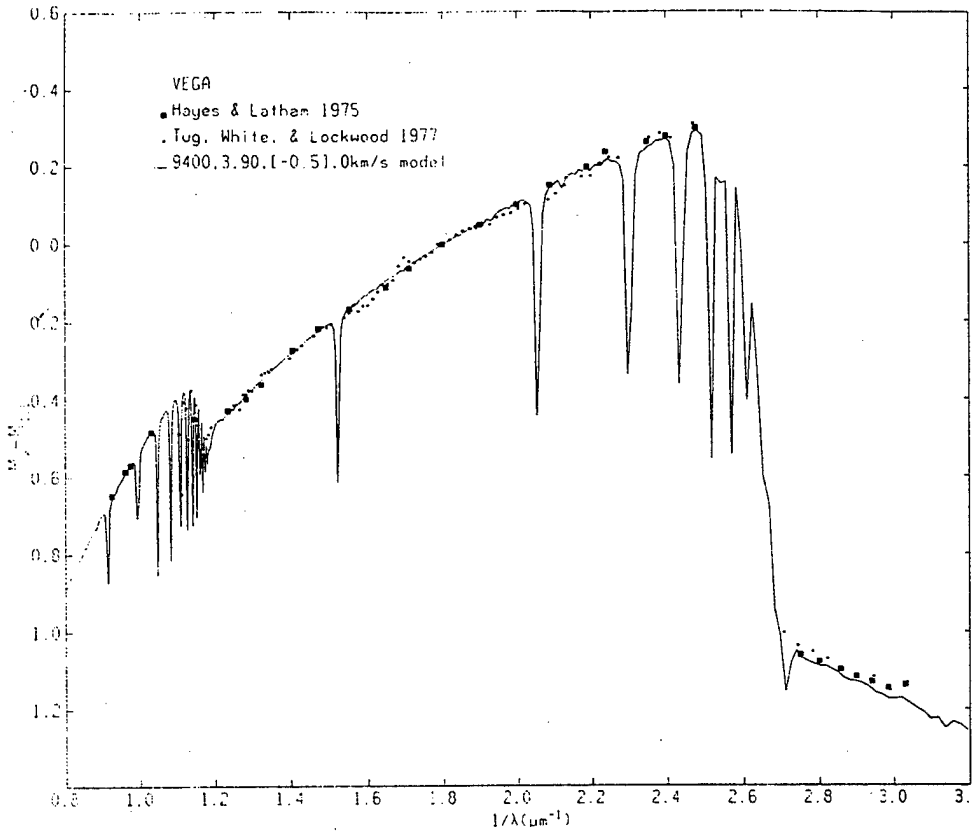

FIG. 1. Kurucz's (1991a) new model for Vega compared with a series of independent UV-optical measurements, specifically those by Hayes & Latham (1985) and by Tug *et al.* (1977).

bration and, for our purposes, continuous wavelength interpolation between the few photometric points available. However, we diverge from their approach in that we base our own calibration scheme on new models by Kurucz (1991a), as yet unpublished, that are briefly described in Sec. 2.

Deacon (1991) and Deacon *et al.* (1992a) have recently tabulated a set of magnitudes for potential infrared calibration standards that come from critical examination of the literature of ground-based measurements. They have also compared (Deacon 1991; Deacon *et al.* 1992b: hereafter DBC) the sensitivity of derived in-band fluxes for Vega to choice of model for that star (e.g., Kurucz 1979; Dreiling & Bell 1980; Kurucz 1991a). The transmission profiles of actual (UKIRT) filters at 77 K that we use are adopted from those within Deacon's dissertation. However, in the present paper we consider only the newest Kurucz models because (1) he himself has tailored the metallicities incorporated into them; (2) he has provided a customized finely-gridded wavelength scale that is suitable for infrared applications; and (3) these models contain much more physics than his 1979 set (for a full description of the physics included see Kurucz 1991b). A further divergence from DBC is that we offer here a more detailed series of comparisons between our own calibration and the original one used by *IRAS*.

2. THE NEW SPECTRA OF VEGA AND SIRIUS

Both these A dwarf stars are sufficiently hot that molecules could not survive in their atmospheres and both have been modeled in the past (Kurucz 1979; Dreiling & Bell 1980; Bell & Dreiling 1981). What distinguishes our latest Kurucz (1991a) models from all previous efforts are the metallicities inherent in Kurucz's new work. After critical examination of detailed high-resolution ultraviolet and visible spectra of Vega, Kurucz finds definite support for the idea that Vega has less than solar metallicity. Sirius, because of mass transfer from its companion, is metal-rich compared with the sun (Latham 1970). It is the presence of dust around Vega and the greater brightness of Sirius that renders the latter a more desirable standard for infrared work. Consequently, we have chosen to work with both Vega—the canonical standard at UV-optical wavelengths—and Sirius.

By strong contrast with the arbitrary adoption of blackbodies, Fig. 1 offers Kurucz's new Vega model in comparison with the UV-optical spectral energy distributions defined from a variety of narrowband observations. It is important to keep the quality of this match firmly in mind when listening to arguments for and against blackbodies as calibration models. Blackbodies do not and cannot represent real stars across the entire ultraviolet, visible, and infrared. The model offered, however, derives its credibility

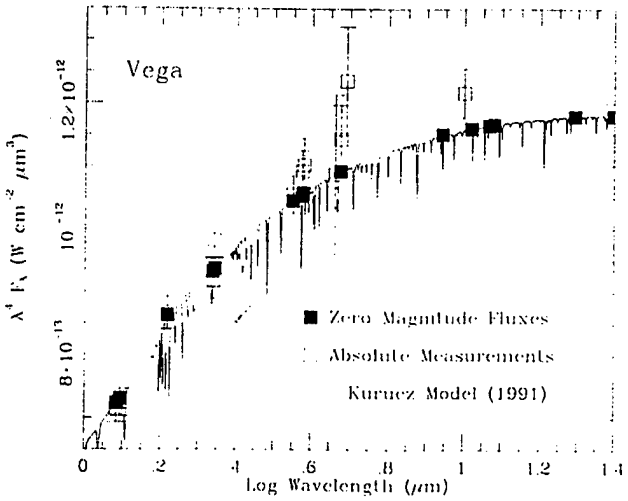

FIG. 2. The new Vega model displayed in the infrared after normalization to the Hayes (1985) average 5556 A monochromatic flux density. Solid squares represent the monochromatic flux densities obtained after integrating this model over the combined atmospheric and filter transmission profiles. Open squares with error bars denote the absolute mountaintop measurements of Vega cited in the text.

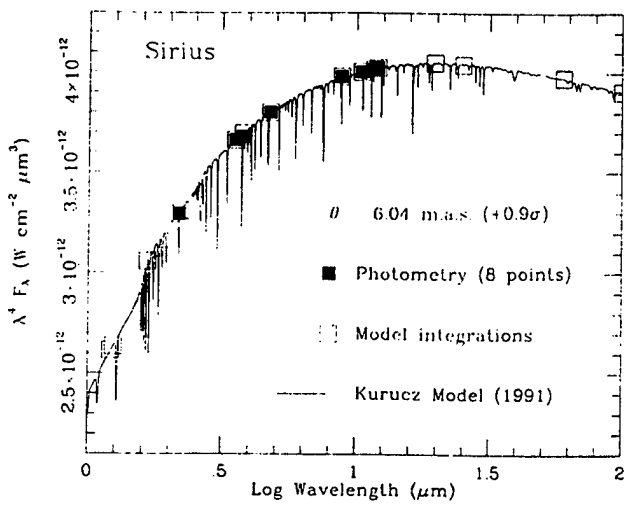

FIG. 3. Kurucz's (1991a) new Sirius model after final normalization. Open squares show actual monochromatic flux densities after integration over this model. Solid squares display the expected flux densities based on the eight magnitude differences between Vega and Sirius noted in the text, and the photometric calibration presented in Table 1(a). The implied angular diameter for Sirius is indicated on the plot along with its value relative to that measured by Hanbury Brown *et al.* (1974), in units of the σ of these authors' determination.

from the excellent reproduction of all these measurements of Vega's energy distribution (and of the Balmer line intensities and profiles). To accept an extrapolation of this model from the difficult and challenging UV-visible realm into the infrared, where lines are more widely separated, molecules negligible, and opacities are better understood than for cool stars, does not require any astrophysical compromise. The new model for Sirius (Kurucz 1991) similarly represents its UV-optical measurements.

Figure 2 presents Vega again, now in the form of a plot of $\lambda^4 F_\lambda$ (so that long and short wavelengths may be conveniently examined with equal ease in a single plot). One can independently validate the shape of this spectrum in the optical by comparison with the energy distribution for Vega tabulated by Hayes (1985: his Table II). Kurucz's new model agrees very well with the colors implied by Hayes' table. To place the model on an absolute footing we have interpolated the wavelength grid to obtain the monochromatic flux density at the astronomical standard wavelength of 5556A, then set this equal to Hayes' (1985) critically evaluated average of six independent measurements made by different groups: $[3.44 \pm 0.05 \times 10^{-9}$ erg $cm^{-2} s^{-1} A^{-1}]$. The filled black squares represent the results of combining both the atmospheric transmission (from a good astronomical site like Mauna Kea) and specific detailed broadband filter transmission profiles (measured at 77 K, their operating temperature: cf. DBC) with the Vega spectrum. Following Deacon, we adopt Vega as zero magnitude at all infrared wavelengths longwards of 1 μm but do not advocate use of real measurements of this star beyond ~ 20 μm for calibration purposes because of the existence of its shell of cold dust grains that first becomes apparent at about this wavelength. Consequently, the solid squares define our system of broadband "zero magnitude fluxes" (plotted with use of isophotal wavelengths: see Sec. 3). However, we do use integrations through the combination of filter and atmospheric transmission profiles over our ideal representation for Vega, namely the new model, to establish what zero magnitude should truly correspond to, even at the longest wavelengths where the real Vega has grossly departed from this ideal.

Figure 3 likewise shows the infrared portion of Kurucz's (1991a) independent model for Sirius. In this figure, open squares represent actual integrations of the stellar spectrum through the atmosphere and relevant filters. We have tested the shape of this Kurucz model in the optical against the colors provided by Davis & Webb (1974): it compares very favorably with their relative energy distribution. Initially we normalized the Sirius model in accordance with the optical interferometric angular diameter measured by Hanbury Brown *et al.* (1974) of 5.89 ± 0.16 milli-arcsec. We compared the ratios of in-band fluxes, between the calibrated Vega spectrum and the Sirius spectrum with this nominal normalization, with the factors corresponding to eight, equally weighted, expected magnitude differences {at K, L, L', M, [8.7], [10], [11.7], and [12], where $[\lambda]$ denotes a magnitude at λ μm, and where we took these magnitude differences from Deacon (1991): $K = L = L' = M = -1.36$; $[8.7] = N = [11.7] = [12] = -1.35$}. We then adjusted the angular diameter of Sirius to bring the observed and expected in-band flux ratios most closely together. This required a further rescaling of the model spectrum by a factor of 1.052 ± 0.002, corresponding to an angular diameter of 6.04 mas. Solid squares in Fig. 3 are derived from the flux densities expected for these magnitude differences (flux ratios) relative to Vega, using the broadband flux calibration illustrated in Fig. 2 and given in Table 1(a).

The two Kurucz models correspond to the following parameters. For Vega: $T_{\rm eff} = 9400$ K; $\log g = 3.90$;

TABLE 1. Monochromatic fluxes for the Vega and Sirius models that define our zero magnitude system.

(a) Vega

Ground-based, narrowband set (Selby *et al.* 1988) with InSb response included at Mauna Kea

Filter name	λ_{iso} (μm)	F_λ (W cm^{-2} μm^{-1})	F_ν (Jy)
Jn	1.243	3.059*E*−13	1575.3
Kn	2.208	3.940*E*−14	640.1
Ln	3.781	5.162*E*−15	246.0

Ground-based, usual set (e.g., UKIRT filters) with InSb response included at Mauna Kea

Filter name	λ_{iso} (μm)	F_λ (W cm^{-2} μm^{-1})	F_ν (Jy)
J	1.215	3.314*E*−13	1631.0
H	1.654	1.151*E*−13	1049.7
K	2.179	4.139*E*−14	655.0
L	3.547	6.590*E*−15	276.4
L'	3.761	5.263*E*−15	248.1
M	4.769	2.107*E*−15	159.7

Ground-based, usual set (e.g., UKIRT filters) at Mauna Kea

Filter name	λ_{iso} (μm)	F_λ (W cm^{-2} μm^{-1})	F_ν (Jy)
8.7	8.756	1.955*E*−16	49.98
N	10.472	9.631*E*−17	35.21
11.7	11.653	6.308*E*−17	28.56
20	20.130	7.182*E*−18	9.70

IRAS bands

		Noncolor-corrected		Color-corrected	
IRAS filter	In-band flux (W cm^{-2})	F_λ (W cm^{-2} μm^{-1})	F_ν (Jy)	F_λ (W cm^{-2} μm^{-1})	F_ν (Jy)
12	5.411*E*−16	8.363*E*−17	40.141	5.616*E*−17	26.966
25	4.585*E*−17	4.265*E*−18	8.886	3.018*E*−18	6.288
60	3.732*E*−18	1.206*E*−19	1.447	9.051*E*−20	1.085
100	4.212*E*−19	1.264*E*−20	0.421	1.159*E*−20	0.386

(b) Sirius

Ground-based, narrowband set (Selby *et al.* 1988) with InSb response included at Mauna Kea

Filter name	λ_{iso} (μm)	F_λ (W cm^{-2} μm^{-1})	F_ν (Jy)	Mag
Jn	1.243	1.105*E*−12	5688.3	−1.39
Kn	2.208	1.392*E*−13	2262.1	−1.37
Ln	3.781	1.806*E*−14	860.9	−1.36

Ground-based, usual set (e.g., UKIRT filters) with InSb response included at Mauna Kea

Filter name	λ_{iso} (μm)	F_λ (W cm^{-2} μm^{-1})	F_ν (Jy)	Mag
J	1.215	1.198*E*−12	5896.4	−1.39
H	1.653	4.099*E*−13	3730.6	−1.40
K	2.179	1.463*E*−13	2315.2	−1.37
L	3.550	2.304*E*−14	967.8	−1.36
L'	3.759	1.843*E*−14	868.4	−1.36
M	4.770	7.350*E*−15	557.5	−1.36

Ground-based, usual set (e.g., UKIRT filters) at Mauna Kea

Filter name	λ_{iso} (μm)	F_λ (W cm^{-2} μm^{-1})	F_ν (Jy)	Mag
8.7	8.758	6.776*E*−16	173.2	−1.35
N	10.472	3.332*E*−16	121.8	−1.35
11.7	11.655	2.178*E*−16	98.62	−1.35
20	20.132	2.466*E*−17	35.31	−1.34

IRAS bands

		Noncolor-corrected		Color-corrected		
IRAS filter	In-band flux (W cm^{-2})	F_λ (W cm^{-2} μm^{-1})	F_ν (Jy)	F_λ (W cm^{-2} μm^{-1})	F_ν (Jy)	Mag
12	1.872*E*−15	2.894*E*−16	138.895	1.941*E*−16	93.159	−1.35
25	1.572*E*−16	1.463*E*−17	30.471	1.034*E*−17	21.542	−1.34
60	1.267*E*−17	4.093*E*−19	4.911	3.066*E*−19	3.679	−1.33
100	1.421*E*−18	4.262*E*−20	1.421	3.906*E*−20	1.302	−1.32

[Fe/H]=−0.5; $v_{microturb}$=0 km s^{-1}. After scaling to the Hayes' 5556 A flux density, the resulting angular diameter is 3.335 mas. The optical angular diameter measured interferometrically by Hanbury Brown *et al.* (1974) for Vega is 3.24±0.07 mas [at 1 μm Leggett *et al.* (1986) obtained 3.25±0.16]. For Sirius corresponding numbers are: 9850 K, 4.25, +0.5, 0 km s^{-1}, and 6.04 mas. Our angular diameter is only 0.9σ above the measurement by Hanbury Brown *et al.* (1974). There is an inherent absolute uncertainty in both models arising from the ±1.45% uncertainty in the Hayes (1985) 5556 A flux for Vega (cited above). The best match of the eight Sirius fluxes to independently determined broadband magnitude differences with respect to Vega introduces another source of error for Sirius, although this is very small (±0.17%: from the standard error in the mean factor given above). This increases the absolute uncertainty inherent in the Sirius spectrum from ±1.45% to ±1.46% (by root sum square combination of these two independent sources of error).

Therefore, these two models, with their current scales, represent our best estimates for absolutely calibrated continuous spectra, from which to determine broad and narrowband stellar flux densities.

3. THE ZERO MAGNITUDE FLUX CALIBRATION

After combining atmosphere and filter profiles and integrating over the two models we obtained a set of in-band fluxes for Vega. In Table 1(a) we present the equivalent monochromatic flux densities (which we define to correspond to zero magnitude) together with the accompanying "isophotal" wavelengths. The choice of isophotal as opposed to effective wavelengths is dictated by our applications to the very broad filters that typify mid-infrared as-

tronomy. We follow the discussion of, rationale for, and definition of isophotal wavelength introduced by Brill (1938), addressed by Stock & Williams (1962), and most clearly explained by Golay (1974). Integration of our calibrated versions of the Kurucz models over a specific filter and atmospheric profile yields an appropriately weighted monochromatic flux density (in units of W cm^{-2} μm^{-1}). Conversion into Jy is achieved using the standard relation between F_ν and F_λ involving the wavelength, here taken to be the isophotal wavelength. For the *IRAS* bands we use nominal wavelengths (12, 25, 60, 100 μm), compute the in-band fluxes, and convert directly into F_ν using the standard bandpasses for these filters. F_λ calibrations again follow from the standard relation: $F_\lambda = 3.0E-16 * F_\nu/\lambda^2$.

Table 1 includes standard ground-based filters and the three very narrow bands used by Selby *et al.* (1988) that support the determinations of angular diameter and effective temperature for 114 stars most recently applied by Blackwell *et al.* (1991) using the Infrared Flux Method. Isophotal wavelengths tabulated are determined by detailed comparison of the actual monochromatic spectral flux densities of the model with the computed monochromatic flux densities. For cool stars these wavelengths will be slightly different from those in Table 1. Table 1 also presents our calibrations for the four *IRAS* bands, in the form of in-band flux, noncolor-corrected flux densities (both F_λ and F_ν), and finally the color-corrected flux densities.

Our primary applications of these zero magnitude calibrations are to the creation of absolutely calibrated cool stellar spectra (cf. CWW). Consequently, the relevant stars are the canonical cool stellar "calibrators" of infrared astronomy. These are all very bright objects in broadband terms and their magnitudes reflect measurements made over the past two decades, largely with bolometers. However, we have also included the wavelength variations of detector quantum efficiency that characterize typical modern InSb detectors (cf. The Infrared Handbook 1978). In practice, this makes very little difference to our calculated numbers: inclusion of the quantum efficiency affects λ_{iso} by $\sim$0.005 μm, and F_λ or F_ν by $<1\%$ over the 1–5 μm region.

Table 1 formally includes the terrestrial atmosphere above Mauna Kea in the determination of isophotal wavelengths and monochromatic flux densities. However, we have also investigated those differences that arise when observing from lower elevation sites and at higher latitudes. We took Kitt Peak to be a representative example of these popular lower elevation sites.

The atmospheric transmittances that we use to represent conditions at Mauna Kea were based initially upon applications of the following: (i) the IRTRANS code (Traub & Stier 1976) by Dr. C. M. Mountain for the 1–6 μm range under the following circumstances: 1.2 mm of precipitable water vapor; an airmass of 1.00; a wavelength gridding of 0.0005 μm with Gaussian convolution to achieve a FWHM of 0.0025 μm; and appropriate values for molecular abundances and partial pressures of H_2O, CO_2, O_3, N_2O, CO, CH_4, and O_2; and (ii) the 6–14 μm atmospheric profile computed by Kyle & Goldman (1975). More recently, we have utilized a complete set of consistent atmospheric calculations based upon a CRAY YMP code ("NWATR") in use at NASA-Ames and derived from the FASCOD2 software. Lord (1992) provides a comparison of the various codes at NASA-Ames that currently all utilize the newest (1991) release of the original HITRAN database (Rothman *et al.* 1987). We used these calculations (carried out for us by J. Simpson) to represent the atmospheres at Mauna Kea and a typical lower elevation site. We find no essential differences between the results yielded by these two approaches but we prefer the homogeneous set of finely gridded models calculated with NWATR at NASA-Ames.

For this direct comparison of sites, we matched Mountain's calculations for Mauna Kea, then computed a similar model for the lower elevation, using 5.0 mm of precipitable water vapor, unit airmass, and fine wavelength gridding. Specific relevant details of the primary molecular constituents in these calculations are as follows: for Mauna Kea, $w(H_2O)=0.418E22$, $w(CO_2)=0.478E22$, $w(O_3)=0.693E19$, $w(N_2O)=0.650E19$, $w(CO)=0.302E19$, $w(CH_4)=0.195E20$, $w(O_2)=0.272E25$ mol cm^{-2}; for Kitt Peak, $w(H_2O)=0.167E23$, $w(CO_2)=0.551E22$, $w(O_3)=0.752E19$, $w(N_2O)=0.837E19$, $w(CO)=0.389E19$, $w(CH_4)=0.251E20$, $w(O_2)=0.350E25$ mol cm^{-2}.

The effects on isophotal wavelengths are generally very small, typically <0.005 μm, although some filters obviously sample poorer "windows" and suffer greater changes. The greatest change is for Q whose λ_{iso} goes from 20.13 μm at Mauna Kea to only 19.58 μm at Kitt Peak. This emphasizes the critical importance of defining a narrower 20 μm band that is blocked at long wavelengths rather than permitting the time-variable atmosphere to dictate both wavelength and observed in-band flux (cf. Young & Milone 1992). For no other filter does λ_{iso} alter by >0.01 μm. This change of site affects the monochromatic flux densities by much less than 1% for all filters except Q, where the great change in λ_{iso} clearly has consequences for the flux density. But it is far preferable to pursue Q photometry only from sites such as Mauna Kea where the Q magnitudes used by CWW of this series were obtained. For practical purposes, we also present this lower elevation calibration (including the effects of InSb wavelength-dependent quantum efficiency) as Table 2, but for Vega alone (i.e., the zero magnitude system).

In order to cope with the photometric calibration of the Strecker *et al.* (1979) spectral database (used by CWW) obtained from high altitude airborne observatories, we have also calibrated all near-infrared filters for altitudes appropriate to airborne observatories. Here the maximal effects occur for the M band whose λ_{iso} diminishes by 0.10 μm (to 4.665 μm) and whose flux density increases $\sim$5%. More typically, however, λ_{iso} changes by <0.02 μm, and flux densities alter by $\sim$2%.

Table 1(b) likewise includes isophotal wavelengths and monochromatic flux densities for Sirius, and its magnitudes relative to Vega=0.0.

In Fig. 2, open squares show the best mountaintop ab-

TABLE 2. Monochromatic fluxes for the Vega model that define our zero magnitude system at lower elevation sites (e.g., Kitt Peak).

Ground-based, narrowband set (Selby *et al.* 1988) with InSb response included

Filter name	λ_{iso} (μm)	F_λ (W cm^{-2} μm^{-1})	F_ν (Jy)
Jn	1.243	3.059*E*−13	1575.2
Kn	2.208	3.940*E*−14	640.1
Ln	3.781	5.162*E*−15	246.0

Ground-based, usual set (e.g., UKIRT filters) with InSb response included

Filter name	λ_{iso} (μm)	F_λ (W cm^{-2} μm^{-1})	F_ν (Jy)
J	1.212	3.341*E*−13	1636.6
H	1.654	1.151*E*−13	1049.5
K	2.182	4.116*E*−14	653.2
L	3.561	6.497*E*−15	274.6
L'	3.751	5.315*E*−15	249.2
M	4.773	2.100*E*−15	159.5

Ground-based, usual set (e.g., UKIRT filters)

Filter name	λ_{iso} (μm)	F_λ (W cm^{-2} μm^{-1})	F_ν (Jy)
8.7	8.765	1.948*E*−16	49.88
N	10.468	9.648*E*−17	35.24
11.7	11.651	6.314*E*−17	28.57
20	19.575	8.026*E*−18	10.25

solute measures of Vega's fluxes (Blackwell *et al.* 1983; Campins *et al.* 1985; Selby *et al.* 1983; Mountain *et al.* 1985; Rieke *et al.* 1985) currently available along with their uncertainties (probably underestimated as between 3% and 10%, increasing with wavelength). To plot the points in this figure we note that some of the measurements were made with spectrometers to isolate carefully chosen "clean" portions of the earth's atmospheric windows: their declared wavelengths were used without modification (e.g., Blackwell *et al.* 1983; Mountain *et al.* 1985). However, the work of Campins *et al.* (1985) refers to the "standard Johnson" system of JHKLM bands: these are broad filters, not selected with detailed consideration of the telluric transmittance, so we chose to plot them in Fig. 2 at their actual isophotal wavelengths for the filter and atmosphere above the Catalina Mts. where the data were obtained. Note that none of these absolute determinations deviates from our calibrated Kurucz model of Vega by more than 2σ.

In spite of this proximity, the disposition of the mountaintop measurements is predominantly above the model. Therefore, it is pertinent to ask whether there is any evidence for a near- or mid-infrared analogue of the known far-infrared excess emission in Vega that could elevate these measurements above the model flux densities. Direct comparison of the *IRAS* Low Resolution spectrum of Vega (after recalibration: see CWW) with our calibrated Kurucz model of the same star indicates that no significant departures from the model are seen shortward of 16.5 μm. Consequently, at least between 7.7 and 16.5 μm and at the few percent level, no departures from the theoretical expectation occur in the real Vega. At present, one cannot definitively exclude some low level of contamination of the observed 1–5 μm energy distribution of Vega by hotter dust grains than those first detected by *IRAS*. However, we note that Bessell & Brett (1988) concluded that the apparent near-infrared excess of Vega, measured from mountaintops, was not real from their own study of the colors of other A0 stars.

Hanner & Tokunaga (1991) present their suggested Vega fluxes in a number of infrared wavebands, apparently based upon these absolute measurements rather than on any stellar model. For the five near-infrared filters in common with our own tabulations (*HKLL'M*) the average ratio of our absolute Vega flux densities to theirs is 0.98 $\pm$0.01, consistent with these authors' reliance on the mountaintop data, which slightly exceed our Kurucz model (Fig. 2). At long wavelengths, Hanner & Tokunaga (1991) adopt "reference wavelengths" different from our isophotal wavelengths for *N* and *Q*. If we treat their wavelengths as isophotal, and extract the flux densities from our Vega model corresponding to 10.10 and 20.00 μm, our flux densities are 0.95 and 1.03 of theirs. We conclude that, within the uncertainties estimated by Hanner & Tokunaga (1991), our calibrated Vega model provides an acceptable set of zero magnitude flux densities. Furthermore, it is essential to utilize such a model in order to obtain wavelength interpolation between the scarce absolute mountaintop data points and hence cope with wavebands that are either unobservable from the ground or simply do not match the filters used in these absolute determinations.

4. THE POINT SOURCE CALIBRATION OF *IRAS*

The issue of the *IRAS* point source calibration is clearly of interest given the wealth of data provided by that satellite. A very careful reading of the *IRAS* Explanatory Supplement (1988: pg. VI-19ff) leads to the conclusion that, until we have studied every star in their Table VI.C.3, we cannot definitely address the *IRAS* point source calibration. However, several comparisons are possible, as described below.

4.1 Comparison with the IRAS Point Source Catalog Version 2 (PSC)

The most direct comparison is with the PSC because this tabulates flux densities in Jy without color-correction. These quantities are readily derived by integration of a given spectrum over the *IRAS* bandpasses and subsequent conversion of the resulting in-band fluxes to monochromatic flux densities using the *IRAS* standard filter bandwidths (*IRAS* Supplement 1988, pg. X-13). In what follows we define $R(\lambda)$ to be the ratio of one of our own flux densities at λ μm to that obtained by *IRAS*. At 12 μm on Vega the PSC gives 41.56$\pm$1.66 Jy (using both the flux density and the quantity "RELUNC" that indicates the relative uncertainty in % of a PSC measurement). Table

1(a) indicates 40.14 Jy, suggesting that $R(12)=0.966 \pm 0.039$. Likewise, for Sirius we obtain $R(12)=0.971 \pm 0.029$ (the PSC indicates $S_\nu=143.1 \pm 4.29$ Jy). (These ratios also appear in Table 3.) At 25 μm we cannot use Vega because of its dust shell. Only Sirius can be used to compare Table 1(b) (30.47 Jy) with the PSC (33.97 ± 1.70 Jy using the 5% figure given for "RELUNC" at this wavelength). This indicates a factor, $R(25)$, of 0.899 ± 0.045. At 60 μm we again cannot use Vega, but Sirius data are still valid. Comparing Table 1(b) (4.911 Jy) with the PSC (4.92 ± 0.39 Jy using the 8% figure given for "RELUNC" at 60 μm) indicates $R(60)=0.998 \pm 0.080$. At 100 μm Vega's dust shell precludes a direct comparison with the Kurucz model and Sirius is contaminated by cirrus, so we cannot evaluate the accuracy of the *IRAS* point source calibration at this longest wavelength using stellar measures.

TABLE 3. Ratios of our calibration stellar fluxes to those measured by *IRAS*.

Star	Wavelength	$R(\lambda)$	Uncertainty	Comparison with
Vega	12	0.966	0.039	PSC
		0.987	0.01	Table VI.C.3
Sirius	12	0.971	0.029	PSC
		0.967	0.01	Table VI.C.3
Combined	12	0.976	0.007	4 values above
Zero mag	12	0.978		
Sirius	25	0.899	0.045	PSC
		0.952	0.025	Table VI.C.3
Combined	25	0.940	0.022	2 values above
Zero mag	25	0.936		
Sirius	60	0.998	0.08	PSC
		0.971	0.02	Table VI.C.3
Combined	60	0.973	0.019	2 values above
Zero mag	60	0.921		
Zero mag	100	0.896		

4.2 Comparison with the IRAS Explanatory Supplement's Subset of Stars

The *IRAS* Explanatory Supplement (1988) places great reliance on developing the *IRAS* point source calibration on the basis of a set of eight stars (Table VI.C.3) which were measured by specific pointed observations. In this special calibration mode of *IRAS*, stars of interest were scanned across optimal "photometric tracks" in the focal plane during the survey (i.e., through the best characterized detectors). These observations had smaller intrinsic dispersion than the normal survey observations. Indeed, Aumanr *et al.* (1984) felt this method offered the most accurate data from *IRAS* on such stars and they quote probable errors of 1%, 2.5%, 2%, and 3% at 12, 25, 60, 100 μm for such flux densities. The Supplement does not offer any information on uncertainties for specific stellar magnitudes cited in Table VI.C.3 so we adopt the probable errors cited by Aumann *et al.* We, therefore, directly compare these most accurate *IRAS* flux densities of Vega (whose 12 μm mag, although not stated, is +0.01 within the context of Table VI.C.3) and Sirius with our own calibrated spectra of these stars. Table VI.C.3 implies 28.04 (Vega) and 99.03 Jy (Sirius) at 12 μm, and 22.70 Jy (Sirius alone) at 25 μm. The Supplement states that all these flux densities have been color-corrected treating each star as "a hot blackbody." We, therefore, assume that the color-correction factors given in Table VI.C.6 of the Supplement were applied, namely 1.45 at 12 μm, and 1.41 at 25 μm (corresponding to a roughly 10 000 K blackbody). Therefore, we deduce that the noncolor-corrected fluxes (the style given in the PSC) were 40.65 Jy (Vega at 12 μm) and 143.6 and 32.01 Jy (Sirius at 12 and 25 μm, respectively) which are to be compared with our own numbers of 40.14, 138.9, and 30.47 Jy, respectively. These comparisons suggest $R(12)=0.987$ (Vega) and 0.967 (Sirius), each with uncertainty of ± 0.01, and $R(25)=0.952 \pm 0.025$ (Sirius).

4.3 Combined Results and Comparison of Zero Point Flux Densities

Table 3 summarizes these several sets of stellar comparisons and presents their combinations, for different wavelengths, using inverse variance weighting.

The three separate determinations (or adoptions) of Vega's [12] by *IRAS* [-0.02 ± 0.06 (survey, mistyped in the Explanatory Supplement on page VI-21 as 0.02), $+0.01 \pm 0.01$ (pointed observations), and -0.01 ± 0.01 (Aumann *et al.* 1984)] are all consistent with our own system in which the Vega model is taken to define zero magnitude at all wavelengths. Consequently, it is meaningful to compare our own zero mag flux densities directly with those adopted by *IRAS*. After removing the color corrections stated to have been made by *IRAS* (1.45, 1.41, 1.32, 1.09 from Table VI.C.6), we deduce the *IRAS* quartet of noncolor-corrected flux densities for zero mag to be (41.04, 9.49, 1.57, 0.47 Jy). Our own values are (40.141, 8.886, 1.447, 0.421 Jy) which yields $R(12, 25, 60, 100)=(0.978, 0.936, 0.921, 0.896)$.

Although incomplete by comparison with the actual process pursued by the *IRAS* Science Team, these figures suggest that the current *IRAS* absolute calibration is too high by 2.4%, 6.5%, 2.9%, and 11.6% in the four wavebands, respectively. These estimates could surely be improved by a more rigorous explanation of, and duplication of, the procedures actually carried out in the calibration of *IRAS*.

5. CONCLUSIONS

We have presented absolutely calibrated versions of realistic model atmosphere calculations by Kurucz for Vega and Sirius on the basis of which we offer a new absolute calibration of infrared broad and narrow filters, and make a preliminary comparison with the current *IRAS* point source calibration. One could explore the influence on these wavelengths and flux densities of varying the site in

question with respect to latitude, longitude, season, even to those profound variations on water vapor (by up to a factor of 10) that can characterize night conditions in some locations. All these circumstances affect λ_{iso} and F_λ for zero mag. However, at this point we feel that equally large changes (if not larger ones) can result from variations in allegedly "standard infrared filters" from observatory to observatory (cf. 2.2.2 of Hanner & Tokunaga 1991), particularly given the past reluctance of most sites to publish cold scans of their filter profiles.

We advocate the use of Sirius as a primary infrared stellar standard; encourage the publication of the corresponding magnitudes of Vega (below 20 μm) and of Sirius whenever new infrared photometric filter systems and standards are developed; and urge the adoption of truly "standard" infrared filters whose transmission profiles, obtained at their actual operating temperatures, have also been published for integration over calibrated stellar models such as the ones we offer here for Vega and Sirius. We note that Young & Milone (1992) argue cogently for a new infrared system of filters that would minimize the variations of λ_{iso} with altitude of observing site.

We thank Bob Kurucz for providing us with the new models of Vega and Sirius on which this effort is based; David Beattie for obtaining and supplying the cold transmission scans of the UKIRT filter set; Jan Simpson for computing the HITRAN model atmospheres to compare MKO and KPNO; and Matt Mountain for his IRTRANS 1–6 μm atmospheric transmission spectrum. We are grateful to Gene Milone and Andy Young for their critical and helpful reading of this paper. Our efforts were supported both by a contract with Lincoln Laboratories, MIT, and by Cooperative Agreement NCC 2-142 between NASA-Ames Research Center and the University of California, Berkeley (M.C.). J.R.D. acknowledges support from Grant No. GR/E94777 from the United Kingdom S.E.R.C.

REFERENCES

Aumann, G., *et al.* 1984, ApJ, 278, L23
Bell, R. A., & Dreiling, L. A. 1981, ApJ, 248, 1031
Bessell, M. S., & Brett, J. M. 1988, PASP, 100, 1134
Blackwell, D. E., Leggett, S. K., Petford, A. D., Mountain, C. M., & Selby, M. J. 1983, MNRAS, 205, 897
Blackwell, D. E., Booth, A. J., Petford, A. D., Leggett, S. K., Mountain, C. M., & Selby, M. J. 1986, MNRAS, 221, 427
Blackwell, D. E., Petford, A. D., Arribas, S., Haddock, D. J., & Selby, M. J. 1990, A&A, 232, 396
Blackwell, D. E., Lynas-Gray, A. E., & Petford, A. D. 1991, A&A, 245, 567
Brill, A. 1938, Zs. f. Astrophys., 15, 137
Campins, H., Rieke, G. H., & Lebofsky, M. J. 1985, AJ, 90, 896
Cohen, M., Walker, R. G., & Witteborn, F. C. 1992, AJ (in press) (CWW)
Cohen, M., Witteborn, F. C., Carbon, D., Augason, G., Wooden, D., Bregman, J., & Goorvitch, D. 1992, AJ (in press)
Davis, J. & Webb, R. J. 1974, MNRAS, 168, 163
Deacon, J. R. 1991, Ph.D. dissertation, University College, London
Deacon, J. R., Barlow, M. J., & Cohen, M. 1992a, in preparation
Deacon, J. R., Barlow, M. J., & Cohen, M. 1992b, in preparation (DBC)
Dreiling, L. A., & Bell, R. A. 1980, ApJ, 241, 737
Golay, M. 1974, Introduction to Astronomical Photometry, Vol. 41 in the Astrophysics and Space Science Library (Reidel, Dordrecht), pp. 39–46
Hanbury Brown, R., Davis, J., & Allen, L. R. 1974, MNRAS, 167, 121
Hanner, M. S., & Tokunaga, A. T. 1991, in Comets in the Post-Halley Era, Vol 1., edited by R. L. Newburn *et al.* (Kluwer, Holland), p. 67
Hayes, D. S. 1985, in Calibration of Fundamental Stellar Quantities, Proc. IAU Symposium No. 111, edited by D. S. Hayes, L. E. Pasinetti, and A. G. Davis Philip (Reidel, Dordrecht), p. 225
Hayes, D. S., & Latham, D. W. 1985, ApJ, 197, 593
IRAS Explanatory Supplement, 1988, IRAS Catalogs and Atlases, Volume 1, NASA RP-1190
Kurucz, R. L. 1979, ApJS, 40, 1
Kurucz, R. L. 1991a, private communication
Kurucz, R. L. 1991b, New lines, New models, New colors, in Proceedings of the workshop on "Precision Photometry: Astrophysics of the Galaxy," edited by A. G. Davis Philip, A. R. Upgren, and K. A. Janes (Davis, Schenectady), p. 27
Kyle, T. G., & Goldman, A. 1975, Atlas of Computed IR Atmospheric Absorption Spectra, NCAR-TN STR-112
Latham, D. W. 1970, Ph.D. dissertation, Harvard University
Leggett, S. K., Mountain, C. M., Selby, M. J., Blackwell, D. E., Booth, A. J., Haddock, D. J., & Petford, A. D. 1986, A&A, 159, 217
Lord, S. D. 1992, A New Software Tool for Computing the Earth's Atmospheric Transmission of Near-Infrared and Far-Infrared Radiation, NASA CR, in preparation
Mountain, C. M., Leggett, S. K., Selby, M. J., Blackwell, D. E., & Petford, A. D. 1985, A&A, 151, 399
Rieke, G. H., Lebofsky, M. J., & Low, F. J. 1985, AJ, 90, 900
Rothman, L. S., *et al.* 1987, Appl. Optics, 26, 4058
Selby, M. J., Mountain, C. M., Blackwell, D. E., Petford, A. D., & Leggett, S. K. 1983, MNRAS, 203, 795
Selby, M. J., Hepburn, I., Blackwell, D. E., Booth, A. J., Haddock, D. J., Arribas, S., Leggett, S. K., & Mountain, C. M. 1988, A&AS, 74, 127
Stock, J., & Williams, A. D. 1962, in Stars and Stellar Systems, Vol. II, Astronomical Techniques, edited by W. A. Hiltner (Univ. of Chicago Press, Chicago), p. 374
Strecker, D. W., Erickson, E. F., & Witteborn, F. C. 1979, ApJS, 41, 501
The Infrared Handbook 1978, edited by W. L. Wolfe and G. J. Zissis (US Govt. Printing Office, Washington, DC), p. 11
Traub, W. A., & Stier, M. T. 1976, Appl. Optics, 15, 364
Tug, H., White, N. M., & Lockwood, G. W. 1977, A&A, 61, 679
Young, A. T., & Milone, E. F. 1992, A&A (in press)

SPECTRAL IRRADIANCE CALIBRATION IN THE INFRARED. II. α TAU AND THE RECALIBRATION OF THE *IRAS* LOW RESOLUTION SPECTROMETER

MARTIN COHEN

Jamieson Science & Engineering, Inc., 5321 Scotts Valley Drive, Suite 204, Scotts Valley, California 95066 and Radio Astronomy Laboratory, 601 Campbell Hall, University of California, Berkeley, California 94720

RUSSELL G. WALKER

Jamieson Science & Engineering, Inc., 5321 Scotts Valley Drive, Suite 204, Scotts Valley, California 95066

FRED C. WITTEBORN

Astrophysics Branch, NASA-Ames Research Center, Mailstop 245-6, Moffett Field, California 94035

Received 20 April 1992; revised 6 July 1992

ABSTRACT

We describe a general technique for assembling continuous calibrated infrared spectra over a wide wavelength range. To demonstrate the method we construct an *absolutely calibrated* 1–35 μm spectrum of α Tau and independently validate the method using new and carefully designed observations. First we investigate the absolute calibration of the *IRAS* low resolution spectrometer (LRS) database by comparing this observed spectrum of α Tau with that assumed in the original LRS calibration scheme. Second, an analysis of asteroidal LRS spectra results in an independent assessment of the calibration problems with the LRS and provides a natural complement to the effort based on α Tau. Stellar studies define the short wavelength problems well; the cool asteroids characterize the long wavelengths. Third, we make a direct comparison of LRS stellar spectra with independently calibrated long-wavelength (~20 μm) airborne and ground-based spectra. These three approaches are complementary and have been combined. Neglect of the SiO fundamental band in α Tau has led to the presence of a specious "emission" feature in *all* LRS spectra near 8.5 μm, and to an incorrect spectral slope between 8 and ~12 μm. We explain the differences between this new LRS recalibration and that due to Volk & Cohen [AJ, 98, 1918 (1989)] and discuss why the present set of "correction factors" is more accurate. Recognition of the influence of the SiO fundamental on both the LRS calibration and on the continua of cool normal giant stars also leads to an understanding of the apparent plethora of classes into which these normal stars fall when assigned by the AUTOCLASS (Cheeseman *et al.* 1989) artificial intelligence scheme applied to the *IRAS* LRS Atlas.

1. INTRODUCTION

This paper is the second in an ongoing series that treats the topic of absolute and continuous infrared spectral calibration. The first (Cohen *et al.* 1992a, hereafter referred to as Paper I) deals with an approach to broadband infrared calibration based on new models of Vega (α Lyr) and Sirius (α CMa) computed by Kurucz (1991), with realistic metallicities chosen by Kurucz on the basis of detailed analyses of their UV-visible spectra; the third (Cohen *et al.* 1992b, hereafter referred to as Paper III) discusses the influence of molecular bandheads (notably CO and SiO) on the near-to-midinfrared spectra of normal giants. In the present paper we demonstrate how these studies may be used both to create absolutely calibrated spectra of cool stars and to repair the critically useful satellite-borne *IRAS* low resolution spectrometer (LRS) database. Only the LRS covers the 14–16 μm region that is still opaque even from airborne observing platforms, such as NASA's Kuiper Airborne Observatory [hereafter referred to as KAO].

The full Dutch *IRAS* LRS database comprises 171 000 extracted spectra and one can place it on the same photometric footing as the *IRAS* Point Source Catalog version 2 (1988, hereafter referred to as PSC). To accomplish this, one should note that the LRS was essentially not intended to provide absolutely calibrated spectra but rather to yield meaningful spectral shapes. One begins by overlapping the independent red and blue spectral halves based on the average flux densities over a common wavelength interval (see Sec. *3.5*). This spliced spectrum is then compared with the in-band flux (W m^{-2}) by integrating the *IRAS* 12 μm system response function [*IRAS* Explanatory Supplement (1988, pp. II–18)] over the LRS spectrum. [In-band flux is implicit in the flux density (Jy) tabulated for a source in the PSC through the bandwidths given in the *IRAS* Explanatory Supplement (1988, pp. X–13)]. This provides a normalization to the PSC photometric scale. (We describe these operations of splicing and normalization in detail in Sec. *3.5*.)

Not all available LRS spectra in the Groningen extracted database are equally useful to the occasional user. One needs to determine that a particular LRS spectrum of interest was obtained at the survey scan rate and not during the staring mode (an "additional observation") or during the special "calibration macros" that were developed to

 0004-6256/92/112030-15$00.90

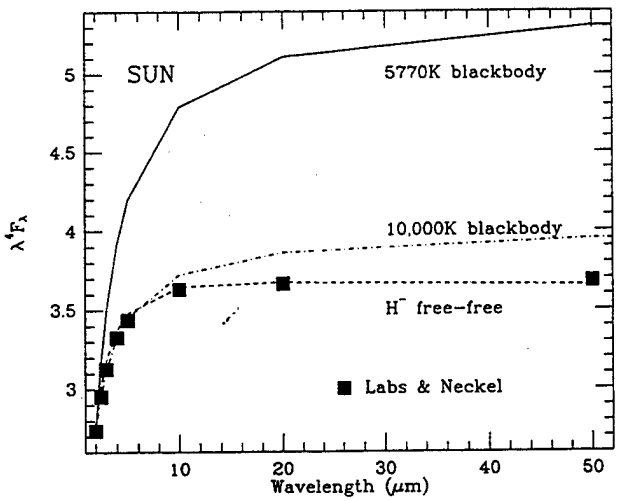

FIG. 1. Energy distribution of absolute solar radiance measurements by Labs and Neckel (1970) compared with blackbodies at the Sun's effective temperature and at 10 000 K, and with Engelke's (1990) approximation.

scan cool "standard" stars slowly over the *IRAS* focal plane for broadband photometric calibration purposes. These nonstandard LRS spectra do not yield to the usual LRS extraction method although all can be recovered at Groningen. Calibration macros affect a number of potentially important calibrators such as α Tau, α Boo, α CMa, etc. The rest of this discussion assumes that standard survey-rate LRS spectra are used.

We now address the issue of the radiance calibration of the LRS. According to the *IRAS* Explanatory Supplement (1988, pp. IX–6), the accuracy of the LRS spectral irradiance calibration rests entirely on the validity of an assumed 10 000 K blackbody for the intrinsic spectrum of α Tau. The stellar continuum of this cool star probably is quite well represented by such a hot blackbody. Indeed, the variations of brightness temperature with wavelength render the broad solar infrared energy distribution (Labs & Neckel 1970) a good match to a hot blackbody (Fig. 1), although a better match is achieved by assuming that the dominant source of opacity is H^- free–free (cf. Engelke 1990). However, the presence of molecular features in α Tau's infrared spectrum would invalidate this method for LRS calibration. The recent recognition of the importance in K–M giants of the SiO fundamental between 7.5 and $\sim$12 μm (Paper III) bears directly on this issue and has motivated our reexamination of the calibration of the LRS.

Therefore, the LRS can be globally recalibrated by dividing each LRS spectrum by the quotient of the real spectrum of α Tau and this 10 000 K blackbody. In this paper we: define the set of correction factors necessary to rectify LRS spectra to an accurate spectral shape; demonstrate the relevance of these corrections by examining the LRS spectra of α CMa and α Lyr, neither of which contains infrared molecular bands; use unpublished 20 μm airborne and newly obtained ground-based spectra to explore the long wavelength rectification of the LRS; and extract essentially the same set of corrections independently of stars by using LRS spectra of asteroids. Finally we indicate, quantitatively, how these corrections naturally account for the apparent diversity of LRS spectra for normal stars, as epitomized by the artificial intelligence "AUTOCLASS" (Cheeseman *et al.* 1989) process applied to the LRS Atlas (1986).

2. DIFFERENTIAL EFFECTS IN THE LRS DATABASE

If one examines the ratios of extracted LRS spectra, interesting patterns emerge that should be independent of any instrumental or calibrational procedures. For example, the ratios of LRS spectra of α Boo, β Peg, or μ Gem to that of α Tau reveal apparent features in the 9 μm region (Fig. 2). Even the LRS spectrum of α CMa has an apparent "emission feature" near 8 μm (Fig. 3). If α Tau were truly in accord with the 10 000 K blackbody assumption (which would be very close to the expected *continuum* if H^- free–free opacity were dominant in this K5III: Fig. 4; cf. Engelke 1990), such features would be mysterious. In order to highlight real features independently of radiance calibration, Paper III examines the ratio of spectra of cool stars to that of α CMa or α Lyr obtained with the same instrument and on the same night or flight. The infrared spectra of these hot dwarf stars do not contain infrared molecular features (Kurucz 1979, 1991; Bell & Dreiling 1981; Dreiling & Bell 1980) and, therefore, provide vital reference spectra for this exercise.

One can, therefore, identify the "feature" in the α CMa LRS spectrum near 8 μm as a consequence of the false assumption that α Tau has a featureless spectrum. The ratios of LRS spectra for M giants to that of α Tau consequently represent the variations between the SiO fundamentals in these cooler stars compared with that in α Tau. Likewise, the ratio of α Boo to α Tau reveals a residual emission feature because α Boo has a weaker SiO absorption band than α Tau [Fig. 2(a)], due to both its higher temperature and lower metal abundance.

3. ASSEMBLY OF A COMPLETE CONTINUOUS ABSOLUTE SPECTRUM FOR α TAU FROM 1.2 TO 35 μm

3.1 Available Infrared Spectra of α Tau

In this section we detail the procedure pursued to construct a complete spectrum of α Tau from fragmentary spectra and preexisting photometry. We aim at a final spectrum containing three attributes: λ, F_λ, and the absolute uncertainty in flux density at each wavelength. The fragments to which we have access are: (1) the 1.2–5.5 μm spectrum presented by Strecker *et al.* (1979, hereafter referred to as SEW); (2) our own 5–8 μm airborne spectral ratio of α Tau to α CMa (cf. Paper III), converted to flux density by multiplying this ratio spectrum by our calibrated Kurucz (1991; Paper I) model for α CMa (smoothed to the same resolution as our observations and regridded to the same wavelength scale); (3) our own 8–13 μm ground-based fragments similarly converted to calibrated spectra from spectral ratios, along with similar data from the UKIRT CGS3 spectrometer (Barlow 1991) that

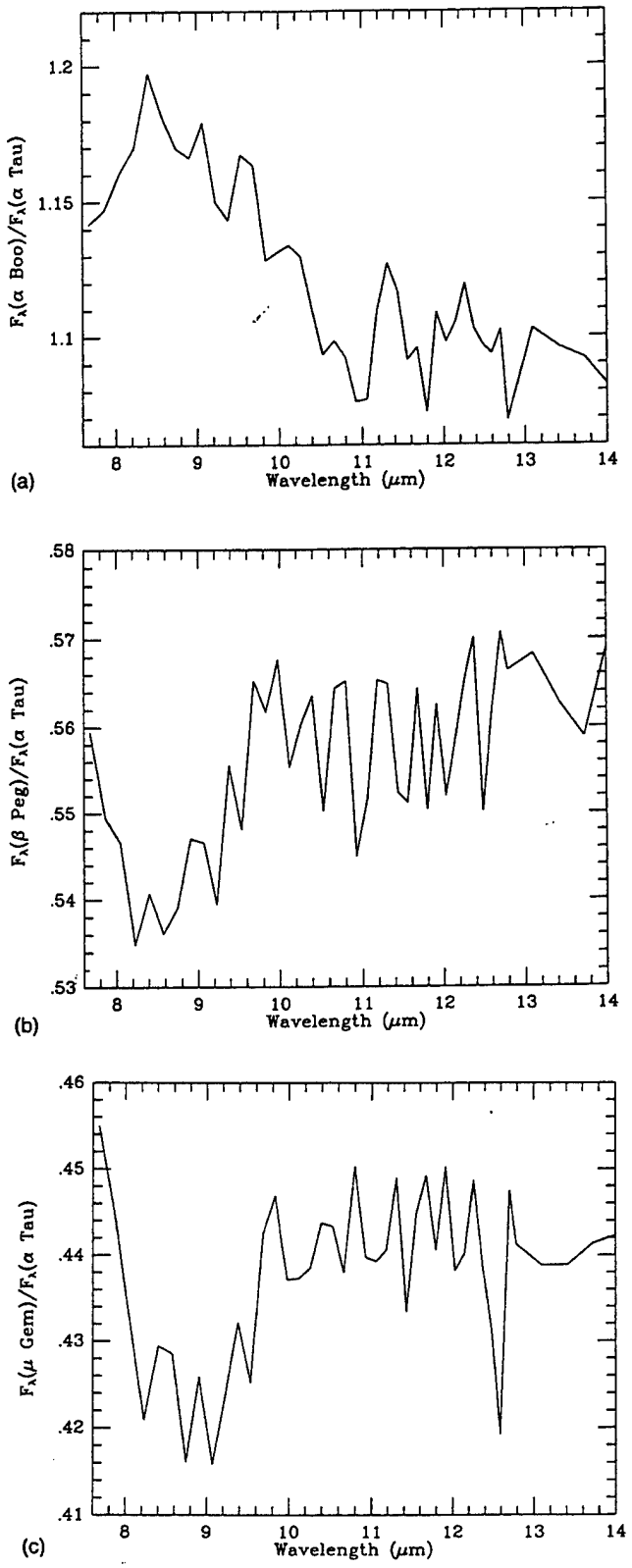

FIG. 2. Differential effects in the LRS database. The ratios of LRS spectra of (a) α Boo and α Tau; (b) β Peg and α Tau; (c) μ Gem and α Tau from 7.7 to 14 μm.

yield the ratios of α Tau to β Peg, and of β Peg to α Lyr; (4) all or part of the LRS spectrum from 7.7–22.7 μm; (5) newly secured UKIRT CGS3 10 and 20 μm spectral ratios of α Tau to α CMa (Secs. *3.4* and *6.3*); and (6) the 20–35 μm spectrum taken by Glaccum (1990), whose irradiance

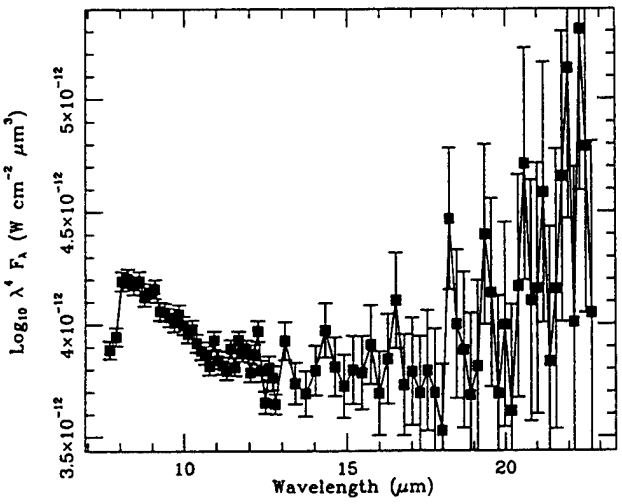

FIG. 3. LRS spectrum of α CMa in $\lambda^4 F_\lambda$ space. Note the emission feature from 8–10 μm.

calibration is based on planetary observations (see Sec. *4.3*). The last three points of Glaccum's spectra tend to have relatively large noise but these cosmetic blemishes in no way lessen the value of this unique database. We now describe in detail how these fragmentary spectra have been assembled into a single complete spectrum for α Tau using newly calibrated broadband ground-based photometry (cf. Paper I) to constrain the absolute levels of fragments whenever possible.

β Peg is characterized as a slowly varying irregular variable in both the General Catalogue of Variable Stars (hereafter referred to as GCVS, Kukarkin *et al.* 1970) and the Bright Star Catalogue (Hoffleit 1982). Although the visual amplitude is given as ~0.4 mag by the GCVS, the remark (on p. 579) indicates at most 0.14 mag in recent years. Despite this, a scrutiny of the infrared photometric literature does not reveal significant scatter in β Peg's adopted magnitudes beyond that expected when an attempt is made to intercompare different authors' zero-point systems (i.e., via their adopted magnitudes for α Lyr and α CMa). For

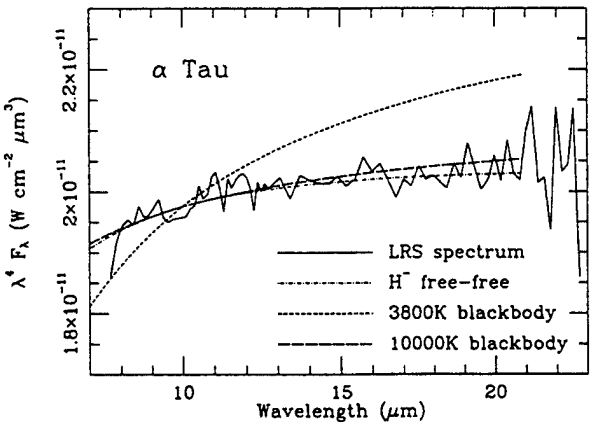

FIG. 4. Assumed LRS spectral shape of α Tau compared with blackbodies near the effective temperature and that adopted for the original LRS calibration, at 10 000 K, and with the H$^-$ free–free approximation made by Engelke (1990).

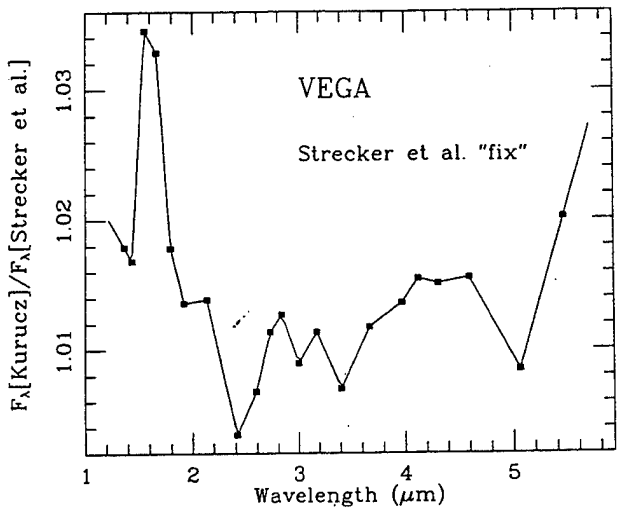

FIG. 5. The factors by which we multiply SEW spectra to convert them to the same reference frame for α Lyr that we use (i.e., the new Kurucz models as opposed to Schild *et al.* 1971).

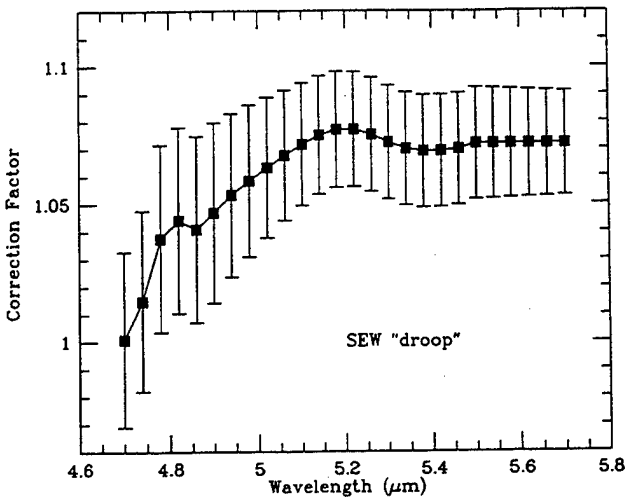

FIG. 6. The factors by which we now multiply SEW spectra to counteract the droop at the longest wavelengths caused by their falling instrumental efficiency. Error bars are 1σ and this function is the final one, determined by using the last iteration of α Tau's spectrum, rather than the one we initially used (from β And data) to construct α Tau.

our purpose here we do not require that β Peg's photometric level be constant; merely that its midinfrared spectrum has maintained a constant shape over time. We find no evidence to the contrary in our database of ratio spectra.

The process of assembling the complete α Tau spectrum involves three iterations. In the first, we employ the ratio of LRS spectra of α Tau and α CMa to assist in the definition of α Tau's true energy distribution by removing any potentially erroneous wavelength-dependent LRS calibration assumptions. In the second, we use an initial set of corrections to the LRS (generated in part by comparison of our first iteration α Tau spectrum with the 10 000 K blackbody originally used to calibrate the LRS) to "fix" the actual α Tau LRS spectrum as part of the process of constructing a more precisely defined energy distribution for α Tau. The second iteration yields a new set of LRS corrections that is indistinguishable from the first, within the uncertainties. The third iteration is described in Sec. 6, and is based on new independent datasets secured to validate the entire process of spectrum assembly.

3.2 The SEW Database

We first examine the pedigree of each spectral fragment with respect to its accuracy of shape. SEW established a system of continuous spectral standards in the near infrared based upon the model then current for the energy distribution of α Lyr (Schild *et al.* 1971). Cross calibration of a few infrared-bright cool giants (like α Tau) against α Lyr provided SEW with secondary standards. Therefore, we can bring their spectrum of α Tau into a form directly comparable with our absolute calibration framework by substituting the Kurucz (1991) α Lyr model for the Schild *et al.* model. Figure 5 presents the factors by which we multiply any SEW spectrum at each of the wavelengths tabulated by SEW for their α Lyr spectrum (any other SEW wavelengths we obtained by linear interpolation). Note that no factor exceeds 1.03 so this rectification makes a relatively small change to the SEW database although it is not negligible at the level of precision we are attempting to attain. To create Fig. 5 we isolated a set of continuum points (not affected by any hydrogen lines) for each of the SEW α Lyr and our Kurucz α Lyr spectra; regridded the Kurucz continuum set onto the wavelength scale representing the set of SEW continuum points (by linear interpolation) after Gaussian smoothing the model to the resolution of the SEW data; and took the direct ratio of the regridded smoothed Kurucz and SEW continuum sets.

A second correction that we found necessary to apply to the SEW database was discovered when we compared our own calibrated spectral shape for β And (derived from the ratio of KAO spectra for β And and α CMa shown in Paper III) with SEW's β And spectrum. We found that SEW's spectrum "drooped" relative to our 1991 January data, longward of about 4.5 μm. This we attribute to a small nonlinearity in the true conversion between wheel rotation and wavelength solely for the longest of SEW's three filter wheels (the 2.9–5.8 μm one); for example, a 2% wavelength error would result in a flux density error of $\sim$8% using either model for α Lyr. We, therefore, regridded our own comparably low-resolution β And spectrum to SEW's wavelength scale and directly compared the two spectra to provide a set of multiplicative factors to apply to all SEW spectra to counteract this droop. Although we used this function to create the first approximations to α Tau's spectrum, we subsequently refined it after creating our final spectrum for α Tau because α Tau provided a smaller set of errors for these multiplicative factors. Figure 6 shows the 0.25 μm FWHM Gaussian smoothed (to clean up the function) version of the correction that we now advocate to remove this effect from the SEW airborne (KAO and Lear Jet) database.

Although SEW do not provide error information specific to each star at every observed wavelength, Dr. Don

Strecker very kindly made available to us his original file of spectra. We have examined these in order to assign individual errors at different wavelengths and have found that the general figure cited by SEW of ±2% suffices for most stars in most wavelength intervals. In general, we have increased this in accordance with the actual scatter we measured in the original spectra obtained by SEW through the strong 2.7 μm CO_2 regime (uncertainties between 2.60 and 2.85 μm can locally attain ±10%). For α Tau, no increase above the nominal adopted ±2% uncertainty was necessary except in the immediate vicinity of the powerful 4.1–4.6 μm terrestrial CO_2 absorption. This region is essentially opaque at its core, even from airborne altitudes. We assigned realistic errors to the points from 4.14 to 4.22, and 4.54 to 4.62 μm and completely dropped all points between 4.23 and 4.50 μm on the basis both of detailed examination of many of our recent KAO 5–8 μm spectra and of atmospheric experiments defined by running NWATER, a NASA–Ames CRAY variant of FASCODE that uses the 1991 release of the HITRAN database (Rothman *et al.* 1987), applied for us by Dr. J. Simpson.

3.3 Airborne 5–8 μm Spectra

We have used several independent sets of spectral observations made from the KAO to determine the 5–8 μm spectrum of α Tau. These led to an indirect determination of the ratio of α Tau to either α CMa or α Lyr because previous "standardizations" did not acknowledge the existence of substantial molecular features in cool stars, nor the importance of obtaining the direct ratios of spectra of cool stars (such as α Tau and α Boo) to hot featureless spectra of stars like α Lyr and α CMa. First we defined the ratio of α Tau to β And between 5.31 and 10.12 μm (in two overlapping grating settings) on our 1985 December 12 flight, and of β And to α CMa on our 1991 January 21 flight that covered 3.38–8.75 μm (in two overlapping regions with two different spectrometers: Paper III shows the 1991 ratios of spectra). After interpolating the more coarsely sampled spectrum onto the more finely sampled wavelength scale and using inverse variance weighting (assuming zero covariance), these yielded the ratio $I(\alpha$ Tau$)/I(\alpha$ CMa), which we converted to flux densities via our calibrated version of Kurucz's (1991) new model for α CMa (Paper I), appropriately smoothed to match the resolution of the Ames Faint Object Grating Spectrograph (Witteborn & Bregman 1984, hereafter referred to as FOGS). Second, we independently constructed the ratio of α Tau to β Peg from 5.50 to 8.95 μm from our 1990 November 28 and 29 flights, and of β Peg to α Lyr between 5.11 and 8.14 μm (two slightly displaced, largely overlapping grating tilts) from our 1986 August 5 KAO flight. These provided the ratio $I(\alpha$ Tau$)/I(\alpha$ Lyr), which we converted to flux densities via our calibrated Kurucz (1991) model for α Lyr (Paper I). We attempted to remove residual small differential airmass effects in the earth's atmosphere by using the Ames HITRAN database and code cited above, although this cleaning resulted only in minimal changes to the observed spectral ratios. We then combined the two separately calibrated α Tau spectra using inverse variance weighting. All our individual spectra are provided with spectrophotometric errors at every wavelength that are defined by the dispersions of a stack of independent spectra. Note that throughout all such manipulations of spectra we: (1) apply inverse variance weighting; (2) augment all error budgets by a root-sum-square procedure applied to the fractional errors at matching wavelengths after interpolation; and (3) interpolate in variance when changing wavelength scales. All Ames spectrometers and the UKIRT CGS3 are multiplex (linear array) devices so that all wavelengths are observed simultaneously. We stress that throughout this effort we rely on these spectrometers to provide accurate *shape* information but only an approximation to the absolute level (as explained below).

We have embarked on an attempt to provide absolute spectral calibration from the KAO with respect to an onboard NIST-referenceable blackbody. During our first flight dedicated to calibration we secured 5.0–9.3 μm spectra of both α Tau and α CMa on 1991 December 20, at closely matched airmasses. These spectra afford totally independent and direct validations of the entire technique described here for constructing continuous infrared spectra because they simultaneously sample part or all of the SEW (1–5 μm), the traditional KAO (5–8 μm), and the ground-based 8–13 μm regions (through use of the new Ames "HIFOGS" instrument that has an array of 120 detectors that offers both higher resolution and broader wavelength coverage than its predecessor, the Ames FOGS). These new KAO data appear in Paper III. We use them in the present paper to examine the likely success of the method that we propose for assembling complete stellar spectra, when applied to stars less aggressively observed than α Tau, and subsequently to define a more accurate α Tau spectrum in this critical wavelength region.

3.4 Ground-Based 8–13 μm Spectra

We have the greatest amount of independent data in the ground-based 8–13 μm window where there exist several independent spectral ratios of α Tau to both α Lyr and α CMa, either direct or indirect: that from the FOGS, 1990 December 8, from the IRTF on Mauna Kea of α Tau to α CMa (Paper III); and a set of 10 μm spectra taken at the UKIRT on Mauna Kea with their CGS3 array spectrometer and very kindly made available to us by Dr. Michael Barlow of University College London. Barlow's CGS3 database yields an excellent pair of spectral ratios of β Peg to α Lyr (1990 July 16), and of β Peg to α Tau (1990 October 5), which we manipulated to provide $I(\alpha$ Tau$)/I(\alpha$ Lyr) that we "fluxed" through our absolutely calibrated α Lyr model by Kurucz (1991, Paper I). We have also secured two new independent sets of both low- and high-resolution CGS3 spectra of α Tau and α CMa taken during UKIRT service observations on 1991 November 9, for which we very carefully matched the airmasses of the two stars to within 0.02. The low-resolution data cover the range $\lambda\lambda$ 7.37–13.35 μm in three overlapping settings of

the grating by oversampling the true resolution. The high-resolution data cover $\lambda\lambda$ 9.09–13.35 μm in six overlapping settings. There is excellent agreement in shape between these low- and high-resolution service-mode datasets which now represent our highest signal-to-noise information on α Tau in the 10 μm window. However, we combined *all* available 8–13 μm data (with inverse variance weighting) to enhance the signal-to-noise ratio overall. We calibrated the ratios of $I(\alpha$ Tau$)/I(\alpha$ CMa) through our calibrated spectrum of α CMa (Paper I), after reducing the spectral resolution of the scaled Kurucz model to the actual observed resolution and regridding to the same wavelength scales as the UKIRT service spectra.

We emphasize the significant fact that we always find the SiO fundamental absorption to be present in the ratio of cool to hot stars (Paper III). In particular, we detect an obvious feature in α Tau in UKIRT CGS3 spectra, both indirectly obtained through ratios against intermediate stars (Barlow's data) and directly secured against α CMa (1991 November service spectra); in IRTF FOGS spectra (Paper III); in KAO direct and indirect spectral ratios that include the 7.5–8.5 μm regime. It is further apparent in other independent datasets such as LeVan's GLADIS spectra taken at Wyoming; and it is present in the *IRAS* LRS database. *We are confident that the reality of this feature in α Tau is not in doubt.*

3.5 Assigning Errors to LRS Spectra

An implicit criterion that we apply to valid spectral fragments is that each is provided with meaningful errors at each wavelength. rms noise figures to accompany each spectrum half can be generated from the Groningen LRS database by using the 20 long wavelength samples that follow each valid half-spectrum (see *IRAS* Explanatory Supplement 1988, p. X–39). Consequently, we now calculate errors within the same routine that we employ to splice together the blue and red LRS spectral segments (this routine also applies absolute flux calibration), following the Supplement's prescription. The fractional error of each spectral element is then calculated. We further disallow any fractional error less than 0.0101 because the quantization limit imposed on the LRS data stream by its least significant bit leads to a maximal signal-to-noise ratio of 98.

Next we splice the overlapping blue and red spectra by comparing the 23 blue points from 10.92 to 13.45 μm with the eight red points from 10.99 to 13.41 μm. This provides an initial estimate for the factor by which to rescale the red segment to match the blue. To determine this more precisely and to generate a formal uncertainty for this splicing procedure we (1) interpolate the eight red flux densities and their variances onto the more finely sampled blue wavelength range; (2) vary the scale factor (red multiplier) from 0.5 to 1.5 times our initial guess in steps of 0.01 times this guess; (3) form the sum of the 23 squared differences between the blue and the rescaled, regridded red flux densities, weighting inversely by the sum of the blue and rescaled red variances; (4) find the minimum of the χ^2 parabola with respect to the red multiplier; (5) determine the red multiplier corresponding to the minimum in χ^2; and (6) examine the half-width in multiplier over which range χ^2 increases by 1 from its minimum value, by fine interpolation in this multiplier. This process gives us both a refined estimate for the red:blue scale factor and a formal "splice error" which is expressed as a fractional error with respect to the optimal value of the scale factor. Because our concern at this point is solely with the shape of the LRS (not its absolute level) we assign one-half this splice error to each of the blue and red spectra by root-sum-squaring this wavelength-independent quantity with the fractional errors already created for blue and red spectral data points. The correct relative scaling of the red part is now determined, along with its uncertainties

We then return to the original LRS wavelength scale, retain the first 38 blue points as far as 12.769 μm and the last 42 red points from 12.812 μm, and combine the last blue and first red points (by inverse variance weighting for both their average flux density and uncertainty), creating a new point at 12.791 μm. This yields a single LRS composite spectrum with 80 wavelengths. Finally we integrate the *IRAS* 12 μm system response function over this unified LRS spectrum and constrain the calculated in-band flux to match that inherent in the tabulated flux density [(in Jy) of the PSC (and we incorporate into this the preliminary absolute rescaling of PSC "Jy" at 12 μm (0.976) defined in Paper I].

This approach, therefore, creates an absolutely calibrated LRS spectrum, with calculated errors. It is at this point in our routine that we will eventually embed the LRS spectral correction factors that we seek to derive in the present paper. The corrections will be made by dividing the LRS spectrum by the wavelength-dependent correction "factors" [following Volk & Cohen (1989), these numbers are actually values to be divided into LRS spectra, rather than multiplicative factors like the rescaling factors common in the present paper].

For the first pass we used the ratio of LRS spectra of α Tau and α CMa but found that, after combining the errors, the resulting calibrated spectrum was too noisy for our purposes, longward of about 17.8 μm. We, therefore, truncated it there and calibrated it through our smoothed Kurucz spectrum of α CMa (Paper I).

3.6 Assembly of a Complete Spectrum for α Tau (First Iteration)

To create our absolutely calibrated spectrum of α Tau and later to validate it against independently calibrated photometry, we shall use broad and narrowband photometry for this star, as follows: the three specially selected narrowbands of Selby *et al.* (1988: these isolate relatively clean, very narrow, regions of the earth's atmosphere) $Jn = -1.95$, $Kn = -2.94$, $Ln = -3.05$; conventional broadbands (cf. Deacon *et al.* 1992a, who surveyed the literature critically for this star and several other potential infrared calibrators) $K = -2.89$, $L = -3.02$, $M = -2.75$, $[8.7] = -2.97$, $N = -3.03$, $[11.7] = -3.05$, and the *IRAS* broad

filters, $[12] = -3.06 \pm 0.06$ and $[25] = -3.01 \pm 0.05$ [our own magnitudes for [12] and [25] were derived from the absolute calibrations of Paper I, flux densities (Jy) given in the PSC, and the uncertainties (RELUNC) cited there]. We averaged the differences between the *Q*-band magnitudes (Tokunaga 1984) of α Tau and those of both α Lyr and α CMa to obtain $[20] = -3.08 \pm 0.02$, taking α Lyr to be 0.0 mag and α CMa to be -1.34 (Paper I). All this photometry was converted from magnitudes to spectral flux densities using the calibrations presented in Paper I.

We now detail the procedure for complete spectral assembly. We scaled the SEW near-infrared spectrum by integrating it through the terrestrial atmosphere and over the *Kn*, *Ln*, and *M* filter transmission profiles (obtained from scans of the UKIRT filter set taken at 77 K: cf. Deacon *et al.* 1992b). Only these three filters are entirely contained within the SEW fragment. We then determined three independent scaling factors for the entire fragment, one for each filter, by constraining the actual in-band fluxes to match those expected from the calibrated photometry; i.e., *we scale the fragment but preserve its shape.* We averaged the three factors (weighted averages can be used, or equal weights, depending on the actual uncertainties in photometric magnitudes at each point: we used unequal weights though little difference in scale factor or error in scale factor results from assigning equal weights). As an indication of the exceptional care taken by SEW we note that their spectrum [after rectification to the new Kurucz (1991) model] required multiplication by 1.003 ± 0.009 to satisfy the fluxes expected through the three filters.

Next we proceed to the combined 8–13 μm dataset and treat it in identical fashion using the magnitudes [8.7] and [11.7] with their zero magnitude absolute calibrations in Paper I (these are the only two filters entirely contained within the fragment; note that the two very broad filters, *N* and IRAS [12], are much broader than our fragment). For the LRS spectrum we can apply two independent procedures: first, the identical match to the 8.7 and 11.7 μm photometry as used for the ground-based 8–13 μm spectrum; second, a direct comparison between almost the entire wavelength interval common to both the LRS and the ground-based 10 μm spectrum. We omit the shortest wavelengths because the poorer resolution of the LRS than the ground-based fragment militates against a valid comparison through the deepest part of the SiO fundamental bandhead. This "splice" was achieved by χ^2 minimization of the sum-squared differences between the two spectra from $\sim$9.0 to 13.1 μm after regridding the more coarsely sampled LRS onto the wavelengths of the more finely gridded ground-based spectrum by linear interpolation in spectral intensity and variance. In practice, the splice yields a far better determined scale factor and is much less prone to propagate errors in the ground-based magnitudes or any uncertainties in the absolute flux density calibration of these. Consequently, we preferred this method rather than the photometric one for the LRS spectrum. Note that, in the overlapping region, we replace the original ground-based spectrum by the appropriately weighted combination of it and the regridded and optimally rescaled LRS. We finally merged the optimally rescaled LRS and the combined LRS/8–13 μm segments so that the former simply extends the latter. However, because we used the flux-calibrated ratio of LRS spectra of α Tau and α CMa in this first iteration, the resulting noise is dominated by that inherent in the LRS spectrum of the fainter star, α CMa. Therefore, we chose to truncate this LRS extension at 17.76 μm (the point at which the fractional error in the resulting irradiance-calibrated α Tau spectrum exceeds 5%). The truncated ratio of LRS spectra was flux calibrated through our absolute α CMa model (Paper I), after smoothing it to the average resolution across the LRS and regridding to the LRS wavelength scale.

The KAO spectrum from 5 to 8 μm cannot be constrained by ground-based photometry, of course. Therefore, we interpose it between the SEW 1.2–5.5 and the merged ground-based/LRS 8–18 μm spectra, both of which we have absolutely calibrated. Formally we seek the scale factor to apply to the 5–8 μm fragment so that we minimiize the χ^2 sum evaluated over *both* the regions of overlap, $\sim\lambda\lambda$4.5–5.5 and 7.3–9.4 μm. Again, we determine an uncertainty in this scale factor through the χ^2 parabola (as described in Sec. *3.5*).

At this point we have assembled a completely observed spectrum of α Tau from 1.22 to 17.76 μm. To this we append Glaccum's (1990) spectroscopy, without rescaling, extending our coverage to 35 μm. We regrid the entire spectral ensemble to a uniform wavelength scale, 2.0–35.0 μm with 0.05 μm spacing. This is convenient to work with (for this first iteration only) and does little violence to the higher resolution data; of course, it oversamples the longest wavelength LRS and Glaccum datasets. Next we integrate the resulting total spectrum over those long wavelength filters whose passbands are so broad that they exceed the range of any single fragment, but now can be explored [*IRAS* 12 and 25, and *Q* filters, including the terrestrial atmospheric contribution (from Mauna Kea) to the *Q* profile]. We iterate the procedure of rescaling the Glaccum spectrum and linearly interpolating for wavelengths between 18 and 20 μm until the inverse variance weighted (by the photometric uncertainties) average scale factor indicated by the set of three passbands best approximates unity.

Next we integrated the resulting complete α Tau spectrum that embodies this rescaled Glaccum portion through all 12 broad and narrow filter transmission profiles including atmospheric attenuation (when relevant). We matched the observed fluxes to those expected from the stellar magnitudes and the zero magnitude calibrations of Paper I, with appropriate weights for each comparison. This first approximation to α Tau's complete spectrum satisfied *all* the photometric constraints, including those of seven filters that were not used to scale any fragment; i.e., it required rescaling by 1.001 ± 0.004, leading us to conclude that this method of spectrum construction had no obvious flaws.

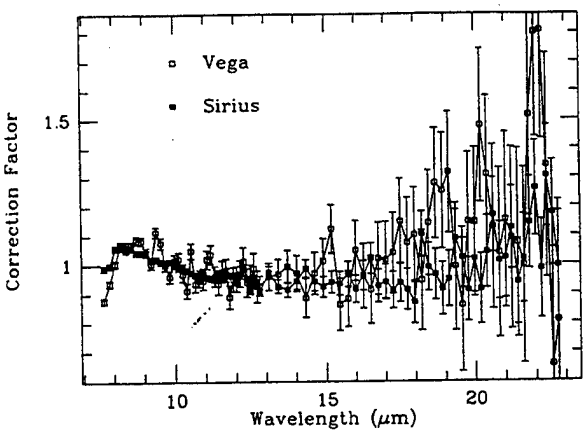

FIG. 7. Ratios of LRS spectra of α Lyr and α CMa to our calibrated versions of the new Kurucz models for these stars. Error bars are 1σ.

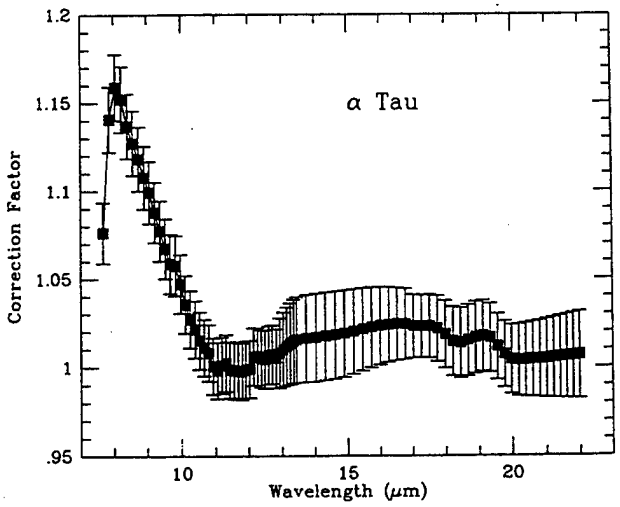

FIG. 8. LRS correction factors resulting from the comparison of the 8–23 μm portion of the complete α Tau spectrum with a 10 000 K blackbody normalized near 12 μm. Error bars are 1σ and the function shown again corresponds to the final pass on α Tau rather than the earlier iterations.

4. DIFFERENT SETS OF LRS CORRECTION FACTORS BASED ON STARS

4.1 A Direct Approach Using α Lyr and α CMa

In Paper I we stress an approach to infrared spectral calibration based on new models for α Lyr and α CMa due to Kurucz (1991). Consequently, we may ask how the midinfrared spectra predicted by these stellar models compares with the uncorrected LRS spectra of α Lyr and α CMa. Figure 7 displays the LRS spectrum of each of these hot stars divided by the appropriately smoothed Kurucz model, regridded to the same wavelength scale. As expected, α Lyr and α CMa are simply too faint to define the character of this quotient curve at long wavelengths. However, one clearly sees the characteristic emission bump due to the neglect of the SiO fundamental in α Tau in the original calibration in these most direct representations of the LRS "correction factors" at each wavelength. Thus, α Lyr and α CMa provide the first two datasets from which to construct an average set of LRS correction factors.

4.2 α Tau (Pass 1: The First Iteration)

We can also use the first iteration spectrum of α Tau in the following manner. We took the 1.2–35 μm spectrum just constructed, convolved it with a Gaussian of FWHM 0.40 μm (equivalent to the approximate LRS spectral resolution near 8 μm), regridded it to the LRS wavelength scale, and divided it by a 10 000 K blackbody normalized to the α Tau spectrum in the continuum between 12 and 13 μm. Figure 8 shows such a set of LRS corrections, actually for the third pass, although there is relatively little variation from pass to pass except that the uncertainties diminish with each successive version. This first iteration of the α Tau spectrum yields the third dataset on LRS corrections.

4.3 Glaccum's KAO Spectra

Glaccum's (1990) long wave KAO spectra provide useful information at the long wavelengths where the LRS spectra of α Lyr, α CMa, and α Tau (first pass) are especially noisy. In particular, we compared his 19.9–35.0 μm spectra of α Ori, α Her, and α Sco with their LRS counterparts. The resulting LRS corrections, after regridding all three sets of correction factors to the LRS wavelength scale and combining these with inverse variance weighting, are also shown in Fig. 9 (the fourth LRS correction dataset). Glaccum also observed four relevant bright objects from 16.3 to 35.0 μm that are eminently suitable for LRS comparison, namely, VY CMa, γ Cru, o Cet, and π^1 Gru. These four yielded the combined correction function (exactly as described above) likewise represented in Fig. 9 (the fifth LRS correction dataset). Glaccum's database has two significant merits. First, its wavelength coverage addresses the longest LRS wavelengths, inadequately repre-

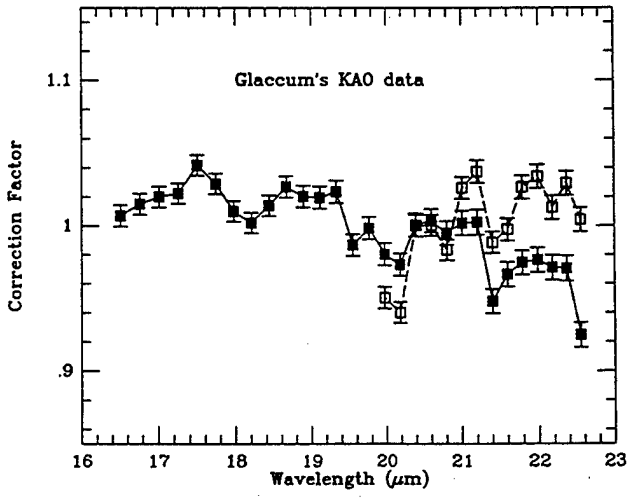

FIG. 9. LRS correction factors defined using Glaccum's long wave KAO spectra. Error bars are 1σ. The filled squares come from combining the comparisons of LRS spectra with Glaccum's data on VY CMa, γ Cru, o Cet, and π^1 Gru. The open squares likewise come from Glaccum's data on α Ori, α Her, and α Sco.

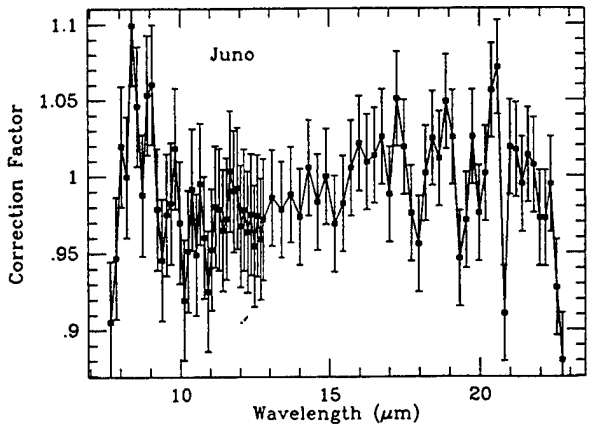

FIG. 10. LRS corrections resulting from comparing Juno's spectrum with that expected from the standard thermal model. Error bars are 1σ.

sented by the noisy α Lyr and α CMa spectra, or by the α Tau (first iteration) spectrum with its 18–20 μm gap. Second, it has a nonstellar calibration approach. A good description of the process of long wavelength KAO spectral calibration is given by Glaccum (1990, cited by Moseley *et al.* 1989). This calibration uses a model of the *Voyager* long wavelength observations of Uranus (Hanel *et al.* 1986) that is transferred to Mars, using Wright's (1976) model for that planet's infrared emission, to provide a secondary standard for KAO flights. Moseley *et al.* (1989) summarize the procedure and demonstrate that cross calibration by Mars, Uranus, and tertiary stellar standards developed for a particular flight series can attain an accuracy of 1%, and that tests of the Mars model against the Uranus model (the primary standard) indicate reproducibility to within 2%–3%. These numbers suggest that the absolute uncertainties inherent in the Glaccum dataset are entirely comparable with the 1.45% (Paper I) that characterizes infrared work based on the new Kurucz stellar models for α Lyr and α CMa. Consequently, we treated all our diverse methods of defining the LRS correction function equally (although, at each wavelength, we employed the real inverse variance weighting to combine the different approaches).

5. THE RELEVANCE OF ASTEROIDAL LRS SPECTRA

A comparison of asteroidal LRS spectra and "standard thermal models" provides a most useful indication of LRS long wave problems (if any) because these cool bodies have spectra that typically peak near 15 μm. They naturally complement the wavelengths at which α Lyr, α CMa, and α Tau yield information on LRS corrections. For best signal-to-noise we used the correction factors obtained by dividing Juno's LRS spectrum by its model spectrum calculated with the *IRAS* standard thermal model (Lebofsky *et al.* 1978; Matson 1986) normalized at 15 μm, although essentially the same shape resulted from combining the normalized corrections from 11 LRS spectra of 7 non-S-type asteroids. The LRS corrections suggested by using Juno's LRS spectrum appear in Fig. 10 (the sixth LRS correction dataset).

6. FINAL LRS CORRECTION FACTORS

6.1 LRS Corrections: The First Estimate

By inverse-variance-weighted combination of the six datasets described in Secs. 4 and 5, we derived a first pass LRS correction function and its uncertainties. To smooth our function, we used polynomials to represent it, as follows: the blue portion (7.67–12.70 μm) was fitted by a χ^2 minimization approach using a sixth order polynomial; the red (10.55–22.74 μm) was found to be best fitted by a constant (1.005 ± 0.005). We combined these two overlapping polynomials and used that function to generate a second pass α Tau using this star's complete fixed LRS spectrum, and incorporating the errors inherent in our correction curve into the LRS spectral errors by root-sum-squaring the fractional errors. We note that the long wave KAO spectra beyond 16.0 μm of Mira (*o* Cet: Glaccum 1990) show no obvious molecular absorptions in the region 16–20 μm. Therefore, we felt it probable that α Tau, a much warmer star than *o* Cet, also suffers no recognizable molecular absorptions. From 13 to 16 μm we expect α Tau to be featureless because no plausible molecule with relevant frequencies in this range is predicted to exist in sufficient abundance in detailed models of α Tau's atmosphere (Carbon 1991). The 14–16 μm region is opaque to all but spaceborne observations (namely, the LRS) and we find that the ratios of LRS spectra of early K to mid-M III stars without dust features reveal no differential effects from 13 to 20 μm, akin to those displayed in Fig. 2. Therefore, a constant (featureless) first estimate for the correction to the LRS spectrum longward of $\sim$13 μm seemed justified.

6.2 LRS Corrections: A Second Estimate

We then recreated the entire 1.2–35 μm spectrum of α Tau, following the procedure detailed in Sec. 3, but this time using its complete fixed LRS spectrum (rather than one ratioed to α CMa) to bridge the gap between the 8–13 μm and 20–35 μm segments. Because this direct approach does not involve the ratio of two LRS spectra, its uncertainties are those of the α Tau spectrum alone, rather than the root-sum-square combination of the errors in both the α Tau and α CMa spectra. In this second pass, we spliced Glaccum's portion directly onto the fixed and correctly scaled LRS portion to provide the right scale factor for the 20–35 μm segment (by a single overlap, again using χ^2 minimization). The procedure of developing α Tau's contribution to the definition of the LRS corrections (Sec. *4.2*) was duplicated using this more complete spectrum and was combined with the other five sets of independent LRS corrections. By the same methods as described above, these LRS corrections now resulted in a second estimate for these factors which, within the two sets of errors, was indistinguishable from the first estimate. To smooth this second estimate we again used a constant at long wavelengths because no significant distinction could be seen between the sum-squared-residuals for a constant fit as compared with

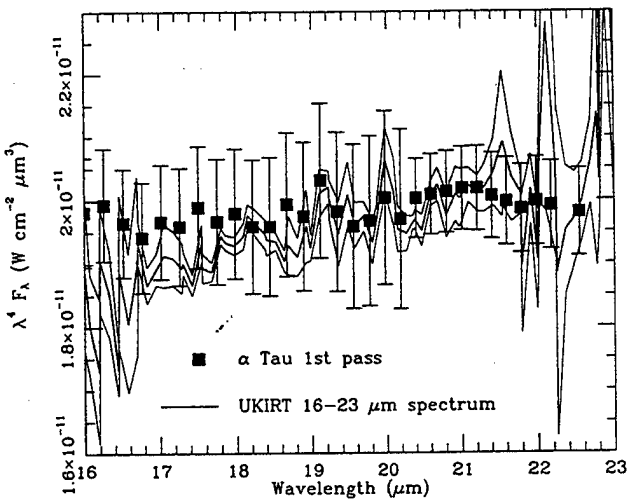

FIG. 11. Comparison of the first pass "LRS fixed" spectrum of α Tau and the newly obtained UKIRT CGS3 service observations from 16 to 23 μm. Filled squares with error bars represent this portion of the first iteration complete α Tau spectrum. Continuous curves show the mean and 1σ bounds on the calibrated UKIRT spectrum.

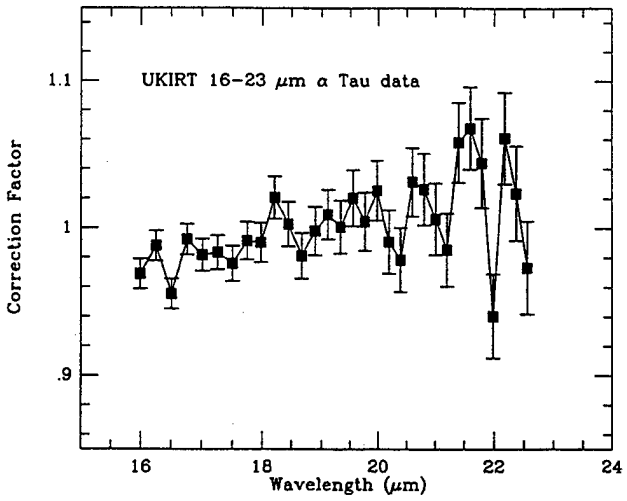

FIG. 12. LRS corrections derived by comparing the UKIRT 16–23 μm spectrum of α Tau itself with its LRS spectrum.

any reasonable order of polynomial fit. We, therefore, adopted the second estimate as the LRS-fixing function for the next attempt on α Tau, because its errors were smaller than those of the first estimate.

6.3 LRS Corrections: Independent Validations and the Final Iteration of α Tau

We then sought independent validation of our second set of LRS corrections by obtaining low-resolution 16–23 μm ground-based spectra of α Tau and α CMa, very closely matched in airmass, through a UKIRT service observation, also on 9 November 1991. This gave a high signal-to-noise ratio spectrum of α Tau to α CMa that we converted to flux densities by multiplying by our calibrated α CMa spectrum, after matching resolutions and regridding to the UKIRT wavelength scale. Figure 11 demonstrates the very close agreement between our second version of α Tau's spectrum and the new UKIRT data. This agreement gave us confidence in our spectrum building and calibrational procedures. Finally, we used the UKIRT 20 μm spectrum in its own right to assemble a third iteration of α Tau's spectrum by: (1) providing an independent appraisal (Fig. 12) of the LRS spectrum in the rather critical 16–23 μm region where we have posited that, within the previous uncertainties, no LRS corrections are necessary; (2) yielding much higher signal-to-noise data than the LRS alone from 17–23 μm; (3) splicing the UKIRT 20 μm fragment onto the merged 8–13 μm/LRS portion and combining all relevant data in this region of overlap; (4) overlapping Glaccum's fragment with the correctly scaled and spliced 17–23 μm data. The most recent and highest signal-to-noise KAO data from 5 to 9 μm (Sec. *3.3*) were also incorporated into this third iteration α Tau spectrum. To provide the highest quality data from the UKIRT 20 μm spectrum, which formally covers $\lambda\lambda$15.14–23.86 μm, we removed all points whose signal-to-noise ratio was less than 10, leaving the cleanest parts of the spectrum, from 17.05 to 23.61 μm.

From this new spectrum of α Tau we recreated LRS correction factors by comparison with a 10 000 K blackbody (cf. Sec. *4.2*). This time we augmented the process by making another direct comparison of part of the LRS spectrum of a star, this time α Tau itself, and an independent spectrum, namely, the complete UKIRT 15–23 μm spectrum (akin to the Glaccum-based information in Sec. *4.3*), rather than just the very limited portion of this which can be identified after splicing into the complete α Tau spectrum. This provided a seventh dataset for LRS corrections by the comparison method in Sec. *4.3*. We again sought separate polynomial fits to overlapping blue and red portions, this time 7.67–12.4 μm for the blue, and 10.8–22.74 μm for the red. In the blue the χ^2 methodology again resulted in a significant preference for a sixth order polynomial fit. This time, with the reduced inherent errors of the complete α Tau spectrum and the inclusion of the direct comparison of the LRS and UKIRT 20 μm spectra, the red was significantly better fit by a parabola rather than by a constant value (or any other polynomial). Such a curve would correct a LRS spectrum by introducing a small ($\sim$1.0%) dip into the red spectral portion. The final set of LRS corrections appears in Fig. 13, and has reduced 1σ errors from about 5–8 and 16–23 μm compared with all earlier iterations due to the new higher quality spectra now available in these regions.

An application of Bloom's one-sided statistics to the long wavelength portion of Fig. 13 shows that the two unusually low points (at 19.98 and 20.19 μm) can be dropped from the distribution. However, the resulting best-fit red polynomial representation (Fig. 13) is still a parabola and is indistinguishable from that derived using *all* the points longward of 10.8 μm (within the error bars portrayed in Fig. 13). Detailed scrutiny of Glaccum's database indicates that these unusually low points in the LRS correction function are directly traceable to an unusually high first point in the KAO spectra of both α Sco and α

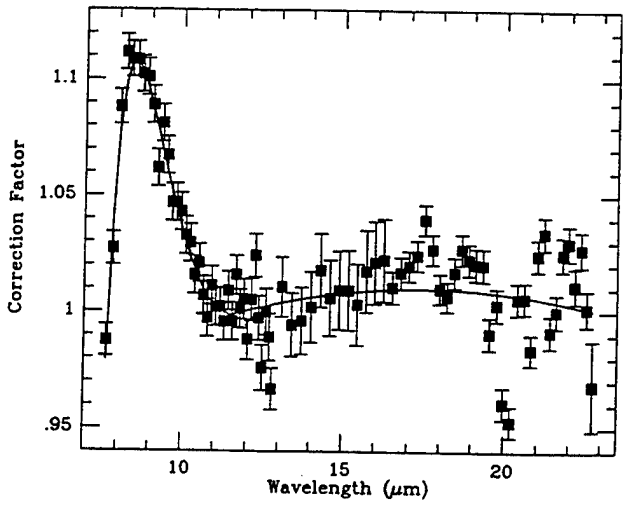

FIG. 13. The final set of LRS correction factors (the squares), with 1σ error bars. The smooth curve represents the combined blue (sixth order) and red (second order) best fitting polynomials, joined at 11.43 μm.

Her (cf. the first two open squares in Fig. 9) that does not match the shape of the corresponding LRS spectrum. These anomalies are not typical of Glaccum's database. In fact, the accord in shape of the corresponding LRS and KAO spectra for *all* other Glaccum spectra (except α Tau's) is within 1%. Consequently, it is both physically meaningful and statistically justified to neglect the two very low points near 20 μm in polynomial fitting of the LRS correction function. We also note that the correction factor for the final wavelength is less than unity (although noisy). This suggests that LRS points at 22.74 μm may be low systematically. One might wish to drop this 80th wavelength for greater accuracy or, at least, treat it with caution.

Polynomial representation of the original data points plotted in Fig. 13 is equivalent to smoothing the original distribution. The operation of smoothing a curve usually results in reduced uncertainties, tantamount to smoothing the running distribution of variances in the same manner as the values themselves are smoothed. However, we feel that a more conservative approach is justified given the central importance of this LRS correction function. Our suggested LRS correction function is represented by the smooth polynomials in the blue and red, overlapped at 11.43 μm where they intersect. However, the actual errors we have assigned to this smoothed function are equivalent, at every wavelength, to the same *fractional* error inherent in the final unsmoothed function. Therefore, we do not claim to have reduced the relative uncertainties of points in the function even though we have effectively smoothed our representation of it. Table 1 summarizes these smooth (polynomial fit) values with their assigned uncertainties.

7. COMPARISON WITH VOLK AND COHEN

Volk & Cohen (1989) attempted to correct the LRS calibration based on examination of a number of cool stellar LRS spectra. They made the simplistic assumption that

TABLE 1. Final set of LRS correction factors: to rectify a LRS spectrum, one divides these factors into the database spectrum.

λ (μm)	Factor	σ	λ (μm)	Factor	σ	λ (μm)	Factor	σ
7.6736	0.9792	0.0067	11.6710	0.9992	0.0082	17.5030	1.0099	0.0064
7.8636	1.0417	0.0072	11.7910	0.9996	0.0083	17.7430	1.0099	0.0065
8.0485	1.0793	0.0074	11.9090	1.0001	0.0085	17.9780	1.0098	0.0066
8.2286	1.0986	0.0075	12.0260	1.0005	0.0089	18.2110	1.0097	0.0066
8.4043	1.1073	0.0076	12.1410	1.0009	0.0090	18.4410	1.0096	0.0066
8.5758	1.1076	0.0077	12.2560	1.0013	0.0091	18.6680	1.0094	0.0066
8.7436	1.1036	0.0078	12.3690	1.0016	0.0096	18.8930	1.0093	0.0067
8.9078	1.0966	0.0078	12.4820	1.0020	0.0100	19.1140	1.0090	0.0069
9.0686	1.0879	0.0079	12.5930	1.0024	0.0100	19.3330	1.0088	0.0070
9.2263	1.0787	0.0080	12.7030	1.0027	0.0103	19.5500	1.0085	0.0071
9.3809	1.0691	0.0079	12.7905	1.0030	0.0093	19.7640	1.0082	0.0071
9.5328	1.0603	0.0080	13.0950	1.0038	0.0128	19.9760	1.0079	0.0071
9.6820	1.0522	0.0081	13.4130	1.0047	0.0139	20.1860	1.0075	0.0070
9.8286	1.0439	0.0081	13.7240	1.0055	0.0147	20.3940	1.0071	0.0068
9.9728	1.0369	0.0081	14.0280	1.0062	0.0154	20.5990	1.0067	0.0066
10.1150	1.0300	0.0081	14.3250	1.0068	0.0158	20.8030	1.0063	0.0067
10.2550	1.0235	0.0081	14.6170	1.0074	0.0166	21.0040	1.0059	0.0067
10.3920	1.0187	0.0081	14.9020	1.0078	0.0171	21.2040	1.0054	0.0068
10.5280	1.0135	0.0081	15.1820	1.0083	0.0176	21.4010	1.0049	0.0069
10.6620	1.0096	0.0081	15.4580	1.0087	0.0181	21.5970	1.0044	0.0071
10.7940	1.0063	0.0081	15.7280	1.0090	0.0181	21.7910	1.0039	0.0071
10.9240	1.0041	0.0081	15.9940	1.0092	0.0183	21.9840	1.0033	0.0072
11.0520	1.0017	0.0081	16.2550	1.0095	0.0184	22.1750	1.0027	0.0074
11.1790	1.0003	0.0081	16.5120	1.0096	0.0069	22.3640	1.0022	0.0074
11.3040	1.0002	0.0082	16.7660	1.0098	0.0067	22.5510	1.0016	0.0076
11.4280	0.9988	0.0082	17.0150	1.0099	0.0066	22.7370	1.0009	0.0196
11.5500	0.9987	0.0082	17.2610	1.0099	0.0065			

TABLE 2. Photometry used to construct the spectrum of α Tau. Filter names and FWHMs, effective wavelengths for α Tau, ground-based magnitudes with uncertainties, and flux densities (F_λ) are presented.

Filter	λ_{eff}	FWHM	Mag.	Uncertainty	F_λ
	μm	μm	mag.	mag.	W cm^{-2} μm^{-1}
Kn	2.205	0.0488	-2.94	0.01	5.91E-13
Ln	3.763	0.1443	-3.05	0.01	8.56E-14
M	4.744	0.6677	-2.75	0.02	2.68E-14
8.7	8.727	1.1576	-2.97	0.01	3.01E-15
11.7	11.622	1.2008	-3.05	0.01	1.05E-15

these stars were well represented by blackbodies at their effective temperatures, which we now recognize to be invalid. However, they noted that their reference stars separated into two groups, a characteristic essentially independent of the relevance of blackbodies. One set yielded LRS shapes basically in agreement with an assumed featureless α Tau; the second (their "set of seven stars") yielded a feature peaking near 8.5 μm that must be removed to obtain the "correct" LRS. With hindsight one can now identify the first group as those stars with essentially the same spectral type as α Tau (e.g., γ Dra) that necessitate no differential correction. The second group corresponds to truly featureless spectra (e.g., A,F,G stars), "damaged" by the neglect of SiO absorption in α Tau. Volk & Cohen also noted that the LRS corrections derived from the two groups differed only between 7.67 and $\sim$11 μm but not at long wavelengths. These authors, therefore, obtained half the solution to the problem of correcting the LRS shapes, namely, the recognition of the peak that we now recognize is caused by SiO absorption in α Tau, although, in the red, the overall change of slope they suggested to correct LRS spectra and the general curvature are not appropriate.

8. THE FINAL SPECTRUM OF α TAU

After determining the LRS corrections shown in Fig. 13 we continued to iterate the process of building the spectrum of α Tau, checking at the end of each iteration that both the α Tau spectrum and the LRS corrections agreed within the 1σ uncertainties with their previous iterations. This was indeed the case for both. The components of the robust spectrum we have developed are summarized in Tables 2–4. These indicate the photometry used to calibrate fragments along with flux densities using the absolute calibrations of Paper I (Table 2); the total wavelength ranges of the available fragments, and the regions actually used when overlaps occur (Table 3); and the scaling factors and uncertainties that result from comparisons of fragments with photometry, and splices of fragments to one another (Table 4). The integration of all 12 broad and narrow filters, using inverse variance weighting and atmospheric attenuation when relevant, over the final complete α Tau spectrum indicates a rescaling by a factor of 1.000$\pm$0.004

TABLE 3. Portions of spectral fragments actually used to build the observed spectrum of α Tau.

Fragment	Reference	Total range μm	Range used μm
SEW	1	1.22- 5.50	1.22- 4.22
KAO/FOGS	2	4.53- 9.38	all
8-13	3	7.33-13.07	all
LRS	4	7.67-22.74	8.91-22.74
15-23	5	15.14-23.86	17.17-23.61
KAO/LONG	6	20.38-35.08	all

Notes to TABLE 1

References: (1) Strecker, Erickson, and Witteborn (1979); (2) NASA-Ames data principally of 1991 Dec. 20 KAO flight; (3) principally UKIRT data of 1991 Nov. 9 "service observations"; (4) IRAS Low Resolution Spectrometer, Groningen database; (5) entirely UKIRT data of 1991 Nov. 9 "service observations"; (6) Glaccum (1990), unpublished Ph.D. dissertation observations

for the 12 filters in order to satisfy all these photometric constraints.

Thus we believe that Fig. 14 represents the best current absolutely calibrated spectrum for α Tau and the most accurate expression of its true spectral shape. Figure 15 summarizes the fractional absolute uncertainties in this composite spectrum as a function of wavelength. These errors are the root-sum-square combinations, at every wavelength, of the wavelength-independent absolute uncertainty in the α Lyr and α CMa spectra that currently underpin our entire effort ($\pm$1.45%), splicing errors, and original spectrophotometric statistics in the set of fragmentary spectra. It suggests that one can achieve absolute calibration by our approach to better than 3% across a very broad wavelength range (1–25 μm, ignoring the very few points that must be observed through almost opaque terrestrial CO_2 absorptions).

After constructing this spectrum, we integrated it through 15 filter profiles (including the atmosphere at Mauna Kea as represented by HITRAN and the detector quantum efficiency of InSb for the 1–5.5 μm range). Table 5 summarizes the resulting broad and narrowband magnitudes, using the calibration flux densities for zero magnitude defined in Paper I. These actual magnitudes determined from our calibrated spectrum are generally in good agreement with those culled from the literature (see Sec. *3.6*), except for the two *IRAS* magnitudes. However, we note that the *IRAS Explanatory Supplement* (1988, Table VI.D.1) showed appreciable discrepancies between *IRAS* and two independent sets of ground-based measurements, which have not yet been resolved.

Engelke (1990) has suggested an approximation to the continuum of cool stars based upon a solar analogue and the assumption that H^- free–free opacity dominates the infrared region. Although only an approximation, it provides an interesting comparison with our observed spectrum of α Tau. One requires only two constants: the stellar

TABLE 4. Scale factors with uncertainties from matching spectral fragments.

Operation	Scale factor	±uncertainty
SEW cf. Kn, Ln, M photometry	1.003	0.009
813 cf. [8.7], [11.7]	1.039	0.007
LRS red half spliced to blue	1.008	0.002
LRS spliced to 813	0.948	0.001
KAO spliced to SEW and LRS+813	1.022	0.001
UKIRT 16-23 spliced to LRS	1.015	0.001
KAO/LONG spliced to 16-23	1.086	0.003

effective temperature and the subtense, or angular diameter, of the star. Engelke himself used $T=3800$ K and $\theta=21.58$ mas. Blackwell *et al.* (1991) applied the infrared flux method to Selby *et al.*'s (1988) narrowband photometry of α Tau and determined $T=3920$ K and an angular diameter of 20.63 mas. We recalculated these parameters using Blackwell *et al.*'s approach and observations, but substituting our own absolute flux calibration (Paper I) rather than Dreiling & Bell (1980) for α Lyr. We deduced $T=3898$ K, and $\theta=20.99$ mas. The best fit to an Engelke function with $T=3898$ K indicates a satisfactory detailed match to the continuum (Fig. 14), and suggests an angular diameter of 21.32 mas. The probable uncertainties in T and θ (using the infrared flux method) have been estimated to be $<1\%$ and $<2\%$, respectively, by Blackwell *et al.* (1991).

9. AN APPLICATION TO AUTOCLASS

Cheeseman *et al.* (1989) applied artificial intelligence techniques to the highest quality spectra selected from the 5425 spectra in the *IRAS* LRS Atlas (*IRAS* Science Team 1985) and developed a categorization of their spectra by shape. The "normal" stars fall primarily into "split class 23/δ0" autoclass subgroups δ0:0–δ0:6. The λ^4F_λ ensemble averages for these separate subclasses show a variety of shapes. In particular, some stars droop between 7.7 and 13 μm relative to others. It is now worthwhile to investigate whether such distinctions can be understood in light of our recalibration of the LRS. We, therefore, seek a quantitative characterization of the uncalibrated ensemble average λ^4F_λ LRS shapes in terms of the differential effects of SiO with spectral type. For each of the nondusty SiO subclasses (δ0:0–δ0:5) we define an average spectral type, assessed as the mean of all the numerically codified spectral types [see Gottlieb's (1978) SKYMAP coding scheme for spectral types: e.g., K0=500; M0=600, etc.] represented by the normal stars among split class 23 (almost all are giants), but excluding the rather infrequently encountered carbon stars. Spectral types are listed by Cheeseman *et al.* in their Table 20. To quantify the residual SiO band absorption we use the fractional depth of the fundamental at 8.0 μm compared with the flat continuum region between 12 and 13 μm, all depths and levels defined on the λ^4F_λ ensemble average plots.

In Fig. 16 we plot $1.00-\{\lambda^4F_\lambda(8.0\ \mu m)/\lambda^4F_\lambda(12.5\ \mu m)\}$ against the difference between the ensemble's mean type and that of α Tau (K5=550); each quantity is also associated with an uncertainty represented by the standard error of the mean spectral type (rounded to the nearest half a spectral class). Figure 16 also overlays the best-fit line estimated from the formal two-parameter χ^2 fit, assigning errors to both ordinate and abscissa, and limit lines corresponding to the $\pm1\sigma$ ranges in the coefficients of this linear fit. The relationship is fairly clean and the origin lies within 2σ of the best-fit line as it should [there should be no residual SiO feature when implicitly comparing an average of K5 with α Tau itself (cf. Volk & Cohen 1989)]. We, therefore, believe that the rather subtle ensemble differences in short wavelength LRS shape that AUTOCLASS has found among these normal stars result essentially from the

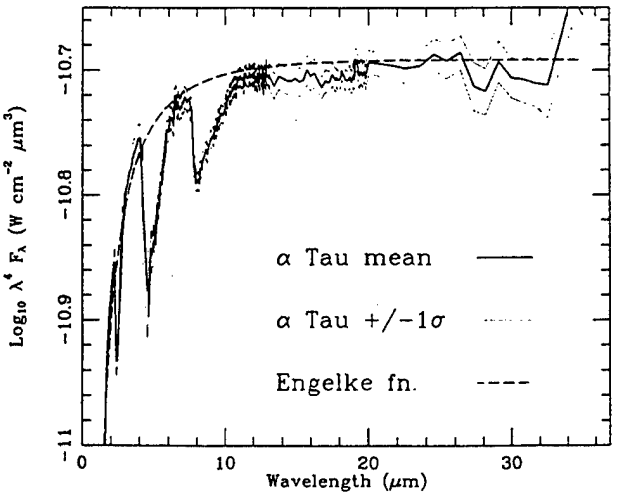

FIG. 14. The final α Tau complete spectrum: heavy line represents the spectrum itself; light continuous lines the $\pm1\sigma$ bounds. Broken line shows the Engelke approximation corresponding to an angular diameter of 21.32 mas.

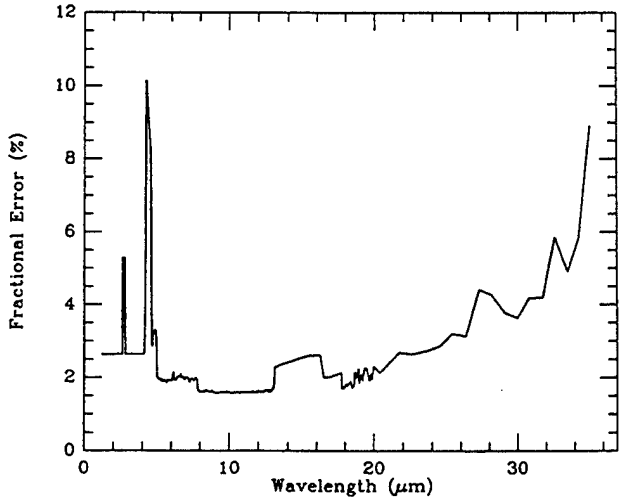

FIG. 15. Fractional errors for the complete α Tau spectrum. "Spikes" at short wavelengths correspond to regions of strong terrestrial CO_2 absorption.

TABLE 5. Derived broad and narrowband magnitudes of α Tau in 15 infrared passbands. Flux density calibrations are those of Paper I.

Filter	Magnitude	Filter	Magnitude	Filter	Magnitude
Jn	-1.97	K	-2.90	N	-3.02
Kn	-2.93	L	-3.04	[11.7]	-3.075
Ln	-3.06	L'	-3.05	Q	-3.08
J	-1.84	M	-2.77	IRAS [12]	-3.08
H	-2.74	[8.7]	-2.95	IRAS [25]	-3.10

differences in depth of SiO fundamental in stars of different spectral type (with some dispersion no doubt attributable to intrinsically different metal abundances in stars of common type). It is clear that all of the ensemble average shapes in this series of AUTOCLASS spectra for normal stars would behave differently after correct LRS recalibration, although the relative distinctions between classes would be preserved. We cannot so readily evaluate whether other AUTOCLASSes, for more exotic objects, might be specious and entirely due to the neglect of SiO in α Tau alone. However, one might expect that this problem would be most severe only for those classes lacking intrinsic spectral content so that the SiO "pseudoemission" feature would dominate the $\lambda^4 F_\lambda$ average for an ensemble.

10. CONCLUSIONS

We have described, demonstrated, and validated a general process for creating complete, continuous, and absolutely calibrated 1–35 μm stellar spectra and have applied this to α Tau, an important infrared calibrator. Our absolute spectrum of this star now rests on the accuracy of our calibrated versions of the pair of new models by Kurucz for α Lyr and α CMa. If the α Lyr model were to be revised, then the zero magnitude calibration flux densities of Paper I would also be revised so that the photometric constraints on spectral fragments would change. Similarly, our spectral fragments represent ratios of the spectra of α Tau to those of either α Lyr or α CMa so that, again, revisions of either of these models would necessitate the creation of newly calibrated fragments from the observed ratio spectra. However, the techniques that we have outlined in this paper would all still be valid and the generation of a new absolutely calibrated spectrum of α Tau, with an altered pedigree, would be straightforward. This represents only the first element in what we envisage as an eventual "atlas" of calibrated stellar spectra drawn from the range of spectral types from K0 to M0 III. It suggests that it is possible, with sufficient care and adequate spectroscopic material, to achieve a fractional uncertainty in the absolutely calibrated spectrum corresponding to a level better than 3% across most of this wavelength range, at least for stars as bright as α Tau.

Using this spectrum of α Tau, and other independent midinfrared data on other stars and asteroids, we have recalibrated the unique and important LRS spectral database by removing artifacts caused by previous neglect of the SiO fundamental in this K5 III star. In our opinion, the approach we have carefully presented in this paper should result in meaningful LRS spectra, with accurate shapes, plausible uncertainties, and capable of absolute calibration in their own right.

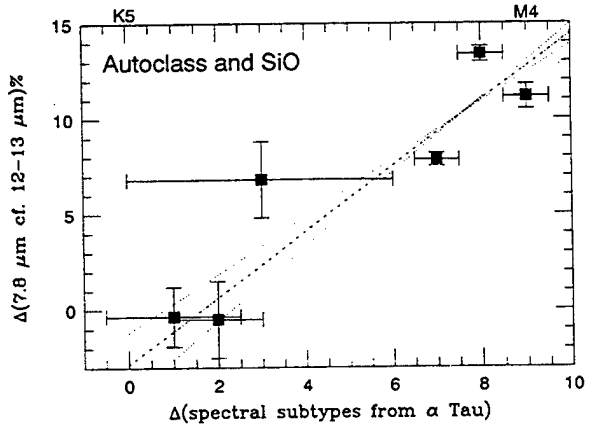

FIG. 16. AUTOCLASS and the SiO band. Abscissa represents the difference between the ensemble average spectral type and K5 III. Ordinate quantifies the degree to which the SiO fundamental has affected the ensemble average spectrum shown by Cheeseman *et al.* (1989) in $\lambda^4 F_\lambda$. Each ensemble represents a nondusty $\delta 0$ subclass of "split class 23". Dash-dot line represents the best-fit line using inverse variance weighting in both axes for each point. Dashed lines indicate the 1σ limit lines that correspond to the mean $+1\sigma$ in slope and the mean -1σ in offset, and vice versa.

It is a pleasure to thank Bob Kurucz, Don Strecker, Mike Barlow, Bill Glaccum, Duane Carbon, Gordon Augason, Dave Goorvitch, and Jan Simpson for their substantive contributions to various aspects of this work. We are most grateful to Tom Geballe and John Davies for their encouragement and vital assistance in obtaining the crucial UKIRT Service Observations in the 10 and 20 μm windows. We are grateful to the entire staff of the KAO for providing us with good support during our crucial 1991 December flight, and to Paul Wesselius for providing NASA–Ames with the Groningen LRS database. We thank Paul LeVan for sending us his ratio of the spectra of α Tau and α CMa obtained from Wyoming Infrared Observatory with the GLADIS array spectrometer for further confirmation of the reality of the SiO fundamental in α Tau. The "Stellar Atlas Panel" convened at the Phillips Laboratory/AFGL by Stephan Price and Paul LeVan has provided a stimulating forum in which to raise issues relevant to our spectrum-building procedure. We thank the referee, Alan Tokunaga, for his very thorough reading of this paper. We were supported in part by Contracts No. NAS 2-13327 with NASA–Ames Research Center and BX-4355 with MIT/Lincoln Laboratories. M.C. thanks NASA–Ames Research Center for partial support of this work under Cooperative Agreement No. NCC 2-142 with Berkeley.

REFERENCES

Barlow, M. J. 1991, private communication
Bell, R. A., & Dreiling, L. A. 1981, ApJ, 248, 1031
Blackwell, D. E., Lynas–Gray, A. E., & Petford, A. D. 1991, A&A, 245, 567
Carbon, D. 1991, private communication
Cheeseman, P., Stutz, J., Self, M., Taylor, W., Goebel, J., Volk, K., & Walker, H. 1989, Automatic Classification of Spectra from the IRAS, NASA RP-1217 (U.S. Government Printing Office, Washington, DC)
Cohen, M., Walker, R. G., Barlow, M. J., & Deacon, J. R. 1992a, AJ, 104, 1650 (Paper I)
Cohen, M., Witteborn, F. C., Carbon, D., Augason, G., Wooden, D., Bregman, J., & Goorvitch, D. 1992b, AJ (now in press) (Paper III)
Deacon, J. R., Barlow, M. J., & Cohen, M. 1992a, in preparation
Deacon, J. R., Barlow, M. J., & Cohen, M. 1992b, in preparation
Dreiling, L. A., & Bell, R. A. 1980, ApJ, 241, 737
Engelke, C. W. 1990, Long Wavelength Infrared Calibration: Infrared Spectral Curves for 30 Standard Stars (Report of Group 51, Lincoln Labs., MIT)
Glaccum, W. 1990, Ph.D. dissertation, University of Chicago, unpublished observations, 1991; private communication to M. C.
Gottlieb, D. M. 1978, ApJS, 38, 287
Hanel, R., *et al.* 1986, Sci, 233, 70
Hoffleit, D. 1982, The Bright Star Catalogue (Yale University Observatory, New Haven)
IRAS Atlas of Low-Resolution Spectra, IRAS Catalogs and Atlases 1986, A&A, 65, 607
IRAS Explanatory Supplement 1988, IRAS Catalogs and Atlases, Volume 1, NASA RP-1190 (U.S. Government Printing Office, Washington, DC)
IRAS Point Source Catalog, version 2 1988, IRAS Catalogs and Atlases, Volumes 2–6, NASA RP-1190 (U.S. Government Printing Office, Washington, DC) (PSC)
Kukarkin, B. V., *et al.* 1970, General Catalogue of Variable Stars (Moscow)
Kurucz, R. L. 1979, ApJS, 40, 1
Kurucz, R. L. 1991, private communication
Labs, D., & Neckel, H. 1970, Solar Physics, 15, 79
Lebofsky, L. A., Veeder, G. J., Lebofsky, M. J., & Matson, D. L. 1978, Icarus, 35, 336
Matson, D. L. 1986, Infrared Astronomical Satellite Asteroid and Comet Survey, version No. 1
Moseley, S. H., Dwek, E., Glaccum, W., Graham, J. R., Loewenstein, R. F., & Silverberg, R. F. 1989, ApJ, 347, 1119
Rothman, L. S., *et al.* 1987, Appl. Optics, 26, 4058
Schild, R., Peterson, D. M., & Oke, J. B. 1971, ApJ, 166, 95
Selby, M. J., *et al.* 1988, A&AS, 74, 127
Strecker, D. W., Erickson, E. F., & Witteborn, F. C. 1979, ApJS, 41, 501
Tokunaga, A. T. 1984, AJ, 89, 172
Volk, K., & Cohen, M. 1989, AJ, 98, 1918
Witteborn, F. C., & Bregman, J. D. 1984, Proceedings Soc. Photo-Opt. Instr. Eng., 509, 123
Wright, E. L. 1976, ApJ, 210, 250

SPECTRAL IRRADIANCE CALIBRATION IN THE INFRARED. III. THE INFLUENCE OF CO AND SiO

MARTIN COHEN

Radio Astronomy Laboratory, 601 Campbell Hall, University of California, Berkeley, California 94720

FRED C. WITTEBORN,[1] DUANE F. CARBON,[2] GORDON AUGASON,[3] DIANE WOODEN,[1] JESSE BREGMAN,[1] AND DAVID GOORVITCH[1]

NASA-Ames Research Center, Moffett Field, California 94035-1000

Received 27 April 1992; revised 10 July 1992

ABSTRACT

We describe first efforts to establish a network of calibrated infrared spectra of "standard stars" suitable for calibration of at least low-resolution infrared spectrometers using ground-based, airborne, and satellite-borne broadband sensors. The focus of this paper is on the crucial 5–8 μm region, inaccessible from the ground, in K and M giants. In this region the fundamental bands of CO and SiO cause substantial departures from featureless pseudo-continua. These departures are, of course, well-known to stellar atmosphere theorists. However, they are still ignored by many astronomical infrared photometrists and spectroscopists who assume that these bright stars can be represented by blackbodies at their effective temperatures. The purpose of this short paper is to draw the attention of infrared observers in the field to the invalidity of the blackbody assumption in the thermal infrared regime. We hope to achieve this end by observationally demonstrating the importance of these molecular features in cool giant stars in the airborne infrared regime, and illustrating their influence on spectra that are calibrated using blackbody assumptions. To help confirm our identifications of the principal molecular features, we present a synthetic spectrum computed using a model atmosphere with the approximate parameters of α Tau. This theoretical synthetic spectrum, which contains line opacity only from CO and SiO, reproduces the observed spectrum of α Tau to within a few percent.

1. INTRODUCTION TO INFRARED SPECTRAL CALIBRATION

In his critical review of the optical absolute calibration of Vega, Hayes (1985) states of the corresponding situation in the infrared: "The calibration of the IR, and the availability of secondary standard stars in the IR, is yet immature, and I recommend more effort... ." While the broadband situation may be immature, the subject of "standard" continuously calibrated stellar spectra has been even more poorly explored. Strecker *et al.* (1979: hereafter referred to as SEW) published a set of calibrated 1.2–5.5 μm stellar spectra obtained from NASA's Lear Jet and Kuiper Airborne Observatories. This airborne platform offers the vital advantage of essentially continuous spectral coverage for the brightest objects, as opposed to ground-based measurements that are constrained by the opaque regions 2.5–2.8 μm (blocked by terrestrial H_2O), 4.2–4.4 (CO_2), ~5–7.5, ~13–17, and the difficult zone from 4–5 μm (highly time-variable transmission). SEW carefully explained their rationale for absolute calibration based on Vega. In spite of these authors' considerable effort, relatively little use has been made of the SEW tabulations by observers, and no one has ventured a comparable effort for the ground-based 8–13 μm window.

Stellar theoreticians are keenly aware of the non-Planckian nature of stellar energy distributions. They have considered the influence of near-infrared CO absorption bands on stellar spectra (e.g., Bell & Gustafsson 1989; Bell & Briley 1991); even the effects of non-LTE conditions on the CO line formation have been examined in considerable detail (e.g., Carbon *et al.* 1976; Ayres & Wiedemann 1989). Effects caused by terrestrial atmospheric absorption features on the calibration of stellar spectra were treated by Bessell & Brett (1988), with specific reference to the SEW database. Of particular importance has been the work applying the Infrared Flux Method (IRFM) to the determination of stellar effective temperature and diameter through calibrated infrared narrowband photometry and considerations of the SEW spectra [Blackwell *et al.* 1986 (and references therein); Blackwell *et al.* 1991]. The IRFM studies provide a bridge between absolute infrared photometric calibration and model atmosphere calculations. However, there appears to be an almost complete separation between two subdisciplines: the theorists who can *ab initio* simulate a stellar atmosphere, replete with non-LTE treatment of molecules; and the observers who simply adopt Planck functions for their calibrators, thereby diminishing the value of their data. Consequently, infrared astronomical calibration by many observers, both spectrally continuous and broadband, has been developed from the completely erroneous assumption that normal stars can be represented by Planck functions at their effective temperatures (although local fits to some blackbody in a restricted region may be an adequate approximation for

[1]Astrophysics Branch, Code SSA, M.S. 245-6.
[2]NAS Systems Development Branch, Code RND, M.S. 258-5.
[3]Space Instrumentation and Studies Branch, Code SFI, M.S. 244-B.

 0004-6256/92/112045-08$00.90

some purposes). A common "consistency check" on this method is to ratio the spectra of two stars, each taken to be a blackbody, and to seek a featureless quotient spectrum. Of course, this does not vindicate the assumption that the original spectra are truly featureless, being equally consistent with the hypothesis that each star suffers approximately the same absorptions.

One might have expected that, as infrared instruments attained higher and higher resolution (at least in the 1–5 μm region) and as stellar atmosphere theory accommodated greater and greater physical complexity, observers' reliance on Planck functions would disappear. However, one has only to peruse the recent infrared astronomical literature to recognize the prevalence of this gross oversimplification in the calibration of both spectroscopy and broadband photometry. Unfortunately, the most striking aspect of most current infrared observational papers is the almost complete absence of any useful details of the calibration procedure (e.g., Wynn-Williams *et al.* 1992). Some authors cite only a general reference in which standard star magnitudes in their broadband system of filters are given, without stating precisely which stars were observed or relating these magnitudes to some absolute calibration for "zero magnitude" (e.g., Margon *et al.* 1992). Neither the true spectroscopic shape nor photometry can be salvaged from such papers. Others state which "standard stars" were used for their spectroscopy but give no details of how the stellar energy distributions were calculated (e.g., Woodward *et al.* 1989): one must presume that the usage of blackbodies at the effective temperatures is implicit but no meaningful quantitative data can be extracted by the more demanding reader. Still other workers list the "standards" used and explicitly cite the blackbodies adopted to represent their energy distributions (see Sec. 5). Although this procedure is erroneous, it at least offers traceability and the prospect of resurrecting the data more accurately under a new calibration approach.

The present paper anticipates the development of an eventual grid of "real" calibrated stellar spectra intended to supplant "calibration" based on Planck functions. This grid should be a resource for both observers and theoreticians. Our coverage will be continuous between at least 2 and 23 μm (the long wave limit of the IRAS Low Resolution Spectrometer) so the grid will be valuable to all modes of infrared observation (from ground, air, and space). Although initially at low spectral resolution, future long-term efforts will be directed toward replacing these initial spectra by ones at higher spectral resolution. The foundation of this stellar grid is a relatively small group of normal stars, typically K0–M0 III, well-observed in a variety of infrared regimes. Their individual spectral fragments in different wavelength regions will be assembled into a single 2 to $\sim$30 μm spectrum for each star and all will be radiometrically calibrated on a common basis, with well-characterized sources of error. Cohen *et al.* (1992) have recently demonstrated this method of complete spectral construction for α Tau.

A search of the infrared literature reveals a plethora of apparently useful spectral fragments relevant to our goal. However, unless a published spectrum can be traced to a single specific "calibration star," these fragments are of no use in the construction of our grid. It is also painfully clear from the literature that the scarcest fragments are those in the 5–8 μm region, accessible only from airplanes or space.

Therefore, we present a series of observed 5–8 μm spectra designed to demonstrate the real and substantial departures from smooth continua in the 4–9 μm range. Such spectra play a fundamental role in the creation of any calibration network and illustrate, observationally, the profound influence of both the CO and SiO fundamentals on the mid-infrared spectra of K and M stars. To justify the identification of these band heads and their spectral extents, we compare the observations with a model atmosphere calculation specifically for α Tau that includes the contributions of these two molecules.

To the sceptic, we stress that the appearance of these molecular features is quite independent of instrumentation. We see the same combination of features in essentially all cool (nondusty) stars we have observed, with our own spectrometers and with the UKIRT CGS3 instrument, and with telescopes in Arizona (the NASA Mt. Lemmon 1.5 m), Hawaii (both the IRTF and the UKIRT), and from the Kuiper Airborne Observatory (hereafter referred to as KAO), where terrestrial atmospheric interference is relatively minimal compared with ground-based measurements.

Consequently, the fundamental purpose of this short paper is to focus the attention of infrared observers in the field on the invalidity of the blackbody assumption in the thermal infrared regime. We hope to create an awareness of "real" stellar atmospheres among observers by illustrating observationally the influence of CO and SiO bands on the emergent infrared spectra of potential calibration stars.

2. THE SPECTRA

It is not the function of the present paper to describe in detail our scheme for absolute flux calibration. These details can be found in Cohen *et al.* (1992a: hereafter referred to as Paper I, on broadband infrared absolute calibration) and in Cohen *et al.* (1992b: hereafter referred to as Paper II, on the assembly of complete calibrated 1–35 μm stellar spectra, and recalibration of the *IRAS* Low Resolution Spectrometer). Our intent here is to discard the notion that "standard stars" are featureless in the infrared. To highlight the potential presence of molecular bands we have established a database of the ratios of the spectra of cool stars compared with those of Sirius and Vega. Both these A dwarf stars are sufficiently hot that these molecules could not survive in their atmospheres. Both have been modeled in the past, providing at least a preliminary absolute calibration (Kurucz 1979; Dreiling & Bell 1980; Bell & Dreiling 1981). The cool stellar spectra we use were taken only during KAO flights on which either Sirius (preferably, because of its brightness and absence of cold dust compared with Vega) or Vega were also observed with the same spectral coverage and resolution.

TABLE 1. Journal of observations represented in Fig. 1.

Flight date	Range (μm)	Grooves/mm	Order	Average Resolution (μm)	Type	Star
4/14/88	6.40-7.18	210	1st	0.043	K1 III	α Boo
4/17/90	5.20-8.00	210	1st	0.043	K3 III	α Hya
12/20/91	5.00-9.30	89	1st	0.043	K5 III	α Tau
1/18/91	3.38-5.30	120	1st	0.062	M0 III	μ UMa
1/18/91	4.79-8.75	75	1st	0.142	M0 III	μ UMa
1/21/91	3.38-5.30	120	1st	0.062	M0 III	β And
1/21/91	4.79-8.75	75	1st	0.142	M0 III	β And
4/14/90	5.54-7.99	210	1st	0.043	M0.5 III	δ Oph
10/24/88	3.82-10.33	90	1st	0.118	M1.5 III	α Cet
11/2/88	5.20-7.83	210	1st	0.043	M1.5 III	α Cet
11/28/90	5.50-9.00	150	1st	0.067	M2.5 III	β Peg
11/29/90	5.50-9.00	150	1st	0.067	M2.5 III	β Peg
4/11/88	3.95-5.37	90	1st	0.118	M3 III	γ Cru
4/5/89	5.25-8.00	210	1st	0.043	M3.5 III	σ Lib
4/17/90	5.20-8.00	210	1st	0.043	M4 III	δ Vir

Most spectra were taken with the NASA-Ames Faint Object Grating Spectrograph (FOGS: Witteborn & Bregman 1974) in the ~5–8 μm range although, in January 1991, we used both this instrument and its short wave counterpart (SIRAS) to provide complete coverage from 3–9 μm. Resolutions varied from ~50 to ~150 depending on the grating and order selected for the primary programs.

It is clear that calibration should not be regarded merely as a necessary evil to be accommodated on such flights or ground-based runs because no object's spectrum can be better determined than the calibration that underpins it.

Table 1 summarizes the observations that define the ratio spectra that are displayed here. Figure 1 shows the resulting spectral ratios to α CMa (for uniformity, all spectral ratios were smoothed to a resolution of 0.20 μm by convolving with a Gaussian of this FWHM). These are displayed in two montages for K1–M0.5 III [Fig. 1(a)] and M1.5–M4 III [Fig. 1(b)].

3. MOLECULAR FEATURES

The January 1991 spectra of β And and μ UMa are particularly valuable because each is an M0 III and because the coverage was continuous (with substantial overlap) from 3 to 9 μm, spanning the difficult edge of the 10 μm ground-based window. For these two stars we can test the working hypothesis that stars of identical spectral type should have very similar, if not identical, spectra. Figure 2 corroborates this hypothesis. We tentatively identify the primary molecular contributors as the fundamental of CO (~4.7 μm) and the fundamental (~8.0 μm) and first overtone (~4.1 μm) of SiO. We shall show in the next section that these identifications are correct in the case of α Tau. In the remainder of this section, we shall assume that the identifications are also correct for the other stars in Fig. 1. Figure 3 illustrates substantially the same spectral signatures in the ratio of spectra of α Tau and α CMa recently

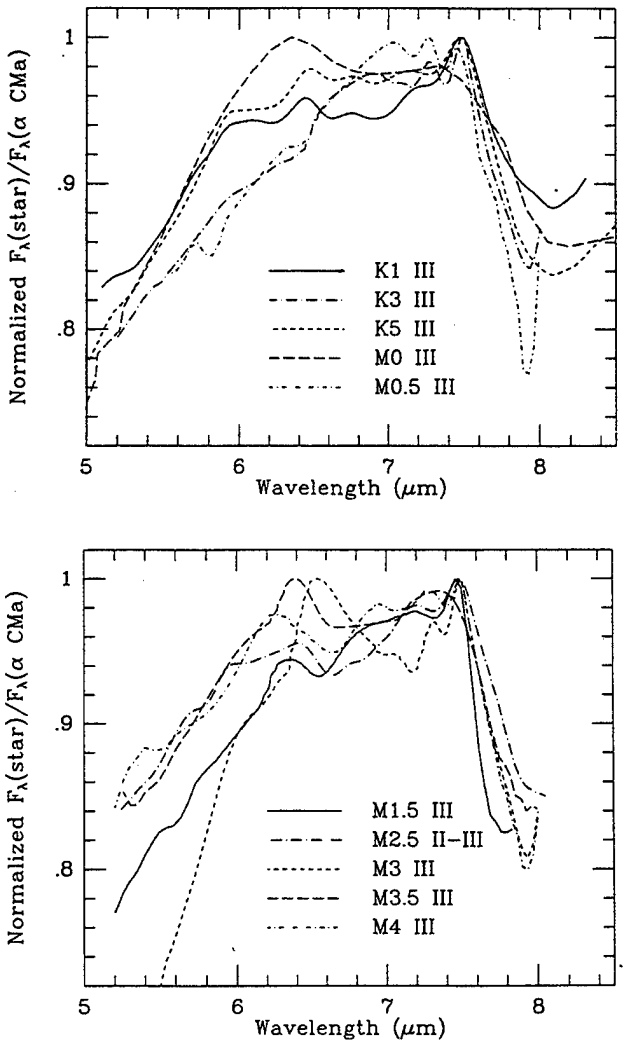

FIG. 1. The normalized profiles of airborne spectra for cool giant stars in the form of ratios to the spectrum of Sirius. Stars in the range K1–M0.5 III are displayed in (a); later types (M1.5–M4 III) in (b). At short wavelengths, spectra emerge from the CO fundamental; at long, they enter the SiO fundamental. All spectra have been smoothed to a common resolution.

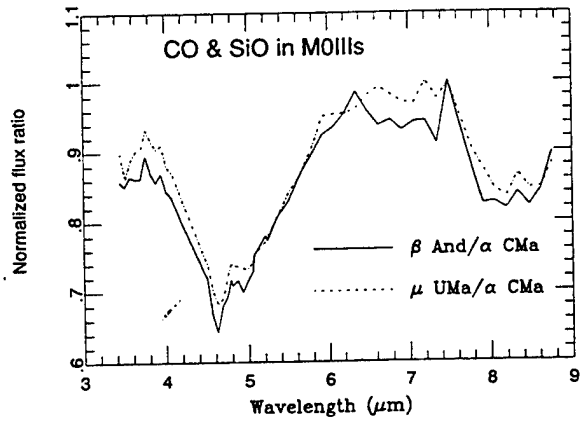

FIG. 2. A comparison of the normalized spectral ratios of two M0 IIIs (β And and μ Uma) to Sirius between 3 and 9 μm (KAO data from 18 and 21 January 1991).

obtained (20 December 1991) from the KAO using the new Ames "HIFOGS" spectrometer, a higher-resolution, 120-detector version of the FOGS instrument. Note that this spectral ratio derives from a single measurement at one grating setting of the HIFOGS: there is no need to blend together fragments of overlapping spectra.

CO was obvious in the SEW spectra and has long been known although its presence has rarely been mentioned in connection with those assumptions that have been made in the past for "calibration" spectra. SiO has enjoyed relatively little discussion in the observational literature since its first tentative identification (in the M supergiant 119 Tau: Knacke *et al.* 1969), no doubt due to its location at the short wave end of the 8–13 μm window where time variations in H_2O can create difficulties for ground-based studies. Indeed, Gillett *et al.* (1970) tried to identify a potentially deep absorption between 7.7 and 9.0 μm in VY CMa with SiO. This "feature" was based critically on the rise in the spectrum $\sim$7.7 μm but subsequent 5–8 μm low-resolution airborne spectroscopy (Cohen *et al.* 1989)

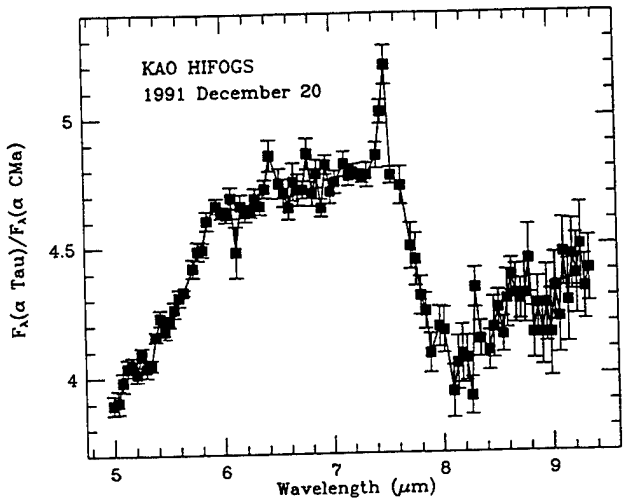

FIG. 3. The spectral ratio of α Tau and α CMa obtained in December 1991 in a single grating setting of the 120-detector HIFOGS instrument.

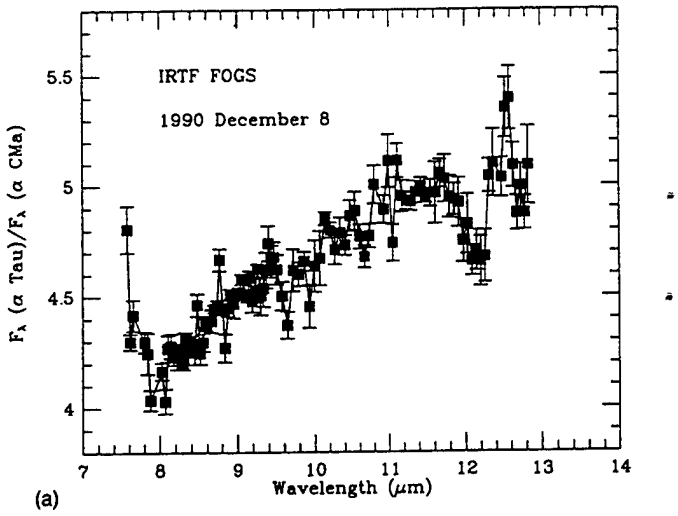

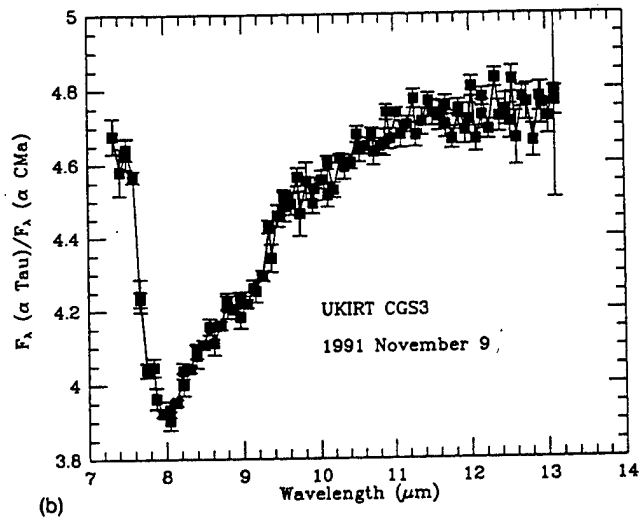

FIG. 4. The ground-based spectral ratio of α Tau to α CMa illustrating the true appearance of the SiO fundamental in the ground-based 8–13 μm window. (a) FOGS data taken at the IRTF on 8 December 1990; (b) CGS3 data taken at the UKIRT on November 1991 in the low-resolution mode and very well matched in airmass.

and high-resolution Fabry-Perot ground-based observations (Geballe *et al.* 1979) have shown any such feature to be far weaker than Gillett *et al.*'s structure. By contrast, the SiO first overtone (2,0) and (3,1) heads have been described in some detail over a range of stellar types by Rinsland & Wing (1982) at moderate resolution, and by Ridgway *et al.* (1984) at high resolution, following the original identification in α Ori by Cudaback *et al.* (1971), in other M giants or supergiants by Wollman *et al.* (1973), and in two Mira variables by Hinkle *et al.* (1976). Given the detections of the $\Delta v=2$ SiO heads just cited, it would be remarkable if the $\Delta v=1$ heads were not also present in these cool stars.

As Fig. 1 illustrates, the influence of SiO on spectral shape is not inconsequential: even in the earliest star represented, α Boo (K1 III), the fundamental head causes a 12% diminution in continuum flux at 7.9 μm. In α Tau [Fig. 1(a)] we observe a 16% feature (cf. Paper II). Figure 4 presents the ratio of ground-based spectra of α Tau and α CMa obtained on two different occasions, with different

spectrometers and on different telescopes. Figure 4(a) shows FOGS data taken at the IRTF on 7–8 December 1990 in three overlapping grating positions. The difference in airmass between the two stars was about 0.11 (α Tau always had the lower airmass) and we have attempted to remove the residual differential effects of the earth's atmosphere through use of a variant of FASCODE, using the 1991 release of the original HITRAN database (Rothman *et al.* 1987). Dr. J. Simpson applied this code for us at NASA-Ames [NWATER on the CRAY: see Lord (1992) for a description of several atmospheric modeling codes in use at NASA-Ames]. Figure 4(b) offers more recent data, obtained during UKIRT Service Observations on 9 November 1991, with rigorous demands on the matching of airmasses (averages were 1.25 for α CMa; 1.22 for α Tau). [Essentially identical material is also available, for example, from the Wyoming Infrared Observatory, where LeVan (1991) has provided us with the same ratio of spectra derived from observations with the GLADIS spectrometer.] These UKIRT data were taken in the low-resolution mode of the CGS3 instrument (resolving power $\sim$50). High-resolution (resolving power $\sim$160) were also secured on the same night at UKIRT and are in excellent agreement with Fig. 4(b) except through the terrestrial ozone, where the higher resolution data actually sample the stellar spectra through "holes" in the ozone absorption. (No HITRAN corrections were applied to the UKIRT data because of the excellent match in airmass.)

Consequently, it is now clear that the major discontinuity shortward of 8 μm and the gradual upward curvature between 8 and $\sim$12 μm are real. Note that neglect of this feature when calibrating with K and M giants at best has a marked effect on the slope of ground-based 8–13 μm spectra (even if one avoids the immediate vicinity of the bandhead) and at worst can create an entirely specious emission feature peaking near 8.5 μm. One might even be misled into the identification of SiO emission in some object calibrated in the typical fashion. It is also apparent when one considers the effect of telluric absorbers between 7 and 8 μm that the KAO data provide a critical complement even to observations from Mauna Kea.

4. A SYNTHETIC SPECTRUM FOR α TAU

4.1 Purpose of the Synthetic Spectrum

We wish to emphasize at the start that it is not our purpose here to present a detailed model atmosphere analysis of the infrared spectrum of α Tau. Such an analysis is certainly interesting, although primarily for what it tells us about the state of theoretical modeling, and we have undertaken it elsewhere (Carbon *et al.* 1992). We have a much more limited goal here. We hope to convince observers that the extended features in the observed spectra of the previous section which we identified as the CO and SiO fundamentals are just what we claim them to be. To accomplish this, we have computed a detailed model atmosphere spectrum for the CO and SiO fundamental regions of one of the infrared "standard stars" shown above, α Tau. We have chosen α Tau for this specific example because it has been the subject of several careful studies and has reasonably well-determined (as cool stars go) atmospheric parameters. We will show that the synthetic spectrum generated using a model atmosphere with the approximate parameters of α Tau follows the observations closely, generally within a few per cent, between 3.5 and 13 μm. Most importantly, the theoretical spectrum shows CO and SiO fundamental absorptions which share the same position, depth, and redward extent as the features we have identified in the previous section. We hope that this agreement will prove we have correctly identified the absorption features in α Tau, and that the CO and SiO fundamentals do, in fact, produce marked deviations from simple Planckian flux distributions.

4.2 Computation of the Synthetic Spectrum for α Tau

The model atmospheres and molecular lines lists used to generate the spectrum discussed later in this section are described in considerable detail in a later paper of this series (Carbon *et al.* 1992). For the spectrum discussed here, we model α Tau with an effective temperature of 3920 K (Blackwell *et al.* 1991), a log g of 1.5 (Smith & Lambert 1985), a microturbulent velocity parameter of 2.0 km/s (e.g., Smith & Lambert 1990; Tsuji 1986; Kovacs 1983), a $^{12}C/^{13}C$ ratio of 10 (Smith & Lambert 1990) and metal abundances based on the latest studies (e.g., Smith & Lambert 1990; Kovacs 1983). This set of atmospheric parameters represents the best of our current understanding of α Tau. As discussed by Carbon *et al.* (1992), the Si/Fe ratio in our model has been raised slightly, by 0.2 dex, relative to the Kovacs (1983) value. Using this enhanced Si abundance, our synthetic spectrum accurately reproduces the high resolution SiO first overtone observations of α Tau presented by Ridgway *et al.* (1984). Only absorption lines from SiO and CO were included in the synthesis calculation. All vibrational–rotational CO lines of the fundamental and first overtone were included to $V''=15$ and $J''=200$ for $^{12}C^{16}O$ and to $V''=12$ and $J''=150$ for $^{13}C^{16}O$. All vibrational–rotational $^{28}Si^{16}O$ lines of the fundamental and first overtone were included to $V''=10$ and $J''=150$; only lines of the $^{28}Si^{16}O$ isotopic species were included.

The model atmosphere for the synthesis calculations was taken from the recent grid of models prepared by Kurucz (1991); a discussion of the spectra obtained using other model atmospheres will be found in Carbon *et al.* (1992). The choice of model atmosphere is not relevant to the arguments of this paper. The spectrum was synthesized using the SOURCE model atmosphere program in essentially the same fashion as described by Carbon *et al.* (1982). For the spectrum that we show here, a variable wavelength mesh was used which gave at least 2 wavelength points per Doppler width. The high-resolution synthetic spectrum was convolved with a Gaussian profile function whose FWHM varied roughly in accord with the wavelength variations in the instrumental profiles of the

TABLE 2. Resolutions adopted for spectral synthesis in different regimes.

Wavelength Interval (μm)	Adopted FWHM (μm)	Mean $\lambda/\Delta\lambda$
1.0 - 4.3	0.066	40
4.3 - 8.0	0.041	150
8.0 - 13.4	0.214	50

observations represented. For simplicity in performing the convolution, we adopted a mean FWHM for each interval; this gives a correct convolution only in the center of each of the tabulated intervals. The errors introduced by this approximation in no way affect our conclusions regarding the deviations of the computed spectrum from a simple Planckian distribution. Table 2 gives the FWHM and mean resolutions we adopted for the convolution.

4.3 Comparison of Observed and Synthetic Spectra for α Tau

In Fig. 5, we compare the synthesized spectrum with the observed composite α Tau spectrum for the interval 3.5–13.0 μm. For comparison, we also show the continuum flux distribution of the theoretical model. Fluxes in the individual spectra have been normalized at 3.8 μm and multiplied throughout by λ^4. The $\pm 1\sigma$ bounds are plotted for the observed spectrum. The theoretical and observed spectra have been shifted so that the theoretical spectrum lies 1.3% above the observed spectrum at 3.80 μm. We have chosen this particular wavelength for the normalization because it is almost completely free of line blanketing. We refer the reader to the region around 2632 cm^{-1} (3.80 μm) in the high-resolution spectrum of α Tau published by Ridgway *et al.* (1984). We measure 1.3% absorption by atomic and molecular lines in the Ridgway *et al.* spectrum for the interval 3.76–3.84 μm sampled by our low-resolution spectral element at 3.80 μm. The atomic and molecular lines in the observed spectrum at 3.80 μm are not included as opacities in our synthesized spectrum (i.e., they do not arise from either CO or SiO). Thus, the synthesized spectrum should be shifted so as to lie 1.3% above the observed at 3.80 μm, a step which we have taken in Fig. 5. This provides the absolute scale for the computed spectrum.

We first discuss the features of the theoretical α Tau spectrum. The continuum flux curve in Fig. 5 has been computed with only continuum opacities. This represents the highest flux that the specified model can emit at the plotted wavelengths. The synthesized spectrum computed by including the opacities of the CO and SiO lines falls distinctly below the continuum level over much of the 3.7–13.0 μm interval. Only near 3.8 μm, 7–7.5 μm, and beyond 11.5 μm, does the synthesized spectrum approach the continuum level. The dominant features of the synthesized

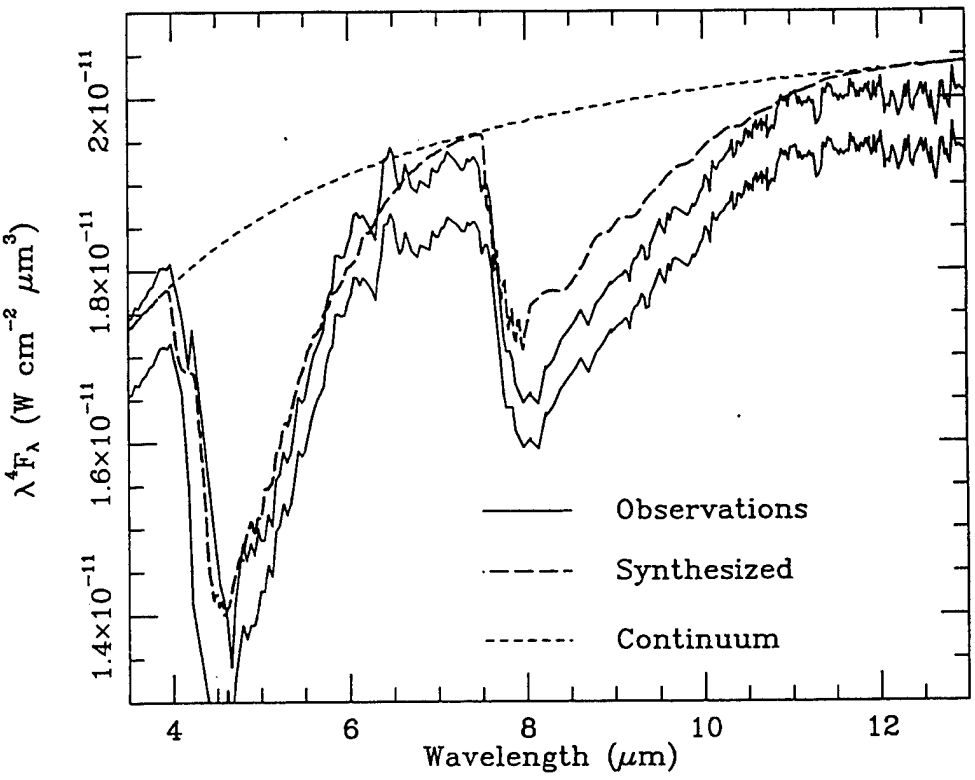

FIG. 5. A comparison of our synthetic model atmosphere for α Tau with a composite spectrum of the same star created from several spectral fragments. The complete spectrum of this star is described by Cohen *et al.* (1992). Long dashed lines: synthetic spectrum; short dashed lines: computed continuum; solid lines: $\pm 1\sigma$ bounds on the observed spectrum.

spectrum are the CO and SiO fundamental vibrational–rotational bands. The CO fundamental reaches maximum absorption near 4.6 μm and the SiO fundamental reaches its maximum near 8.0 μm. The SiO first overtone bands are apparent in the synthesized spectrum as a notch on the blue wing of the CO fundamental. These are the SiO overtone bands which were described at moderate resolution by Rinsland & Wing (1982) and which may be seen at high resolution in the α Tau spectrum presented by Ridgway *et al.* (1984).

The agreement between this single synthesized spectrum and the observed α Tau spectrum is generally good. With the relative placement of synthesized and observed spectra that we have chosen, the observed spectrum tends to lie systematically below the computed spectrum, generally by only ~4%. At least part of this discrepancy is probably due to additional line opacities in α Tau which were not included in our model calculations. This issue is discussed by Carbon *et al.* (1992) who also discuss in detail and quantify other uncertainties in the synthesized spectrum and in the underlying model atmosphere which generated it. Nevertheless, it is apparent from the comparison in Fig. 5 that the spectrum of α Tau is impacted significantly by absorption from the CO and SiO fundamentals. The computed CO and SiO bands generally match the observed absorption features in location, depth, and redward extent. Thus, at least in the specific example of α Tau, the features which we identified in Sec. 3 as CO and SiO fundamental band absorptions can be largely explained by those two species. Since both CO and SiO are abundant molecular species in oxygen-rich cool stars over a wide range of temperatures, gravities, and compositions, it is probable that CO and SiO will contribute significantly to the absorptions seen in Fig. 1. Caution must be exercized, however, in assuming that *all* the absorption in all the stars of Fig. 1 is due only to CO and SiO. Other species might contribute, particularly in the cooler stars. Barring direct observational evidence, preferably at high resolution, this question can be resolved best by synthesizing the spectra for other representative stars as we have done for α Tau.

5. ERRORS INHERENT IN CALIBRATION UNDER THE BLACKBODY ASSUMPTION

We have constructed a complete infrared spectrum for α Tau, both empirically (Paper II), and *ab initio* (Sec. 4), and have demonstrated the relevance of the CO and SiO absorptions to all cool giants of types K and M. We now detail and quantify the types of error that are inherent in calibration by blackbody assumption. First, the infrared continuum slope is substantially different from a Planckian slope in near- and mid-infrared, even for solar-type stars (cf. Fig. 1 of Paper I). This leads to a derived slope that is systematically too steep and grows monotonically with decreasing wavelength. Typical continuum errors made by assuming that α Tau is represented by a 3920 K blackbody are 21% at 4 μm when the real and assumed distributions are normalized near 2.0 μm, and 9% error at 25 μm when pinning real and assumed distributions to photometry at 12 μm. (We now cite typical astronomical applications, drawn from the recent literature, to illustrate the various ways in which blackbody assumptions are currently being used.) This first category of problem is particularly prevalent in current reductions of astronomical spectroscopy (e.g., Suto, *et al.* 1992; Zhang & Kwok 1992; Lowe *et al.* 1991; Graham & Chen 1991). It also affects any attempt to predict photometric flux densities in nonstandard filters by interpolating between supposedly known values in adjacent broadband filters (e.g., Telesco & Knacke 1991). The severity of this kind of error increases with decreasing stellar effective temperature of the "calibrator" (e.g., Courvoisier *et al.* 1992). The most common blackbody assumption made is to approximate some late B or early A dwarf by a 10 000 K blackbody. If we normalize this Planck function and the calibrated Vega spectrum from Paper I at 2.0 μm, then the continuum values drawn from the Planck curve will overestimate the model atmosphere values by 5% near 3.5 μm, 6% near 5 μm, 9% near 10 μm, and 11% near 20 μm.

Second, neglect of atomic and especially molecular absorptions in cool stellar calibrators leads to spurious emission features at the locations of the ignored absorptions, a much more insidious failing than incorrectly sloping continua. For the CO fundamental, such spurious peaks can attain 40% of the interpolated smooth continuum near 4.6 μm; for SiO, the effect varies from 12%–30% at 7.9 μm across the range of spectral types we have so far observed. In the *IRAS* Low Resolution Spectrometer database, neglect of the SiO fundamental has created an 11% feature at its peak. Both fundamentals are sufficiently broad that their influence is felt over almost 2 μm (CO) and almost 4 μm (SiO). This type of problem may be recognized explicitly by the presence of artificial "emission features," often near 8 μm (e.g., Vardya *et al.* 1990). But it is also *implicit* in most photometry of cool "calibration stars" in those filters that sample molecular heads (K, M, [8.7], N, [11.7], *IRAS* [12]). In particular, it is dangerous to interpolate adopted stellar magnitudes between bands that sample dominantly infrared continuum and bands influenced by molecular absorptions, in order to represent the continuous spectrum of a calibrator (e.g., Telesco & Knacke 1991; Hanner *et al.* 1990).

We trust that these cautionary notes will lead to a decreased reliance on assumed blackbodies for reductions of infrared astronomical observations.

We thank Amara Graps for her assistance obtaining the newest spectral ratio data of α Tau to α CMa in December 1991. The airborne observations we described were obtained through NASA's Airborne Astronomy program during fiscal years 1988–92 and we thank the entire staff of the KAO for their assistance in securing so many valuable spectra. M.C. was supported by NASA-Ames through Co-Operative Agreement NCC 2-142 with the University of California at Berkeley.

REFERENCES

Ayres, T. R., & Wiedemann, G. R. 1989, ApJ, 338, 1033
Bell, R. A., & Briley, M. M. 1991, AJ, 102, 763
Bell, R. A., & Dreiling, L. A. 1981, ApJ, 248, 1031
Bell, R. A., & Gustafsson, B. 1989, MNRAS, 236, 653
Bessell, M. S., & Brett, J. M. 1988, PASP, 100, 1134
Blackwell, D. E., Booth, A. J., Petford, A. D., Leggett, S. K., Mountain, C. M., & Selby, M. J. 1986, MNRAS, 221, 427
Blackwell, D. E., Lynas-Gray, A. E., & Petford, A. D. 1991, A&A, 245, 567
Carbon, D. F., Augason, G. C., Cohen, M., Witteborn, F. C., Wooden, D., & Goorvitch, D. 1992, in preparation
Carbon, D. F., Langer, G. E., Butler, D., Kraft, R. P., Trefzger, Ch. F., Suntzeff, N. B., Kemper, E., & Romanishin, W. 1982, ApJS, 49, 207
Carbon, D. F., Milkey, R. W., & Heasley, J. N. 1976, ApJ, 207, 253
Cohen, M., Tielens, A. G. G. M., Bregman, J. D., Witteborn, F. C., Rank, D. M., Allamandola, L. J., Wooden, D. H., & Jourdain de Muizon, M. 1989, ApJ, 341, 246
Cohen, M., Walker, R. G., Barlow, M. J., & Deacon, J. R. 1992a, AJ, 104, 1653 (Paper I)
Cohen, M., Walker, R. G., & Witteborn, F. C. 1992b, AJ, 104, 2030 (Paper II)
Courvoisier, T. J.-L., Bouchet, P., & Robson, E. I. 1992, A&A, 258, 272
Cudaback, D. D., Gaustad, J. E., & Knacke, R. F. 1971, ApJ, 166, L49
Dreiling, L. A., & Bell, R. A. 1980, ApJ, 241, 737
Geballe, T. R., Lacy, J. H., & Beck, S. C. 1979, ApJ, 230, L47
Gillett, F. C., Stein, W. A., & Solomon, P. M. 1970, ApJ, 160, L173
Graham, J. A., & Chen, W. P. 1991, AA, 102, 1405
Hanner, M. S., Newburn, R. L., Gehrz, R. D., Harrison, T., Ney, E. P., & Hayward, T. L. 1990, ApJ, 348, 312
Hayes, D. S. 1985, in Calibration of Fundamental Stellar Quantities, Proceedings of the IAU Symposium No. 111, edited by D. S. Hayes, L. E. Pasinetti, and A. G. Davis Philip (Reidel, Dordrecht), p. 225
Hinkle, K. H., Barnes, T. G., Lambert, D. L., & Beer, R. 1976, ApJ, 210, L141
Knacke, R. F., Gaustad. J. E., Gillett, F. C., & Stein, W. A. 1969, ApJ, 155, L189
Kovacs, N. 1983, A&A, 120, 21
Kurucz, R. L. 1979, ApJS, 40, 1
Kurucz, R. L. 1991, in Precision Photometry: Astrophysics of the Galaxy, edited by A. G. Davis Philip, A. R. Upgren, and K. A. Janes (Davis, Schenectady)
LeVan, P. 1991, personal communication
Lord, S. 1992, Contractor's report to NASA (in preparation)
Lowe, R. P., Moorhead, J. M., Whelau, W. H., & Maillard, J.-P. 1991, ApJ, 368, 195
Margon, B., Phillips, A. C., Ciardullo, R., & Jacoby, G. H. 1992, AJ, 103, 924
Ridgway, S. T., Carbon, D. F., Hall, D. N. B., & Jewell, J. 1984, ApJS, 54, 177
Rinsland, C. R., & Wing, R. F. 1982, ApJ, 262, 201
Rothman, L. S., *et al.* 1987, Appl. Optics, 26, 4058
Smith, V. V., & Lambert, D. L. 1985, ApJ, 294, 326
Smith, V. V., & Lambert, D. L. 1990, ApJS, 72, 387
Strecker, D. W., Erickson, E. F., & Witteborn, F. C. 1979, ApJS, 41, 501 (SEW)
Suto, H., Mizutani, K., & Maihara, T. 1992, AJ, 103, 927
Telesco, C. M., & Knacke, R. F. 1991, ApJ, 372, L29
Tsuji, T. 1986, A&A, 156, 8
Vardya, M. S., de Jong, T., & Willems, F. J. 1990, ApJ, 304, L29
Witteborn, F. C., & Bregman, J. D. 1984, Proc. Soc. Photo.-Opt. Eng., 509, 123
Wollman, E. R., Geballe, T. R., Greenberg, L. T., Holtz, J. Z., & Rank, D. M. 1973, ApJ, 184, L85
Woodward, C. E., Pipher, J. L., Shure, M., & Forrest, W. J. 1989, ApJ, 342, 860
Wynn-Williams, C. G. *et al.* 1992, ApJ, 377, 426
Zhang, C. Y., & Kwok, S. 1992, ApJ, 385, 255

ERRATUM: "SPECTRAL IRRADIANCE CALIBRATION IN THE INFRARED." PAPERS I, II, AND III [ASTRON. J. **104**, 1650, 2030, 2045 (1992)]

MARTIN COHEN

Radio Astronomy Laboratory, University of California, Berkeley, California 94720, and Jamieson Science & Engineering, Inc., 5321 Scotts Valley Drive, Suite 204, Scotts Valley, California 95066
Electronic mail: cohen@bkyast.berkeley.edu

RUSSELL G. WALKER

Jamieson Science & Engineering, Inc., 5321 Scotts Valley Drive, Suite 204, Scotts Valley, California 95066
Electronic mail: jamieson@bkyast.berkeley.edu

MICHAEL J. BARLOW AND JOHN R. DEACON

Department of Physics & Astronomy, University College London, Gower Street, London WC1E 6BT, United Kingdom
Electronic mail: 19752:mjb, 19752:jrd

FRED C. WITTEBORN, DUANE F. CARBON, GORDON AUGASON, DIANE WOODEN, JESSE BREGMAN, AND DAVID GOORVITCH

NASA-Ames Research Center, Moffett Field, California 94035-1000
Electronic mail: witteborn@gal.arc.nasa.gov, dcarbon@nas.nasa.gov, augason@gal.arc.nasa.gov, woden@gal.arc.nasa.gov, bregman@gal.arc.nasa.gov, goorvitch@gal.arc.nasa.gov

Received 1992 December 23

Due to an unfortunate oversight, a direct acknowledgment of the source of support and sponsorship for this entire program of work on infrared calibration was omitted from the papers although the separate contract numbers appear. The authors of these three articles wish to thank Dr. Stephan D. Price and the Phillips Laboratory for direct financial support and continued encouragement, both personally and via the Stellar Atlas Panel, for these ongoing efforts.

 0004-6256/93/052008-01$00.90

SPECTRAL IRRADIANCE CALIBRATION IN THE INFRARED. IV. 1.2–35 μm SPECTRA OF SIX STANDARD STARS

MARTIN COHEN

Jamieson Science and Engineering, Inc., Suite 204, 5321 Scotts Valley Drive, Scotts Valley, California 95066 and Radio Astronomy Laboratory, 601 Campbell Hall, University of California, Berkeley 94720
Electronic mail: cohen@bkyast.berkeley.edu

FRED C. WITTEBORN

NASA–Ames Research Center, Mailstop 245-6, Moffett Field, California 94035-1000
Electronic mail: witteborn@ssal.arc.nasa.gov

RUSSELL G. WALKER

Jamieson Science and Engineering, Inc., Suite 204, 5321 Scotts Valley Drive, Scotts Valley, California 95066
Electronic mail: jse@netcom.com

JESSE D. BREGMAN, AND DIANE H. WOODEN

NASA–Ames Research Center, Mailstop 245-6, Moffett Field, California 94035-1000
Electronic mail: bregman@ssal.arc.nasa.gov, wooden@ssal.arc.nasa.gov

Received 1994 December 19; revised 1995 April 3

ABSTRACT

We present five new absolutely calibrated continuous stellar spectra from 1.2 to 35 μm, constructed as far as possible from actual observed spectral fragments taken from the ground, the Kuiper Airborne Observatory (KAO), and the *IRAS* Low Resolution Spectrometer (LRS). These stars—β Peg, α Boo, β And, β Gem, and α Hya—augment our already created complete absolutely calibrated spectrum for α Tau. All these spectra have a common calibration pedigree. The wavelength coverage is ideal for calibration of many existing and proposed ground-based, airborne, and satellite sensors. © *1995 American Astronomical Society.*

1. INTRODUCTION

In a previous paper of this series we have described a consistent effort to provide absolutely calibrated broad- and narrow-band infrared photometry based upon a carefully selected, infrared-customized pair of stellar models for Vega and Sirius, created by Kurucz, and absolutely calibrated by Cohen *et al.* (1992a: hereafter referred to as Paper I). These hot stellar models have been employed as reference spectra to calibrate cool stars by the methods detailed by Cohen *et al.* (1992, hereafter referred to as Paper II), and applied to the K5III star, α Tau. This approach yields a valuable infrared-bright secondary stellar standard with a calibration pedigree directly traceable to our primary radiometric standard, namely, α CMa. This cool giant spectrum is totally unlike any blackbody in its energy distribution, and is dominated by the fundamental absorption and overtones of CO and SiO. These molecular bands are common among cool giants and supergiants (Cohen *et al.* 1992b; hereafter referred to as Paper III). By following identical procedures to those described in Paper II, we have assembled spectra for five other popular infrared "calibrators," namely β Peg, α Boo, β And, β Gem, and α Hya. In this paper we (1) graphically illustrate the techniques involved in our process of spectral assembly; (2) present all five newly built "composite" spectra, and discuss their calibration pedigrees; and (3) from them derive magnitudes in several commonly used infrared passbands. We also discuss our adopted method for extrapolation of stellar spectra to 35 μm in the absence of an observed spectral fragment, or given only a noisy spectrum, and vindicate the procedure using long-wavelength KAO data by Glaccum (1990).

2. THE NEW COMPOSITE SPECTRA

Our methodology for creating a complete and continuous composite spectrum from 1.2–35 μm is precisely described in Paper II. By exactly following the procedures laid down there we have been able to construct several more composites for β Peg (M2.5II–III, and the latest type we have treated), α Boo (K1III), β And (M0III), β Gem (K0III), and α Hya (K3II–III), in chronological order of actual construction. In some cases, earlier composites have been replaced by subsequent and better products, as we have acquired new and higher signal-to-noise spectral fragments either from the KAO (~5–9 μm) or from the ground (~7.5–13 μm). Cohen & Davies (1995, Paper V in this series) separately assess the calibration pedigree of the UKIRT CGS3 spectrometer that has provided most of our 10 μm spectra. Table 1 will serve as a guide to the currently available and most reliable composites and models for the eight stars within our calibration context.

We emphasize the following key points concerning spectrum assembly.

(i) We define flux density calibrations only for filters with known transmission profiles scanned at their cold operating

TABLE 1. Model and composite spectra currently available.

Star	Spectral type	Date of assembly
α Lyr	A0 V	July 23, 1991
α CMa	A1 V	July 29, 1991
α Tau	K5 III	March 5, 1992
β Peg	M2.5 II-III	March 10, 1992
α Boo	K1 III	April 28, 1993
β And	M0 III	October 15, 1993
β Gem	K0 III	September 12, 1994
α Hya	K3 II-III	December 12, 1994

points, and we incorporate the effects of terrestrial site-specific transmission through the atmosphere, and of detector quantum efficiency.

(ii) We use photometry from the literature only if errors and magnitudes of standard stars are given so we can calculate the relevant "zero point offsets" (i.e., we define Vega to have zero magnitude at all infrared wavelengths; others may not do so, thereby creating an "offset" from zero in their system relative to our own).

(iii) All fragments are calibrated by multiplying the observed ratios of matched airmass spectra of a cool star and a reference star (Sirius or Vega) by the calibrated Kurucz hot star model, after convolution with a Gaussian that represents the combined effects of the instrumental profile with the actual spectral observations (cf. Appendix B and Fig. 14 of Wooden *et al.* 1993).

(iv) We stress independent photometric calibration of every possible spectral fragment by all possible filters whose passbands are entirely contained within the observed fragment.

(v) In the regions of overlap of two independent spectral fragments, both are combined using inverse variance weighting.

(vi) No fragment is ever changed in shape (except where it overlaps another fragment), only shifted in the absolute level.

(vii) The order of operations (Paper II) is logical but not important to the end product: we normalize the 1–5 μm fragment to near-infrared photometry; we separately but identically treat the 7.5–13 μm fragment using narrow band photometry in the 10 μm region; we splice the LRS 7.7–22.7 μm spectrum to the higher resolution CGS3 10 μm fragment (degrading the resolution of the CGS3 spectrum to match that of the LRS before splicing); we doubly splice the KAO 5–9 μm fragment to both the radiometrically calibrated 1–5 and 8–23 μm pieces; we then splice other long wave fragments to the long-wavelength observations.

We illustrate the following three primary procedures explicitly. (Note that in our graphics we make use of $\lambda^4 F_\lambda$ vs λ plots; these mitigate the intrinsically very steep falloff of stellar continua and enable us to display spectral fragments linearly for clarity.)

(viii) Normalization of a fragment with respect to photometry—Fig. 1 shows the Strecker *et al.* (1979, hereafter referred to as SEW) α Tau fragment placed relative to the

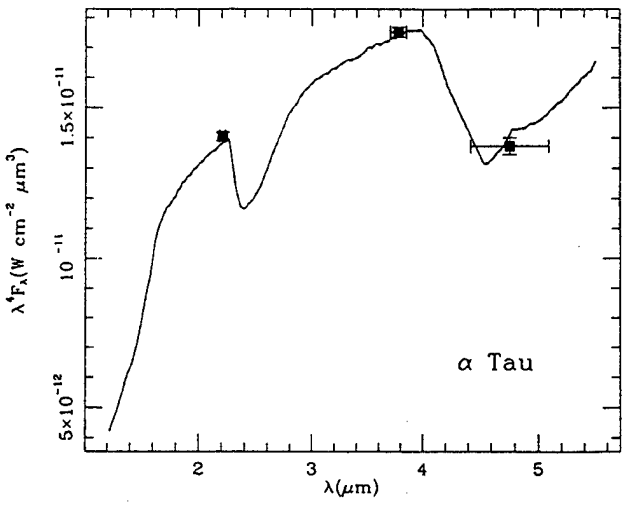

FIG. 1. Strecker *et al.* (1979) 1.2–5.5 μm KAO fragment for α Tau located with respect to photometry (Kn, Ln, M). The ±HWHMs of the relevant passbands are plotted. The short dashed line (barely distinguishable from the solid) is the SEW fragment; the solid line is the result of scaling it by 1.003 to fit this photometry.

Selby *et al.* (1988) "Kn" and "Ln" points, and the UKIRT (Deacon 1991) "M" point. The multiplier for the fragment is the inverse variance weighted result of simultaneously matching (in a least-squares sense) the three in-band flux ratios (KnLnM) defined from the α Tau fragment ratioed to the α Lyr calibrated model (Paper I). The short-dashed line represents the SEW fragment (after correction to the context of our 1991 Kurucz Vega model and for the influence of the potential nonlinearity in wavelength in the SEW longest filter wheel: cf. Figs. 5 and 6 of Paper II); solid line, barely perceptibly different from the solid (the scale factor applied was 1.003), is our rescaled version of the SEW spectrum.

(ix) A single-sided splice—in Fig. 2, the UKIRT CGS3

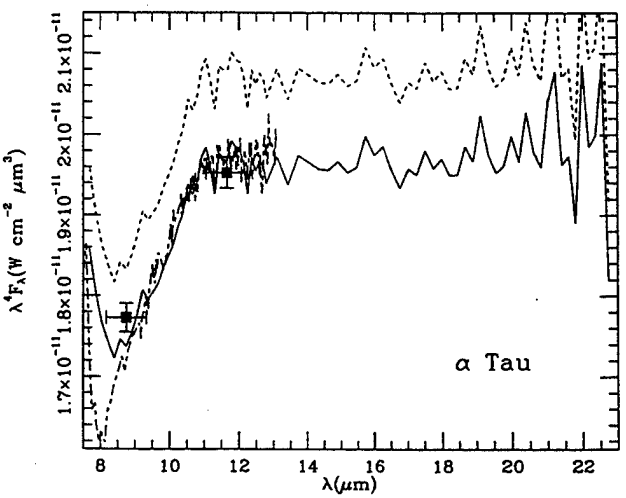

FIG. 2. A single-sided splice of the *IRAS* LRS spectrum of α Tau with the higher resolution UKIRT CGS3 spectrum (long-dashed–short-dashed line), which was previously "locked" to photometry from UKIRT ([8.7], [11.7]). The short-dashed line is the original LRS fragment; the solid line is the LRS scaled by 0.95. Note the close accord of the shapes of the rescaled LRS spectrum and the ground-based CGS3 spectrum. Deacon's (1991) photometry is included (along with the ±HWHMs of the passbands).

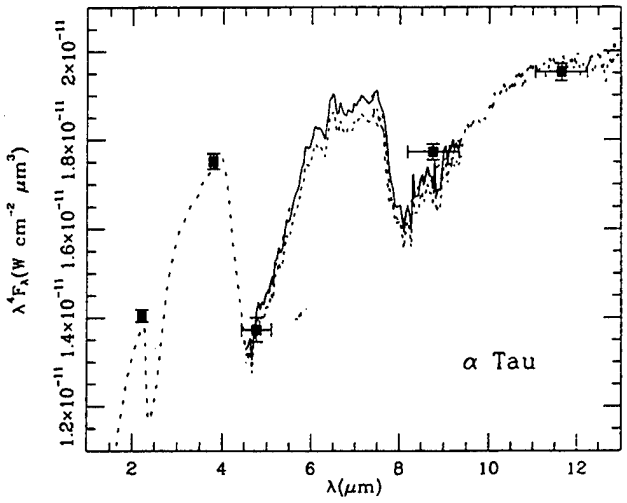

FIG. 3. Double-sided splice of the KAO fragment of α Tau to the radiometrically calibrated 1.2–5.5 and 7.5–22.7 μm pieces. The KAO fragment fits between the other two; the unscaled KAO portion is the short-dashed 5–9 μm piece; the solid line is the same fragment scaled by 1.022. All the photometry used to assemble the complete α Tau spectrum appears here, together with the passband ±HWHMs.

fragment is first "locked" to the [8.7] and [11.7] magnitudes shown in this figure (rescaling by 1.039) then α Tau's original LRS spectrum (short dashed line) is spliced to the CGS3 spectrum giving the solid line (the multiplier was approximately 0.95). Note that the higher resolution CGS3 spectrum was first degraded to match the LRS in resolution, before splicing. This figure details the region of overlap between these two fragments.

(x) A double-sided splice—in Fig. 3, α Tau's KAO spectrum is inserted between the radiometrically calibrated near- and mid-infrared spectra, simultaneously minimizing differences in the pair of jointly overlapping wavelength regions in a least-squares sense. The multiplier here is 1.022, moving the KAO fragment from the short dashed line to the solid line.

Figure 4 presents all six cool stellar composites in the form of absolute $\log(\lambda^4 F_\lambda)$ plots against $\log(\lambda)$. In each spectrum, the $\pm 1\sigma$ error range is indicated. Note that, for α Tau, the entire 1.2–35 μm range was spanned by observations through the fortuitous efforts of Glaccum (1990) who obtained 16–35 μm KAO spectra, which usefully extended the typical observation limit of 22.7 μm of the LRS instrument, or ~24 μm from UKIRT CGS3 long-wavelength spectroscopy from Mauna Kea. No other star among our composites has such a long-wavelength KAO fragment although occasionally we can extend the LRS range slightly using CGS3 data from 16 to 24 μm. Therefore, we need a method of extrapolation beyond the 20 μm domain.

After careful examination of all our spectral fragments, and of a number of model atmospheres for α Tau built by D. Carbon (1994), we decided to adopt the Engelke (1992) function as an extrapolator for the stellar continuum. The long dashed curves in Fig. 4 represent the relevant Engelke functions for the five composites. This analytic approximation to real stellar continua was derived assuming that the dominant source of infrared continuum opacity in these cool giant stars is H^- free–free. The intensive CRAY computations of α Tau's atmosphere by Carbon (1994) demonstrate that the Engelke function is a reasonably good approximation to the theoretical continuum at all wavelengths between 2 and 35 μm (it lies within ~±5% of the full-blown calculation). It is pertinent to ask whether we have substantive evidence that real stars behave in the way suggested by any of these models or approximations. Glaccum (1990) has observed the spectra of two normal stars (not known variables and without dust shells) between 16 and 35 μm from the KAO. Both the Engelke function and the CRAY models represent quite well the *observed* continuum in α Tau (Fig. 14 of Paper II; Fig. 5 of Paper III) and in the M3.5III γ Cru (Fig. 5). The importance of these KAO measurements is that their calibrational pedigree is entirely independent of any aspect of stars and their behavior. It is founded on observations and models for Uranus and Mars (cf. Moseley *et al.* 1989). Paper II illustrates the observed featureless and Rayleigh–Jeans character (flat in $\lambda^4 F_\lambda$ space) of the α Tau spectrum as far as 35 μm. Figure 5 demonstrates the same behavior for γ Cru, comparing the observed LRS and Glaccum KAO spectra with the shape of the Engelke function for this star. These long-wavelength KAO spectra materially strengthen our belief in the validity of these flat extrapolations of stellar spectra in the limited domain over which we use them (10–35 μm at most). By splicing Engelke functions to the actual composite observations longward of the SiO fundamental (typically, between about 12 and 22 μm), we can establish the flux density level of this spectral approximation, and hence estimate the stellar angular diameter.

We have also chosen to substitute this best-fitting Engelke function for noisy LRS and/or 20 μm CGS3 data when appropriate. Figure 6 exemplifies this substitution process for β And where both LRS and long-wave CGS3 fragments are available, but both are noisy in this amplified portrayal in a $\lambda^4 F_\lambda$ plot. There is no meaningful overlap between the two fragments; i.e., the 20 μm CGS3 fragment is unconstrained in the absolute level. The Engelke function seems to represent the *shape* of these two fragments very well. Even though noisy, these observed spectra are flat overall, or we would not be justified in using this simplistic substitution. (The same situation arises for β Gem.)

The essential parameters for the Engelke function, namely effective temperature and angular diameter, are initially fixed by reference to the work of Blackwell *et al.* (1991). $T_{\rm eff}$ is never altered; only the angular diameter is (slightly) rescaled when the Engelke function is spliced to our observed spectra. We do, however, assign a conservative uncertainty of a few percent to any usage of this approximation, driven largely by the uncertainties in both $T_{\rm eff}$ and angular diameter estimated by Blackwell *et al.* (1991), but also taking note of the change in infrared slope of the Engelke function engendered by the uncertainty in stellar temperature. We note that Blackwell & Lynas-Gray (1994) have recently recalibrated their narrow band near-infrared photometry of bright stars to which they apply the "Infrared Flux Method." They have redetermined both $T_{\rm eff}$ and angular diameter for many stars, including β Gem, where their new determination (8.03 milliarcsec [mas])

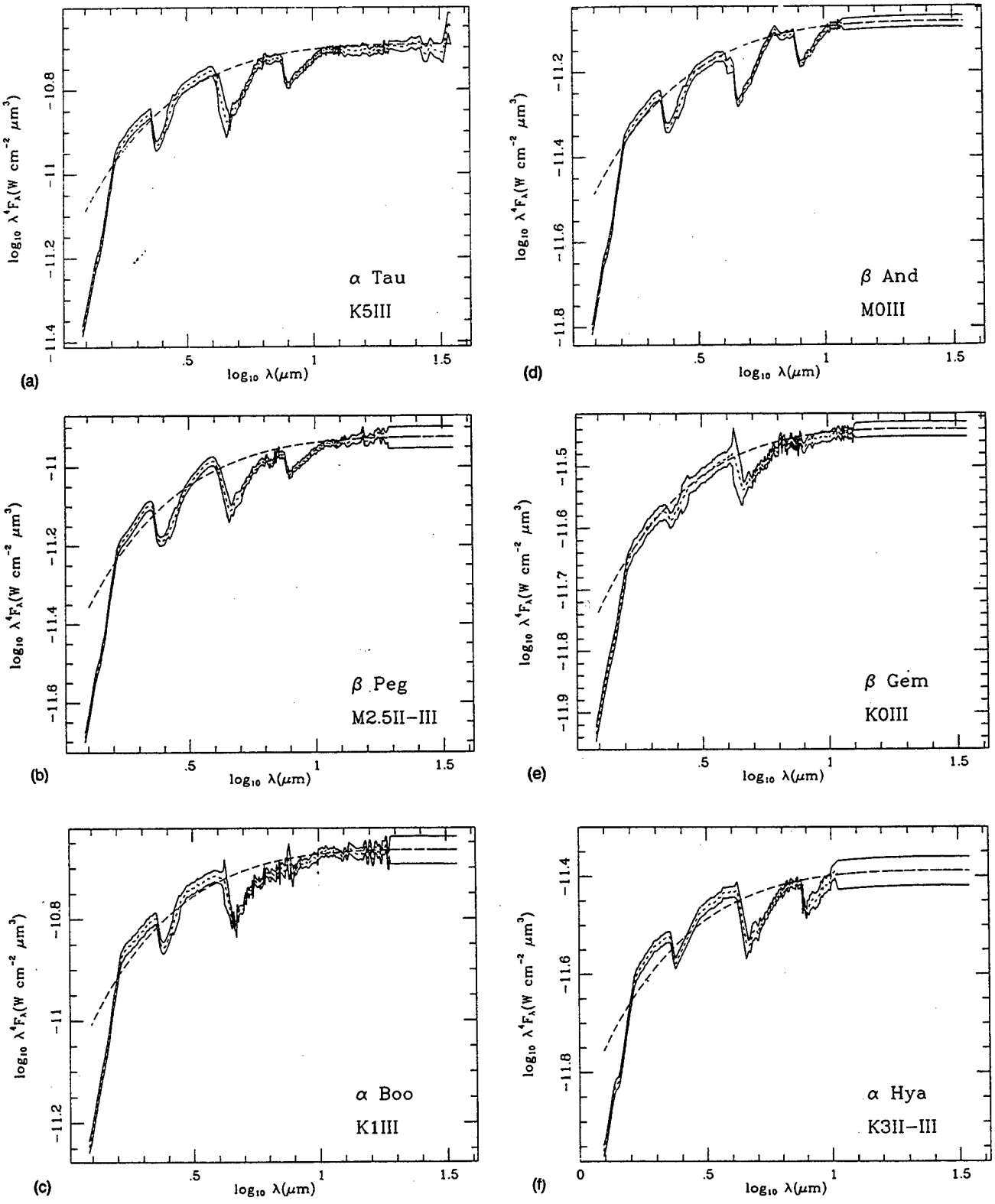

FIG. 4. All six cool stellar composites in the form of logarithmic plots of absolute $\lambda^4 F_\lambda$ against λ. In each spectrum, the $\pm 1\sigma$ error bars are indicated by the pair of solid lines, with the mean spectrum represented by the short-dashed line. The long-dashed line is the best-fitting Engelke approximation. (a) α Tau; (b) β Peg; (c) α Boo; (d) β And; (e) β Gem; and (f) α Hya.

agrees very well with our own, via normalization of an Engelke function (8.07 mas).

These functions play a useful role in all five new stellar composites, to varying degrees, depending essentially on the quality of the longest-wavelength LRS data. Table 2 summarizes details of these substitutions in our composites (or, for the completely observed α Tau, the value of the best-fitting Engelke function for the overall spectrum, even though one is not used in the actual spectrum assembly). Of those molecules that one would incorporate into a full model atmosphere calculation, only CO_2 might be relevant and has any strong absorption bands between about 12 μm (by which

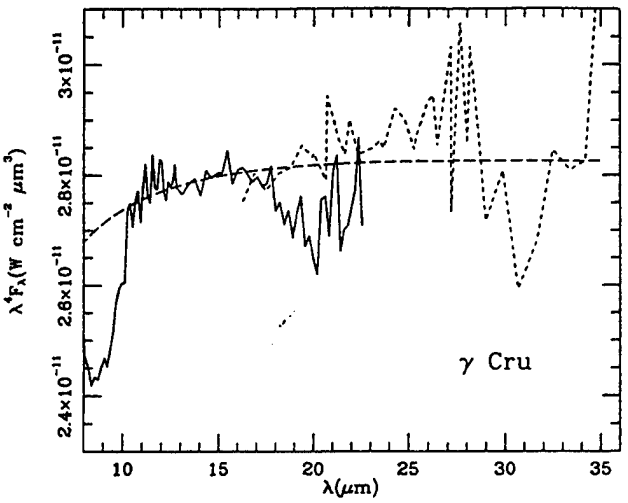

FIG. 5. The two independently calibrated long-wavelength fragments of the mid-M giant, γ Cru. The shorter spectrum is from the *IRAS* LRS; the longer from Glaccum's (1990) work. In spite of the noise (note that a $\lambda^4 F_\lambda$ plot acts as an amplifier of any inherent noise), one definitely sees indications in these axes of a sustained "flat" spectrum out to 35 μm, as for α Tau; i.e., a Rayleigh–Jeans character.

wavelength the SiO fundamental has essentially disappeared at our relatively low resolution) and 35 μm. However, its expected abundance in these cool giants is orders of magnitude below those of CO and SiO. It is, therefore, very plausible that a pure continuum extrapolation of these composites is justified at long wavelengths. While the Engelke function matches the continuum regions of our warmest star (β Gem) very well and those of our coolest (β Peg) most poorly (Fig. 4), we see no overall systematics with respect to effective temperature. These functions seem to fit all these cool giants equally though they are at best only approximations at the 3σ level, sometimes above and at other times below the observed continua. There is a tendency for the function that best fits the long wavelengths to fall significantly below the

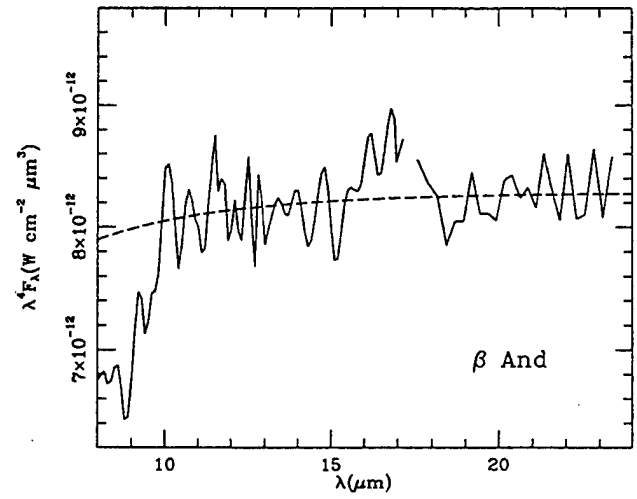

FIG. 6. The two observed, but noisy, long-wavelength fragments of β And and the Engelke function used as their substitute. The portion from 8 to about 17 μm is the LRS which was truncated due to high noise beyond 17 μm; that longward of about 17.5 μm represents the useful part of a UKIRT CGS3 spectrum in the 16–24 μm range.

TABLE 2. Engelke functions used in, or relevant to, composite spectra.

Star	Effective Temperature (K)	Angular diameter milliarcsec
α Tau	3898	21.32
β Peg	3600	16.98
α Boo	4362	20.80
β And	3839	13.71
β Gem	4866	8.07
α Hya	4141	9.27

near-infrared continua, perhaps reflecting the fact that the approximation is strictly valid only in the context of solar-type stars. In these cooler objects, one might well expect H^- free–free opacity to lose its dominating influence to molecular opacity.

3. NEW SPECTRAL FRAGMENTS

All the new spectral fragments incorporated into this paper were secured with one or more of the following instruments: the NASA–Ames "SIRAS" (Short-Wavelength Infrared Array Spectrometer; Wooden 1989), "FOGS" (Faint Object Grating Spectrometer; Witteborn & Bregman 1984), or "HIFOGS" (High-efficiency Infrared Faint Object Grating Spectrometer; Witteborn *et al.* 1995) on the KAO or with the NASA 1.5 m Mount Lemmon telescope; or the CGS3 spectrometer on the 3.8 m UKIRT. The Ames spectrometers are doubly sampled by using two different grating settings spaced a few detectors apart to achieve Nyquist sampling and to provide coverage of occasional dead detectors. CGS3 is either doubly or triply sampled, likewise to achieve the full theoretical resolution. For the CGS3 fragments (cf. Cohen & Davies 1995) we have always stressed close matching of airmasses between the target (cool) star and the hot reference object (Sirius or Vega). From the KAO we cannot always exert such control over stellar airmasses at the time of observation due to the relative brevity and constraints of the actual observing time at altitude. Therefore, we remove the residual effects of the terrestrial atmosphere (particularly important from 5–8 μm) *post facto* from the spectra, through use of precomputed standard atmospheric transmission curves relevant to different amounts of precipitable water vapor (currently between 6 and 12 μm). Actual water vapor is measured on each flight with a radiometer. These transmissions are calculated using Lord's (1992) ATRAN tool.

One of the goals of our overall effort has been to provide a composite spectrum for every cool giant spectral type. Therefore, we have for some time been trying to secure observations of a K3 III. SEW provide coverage in the 1.2–5.5 μm range for only γ^1 And, of type K3-IIb, but we have never been able to acquire adequate 5–9 μm data of this star. However, α Hya (K3 II–III) was frequently observed during KAO expeditions to New Zealand to monitor SN 1987A, and Sirius was usually observed on the same flights. Consequently, we have elected to construct a composite for α Hya whose NIR fragment is actually that of γ^1 And, very closely matched in type. In defense of this procedure we note that the bias associated with the normalization of γ^1 And's NIR

spectrum to the actual photometry of α Hya is only 0.50% (Table 8), implying that these five photometric points for α Hya accurately match the shape defined by this miniature template.

4. PHOTOMETRY USED

Supporting photometry for these spectral assemblies comes, as in Paper II, almost entirely from Deacon's (1991) tabulations for the UKIRT M, 8.7 and 11.7 μm passbands, and from Selby *et al.* (1988) for the extremely valuable narrow band Kn and Ln measurements. All photometry that we use to construct a composite appears in the individual informational header (see Tables 4–8). A final check is later performed on each composite to see how well it fits *all* available characterized filter photometry, as opposed to just the five measurements already employed. Typically this involves 12–20 measurements between 1.6 and 25 μm. The normalization factors for each composite lie within $\pm$0.004 of unity, thereby validating the overall construct and ruling out conspicuous infrared photometric variability in any of these stars within the period covered by the available characterized photometry. After construction we also integrate the composite over all available combinations of filter and detector and atmosphere that we have archived, thereby providing a refined set of actual magnitudes (as opposed to those estimated from the literature). Because of their widespread usefulness, we have included a subset of these magnitudes in Table 3. These refer strictly to the passbands characterized in Paper I but will also represent the magnitudes (within 0.01–0.02 mag) at typical lower elevation sites. We can, of course, create "customized" photometry for *any* triad of filter, detector, and atmosphere given the actual system (or separate passband) profile(s) measured cold.

It is important to distinguish between the photometry that is instrumental in creating the complete spectrum, and that used *post facto* to validate the composite spectrum. The former includes two of the narrow bands created by Selby *et al.* (1988), namely Kn and Ln, and three UKIRT bolometer points for M, [8.7], and [11.7]. Due to the anchoring role played by these filters, we discuss the out-of-band rejection of these passbands, and give some history of the actual magnitudes used for most of our stars.

It is the fundamental tenet of our calibration philosophy that photometry produces the most accurate radiometric levels while one tasks a spectrometer with providing accurate spectral shapes. This belief stems from the all too frequent usage with IR spectrometers of small apertures that cannot capture all the light (cf. Cohen & Davies 1995), and from the strong likelihood that different seeing conditions will prevail while target and reference stars are being separately observed. In Paper II we, therefore, developed a procedure of using independently obtained and calibrated photometry to normalize IR spectral shapes to their correct radiometric levels. *This tenet and our broad-wavelength, multifragment method distinguish our approach from all other efforts in this field.*

Our procedure is first to lock the SEW (1.2–5.5 μm) KAO fragment to Selby *et al.*'s (1988) narrow band photometry in the Kn and Ln bands, and to UKIRT M photometry. These two Selby filters were very carefully selected to sample the cleanest parts of the terrestrial atmospheric transmission curve in the general vicinities of the conventional broadband K and L′ passbands. They are only 0.05 and 0.14 μm in FWHM, respectively, and we have vindicated the contention that these are robust bandpasses by calculating the isophotal wavelengths and transmission-weighted monochromatic flux densities for these when used at Mauna Kea and at a lower elevation site (Tables 1 and 2 of Paper I). There are no differences with site (using annual average transmission curves for each site's observing season) in either isophotal wavelength (Paper I) or F_λ. The choice of the filters was originally motivated by equally rigorous work on the absolute IR calibration of Vega (Mountain *et al.* 1985; Leggett *et al.* 1986; Blackwell *et al.* 1991).

Both Kn and Ln are defined by tandem filters, one narrow band, and the other conventional (the latter are the UKIRT standard K and L′ bands), each component separately specified to have out-of-band rejections of 10^{-4} or better from the UV to at least 10 μm (Leggett 1994; Mountain 1994; Petford 1994) The separate transmission curves of the filter elements of these tandem combinations were measured in the laboratory at 78 K by Selby (documentation is most complete for the laboratory sessions of July 1, 1981, July 12, and September 13, 1982), using a specially designed monochromator and an absolutely calibrated furnace (typically run at 1254 K). He determined there were no out-of-band leaks greater than 10^{-4} of the peak transmission in any of the standard UKIRT filter set (JHKLL′M), which includes the two (K,L′) used as broadband blocking filters for Kn and Ln. The narrow band tandem combinations were regularly measured in their usual cryostat before and after observing sessions at Tenerife by Selby (Petford 1994), with the same equipment and yielded similar results. Best documented are actual mea-

TABLE 3. (a) Refined near-infrared magnitudes derived *post facto* from our model and composite spectra. Passbands are as declared in Paper I. (b) Refined mid-infrared magnitudes derived *post facto* from our model and composite spectra. Passbands are as declared in Paper I.

(a)

Star	Jn	Kn	Ln	J	H	K	L	L′	M
α Lyr	0.00	0.00	0.00	0.00	0.00	0.00	0.00	0.00	0.00
α CMa	-1.39	-1.37	-1.36	-1.39	-1.40	-1.37	-1.36	-1.36	-1.36
β Gem	-0.55	-1.14	-1.23	-0.40	-1.04	-1.12	-1.20	-1.22	-1.09
α Boo	-2.27	-3.07	-3.17	-2.14	-2.96	-3.04	-3.15	-3.15	-2.93
α Hya	-0.44	-1.26	-1.38	-0.30	-1.11	-1.22	-1.35	-1.36	-1.12
α Tau	-1.97	-2.93	-3.06	-1.84	-2.74	-2.90	-3.04	-3.05	-2.77
β And	-0.89	-1.93	-2.05	-0.78	-1.73	-1.89	-2.02	-2.02	-1.78
β Peg	-1.18	-2.33	-2.49	-1.09	-2.09	-2.29	-2.45	-2.47	-2.20

(b)

Star	8.7	N	11.7	Q	IRAS12	IRAS25
α Lyr	0.00	0.00	0.00	0.00	0.00	–
α CMa	-1.35	-1.35	-1.35	-1.34	-1.35	-1.34
β Gem	-1.21	-1.22	-1.22	-1.23	-1.22	-1.22
α Boo	-3.12	-3.14	-3.16	-3.16	-3.15	-3.16
α Hya	-1.25	-1.31	-1.35	-1.35	-1.35	-1.35
α Tau	-2.95	-3.02	-3.07	-3.08	-3.08	-3.10
β And	-1.96	-2.05	-2.11	-2.12	-2.11	-2.12
β Peg	-2.37	-2.44	-2.49	-2.51	-2.48	-2.51

surements made on November 17, 1980 with the furnace and monochromator. Blocking of Kn and Ln were found to be superior to 10^{-5} and likely to be no poorer than 10^{-6}. Such values are also cited by both Leggett (1994) and Mountain (1994), whose Ph.D. dissertations depended on these passbands. For example, Leggett's thesis stipulates "The narrow band filters were blocked by wider filters to reduce any filter leakage. We searched for leakage on site using the furnace with combinations of warm and cold filters. The leakage of *unblocked* filters was estimated to be $\leq$0.01%." Hence, blocked filter leakage was much superior to this figure of 0.01%.

Realizing just how difficult and important were their attempts to calibrate Vega absolutely, Blackwell, Selby, Mountain, and Leggett in their various efforts and publications were at pains to detail all possible sources of uncertainty, down to the component level. The DC linearity of the InSb system overall was of great concern (cf. Mountain *et al.* 1985) and forms the substance of a separate and detailed document (McGregor 1977). In particular, the Ohmic properties of the Victoreen feedback resistors (the dominant source of potential concern) were established to be linear to better than 0.5%. The detectors were (and still are) run in low voltage and low-current circumstances. High voltages would occasion far more concern in terms of possible nonlinearities and the figure of <0.5% was obtained even when measuring signals far higher than those due to stars on the relevant telescope. The amplifier chains have been, and are still, regularly measured and found to harbor no nonlinearities above the 0.01% level and their gains are well calibrated (Hammersley 1994). Questions of potential saturation, and hence nonlinearities, may also arise in the context of a comparison between stars as bright as α Tau with Vega. The InSb system in question has a very large dynamic range. This multichannel narrow band system is still in frequent use in The Canaries on both 1.5 m and 4.5 m telescopes. No saturation effects have been detected in use on stars with the flux densities of α Tau even on the 4.5 m (William Herschel) telescope. Stars as faint as K=18 or fainter are routinely measured so the dynamic range in the linear regime of detector/system behavior is established to be far larger than the span between infrared-bright stars like α Tau and Vega. The use of the doubly blocked narrow band filters on the 1.5 m telescope employed by Blackwell and colleagues, *a fortiori* excludes any possibility of detector saturation. In addition, as detailed by Mountain *et al.* (1985), the original calibration work involved direct comparison of Vega with an absolute furnace on the telescope. The issues of dynamic range and saturation were, therefore, central to the measurements made by these authors, hence their painstaking efforts to assure that no source of potential error was overlooked.

In our spectral assembly scheme (Paper II) we next lock the CGS3 fragment (typically from 7.4–13.4 μm) to [8.7] and [11.7] photometry obtained from the UKIRT using their standard bolometer (UKT8) with characterized cold filter transmission curves. Rejection was measured in July 1982 by Beattie at the Royal Observatory Edinburgh at the request of Barlow and Cohen. A series of documented experiments was also carried out at Mauna Kea using UKIRT on July 27, 1982 and combining these internal cold filters with external warm ones in the 10 μm region. Memoranda indicate "zero" signals were detected through these combinations, with implied rejections of at least 3×10^{-5}, or better, out of band. Issues of linearity were again covered in McGregor's (1977) report.

The actual magnitudes of the five stars in the Kn, Ln, M, 8.7, and 11.7 μm filters (in a context in which Vega is 0.000 at all wavelengths) that we used to assemble their composite spectra are summarized in Tables 4–8 (and Paper II). The sources for photometry and assigned uncertainties are Selby *et al.* (1988) and Deacon (1991). The 8.7 and 11.7 μm pair of filters is critical to calibrating our 10 μm spectral fragments for any star. Therefore, we append here the typical details of this narrow band 10 μm photometry for one star in order to characterize the dataset that constitutes Deacon's table of photometry for "standard stars." Because we use α Tau to illustrate spectrum assembly we will also use its photometry to exemplify the pedigree of Deacon's tabulated magnitudes.

There are several distinct elements to this photometry, one of which is based on measurements with germanium bolometers actually made by Cohen and Barlow over a 13 yr period (August 1976–August 1989) from several telescopes: the 3.8 m UKIRT, the 1.5 m at Cerro Tololo, the 1.3 m at Kitt Peak, and the Minnesota–San Diego Mount Lemmon Observatory 1.5 m. Cohen and Barlow were able to construct a set of midinfrared magnitudes from these hundreds of standard star measurements akin to those by Thomas *et al.* (1973), Gehrz *et al.* (1974), Cohen & Barlow (1974, 1980). Of these measurements, the magnitudes relevant to our spectral calibration effort are solely those for M, [8.7], and [11.7]. For M. Deacon (1991) took the published spectrophotometry of SEW for bright standard stars and integrated these spectra through the combination of the cold system (UKIRT) passband and the Mauna Kea atmosphere. These provided M data for stars such as α Tau and β Peg relative to Vega (adopted to be zero magnitude at all wavelengths shortward of 20 μm). The reproducibility of the SEW dataset was found to be no worse than 2% in absolute signal and shape (cf. SEW) so these relative magnitudes are felt to be good to about $\pm$0.02, a value defensible by comparison with the Cohen and Barlow broadband archive. Use of an airborne spectral archive to define stellar M brightness with respect to Vega (zero magnitude) leads to a much more reliable determination even for relative magnitudes than typical ground-based observations. The 5 μm "window" is notoriously variable in time from the ground but observations are considerably more reproducible from 12.5 km altitude.

The second element is the set of [8.7] magnitudes. These were most precisely systematized during 1980 and 1981 using the UKT8 bolometer on the UKIRT telescope, although values good to $\pm$0.02–0.03 were already available in the literature. Nights were clear, calm, and mostly quite transparent. During six nights (UT 1980 September 1 and 3, 1981 October 18, 19, 20, and 21) we made 92 measurements of standard stars, referring the cool giants to both Vega and Sirius to establish accurate and traceable zero points for [8.7]. Conditions were quite stable: zero points reproduced to within a few percent and resulted in sensible extinction val-

ues. Extinction in this filter varied during the overall observing runs between 0.05 and 0.60 mag/AM, but the average value for the relevant six nights was better defined, at 0.11 ±0.05 mag/AM. We concentrated on defining relative magnitudes between a cool giant and either Vega or Sirius, with minimal airmass differences between the pairs. A typical cool star had ten measurements relative to either Vega or Sirius, and we used an aperture of diameter 8 arcsec with UKT8. Below we summarize the salient measurements for α Tau in [8.7].

1980, August 31. The observed values of Δ[8.7] between α Tau and α Lyr were −3.03±0.03 with airmasses of 1.02 and 1.06, respectively, while a second set gave −3.00±0.01 with airmasses of 1.03 and 1.10, respectively (extinction at 8.7 μm was measured at 0.05±0.05 mag/AM). With Vega as 0.00 these magnitude differences translate directly into the magnitude of α Tau.

1981, October 17. The observed value of Δ[8.7] between α Tau and α CMa was −1.61±0.01, with airmasses of 1.37 and 1.26, respectively. Extinction was measured at 0.16 ±0.05 mag/AM for the October 17–19, 1981 period so from this we find α Tau has [8.7]=−2.98±0.01, with α CMa as [8.7]=−1.35 (Paper I). A second set of measurements between the same pair of stars on this night yielded Δ[8.7]= −1.68±0.01 with airmasses of 1.05 and 1.64, respectively, when [8.7]=−2.93±0.03.

1981, October 18. The observed value of Δ[8.7] between α Tau and α CMa was −1.63±0.01, with airmasses of 1.18 and 1.25, respectively. From this we find α Tau has [8.7]= −2.97±0.01.

1981, October 19. The observed value of Δ[8.7] between α Tau and α Lyr was −2.97±0.01, with airmasses of 1.14 and 1.02, respectively. From this we find α Tau has [8.7]= −2.99±0.02. On the same night, Δ[8.7] between α Tau and α CMa was −1.59±0.01, with airmasses of 1.02 and 1.25, respectively; whence [8.7]=−2.90±0.02.

By inverse variance weighting we finally obtain α Tau's [8.7] as −2.97±0.01.

We note that recent independent determinations by Hanner (1994) at the IRTF yield [8.7]=−2.97±0.02 for α Tau, in a filter similar to the cold characterized UKIRT 8.7. This, too, is in the context of Vega as zero magnitude.

The third element is [11.7] data. Because a homogeneous exoatmospheric archive like *IRAS* is not subject to the vagaries of transparency or extinction changes which occur even on Mauna Kea, and due to the close proximity of central wavelengths between the *IRAS* 12 and the UKIRT 11.7 μm bands, we believe it to be far more secure to derive the precise value of [11.7] for α Tau directly from [12]. Deacon (1991) has presented an analysis of *IRAS* flux densities obtained for a number of IR-bright "calibrators." He placed heavy reliance on the *IRAS* Pointed Observation archive at Rutherford Laboratory, in particular on measurements with the "DPP" macros taken by Barlow and Willis, augmented by "DPS" macros (cf. Tables 3.1 and 3.2 on Young *et al.* 1985) and later by the body of the Serendipitous Survey Catalog (Kleinmann *et al.* 1986). Although Point Source Catalog (1988, hereafter referred to as PSC) data were also used these *IRAS* Pointed Observations (PO) clearly have higher significance. The issue is not one of signal to noise ratio (SNR): all these bright cool giants have large formal SNR in the PSC but their "RELUNC" values (the relative uncertainties taking into account any systematics and the time since the last internal stimulator flashes) are generally a few percent. By contrast, the PO data have less intrinsic scatter than PSC measurements and contain their own contemporaneous stimulator flashes. Indeed, Aumann *et al.* (1984) have documented the accuracy of PO at 1% in [12], rather better than the precision attainable from the ground even with large telescopes. Consequently, Deacon was able to determine that α Tau has a [12] of −3.05±0.01.

In his dissertation Deacon used standard IR philosophy in extrapolating monochromatic flux densities from 12 to 11.7 μm, namely to posit that α Tau behaves as a Planck function at its effective temperature. With hindsight (e.g., Paper II) we would now argue that a far better representation for α Tau is to assert that, longward of the obvious SiO fundamental absorption in K and M giants, stars are already in the domain where $F_\lambda \propto \lambda^{-4}$. This asymptotic domain is not attained by Planck functions or stellar models for stellar temperatures by 12 μm, but real stars appear to have true Rayleigh–Jeans (RJ) spectra by this wavelength. Because the wavelength difference between 11.7 and 12 μm is so tiny, the difference between a true RJ slope in this wavelength region and an actual model atmospheric spectrum (or even a Planck function) for cool giants is virtually negligible. Hence the difference in deduced [11.7] between the strictly incorrect blackbody assumption and the more accurate RJ method is only 0.004 mag in modulus. This calculation indicates that Deacon's methodology and tabulated magnitudes (for all relevant K and M giants in his Table 2.4) are meaningfully converted from [12] to [11.7], to much better than 0.01 mag.

For photometry to support α Hya we have cast further afield, using high-precision observations made in support of our efforts by Carter (1994) in the South African Astronomical Observatory's *HKL* passbands, and measurements made in the ESO narrow band 10 μm filters (Bouchet *et al.* (1991), to whose published passbands (ESO User's Manual) we have added our calculated representative atmosphere for the La Silla site. To provide a traceable 5 μm magnitude for α Hya, we have used Koornneef's (1983) old ESO "M", with Bessell & Brett's (1988) recommended combination of this filter passband and atmosphere. In addition, we found the broad "N" magnitude by Thomas *et al.* (1973) to be useful. In order to use these photometric systems we required not only that cold filter profiles were available but also that zero points were traceable. This was facilitated by published observations of Sirius in all these passbands.

In this section we have fully described the pedigree of the photometry in Tables 4–8 and in Paper II, on which basis we adjusted the radiometric levels of spectral fragments from relative to absolute irradiances prior to the splicing procedures, and generated local "biases" (see below).

5. OUR ARCHIVE OF COMPOSITES

Tables 4–8 reproduce the header information that accompanies all five new composite spectra (cf. Paper II, Tables 2,

TABLE 4. "Header" information accompanying β Peg composite.

3-10-92 OBSERVED SPECTRUM OF BETA PEGASI

β Peg photometry file: photometry actually used to construct the spectrum

Name	FWHM (μm)	Mag.±Unc.	Eff Wvl (Vega) (μm)	Eff Wvl (star) (μm)	F_λ W cm^{-2} μm^{-1}
Kn	0.0488	-2.33±0.01	2.208	2.205	3.37E-13
Ln	0.1443	-2.49±0.01	3.782	3.763	5.11E-14
M	0.6677	-2.12±0.02	4.758	4.720	1.50E-14
8.7	1.1576	-2.39±0.01	8.753	8.727	1.77E-15
11.7	1.2008	-2.47±0.01	11.650	11.621	6.14E-16

Spectral fragments and portions of these actually used in observed spectrum (''used" may include combination with other data where overlaps occur)

Fragment	Reference	Total range (μm)	Start and stop wavelengths (μm)	Average resolving power
NIR	1	1.22-5.70	1.22-5.14	50
KAO	2	5.23-8.06	5.23-8.06	65,100
8-13	3	7.50-13.07	8.03-13.07	55,55,55
LRS	4	7.70-22.74	13.10-21.00	30
LONG	5	1.25-35.00	19.45-35.00	-

References:

- 1. Strecker, Erickson, and Witteborn 1979, Ap.J. Suppl., 41, 501.
- 2. FOGS data of August 5, 1986 KAO flight [β Peg/α Lyr]; and Nov. 27-28 and 28-29, 1990 KAO flights [β Peg/α Tau].
- 3. CGS3 UKIRT data of July 16, 1990 of M. Barlow (priv. comm. to MC) and Mt Lemmon FOGS data of Oct. 11 and 14, 1989 [β Peg/α Lyr]; Barlow's CGS3 UKIRT data of Oct. 5, 1990 [β Peg/α Tau]; and our previously defined α Tau 8--13 μm data.
- 4. LRS raw data extracted from ''LRSVAX" Groningen archive at NASA-Ames
- 5. Engelke Fn. used for T=3600K (see Blackwell, Lynas-Gray, and Petford 1991, A&A, 245, 567) and ang. diam. of 16.727 mas; we rescaled this to 16.98 mas. This Engelke Function was locked to the photometrically scaled combination of 8-13 and LRS spectra by splicing and used to replace the observations from 19.45 μm. A conservative error of 6.0% in EFn. due to effective temperature uncertainty was input for this fragment.

INFORMATION ON SPLICES AND BIASES INCURRED

Process	Factor determined	±Bias (%)
NIR cf. photometry	1.025	0.90
813 cf. photometry	1.029	0.64
LRS blue/red bias	-	0.16
LRS splice to 813	0.995	0.01
KAO joint splice to NIR and merged 813/LRS	1.007	0.11
Engelke Fn. splice to combined 813/LRS	1.030	0.77

3, and 4 for the same pedigree for the α Tau composite). The date of original assembly appears, along with details of the photometry used to calibrate the composite radiometrically. The FWHM of the relevant passbands and their effective wavelengths for the Vega spectrum and for the star in question are recorded, along with the monochromatic specific intensities. All archival spectral fragments are detailed, with their total spectral ranges, the ranges of their data that were actually utilized, and their average resolving power over that spectral range (expressed as the resolving power, $\lambda/\Delta\lambda$). When several spectra are available, the relevant resolving powers are presented in the order in which the fragments are

TABLE 5. "Header" information accompanying α Boo composite.

4-28-93 OBSERVED SPECTRUM OF ALPHA BOOTIS

α Boo photometry file: photometry actually used to construct the spectrum

Name	FWHM (μm)	Mag.±Unc.	Eff Wvl (Vega) (μm)	Eff Wvl (star) (μm)	F_λ W cm^{-2} μm^{-1}
Kn	0.0488	-3.07±0.01	2.208	2.205	6.66E-13
Ln	0.1443	-3.15±0.01	3.782	3.762	9.39E-14
M	0.6677	-2.97±0.02	4.758	4.736	3.25E-14
8.7	1.1576	-3.12±0.01	8.753	8.730	3.46E-15
11.7	1.2008	-3.19±0.03	11.650	11.621	1.19E-15

Spectral fragments and portions of these actually used in observed spectrum (''used" may include combination with other data where overlaps occur)

Fragment	Reference	Total range (μm)	Start and stop wavelengths (μm)	Average resolving power
NIR	1	1.22-5.70	1.22-4.22	50
KAO	2	3.65-9.39	4.44-8.17	150
8-13	3	7.65-13.17	7.65-10.96	220,55
LRS	4	7.80-22.70	11.10-19.00	30
LONG	5	1.25-35.00	19.10-35.00	–

References:

- 1. Strecker, Erickson, and Witteborn 1979, Ap.J. Suppl., 41, 501.
- 2. FOGS data of May 11, 1992 KAO flight [α Boo/α Lyr].
- 3. FOGS Mt Lemmon data of Feb. 24, 1992 [α Boo/α Lyr] and CGS3 UKIRT data of May 24 and 25, 1991 (Barlow, priv. comm. to MC) [α Boo/β Peg].
- 4. LRS raw data extracted from the new Groningen IRAS database and recalibrated with ''LRSCAL" routine in ''GIPSY" package.
- 5. Engelke Fn. used for T=4362K (see Blackwell, Lynas-Gray, and Petford 1991, A&A, 245, 567) and angular diameter=20.430 mas; we rescaled this to 20.80 mas. This Engelke Function was locked to the photometrically scaled combination of 8-13 and LRS spectra by splicing and used to replace the observations beyond 19.10 μm. A conservative error of 6.0% in EFn. due to effective temperature uncertainty was input for this fragment.

INFORMATION ON SPLICES AND BIASES INCURRED

Process	Factor determined	±Bias (%)
NIR cf. photometry	1.002	0.89
813 cf. photometry	1.056	0.85
LRS blue/red bias	–	0.03
LRS splice to 813	0.933	0.03
KAO joint splice to NIR and merged 813/LRS	0.850	0.32
Engelke Fn. splice to combined 813/LRS	1.037	0.26

described in the "Reference" section accompanying each table. Although the actual spectral resolution is variable with wavelength in a composite spectrum, the degradation of higher resolution spectrum to match the resolutions of lower resolution spectra effectively leads to a low-resolution archive.

These six composites are rather similar at all wavelengths in their overall effective resolving powers, typically around 50. Of course, mere usage of a high-resolution grating does not of itself provide a high resolution product, because seeing conditions and spectrometer aperture all lead to a degradation in the resolution actually achieved. For example,

TABLE 6. "Header" information accompanying β And composite.

10-15-93 OBSERVED SPECTRUM OF BETA ANDROMEDAE
β And photometry file: photometry actually used to construct the spectrum

Name	FWHM (μm)	Mag.±Unc.	Eff Wvl (Vega) (μm)	Eff Wvl (star) (μm)	F_λ W cm^{-2} μm^{-1}
Kn	0.0488	-1.93±0.01	2.208	2.205	2.33E-13
Ln	0.1443	-2.06±0.01	3.782	3.762	3.44E-14
M	0.6677	-1.74±0.02	4.758	4.749	1.04E-14
8.7	1.1576	-1.98±0.01	8.753	8.736	1.21E-15
11.7	1.2008	-2.09±0.01	11.650	11.622	4.28E-16

Spectral fragments and portions of these actually used in observed spectrum ("used" may include combination with other data where overlaps occur)

Fragment	Reference	Total range (μm)	Start and stop wavelengths (μm)	Average resolving power
NIR	1	1.22-5.50	1.22-4.14	50
KAO	2	3.38-10.12	4.26-7.89	50,50,45,70,150
8-13	3	7.59-13.06	7.59-13.06	65,55
LRS	4	7.70-22.60	7.70-16.90	30
LONG	5	15.52-24.09	16.95-23.37	73
VERY-LONG	6	1.25-35.00	12.00-35.00	–

References:

- 1. Strecker, Erickson, and Witteborn 1979, Ap.J. Suppl., 41, 501.
- 2. FOGS data of Nov. 29, 1983, Dec. 1, 1983, and Dec. 12, 1985 KAO flights [β And/α Tau]; Jan. 18, 1991 FOGS and SIRAS data [β And/α CMa]; and HIFOGS KAO flight of July 21, 1993 [β And/α Lyr].
- 3. FOGS Mt Lemmon data of Sept. 17, 1985 [β And/β Peg] and UKIRT CGS3 data of August 29, 1993 [β And/α CMa] and [β And/α Tau].
- 4. LRS raw data extracted from the new Groningen IRAS database and recalibrated with "LRSCAL" routine in "GIPSY" package.
- 5. UKIRT CGS3 20 um ratio of [β And/α Tau] of Oct. 5, 1990.
- 6. Engelke Fn. used for T=3839K (see Blackwell, Lynas-Gray, and Petford 1991, A&A, 245, 567) and angular diameter=13.219 milliarcsec; we rescaled this to 13.71 mas. This Engelke Function was locked to the photometrically scaled combination of 8-13, LRS, and LONG spectra by splicing and used to replace the observations beyond 12.00 μm (bias only ±0.16%). The uncertainty in EFn. due to an effective temperature error of 100K is 2.7% which was input as the error of this fragment because of the additional shape constraints available from the LONG spectral fragment.

INFORMATION ON SPLICES AND BIASES INCURRED

Process	Factor determined	±Bias (%)
NIR cf. photometry	0.983	0.90
813 cf. photometry	0.997	0.66
LRS blue/red bias	–	0.07
LRS splice to 813	0.941	0.14
KAO joint splice to NIR and merged 813/LRS	0.881	0.05
Engelke Fn. splice to combined 813/LRS/CGS3-20μm	1.075	0.16

SEWs circular variable filter wheel was a 1.5% device, capable of a formal resolving power of 70. But its use on the KAO with apertures of 30–40″ surely lowered this power to around 50.

Note that the maximum possible wavelength coverage was used to constrain any splice and to enhance signal-to-noise ratios in regions of overlapping independent data. Subsequently, we select a specific wavelength above which we use one fragment, and below, the other. However, the lower spectral resolution fragment at this juncture may embody

TABLE 7. "Header" information accompanying β Gem composite.

09-12-94 OBSERVED SPECTRUM OF BETA GEMINORUM
β Gem photometry file: photometry actually used to construct the spectrum

Name	FWHM (μm)	Mag.±Unc.	Eff Wvl (Vega) (μm)	Eff Wvl (star) (μm)	F_λ W cm^{-2} μm^{-1}
Kn	0.0488	-1.14±0.02	2.208	2.205	1.13E-13
Ln	0.1443	-1.21±0.02	3.782	3.762	1.57E-14
M	0.6677	-1.13±0.02	4.758	4.733	5.95E-15
8.7	1.1576	-1.21±0.02	8.753	8.725	5.96E-16
11.7	1.2008	-1.22±0.02	11.650	11.623	1.94E-16

Spectral fragments and portions of these actually used in observed spectrum (''used" may include combination with other data where overlaps occur)

Fragment	Reference	Total range (μm)	Start and stop wavelengths (μm)	Average resolving power
NIR	1	1.22-5.66	1.22-4.90	50
KAO	2	4.92-9.39	4.92-7.63	150
8-13	3	7.67-12.83	7.67-10.38	55
LRS	4	7.80-22.60	10.39-12.94	30
LONG	5	16.14-24.61	16.26-24.02	73
VERY-LONG	6	1.25-35.00	12.95-35.00	–

References:

- 1. Strecker, Erickson, and Witteborn 1979, Ap.J. Suppl., 41, 501.
- 2. HIFOGS data of Dec. 21, 1991 KAO flight [β Gem/α CMa].
- 3. CGS3 UKIRT data of Nov. 5, 1993 [β Gem/α Tau] (multiplied by CGS3 UKIRT [α Tau/α CMa] from Nov. 9, 1991). Confirmed by UKIRT CGS3 [β Gem/α CMa] of Nov. 3 and 4, 1993.
- 4. LRS raw data extracted from the new Groningen IRAS database and recalibrated with ''LRSCAL" routine in ''GIPSY" package.
- 5. CGS3 UKIRT 20 μm ratio of [β Gem/α CMa] of Feb. 7, 1994 from the UKIRT archives.
- 6. Engelke Fn. used for T=4866K (see Blackwell, Lynas-Gray, and Petford 1991, A&A, 245, 567) and ang. diam.=7.807 milliarcsec; we rescaled this to 8.07 mas. This Engelke Function was locked to the photometrically scaled combination of 8-13, LRS, and LONG spectra by splicing and used to replace the observations beyond 12.95 μm (bias ±0.14%). The uncertainty in EFn. due to an effective temperature error of 100K is 2.1% which was input as the uncertainty in this extrapolating fragment because of the additional shape constraints available from the LONG spectral fragment.

INFORMATION ON SPLICES AND BIASES INCURRED

Process	Factor determined	±Bias (%)
NIR cf. photometry	1.020	1.26
813 cf. photometry	1.019	1.03
LRS blue/red bias	–	0.09
LRS splice to 813	1.115	0.33
KAO joint splice to NIR and merged 813/LRS	1.025	0.06
Engelke Fn. splice to combined 813/LRS/CGS3-20μm	1.052	0.14

inverse-variance weighted combined data from both spectra in the overlap region, changing the original fragment (as described above in Sec. 2), so these wavelength cutoffs are not rigid. Information also appears on all processes undertaken during assembly, with their results (scale factor and uncertainties or "biases"). Scale factors best match spectral fragments to the observed in-band fluxes from photometry, while biases represent the uncertainties associated with each scale

TABLE 8. "Header" information accompanying α Hya composite.

12-12-94 OBSERVED SPECTRUM OF ALPHA HYDRAE
α Hya photometry file: photometry actually used to construct the spectrum

Name	FWHM (μm)	Mag.±Unc.	Eff Wvl (Vega) (μm)	Eff Wvl (star) (μm)	F_λ W cm^{-2} μm^{-1}	Source
SAAO-H	0.2896	-1.074±0.015	1.655	1.638	3.09E-13	Carter 1994
SAAO-K	0.3902	-1.223±0.016	2.221	2.219	1.19E-13	Carter 1994
SAAO-L	0.5648	-1.341±0.010	3.474	3.459	2.46E-14	Carter 1994
M	0.5418	-1.107±0.042	4.748	4.764	5.87E-15	Koornneef 1983
ESO-M	0.3588	-1.166±0.042	4.733	4.714	6.28E-15	Bouchet et al. 1989
ESO-N1	0.8954	-1.280±0.051	8.373	8.369	7.50E-16	Bouchet et al. 1989
ESO-N2	1.2949	-1.324±0.039	9.849	9.860	3.74E-16	Bouchet et al. 1989
ESO-N3	1.2381	-1.424±0.054	12.567	12.538	1.72E-16	Bouchet et al. 1989
N	5.1318	-1.32 ±0.036	10.161	10.219	3.25E-16	Thomas et al. 1973

Spectral fragments and portions of these actually used in observed spectrum (''used" may include combination with other data where overlaps occur)

Fragment	Reference	Total range (μm)	Start and stop wavelengths (μm)	Average resolving power
NIR	1	1.24-5.46	1.24-5.46	50
KAO	2	5.20-8.00	5.20-8.00	150
8-13	3	7.59-13.31	7.59-13.31	55
LRS	4	7.67-22.74	8.05-22.74	30
LONG	5	1.25-35.00	10.65-35.00	–

References:

- 1. Strecker, Erickson, and Witteborn 1979, Ap.J. Suppl., 41, 501; actually used fragment for γ^1 And, K3-IIb.
- 2. FOGS data of April 17, 1990 KAO flight [α Hya/α CMa] in New Zealand.
- 3. CGS3 UKIRT data of Feb. 9, 1993 [α Hya/α CMa].
- 4. LRSVAX version of Groningen database at NASA-Ames; spliced and recalibrated.
- 5. Engelke Fn. used for T=4141K (see Bell 1993, MNRAS, 264, 345); we found the best fitting ang. diam. to be 9.27 milliarcsec. This Engelke Function was locked to the photometrically scaled combination of 8-13 and the LRS, by ''splicing" and used to replace the observations beyond 10.65 μm with a conservative estimated uncertainty in EFn. of 6%.

INFORMATION ON SPLICES AND BIASES INCURRED

Process	Factor determined	±Bias (%)
NIR cf. photometry	1.473	0.50
813 cf. photometry	0.777	2.61
LRS blue/red bias	–	0.23
LRS splice to 813	0.888	0.40
KAO joint splice to NIR and merged 813/LRS	0.993	0.63
Engelke Fn. splice to combined 813/LRS/CGS3-20μm	0.860	0.37

factor. Biases, therefore, are correlated errors that represent entire ranges of the overall spectrum, rather than the uncorrelated errors that are specific to each individual wavelength point. Two kinds of bias occur: "local" biases arising from scaling of spectral fragments; and "global" that derive directly from the underpinning uncertainty in the absolute calibrations of Vega and Sirius (Paper I).

We prefer to provide pristine data whenever possible, rather than to regrid each composite to some equally spaced or common wavelength scale. Each composite, therefore, has a different set of wavelengths. We tabulate wavelength; monochromatic specific intensity (F_λ in units of W cm^{-2} μm^{-1}); total uncertainty (also in units of W cm^{-2} μm^{-1}) associated with this value of F_λ; local bias;

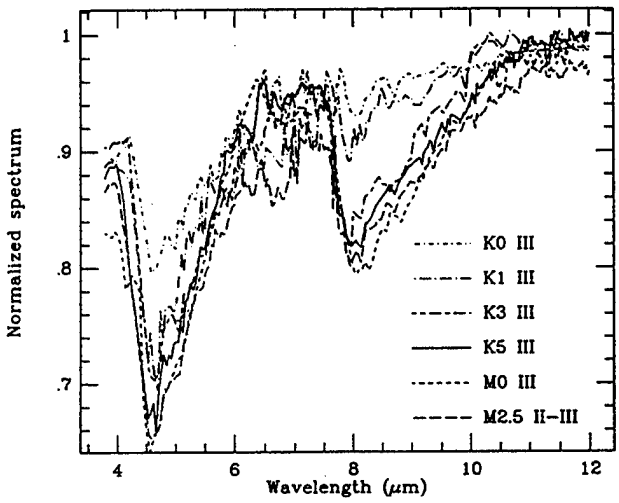

FIG. 7. The six observed composite spectra in the regions of the CO and SiO fundamentals, plotted in $\lambda^4 F_\lambda$ space, each normalized by their mean level between 12 and 35 μm. Each star has a different line type and one can see a progression of deeper bands with cooler stars.

and global bias. For most applications, "total uncertainty" is the error term most appropriate to use. It is the standard deviation of the spectral irradiance and includes the local and global biases. Local and global biases are given as a percent of the irradiance. The global bias does not contribute error to flux ratios or color measurements, and may be removed (in the root-sum-square sense) from the total error.

Figure 7 offers a direct comparison of these six composite spectra in the region containing the dominant spectral structure due to the fundamentals of CO and SiO. To intercompare different stars one would ideally normalize all spectra using a subregion of the wavelength region of interest. One might think that the 6.5–7.5 μm region between CO and SiO would be the natural region in which to normalize. However, the onset of water vapor absorption near 6.5 μm makes this region unsuitable (the absorption is clearest for the coolest star, β Peg, but is also shown by β And). Consequently, we have adjusted them according to their average levels between 12 and 35 μm, where there is no significant observed structure. To mitigate the very steep decay of flux densities in these stellar spectra we have again treated all spectra in $\lambda^4 F_\lambda$ space. There are some slight differences in overall curvature between stars in Fig. 7, solely due to their different temperatures, but one can clearly see that there is an essentially monotonic progression in absorption band depths with lateness of spectral type (although β Peg does not always have the lowest spectrum—perhaps its higher luminosity class invalidates this direct comparison with the other class III giants).

6. CONCLUSIONS

We have assembled absolutely calibrated, complete, continuous stellar spectra for six stars: α Tau, β Peg, α Boo, β And, β Gem, and α Hya. These spectra are tightly constrained by carefully characterized photometry and have an estimated absolute uncertainty of order 3% (1σ) across most of the 1.2–35 μm range. Such spectra establish the pedigree for secondary stellar standards and thereby the flexibility to calibrate arbitrary filter systems and sensors on the ground, from airplanes, or satellites. These composite spectra with their associated pedigree files can be obtained through NASA's ADC at the Goddard Space Flight Center.

We thank Phillips Laboratory for its support of this effort through Dr. S. D. Price under Contract No. F19628-92-C-0900 with JS&E, Inc. (MC, RGW). We are grateful to NASA's Airborne Astronomy program for its continued support and to the staff of the entire KAO program for their sterling efforts throughout the flights dedicated to this calibration study. MC also thanks the NASA–Ames Research Center for partial support under Co-Operative Agreement No. NCC 2-142 with Berkeley. We are grateful to Dr. W. Glaccum for providing access to his uniquely valuable KAO archive of stellar spectra.

APPENDIX

1. Data Available on the AAS CD-ROM Series

The digital (ASCII) version of the six calibrated stellar spectra portrayed in Fig. 4 can be found in the Fifth volume of the AAS CD-ROM series. These are represented as five-column files, with the detailed structure given in Sec. 5, paragraph 4. In addition, we have archived the two calibrated Kurucz model spectra for Vega and Sirius on the CD-ROM. These appear as five-column files with the same structure as the six stellar spectra.

REFERENCES

Aumann, G., *et al.* 1984, ApJ, 278, L23
Bell, R. 1993, MNRAS, 264, 345
Bessell, M. S. & Brett, J. M. 1988, PASP, 100, 1134
Blackwell, D. E., & Lynas-Gray, A. E. 1994, A&A, 282, 899
Blackwell, D. E., Lynas-Gray, A. E., & Petford, A. D. 1991, A&A, 245, 567
Bouchet, P., Moneti, A., Slezak, E., Le Bertre, T., & Manfroid, J. 1991, A&AS, 80, 379
Carbon, D. F. 1994 (private communication)
Carter, B. 1994 (private communication)
Cohen, M., & Barlow, M. J. 1974, ApJ, 193, 401
Cohen, M., & Barlow, M. J. 1980, ApJ, 238, 585
Cohen, M., & Davies, J. K. 1995, MNRAS (in press) (Paper V)
Cohen, M., Walker, R. G., Barlow, M. J., & Deacon, J. R. 1992a, AJ, 104, 1650 (Paper I)
Cohen, M., Witteborn, F. C., Carbon, D. F., Augason, G. C., Wooden, D., Bregman, J., & Goorvitch, D. 1992b, AJ, 104, 2045 (Paper III)
Cohen, M., Walker, R. G., & Witteborn, F. C. 1992, AJ, 104, 2030 (Paper II)
Deacon, J. R. 1991, Ph.D. dissertation, University College London
Engelke, C. W. 1992, AJ, 104, 1248
Gehrz, R. D., Hackwell, J. A., and Jones, T. W. 1974, ApJ, 191, 675
Glaccum, W. 1990, Ph.D. dissertation, University of Chicago
Hammersley, P. L. 1994 (private communication of October 26, 1994)
Hanner, M. S. 1994 (private communication of May 25, 1994)
IRAS Point Source Catalog, version 2, 1988, IRAS Catalogs and Atlases, Volumes 2–6, NASA RP-1190 (GPO, Washington, DC)

Kleinmann, S. G., Cutri, R. M., Young, E. T., Low, F. J., & Gillett, F. C. 1986, Explanatory Supplement to the IRAS Serendipitous Catalog (GPO, Washington, DC)
Koornneff, J. 1983, A&AS, 51, 489
Leggett, S. K. 1994 (private communication of June 18, 1994)
Leggett, S. K., Mountain, C. M. Selby, M. J., Blackwell, D. E., Booth, A. J., Haddock, D. J., & Petford, A. D. 1986, A&A, 159, 217
Lord, S. D. 1992, A New Software Tool for Computing the Earth's Atmospheric Transmission of Near-Infrared and Far-Infrared Radiation, NASA TM-103957
McGregor, A. D. 1977, Imperial College of Science & Technology UK Detector Testing Contract: Final Report, Royal Observatory of Edinburgh
Moseley, S. H., Dwek, E., Glaccum, W., Graham, J. R., Loewenstein, R. F., & Silverberg, R. F. 1989, ApJ, 347, 1119
Mountain, C. M. 1994 (private communication of June 24, 1994)
Mountain, C. M., Leggett, S. K., Selby, M. J., Blackwell, D. E. & Petford, A. D. 1985, A&A, 151, 399
Petford, A. D. 1994 (private communication of June 20, 1994)
Selby M. J., *et al.* 1988, A&AS, 74, 127
Strecker, D. W., Erickson, E. F., & Witteborn, F. C. 1979, ApJS, 41, 501
Thomas, J. A., Hyland, A. R., & Robinson, G. 1973, MNRAS, 165, 201
Witteborn, F. C., & Bregman, J. D. 1984, Proc. Soc. Photo-Opt. Instrum. Eng., 509, 123
Witteborn, F. C., Cohen, M., Bregman, J. D., Heere, K. R., Greene, T. P., & Wooden, D. H. 1995, in Proceedings of the Airborne Astronomy Symposium on the Galactic Ecosystem, edited by M. Haas, E. F. Erickson, and J. Davidson, ASP Conf. Ser. Vol. 73, p. 573
Wooden, D. H. 1989, in Proceedings of the ESO/SIPC Workshop, SN 1987A and Other Supernovae, edited by I. J. Danziger and K. Kjar (ESO, Garching), p. 531
Wooden, D. H., *et al.* 1993, ApJS, 88, 477
Young, E. T., Neugebauer, G., Kopan, E. L., Benson, R. D., Conrow, T. P., Rice, W. L., & Gregorich, D. T. 1985, A User's Guide to IRAS Pointed Observation Products (Ipac, Pasadena)

Mon. Not. R. Astron. Soc. 276, 715-722 (1995)

Spectral irradiance calibration in the infrared – V. The role of UKIRT and the CGS3 spectrometer

Martin Cohen[1,2] and John K. Davies[3]

[1] *Radio Astronomy Laboratory, 601 Cambell Hall, University of California, Berkeley, CA 94720, USA*
[2] *Jamieson Science and Engineering, Inc., 5321 Scotts Valley Drive, Suite 204, Scotts Valley, CA 95066, USA*
[3] *Joint Astronomy Centre, 660 N. A 'ohōkū Place, Hilo, HI 96720, USA*

Accepted 1995 April 12. Received 1995 March 15

ABSTRACT

We describe, illustrate, and quantify the performance achieved by the combination of CGS3 and UKIRT, with emphasis on the role already played by CGS3 in the field of spectrally continuous, absolute, infrared radiance calibration. The focus of the paper is on the reliability and reproducibility of the spectral shapes obtained by CGS3. We offer an electronically available data base of calibration spectra taken with UKIRT and CGS3 of a variety of infrared-bright cool K and M giants. These highlight the influence of the SiO fundamental absorption on the stellar spectra as effective temperature is varied. The calibration archive has an absolute pedigree traceable directly to Cohen et al.

Key words: techniques: spectroscopic – infrared: general.

1 INTRODUCTION

The purpose of this paper is threefold. First, we describe the role currently being fulfilled by UKIRT's CGS3 spectrometer in creating absolutely calibrated continuous infrared spectra. The key importance of CGS3 to this programme (Cohen, Walker & Witteborn 1992b) requires that its credentials be explained. Secondly, we present 7.5–13 μm spectral fragments secured with CGS3 of a wide variety of stellar spectral types in the form of the ratios of cool stellar spectra to hot stellar spectra. Thirdly, we describe an effort to calibrate these spectra absolutely using independent photometry, thereby providing an archive of calibrated CGS3 spectra, electronically available to the astronomical community for use either with CGS3 or other 10-μm instruments.

In Section 2 we briefly describe the physical attributes of the CGS3 instrument. Section 3 illustrates the actual performance achieved on UKIRT, focusing on issues of reproducibility of spectral shape as a function of time, aperture, and spectral resolution. Section 4 presents a series of ratios of stellar spectra between 7.5 and 13 μm, reinforcing the importance of the SiO fundamental absorption and its influence on normal stellar spectral energy distributions in this wavelength region (Cohen et al. 1992c) and its effects on photometry between 8 and 10 μm. Section 5 emphasizes the role of independently calibrated broad- and narrow-band photometry in normalizing spectral shapes.

We will conclude that the combination of CGS3 and UKIRT, with apertures of at least 5.5 arcsec (which is unfortunately not universal on large infrared telescopes working spectroscopically) and the routine use of an autoguider, offers an extraordinarily robust calibration tool for 10-μm spectroscopy at low (and modest) resolution.

2 A DESCRIPTION OF CGS3

CGS3 is a liquid-helium-cooled grating spectrometer which employs a linear array of 32 Si:As photoconductive detectors for spectroscopy in the 10- and 20-μm windows. A spectrum taken by CGS3 at a given grating position is sampled once per resolution element. In order to obtain full (Nyquist) or greater sampling, the number of subspectra must be two or more. Typically, double or triple sampling is used to achieve the expected resolution. Consequently, CGS3 spectra are composed of several interleaved subspectra, each of which is the average of several individual beamswitch observation pairs, each of which may have been divided by an optional sky spectrum. (Note that this implies that not all subspectra are obtained simultaneously so some minutes or even tens of minutes can intervene between acquisition of one subspectrum and the next.)

There is a rotating sector chopper, mounted on the CGS3 optical platform, which provides the instrument with alternating views through the telescope and of the ambient-temperature blackbody emission (i.e. the blades themselves).

This is used for sky-spectra, flat-fielding, and lamp spectra. Optional sky spectra are taken with the instrument set up in the same configuration that will be used to observe the astronomical source. These spectra are formed by modulating the sky's emission spectrum with the chopper, so are strictly only true sky spectra if the sky column is at the same temperature as the chopper blade.

Beamswitching and the taking of sky and source spectra are all done automatically. Sky division, if used, approximately removes the detector array's flat-field response and eliminates the gross effects of variations in sky transmission with wavelength. It is ideally used in addition to the division of the spectrum by a standard star (which has also been divided by the sky). Aperture diameters range from 1.5 to 9 arcsec. Three gratings are available in the spectrometer, and provide coverage and resolutions as listed in Table 1 for measurements made in the nominal 5.5-arcsec aperture (5.5 arcsec FW at 10 per cent, 4.8 arcsec FWHM). The spectral profile of CGS3 is roughly rectangular. Fig. 1 illustrates two orthogonal scans of the spatial profile of the 5.5-arcsec aperture in CGS3 to demonstrate the flat-topped character of the beam profiles.

The longer process of integrating on-source then begins, with the telescope chopping from source to nearby blank sky at the chop frequency, then nodding to remove thermal offsets between the two beams every dwell-time period (typically 10 s). For each beamswitch pair the coadded source spectrum divided by the sky is plotted for the observer to see. This spectrum is known as a 'subspectrum'. In order to produce a final spectrum that is fully sampled in wavelength, it is necessary to interleave several subspectra taken at nearby grating positions, and so the steps above are repeated at least once to produce the final observation.

Wavelength calibration is accomplished by observing high orders of the dominant line of Krypton at 2.1908 μm. For use with a 10-μm grating, the fourth, fifth, and sixth orders of this line at 8.763, 10.954, and 13.145 μm are useful; if the 20-μm grating is selected, a strong line will be seen in ninth order at 19.72 μm, flanked by about four other weaker lines.

3 THE ACTUAL PERFORMANCE OF CGS3 ON THE UKIRT

The critical issue for any spectrometer is whether it delivers the correct shape of a spectrum. Because it can be used with a variety of apertures, and because smaller apertures mean less background and hence greater sensitivity, users are apt to use spectrometers with apertures too small to assure spectrophotometric accuracy, according to accepted views. The danger in spectroscopy is that too small an aperture will preferentially shed light at the longer wavelengths where the Airy disc is significantly larger than at the shorter wavelengths on the CGS3 gratings. This leads to a tilt in the slope of the spectrum obtained. We encourage the use of at least the 5.5-arcsec aperture with CGS3, which is also approximately the beamsize used with the UKIRT bolometer (UKT8) system.

In the scheme recommended in Cohen et al. (1992b), one demands only that a spectrometer yields an accurate shape, albeit for the ratio of two spectra, not necessarily absolutely accurate photometric signals at each wavelength. How closely does CGS3 achieve this primary requirement, as a function of several pertinent variables: (1) stability and reproducibility on short and long time-scales; (2) spectral resolution; and (3) aperture? Secondly, how closely can CGS3 approach precise radiometric accuracy in these spectral ratios?

3.1 Reproducibility

The model of operation is to set the grating to the first required position, acquire all necessary 'subspectra', then move the grating and repeat this procedure for the one or two remaining grating settings. Note that the separate grating settings result in raw data files that are interlaced in wave-

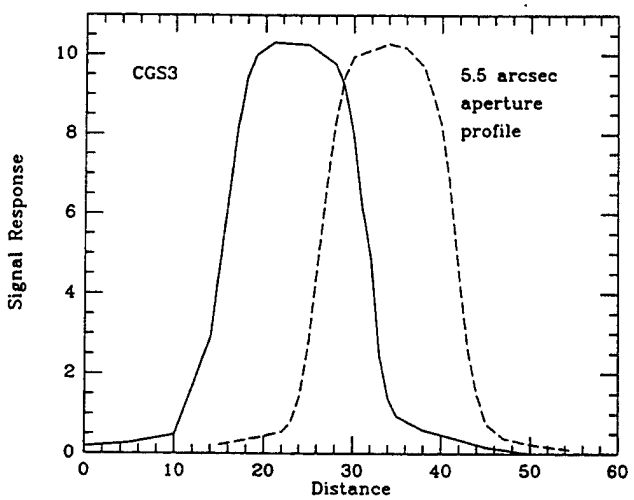

Figure 1. Two orthogonal cuts through the 5.5-arcsec CGS3 aperture to show the beam profiles. 5.5 arcsec represents the FW at 10 per cent intensity of the flat-topped profiles.

Table 1. Gratings and resolutions available with CGS3.

Grating Name ruling	Available Wavelengths μm	Spectral range μm	Optimum Filter μm	Detector spacing μm	Resolution FWHM μm	Sensitivity 1σ 1 sec		
						mag	Jy	W m^{-2}
HIRES_10 105 l mm^{-1}	7–15	1.6	7–22	0.05	0.060	2.3	5.0	0.8×10^{-14}
LORES_10 35 l mm^{-1}	7–15	5.8	7–22	0.19	0.20	3.0	2.5	1.5×10^{-14}
20 25 l mm^{-1}	16–24	8.3	15–24	0.27	0.275	0.4	7.0	1.6×10^{-14}

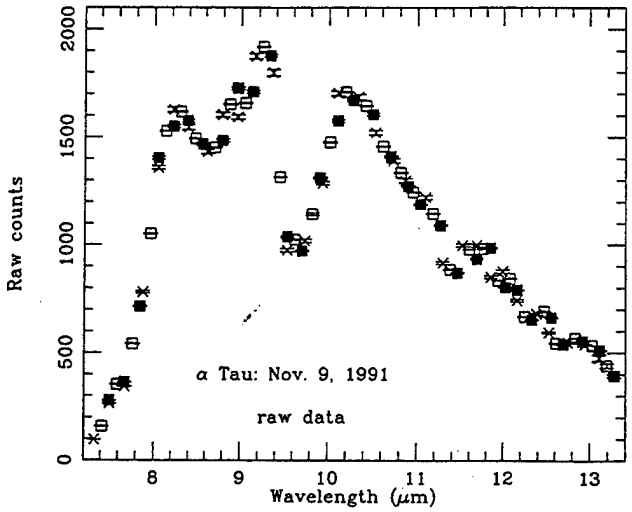

Figure 2. Raw counts from three separate subspectra of α Tau taken consecutively on 1991 November 9. 1σ error bars are plotted but are generally smaller than the symbols used to denote the data points.

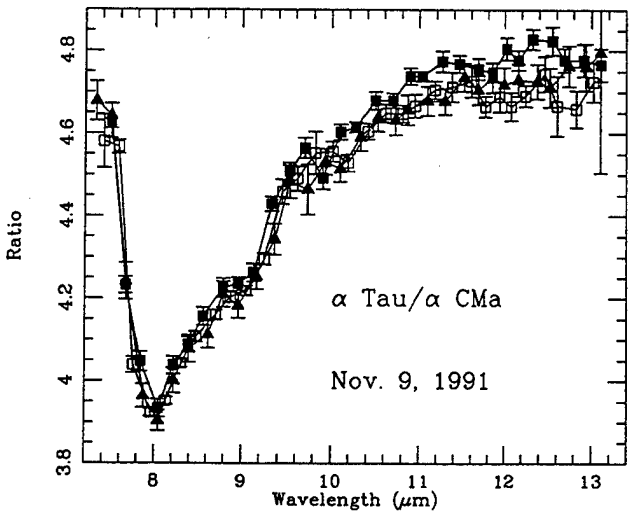

Figure 3. Ratios of raw counts of α Tau and α CMa from three pairs of consecutive subspectra on 1991 November 9 with matched airmasses. Note the very close accord of these unadjusted low-resolution spectral ratios. 1σ error bars are plotted.

length, each covering identical total ranges, with wavelength scales offset by $\frac{1}{3}$ (or $\frac{1}{2}$ in double sampling mode) of a resolution element. If all is stable instrumentally (including the guiding, a most critical item in the overall system), the sky stability and seeing are good, and the aperture is not too small, then these consecutively taken, independent raw spectra should be interlaced perfectly. Fig. 2 illustrates this for three spectra of α Tau (taken 1991 November 9 with a 5.5-arcsec aperture). The same shape is conspicuously well reproduced by all three independent spectra and the total spread between the three raw spectral shapes is ~0.7 per cent.

An even more demanding criterion is to compare the three *ratios* of spectra of two stars, obtained from the three distinct pairs of subspectra. Fig. 3 illustrates this more rigorous test in the case of ratios of α Tau to α CMa, also from 1991 November 9, again in the 10-μm window, at low resolution. Airmasses (AMs) of the two stars were deliberately well matched to have a difference in AM < 0.02. These three interlaced ratio subspectra have not been adjusted in any way, yet all match within 3 per cent, even at the longest wavelengths. This tests stability and fidelity of spectral shape on two short time-scales: that associated with a single grating setting on these bright stars (about 2–5 min); and that within a night, on a scale of a few hours.

Fig. 4 examines reproducibility on a night-to-night time-scale using an aperture with an even smaller diameter. We present this figure for two reasons. First, it is indicative of those places in a 10-μm spectrum where unmatched airmasses can give rise to specious structure; it speaks eloquently of the need to take great care in scheduling observations unless one is willing post facto to remove atmospheric features arising from differential airmass using an appropriate code [e.g. FASTCODE (Rothman et al. 1987); or IRTRANS (Traub & Stier 1976)]. Secondly, outside those regions contaminated by time-varying water vapour (below about 8.2 μm) and ozone (roughly 9.3–9.8 μm), note the match both of shape and level between these spectral ratios of β Gem to α Tau obtained on 1993 November 4 and 1993 November 5

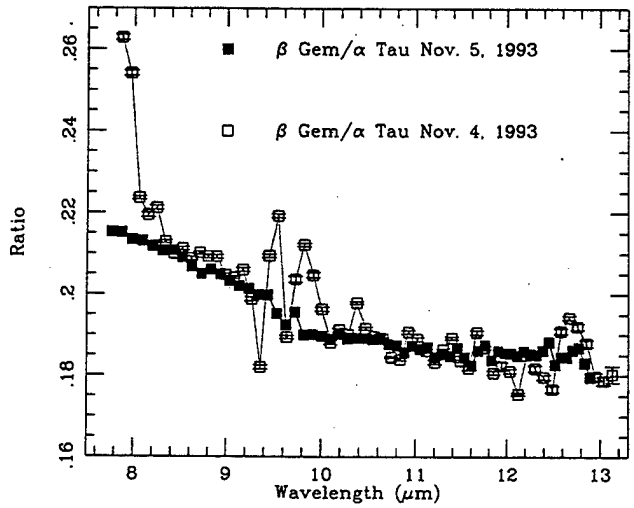

Figure 4. Ratios of raw counts of β Gem and α Tau taken on two consecutive nights in 1993 November. 1σ error bars are plotted. Observations on November 5 were closely matched in airmass; those on November 4 were not. Note the effects at the band edge below 8.2 μm, where telluric water vapour enters, and in the ozone between 9.3 and 9.9 μm.

with only 3.3-arcsec apertures throughout. Shape and level agree to better than about 2.5 per cent except near 13 μm where the difference rises to some 6 per cent. The airmasses were perfectly matched on November 5, but differed by about 0.3 airmass on November 4. We feel that the lack of airmass match on the earlier spectral pair has caused not only spurious spectral 'features' but also any wavelength-dependent differences in spectral shape between the ratio spectra. The enhanced level of noise on November 4 also betrays the difference of airmass. Of course, we note that, while airmass matching is clearly important, atmospheric changes within a night (in transparency, or water vapour) can invalidate even an airmass-matched ratio of stellar spectra.

3.2 Aperture effects

Fig. 5 investigates the effects of defining spectral ratios using different aperture measurements to secure the same ratios of α Tau to α CMa taken at low resolution on 1991 November 9 (triply sampled) and 1993 November 7 (doubly sampled this time). The actual levels of the ratio spectra are well reproduced (within 4.4 per cent). The shapes are in excellent agreement, as shown in Fig. 6, where the 1991 data are compared with those from 1993 rescaled by 0.958 (the best-fitting matching of the levels). Differences in shape are generally <2 per cent, rising to 3.2 per cent at the longest wavelengths. We emphasize that in each of these sets of observations: (1) great care was taken to match airmasses of the two stars closely; and (2) an autoguider was used throughout to supply objective and high-frequency guiding of the stellar images. Apertures used were 5.5 arcsec in 1991 but only 3.3 arcsec in 1993. Shape is clearly very well reproduced but radiometric level has suffered at the roughly 5 per cent level. The 1993 data show a higher level in raw spectral ratio which we attribute to signal from Sirius (in this case the fainter star) being preferentially lost due to effects of seeing, guiding, etc. We stress, however, that we would not be surprised to see this raw ratio show the inverse behaviour, so dependent is it upon differential external conditions (seeing, haze, transmission) for the several independent data sets required. Incidentally, this good agreement also provides an end-to-end test of CGS3 on the long term (years) time-scale, showing that no instrumental effects have varied (e.g., the individual detectors' responsivities as a function of background) to the point where short-term ratios of spectra cannot remove them.

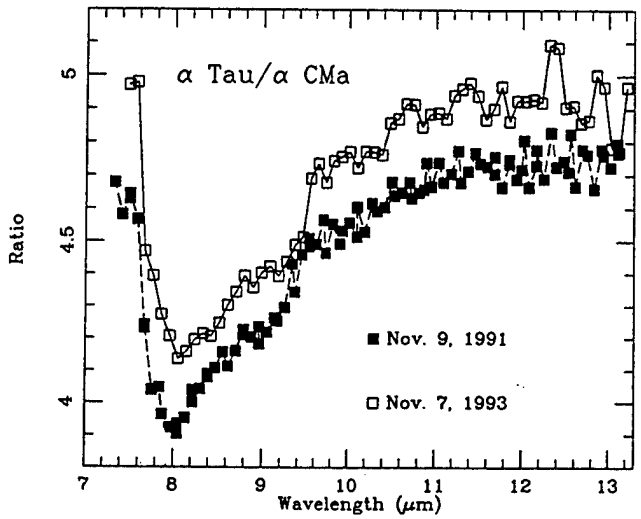

Figure 5. Ratios of low-resolution merged subspectra of α Tau and α CMa taken with different apertures, but each with matched airmasses. The 1991 data are triply sampled with 5.5-arcsec aperture; those of 1993 are doubly sampled with only 3.3-arcsec aperture. Note that the shapes are extremely well reproduced and the actual levels are only about 4 per cent different.

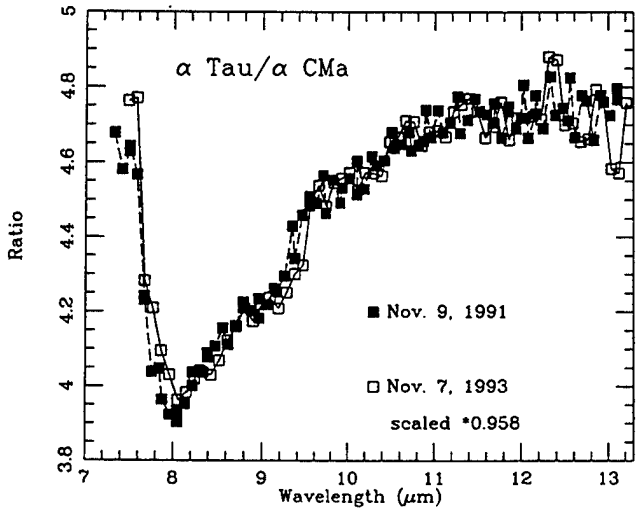

Figure 6. As in Fig. 5, but after merging the 1991 ratio with the 1993 observations, rescaled by the best-fitting factor of 0.958 to the 1991 spectrum. These observations illustrate what can be expected if one uses different apertures in CGS3.

Very recently, a theoretical analysis was carried out to determine the effect of aperture size on the calibration of CGS3, taking into account the influence on the Airy pattern of the central obscuration in the telescope. This report (Rees 1994) concludes that, at 10 μm, the 3.3-arcsec aperture so popular for spectroscopy of faint objects cannot include more than 95 per cent of the total light, whereas the 5.5-arcsec diameter aperture we use with CGS3 on UKIRT attains ~97 per cent. Rees also demonstrates that there is an effect on spectral shape such that systematically more light is lost at shorter wavelengths, leading to a spectral curvature. For these two apertures, the magnitude of this change in spectral shape across the whole range from 7.5 to 13 μm is ~3 per cent. This analysis pertains to ideal conditions, when the qualitative phenomenon is a sharpening of the Airy disc with a simultaneous translation of energy outwards into the diffraction pattern, so the contrast between peak and rings is diminished. Under real seeing conditions, however, there is already softening of the ideal diffraction pattern and one might expect the actual spectral curvature to be less than estimated above. Likewise, any such wavelength-dependent effects are removed or at least greatly reduced by dividing one stellar spectrum by another. Only the differential light loss with wavelength remains, as a consequence of the potentially different seeing conditions under which the two stars were observed. There is, of course, no doubt that smaller apertures are still appreciably less capable of including all the light available in a CGS3 spectrum than are larger apertures.

3.3 Spectral resolution

During these 1991 November observations, both low- and high-resolution spectra of α Tau and α CMa were secured with CGS3. Apertures were 5.5 arcsec throughout the night which was clear, dry and calm. Airmasses were matched closely, though more closely on the low-resolution pair due to the rigours of meeting all the detailed demands of scheduling, so that these observations could serve as an unambiguous demonstration of what can be attained with sufficient care. Fig. 7 presents the raw ratios of spectra, α Tau/α CMa, distinguishing high from low resolution. Note the faithful reproduction of shape (a handful of discrepant points are

identifiable in the ozone region because the higher-resolution data sample the same terrestrial ozone lines more sharply than the low and were not so well matched in airmass as the low). The raw ratio levels differ by only 3.5 per cent, again probably due to differential sky conditions from star to star. When rescaling the high-resolution data by a factor of 1.035, they merge well with the low-resolution data (Fig. 8), allowing for the better signal-to-noise ratios of the low-resolution data.

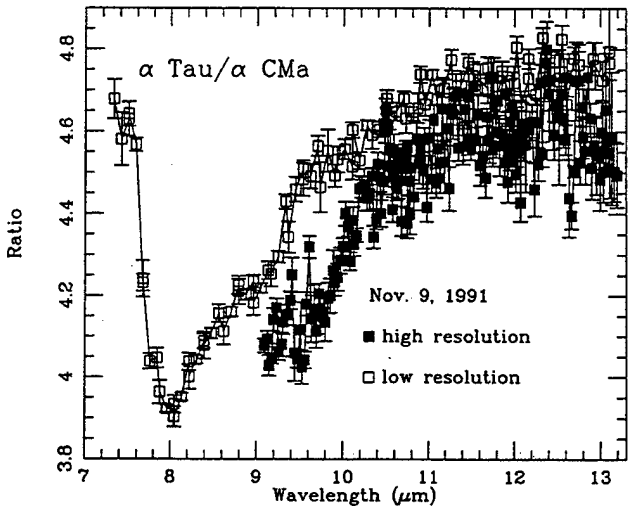

Figure 7. Comparison of low- and high-resolution spectral ratios of α Tau and α CMa on 1991 November 9. The low-resolution data represent triply sampled subspectra; those at high resolution correspond to three separate grating settings, each double sampled, all merged by the same techniques described by Cohen, Walker & Witteborn (1992b). The two sets of unadjusted spectral ratios are only 3.5 per cent apart. 1σ error bars in the ratios are plotted.

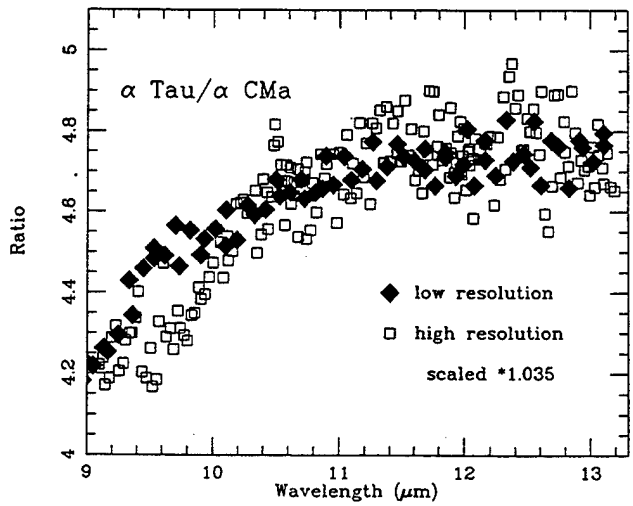

Figure 8. As in Fig. 7 but after merging the low- and high-resolution observations, and after rescaling the latter by the best-fitting factor of 1.035 to the low-resolution spectrum. Note the excellent agreement between the two spectra, except in the ozone region (~9.3–9.8 μm). The high-resolution observations were not matched quite as closely in airmass as the low.

4 SPECTRAL TYPE AND MOLECULAR FEATURES

The stars selected for discussion and for building the archive of calibrated spectra are all 'normal', without dust shells, and not of extreme luminosity or metal abundance. Table 2 summarizes the details of the spectra taken of these selected stars whose ratios with respect to either Vega or Sirius are presented in Fig. 9. These were constructed from the products of the ratios in Table 2 (possibly combined to enhance the signal-to-noise ratio when more than one ratio is available for a given star) with 'basic' ratios such as α Tau/α CMa and α Boo/α Lyr, because one cannot always take a spectrum of either Vega or Sirius on a particular night, and because higher signal-to-noise spectra always result from comparisons with infrared-bright comparison stars like α Tau or α Boo. When there are a few discrepant points at wavelengths that suffer from the greatest sensitivity to time variations in ozone or water vapour, these have been omitted from the individual plots. This can occur in products of spectral ratios even when the separate component ratio spectra already involve close airmass matching. The product of spectra can effectively amplify any slight mismatches in telluric molecular absorptions. These effects are not, however, detrimental in any way to the bulk of the points in a spectrum (see Section 3.1), and are confined to a handful of points either at the shortest, or longest, wavelengths or near the 9.6-μm ozone feature.

We have attempted to show spectra in Fig. 9 that span a significant range of spectral types although there is essentially no low-resolution spectral content of interest until late G-K0 giant types. Note the featureless nature of the hot stellar spectra (e.g. α Aql), and the growth of the P-branch of the SiO fundamental absorption (deepest at our low resolution near 7.9 μm in ratio plots) with lateness of spectral type. In Fig. 10 we have attempted to quantify the dependence of the SiO fundamental depth on spectral type (cf. Cohen et al. 1992c) by plotting the strength of the absorption near 7.9 μm relative to a reference level in the continuum. Ideally we would combine airborne 5–9 μm spectra with the CGS3 data to construct continuous 5–13 μm spectra, from which we could derive an interpolated continuum also at 7.9 μm. In the absence of airborne data for most of the stars in Fig. 9, we have, however, chosen to assess the relevant continuum based on the approximate mean level of the spectral ratios in the 11–13 μm range. Such a choice also obviates any dependence on those points most vulnerable to problems with telluric water, below 8 μm. The resulting deficits near 7.9 μm are attributed to SiO absorption and should coarsely assess the real strengths of this band in our stars. Fig. 10 also includes estimated errors in these strengths. All stars are of luminosity class III except for α Hya and β Peg, which have class 'II–III' and are distinguished by open squares in the figure. The SiO feature grows essentially linearly for the class III giants, reaching a maximum between K5III and M0III, beyond which it remains constant, as if saturation has occurred in these cool atmospheres. We can find no clear evidence for its presence in stars earlier than K0III. A similar trend was found by Rinsland & Wing who observed the first overtone bandheads in a number of late-type stars (Rinsland & Wing 1982). The spectrum of α Aur (G5III + G0III) plays a pivotal role in this pattern because the absence of recogniz-

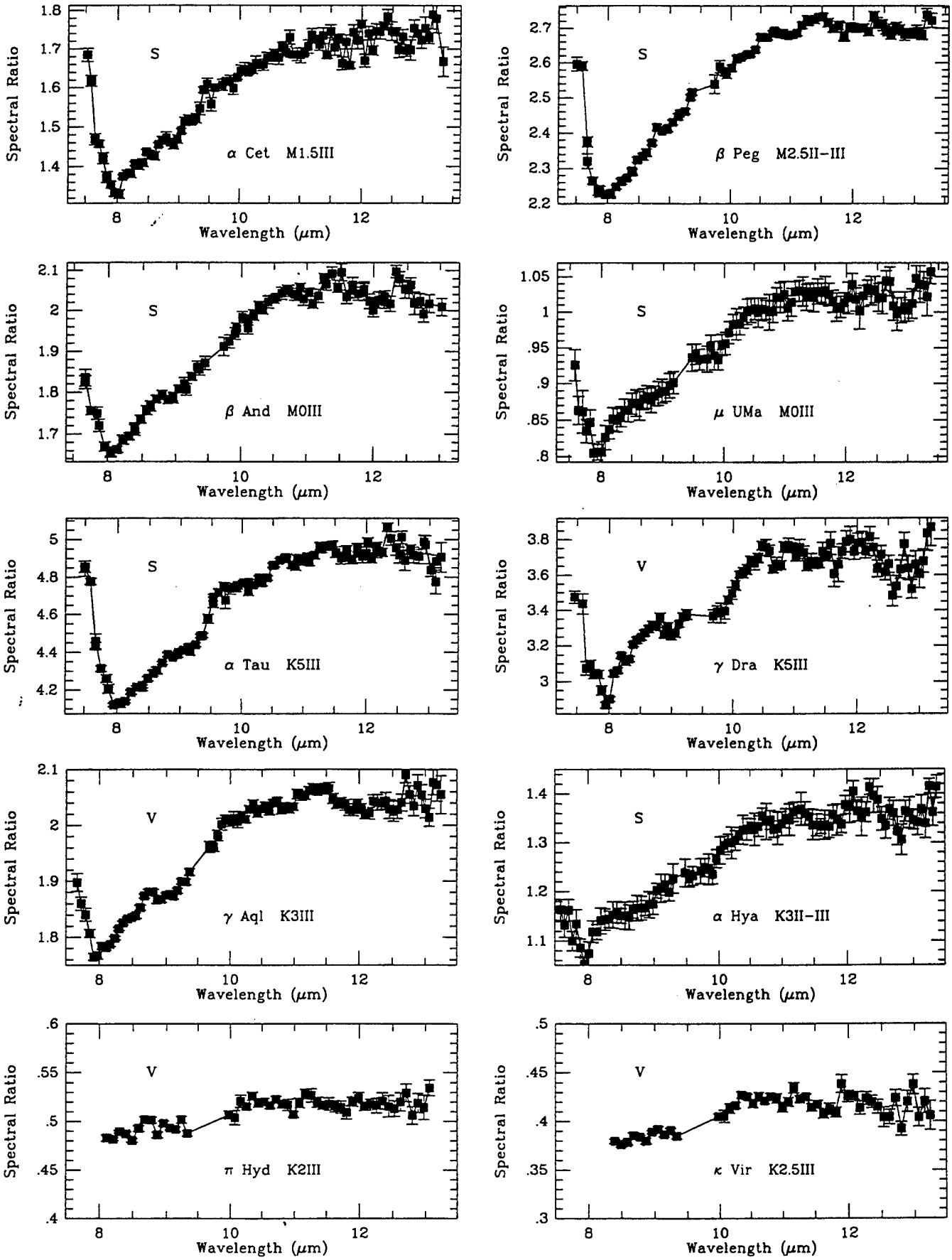

Figure 9. Montage of ratio spectra from CGS3 comparing stars with either Vega or Sirius. Each plot carries labels that indicate the star, spectral type, and reference star (the latter by the single-letter code 'V' for Vega, 'S' for Sirius in the upper-left corner).

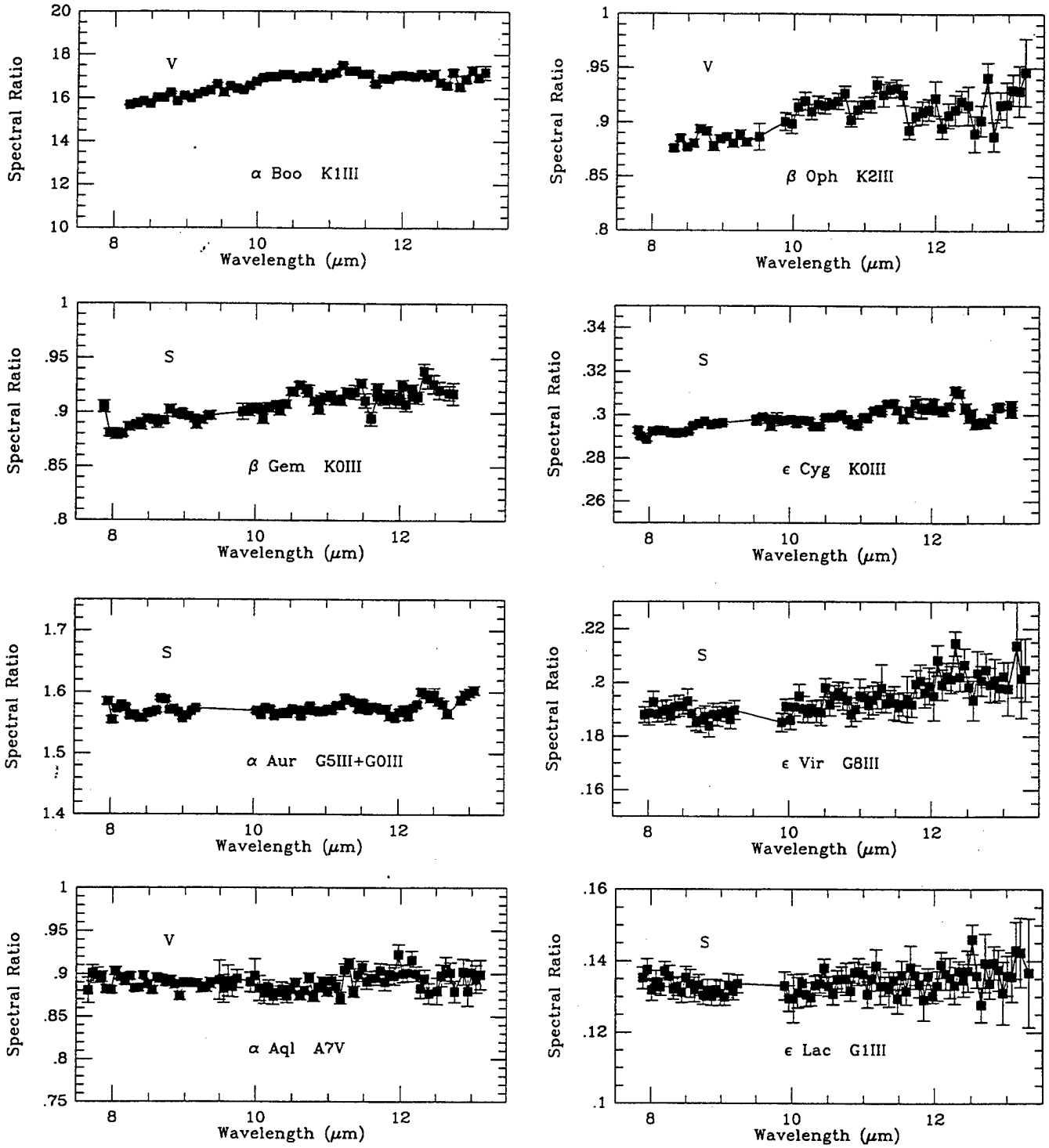

Figure 9 – *continued*

able SiO absorption in this star rules out measurable SiO absorption in typical middle and early G giants.

5 THE ABSOLUTELY CALIBRATED PRODUCTS

It is quite straightforward, given the ratios of stellar spectra to those of Vega and Sirius, to proceed from Fig. 9 to absolutely calibrated stellar spectra. We require only two procedures. First, we multiply the ratio spectra by the absolutely calibrated Vega or Sirius spectra in Cohen et al. (1992a), after smoothing the latter to match the instrumental resolution actually achieved by CGS3. Secondly, we integrate narrowband filters in the 10-μm region, with known cold transmission profiles, over the resulting 'fluxed' spectra, including the effects of the (mean) atmosphere for Mauna

Table 2. Selected stars observed with CGS3 and absolutely calibrated.

STAR	Spectral type	AM	Reference	AM	Date	Sampling
α Aql	A7V	1.03	α Lyr	1.06	May 13, 1994	3
α Aql	A7V	1.16	α Lyr	1.09	Nov. 3, 1993	2
ϵ Leo	G1III	1.00	α CMa	1.26	Feb. 9, 1993	3
α Aur	G5III+G0III	1.17	α CMa	1.44	Oct. 4, 1992	2
α Aur	G5III+G0III	1.17	α Tau	1.09	Aug. 29, 1993	2
ϵ Vir	G8IIIab	1.02	α CMa	1.26	Feb. 9, 1993	3
β Gem	K0III	1.15	α Tau	1.14	Nov. 5, 1993	2
ϵ Cyg	K0III	1.23	α CMa	1.24	Nov. 7, 1993	2
α Boo	K1III	1.51	α Lyr	1.75	May 29, 1991	2
β Oph	K2III	1.75	α Lyr	1.75	May 29, 1991	2
β Oph	K2III	1.51	α Boo	1.51	May 29, 1991	2
π Hyd	K2III	1.54	α Boo	1.51	May 29, 1991	2
κ Vir	K2.5III	1.01	α Boo	1.06	May 29, 1991	2
κ Vir	K2.5III	1.51	α Boo	1.51	May 29, 1991	2
γ Aql	K3III	1.75	α Lyr	1.75	May 29, 1991	2
γ Aql	K3III	1.16	α Boo	1.17	May 29, 1991	2
γ Aql	K3III	1.07	α Lyr	1.06	May 13, 1994	3
α Hya	K3II	1.26	α CMa	1.26	Feb. 9, 1993	3
α Tau	K5III	1.22	α CMa	1.25	Nov. 9, 1991	3
α Tau	K5III	1.20	α CMa	1.24	Nov. 7, 1993	2
γ Dra	K5III	1.17	α Lyr	1.09	Aug. 26, 1994	3
β And	M0III	1.08	α Tau	1.09	Aug. 29, 1993	3
μ UMa	M0III	1.25	α CMa	1.26	Feb. 9, 1993	3
α Cet	M1.5III	1.32	α CMa	1.28	Nov. 3, 1993	3
β Peg	M2.5II-III	1.01	α Tau	1.12	Oct. 5, 1990	2

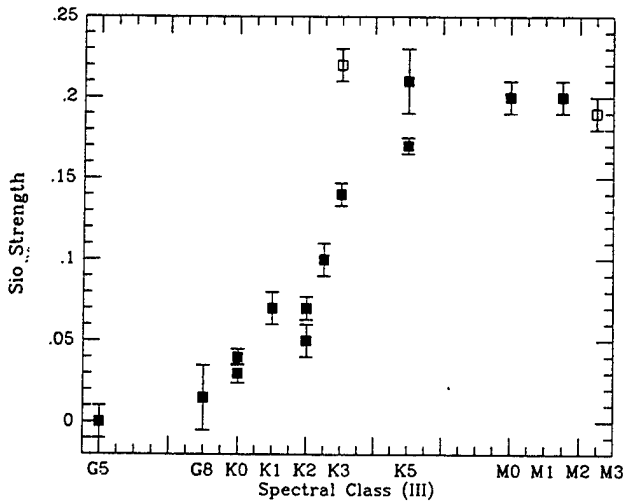

Figure 10. A coarse measure of the strength of the SiO fundamental absorption in middle G to early M giants. Solid squares represent stars of class III; open squares those of class II–III.

Kea (cf. Cohen et al. 1992a). The in-band fluxes of the stellar spectrum are then best matched to the in-band fluxes expected, given the star's magnitudes. We prefer to carry out this procedure using the UKIRT 8.7- and 11.7-μm filters, cold characterized and calibrated by Cohen et al. (1992a), rather than through use of the very broad N passband. The N filter extends to longer wavelengths than those offered by typical CGS3 grating settings; also, the signal-to-noise ratio spectroscopically is rather poor beyond 13.3 μm compared with shorter wavelengths. Further, having two passbands to satisfy provides an estimate of uncertainty beyond that of just the photometry measurement (cf. Cohen et al. 1992b).

As we secure these photometric measurements we will be able to calibrate our CGS3 spectra absolutely and such products can be obtained by e-mail to JKD at the Joint Astronomy Centre, Hawaii. We note that this procedure is precisely that detailed by Cohen et al. (1992b). Therefore, given the central role of the CGS3 10-μm spectral fragments in the entire process of assembling a complete 1.2–35 μm spectrum, the same absolute calibration results whether we treat the CGS3 fragment in isolation (as in the present paper) or abstract it from an already generated complete spectrum. This ensures consistency of the CGS3 calibration archive and the archive of complete spectra (which, of necessity, involves a much smaller set of stars than treated here because of the requirement for continuous 1–5.5 and 5–9 μm spectral fragments). We have considered using *IRAS* flux densities in the 12-μm band but the relevant system response spans a wavelength range greater than that available from the CGS3 spectra. Consequently, in the absence of photometry through characterized narrow passbands, we can provide stellar spectra whose shape is reliable but whose radiometric level is uncertain at the level of at least a few to 10 per cent.

ACKNOWLEDGMENTS

MC thanks US Air Force Phillips Laboratory for partial support of this work through Dr S. D. Price under contract number F19628-92-C-0090 with Jamieson Science and Engineering, Inc. MC also thanks NASA-Ames for partial support under cooperative agreement NGCC 2-142 with UC Berkeley. We thank Dr Tom Geballe for providing many of the excellent CGS3 spectra obtained under the Service programme and contained in the UKIRT archives, for his comments and insight on the manuscript, and Drs A. J. Adamson, M. J. Barlow, M. Hanner and Mr C. Dudley who kindly made observations available to us and encouraged us in this effort.

REFERENCES

Cohen M., Walker R. G., Barlow M. J., Deacon J. R., 1992a, AJ, 104, 1650
Cohen M., Walker R. G., Witteborn F. C., 1992b, AJ, 104, 2030
Cohen M., Witteborn F. C., Carbon D. F., Augason G. C., Wooden D., Bregman J., Goorvitch D., 1992c, AJ, 104, 2045
Rees N., 1994, report to the Science and Engineering Research Council, UKIRT Upgrades Project (1994 November 20)
Rinsland C. P., Wing R. F., 1982, ApJ, 262, 201
Rothman L. S. et al., 1987, Appl. Opt., 26, 4058
Traub W. A., Stier M. T., 1976, Appl. Opt., 15, 364

SPECTRAL IRRADIANCE CALIBRATION IN THE INFRARED. VI. 3–35 μm SPECTRA OF THREE SOUTHERN STANDARD STARS

MARTIN COHEN

Jamieson Science and Engineering, Inc., Suite 204, 5321 Scotts Valley Drive, Scotts Valley, California 95066, and Radio Astronomy Laboratory, 601 Campbell Hall, University of California, Berkeley, California 94720
Electronic mail: cohen@bkyast.berkeley.edu

FRED C. WITTEBORN, JESSE D. BREGMAN, AND DIANE H. WOODEN

Space Science Division, Mailstop 245-6, NASA-Ames Research Center, Moffett Field, California 94035
Electronic mail: (witteborn, bregman, wooden)@ssa1.arc.nasa.gov

ALBERTO SALAMA AND LEO METCALFE

ISO Science Operations Centre, Astrophysics Division of ESA, Villafranca, Spain
Electronic mail: (asalama, lmetcalf)@iso.vilspa.esa.es

Received 1995 December 27; revised 1996 March 27

ABSTRACT

We present three new absolutely calibrated continuous stellar spectra from 3 to 35 μm, constructed as far as possible from actual observed spectral fragments taken from the *Kuiper Airborne Observatory (KAO)*, and the *IRAS* Low Resolution Spectrometer (LRS). These stars—α^1 Cen, α TrA, and ϵ Car—augment our previous archive of complete absolutely calibrated spectra for northern K and M giants. All these spectra have a common calibration pedigree. The wavelength coverage is ideal for calibration of many existing and proposed ground-based, airborne, and satellite sensors. *KAO* and *IRAS* data in the 15–30 μm range suggest that the spectra of cool giants are close to Rayleigh–Jeans slopes. Our observations of α^1 Cen, absolutely calibrated via our adopted Sirius model, indicate an angular diameter in very good agreement with values in the literature, demonstrating "closure" of the set of spectra within our absolute framework. We compare our observed α^1 Cen spectrum with a published grid of theoretical models from Kurucz, and adopt a plausible theoretical shape, that fits our spectrum, as a secondary reference spectrum in the southern sky.

1. INTRODUCTION

In this ongoing series of papers we have described a consistent effort to provide absolutely calibrated broad and narrowband infrared photometry based upon a carefully selected, infrared-customized pair of stellar models for Vega and Sirius, created by Kurucz, and absolutely calibrated by Cohen *et al.* (1992, hereafter referred to as Paper I). These hot stellar models have been employed as reference spectra to calibrate six K and M giants using the methods detailed by Cohen *et al.* (1992, hereafter referred to as Paper II) and Cohen *et al.* (1995, hereafter referred to as Paper IV).

In the present paper we extend these techniques to the southern hemisphere to meet several different objectives. Our primary standard, Sirius, is best observed from the south, and we wished to intercompare this star and the infrared-brighter solar-type star, α^1 Cen (HR 5459=HD 128620; G2 V), for which Kurucz (1995) has kindly provided us with his grid of atmospheric models (published by Furenlid & Meylan 1990). The salient issue is that we wished to find, empirically, a model that fits our low-resolution infrared spectral observations and to use it as an interpolator to smoothe our spectrum of α^1 Cen, and as an extrapolator to somewhat longer wavelengths. Our finally adopted model (Sec. 4) not only provides an adequate match to the CO fundamental region, its overall shape also satisfies the independent photometry between 1.2 and 12.5 μm. To this extent, we have achieved our goal of offering a brighter calibrator in the south than Sirius, for use at low resolution and on small telescopes such as those on satellites. The purpose of this paper is not to determine atmospheric abundances in α^1 Cen, nor to offer the definitive model for this star, but merely to use our observations to select a plausible theoretical shape for its spectral energy distribution.

We wanted to increase the spectral resolution of our calibration standards beyond the lower-resolution products recently released as Paper IV, and to enlarge the set of K-giant spectral types so far studied. The cool stars α TrA (HR 6217=HD 150798: K2 III), and ϵ Car (HR 3307=HD 71129: K3 III) were judged ideal candidates for the *KAO* flights focusing on Sirius, so that they could be compared directly with our primary standard.

A particular goal of these flights was the acquisition of 15–30 μm spectra from the *KAO* through the use of Si:P BIB detectors provided by ESTEC. However, we found that Sirius, our primary reference, provided insufficient signal-to-noise ratios for work at these long wavelengths. We, therefore, made an effort to use the brighter α^1 Cen as a secondary

 0004-6256/96/112(1)/241/11/$6.00

reference star for these difficult observations. We hoped to test the general conclusion reached in Papers II and IV that cool giants appear essentially flat in $\lambda^4 F_\lambda$ space, justifying our use of the Engelke (1992) approximation to smoothe and/or extrapolate our observed spectra as far as 35 μm (see Sec. 5).

2. THE NEW SPECTRAL FRAGMENTS

All the new spectral fragments incorporated in this paper were secured with the NASA-Ames "HIFOGS" (High-efficiency Infrared Faint Object Grating Spectrometer: Witterborn *et al.* 1995) on the *KAO*. We augmented our usual 1×120 set of Si:Bi linear arrays by two Batelle 1×32 Si:P detectors, combining the Si:P arrays into 32 separate readouts of two detectors each. These observations were secured during three flights of the *KAO* while based in Christchurch, New Zealand. The flight dates were 1993 April 7, 9, and 12 UT. Confirming data on the ratios of α^1 Cen and α TrA to α CMa were acquired in 1994 July with HIFOGS from Australia, during *KAO* flights to observe the encounter of Comet Shoemaker–Levy with Jupiter. While these later flights do support the spectral shapes and flux density levels for these two program stars obtained from New Zealand, the observing time per star was significantly less in Australia. These 1994 data thus confirm our 1993 work but without contributing much statistical significance to a combination with the 1993 spectra.

Our methodology for creating a complete and continuous composite spectrum from 1.2 to 35 μm is described in detail in Papers II and IV. However, the paucity of infrared photometric and spectral measurements of these southern objects dictated a modified approach to the assembly of complete spectra. It is unfortunately the case that the vital northern archive constructed from the Lear jet and *KAO* by Strecker *et al.* (1979) using CVF spectrometers has no counterpart in the south, nor has the work been extended to any other stars even in the north. Consequently, we secured a grating and appropriate order-sorting filter to provide our own contemporaneous 2.9–5.5 μm spectral fragments.

No preexisting, ground-based 10 μm spectral observations could be located so we employed a grating to provide *KAO* 9–13 μm spectroscopy. We realized that on the *KAO* these were likely to have quite poor signal-to-noise but felt that they offered an independent appraisal of the LRS spectra and might assist in splicing 5–9 μm fragments to the LRS spectra. LRS data already existed for all three stars. To extend the wavelength coverage toward 30 μm, and supplement noisy LRS data, we used four overlapping grating settings for the 15–30 μm region. These provided coverage from 15.0 to 18.5 μm on the Si:Bi array (two settings), and 19.5–27.2 μm on the Si:P arrays (two settings).

The method used to build the new composites varied according to the existence or absence of characterized mid-infrared photometry. Given narrowband photometry in the 10 μm region, we proceeded exactly as in Papers II and IV. In the absence of such photometry we resorted to an "end-to-end" method by splicing the 5–9 μm piece onto the photometrically constrained 2.9–5.5 μm fragment, then further splicing the 9–13 μm and LRS pieces onto these. This latter scheme clearly provides less control over the radiometric aspect of a composite. Everything now turns on the near-infrared photometry (which might be in a single passband) and the fidelity of the shapes of the succeeding fragments in their regions of overlap. But this was judged to be the sole approach available to us in the absence of 10 μm photometry.

TABLE 1. Engelke functions used in our composite spectra.

Star	Effective temperature (K)	Angular diameter (mas)
α^1 Cen	5770	8.58
α TrA	4140	9.55
ϵ Car	4064	12.67

As in Paper IV, we chose to substitute the best-fitting Engelke function for noisy 10–20 μm data. The essential parameters for the Engelke approximations, namely, effective temperature and angular diameter, were initially fixed by reference to the literature. Specifically, we took the following parameters: for α^1 Cen, 5770 K and a radius from Lydon *et al.* (1993), and a distance from Demarque *et al.* (1986), implying an angular diameter of 8.66 milliarcsec (mas); for α TrA, 4140 K and 12.4 mas (Harper 1992); for ϵ Car, 4064 K (Pasquini & Brocato 1992), and we guessed 12.5 mas. As in previous work, $T_{\rm eff}$ is never altered; and the angular diameter is redetermined when the Engelke function is spliced to our observed spectra. We do, however, assign an additional uncertainty to any usage of this approximation, driven by the uncertainties in both $T_{\rm eff}$ and angular diameter (cf. Blackwell *et al.* 1991), but also taking note of the change in infrared slope of the Engelke function engendered by a typical uncertainty of ±100 K in stellar effective temperature.

Table 1 summarizes our adopted values of $T_{\rm eff}$ and our determination of angular diameters via Engelke approximations fitted to our observed spectra. For α^1 Cen, our estimate is very close to expectation yet that for α TrA is highly discrepant with Harper's (1992) value. However, Harper is vague on the method used to determine α TrA's diameter. This star entirely lacks any published near-infrared photometry so his reference to use of the "infrared flux method" (hereafter referred to as IRFM) is odd, to say the least. From the language of the relevant paragraph of Harper (1992) we deduce that he used V with Johnson colors to estimate near-infrared photometry, for a spectral type of K4 III. The literature on this star prefers a type of K2 and we estimate that the application of Johnson K4 colors rather than those for type K2 could have led to overestimates of the "observed" near-infrared flux densities by about 60%, thereby raising the monochromatic derivations of angular diameter (following Blackwell *et al.* 1991) by about 26%. Correcting Harper's diameter for this overestimate yields about 9.8 mas, close to our value. Whether this is the correct reconstruction of Harper's line of reasoning or not, it is clear that any method that applies the IRFM to a star without observed infrared magnitudes must be regarded as highly unreliable. There is also support for a much lower value than Harper's in the work of Kovacs (1983), where a value of 15 mas is cited for this star

solely based on Wesselink *et al.*'s (1972) $(V,B-V)$ approach. The equivalent parallax deduced by these authors is 0.043 arcsec, yet the average of the three values now available in the literature [0.024, 0.027 (from SIMBAD), and 0.031 arcsec from the *Yale Bright Star Catalog* (Hoffleit 1982)] is 0.027 arcsec. Following Kovacs' (1983) approach, such a parallax would then be equivalent to a diameter of 9.4 mas, very close to our deduced value.

3. SUPPORTING PHOTOMETRY AND THE NEW COMPOSITES

The absence of high-quality near-infrared photometry through characterized passbands was addressed through *JHKL* measurements made for this study by Carter (1994) at the *South African Astronomical Observatory* (hereafter referred to as *SAAO*). For α^1 Cen, we also used the *ESO L* and *M* magnitudes of Engels *et al.* (1981), and two measurements made in the 10 μm region with the *ESO* narrowband filters "*N*1" and "*N*2" (Bouchet *et al.* 1989). We have multiplied these published passbands (*ESO User's Manual*) by our calculated representative atmosphere for the La Silla site. Zero points were traced for all the *ESO* passbands through published observations of Sirius by these same authors. All photometry used to construct the three composites appears in the individual informational headers in Tables 2–4, after correction for zero points. These data provided the scale factors that best match spectral fragments to the observed in-band fluxes from photometry, and the local "biases" of those fragments, i.e., the uncertainties associated with each scale factor. Biases, therefore, are correlated errors that refer to entire ranges of the overall spectrum, rather than the uncorrelated errors that are specific to each individual wavelength point. Two kinds of bias occur: "local" biases arising from scaling of spectral fragments; and "global" that derive directly from the underpinning uncertainty in the absolute calibrations of Vega and Sirius (Paper I).

The standard technique of Papers II and IV was applied to the composite of α^1 Cen. For α TrA and ϵ Car, where we have no ground-based photometry beyond 4 μm, we pinned our 3–5.5 μm *KAO* fragment to Carter's *L* point and employed the end-to-end approach described above. Tables 2–4 reproduce the calibration pedigrees that accompany the three new composite spectra, including all pertinent information on the processes undertaken during assembly of these composites, with their results (scale factors and biases). The date of original assembly appears, along with details of the photometry used to calibrate the composite radiometrically. The FWHM of the relevant passbands and their effective wavelengths for our Vega spectrum and for the star in question are recorded, along with the monochromatic specific intensities. All archival spectral fragments are detailed, with their total spectral ranges, the ranges of their data that were actually utilized, and their average resolving power over that spectral range (expressed as the ratio of $\lambda/\Delta\lambda$).

All the *KAO* spectral fragments were processed so as to remove residual terrestrial atmospheric features by computing atmospheric transmission spectra [through use of Lord's (1992) "ATRAN" tool] pertinent to the actual airmass and column of precipitable water vapor in the line of sight at the time of each stellar observation. In the wavelength region of principal interest, where our spectra were used to construct the composites, these corrections for residual telluric absorptions did not exceed about 3% (we exclude the CO_2 region near 4.3 μm, opaque even at *KAO* altitudes). At the longest wavelengths where water vapor dominates, the maximum typical correction was about 5% (near 28 μm), excluding the CO_2 near 15 μm, also opaque from the *KAO*.

We prefer to provide pristine data whenever possible, rather than to regrid each composite to some equally spaced or common wavelength scale. In the AAS CD-ROM series that will carry the tables from the present paper, each stellar composite spectrum, therefore, has a different set of wavelengths. We tabulate: wavelength (in μm); monochromatic specific intensity (F_λ in units of W cm^{-2} μm^{-1}); total uncertainty (also in units of W cm^{-2} μm^{-1}) associated with this value of F_λ; local bias (in %); and global bias (in %). For most applications, "total uncertainty" is the error term most appropriate to use. It is the standard deviation of the spectral irradiance and includes the local and global biases. Local and global biases are given as a percentage of the irradiance. The global bias does not contribute error to flux ratios or color measurements, and may be removed (in the root-sum-square sense) from the total error.

Some remarks are in order with respect to α Cen, because of its composite character. The star consists dominantly of a G2 V, with a K1 V companion separated by about 18″, and differing in *V* mag by 1.34^m. On the *KAO* we used a 20″ diameter aperture which avoided the K dwarf star. For identical reasons, the *SAAO* photometry was taken with a 17″ aperture (half the usual diameter for Carter's work). But the *IRAS* flux densities at 12 and 25 μm will clearly refer to both G and K dwarf components, as will the LRS spectrum. It is, therefore, important to assess the degree of contamination of the LRS spectrum by the K star and to determine whether the K star and G star may have differently shaped energy distributions. For this purpose we have reviewed the photometry for the two separate components of α Cen secured by Thomas *et al.* (1973) at wavelengths from *J* to 11.2 μm. Below *J*, one expects strong temperature-related differences in the stellar energy distributions but, between 1.6 and 11.2 μm, the average difference in brightness between the G and K stars is 0.91^m, and it appears independent of wavelength, within the estimated uncertainties. In particular, the same difference in magnitude is observed at 8.4 as at 11.2 μm. Therefore, we deduce: (i) that the G2 V and K1 V components contribute 70% and 30% of the light, respectively, at all wavelengths between 1.6 and 11.2 μm, and (ii) that neither star has the SiO band in absorption, or there is no difference in SiO fundamentals between the two stars. Consequently, the LRS spectrum has the correct shape for the G2 V component even though the flux density level is wrong (based on simulations with Kurucz model atmospheres for the two dwarf components). Therefore, we were able to construct the 3–35 μm spectrum of α^1 Cen by our normal techniques, using spectra calibrated through ratios to Sirius in the several spectral regions, extended by an appropriate Engelke approximation [Fig. 1(a)], but not using the new long wave (>15 μm) *KAO* measurements (Sec. 5).

TABLE 2. "Header" information accompanying α^1 Cen composite.

5-9-95 OBSERVED SPECTRUM OF ALPHA^1 CENTAURI

α^1 Cen photometry file: photometry actually used to construct the spectrum

Name	FWHM (μm)	Mag.±Unc.	Eff Wvl (Vega) (μm)	Eff Wvl (star) (μm)	F_λ (W cm^{-2} μm^{-1})	Source
SAAO-L	0.5648	−1.559±0.015	3.475	3.450	3.00E-14	Carter 1994
ESO-L	0.6509	−1.552±0.021	3.768	3.768	2.18E-14	Engels *et al.* 1981
ESO-M	0.5418	−1.437±0.028	4.748	4.759	7.95E-15	Engels *et al.* 1981
ESO-N1	0.8954	−1.557±0.023	8.394	8.394	9.68E-16	Bouchet *et al.* 1989
ESO-N2	1.2949	−1.553±0.026	9.886	9.853	5.06E-16	Bouchet *et al.* 1989

Spectral fragments and portions of these actually used in observed spectrum ("used" may include combination with other data where overlaps occur)

Fragment	Reference	Total range (μm)	Start and stop wavelengths (μm)	Average resolving power
KAO-NIR	1	3.04–5.53	3.04–5.53	160
KAO-5–9	2	5.07–9.28	5.07–9.28	190
KAO-8–13	3	8.80–13.07	...	250
LRS	4	7.67–22.74	7.67–11.55	30
KAO-Si:Bi	5	15.00–18.51	...	80
KAO-Si:P	6	19.48–27.20	...	180
LONG	7	1.25–35.00	12.20–35.00	

References:
(1),(5),(6) HIFOGS data of 1993 April 10 & 12 *KAO* flights [α^1 Cen/α CMa].
(2),(3) HIFOGS data of 1993 April 7 *KAO* flight [α^1 Cen/α CMa]. Spectral ratios in both these wavelength ranges are additionally confirmed by HIFOGS data of 1994 July 22 *KAO* flight from Australia.
(4) LRS raw data extracted from "LRSVAX" Groningen archive at NASA-Ames.
(7) Engelke Fn. used for T=5770 K and ang. diam. of 8.66 mas [see Lydon *et al.* (1993) and Demarque *et al.* (1986)]; we rescaled this to 8.59 mas. This Engelke function was locked to the photometrically scaled LRS spectrum by splicing and used to replace the observations from 12.20 μm. An error of 2.0% in EFn. due to effective temperature uncertainty was input for this fragment.

INFORMATION ON SPLICES AND BIASES INCURRED

Process	Factor determined	±Bias (%)
NIR cf. photometry	0.796	1.31
LRS blue/red bias	...	0.09
LRS cf. photometry	0.778	2.07
5–9 joint splice to NIR and LRS	...	
	0.995	0.16
Engelke Fn. splice to LRS	0.989	0.38

We proceeded to assemble composites for α TrA and ϵ Car based on calibration of their spectra ratioed to that of Sirius. However, once we had selected a model atmosphere for α^1 Cen (see Sec. 4), we were able to recalibrate the observed spectral fragments for these two K giants using ratios to α^1 Cen instead, which yielded higher signal-to-noise data. The overall shapes of the composites based entirely on Sirius agree well with the less noisy ones built through α^1 Cen. In this paper we present solely the latter spectral composites for α TrA and ϵ Car. Figure 1 presents all three stellar composites in the form of absolute $\log(\lambda^4 F_\lambda)$ plots against $\log(\lambda)$. In each spectrum, the $\pm 1\sigma$ error range is indicated, as is the relevant scaled Engelke approximation used for smoothing and extrapolation purposes. Overplotted in each figure are the photometric points used to assemble the relevant spectrum (filled squares), together with the *IRAS* Faint Source Survey (Moshir *et al.* 1992) points (unused in the process of spectral assembly: filled triangles), and the long-wavelength points we derived from our *KAO* spectra (see Sec. 5: open squares). Each photometry point is plotted at its isophotal wavelength for the particular star, with horizontal bars that represent the extent of its FWHM (not necessarily symmetric with respect to the isophotal wavelength), and vertical bars that indicate the uncertainty in the photometry.

Figure 1(a) shows an apparent discrepancy between the *M*-band point of Engels *et al.* (1981) and our *KAO* spectroscopy of α^1 Cen. However, Table 2 indicates that the 1σ uncertainty of this 4.7 μm point is the largest of the errors for the five photometric points that we used to build the composite spectrum. The difference between the integrated in-band flux when this passband is run over our spectrum and the ground-based 4.7 μm in-band flux is significant only at the 2σ level. Further, photometry in the 5 μm window is notoriously difficult from relatively low-altitude sites on the ground such as La Silla. It has also been somewhat problem-

TABLE 3. "Header" information accompanying α TrA composite.

12-5-95 OBSERVED SPECTRUM OF ALPHA TRIANGULI AUSTRALIS

α TrA photometry file: photometry actually used to construct the spectrum

Name	FWHM (μm)	Mag.±Unc.	Eff Wvl (Vega) (μm)	Eff Wvl (star) (μm)	F_λ (W cm^{-2} μm^{-1})	Source
SAAO-L	0.5648	−1.338±0.008	3.475	3.463	2.45E-14	Carter 1994

Spectral fragments and portions of these actually used in observed spectrum ("used" may include combination with other data where overlaps occur)

Fragment	Reference	Total range (μm)	Start and stop wavelengths (μm)	Average resolving power
KAO-NIR	1	2.90–5.51	2.90–5.51	160
KAO-5–9	2	4.94–9.36	4.94–9.36	190
KAO-8–13	3	8.80–13.08	···	250
LRS	4	7.67–22.74	7.67–12.59	30
KAO-Si:Bi	5	15.00–18.51	···	80
KAO-Si:P	6	21.90–27.08	···	180
LONG	7	1.25–35.00	11.00–35.00	

References:

(1),(5),(6) HIFOGS data of 1993 April 10 & 12 *KAO* flights [α TrA/α^1 Cen] and [α TrA/α CMa].

(2),(3) HIFOGS data of 1993 April 7 *KAO* flight [α TrA/α^1 Cen] and [α TrA/α CMa]. The 5–9 μm spectral ratio is additionally confirmed by HIFOGS data of 1994 July 22 *KAO* flight from Australia.

(4) LRS raw data extracted from "LRSVAX" Groningen archive at NASA-Ames.

(7) Engelke Fn. used for T=4140 K and ang. diam. of 12.40 mas (Harper 1992); we rescaled this to 9.55 mas. This Engelke function was locked to the photometrically scaled LRS spectrum by splicing and used to replace the observations from 11.00 μm. An error of 2.6% in EFn. due to effective temperature uncertainty was input for this fragment.

INFORMATION ON SPLICES AND BIASES INCURRED

Process	Factor determined	±Bias (%)
KAO-NIR cf. photometry	1.004	0.74
KAO-5–9 splice to NIR	1.050	0.14
LRS blue/red bias	···	0.06
LRS splice to *KAO*	1.009	0.40
Engelke Fn. splice to LRS	0.593	0.78

atic to trace the exact cold filter profiles for the *ESO* photometers due to their rapid evolution during the late 1970s and early 1980s (van Dijsseldonk 1994). We, therefore, see no reason for concern at this separation in the figure.

4. THE SPECTRUM OF α^1 CEN AND THE KURUCZ MODEL

Although it had been our original intention to compare all stars directly with Sirius, the signal-to-noise actually obtained on Sirius longward of the 10 μm region was rather poor for this purpose. Consequently, we decided to compare program stars also with α^1 Cen, which is significantly brighter.

We wanted to test the internal consistency of our spectra of Sirius and α^1 Cen, in order to establish the latter as a viable southern reference star. Examination of the generic grid of model atmospheres by Kurucz (1991) indicated that models for 5770 K and log g of 4.30 with varying metallicities differ almost negligibly in the shape of their infrared continua; the only obvious distinction is in the strengths of the CO bands, primarily the fundamental. It was clear from the Kurucz grid that generic models of α^1 Cen with normal solar abundances would fit our data better than those with nonsolar abundances.

To assess the probable value of the Kurucz model for α^1 Cen in the infrared, one should directly test the Kurucz model of the Sun against the highest-resolution solar infrared observations. The great similarity of physical characteristics of the Sun and α^1 Cen suggests the relevance of such a test, particularly if it addresses the 5 μm region, where ground-based spectroscopy is scarce. Farmer & Norton (1989) observed the Sun from the Space Shuttle, using the "ATMOS" Fourier Transform Spectrometer. They have provided us with their archival spectra of the solar intensity integrated through a circular diaphragm centered on the disk and extending out to μ=0.951. We have abstracted portions of their data in the 5 μm region where a plethora of CO lines dominates the solar spectrum. In this wavelength region, the resolving power is 136 000. Kurucz (1996) has very kindly computed his spectrum of the Sun using the SYNTHE spectrum synthesis program and line data from the CD-ROM 18 (Kurucz 1993a). The model is the theoretical solar model from the CD-ROM 13 (Kurucz 1993b). The spectrum was computed for a range of angles on the disk and rotationally

TABLE 4. "Header" information accompanying ϵ Car composite.

12-5-95 OBSERVED SPECTRUM OF EPSILON CARINAE

ϵ Car photometry file: photometry actually used to construct the spectrum

Name	FWHM (μm)	Mag.±Unc.	Eff Wvl (Vega) (μm)	Eff Wvl (star) (μm)	F_λ (W cm^{-2} μm^{-1})	Source
SAAO-L	0.5648	−1.914±0.016	3.475	3.464	4.16E-14	Carter 1994

Spectral fragments and portions of these actually used in observed spectrum ("used" may include combination with other data where overlaps occur)

Fragment	Reference	Total range (μm)	Start and stop wavelengths (μm)	Average resolving power
KAO-NIR	1	2.90–5.50	2.90–5.50	160
KAO-5–9	2	4.94–9.30	4.94–9.30	190
KAO-8–13	3	8.80–13.22	···	250
LRS	4	7.67–22.74	7.67–17.98	30
KAO-Si:Bi	5	15.87–18.53	···	80
KAO-Si:P	6	21.90–27.20	···	180
LONG	7	1.25–35.00	11.00–35.00	

References:

(1),(5),(6) HIFOGS data of 1993 April 10 & 12 *KAO* flights ϵ Car/[α^1 Cen] and [ϵ Car/α CMa].

(2),(3) HIFOGS data of 1993 April 7 *KAO* flight [ϵ Car/α^1 Cen] and [ϵ Car/α CMa]. The 5–9 μm spectral ratio is additionally confirmed by HIFOGS data of 1994 July 22 *KAO* flight from Australia.

(4) LRS raw data extracted from "LRSVAX" Groningen archive at NASA-Ames.

(7) Engelke Fn. used for T=4064 K (Pasquini & Brocato 1992), and we guessed an ang. diam. of 12.50 mas; we rescaled this to 12.67 mas. This Engelke function was locked to the photometrically scaled LRS spectrum by splicing and used to replace the observations from 11.00 μm. An error of 2.6% in EFn. due to effective temperature uncertainty was input for this fragment.

INFORMATION ON SPLICES AND BIASES INCURRED

Process	Factor determined	±Bias (%)
KAO-NIR cf. photometry	1.051	1.49
KAO-5–9 splice to NIR	1.082	0.57
LRS blue/red bias	···	0.07
LRS splice to *KAO*	0.989	0.73
Engelke Fn. splice to LRS	0.956	0.58

broadened for the area covered by the diaphragm. It was broadened with 1.75 km s^{-1} macroturbulent velocity and a $\sin x/x$ instrumental function. We emphasize that the computation has *not* been fitted to the observed spectrum: it is simply as calculated.

Figure 2 illustrates a representative small section from the ATMOS archive, with the Kurucz calculation superimposed. The comparison is persuasive of the capability of this model to represent the real Sun, as observed by ATMOS. Bell (1994) has criticized gf values from at least one version of Kurucz's line list for not yielding a good match to the observed solar spectrum. However, this test was performed with synthetic spectra in the optical, where the fidelity of gf values of atomic lines is of paramount importance. For our low-resolution application in the infrared, blanketing by atomic lines is almost negligible compared with the myriad CO lines (e.g., every line in Fig. 2 is a CO line). The demonstrated quality of the accord (Fig. 2) between the computed and observed spectra shows that the Kurucz solar model is relevant and of adequate fidelity to reproduce the solar spectrum at very high resolution. The computed lines in Fig. 2 do seem to be systematically slightly too deep. However, many aspects of the real Sun are not dealt with by this model: for example, non-LTE effects; the need for a two-component treatment, i.e., a chromosphere, and departures from plane parallelism. Inclusion of a chromosphere alone would lead to shallower predicted CO line cores.

But, even if we posited that the Kurucz model had no such mitigating circumstances, the maximum systematic error in these lines is only about 5% in equivalent width (hereafter referred to as EW). At high resolution one is concerned with line depths but, at low resolution, our observations are sensitive to the EWs of the CO lines, and individual line depths are unimportant. In the region most crucial to us (4–6 μm), one can estimate that the integrated line blanketing from the ATMOS spectra is roughly 10% of the continuum level. The 5% errors in EWs at high resolution would, therefore, be manifest only as <0.5% errors in the low resolution spectral energy distribution, well below the observational uncertainties at these wavelengths. In these terms, the Kurucz solar model is an excellent match to the solar spectrum. Consequently, a low-resolution version of his α^1 Cen model is *a fortiori* applicable to our need, and promises comparable fidelity.

There has been widespread agreement in the literature (see Table 3 of Chmielewski *et al.* 1992) that α^1 Cen is metal

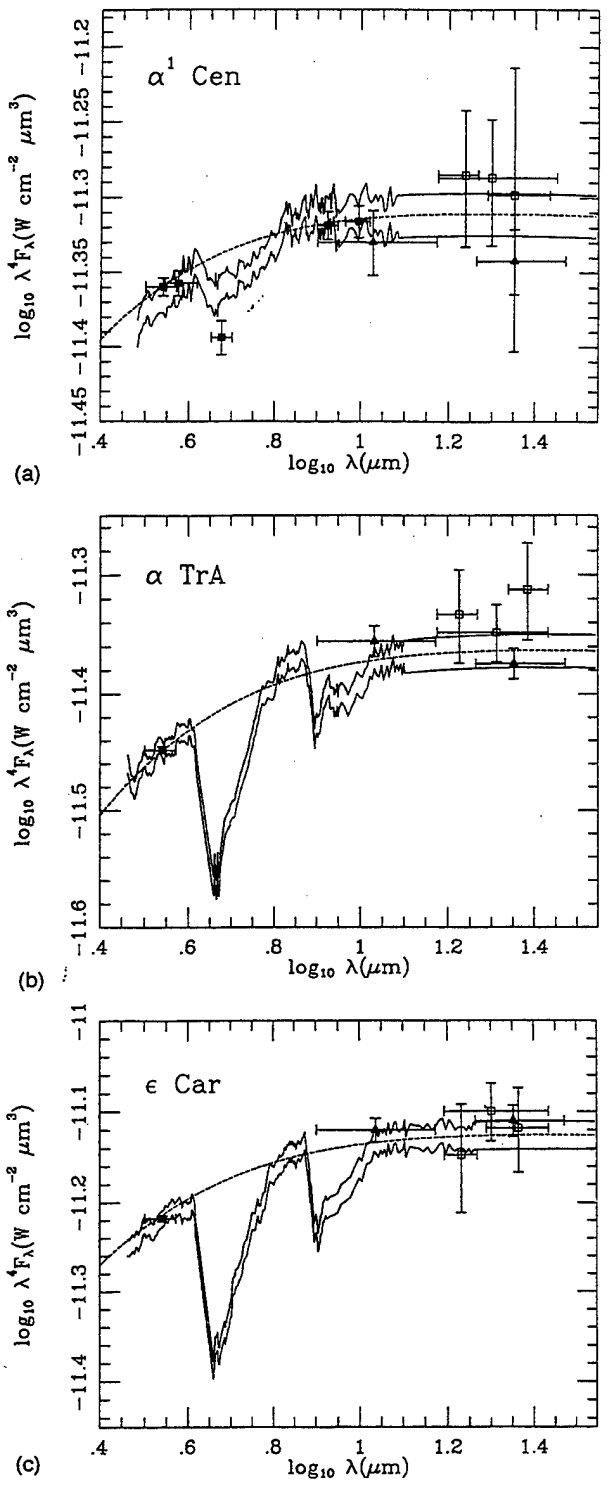

FIG. 1. The three new stellar composites in the form of logarithmic plots of absolute $\lambda^4 F_\lambda$ against λ. In each plot, the $\pm 1\sigma$ error bars are indicated by the pair of solid lines, and a short dashed line represents the best-fitting Engelke approximation: (a) α^1 Cen, (b) α TrA, (c) ϵ Car. Photometry used to essemble the composites is represented by filled squares; *IRAS* 12 and 25 μm data by filled triangles; and our long-wavelength *KAO* pseudophotometry by open squares.

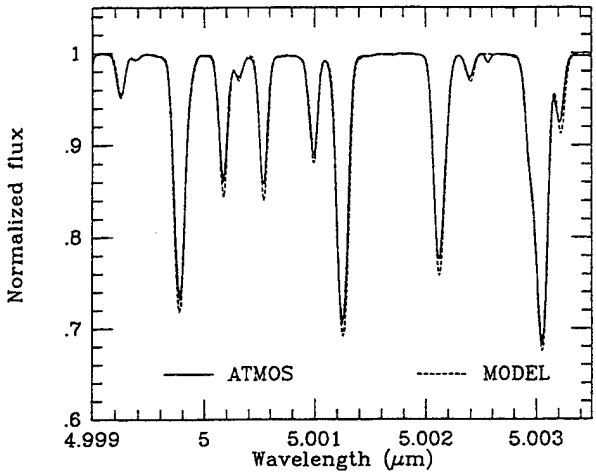

FIG. 2. Direct comparison between a portion of the ATMOS Shuttleborne infrared spectrum of the Sun (heavy solid line) and the computed Kurucz solar spectrum (dashed line) in the general vicinity of the CO fundamental. This section is typical of the overall quality of the calculations. Every line is a CO line.

rich compared with the Sun, with [Fe/H] about +0.2 dex. From their own spectroscopic material, Furenlid & Meylan (1990) determined abundances of many elements in α^1 Cen, finding a general enhancement of the important electron donors (Fe,Mg,Si). Their table of abundances for this star also suggested that both C and O were enhanced, C by +0.14 ±0.04 and O by +0.10±0.06 dex, compared with solar. However, these derived overabundances are marginal at best, and this part of their analysis used values of 5710 K and log gravity of 4.10 (not 5770 and 4.30) to determine the enhancements. Note that this Furenlid–Meylan grid of Kurucz models was used in a strictly differential context, and yielded actual solar abundances from the Kurucz solar log gf values, through use of "corrections." Therefore, while we clearly cannot assert quantitatively that C and O are equally enhanced in α^1 Cen, we do accept the qualitative result from the Furenlid–Meyland differential analysis that the abundances of these elements are not totally decoupled. In what follows, we have implicitly assumed that the C and O abundances scale together. This assumption is necessary because, as Bell *et al.* (1992) have shown, the strengths of the CO bands cannot simultaneously yield information on the separate abundances of C and O (unless CN strengths are also available). However, in stars as warm as α^1 Cen, CO band strength does depend on the product of C and O abundances (Bell & Briley 1991).

Consequently, we needed a grid of models computed for this metal-rich environment in which to test the CO fundamental's appearance. In their analysis of this star, Furenlid & Meylan (1990) cited precisely such a grid, computed by Kurucz to satisfy their requirements. Kurucz (1995) has very kindly supplied us with a subset of that grid, for effective temperature 5770 K, log g of 4.30, [Fe/H] set at +0.2, with C and O varied in unison with respect to their abundances in the Sun. All calculations were done using the CO line list based on the theoretical calculations by Kirby-Docken & Liu (1978), one of several contemporaneous papers providing changed energy levels and filling out the isotopomers. Goorvitch (1994) has recomputed CO but the improvements inherent in the use of his calculations, as opposed to those by Kirby-Docken & Liu (1978), principally affect lines that are high up on the potential and so have small Boltzman factors in solar-type stars; therefore, one might not expect a large

overall effect if Kurucz had switched line lists in these models. [It is, of course, possible that the newer CO line strengths might be systematically different from those of Kirby-Docken & Liu (1978), and an updated CO archive alone could remove the small discrepancies between computed and observed line depths in Fig. 2.]

Microturbulent velocity in all models is 2.0 km s^{-1} and convection is treated using L/H of 1.25. Although Furenlid & Meylan determined a *vturb* of 1 km s^{-1}, our increase makes up for missing line opacity in the model due to the under-representation in the line list of the heavy elements. Because all our potential applications for this model are at low resolution, we chose this model's *vturb*. However, we have examined the consequences had we used a grid with 1 km s^{-1}, instead of the 2 km $^{-1}$ version. To quantify the maximum expected effect, we have compared two models with C and O both enhanced by +0.2 over solar, one with 2 km s^{-1}, and its otherwise identical counterpart with 1 km s^{-1}, to see by how much the 1 km s^{-1} model would have reduced the CO fundamental's depth computed for *vturb* of 2 km s^{-1}. In the IR region where we have data, we find essentially no difference between the two full-resolution calculations that exceeds 0.9%, and degradation of the two models to match our observed resolution lessens this maximal difference to only 0.6%. For the model we finally selected, with much less C and O than this trial calculation (solar, or 0.1 dex below solar), this difference would be appreciably diminished. The maximum expected difference, of course, always occurs close to 4.6 μm and, for our adopted model, is much smaller than both the difference between models with [0.0] and [−0.1], and our observational 1σ uncertainties. Consequently, we would not have selected a model with significantly different attributes were we to have used the grid with 1 km s^{-1}.

Figure 3 compares the emergent spectra for four of the models in our grid (with C and O abundances of −0.2, −0.1, 0.0, and +0.1 with respect to solar) with the *KAO* spectrum of α^1 Cen near the CO fundamental (to facilitate direct comparison we smoothed the *KAO* data and each model by a Gaussian with FWHM of 0.2 μm, and regridded the models to exactly the same wavelength scale as the observed spectra. To the eye, the two models closest in shape to the observations are those with solar C and O, and with C and O both set 0.1 dex below solar. The other two models bracket the observed spectral shape and serve to quantify the variation in the CO fundamental band with these different abundances.

We have compared the shapes of the emergent spectra for these four models with our *KAO* spectrum for α^1 Cen by performing a differential quantitative analysis of the match of shape between each model and the observed spectrum to determine the best-fitting model. In this analysis, each model is allowed to vary up and down freely of the others in order to provide the best fit for that model. Figure 3 simply presents the spectra in such a way as to enhance their differences in the CO fundamental and show their great similarity outside this region. Figure 3 does *not* indicate the actual best-fit scale factors obtained. The nature of these tests was to find both the best multiplier (equivalent to the stellar angular subtense: corresponding to the χ^2 minimum over the

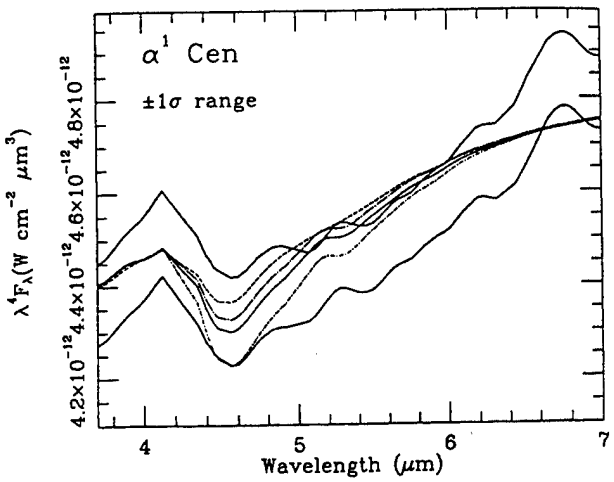

FIG. 3. The ±1σ range around our observed composite spectrum of α^1 Cen in the region of the CO fundamental, plotted in $\lambda^4 F_\lambda$ space, and compared with four models from our Kurucz grid for this star. Each model is scaled to the same solid angle (corresponding to 8.58 mas) and smoothed by a Gaussian of 0.2 μm FWHM, as is the observed spectrum in this figure. The models, from top to bottom, are for C and O abundances of −0.2, −0.1, 0.0, and +0.1 dex, with respect to solar.

set of possible scale factors) and, more importantly, the "bias" (the uncertainty in scaling factor for the best fit: cf. Paper IV). A large uncertainty implies a poor match in shape because the range of acceptable multipliers is wide, whereas a small uncertainty implies a good match in shape. This uncertainty is determined directly from the formal χ^2 parabola and is related to the breadth of the parabola and, as such, is an independent assessment.

These tests were applied to several wavelength ranges. When tested over a broad wavelength range (e.g., 3–12 μm), essentially all models fit equally well. However, emphasizing the region with the greatest observed spectral structure (Fig. 3) provides quantitative discrimination. In particular, varying the wavelength region of comparison from a minimum range of 4.1–5.2 μm to a maximum of 3.3–7.1 μm produced curves of minimum χ^2 value and uncertainty in multiplier with well-defined minima lying between the [0.0] and [−0.1] models, while the [+0.1] and [−0.2] models always fit significantly more poorly. We see no statistically significant distinction between the [0.0] and [−0.1] and are, therefore, unable to discriminate more precisely between the two closest matching models, given the uncertainties in our observed spectral shape. Therefore, we simply averaged the two emergent spectral energy distributions, which differ by at most 1% across our entire observed range, 3–30 μm (the greatest divergence is, of course, confined to the region near 4.6 μm). We took this averaged emergent spectral shape as the best model representation for this star. Figure 4 represents the ratio of our observations to the absolutely calibrated version of this model (see below), near the CO fundamental; observations and model were smoothed by a Gaussian with 0.2 μm FWHM to produce Fig. 4. This presumably corresponds to values of C and O enhancement between 0.0 and −0.1, if these were to vary in unison, as we have assumed. We emphasize that we have not determined the C and O abundances for this star; rather, we have chosen a physically defensible

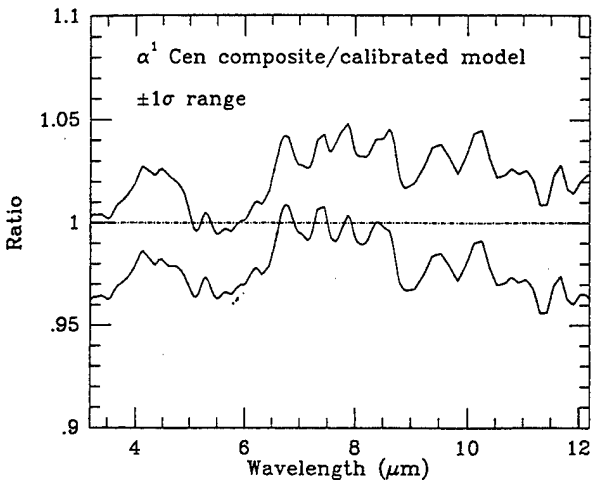

FIG. 4. The ratio of our composite to the calibrated α^1 Cen model in the vicinity of the CO fundamental. The $\pm 1\sigma$ range around the observations is shown and this plot was constructed from the smoothed spectra shown in Fig. 3.

model shape to serve as a smooth interpolator, and plausible extrapolator, of our observations.

To achieve an absolutely calibrated version of the adopted model for α^1 Cen we have directly spliced (by our standard technique: see Papers II and IV) the part of our composite spectrum that is observed (as opposed to that represented by the best-fitting Engelke function) to the model, namely, the 3.0–12.1 μm range. The best-fit scaling factor yields an equivalent angular diameter of 8.58±0.01 mas (the error is determined simply from the χ^2 parabola and represents only the internal precision of this operation). Exactly the same value results from a splice of the model, smoothed by a Gaussian of FWHM 0.2 μm, to an identically smoothed version of the observed spectrum.

To sample a wider spectral range we have also normalized the model to photometry of α^1 Cen in characterized system passbands (see Sec. 3 above). Because we have a continuous model spectrum between 1 and 200 μm and are no longer limited to small fragments within the 3–30 μm region, we have chosen to use all Carter's high-precision measurements for the *JHKL* region, supplemented by the three *ESO* 10 μm narrowbands (*N*1, *N*2, and *N*3: Bouchet *et al.* 1989). After correction for zero points, the actual photometry we used, that does not already appear in Table 2, is: *SAAO-J*−1.138±0.005, *SAAO-H*−1.470±0.005, *SAAO-K* −1.524±0.009, and *ESO-N3*−1.596±0.057. The scaling factor resulting from this normalization is equivalent to an angular diameter of 8.57±0.04 mas (internal precision); an excellent, and somewhat independent accord (because only half the photometry was used to build the composite for α^1 Cen), with that found by comparison of the observed and modeled energy distributions. This compares extremely favorably with the value of 8.62±0.23 mas, derived by Blackwell & Shallis (1977), by application of the IRFM (based on a stellar atmosphere code but not on Kurucz models), but using heterogeneous infrared photometry with diverse absolute calibrations.

It is noteworthy that one can challenge the shape of a model's emergent spectrum solely by use of infrared continuum photometry, provided that one has photometry available over a sufficiently wide range of wavelengths. For example, we experimented with generic Kurucz (1991, 1993a) spectra for F2 V and K2 V stars by testing how well they fitted the actual photometry for α^1 Cen. The relevant parameter is, of course, the bias of the scale factor as one compares the set of in-band fluxes derived from integration over the spectra with those from the independently secured and calibrated ground-based photometric measurements. We found that, while the bias of the best fit of our adopted model for α^1 Cen to this photometry is only about 0.5%, the F and K dwarfs yielded biases of order 3%–4%, substantially poorer. The need for a broad wavelength range arises because of the sensitivity in the computed shapes of stellar infrared energy distributions to effective temperature, which can be measured principally by comparing the *J* band with photometry in the 10 μm window. This sensitivity of real stars and of computed model atmospheres can also be recognized as one of the shortcomings of the Engelke function. In Paper IV one can see how every Engelke approximation predicts far too much flux at wavelengths below about 2 μm because of the analytic oversimplification. While we advocate the selection of relevant theoretical models through use of observed and continuous infrared spectroscopy, it is possible that this rather simplistic approximation could yield adequate results (±10% in irradiance values) for the establishment of rough and ready "standards" in the total absence of any infrared spectroscopy, at least at long infrared continuum wavelengths (cf. Fig. 1).

We conclude that the absolutely calibrated version of our model for α^1 Cen represents the angular diameter of this star as 8.58±0.13 mas, where the uncertainty now includes the external error that arises from the fundamental uncertainty of 1.46% in our Sirius absolute calibration (Paper I). The global bias associated with the calibrated α^1 Cen model is 1.464%. Figure 5 presents the absolutely calibrated model of α^1 Cen in the same format, and on the same wavelength scale, as the models of Vega and Sirius that we showed in Paper I.

There seems to be no direct measurement of α^1 Cen's apparent angular diameter, by an intensity interferometer, presumably because of its binarity and the resulting complex visibility curves. However, there are two recent values for its physical radius determined through atmospheric modeling for an effective temperature of 5770 K. These are 1.21±0.02 $R_\odot$ (Kjellsen & Bedding 1995) and 1.24±0.025 $R_\odot$ (Lydon *et al.* 1990). The most precise parallax is that by Demarque *et al.* (1986: 0.7506±0.0046″). From the implied distance to the star these two radii yield apparent angular diameters of 8.45±0.15 and 8.66±0.19 mas, respectively, where these errors are the root-sum-square combination of the error in the parallax and that in the estimated stellar radius. Combining these results with the diameter of Blackwell & Shallis (1977), using inverse variance weighting, implies that the literature supports a value of 8.55±0.11 mas, vindicating our own estimate.

Therefore, we conclude that both our observed α^1 Cen spectrum, calibrated from our Sirius spectrum, and the shape of our adopted, plausible, independently calculated, α^1 Cen model spectrum are in good agreement (well within 1σ) with

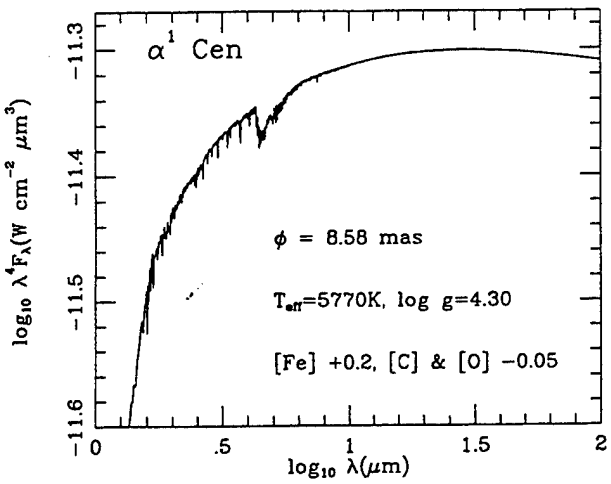

FIG. 5. The adopted, calibrated, theoretical shape for α^1 Cen. Wavelength scale is identical to that used in Paper I to portray our calibrated Vega and Sirius spectra.

infrared photometry and with estimates of the stellar angular diameter. Consequently, this provides an effective closure within our scheme of calibrated infrared spectra, as well as offering a brighter reference star with which to calibrate objects observed in the southern hemisphere.

5. THE LONG-WAVELENGTH SPECTRA

In reality, all our long-wave spectra lacked enough signal-to-noise to use as spectral fragments in their entirety and we resorted instead to combining the data from all the channels on the Si:Bi array and similarly from all the Si:P detectors. To increase signal-to-noise further, we also combined the ratio spectra from all the Si:Bi and Si:P detectors. By this means we were able to derive pseudophotometric points to check our assembled complete spectra because these long-wavelength data were not used in the process of spectral assembly. These photometric points were then converted to flux densities via our calibrated models for Sirius and α^1 Cen. Although the spectra were noisy, we still applied our usual techniques to these spectral fragments, bringing together overlapping ranges by routine splices and augmenting the formal photometric errors by root-sum-squaring with the associated uncertainties (biases) in scale factors for the best overlaps. It is these latter uncertainties that increase the final errors even after combining all the Si:Bi or all the Si:P detectors into a single number, but the methodology is then consistent throughout our work.

We compared α^1 Cen directly to α CMa but were able to use ratios with respect to α^1 Cen and to α CMa for the two K giants, using the absolutely calibrated α^1 Cen spectrum in Fig. 5. The binned long-wave spectral ratios yielded flux densities across the Si:Bi (15.0–18.5 μm) and Si:P (19.5–27.2 μm) ranges. Table 5 summarizes these flux densities for the stars discussed in this paper, indicating which calibrator was used. These flux densities are plotted in Fig. 1 along with the photometry used to assemble the composite spectrum, and the *IRAS* flux densities. Note that although the long-wavelength *KAO* and the *IRAS* data were not used to construct any of these spectral composites they are in good agreement (within 1σ) with our calibrated spectra, as is the *ESO-N3* point for α^1 Cen. To present the *IRAS* flux densities we used the somewhat more precise *IRAS* Faint Source Survey photometry. All the measurements beyond 15 μm are consistent with our extrapolated Engelke functions. The uncertainties in the observed photometry points are rather large but suffice to preclude any radical departures of real stellar spectra from a Rayleigh–Jeans slope within our observed wavelength range.

6. CONCLUSIONS

We have assembled absolutely calibrated, complete, continuous stellar spectra between 3 and 30 μm for three stars: α^1 Cen, α TrA, and ϵ Car. We have created an absolutely calibrated theoretical emergent spectrum derived from Kurucz model atmospheres for α^1 Cen, whose shape is in agreement with our observations of this star. We recommend use of this star when a southern spectral standard brighter than Sirius is needed. The two K giants show deep absorptions of CO and SiO. Our long-wave *KAO* measurements, and those from *IRAS*, are consistent with our extrapolations of observed but noisy stellar spectra by means of the Engelke

TABLE 5. Long-wavelength (>15.00 μm) flux densities derived from the absolutely calibrated α^1 Cen and/or α CMa models.

Star	Data	$\langle\lambda\rangle$ (μm)	$\lambda^4 F_\lambda$ (W cm^{-2} μm^{-1})	$\pm\epsilon(\lambda^4 F_\lambda)$ (W cm^{-2} μm^{-1})	Calibrator
α^1 Cen	Si:Bi	17.30	5.79E-17	0.60E-17	α CMa
α^1 Cen	Si:P	22.50	1.96E-17	0.42E-17	α CMa
α^1 Cen	All	19.90	3.29E-17	0.32E-17	α CMa
α TrA	Si:Bi	16.83	5.79E-17	0.52E-17	α^1 Cen
α TrA	Si:P	24.29	1.40E-17	0.13E-17	α^1 Cen
α TrA	All	20.50	2.69E-17	0.17E-17	α^1 Cen
α TrA	All	20.50	2.17E-17	0.27E-17	α CMa
α TrA	All	20.50	2.54E-17	0.14E-17	α^1 Cen and α CMa
ϵ Car	Si:Bi	17.06	8.41E-17	1.15E-17	α^1 Cen
ϵ Car	Si:P	23.18	2.64E-17	0.28E-17	α^1 Cen
ϵ Car	All	20.12	4.54E-17	0.43E-17	α^1 Cen
ϵ Car	All	19.86	5.75E-17	0.63E-17	α CMa
ϵ Car	All	20.00	4.98E-17	0.36E-17	α^1 Cen and α CMa

approximation; i.e., the energy distributions of cool giants in this mid-infrared region are close to their Rayleigh–Jeans slopes.

We are deeply grateful to Dr. R. Kurucz for generating the mini-grid of model atmospheres that underpin our work on α^1 Cen, for creating the special computations necessary to compare his model with the ATMOS data, and for many valuable discussions concerning our work. It is likewise a pleasure to acknowledge Dr. D. Carbon for a wealth of vital advice, and Dr. B. Carter for obtaining the precision photometry used to construct our composite spectra. M.C. thanks Phillips Laboratory for its support of this effort through Dr. S. D. Price under Contract No. F19628-92-C-0090 with JS&E, Inc. We are grateful to NASA's Airborne Astronomy program and to the entire staff of the *KAO* for their sterling efforts throughout the flights dedicated to this calibration study. M.C. also thanks NASA-Ames Research Center for partial support under Co-Operative Agreement NCC 2-142 with Berkeley. This research has made use of the SIMBAD database, operated at CDS, Strasbourg, France.

REFERENCES

Bell, R. A. 1994, MNRAS, 268, 771
Bell, R. A., & Briley, M. M. 1991, AJ, 102, 763
Bell, R. A., Briley, M. M., & Norris, J. E. 1992, AJ, 104, 1127
Bessell, M. S., & Brett, J. M. 1988, PASP, 100, 1134
Blackwell, D. E., Lynas-Gray, A. E., & Petford, A. D. 1991, A&A, 245, 567
Blackwell, D. E., & Shallis, M. J. 1977, MNRAS, 180, 177
Bouchet, P., Moneti, A., Slezak, E., Le Bertre, T., & Manfroid, J. 1989, A&AS, 80, 379
Carter, B. 1994 (private communication)
Chmielewski, Y., Friel, E., Cayrel de Strobel, G., & Bentolila, C. 1992, A&A, 263, 219
Cohen, M., Walker, R. G., Barlow, M. J., & Deacon, J. R. 1992, AJ, 104, 1650 (Paper I)
Cohen, M., Walker, R. G., & Witteborn, F. C. 1992, AJ, 104, 2030 (Paper II)
Cohen, M., Witteborn, F. C., Walker, R. G., Bregman, J., & Wooden, D. 1995, AJ, 110, 275 (Paper IV)
Demarque, P., Guenther, D. B., & van Altena, W. F. 1986, ApJ, 300, 773
van Dijsseldonk 1994 (private communication)
Engelke, C. W. 1992, AJ, 104, 1248
Engels, D., Sherwood, W. A., Wamsteker, W., & Schultz, G. V. 1981, A&AS, 45, 5
Farmer, C. B., & Norton, R. H. 1989, A High-Resolution Atlas of the Infrared Spectrum of the Sun and Earth Atmosphere from Space, NASA RP-1224
Furenlid, I., & Meylan, T. 1990, ApJ, 350, 827
Goorvitch, D. 1994, ApJS, 95, 535
Harper, G. M. 1992, MNRAS, 256. 37
Hoffleit, D. 1982, Yale Bright Star Catalog, 4th ed. (Yale University Obs., New Haven)
Kirby-Docken, K., & Liu, B. 1978, ApJS, 36, 359
Kjeldsen, H., & Bedding, T. R. 1995, A&A, 293, 87
Kovacs, N. 1983, A&A, 120, 21
Kurucz, R. L. 1991, New lines, new models. new colors, in Precision Photometry: Astrophysics of the Galaxy, edited by A. G. Davis Philip, A. R. Upgren, and K. A. Janes (Davis, Schenectady), p. 27
Kurucz, R. L. 1993a, ATLAS9 Stellar Atmosphere Programs and 2 km/s grid, Kurucz CD-ROM No. 13
Kurucz, R. L. 1993b, SYNTHE Spectrum Synthesis Programs and Line Data, Kurucz CD-ROM No. 18
Kurucz, R. L. 1995 (private communication)
Kurucz, R. L. 1996 (private communication)
Lord, S. D. 1992, A New Software Tool for Computing the Earth's Atmospheric Transmission of Near-Infrared and Far-Infrared Radiation, NASA TM-103957
Lydon, T. S., Fox, P. A., & Sofia, S. 1993, ApJ, 413, 390
Moshir, M., *et al.* 1992, Explanatory Supplement to the *IRAS* Faint Source Survey, Version 2, JPL D-10015 (JPL, Pasadena)
Pasquini, L., & Brocato, E. 1992, A&A, 266, 340
Strecker, D. W., Erickson, E. F., & Witteborn, F. C. 1979, ApJS, 41, 501
Thomas, J. A., Hyland, A. R., & Robinson, G. 1973, MNRAS, 165, 201
Wesselink, A. J., Paranya, K., & DeVorkin, K. 1972, A&AS, 7, 257
Witteborn, F. C., Cohen, M., Bregman, J. D., Heere, K. R., Greene, T. P., & Wooden, D. H. 1995, in Proceedings of the Airborne Astronomy Symposium on the Galactic Ecosystem, ASP Conf. Ser. 73, edited by M. Haas, E. F. Erickson, and J. Davidson (ASP. San Francisco), p. 573

SPECTRAL IRRADIANCE CALIBRATION IN THE INFRARED. VII. NEW COMPOSITE SPECTRA, COMPARISON WITH MODEL ATMOSPHERES, AND FAR-INFRARED EXTRAPOLATIONS

MARTIN COHEN

Radio Astronomy Laboratory, 601 Campbell Hall, University of California, Berkeley, California 94720, and Jamieson Science and Engineering, Inc., Suite 204, 5321 Scotts Valley Drive, Scotts Valley, California 95066
Electronic mail: cohen@bkyast.berkeley.edu

FRED C. WITTEBORN

Space Science Division, Mailstop 245-6, NASA-Ames Research Center, Moffett Field, California 94035
Electronic mail: witteborn@ssa1.arc.nasa.gov

DUANE F. CARBON

NAS Systems Division, Mailstop 258-5, NASA-Ames Research Center, Moffett Field, California 94035
Electronic mail: dcarbon@nas.nasa.gov

JOHN K. DAVIES

Joint Astronomy Centre Hawaii, 660 N. Aohoku Place, University Park, Hilo, Hawaii 96720
Electronic mail: jkd@jach.hawaii.edu

DIANE H. WOODEN

Space Science Division, Mailstop 245-6, NASA-Ames Research Center, Moffett Field, California 94035
Electronic mail: wooden@ssa1.arc.nasa.gov

JESSE D. BREGMAN

Space Science Division, Mailstop 245-6, NASA-Ames Research Center, Moffett Field, California 94035
Electronic mail: bregman@ssa1.arc.nasa.gov

Received 1996 May 21; revised 1996 July 17

ABSTRACT

We present five new absolutely calibrated continuous stellar spectra constructed as far as possible from spectral fragments observed from the ground, the *Kuiper Airborne Observatory* (*KAO*), and the *IRAS* Low Resolution Spectrometer. These stars—α Boo, γ Dra, α Cet, γ Cru, and μ UMa—augment our six, published, absolutely calibrated spectra of K and early-M giants. All spectra have a common calibration pedigree. A revised composite for α Boo has been constructed from higher quality spectral fragments than our previously published one. The spectrum of γ Dra was created in direct response to the needs of instruments aboard the *Infrared Space Observatory (ISO)*; this star's location near the north ecliptic pole renders it highly visible throughout the mission. We compare all our low-resolution composite spectra with Kurucz model atmospheres and find good agreement in shape, with the obvious exception of the SiO fundamental, still lacking in current grids of model atmospheres. The CO fundamental seems slightly too deep in these models, but this could reflect our use of generic models with solar metal abundances rather than models specific to the metallicities of the individual stars. Angular diameters derived from these spectra and models are in excellent agreement with the best observed diameters. The ratio of our adopted Sirius and Vega models is vindicated by spectral observations. We compare *IRAS* fluxes predicted from our cool stellar spectra with those observed and conclude that, at 12 and 25 μm, flux densities measured by *IRAS* should be revised downwards by about 4.1% and 5.7%, respectively, for consistency with our absolute calibration. We have provided extrapolated continuum versions of these spectra to 300 μm, in direct support of *ISO* (PHT and LWS instruments). These spectra are consistent with *IRAS* flux densities at 60 and 100 μm.

1. INTRODUCTION

The previous papers of this series have presented a consistent effort to provide absolutely calibrated broadband and narrowband infrared photometry and spectra based upon a carefully selected, infrared-customized pair of stellar models for Vega and Sirius, created by Kurucz, and absolutely calibrated by Cohen *et al.* (1992a, hereafter referred to as Paper I). These hot stellar models have been employed as reference spectra to provide continuous (i.e., uninterrupted in wave-

 0004-6256/96/112(5)/2274/12/$10.00

length), observed, absolutely calibrated spectra ("composites") of cool stars by the methods detailed by Cohen *et al.* (1992, hereafter referred to as Paper II) and Cohen *et al.* (1995, hereafter referred to as Paper IV). This approach has yielded six infrared-bright secondary stellar standards with calibration pedigrees directly traceable to our primary radiometric standard, namely, α CMa. Molecular bands of CO and SiO dominate these observed infrared spectra of cool giants and supergiants (Cohen *et al.* 1992b, hereafter referred to as Paper III).

In the present paper we update the spectrum of α Boo to take account of newer and higher quality spectral fragments, and we augment the six composites by spectra of four additional stars assembled by the identical procedures to those described in Papers II and IV (Sec. 2). Note that two of these new composites do not start at 1.2 μm because there has never been any further development of the unique Strecker *et al.* (1979, hereafter referred to as SEW) archive of airborne 1.2–5.5 μm spectra. The composite of μ UMa starts at about 3.1 μm, and that for γ Cru at about 3.9 μm. However, these can still provide valuable calibrators (cf. Cohen *et al.* 1996a, hereafter referred to as Paper VI which offers 3.0–29 μm coverage).

In a future paper (Cohen *et al.* 1996b, hereafter referred to as Paper VIII), we will describe how we have converted this limited set of stars with abundant spectral observations into a network of nearly 300 calibrators across the sky by using the "template assumption," namely, that the dereddened infrared spectrum of any observed K-M giant accurately represents the intrinsic spectrum of any other giant with the identical spectral type as the composite, and so serves as a "template." Given our intended dependence upon these few observed continuous spectra (now covering the range K0 −M3.4 III), it is appropriate to make direct comparisons with a grid of model atmospheres. We, therefore, compare Kurucz (1991, 1993) models for our stars with composite spectra, and ratio these calibrated spectra to the models (Sec. 3).

We have several objectives in these comparisons: to test the goodness of fit (shape) of theory and observations (these cool stellar models are totally independent of the data and procedures used to assemble the composites); if well matched in shape, to determine angular diameters from the normalization of models that match the composites; to compare these empirical angular diameters with those observed by Michelson (intensity) interferometry or lunar occultation; and to attempt the extrapolation of these observed spectra to the far-infrared, using *IRAS* measurements to attempt to validate these extrapolations. Despite the conspicuous omission of the SiO fundamental (whose presence locally dominates these spectra between about 7.5 and 12 μm), we find that the Kurucz models are capable of replicating these complete spectral shapes to within a few percent. Our derived angular diameters are in good accord with the best, observationally determined, diameters for these stars (Sec. 4).

We have sought direct observational evidence on the ratio of our adopted spectra of Sirius and Vega, both photometrically and through 10 μm spectroscopy, and find support for this ratio (Sec. 5).

TABLE 1. New composite spectra described in this paper.*

Star	Spectral type	Date of assembly
α Boo	K1 III	December 21, 1995
γ Dra	K5 III	December 22, 1995
α Cet	M1.5 III	March 26, 1996
γ Cru	M3.4 III	March 13, 1996
μ UMa	M0 III	April 2,1996

*Table 1 can be found in the AAS CD-ROM Series, Vol. 7, 1996.

In Sec. 6, we return to the issue of the mid-infrared behavior of real giants, as opposed to model atmospheres, and present empirical evidence in favor of the locally Rayleigh–Jeans character of K and M giants beyond 10 μm.

Finally, we again probe the absolute calibration of *IRAS* (cf. Paper I) by synthesizing *IRAS* flux densities for all our composites in the 12 and 25 μm bands (Sec. 7) and, from theoretical continuum extrapolations of their spectra using a grid computed by one of us (D.F.C) (Sec. 8), in the 60 and 100 μm bands (Sec. 9). We find good agreement between these extrapolated models and observed *IRAS* long-wavelength flux densities, encouraging us to provide stellar calibration spectra in support of *ISO*'s absolute calibration.

2. NEW COMPOSITE SPECTRA

Our methodology for creating a complete and continuous composite spectrum from 1.2 to 35 μm follows that described in Papers II and IV. Except for that of γ Cru, these new complete spectra were made possible through a fruitful collaboration with the UKIRT Service Observing program (cf. Cohen & Davies 1995, hereafter referred to as Paper V) that has provided high quality 10 and 20 μm spectral fragments. Table 1 summarizes the new composites. Full details of the process of assembly for each composite appear in the AAS CD-ROM Series, Vol. 7, 1996 associated with this paper, including the independent photometry used to support the normalization of spectral fragments. To illustrate the calibration pedigree that accompanies each new composite spectrum, we present only one table here, corresponding to α Boo. Figure 1 presents the spectra themselves in the form of $\log \lambda^4 F_\lambda$ vs $\log \lambda$ plots. We show the three composites with fullest wavelength coverage before those with more restricted ranges.

All the new spectral fragments incorporated into this paper were secured with two or more of the following instruments: the NASA-Ames "SIRAS" (Short Wavelength Infrared Array Spectrometer: Wooden 1989), "FOGS" (Faint Object Grating Spectrometer: Witteborn & Bregman 1984), or "HIFOGS" (High-efficiency Infrared Faint Object Grating Spectrometer: Witteborn *et al.* 1995) on the *KAO* or with the NASA 1.5 m Mt Lemmon telescope; the CGS3 spectrometer on the 3.8 m UKIRT; or the *IRAS* Low Resolution Spectrometer-(hereafter referred to as LRS). The Ames spectrometers are doubly sampled by using two different grating settings spaced an integral number plus one half detectors apart to achieve Nyquist sampling and to provide coverage of occasional dead detectors. CGS3 is always either doubly

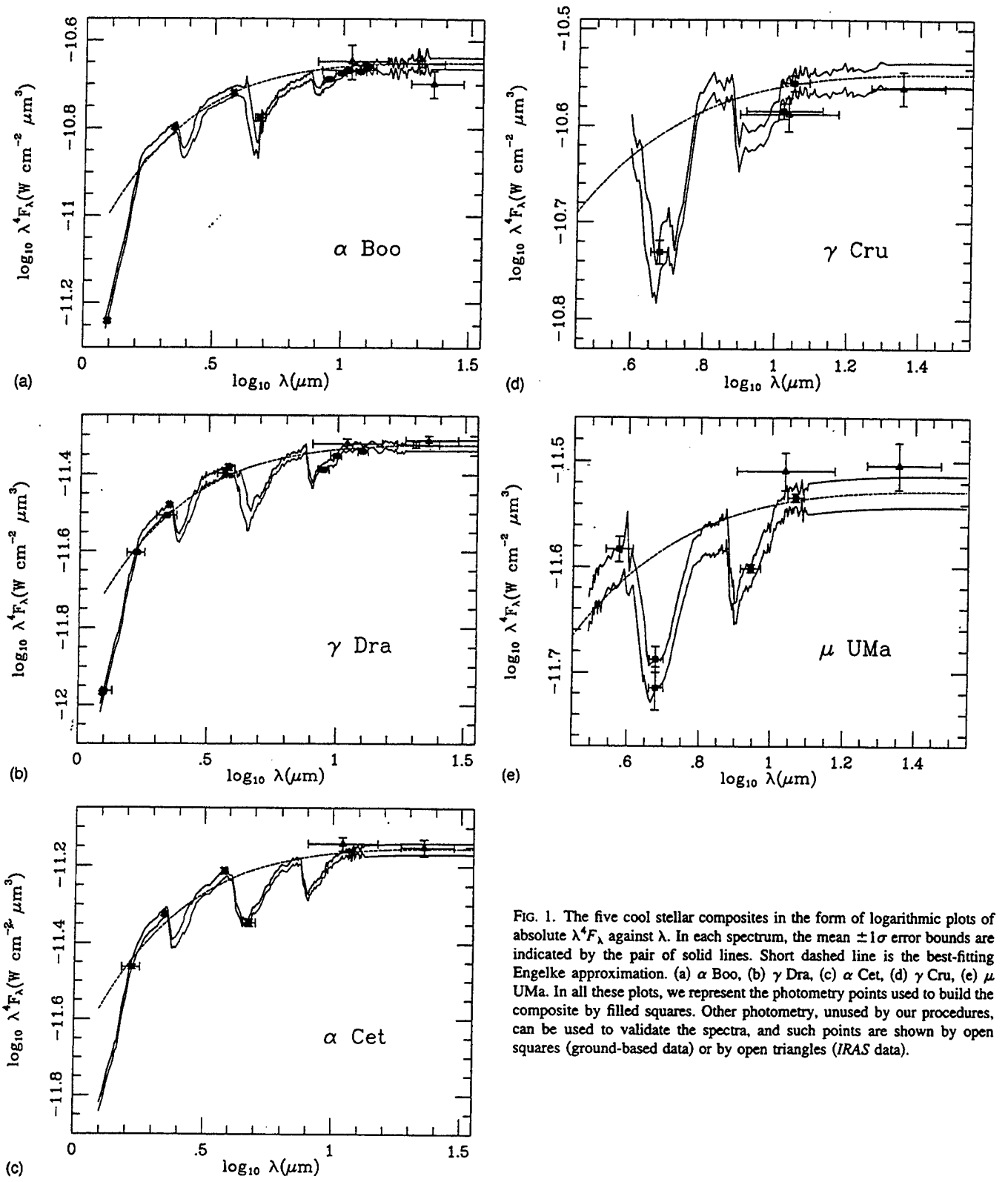

FIG. 1. The five cool stellar composites in the form of logarithmic plots of absolute $\lambda^4 F_\lambda$ against λ. In each spectrum, the mean $\pm 1\sigma$ error bounds are indicated by the pair of solid lines. Short dashed line is the best-fitting Engelke approximation. (a) α Boo, (b) γ Dra, (c) α Cet, (d) γ Cru, (e) μ UMa. In all these plots, we represent the photometry points used to build the composite by filled squares. Other photometry, unused by our procedures, can be used to validate the spectra, and such points are shown by open squares (ground-based data) or by open triangles (*IRAS* data).

or triply sampled, likewise to achieve the full theoretical resolution. For the CGS3 fragments (cf. Paper V) we have continued to emphasize close matching of airmasses between the cool target stars and the reference object (preferably Sirius, or one of our already established cool composites). From the *KAO* we could not always exert such control over stellar airmasses at the time of observation due to the relative brevity and constraints of the actual observing time at altitude. Therefore, we remove the residual effects of the terrestrial atmosphere (particularly important from 5 to 8 μm) post facto from the spectra, through use of precomputed standard atmospheric transmission curves relevant to different amounts of precipitable water vapor (currently between 6 and 12 μm). Actual water vapor was measured on each flight with a radiometer. These transmissions were calculated using Lord's (1992) "ATRAN" software tool. Any corrections to

TABLE 2. Engelke functions used in, or relevant to, composite spectra.*

Star	Effective Temperature (K)	Angular diameter milliarcsec
α Boo	4362	21.12
γ Dra	3986	10.17
α Cet	3745	12.77
γ Cru	3626	26.14
μ UMa	3735	8.32

*This table can be found in the AAS CD-ROM Series, Vol. 7, 1996.

measured spectral points were ~3%–5% in molecular lines.

As in Paper IV, we have substituted the best-fitting Engelke (1992) function for noisy LRS, 16–24 μm CGS3, and/or 16–35 μm *KAO* data to provide meaningful extrapolations of our new composites out to 35 μm. This analytic approximation to real stellar continua is derived assuming that the dominant source of infrared continuum opacity in these cool giant stars is H^- free-free (cf. Engelke 1992). There is only one essential input to the shape of an Engelke function, namely the effective temperature, which we fixed by reference to the literature (see Tables 2, 3, and the AAS CD-ROM Series). The normalizing scale factors for these functions, namely their angular subtenses, are determined by the fit of the Engelke function shape to our composite spectra.

We document the full calibrational information for these new composites (see Table 4 and the CD-ROM), namely, date of assembly (i.e., the version of this spectrum); details of the photometry used to calibrate the composite radiometrically including the FWHM of the relevant passbands and their effective wavelengths for the Vega spectrum and for the star in question, and the monochromatic flux densities; all archival spectral fragments, with total spectral ranges, ranges actually utilized, and average resolving power over that spectral range (expressed as the resolving power, $\lambda/\Delta\lambda$). We had access to adequate photometry to assemble the composites for α Boo, γ Dra, μ UMa, and γ Cru by precisely the same technique used for that of α Tau (Paper II) and the 1.2–35 μm spectra detailed in Paper IV. For α Cet we lacked any traceable photometry in characterized passbands in the 10 μm window and were, therefore, obliged to assemble this star's composite using the "end-to-end" method used in Paper VI for the composite spectrum of α^1 Cen.

The star μ UMa is now designated as a new suspected variable (NSV 4829) by Kholopov *et al.* (1992), although details are minimal. Hoffleit & Warren (1991) indicate it to be a spectroscopic binary, possibly an eclipsing variable, with visual amplitude about 0.3 mag. Examination of the infrared literature (Gezari *et al.* 1993) does not suggest infrared variation above a few hundredths of magnitude, after allowance for the diverse zero points of the references cited therein, although Sinton & Tittemore (1984) indicate qualitatively that they saw some variation at M. Consequently, we have retained this star as a secondary standard because of its popularity as an-infrared calibrator, due as much to its northerly location as to its mid-infrared brightness.

In addition to the photometry used for the actual assembly of composites (the filled squares in Fig. 1), we sometimes have other photometry in well-characterized passbands that can be used to validate the spectra, precisely because it was unused by our procedures. Any such points are distinguished, in Fig. 1, by open squares (ground-based data) or by open triangles (*IRAS* data, similarly not used in composite assembly). All photometry points are plotted at their isophotal wavelengths for these stellar spectra. These validating data points are as follows. For α Boo we have: narrowband Jn (Selby *et al.* 1988; Hammersley 1995, described in Paper VIII); UKIRT broad N-band (10 μm) and Q-band (20 μm) points (too wide to be integrated over the CGS3 10/20 μm fragments but valid post factor; and the *IRAS* FSS flux densities at 12 and 25 μm. For γ Dra, these are narrowband Jn (Selby *et al.* 1988; Hammersley 1995) and broadband Tenerife J (Hammersley 1995); a UKIRT Q-band point; and *IRAS* FSS points. For the other three stars, we have only *IRAS* flux densities as external checks of the composites. In all five cases, these additional photometry values confirm the accuracy of the new composites at the 1σ level or better.

We prefer to provide pristine data whenever possible, rather than to regrid each composite to some equally spaced or common wavelength scale. Each composite (on the CD-ROM), therefore, has a different set of wavelengths. We tabulate: wavelength; monochromatic flux density (F_λ in units of W cm^{-2} μm^{-1}); total uncertainty (also in units of W cm^{-2} μm^{-1}) associated with this value of F_λ; local bias; and global bias. For most applications, "total uncertainty" is the error term most appropriate to use. It is the standard deviation of the spectral irradiance and includes the local and global biases. Local and global biases are tabulated as percentages of the irradiance; their corresponding absolute quantities are already included in the total uncertainty. The global bias does not contribute error to flux ratios or color measurements, and may be removed (in the root-sum-square sense) from the total error.

3. COMPARISON WITH KURUCZ MODEL ATMOSPHERES

De Jager & Nieuwehuisen (1987) tabulate statistical relations between effective temperature and bolometric luminosity for all spectral types, assigning algebraic variables, that can be interpolated, to the qualitative descriptors of "spectral class" and "luminosity class." Following the approach and work of de Jager & Nieuwehuisen, Cohen (unpublished) has constructed similar tables that correspond to stellar mass and radius, using values drawn from the literature, whence a derivative relation between gravity and spectral type was obtained. Adopting solar metallicities, appropriate effective temperatures, and these gravities (corresponding solely to the spectral types of our stars), we have extracted theoretical spectra from the Kurucz grid. To provide a generic model for each selected set of values for temperature and gravity, we interpolated bilinearly in log $T_{\rm eff}$ and log g within the Kurucz archive.

Each pair of model and composite spectra was then convolved with a Gaussian and the model regridded to the same wavelength scale as the corresponding composite. We then fitted the complete emergent spectrum from the model atmosphere to the composite, omitting only the region 7.43–11.25

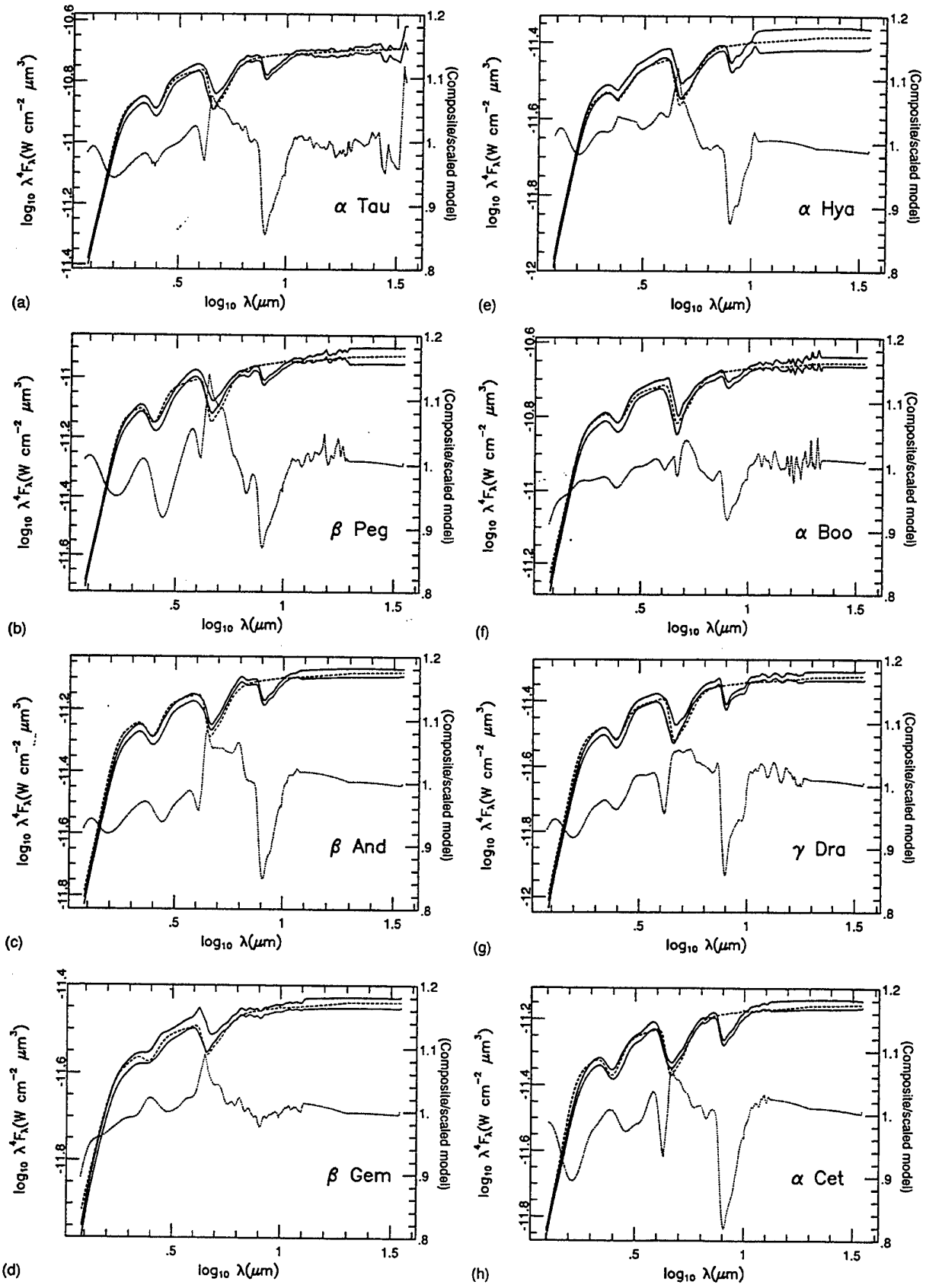

FIG. 2. Eight 1.2–35 μm composites, smoothed by a Gaussian with FWHM of 0.3 μm, showing their $\pm 1\sigma$ ranges (pairs of solid lines), compared with the identically smoothed relevant Kurucz models (short dashed lines), scaled optimally to match each composite spectrum, excluding only the region of the SiO fundamental ($\log \lambda \sim 0.90$). (These curves are to be read against the left-hand axes.) The major CO bands occur at $\log \lambda \sim 0.67$ (fundamental) and $\log \lambda \sim 0.36$ (first overtone) in these plots. The ratios of these smoothed spectra are also plotted in these figures (the dotted curves), in the form of composite divided by scaled model. These dotted ratio curves are associated with the right-hand axes. Note the SiO ratio absorption due to the absence of the lines of this fundamental band ($\log \lambda \sim 0.90$) from the grid of models, and the apparent "emissions" in the CO fundamental ($\log \lambda \sim 0.67$), where the models' bands are too deep. (a) α Tau, (b) β Peg, (c) β And, (d) β Gem, (e) α Hya, (f) α Boo, (g) γ Dra, (h) α Cet.

TABLE 3. Fundamental parameters adopted for the generic Kurucz models.*

Star	Spectral Type	T_{eff}	*log g*
α Tau	K5III	3898	2.0
β Peg	M2.5II-III	3600	1.4
β And	M0III	3839	1.5
β Gem	K0III	4844	2.5
α Hya	K3II-III	4141	2.2
α Boo	K1III	4362	2.4
γ Dra	K5III	3986	2.0
α Cet	M1.5III	3745	1.3

*This tale can be found in the AAS CD-ROM Series, Vol. 7, 1996.

μm, where the SiO fundamental is apparent in the observations but lacking in the Kurucz models. The "fit" was accomplished simply by treating the smoothed model and the smoothed composite as two independent spectral fragments that we wished to "splice." This procedure (described in detail in Paper II) involves χ^2 minimization of the sum-squared differences between the two spectral shapes, taking into account the variances of the observed points. The method provides the overall optimal scale factor for the model, and hence provides a value for the angular diameter. The results showed minimal sensitivity to sensible values of the FWHM used for the smoothing (i.e., in the range 0.1–0.3 μm).

Figure 2 illustrates the results of these direct comparisons, where we present the ratios of eight of our twelve composites (those with fullest wavelength coverage) to the optimally-scaled relevant Kurucz models. The fundamental parameters we used for the eight stars presented in these figures are summarized in Table 3. (The four spectra not shown present similar comparisons though the quality of fit is higher when we have a broader spectral range in the observations.) Apart from the SiO fundamental region ($\lambda\sim8.0$ μm), the models fit well, and the ratio spectra are essentially featureless (allowing for the 1σ absolute uncertainties in our spectra), except for deviations of order 10% through the CO fundamental ($\lambda\sim4.7$ μm) and occasional, smaller, more ambiguous, features in the CO first overtone bands ($\lambda\sim2.3$ μm). We conclude that the Kurucz models provide good predictors of stellar spectral energy distributions for these cool giants, at better than the $\pm2\%$–3% level outside the major CO and SiO absorption features, and about 5%–10% in the CO bands. We recognize that α Boo is anomalous for its spectral type by virtue of its metal-poor character, yet this appears predominantly to affect the strong bands and not the less heavily blanketed regions where the spectrum approaches the true continuum.

The discrepancies in CO might arise for a number of reasons, including our use of generic, as opposed to customized, models for these individual stars, Kurucz's use of comparatively old CO line strengths (i.e., Kirby-Docken & Liu 1978), and the omission of H_2O opacity in the Kurucz models. Further investigation will be needed to sort this out. It is interesting to note that there is no clear tendency for stars of lower temperature to have systematically greater deviations from expectation, in spite of the absence of H_2O lines from the Kurucz models. In the near future, we plan a much more extensive investigation of the influence of all the H_2O, CO, and SiO lines that must be present in these giants on their emergent spectra. The overriding impression conveyed by Fig. 2, however, is of the strong predictive power of these models in representing these observed spectra.

TABLE 4. "Header" information accompanying new α Boo composite.*

12-21-95 OBSERVED SPECTRUM OF ALPHA BOOTIS
α Boo photometry file: photometry actually used to construct the spectrum

Name	FWHM (μm)	Mag.±Unc.	Eff Wvl (Vega) (μm)	Eff Wvl (star) (μm)	F_λ W cm^{-2} μm^{-1}	Source
Kn	0.0488	-3.07±0.01	2.208	2.205	6.69E-13	Selby,Hammersley
Ln	0.1443	-3.15±0.01	3.782	3.762	9.35E-14	Selby,Hammersley
M	0.6677	-2.97±0.02	4.758	4.738	3.24E-14	Strecker *et al.* 1979
UKIRT87	0.8611	-3.13±0.01	8.770	8.779	3.43E-15	UKIRT Service data
UKIRT98	0.9455	-3.16±0.01	9.843	9.828	2.23E-15	UKIRT Service data
UKIRT11	1.1198	-3.16±0.01	11.641	11.639	1.15E-15	UKIRT Service data
UKIRT12	1.1782	-3.19±0.01	12.432	12.427	9.13E-16	UKIRT Service data

This UKIRT filter set represents a series of narrowband 10 μm passbands provided in common to UKIRT, Univ. Minnesota, and IRTF for "silicate" work. The "11" filter is centered near 11.7 μm, the "12" filter is centered near 12.5 μm.

Spectral fragments and portions of these actually used in observed spectrum ("used" may include combination with other data where overlaps occur)

Fragment	Reference	Total range (μm)	Start and stop wavelengths (μm)	Average resolving power
NIR	1	1.22–5.70	1.22–5.58	50
KAO	2	3.65–9.39	4.44–8.99	150
8–13	3	7.65–13.43	7.65–13.43	55
LRS	4	7.80–22.70	9.30–21.90	30
LONG	5	15.73–23.85	15.73–23.85	73
VLONG	6	1.25–35.00	21.80–35.00	–

References:

- 1. Strecker, Erickson, & Witteborn 1979, Ap.J. Suppl., 41, 501.
- 2. FOGS data of May 11, 1992 KAO flight [α Boo/α Lyr], and HIFOGS data of April 14, 1995 KAO flight [α Boo/α Lyr].
- 3. FOGS Mt Lemmon data of Feb. 24, 1992 [α Boo/α Lyr], CGS3 UKIRT data of May 24 and 29, 1991 [α Boo/β Peg], August 12, 1995 [α Boo/β Peg] and [α Boo/β And]. The CGS3 spectra have the greatest weight in this combined data set.
- 4. LRS raw data extracted from the new Groningen IRAS database and recalibrated with "LRSCAL" routine in "GIPSY" package.
- 5. 20 μm UKIRT CGS3 data of May 24/25, 1991 for [α Boo/β Peg].
- 6. Engelke Fn. used for T=4362K (see Blackwell, Lynas-Gray, & Petford 1991, A&A, 245, 567) and angular diameter=20.430 mas; we rescaled this to 21.12 mas. This Engelke Function was locked to the photometrically scaled combination of 8--13 and LRS spectra by splicing and used to replace the observations beyond 21.80 μm. We applied an estimated uncertainty in EFn. of 2.4%, allowing for the change in shape of the EFn. for a temperature uncertainty of 100K at this effective temperature.

INFORMATION ON SPLICES AND BIASES INCURRED

Process	Factor determined	±Bias (%)
NIR cf. photometry	1.003	0.87
813 cf. photometry	1.031	0.45
LRS blue/red bias	–	0.03
LRS splice to 813	0.950	0.02
KAO joint splice to NIR and merged 813/LRS	0.862	0.41
LONG splice to merged 813/LRS	1.124	0.66
Engelke Fn. splice to combined 813/LRS/LONG	1.017	0.40

*Actual spectra for other stars can be found in the AAS CD-ROM Series, Vol. 7, 1996.

4. STELLAR ANGULAR DIAMETERS

Table 5 (this table can also be found in the AAS CD-ROM Series, Vol. 7, 1996) summarizes four estimates of angular diameter for these stars: (i) from the multiplicative scale of the best-fitting Kurucz model appropriate to each star (as just described); (ii) from our Engelke approximations; (iii) from the independent work of Blackwell *et al.* (1990), Blackwell *et al.* (1991) using the MARCS model atmosphere code and a different absolute calibration for Vega

TABLE 5. Comparison of derived angular diameters with measured values.*

Star	Kurucz model	Our Engelke function	Blackwell *et al.* IRFM	Observed	Reference
α Tau	20.92	21.32	20.63	20.88	Ridgway *et al.* 1982
	±0.21	±0.58	±0.41	±0.10	
β Peg	16.49	16.98	16.73	16.75	Di Benedetto & Rabbia 1987
	±0.16	±0.51	±0.33	±0.24	
β And	13.47	13.71	13.22	13.81	Mozurkewich *et al.* 1991
	±0.13	±0.37	±0.26	±0.11	
β Gem	8.01	8.07	7.87	8.03	Mozurkewich *et al.* 1991
	±0.08	±0.17	±0.16	±0.08	
α Boo	20.76	21.12	20.43	20.95	Di Benedetto & Foy 1986
	±0.21	±0.51	±0.41	±0.20	
γ Dra	10.04	10.17	10.00	10.13	Di Benedetto & Rabbia 1987
	±0.10	±0.27	±0.20	±0.24	
α Cet	12.52	12.66	12.64	13.23	Mozurkewich *et al.* 1991
	±0.13	±0.36	±0.25	±0.20	
γ Cru	25.49	26.14	-	-	
	±0.25	±0.86	-	-	
α Hya	9.21	9.27	-	-	
	±0.09	±0.24	-	-	
α TrA	9.51	9.55	-	-	
	±0.10	±0.26	-	-	
μ UMa	8.16	8.32	-	-	
	±0.08	±0.28	-	-	
ϵ Car	12.39	12.67	-	-	
	±0.12	±0.33	-	-	

*This table can be found in the AAS CD-ROM Series, Vol. 7, 1996.

than our own, or Blackwell & Lynas-Gray (1994), who revised their earlier results to use the Kurucz model grid and adopted our absolute calibration of the Selby narrowbands (Paper I); and (iv) from Michelson intensity interferometry. For the latter, we have used the "true" (limb-darkened) angular diameters (as opposed to those based on interpretation of the observed visibility fringes with the "uniform diameter" assumption). Details of the calculations used to convert observed to true angular diameters are presented by Di Benedetto & Rabbia (1987), Mozurkewich *et al.* (1991), and in the more recent summary by Di Benedetto (1993). For α Tau, there is also an extensive series of measurements based upon lunar occultations (see White & Feierman 1987) with the best weighted value for this star being 20.88 mas (Ridgway *et al.* 1982). (In the lower part of Table 5, we have included the five stars apparently without direct observations, or IRFM-based estimates of diameter.) There is good accord between all four estimates for the seven stars for which all this information is available. The existence of such an accord makes a profound statement because each estimate is based on a very different spectral region. Our match to Kurucz models assesses the quality of fit over each entire composite (excluding the SiO fundamental), but this effectively assigns greatest weight to the shorter wavelengths (below ~7.5 μm), where our total uncertainties are relatively small. By contrast, our Engelke approximations are fitted to the observed spectra longward of the SiO fundamental, typically beyond 12 μm. Blackwell and colleagues treat only narrowband photometry in the 1.2–3.8 μm region. Yet all these methodologies agree with the direct observations within the stated errors, and the technique of matching generic Kurucz models to composites provides meaningful diameters and formal uncertainties in these diameters.

The third column in Table 5 presents the most recent determination of angular diameter by Blackwell and colleagues for each of these stars. This corresponds to the Blackwell *et al.* (1991) paper for all stars except β Gem, for which Blackwell & Lynas-Gray (1994) provide a new value of 8.03 mas with a methodology that is closest to our own (Kurucz models; our calibration of the Selby passbands). This value is essentially identical to our own diameter (8.01 mas). Unfortunately, these authors have not published similarly recalibrated diameters for the other stars in Table 5. It is difficult to make accurate estimates of what values they would have obtained by application of their most recent method but, based on β Gem, their diameters would have been quite close to our values.

We note from Table 5 that the Kurucz models lead to systematically smaller angular diameters than indicated by the observations. We can speculate on possible causes of this phenomenon but we cannot fully account for it in the present paper. Several factors may contribute. First, the particular technique used here is designed to treat stars as though we lacked individual knowledge of their fundamental parameters, including elemental and isotopic abundances (in readiness for application of the generic "template" scheme in the future). Perhaps, in this manner, or through our effective temperature-spectral class transformation, we have systematically misrepresented the actual stars. Second, perhaps our attempt to fit the entire observable spectral region, without the SiO fundamental, has made our result more vulnerable to any inadequacies in the representation of the absorption strengths of the myriad molecular lines. (Recall in particular that the Kurucz and MARCS models do not include the potentially important H_2O opacity.) Use of a different scheme which weights the relative continuum portions of the spectrum more heavily might lead to more secure diameters. However, even this is unclear since the fluxes in these "continuum" regions are affected in reality both by a veil of molecular lines and by the brighter true continuum levels which arise when deeper atmospheric layers are heated by line blanketing. The Selby narrowband filters used to support the IRFM have isophotal wavelengths close to 1.25, 2.21, and 3.78 μm (logarithmic values of 0.10, 0.34, 0.58). These tend to correspond to local maxima close to unity in the ratio plots shown in Fig. 2. Therefore, basing our scaling of models on the fluxes at these wavelengths might improve the agreement with the observations.

The diameters implied by the Engelke approximations are generally bigger than those from using real models. This arises because Engelke functions are essentially Rayleigh–Jeans in character in the domain in which we employ them, whereas true model spectra decline more slowly with increasing wavelength. Therefore, to match the level of a given observed spectrum, one requires larger scale factors for Engelke functions.

It is worth emphasizing that the diameters derived from both the Kurucz and MARCS models generally accord, at the 1σ level, with the observed diameters. This level of agreement implies discrepancies in diameter at only the 1% level, yet Blackwell & Lynas-Gray (1994) estimated conservative uncertainties in diameters derived by the IRFM of 4%. It is interesting that neither model grid reproduces the observed subtense of α Cet, but one must recall that angular diameters of resolved stars depend on limb darkening corrections to derive the "true" diameter from the observed. Such corrections might plausibly be suspect on very cool giants such as α Cet. An informative discussion of the complexity

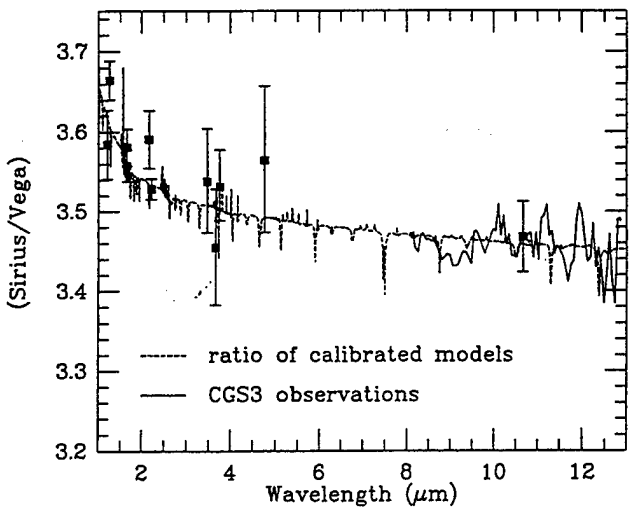

FIG. 3. Ratio of calibrated models of Sirius and Vega (short dashed line), compared with CGS3 direct spectral observations (solid line), and with the measured broad and narrowband ratios (filled squares with $\pm 1\sigma$ error bars) in well-characterized infrared photometric bandpasses.

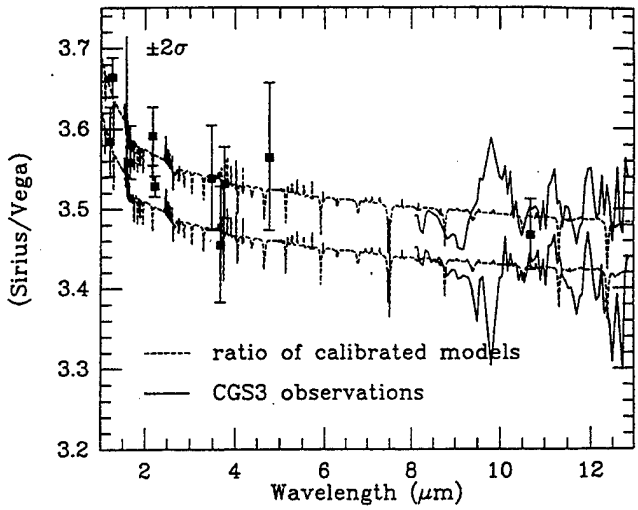

FIG. 4. As for Fig. 3, but now combining direct and indirect CGS3 spectroscopy of Sirius/Vega, and illustrating the $\pm 2\sigma$ bounds on the ratio of the model spectra.

of limb-darkening in cool photospheres may be found in Scholtz & Takeda (1987).

Finally, for γ Cru, our angular diameter is quite different from the 41.1 mas cited by Judge & Stencel (1991). However, their value was an indirect one, based upon adopting colors similar to those of other very cool M giants and applying relations due to Barnes *et al.* (1978) between color and visual surface flux (Stencel 1996; cf. Judge & Stencel 1991, Appendix A, Sec. 2, last sentence).

5. THE SPECTRAL RATIO OF SIRIUS/VEGA

The derivation of plausible angular diameters from our composites provides external validation of their accuracies. This, in turn, vindicates the procedures we have devised to assemble composite spectra. The derivation (Paper VI) of an angular diameter for α^1 Cen, that is consistent with the literature for that star, is a further indirect check on the adopted, calibrated model for Sirius. As a final cross check on the overall scheme we have sought data not used in Paper I on the ratio of Sirius to Vega. Two kinds of data are of value: independent photometric measurements of Sirius compared with Vega; and the ratio of their spectra.

Our calibration of the Kurucz Sirius model relative to the calibrated model for Vega (Paper I) was based upon the bolometry of Cohen & Barlow, published by Deacon (1991). Therefore, we sought other well-characterized photometric systems for which the difference in magnitude between these hot stars has been measured. We require detailed cold-scanned filter transmission profiles for these systems, and we have applied an atmosphere appropriate to each site (cf. Paper I). Of particular value are data by Carter (1996: detailed in Paper VIII) in the *SAAO JHKL* system [as characterized for us by Glass (private communication)], and by Hammersley (1995: *JHK*; to be represented in detail in Paper VIII) and Alonso *et al.* (1994: *JHKL'*) in the Tenerife broadband InSb passbands. The *JHK* data of Alonso *et al.* are already included in Hammersley's reanalysis of the entire photometric archive of the Telescopio Carlos Sanchez (Paper VIII) so only these authors' L' result is separately represented here. Additional photometry can be found in Sinton & Tittemore (1984) using L' and M passbands which, from their descriptions, are identical with the UKIRT bolometer passbands of the same name that we calibrated in Paper I (although Sinton and Tittemore's measurements were never used in Paper I). We emphasize that we have taken great pains to avoid circularity: we do not use our expectation for Sirius' magnitudes in these passbands from a recalibration of the authors' systems, but focus strictly on the observed differences in magnitude as measured by these authors. Figure 3 illustrates the ratios equivalent to each of these magnitude differences between Sirius and Vega. Filled squares represent the photometry with $\pm 1\sigma$ error bars, defined as the root-sum-square of the observed magnitude uncertainties of these two stars, in each passband. Points are plotted at their isophotal wavelengths (almost identical in these bands for Sirius and Vega: cf. Paper I). The longest wavelength point plotted in Fig. 3 and 4 is the high precision measurement made by *IRAS* at 12 μm (from Table VI.C.3 in the *IRAS* Explanatory Supplement 1988).

We wish to make a comparison of our adopted ratio of the two model spectra, and to assign meaningful uncertainties to their ratio. The relevant uncertainty for the spectral ratio of Sirius to Vega is the uncorrelated error, rather than the underpinning 1.45% absolute uncertainty in Vega's calibration which is directly transferred, as a bias (a correlated uncertainty), when we calibrated Sirius relative to Vega. If we assign uncertainties of $\pm 0.01^{\rm m}$ to each of Deacon's magnitudes, then the root-sum-square of these random errors with the small bias associated with locking the Sirius model to the expected photometry of Deacon, yields a conservative estimate of $\pm 0.5\%$. Figure 4 compares this photometry with the $\pm 2\sigma$ bounds in the mean ratio of our adopted calibrated spectra for these stars (short dashed lines). The photometry points appear to follow the upward trend (with decreasing wavelength) in the models' spectral ratio very well. This is

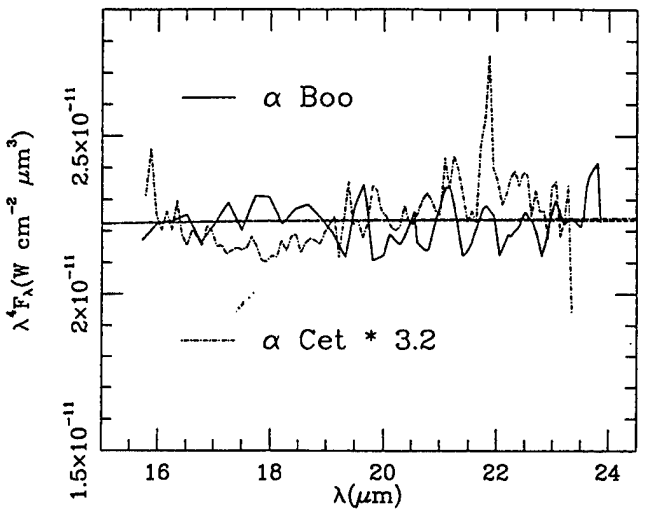

FIG. 5. Further evidence for the Rayleigh–Jeans character of cool stellar spectra in the form of spectral "flatness" in $(\lambda,\lambda^4 F_\lambda)$ space. UKIRT CGS3 16–24 μm spectra for α Boo (unscaled, solid line) and α Cet (scaled by a factor 3.2, dash-dot line) are compared with their relevant Engelke approximations (dashed lines across the middle of the plot). That for α Boo appears slightly above that for α Cet.

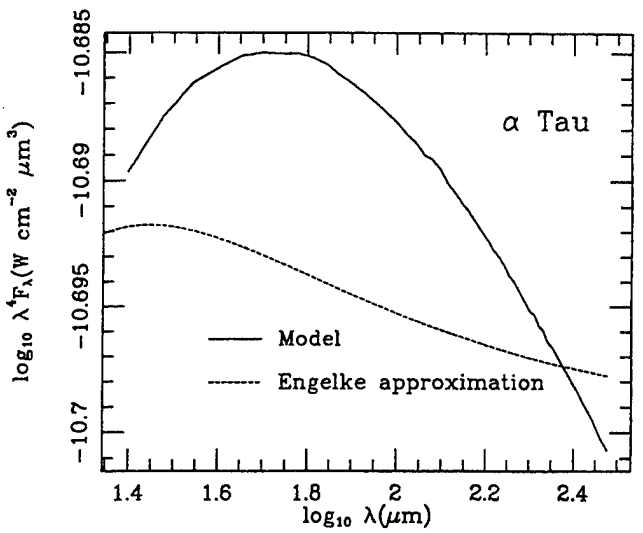

FIG. 6. Far-infrared model continuum extrapolation (solid line) of our α Tau composite, compared with the extrapolated Engelke approximation (short dashed line) for this star. The maximum difference between these two spectra occurs near 65 μm, where it attains almost 2%.

entirely due to differences in the two adopted stellar effective temperatures.

What observational spectroscopic evidence can we adduce in support of our models' ratio? There are two kinds of measurement to discuss, because it is a challenging observation to secure spectra of Sirius and Vega in a single night. Given data on the two stars in one night, one can construct the direct spectral ratio. The second, indirect, measurement of spectral ratio that we consider is formed by use of intermediate stars, so that one compares an airmass-matched ratio (cf. Papers II, V) of Sirius to a bright star, and of Vega to the same bright star, also matched in the airmasses of observation. The indirect method offers the advantage of being able to choose good bright intermediaries and to secure close matches in airmass, at the cost of added noise in the eventual ratio of Sirius to Vega, attendant on the products or quotients of these intermediate ratio spectra.

We have found one direct measurement of Sirius to Vega from the UKIRT archives. This is constructed from 10 μm spectra taken with the CGS3 spectrometer, by Skinner and Sylvester on 1992 October 4, and kindly furnished for our use by Sylvester (1996). The two stars were not closely matched in airmass (Vega $z=1.29$; Sirius $z=1.55$). Consequently, the short-wavelength edge was lost to water vapor differences and the 9.6 μm telluric ozone feature was uncanceled. This necessitated deletion of the affected data (7.5–7.7 and 9.75–9.9 μm). The resulting spectrum was normalized using photometry from Deacon (1991) in the UKIRT 8.7 μm "narrowband" filter. Figure 3 presents this direct spectral ratio, as the simplest comparison we can make with the models' ratio.

To enhance signal to noise, we needed to secure additional indirect spectral ratios, so we sought airmass matching with bright intermediaries. Two such indirect routes are available to us from the UKIRT CGS3 archives. One involves the quotient of ratios of spectra, [β Peg/α Lyr] (1995 August 12) and [β Peg/α Tau] (1993 November 4 and 5), from which we derive an estimate of the spectral ratio [α Tau/α Lyr]. The second similarly involves [β And/α Lyr] (1995 August 11 and 12) and [β And/α Tau] (1993 August 28), whose quotient gives another estimate of [α Tau/α Lyr]. We combined these two ratio spectra (with inverse-variance weighting) to yield a cleaner [α Tau/α Lyr], which we divided by our published ratio of [α Tau/α CMa] (from 1991 November 9: Fig. 4 of Paper III), to create [α CMa/α Lyr]. Finally, we combined this indirect ratio (which has broader wavelength coverage than the direct method because of the close matching in airmasses of the quotient spectra) with the direct approach, using inverse variance weighting. Essentially the same spectral ratio results as from the direct measurement alone, but now it is seen with higher signal to noise and over a larger and more completely sampled wavelength interval. The resulting ratio spectrum appears in Fig. 4, where we have indicated the $\pm 2\sigma$ bounds on this observed spectrum, exactly as shown for the ratio of model spectra. The two $\pm 2\sigma$ swathes (model and CGS3) overlap significantly.

Therefore, we conclude that both independent photometry and spectroscopy support the ratio of our two, independent, adopted models for the spectra of Sirius and Vega.

6. THE BEHAVIOR OF REAL GIANT STARS FROM 10 TO 35 μm

The agreement between cols. (1) and (2) of Table 5 suggests that the simplistic Engelke function is a reasonable approximation to the general shape of emergent spectra predicted by fully detailed model atmosphere calculations. Closer inspection reveals that the diameter implied by the Engelke approximations is invariably larger than that from matching to real models. This happens because Engelke functions decline slightly faster with wavelength than model spectra, and therefore require slightly greater multipliers to match a given observed spectrum. What of real stars?

Only two normal giant stars, α Tau and γ Cru, were observed by Glaccum (1990) from the *KAO*, and these spectral fragments owe their shapes to standard planetary absolute calibration techniques (Paper II; Moseley *et al.* 1989). These two stars do seem to behave in a Rayleigh–Jeans fashion once the spectrum rises out of the strong SiO fundamental absorption; i.e., in $\lambda^4 F_\lambda$ space, their observed spectra are essentially independent of wavelength beyond about 12 μm. Additional support for the observed "flatness" of real stellar spectra in this space (Figs. 1 and 2) comes from our CGS3 20 μm spectra taken at the UKIRT and, to a lesser extent (due to the noise at the longest wavelengths), from the LRS too (cf. for α Tau in Fig. 11 and 12 of Papers II; for γ Cru, Fig. 5, and β And, Fig. 6, both in Paper IV). In the present paper, we adduce additional evidence for the Rayleigh–Jeans nature of real stellar spectra from 20 μm CGS3 spectra of α Boo and α Cet. These are compared, in Fig. 5, with the relevant Engelke approximations. The spectral "flatness" is emphasized by these direct plots of the calibrated stellar spectra in $\lambda^4 F_\lambda$ space.

7. SYNTHESIZING IRAS 12/25 μm FLUX DENSITIES

We hoped further to probe this apparent and persistent discrepancy between the long-wavelength (beyond $\sim$12 μm) behavior of real and model stars, by comparing our composite spectra with *IRAS* observations. Every composite is fundamentally built from observations based on our model spectra for Sirius and Vega. Therefore, we would expect to conclude in favor of the same "recalibration" factors for *IRAS* flux densities deduced from photometry alone in Paper I, by use of *IRAS* flux densities synthesized from our composites, unless real stars deviated significantly from Rayleigh–Jeans slopes. The procedure is straightforward, requiring only the integration of the *IRAS* system response functions for the 12 and 25 μm passbands over our spectral composites, and direct comparison with the *IRAS* in-band fluxes, and the flux densities derived from these upon division by the bandwidths (cf. Paper I).

Table 6 (also found in the AAS-CD-ROM Series, Vol. 7, 1996) summarizes the results of these direct comparisons with the *IRAS* Faint Source Survey (Moshir *et al.* 1992), reputedly of higher quality than the *IRAS* Point Source Catalog (1988: hereafter referred to as PSC) fluxes, and with the PSC itself. Table 6 incorporates both the uncertainties that attend our derived fluxes and those inherent in the *IRAS* measurements ("RELUNC" quantities in these catalogs). The comparison suggests that these *IRAS* point source products overestimate 12 and 25 μm flux densities by statistically the same amount in the PSC and the FSS, namely, by 4.1% at 12 and by 5.7% at 25 μm. From this we conclude that our spectral composites, based on the calibrated spectra of Sirius and Vega (Paper I), represent self-consistent products because these factors for *IRAS*'s calibration, derived here from cool stellar spectra (0.96 ± 0.01 and 0.94 ± 0.01), are in accord (at the 1σ level) with those determined purely from our basis models for Sirius and Vega (12 μm: 0.98 ± 0.01; 25: 0.94 ± 0.02). It is also tempting to conclude that, in the ensemble average, *IRAS* measurements vindicate the essentially Rayleigh–Jeans character of the infrared photospheric emission from these cool giants in the 7–35 μm range, although the actual *IRAS* uncertainties on any star are too large to reach this conclusion for an individual object.

TABLE 6. Ratios of *IRAS* flux densities synthesized by integration of the *IRAS* passbands over our observed composite spectra (12,25 μm), extrapolated by model atmospheres (60,100 μm), to those actually observed by *IRAS*.*

IRAS data	12 μm	σ	25 μm	σ	60 μm	σ	100 μm	σ
FSS	0.961	0.012	0.946	0.013	0.997	0.015	1.038	0.040
PSC	0.961	0.010	0.943	0.010	0.985	0.029	1.015	0.026

*This table can be found in the AAS CD-ROM Series, Vol. 7, 1996.

8. EXTRAPOLATION OF COMPOSITES TO 300 μm

The 35 μm limit of our standard composite spectra does not afford the same test with longer wavelength *IRAS* data. Consequently, we have adopted the emergent spectral shapes of a grid of mid- to far-infrared continuum models of red giant branch stars, computed as described below. We interpolated in this grid to provide a model that matched the correct effective temperature for each composite (and we assumed the red giant branch gravities interpolated were correct for our observed giants). The attributes of the giants come from VandenBerg & Laskarides (1987) and are close to the expected gravities for our giants. By fitting these shapes to the *observed portions* of composites, longward of the SiO fundamental's influence, but shortward of the wavelength where we chose to replace noisy data by Engelke functions, we created best-fitting extensions of each composite.

In order to obtain representative effective temperature-log(gravity) ($T_{\rm eff}$,log g) combinations for the late-K and early-M giant branch stars of the disk in our observed sample, we adopted the theoretical red giant branch tracks computed by VandenBerg & Laskarides (1987). We chose the particular track with the following model parameters: $\mathcal{M}/\mathcal{M}_\odot=1.3$; $Y=0.25$; $Z=0.0169$; [M/H]=0.0.

Stellar evolution models with these parameters have an age of 5.28 Gyr at the He flash and, thus, should be reasonably representative of evolved stars of the disk. To obtain the ($T_{\rm eff}$,log g) needed for the stellar model atmosphere calculations, we selected three combinations of ($T_{\rm eff}$,log g), spaced by 500 K, on the aforementioned VandenBerg & Laskarides track: (4500,2.86), (4000,1.87), and (3500,0.975).

To obtain a model which might be appropriate for the hottest star in our sample, β Gem, we adopted the specific parameters of $T_{\rm eff}=4844$ K and log $g=2.24$, which are in excellent agreement with the analyses of this star by Blackwell & Lynas-Gray (1994), Di Benedetto (1993), and Ruland *et al.* (1980).

To obtain the temperature vs. continuum optical depth at 1 μm relations [$T(\tau^c_{1\ \mu{\rm m}})$], needed to compute emergent fluxes for our four desired models, we began with published model grids and proceeded in the following fashion for each of the desired models:

(1) the temperature–pressure relation of the grid model

nearest in $T_{\rm eff}$ and log g to the desired model was used to obtain the grid model's $T(\tau^c_{1\ \mu m})$;

(2) the grid model's $T(\tau^c_{1\ \mu m})$ relation was then scaled by the ratio $T_{\rm eff}$(desired)/$T_{\rm eff}$(grid model). The validity of this procedure over moderate ranges in $T_{\rm eff}$ has been demonstrated by Carbon & Gingerich (1969) and Gustafsson *et al.* (1975);

(3) and, finally, using the resultant $T(\tau^c_{1\ \mu m})$, the equation of hydrostatic equilibrium was reintegrated using the log g of the desired model.

All the calculations were carried out using the set of solar abundances adopted by the authors of the respective model grids.

For the three coolest models, (4500,2.86), (400,1.87), and (3500,0.975), we interpolated in the model atmosphere grid published by Brown *et al.* (1989). For the β Gem model, (4844,2.24), we interpolated in Kurucz's (1991, 1993) model grid to obtain the required T–P relation. For each of the four models, we computed continuum spectral energy distributions at 101 wavelengths from 1.0 to 300 μm using the SOURCE model atmosphere program described in Carbon *et al.* (1982). For *ISO* purposes, we created products gridded every 5 μm from 25 to 300 μm to supplement and extend our absolute calibrated composites out to the longest wavelengths relevant to *ISO*.

We assessed uncertainties in these extrapolations based on the recent study of the sensitivity of far-infrared continua to fundamental stellar parameters by van der Blieck *et al.* (1996). Explicitly, at 100 μm, these are ~2% (corresponding to ±100 K in effective temperature), ~0.2% (±0.3 in log g), and ≤1% (±0.2 in metallicity). In fact, as these authors point out, errors in gravity are even greater for late-type giants than for ensembles of warmer stars, typically attaining ±0.5 in log g. Van Blieck *et al.* (1996) also simulated chromospheres and considered the influence of circumstellar dust. We examined their estimates for uncertainties in far-infrared flux due to errors in fundamental parameters, in temperature structure, and other causes, and adopted 4.8% as typical for the root-sum-square combination of all these components for the mid-G to early-M giants they considered. To these we have appended an extra 3% to account for the typical expected contributions to the spectra of molecular line blanketing due to the copious lines of water vapor, CO, and SiO, and their isotopes.

9. SYNTHESIZING IRAS 60/100 μm FLUX DENSITIES

These extrapolated composites permit integration over the 60 and 100 μm *IRAS* bands. Table 6 presents the results of direct comparison of long-wavelength flux densities synthesized from our spectra with those measured by *IRAS*. In spite of the rather larger relative uncertainties, "RELUNCs," associated with the *IRAS* long-wavelength measurements we can, nevertheless, determine from this ensemble of composites that *IRAS* measurements are consistent with our calibrated observed spectra, extrapolated through theoretical model atmospheres.

It is, perhaps, also of interest to examine the long-wavelength quality of the simplistic Engelke approximations. The absolute difference in emergent spectra of these giants, between their best-fit Engelke approximations and our grid of far-infrared continua, is always small. In fact, as Fig. 6 illustrates, for α Tau it amounts to a mere 2% over the range 25–200 μm. For the set of 12 composites now available, this maximum difference between Engelke approximations and model continua lies in the range 2%–5%, and always occurs between 60 and 70 μm. As a further test, we also continuedthe same Engelke functions that best fitted each composite (see Papers IV, VI, and this paper) to wavelengths long enough to synthesize *IRAS* flux densities by integrating these extended spectra over the long *IRAS* system passbands. The corresponding ratios of synthetic 60 and 100 μm flux densities predicted by Engelke functions to those observed by *IRAS* (the FSS) are: 0.964±0.013 (60 μm) and 0.976±0.037 (100 μm). These should be compared with the corresponding numbers in the first line of Table 6. Differences are only at the 1.6σ level, so we could not discriminate statistically between Engelke approximations and true models of the infrared continuum solely on the basis of *IRAS* flux densities. The fundamental limitation again lies in the "RELUNCs."

10. CONCLUSIONS

We have assembled absolutely calibrated, complete, continuous stellar spectra for five cool stars: α Boo (updated), γ Dra, α Cet, γ Cru, and μ UMa. These spectra are constrained by carefully characterized photometry and have an estimated absolute uncertainty (within our adopted absolute framework: Paper I) of order 3% (1σ) across most of the 1.2–35 μm range. Such spectra establish the pedigree for secondary stellar standards and thereby the flexibility to calibrate arbitrary filter systems and sensors on the ground, from airplanes, or satellites. We find good agreement in shape between these spectra and generic Kurucz model atmosphere spectra, with the obvious exception of the SiO fundamental and some systematic small (~10%) deviations associated with the CO fundamental. Stellar angular diameters derived from our spectra are in accord with directly measured diameters.

Using a grid of computed stellar model continua, we have extrapolated our observed spectra as far as 300 μm, maintaining our absolute context, to provide calibration support for the *ISO* PHT and LWS instruments. Tests of these extrapolations using *IRAS* 60 and 100 μm point source flux densities show consistency with our predictions. The composite spectra with their associated pedigree files will appear on an AIP Journal CD-ROM and eventually will be obtainable through NASA's NSSDC at Goddard Space Flight Center.

We are grateful for the invaluable legacy of NASA's Airborne Astronomy program and to the staff of the former *KAO* program for their support throughout the flights dedicated to this calibration work. We thank Phillips Laboratory for its ongoing support of this effort through Dr. S. D. Price under Contract No. F19628-92-C-0090 with JS&E, Inc., and NASA for partial support through a subcontract with the University of Florida at Gainesville under Grant No. NAGW-4201. M. C. thanks NASA-Ames Research Center

for partial support under Co-Operative Agreement NCC 2-142 with UC Berkeley. We are grateful to Drs. D. Strecker and W. Glaccum for providing access to their uniquely valuable *KAO* archives of stellar spectra, to Dr. R. Kurucz for his ongoing help and guidance, and to the UKIRT Service Observing program for providing us with high-quality 10 (and 20) μm CGS3 spectra that constitute a vital part of our observational spectral archive. It is a pleasure to thank those of our colleagues who contributed their own CGS3 spectra to this effort, namely, Professor M. J. Barlow and Drs. T. Geballe, M. Hanner, C. Dudley, C. Skinner, and R. Sylvester. We thank Dr. P. Wesselius of SRON, Groningen, for providing NASA-Ames with its copy of the "LRSVAX" archive which constitutes a vital resource in our ongoing effort in infrared calibration.

REFERENCES

Alonso, A., Arribas, S., & Martinez-Roger, C. 1994, A&A, 282, 684
Barnes, T. G., Evans, D. S. & Moffett, T. J. 1978, MNRAS, 183, 285
Blackwell, D. E., & Lynas-Gray, A. E. 1994, A&A, 282, 899
Blackwell, D. E., Lynas-Gray, A. E., & Petford, A. D. 1991, A&A, 245, 567
Blackwell, D. E., Petford, A. D., Arribas, S., Haddock, D. J., & Selby, M. J. 1990, A&A, 232, 396
Brown, J. A., Johnson, H. R., Alexander, D. R., Cutright, L. C., & Sharp, C. M. 1989, ApJS, 71, 623
Carbon, D. F., & Gingerich, I. 1969, in Theory and Observations of Normal Stellar Atmospheres, edited by O. Gingerich (MIT Press), p. 377
Carbon, D. F., Langer, G. E., Butler, D., Kraft, R. P., Trefzger, Ch. F., Suntzeff, N. B., Kemper, E., & Romanishin, W. 1982, ApJS, 49, 207
Carter, B., 1996 (an Appendix in Paper VIII)
Cohen, M., & Davies, J. K. 1995, MNRAS 276, 715 (Paper V)
Cohen, M., Walker, R. G., Barlow, M. J., & Deacon, J. R. 1992a, AJ, 104, 1650 (Paper I)
Cohen, M., Walker, R. G., Carter, B., Hammersley, P. L., Kidger, M., & Noguchi, K. 1996b, in preparation (Paper VIII)
Cohen, M., Walker, R. G., & Witteborn, F. C. 1992, AJ, 104, 2030 (Paper II)
Cohen, M., Witteborn, F. C., Bregman, J., Wooden, D., Salama, A., & Metcalfe, L. 1996a, AJ, 112, 241 (Paper VI)
Cohen, M., Witteborn, F. C., Carbon, D. F., Augason, G. C., Wooden, D., Bregman, J., & Goorvitch, D. 1992b, AJ, 104, 2045 (Paper III)
Cohen, M., Witteborn, F. C., Walker, R. G., Bregman, J., & Wooden, D. 1995, AJ, 110, 275 (Paper IV)
Deacon, J. R. 1991, Ph.D. distertation, University College London
Di Benedetto, G. P. 1993, A&A, 270, 315
Di Benedetto, G. P., & Rabbia, Y. 1987, A&A, 188, 114
Engelke, C. W. 1992, AJ, 104, 1248
Gezari, D. Y., Schmitz, M., Pilts, P.S., & Mead, O. M. 1993, "Catalog of Infrared Observations," 3rd. ed., NASA RP-1294.
Glaccum, W. 1990, Ph.D. dissertation, University of Chicago
Gustafsson, B., Bell, R. A., Eriksson, K., & Nordlund, A. 1975, A&A, 42, 407
Hammersley, P. L. 1995 (an Appendix in Paper VIII)
Hoffleit, D., & Warren, Jr., W. H. 1991, Yale Bright Star Catalog, 5th revised ed. (NSSDC)
IRAS Explanatory Supplement 1988, "*IRAS* Catalogs and Atlases. Volume 1," NASA RP-1190 (GPO, Washington, DC)
IRAS Point Source Catalog, version 2, 1988, "*IRAS* Catalogs and Atlases. Volumes 2–6," NASA RP-1190 (GPO, Washington, DC) (PSC)
de Jager, C., & Nieuwehuizen, H. 1987, A&A, 177, 217
Judge, P. G., & Stencel, R. S. 1991, ApJ, 371, 357
Kholopov, P. N., *et al.* 1992, General Catalogue of Variable Stars, 4th ed. .(Mauka Publishing House, Moscow)
Kirby-Docken, K., & Liu, B. 1978, ApJS, 36, 359
Kurucz, R. L. 1991, "New lines, new models, new colors," in Precision Photometry: Astrophysics of the Galaxy, edited by A. G. Davis Philip, A. R. Upgren, and K. A. Janes (L. Davis Press, Schenectady), p. 27
Kurucz, R. L. 1993, CD-ROM series; "ATLAS9 Stellar Atmosphere Programs and 2 km/s grid" (Kurucz CD-ROM No. 13); "SYNTHE Spectrum Synthesis Programs and Line Data" (Kurucz CD-ROM No. 18)
Lord, S. D. 1992, "A New Software Tool for Computing the Earth's Atmospheric Transmission of Near-Infrared and Far-Infrared Radiation," NASA TM-103957
Moseley, S. H., Dwek, E., Glaccum, W., Graham, J. R., Loewenstein, R. F., & Silverberg, R. F. 1989, ApJ, 347, 1119
Moshir, M., *et al.* 1992, Explanatory Supplement to the *IRAS* Faint Source Survey, Version 2, JPL D-10015 JPL, Pasadena
Mozurkewich, D., Johnston, K. J., Simon, R. S., Bowers, P. F., & Gaume, R. 1991, AJ, 101, 2207
Ridgway, S. T., Jacoby, G. H., Joyce, R. R., Siegel, M. J., & Wells, D. C. 1982, AJ, 87, 1044
Ruland, F., Biehl, D., Holweger, H., Griffin, R., & Griffin, R. 1980, 92, 70
Scholtz, M., & Takeda, Y. 1987, A&A, 186, 200
Selby, M. J., Hepburn, I., Blackwell, D. E., Booth, A. J., Haddock, D. J., Arribas, S., Leggett, S. K., & Mountain, C. M. 1988, A&AS, 74, 127
Sinton, W. M., & Tittemore, W. C. 1984, AJ, 89, 1366
Stencel, R. S. 1996 (private communication)
Strecker, D. W., Erickson, E. F., & Witteborn, F. C. 1979, ApJS, 41, 501
Sylvester, R. 1996 (private communication)
VandenBerg, D.A., & Laskarides, P. G. 1987, ApJS, 64, 13
van der Blieck, N. S., Gustafsson, B., & Eriksson, K. 1996, A&A (in press)
Witteborn, F. C., & Bregman, J. D. 1984, Proc. Soc. Photo-Opt. Instr. Eng., 509, 123
White, N. M., & Feierman, B. H. 1987, AJ, 94, 751
Witteborn, F. C., Cohen, M., Bregman, J. D., Heere, K. R., Greene, T. P., & Wooden, D. H. 1995, in Proceedings of the Airborne Astronomy Symposium on the Galactic Ecosystem, edited by M. Haas, E. F. Erickson, and J. Davidson (in press)
Wooden, D. H. 1989, in Proceedings of ESO SIPC Workshop, SN 1987A and Other Supernovae, edited by I. J. Danziger and K. Kjar (ESO, Garching), p. 531

THE ASTRONOMICAL JOURNAL, 115:1671–1679, 1998 April

SPECTRAL IRRADIANCE CALIBRATION IN THE INFRARED. VIII. 5–14 MICRON SPECTROSCOPY OF THE ASTEROIDS CERES, VESTA, AND PALLAS

MARTIN COHEN
Radio Astronomy Laboratory, 601 Campbell Hall, University of California at Berkeley, Berkeley, CA 94720; and Vanguard Research, Inc., Suite 204, 5321 Scotts Valley Drive, Scotts Valley, CA 95066; mcohen@astro.berkeley.edu

FRED C. WITTEBORN
Space Science Division, Mail Stop 245-6, NASA Ames Research Center, Moffett Field, CA 94035; witteborn@aol.com

TED ROUSH
Space Science Division, Planetary Systems Branch, Mail Stop 245-3, NASA Ames Research Center, Moffett Field, CA 94035; and Department of Geosciences, San Francisco State University, 1600 Holloway Avenue, San Francisco, CA 94132; roush@barsoom.arc.nasa.gov

AND

JESSE BREGMAN AND DIANE WOODEN
Space Science Division, Mail Stop 245-6, NASA Ames Research Center, Moffett Field, CA 94035; bregman@ssa1.arc.nasa.gov, wooden@ssa1.arc.nasa.gov

Received 1997 May 23; revised 1997 December 31

ABSTRACT

We describe our efforts to seek "closure" in our infrared absolute calibration scheme by comparing spectra of asteroids, absolutely calibrated through reference stars, with "standard thermal models" and "thermophysical models" for these bodies. Our use of continuous 5–14 μm airborne spectra provides complete sampling of the rise to, and peak, of the infrared spectral energy distribution and constrains these models. Such models currently support the absolute calibration of the *Infrared Space Observatory* Imaging Photopolarimeter (ISOPHOT) at far-infrared wavelengths (as far as 300 μm) and contribute to that of the Mid-Infrared Spectrometer on the *Infrared Telescope in Space* in the 6–12 μm region. The best match to our observed spectra of Ceres and Vesta is a standard thermal model using a beaming factor of unity. We also report the presence of three emissivity features in Ceres that may complicate the traditional model extrapolation to the far-infrared from contemporaneous ground-based *N*-band photometry that is used to support calibration of, for example, ISOPHOT. While identification of specific materials that cause these features is not made, we discuss families of minerals that may be responsible.

Key words: infrared radiation — minor planets, asteroids

1. INTRODUCTION

There are very few published midinfrared (MIR; 7–14 μm) spectroscopic investigations of asteroids (e.g., Gillett & Merrill 1975; Hansen 1976; Feierberg, Witteborn, & Lebofsky 1983; Green et al. 1985), and earlier studies usually presumed that their stellar "calibrators" radiated like blackbodies, thereby introducing spurious emission features, typically corresponding to neglect of the SiO fundamental absorption in stellar photospheres (Cohen et al. 1992c). Now that we have established rigorous stellar calibration spectra between 1.2 and 35 μm for a set of secondary IR standards (Cohen et al. 1992a; Cohen, Walker, & Witteborn 1992b; Cohen et al. 1992c; Cohen et al. 1995; Cohen & Davies 1995; Cohen et al. 1996a, 1996b; hereafter Papers I–VII, respectively), we examine our airborne asteroid spectra, which we have archived as ratios of asteroidal to stellar spectra.

Their proximity to Earth and low surface temperatures make asteroids far brighter in the MIR and far-infrared (FIR) than normal stars, leading to consideration of their potential role as flux calibrators. Our interest in their spectra, therefore, stems partly from a need to intercompare absolute calibration based on stars and on asteroids. The NASA Ames HIFOGS spectrometer (Witteborn et al. 1995), working from the Kuiper Airborne Observatory (KAO), offered coverage of the otherwise inaccessible 5–8 μm regime. Without complete observation both of the rapid rise of flux density with wavelength and of the peak in the infrared spectral energy distribution, it is impossible to constrain models of the thermal emission from asteroids.

Continuum thermal models of asteroids (e.g., Morrison 1973; Jones & Morrison 1974; Matson, Veeder, & Lebofsky 1978; Morrison & Lebofsky 1979; Lebofsky et al. 1986; Lebofsky & Spencer 1989) are, therefore, highly relevant to the absolute calibration of both the *Infrared Space Observatory* (*ISO*) (Kessler et al. 1997) and of the Mid-Infrared Spectrometer (MIRS; Roellig et al. 1994) on the joint ISAS-NASA *Infrared Telescope in Space* (*IRTS*). The newest data on Ceres that we present in this paper were secured on KAO flights while *IRTS* was in orbit and observing the sky. Therefore, these spectra offer vital calibration information for MIRS because Ceres is much brighter longward of about 7 μm than the normal stars that we have provided for the calibration of MIRS and its near-infrared counterpart on *IRTS*. Both the photometer (ISOPHOT) and the long-wavelength spectrometer (LWS) on *ISO* have observed asteroids, including Ceres, to provide absolute flux calibration beyond about 50 μm and as far as 300 μm (although the basis for calibration of the LWS was switched to planets, notably Uranus and Neptune). It is no longer possible to secure contemporaneous airborne infrared spectroscopy or 50–150 μm radiometry to support satellite sensors. Therefore, one must either place complete reliance on thermal models of asteroids or, at least, extrapolate from ground-based 10 (and/or 20) μm broadband measurements to these very long wavelengths using such models. Our

investigation of the spectrum of Ceres, in particular, was designed to explore how accurately such "standard thermal models" (STMs) can predict the observed asteroidal spectral energy distributions.

There have been a few reports in the literature of structure in the thermal spectra of asteroids (e.g., Feierberg et al. 1983). We had hoped to identify the specific surface mineralogy of several of these rocky bodies through such infrared signatures but were able to observe only Ceres at sufficiently high signal-to-noise ratio on the KAO to seek features.

We offer a pragmatic way to predict the spectral energy distribution of Ceres that includes these emission features.

2. OBSERVATIONS

Table 1 summarizes the KAO HIFOGS spectra we have obtained of Ceres, Vesta, and Pallas since 1992. On any flight we took overlapping spectra displaced by a half-integral number of detector elements to achieve the full instrumental resolution and to cover dead detectors. Thus a "5–14 μm" spectrum actually consists of at least four such spectra that we have overlapped by the splicing technique described in Paper II. Consequently, four distinct components of error enter into the ratio of an asteroid spectrum to that of our stellar calibrator. First, there are the individual photometric uncertainties from the statistics of all measurements of the asteroid by a single detector element in HIFOGS's arrays. Second are the corresponding errors in the spectra of the stellar standard. Third are the local "biases" (see Papers II, IV) that arise whenever two spectral fragments are spliced and overlapped. Finally, there are uncertainties in the adopted absolute calibration of the stellar standard (which are derived from the same considerations applied to the secondary standard and to our KAO data of Sirius or Vega). We combine all these components in a root sum square sense into the total absolute uncertainty of the asteroid's spectrum. As in previous work, we remove any residual terrestrial atmospheric effect due to the imperfectly matched air masses of asteroid and stellar spectra using Lord's (1992) ATRAN software. The pedigree of the two stellar calibrators used in this study of asteroids is documented in Paper II (α Tau) and Paper VII (α Boo).

In addition to these airborne data, we took a series of HIFOGS spectra of Vesta from the Mount Lemmon Observatory (MLO) in 1992 February that provide much more rigorous tests of model energy distributions. These are also summarized in Table 1.

3. COMPARISON OF MODELS AND OBSERVATIONS

3.1. *Thermal and Thermophysical Models*

The STM is a very simple model that treats asteroids as nonrotating spherical bodies with a smooth surface, observed at zero phase angle. Its lineage (L. A. Lebofsky 1997, private communication) is that of a model originally applied strictly to broadband 10 μm photometry, in which the true temperature distribution of an asteroid is not known, but assumed. Allowance for nonzero phase angles depends on an adopted phase coefficient whose typical value (0.01 mag deg^{-1}), in combination with that for the "beaming" parameter (allowance for preferential directing of radiation toward the Sun), is adjusted to match the absolute N-band flux level and occultation diameters of specific asteroids. Its application to wavelengths both shorter and longer than the broad 10 μm N band has been problematic (e.g., Lebofsky 1989). The mere existence of beaming implies that an excess of radiation is emitted in the zero phase direction and consequently less at larger phase angles, to conserve energy. Further, it is known (Lebofsky et al. 1984) that the prograde rotation of Ceres leads to different phase coefficients before and after opposition, although the average coefficient is preserved. Thus, spectra taken after opposition (phase greater than 22°) sample lower temperatures than those predicted by the STM, even allowing for phase correction. This morning/evening effect alone results in a systematic variation of order 10% in flux received from Ceres. These problems all highlight the importance of thermal inertia, the neglect of which, in the

TABLE 1

JOURNAL OF 5–14 μm HIFOGS ASTEROID SPECTRA

Date	Site	UT Range	Phase Angle (deg)	Asteroid	Calibrator	Wavelengths (μm)	Resolving Power
1992 Feb 24	MLO	8.30–8.50	8.2	Vesta	α Boo	7.47–13.16	200
		10.50–11.10			α Boo	7.47–13.16	200
		11.51–12.11			α Boo	7.47–13.16	200
1992 May 12.....	KAO	5.27–6.44	25.1	Vesta	α Boo	4.86–9.28	150
					α Boo	4.90–9.41	150
					α Boo	7.83–14.18	110
1993 Nov 9	KAO	2.25–4.05	17.7	Pallas	α Tau	4.88–9.37	170
					α Tau	4.94–9.44	170
					α Tau	8.80–14.22	230
					α Tau	9.08–14.27	230
1993 Nov 9	KAO	4.22–5.54	8.0	Ceres	α Tau	4.88–9.37	170
					α Tau	4.94–9.44	170
					α Tau	8.80–14.22	230
					α Tau	9.08–14.27	230
1995 Apr 14	KAO	5.09–5.30	22.3	Ceres	α Boo	4.92–9.37	170
					α Boo	4.94–9.40	170
1995 Apr 19	KAO	4.45–5.20	22.7	Ceres	α Boo	4.92–9.37	170
					α Boo	4.94–9.40	170
1995 May 5	KAO	3.35–4.25	23.2	Ceres	α Boo	4.92–9.37	170
					α Boo	4.94–9.40	170
					α Boo	8.03–13.75	230
					α Boo	8.41–14.14	230

STM, renders calculated flux densities unreliable below about 8 μm. D. Osip, of the University of Florida, kindly furnished us with a set of model spectra from the "canonical STM" (i.e., with beaming parameter of 0.756; Lebofsky et al. 1986) for our times of observation of these asteroids (these models were calculated exactly as described by Lebofsky).

Recently, Lagerros (1996, 1997) has described "thermophysical models" (TPMs) for asteroids that specifically address the issues of shape, heat conduction, orientation of the pole of rotation, and the beaming effect. Echoing the thermophysical approach of Wesselink (1948), who modeled diffusion of heat through the lunar surface, Lagerros treats spinning ellipsoidal asteroids with cratered surfaces, using roughness to create the beaming. His application is to broad *N*-band and millimeter fluxes. Müller (1997) has recently applied Lagerros models to a set of asteroids, gathering geometric, optical, and thermal information from the literature, specific to each of these particular asteroids, to render the TPMs most relevant to them. He has kindly supplied us with TPMs for Ceres computed for our actual times of observation, and normalized to fit a set of 92 measurements of Ceres at 10, 20, 200, 400, 800, and 1000 μm.

Note that even the TPMs do not include any surface emissivity features of real materials, nor do they treat the influence on the emitted radiation of temperature gradients in the immediate surface layers of asteroids (see e.g., Henderson & Jakosky 1997).

3.2. *Observations*

The "splicing technique" (Paper II) is used to combine independent spectra that have some overlap in spectral coverage. The method is designed to scale fainter fragments up to match brighter ones during the overlap procedure. It attributes lower intensity spectra to the effects of differential seeing, poor guiding, and/or loss of the position of maximum signal in the KAO's autoguider. Our brightest 1995 spectra of Ceres were those taken on April 14. Consequently, we have chosen to compare our composite (i.e., constructed from splicing together all the separate spectral fragments from all the flights) Ceres spectrum with models pertinent to 1995 April 14. This decision can be justified as follows:

The total amplitude of the visual light curve of Ceres is only about 4%, as a result of the combination of varying projected cross section (cf. Millis et al. 1987), variable surface reflectivity, and inclination of the pole of rotation (essentially lying in the plane of the sky; Millis et al. 1987; Spencer, Lebofsky, & Sykes 1989; Saint-Pé, Combes, & Rigaut 1993). Therefore, we expect essentially no variation in the absolute level of the thermal flux of Ceres. Further, the rotation period of Ceres is about 9 hr, leading to only minimal expected variation over the duration of acquisition of a single spectral fragment (typically about 20 minutes). In fact, we carried out an experiment seeking rotational modulation of the midinfrared spectrum of Vesta, whose period (5.3 hr) is much shorter than that of Ceres and whose visual amplitude is between 10% and 14%. On 1992 February 24, we secured three HIFOGS spectra during an interval of 3 hours and 40 minutes, a significant fraction of Vesta's rotation period. The three spectra are identical in shape, within their 1 σ errors, and their absolute levels span a total range of only 4% of the mean spectral level at any wavelength. This indicates that at least Vesta shows no significant variations in thermal emission properties across its disk.

Most of the changes we have observed in our spectra of Ceres arise from the steady increase in geocentric distance of the asteroid between the three 1995 flights. However, in this period the heliocentric distance did not vary significantly, so the temperature at the subsolar point on Ceres was essentially constant and the shape of the single model from April 14 (the closest geocentrically) can be used to represent our expectation of Ceres during this flight series. This conclusion is also supported by the absence of spatial variations ($\lesssim 5\%$) across the surface of Ceres in the images observed at 2.2 and 3.8 μm, with adaptive optics, by Saint-Pé et al. (1993).

We have tested this conclusion in two ways. First, we compared the shapes of overlapping spectral fragments from different flights in the 1995 series and from the "half-integral bin shifted" fragments within each flight. We see no statistically significant distinctions between these fragments, above the $\pm 1\ \sigma$ level. Next we ratioed the three STMs for April 14 and 19 and May 5 and found that these have identical shapes, and identical levels if one simply multiplies these by 1, 1.06, and 1.26, respectively. These factors are roughly what one expects from the varying geocentric distance of Ceres, coupled with its essentially constant heliocentric distance.

Our methodology for spectral assembly applied to stars depends on the use of independent photometry through well-characterized passbands so that one can normalize (some) spectral fragment(s) to the observed in-band fluxes. For Ceres, however, we have been unable to locate any such photometry during the spring of 1995 that is contained within the 5–14 μm region. We doubt that our KAO spectral levels could be inaccurate by more than about 10%–15%. Indeed, there is good support (at the ~10% level) for the absolute calibration of the Ceres spectrum in Figure 1 through the continuity of the flux calibration of the *IRTS* MIRS on the basis of Ceres and of stars (cf. Tanabé et al. 1997). But, because we cannot quantify our accuracy by contemporary independent photometry, in subsequent discussions we emphasize the *shape* of the energy distributions predicted by the STMs, renormalizing these to facilitate comparison with our observed spectra.

Figure 1 compares the observed spectrum (the mean $\pm 2\ \sigma$) with Osip's STM. The shape is rather poorly represented by such a model, particularly below 8 μm (as expected because of the effects of thermal inertia). The STM was originally cast in terms of the brightness temperature and was intended to be normalized to the broadband 10 μm flux of an asteroid (L. A. Lebofsky 1997, private communication). The beaming parameter was adjusted, as needed, to match the broad *N*-band modeled and observed fluxes at zero phase to known occultation diameters. But this very broadband approach means that one does not know the real temperature distribution of the surface. With our higher spectral resolution we are sensitive to color temperature, and this simply does not agree with the *N*-band brightness temperature. Many other factors enter into thermal models for asteroids, not the least of which is the phase correction. Our 1993 Ceres observations were taken at a phase angle of 8°; those from 1995 were made after opposition at phase angles greater than 22°. Ceres is a prograde rotator, so that we observed its morning side in 1995. In such circumstances, the actual phase coefficient would be

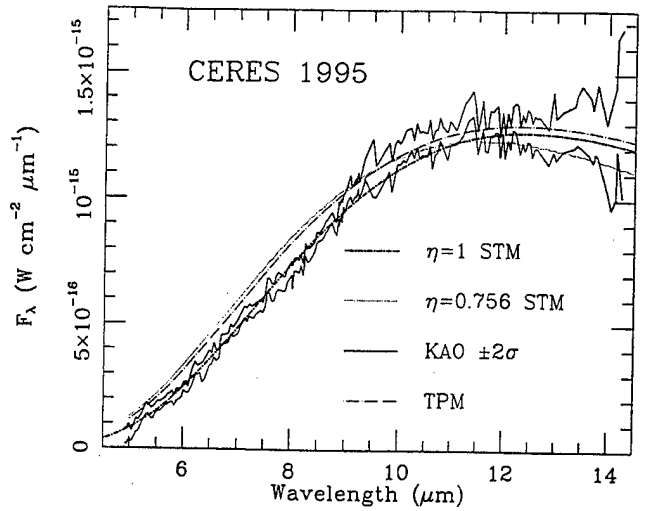

FIG. 1.—Combined KAO spectrum of Ceres from 1995 April–May compared with the STM for the time of observations computed with beaming factors of 0.756 (the canonical value) and 1. Also shown is the TPM calculated by T. G. Müller (1997, private communication).

quite different from the adopted mean value of 0.01 mag deg^{-1}, and the temperature significantly lower than that predicted by the canonical STM. Even a photometric renormalization of the STM would not then match an observed spectrum, and the discrepancies would grow with distance from the wavelength of the thermal flux peak.

The value of η (the beaming parameter) is also controversial (cf. Morrison 1973). We note that Green et al. (1985) successfully modeled their MIR spectra of 12 main-belt asteroids using the STM with $\eta = 0.9$. There is even precedent for the use of $\eta = 1$ (cf. Paper II, for Juno). Both these previous applications of the STM were to MIR spectroscopy. By contrast, the canonical beaming parameter of 0.756 for Ceres was determined solely from *N*-band data (Lebofsky et al. 1986), even though 5 and 20 μm photometry was also available. When we compute such an STM with $\eta = 1$ by Morrison's or Lebofsky's prescription, we obtain a quite differently shaped energy distribution from that from the canonical STM (Fig. 1, *short-dash–dotted line*), at a level that actually replicates the observed KAO composite for 1995 April 14 to within 1% (perhaps fortuitously). This factor was determined by calculating a formal splice of the KAO composite spectrum to the model, using solely the range 6–9 μm to avoid the very noisy KAO data on Ceres below about 6 μm and the apparent emission feature longward of 9 μm. Our observed Ceres spectrum, scaled by a factor of 0.99, both is the formal best fit to the STM with $\eta = 1$ and clearly follows this model's shape. Therefore, empirically, a value for η of unity results in the most accurate STM for Ceres. Note that, for whatever reason, this modified STM matches the KAO spectrum over our *entire* spectral range, presumably because of the interplay between the influences of thermal inertia and beaming on the modeled temperature distribution.

The energy distribution of Müller's TPM for Ceres (Fig. 1, *long-dash–dotted line*) greatly resembles that from the canonical STM and results in a poorer fit to our observations than that from the much simpler $\eta = 1$ STM. Our 1993 Ceres data offer confirmation of this conclusion. Figure 2 (from which a handful of noisy points in the terrestrial ozone near 9.6 μm have been removed) compares the STM with unit beaming factor and the appropriately computed TPM (T. G. Müller 1997, private communication).

The identical procedure applied to our KAO observations of Vesta (Fig. 3*a*; from 1992) results in an ambiguous conclusion: the STM with $\eta = 0.756$ fits beyond 10.5 μm better than the $\eta = 1$ although, again, the $\eta = 1$ STM fits better at short wavelengths. Our KAO Pallas data (Fig. 3*b*; 1993) are rather noisy but suggest that the canonical STM fits the spectral shape adequately. From these spectra, we can identify no obvious deviations from a canonical STM for Pallas at the 20% level or for Vesta at the 15% level, although these data are much noisier than those for Ceres (bad points were again removed in the O_3 region).

However, our MLO ground-based spectra of Vesta provide a more rigorous test of models. These three energy distributions (Table 1) span almost a 4 hr period and reveal identically shaped spectra within their errors. Therefore, we have combined them using inverse variance weighting, resulting in the spectrum shown in Figure 3*c*. This more accurately defined energy distribution clearly favors the STM with unit beaming factor over the canonical version.

4. EMISSION FEATURES

To amplify any deviations from the STM, we have matched the shape of the observed spectrum of Ceres to the best-fitting STM, with $\eta = 1$, appropriate to each epoch of observation (as described above). This necessitated minor rescaling of each KAO spectrum to fit the several observed peaks (the 1993 spectrum was multiplied by 1.07, the 1995 by 1.04). We subtracted the STM from the scaled observations and ratioed the spectral differences in 1993 and 1995 to these STMs, then combined the two spectral deviations using inverse variance weighting. Figure 4 represents the result of this process. Three statistically significant "emission features" are recognizable: two narrow peaks near 6.6 and 11.4 μm, and a broader one centered near 10 μm. It is interesting to reexamine the observations of Ceres by Gillett & Merrill (1975) and by Green et al. (1985). These authors adopted blackbody continua for their standard stars, which introduce spurious structure in the 10 μm region due to the neglect of the SiO fundamental in their reference stars (of order 15% in α Tau and 8% in α Boo at their resolutions). The primary SiO structure in their two

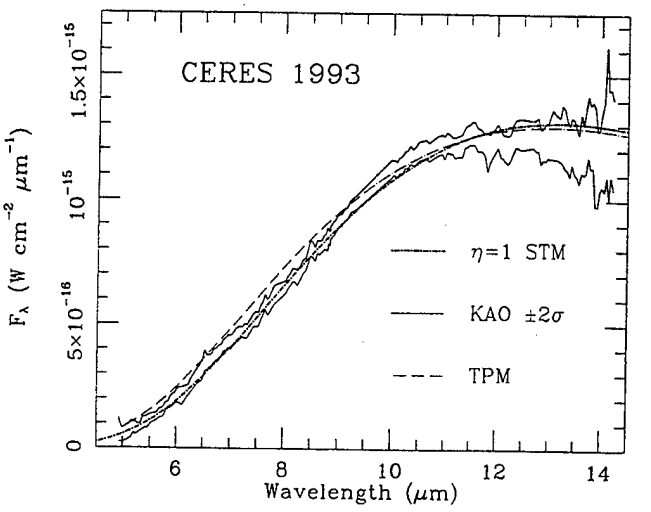

FIG. 2.—KAO spectrum of Ceres from 1993 compared with an STM with η of unity and Müller's computed TPM.

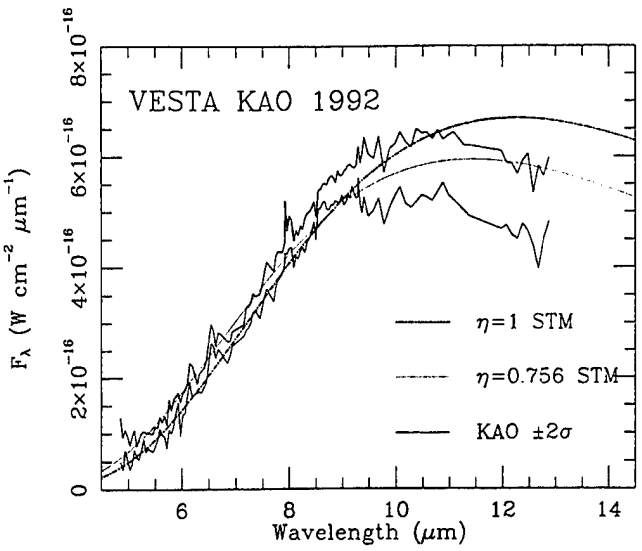

FIG. 3a

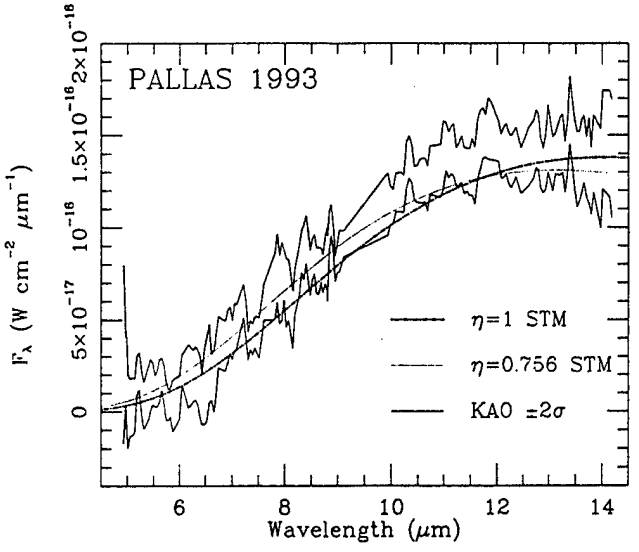

FIG. 3b

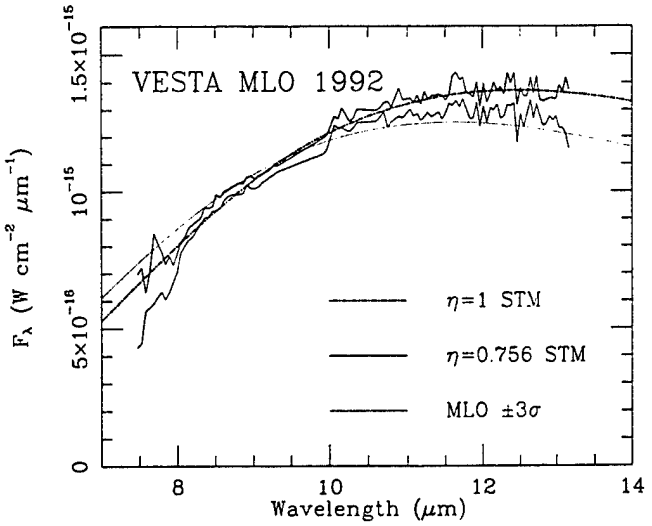

FIG. 3c

FIG. 3.—KAO spectra (*a*) of Vesta from 1992 May and (*b*) of Pallas from 1993 November, each compared with canonical ($\eta = 0.756$) and unit beaming factor STMs. (*c*) MLO spectroscopy of Vesta from 1992 February, which matches only the STM with unit beaming factor.

calibration stars is in the 7.9–8.5 μm range, yet the Ceres spectrum by Gillett & Merrill shows an emission feature remarkably similar to our own in the 9–11 μm. If this were not attributable to problems with telluric ozone cancellation, then these data also would support the existence of a broad emission feature in this asteroid. Likewise, correction of the Ceres spectra of Green et al. for neglect of the SiO fundamental in α Boo leads to the conclusion that they too saw a weak emission feature rising above the continuum beyond 8.5 μm.

To facilitate direct comparison with laboratory spectra, we also divided each set of scaled observations by the relevant STM continuum to create an emittance spectrum for Ceres. Specifically, we normalized the wavelength regions where the emittance approaches unity to the *high* points in both the 1993 and 1995 calibrated spectra of Ceres. The two emittances were combined with inverse variance weighting to produce the curve in Figure 5. Error bars associated with the combined emittance spectrum are also shown.

5. IDENTIFICATIONS OF MATERIALS AND CHRISTIANSEN FREQUENCIES

In the MIR, mineralogical information is related to the wavelength (frequency) position of the observed emittance maximum, which defines the Christiansen frequency (CF; Salisbury 1993; Kahle, Palluconi, & Christensen 1993). The CF is defined as the frequency at which the real index of the sample (n_s) equals the index of the surrounding medium (n_m, i.e., vacuum or air). It has been demonstrated recently that the emissivity maximum does not occur at the exact wavelength where $n_s = n_m$ (Hapke 1996). Here we use the term "CF" to refer to the position of the emittance maximum. For silicate minerals the CF has been related to the degree or extent of polymerization of the SiO_4 tetrahedra. Highly polymerized silicates (e.g., quartz, feldspars) have CFs that occur at shorter wavelengths than those of silicates with lower degree of polymerization (e.g., olivines; Salisbury 1993; Kahle et al. 1993). Systematic characterization of the

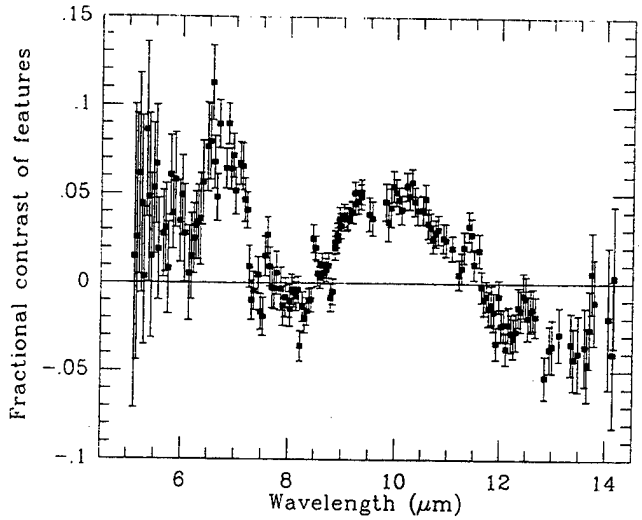

FIG. 4.—Emission features found in the spectrum of Ceres, combining our 1993 and 1995 data. Fractional contrast is shown, namely, the percentage of the flux predicted by the STM with $\eta = 1$ by which the observations exceed the STM continuum.

CF behavior of nonsilicates (e.g., oxides, metals, ices, organics) has not been discussed in the literature. For the MIR data of Ceres, we associate the maximum near 9.5 μm with the CF.

For solid particulate surfaces, the spectral contrast of MIR *restrahlen* features is inversely correlated with particle size and porosity (Salisbury 1993). There is no direct information regarding the particle size distribution of the materials on Ceres's surface. The lunar regolith, directly sampled during the Apollo missions, has a median particle diameter of 40–130 μm, with an average particle diameter of 70 μm (Carrier 1973). Here we *assume* that a similar particle size distribution exists on Ceres.

The polarimetric signature for small asteroids is consistent with a coarse regolith depleted in the smallest particles (Dollfus et al. 1989). This depletion is attributed to low surface gravity. Polarimetry of Vesta (diameter 550 km) indicates some depletion of small particles, but particles larger than 50 μm appear to be coated with particles smaller than 10 μm (Le Bertre & Zellner 1980). Ceres (diameter 934 km) could be assumed to have retained even more fine particles, thus resembling the Moon more than small asteroids in this respect. Furthermore, the nature of the small particles may be different since the polarization studies sample only optical radiation. In the MIR, the polarized light may result primarily from reflections from larger particles.

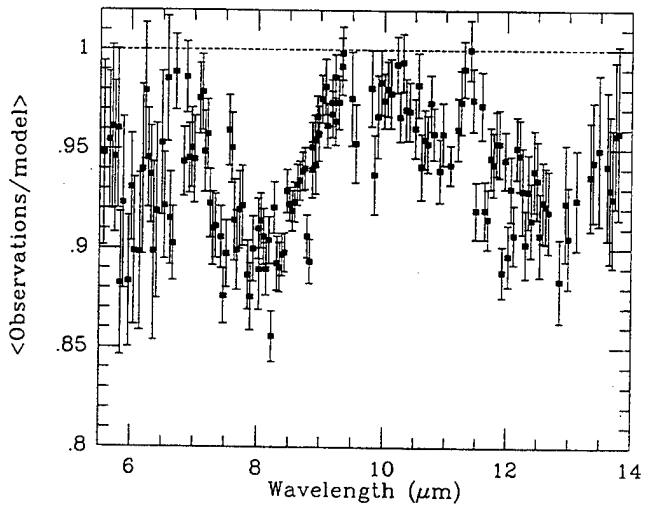

FIG. 5.—Emittance spectrum of Ceres from 1993 and 1995 data combined.

MIR emissivity (ϵ) spectra for a variety of materials exist in the literature (Lyon 1964; Conel 1969; Logan et al. 1973; Arnold & Wagner 1988; Christensen & Harrison 1993; Roush & Bell 1995; Moersch & Christensen 1995; Wagner & Schaade 1996; Roush & Orenberg 1996), but reflectance (r) spectra for a wider variety of samples are readily available (e.g., Salisbury et al. 1991). Under ideal conditions the reflectance spectra can be used to simulate emittance spectra via Kirchoff's law ($\epsilon = 1 - r$; see Salisbury 1993), an approach that we will adopt to compare laboratory spectra with those of Ceres. Our initial comparison uses data from Salisbury et al. (1991) for the finest particle sizes (0–74 μm). By visual inspection of these authors' figures, we identified samples whose reflectance minima were near Ceres's emission maximum and had spectral features with widths similar to the 9–11 μm feature seen in the Ceres data. About a dozen samples met these criteria, dominantly silicates with a low degree of silica polymerization, consistent with the position of the CF of the Ceres data, but none exactly matched the Ceres emittance spectrum.

Lebofsky et al. (1981) suggested the presence of phyllosilicates on Ceres, covered by a fine layer ($\approx$0.01 μm thick) of water ice, based on observations of Ceres near 3 μm. From visual and near-infrared observations of Ceres, Gaffey, Bell, & Cruikshank (1989) suggest a surface composition containing iron-poor phyllosilicates, with magnetite and/or carbonaceous opaque phases. From spectra of Ceres in the 3 μm region, King et al. (1992) concluded that the observed features were poorly matched by water ice, and preferred ammoniated phyllosilicates.

At the MIR wavelengths of the observations obtained from KAO, silicates would be expected to exhibit spectral features due to SiO_4 polymerization (7–10 μm) and, because molecular water is associated with some phyllosilicate structures, possibly near 6 μm. In addition, NH-bearing materials could exhibit spectral features between 6 and 7 μm and carbonaceous phases could have features in the 6–7 μm and 11–11.5 μm regions. By contrast, magnetite does not exhibit distinctive spectral features over the wavelength range of the KAO data (Salisbury et al. 1991). T. V. V. King (1997, private communication) has measured the MIR reflectance of ammoniated phyllosilicates, and both D. Cruikshank (1997, private communication) and W. Calvin (1997, private communication) have measured the MIR reflectance of organic materials. Kirchoff's law was used to calculate the emittance from the digital reflectance data (King 1997, Cruikshank 1997, Calvin 1997, private communications), and the results for a subset of all these samples are compared with the Ceres spectrum in Figure 6. No single material can adequately explain the spectral features seen in the Ceres data. Nevertheless, there are some interesting correspondences.

For example, the ammoniated saponite spectrum in Figure 6 exhibits maxima near 6.2 and 6.9 μm that are near the emissivity peaks seen in the Ceres data near 6.2 and 7.1 μm. However, because phyllosilicates have a relatively high

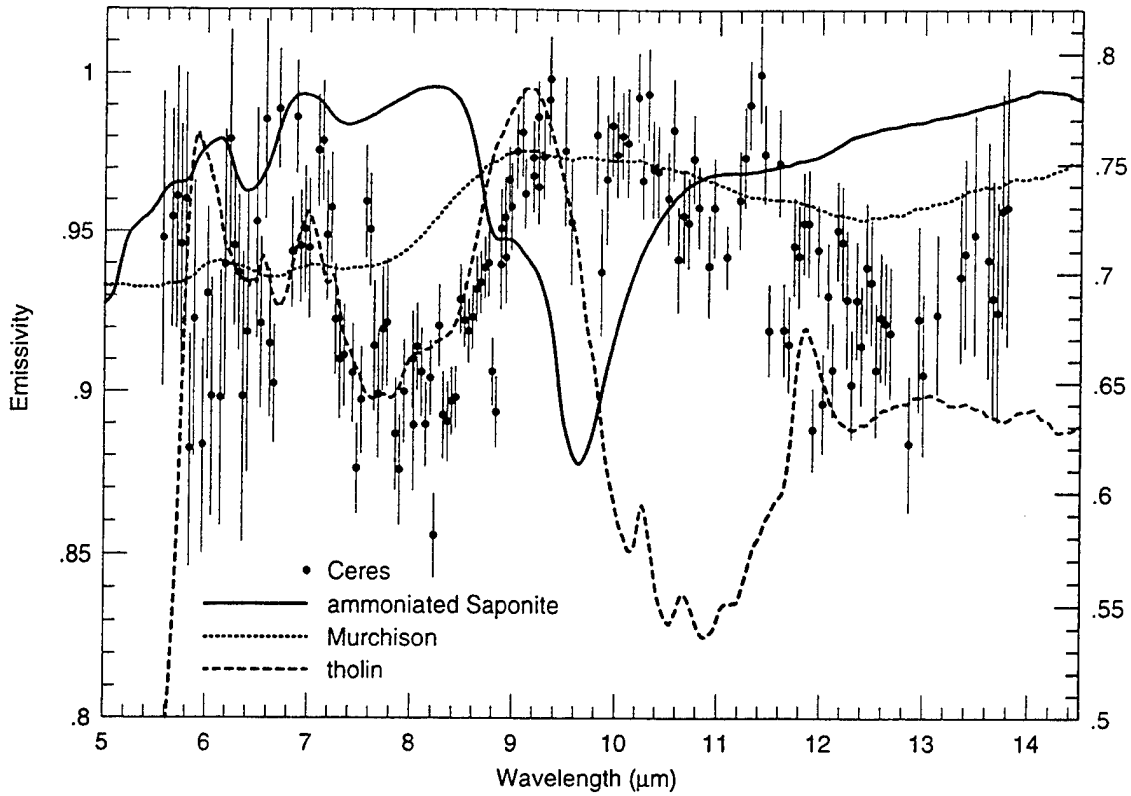

FIG. 6.—Ceres relative emittance spectrum compared with the emittance of several materials calculated from laboratory measurements. The right ordinate corresponds to the calculated emissivity of tholin; the left, to all the other curves.

degree of SiO_4 polymerization, the CF of the saponite occurs near 8.4 μm, compared with ~9.5 μm seen for the Ceres data. The spectrum of tholin, a solid organic residue produced by plasma irradiation of hydrocarbon gases, is also shown in Figure 6. It exhibits emissivity peaks near 7.0 and 11.9 μm that correspond to similar features seen in the Ceres spectrum, but shows greater spectral contrast in the 10–12 μm region and additional maxima near 5.9 and 6.5 μm. The CF of the tholin occurs near 9.2 μm, which is close to, but not an exact match to, that observed for Ceres. The overall emissivity of the tholin is too low compared with the Ceres data. Such disagreement could perhaps be mitigated by a finer grain size or mixing of the tholin with a higher emissivity material, but such measurements are not available, and theoretical calculations of such mixtures are beyond the scope of this paper. Ceres is a C-type asteroid, which are commonly associated with carbonaceous chondrite meteorites. Also shown in Figure 6 is the calculated emissivity of the bulk powder of the Murchison meteorite. The spectral contrast exhibited by Murchison's emissivity spectrum is very low compared with the Ceres data. The CF in the 9–9.2 μm region is close to, but not at, the position of the CF in the Ceres data.

The comparison of laboratory data with the Ceres observations remains the greatest shortcoming here, as in Lebofsky et al. (1981) and King et al. (1992). Lebofsky et al. measured pure materials without any indication of their grain sizes but at a temperature appropriate for Ceres. King et al. measured a single mixture with no indication of grain sizes of the components and at room temperature. Here we have used laboratory data from the literature; no mixtures of appropriate materials are available, much less at the appropriate temperatures. The problem with the Murchison data is that the obvious mechanism to increase the spectral contrast, by increasing the grain size, is in seeming conflict with the inferred presence of abundant fine-grained materials on like-sized bodies, e.g., Vesta.

Consequently, we cannot provide an exact spectral match to the Ceres data. Phyllosilicates exhibit CFs that, for the available spectra, occur at too short a wavelength to be consistent with the Ceres spectrum. Organic materials do exhibit spectral features that are consistent with those seen in Ceres, although none of the available spectra provides a convincing comparison to the Ceres data. We note that organic materials exhibit a wide range of compositional variation and we have compared only with a few examples.

6. ABSOLUTE CALIBRATION OF *ISO* AND *IRTS*

The major focus of this paper is on the consequences of the spectral structure in Ceres for calibration based on the STM. Therefore, we address the pragmatic issues of how to use Ceres for MIR calibration of the *IRTS* MIRS in 1995 April and for FIR calibration of ISOPHOT during the lifetime of *ISO*. The features we have found in Ceres's spectrum appear to be real, and reproduce on both long and short timescales, so they should not be neglected. There is some evidence in our 1993 and 1995 observations for variation in the relative strengths of the 6.6 and 10 μm features, but their influence on the observed spectral energy distribution is always local, and at the 10% level at most.

6.1. *MIRS*

We believe that any MIRS calibration using Ceres should be accomplished in two steps. The zeroth-order expectation is a continuum spectrum based on the STM with $\eta = 1$.

First-order modifications to this STM should then be made by the addition of three discrete emission features, in accord with Figure 4. This procedure should work for other detectors observing in the 6–14 μm regime too. We are well aware that our usage of the STM in this fashion is an oversimplification of the real situation, yet, empirically, it seems to replicate the observed thermal continua in Ceres (and Vesta) better than either the canonical STM or a TPM. Perhaps the neglect of thermal inertia in the STM is mitigated because of the large phase angles in the 1995 flight series on Ceres (L. A. Lebofsky 1997, private communication).

6.2. *ISOPHOT*

There are two fundamental questions here: (1) How does the existence of these MIR features affect ground-based 10 μm photometry of Ceres that is used in the context of extrapolation to longer wavelengths? (2) What quantitative discrepancies does $\eta = 1$, as opposed to 0.756, introduce into FIR extrapolations by the STM?

For measurements from the ground, only the broad 9–11 μm and narrow 11.4 μm features are relevant. A typical *N*-band filter (very broad) will receive an in-band flux enhancement due to these features of 5.0%. Narrowband 8.8 and 11.3 μm passbands (common to the few extant IR bolometer photometers, and to Si:As and Si:Bi imagers) are similarly afflicted, with expected enhancements of 4.4% and 5.2%, respectively. All these enhancements appreciably exceed the levels of typical spectrophotometric uncertainties inherent in these measurements. Whether using the canonical STM for Ceres or incorporating a value of 1 for the beaming factor, absolute errors will propagate solely as a result of the contamination of the assumed continuum thermal flux by these features. If one extrapolates these ground-based measurements by the shape of an STM, these errors will appear at the level of +4% to +5% between 10 and 300 μm, because one will have normalized a featureless model at too high a flux level.

The spectral *levels* of STMs with $\eta = 1$ and 0.756 differ substantially, essentially by a factor of 1.4 in peak flux, all other parameters being unchanged. Renormalization of the STM using its shape fitted to the measured in-band fluxes of filters such as *N* or *Q* will partially offset this effect. But, even after renormalization, the difference in flux levels between the two STMs will amount to −12% and −17% at 20 and 30 μm, respectively (a negative value implies an extrapolated flux for the $\eta = 0.756$ model that is too low relative to the $\eta = 1$ model) and asymptotically approaches a deficit of about 25% by 300 μm. The very existence of the beaming parameter implies that there is less flux emitted at appreciable phase angles than near zero phase, yet the simple STM does not address this decline in the mean temperature distribution. The errors associated with the neglect of this effect will increase at wavelengths further from the peak of the thermal emission curve of Ceres. Such phenomena bear directly on the absolute calibration of satellites that depend on thermal modeling of Ceres.

7. CONCLUSIONS

We report the existence of MIR emission features in the spectrum of Ceres. Empirically (we stress), we find the MIR continuum energy distribution of Ceres (and Vesta) to be better fitted by an STM with a beaming factor of 1 than by either an STM with the canonical beaming parameter of 0.756 or a TPM. The consequences of the presence and strengths of these features, and of using an STM with unity beaming factor, on the absolute calibration of Ceres are discussed and quantified. We propose a pragmatic method that should provide an adequate fit to the spectral energy distribution of Ceres beyond 5 μm, including these emission features.

Distinct mineralogical identification on Ceres is difficult for the following reasons: spectra due to mixtures of fine grain sizes are not theoretically tractable; any spectral features are a strong function of many parameters that are poorly constrained for Ceres, such as particle size, surface porosity, and thermal gradients (Henderson, Lucey, & Jakosky 1996; Henderson & Jakosky 1997); laboratory spectra (emission or reflectance) of candidate materials are not available at temperatures and pressures pertinent to Ceres's surface.

We are grateful to NASA's airborne astronomy program and to the staff of the entire KAO program for their past support of these flights. M. C. also acknowledges the support at Vanguard Research of the University of Florida through a subcontract of NASA grant NAG 5-3343. We thank David Osip for providing us with the University of Florida STMs for all three asteroids, and Kin-Wing Chan for providing algorithms for computing the $\eta = 1$ STMs of Ceres and for drawing our attention to the quality of fit between these models and our KAO spectra. The referee, Larry Lebofsky, provided valuable comments and substantive follow-up discussions. We are also grateful to Thomas Müller for communicating to us the results of his computations of TPMs for Ceres. Ann Sprague was the principal investigator of the 1992 February HIFOGS observations of Vesta that were taken by her and by two of the authors of the present paper.

REFERENCES

Arnold, G., & Wagner, C. 1988, Earth Moon Planets, 41, 161
Carrier, W. D., III. 1973, Moon, 6, 250
Christensen, P. R., & Harrison, S. T. 1993, J. Geophys. Res., 98, 19819
Cohen, M., & Davies, J. K. 1995, MNRAS, 276, 715 (Paper V)
Cohen, M., Walker, R. G., Barlow, M. J., & Deacon, J. R. 1992a, AJ, 104, 16 (Paper I)
Cohen, M., Walker, R. G., & Witteborn, F. C. 1992b, AJ, 104, 2030 (Paper II)
Cohen, M., Witteborn, F. C., Bregman, J. D., Wooden, D. H., Salama, A., & Metcalfe, L. 1996a, AJ, 112, 240 (Paper VI)
Cohen, M., Witteborn, F. C., Carbon, D. F., Augason, G. C., Wooden, D. H., Bregman, J. D., & Goorvitch, D. 1992c, AJ, 104, 2045 (Paper III)
Cohen, M., Witteborn, F. C., Carbon, D. F., Davies, J. K., Wooden, D. H., & Bregman, J. D. 1996b, AJ, 112, 2274 (Paper VII)
Cohen, M., Witteborn, F. C., Walker, R. G., Bregman, J. D., & Wooden, D. H. 1995, AJ, 110, 275 (Paper IV)
Conel, J. E. 1969, J. Geophys. Res., 74, 1614
Dollfus, A., Wolff, M., Gaeke, J. E., Lupishko, D. F., & Dougherty, L. M. 1989, in Asteroids II, ed. R. P. Binzel, T. Gehrels, & M. S. Matthews (Tucson: Univ. Arizona Press), 594
Feierberg, M. A., Witteborn, F. C., & Lebofsky, L. A. 1983 Icarus, 56, 393
Gaffey, M. J., Bell, J. F., & Cruikshank, D. P. 1989, in Asteroids II, ed. R. P. Binzel, T. Gehrels, & M. S. Matthews (Tucson: Univ. Arizona Press), 98
Gillett, F. C., & Merrill, K. M. 1975, Icarus, 26, 358
Green, S. F., Eaton, N., Aitken, D. K., Roche, P. F., & Meadows, A. J. 1985, Icarus, 62, 282
Hansen, O. L. 1976, Icarus, 27, 453
Hapke, B. 1996, J. Geophys. Res., 101, 16833
Henderson, B. G., & Jakosky, B. M. 1997, J. Geophys. Res., 102, 6567
Henderson, B. G., Lucey, P. G., & Jakosky, B. M. 1996, J. Geophys. Res., 101, 14969
Jones, T. J., & Morrison, D. 1974, AJ, 79, 892

Kahle, A. B., Palluconi, F. D., & Christensen, P. R. 1993, in Remote Geochemical Analysis, ed. C. M. Pieters & P. A. J. Englert (Cambridge: Cambridge Univ. Press), 99
Kessler, M. F., et al. 1997, A&A, 315, L27
King, T. V. V., Clark, R. N., Calvin, W. M., Sherman, D. M., & Brown, R. H. 1992, Science, 255, 1551
Lagerros, J. S. V. 1996, A&A, 310, 1011
———. 1997, A&A, 325, 1226
Le Bertre, T., & Zellner, B. 1980, Icarus, 43, 172
Lebofsky, L. A. 1989, Icarus, 78, 355
Lebofsky, L. A., Feierberg, M. A., Tokunaga, A. T., Larson, H. P., & Johnson, J. R. 1981, Icarus, 48, 453
Lebofsky, L. A., et al. 1984, BAAS, 16, 698
Lebofsky, L. A., & Spencer, J. R. 1989, in Asteroids II, ed. R. P. Binzel, T. Gehrels, & M. S. Matthews (Tucson: Univ. Arizona Press), 128
Lebofsky, L. A., et al. 1986, Icarus, 68, 239
Logan, L. M., Hunt, G., Salisbury, J., & Balsamo, S. 1973, J. Geophys. Res., 78, 4983
Lord, S. D. 1992, A New Software Tool for Computing Earth's Atmospheric Transmission of Near- and Far-Infrared Radiation (NASA TM-103957) (Moffett Field, CA: NASA)
Lyon, R. J. P. 1964, Evaluation of Infrared Spectrophotometry for Compositional Analysis of Lunar and Planetary Soils, Vol. 2, Rough and Powered Surfaces (NASA CR-100) (Washington: Off. Tech. Serv.)
Matson, D. L., Veeder, G. J., & Lebofsky, L. J. 1978, in Asteroids: An Exploration Assessment, ed. D. Morrison & W. C. Wells (NASA CP-2053) (Washington: NASA), 127
Millis, R. L., et al. 1987, Icarus, 72, 507
Moersch, J. E., & Christensen, P. R. 1995, J. Geophys. Res., 100, 7465
Morrison, D. 1973, Icarus, 19, 1
Morrison, D., & Lebofsky, L. A. 1979, in Asteroids, ed. T. Gehrels (Tucson: Univ. Arizona Press), 184
Müller, T. G. 1997, Ph.D. thesis, Univ. Heidelberg
Roellig, T. L., Onaka, T., McMahon, T. G., & Tanabé, T. 1994, ApJ, 428, 370
Roush, T. L., & Bell, J. F., III. 1995, J. Geophys. Res., 100, 5309
Roush, T. L., & Orenberg, J. B. 1996, J. Geophys. Res., 101, 26111
Saint-Pé, O., Combes, M., & Rigaut, F. 1993, Icarus, 105, 271
Salisbury, J. W. 1993, in Remote Geochemical Analysis, ed. C. M. Pieters & P. A. J. Englert (Cambridge: Cambridge Univ. Press), 79
Salisbury, J. W., Walter, L. S., Vergo, N., & D'Aria, D. M. 1991, Infrared (2.1–25 μm) Spectra of Minerals (Baltimore: Johns Hopkins Univ. Press)
Spencer, J. R., Lebofsky, L. A., & Sykes, M. V. 1989, Icarus, 78, 337
Tanabé, T., Yamamura, I., Onaka, T., Chan, K.-W., Roellig, T. L., & Cohen, M. 1997, in ASP Conf. Ser. 124, Diffuse Infrared Radiation and the *IRTS*, ed. H. Okuda, T. Matsumoto, & T. Roellig (San Francisco: ASP), 12
Wagner, C., & Schaade, U. 1996, Icarus, 123, 256
Wesselink, A. J. 1948, Bull. Astron. Inst. Netherlands, 10, 351
Witteborn, F. C., Cohen, M., Bregman, J. D., Heere, K. R., Greene, T. P., & Wooden, D. H. 1995, in ASP Conf. Ser. 73, Airborne Astronomy Symposium on The Galactic Ecosystem, ed. M. R. Haas, J. A. Davidson, & E. F. Erickson (San Francisco: ASP), 573

THE ASTRONOMICAL JOURNAL, 115:2092–2096, 1998 May

SPECTRAL IRRADIANCE CALIBRATION IN THE INFRARED. IX. CALIBRATED STELLAR SPECTRA USING DIRBE RADIOMETRY

MARTIN COHEN
Vanguard Research Incorporated, 5321 Scotts Valley Drive, Suite 204, Scotts Valley. CA 95066; and Radio Astronomy Laboratory, 601 Campbell Hall, University of California at Berkeley, Berkeley, CA 94720; mcohen@astro.berkeley.edu
Received 1997 December; revised 1998 January 26

ABSTRACT

The absolute calibration of the *COBE*/DIRBE data in the range 1–25 μm is examined through the in-band fluxes of DIRBE's own set of point-source calibration objects. Using the values of DIRBE fluxes expected for Sirius and for 10 of our published set of absolutely calibrated K and M giants that are in common with DIRBE's own calibration network, I find consistency with the project's formal basis, namely, our published calibrated spectrum of Sirius. This consistency means that one can use the DIRBE radiometry to construct absolutely calibrated "stellar templates" (i.e., continuous calibrated spectra from 1 to 35 μm) on the assumption that the intrinsic stellar spectrum of a star of given spectral class matches the intrinsic spectrum for the star of the same spectral class among the set of K and M giants, the spectrum of which has been absolutely defined. This technique is validated using a set of early M giants with well-characterized ground-based photometry and confirmed with *IRAS* low-resolution spectra.

Key words: infrared radiation — methods: miscellaneous — stars: late-type

1. INTRODUCTION

Whether the issue is the *qualitative* existence of weak emission or absorption features (i.e., an accurate spectral *shape*) or the *quantitative* identification of the faint cosmic background (i.e, an accurate *level*), every space-based and ground-based observation benefits from a robust and reliable calibration framework.

Several infrared satellites were launched in the period 1995–1996: the joint ISAS/NASA *Infrared Telescope in Space* (*IRTS*; Murakami et al. 1994, 1996) that surveyed about 8% of the sky in 1995; the European Space Agency's *Infrared Space Observatory* (*ISO*; Kessler et al. 1996), with the involvement of the USA and Japan; and the US *Midcourse Space Experiment* (*MSX*: Mill et al. 1994), launched in spring 1996. NASA's *WIRE* (*Wide-Field Infrared Explorer*) mission is scheduled for a 1998 launch, and the stratospheric observatory project (SOFIA) is fast proceeding. There is an urgent need not only to rationalize IR calibration and place it in a common and well-defined context, but also to provide a network of calibrators well distributed across the sky, with a common traceable pedigree. This should be sufficiently dense to have a member relatively close to an arbitrary direction because satellites and planes cannot afford major excursions in pointing to secure measurements of the few traditional calibration objects. Dynamic range, too, is an issue and such a network should include stars fainter than today's popular "standard" stars.

In a series of papers we have described a fresh approach to a self-consistent absolute framework within which photometry and spectroscopy are unified, with wavelength coverage ideal for calibrating many satellite, airborne, and ground-based sensors. The zero points are well defined and bypass the plethora of heterogeneous, poorly specified, and often mutually conflicting "calibrators" that have plagued IR astronomy. This approach is based upon a carefully selected pair of stellar models for Vega and Sirius, created by Kurucz, and absolutely calibrated (Cohen et al. 1992a; hereafter Paper I). These hot stellar models have been employed as reference spectra to calibrate cool giants as detailed by Cohen, Walker, & Witteborn (1992b; hereafter Paper II) and amplified by Cohen et al. (1995, 1996b; hereafter Papers IV and VII). This approach has yielded a valuable set of IR-bright secondary stellar standards with calibration pedigrees directly traceable to the two primary radiometric standards. These *observed* giant spectra are totally unlike any blackbody and are dominated by the fundamental absorption and overtones of CO, SiO, and water vapor. These molecular bands are common among cool giants and supergiants (Cohen et al. 1992c; hereafter Paper III). Thus the ideal (IR-bright) calibrators have significant spectral structure, not yet adequately modeled by stellar atmospheric codes.

This paper describes an attempt to validate the self-consistency of this absolute IR calibration using space-based measurements, and to extend it to more reference stars. My goal was not to "recalibrate" the Diffuse Infrared Background Experiment (DIRBE) but simply to verify its declared zero points then to use DIRBE data to strengthen the foundation of this new self-consistent absolute framework, which has already been applied to the calibration of four satellites: *COBE*/DIRBE (through Sirius, the basis star), the *IRTS*, *ISO*, and *MSX*; Kuiper Airborne Observatory spectroscopy from 3 to 30 μm (e.g., Cohen et al. 1996a; hereafter Paper VI); and several ground-based IR spectrometers (e.g., Cohen & Davies 1995). The objectives of the present paper are to employ DIRBE data to vindicate, or highlight any potential inconsistencies in, the current set of calibration spectra; and to create and test calibrated spectra of potential new reference stars. This work represents a preliminary test of our technique for creating faint calibrators that is described in detail and applied to the production of over 400 absolute calibration stars by Cohen et al. (1998; hereafter Paper X).

2. DIRBE's CALIBRATORS

The fundamental calibrator for the absolute calibration of DIRBE between 1 and 12 μm is Paper I's absolute Sirius

spectrum (W. Reach 1995, private communication). The extension of DIRBE's calibration across the sky is embodied in a set of measurements of 92 sources (Mitchell et al. 1996) that empirically furnished stable external references on short and long timescales over the roughly 10 month cold mission of DIRBE by comparison with the highly reproducible internal reference sources on board. I have specifically examined DIRBE measurements of this set of bright sources to compare the in-band fluxes predicted for DIRBE's passbands with actual DIRBE measurements of stable reference stars common to our published set of K and M giant absolute spectra. This analysis was extended to DIRBE bands 5 and 6 to check for consistency with bands 1–4.

The pertinent *COBE* data is designated as "BCC." The prefix "B" denotes a DIRBE routine that is used for "CC" (celestial calibration), by reading the output from the photometry routine applied to individual sources, namely "BCO" (calibration objects). Details can be found in the *COBE*/DIRBE Explanatory Supplement (1997). DIRBE offers broad spectral coverage with a valuable set of passbands; for example, its bands 4 and 2 sample the CO fundamental and first-overtone absorptions, respectively. DIRBE is compromised solely by its very large beam but the BCC data base already includes those point sources *well measured by DIRBE itself*, making it the ideal subset for any calibration study that builds on DIRBE data.

For 10 of the BCC calibrators, complete, continuous, absolutely calibrated 1.2–35 μm observed spectra, so-called composites (due to their method of construction), have already been created and published (Papers II, IV, VI, VII). The commonality of the basis for calibration of these spectra (Sirius) and of DIRBE itself means that DIRBE can provide vital checks on the accuracy of the composites. Its data offer a unique, independent appraisal of the quality of our calibration spectra because these exoatmospheric passbands are quite different from their ground-based counterparts. *IRAS* data, in principle, also provide valuable clues to the accuracy of templates. However, (1) *IRAS* data suffer from relatively large formal uncertainties, even for the bright objects for which we have assembled composite spectra (e.g., the "RELUNC" for α Tau at 12 μm is 6% in the Point-Source Catalog and 5% in the Faint Source Survey); (2) *IRAS* cannot supply the vital short-wavelength data that sample the regions with the most obvious spectral structure in these cool giants, particularly the 4.6 and 2.3 μm regions that include the CO fundamental and first overtones, respectively; and (3) *IRAS* was not calibrated on the basis of a single star, such as Sirius, but rather through an ensemble of stars, with assumptions as to their real behavior. None of our bright stars with composites was used for calibration in DIRBE bands 5 and 6, but *IRAS*'s far smaller beams at 12 and 25 μm made midinfrared photometry of these same sources viable. The combination of DIRBE data from 1–5 μm with *IRAS* data at 12/25 μm therefore provides a suitable set of photometry for our purposes.

It is of interest that the BCC archive includes a significant proportion of optical variable stars, some recognizable by name, others through the long-term *UBV* compilations of Mermiliod (1994). None are Mira variables. They are long-period irregular or semiregular variables, with visual amplitudes typically of 0.1–0.2 mag. Nevertheless, there are stars as late as M5 and M6 III that were found to be *stable* calibrators, in spite of the widespread impression that most stars later than M4 III are apt to be variable and even to have dust shells. The periods of these BCC stars often exceeded the cold mission of DIRBE yet this roughly 10 month duration should certainly have provided good sampling of their variations. What DIRBE tells us is that there are at least some of these late-type stars whose infrared variability is less than 2% over about 1 yr, sometimes even in bands that include strong photospheric absorption features. Consequently, there is hope that one could use carefully selected examples of such objects as tertiary calibrators for future space or airborne missions, although it is surely more conservative to depend only on nonvariable K and early M giants.

3. ZERO POINTS FOR ABSOLUTE IR CALIBRATION

3.1. *Traceability*

Paper I establishes the absolute calibration and magnitudes of the primary standards (Sirius and Vega) for several sets of passbands, including terrestrial transmission specific to the observing sites and generic detector radiance response curves. One needs detailed *cold* system passbands and individual measurement errors to provide the requisite traceability.

To use photometry in other filter systems, one also requires the basis star(s) of any set of measurements. For many northern observers, Vega fulfills this role. Consequently, if an observer publishes system magnitudes for Vega and these are not all zero, one can readily translate them into another context by forcing Vega to be zero. The algebraic quantities needed to achieve this are the "zero-point offsets." Not every basis set includes Vega. Sirius can equally well provide the offsets once its spectrum has been integrated over the system passbands. Any well-characterized system must demonstrate "closure," that is, its magnitudes for the composites must yield exactly what is expected when integrating its passbands over these cool stellar spectra. Consequently, one can also assess the offsets if a set of measurements includes only cool giant stars for which composite spectra have been created.

DIRBE measurements satisfy all the criteria for a traceable photometric system. Well-defined passbands are archived at NSSDC. The fundamental basis star is Sirius, and the BCC archive extends Sirius's calibration around the sky. There are no terrestrial atmospheric complications.

3.2. *Testing the Zero Points of the DIRBE Calibrators*

The set of bright stars that affords a test of the correct implementation of the Sirius absolute calibration for DIRBE is as follows, where each star was found stable (between 0 and less than $\sim$2% variability) over the cold mission of DIRBE (from 1989 December through 1990 September), in the parenthesized bands: α CMa (1–4: the declared fundamental calibrator in this range); the published composite spectra for α Tau (1–5); α Boo (1, 3–6); α Hya (1–4); β Peg (5); β And (1–5); γ Dra (1–4); γ Cru (1–4, 6); α Cet (1–4); ϵ Car (1–3); and μ UMa (2–4). The results of this analysis appear in Table 1 in the form of the ensemble averaged ratios of the DIRBE inband fluxes to those predicted by integrating the published DIRBE system responses over these stellar spectra. (Note that the BCC archive tabulates flux densities, so one must reconstruct the observed DIRBE in-band fluxes using the bandwidths published by the project for each of bands 1–6.) Not every

TABLE 1

MEAN RATIOS OF OBSERVED DIRBE IN-BAND FLUXES TO THOSE PREDICTED FROM COOL GIANT COMPOSITE SPECTRA AND THE MODEL FOR SIRIUS

Band	Average Ratio	σ	Number of Stars
DIRBE-1.....	1.00	0.02	1
DIRBE-2.....	0.98	0.02	6
DIRBE-3.....	0.97	0.02	8
DIRBE-4.....	0.98	0.02	9
DIRBE-5.....	0.96	0.02	4
DIRBE-6.....	1.07	0.04	2

DIRBE band is usable for all of these bright stars because, with the exception of Sirius, our calibrated spectra begin longward of 1.2 μm (or even 3.9 μm; e.g., γ Cru) so that DIRBE band 1 cannot be integrated fully over our composite spectra.

I conclude from Table 1 that this subset of composites is self-consistent; i.e., starting from the adopted Sirius spectrum, our published ensemble of absolute spectra of cool giants is vindicated in both spectral shape (within these six DIRBE bands), and absolute level, by the independent exoatmospheric measurements of DIRBE. Equivalently, the procedures inherent in the creation of the BCC archive have indeed maintained the integrity and traceability of the DIRBE calibration to the basis spectrum of Sirius.

4. BUILDING CALIBRATED SPECTRA USING DIRBE DATA: "STELLAR TEMPLATES"

One fully observed K/M giant spectrum can be used to create many calibrated stellar spectra if one makes the fundamental "template assumption" that the dereddened spectral shape of any observed K0–M2.5 giant accurately represents the intrinsic spectrum of any other giant with the same two-dimensional MK spectral type as the star from which the "template" is created. To customize the adopted template (i.e., the spectral shape) for any star requires photometry in a well-characterized system such as that of DIRBE (or *IRAS*), together with pertinent uncertainties.

Every 1.2–35 μm K/M giant spectrum is dereddened according to its own extinction (actually all the bright cool giants relevant to the present paper have zero reddening), and lightly smoothed in an information-preserving fashion (Jacobson 1990) that eliminates inappropriate high-frequency noise (i.e., beyond the resolution of the spectrometers used for the original observations). The smoothed, intrinsic spectral shapes thereby provide calibrated "spectral templates" for giants of spectral types K0, K1.5, K3, K5, M0 and M2.5. Specifically, the correspondence between spectral type, template, and the latest published absolute spectrum is as follows: K0, β Gem (Paper IV); K1.5, α Boo (Paper VII); K3, α Hya (Paper IV); K5, α Tau (Paper II); M0, β And (Paper IV); and M2.5, β Peg (Paper IV).

The procedure for templating a target star that is spectroscopically unobserved in the IR is to select the appropriate intrinsic template shape, apply reddening according to the target star's extinction [determined from $E(B-V)$], and normalize the resulting reddened template by photometry specific to the star through fully characterized, absolutely calibrated combinations of detector radiance response, filter passband, and site-specific mean terrestrial atmosphere (for ground-based data) or overall system response functions (for space-based data) such as those provided by *IRAS* and DIRBE. The result is a scaled spectral template, with a mean scale factor determined from the set of comparisons of expected in-band fluxes to those actually observed, and an associated uncertainty, assessed from the inverse variance weighted set of multipliers for a star (one multiplier and associated uncertainty for each characterized passband used). Each template is as complete in its wavelength coverage as the pristine composite from which it was derived, namely, 1.2–35 μm. No attempt is made to regrid these composites or templates to a common wavelength scale because the requisite interpolation would itself constitute an additional source of uncertainty. Note that the mean scale factor for a given template is relative to the appropriate K/M giant's stellar spectrum, so that two stars with the same scale factor, but made from different spectral templates, will not have the same angular diameter.

When utilizing BCC data, I have made use of the information provided on the level of background emission that was removed to determine each star's fluxes, in addition to the formal DIRBE "uncertainty" (in janskys) that is given. Because BCC stars were observed a great many times, these formal uncertainties can be inappropriately small ($<0.1\%$). It is clearly of consequence to know just how difficult was the extraction of each source from the (mean) background (presumably caused by the scattered component of the zodiacal light in bands 1, 2, 3 and by the onset of zodiacal thermal radiation in band 4, and assessed by interpolation from neighboring DIRBE beams). I quantified the difficulty of this extraction by assigning a fractional uncertainty inversely proportional to the square root of the background flux, and combined this in quadrature with the fractional error given in the DIRBE Explanatory Supplement for each band's effective field of view (also required to convert any BCC star's given background radiance from MJy sr^{-1} to Jy). The BCC's formal (fractional) uncertainty in the value of source-over-background flux density was also root sum squared with these other components to provide the final estimate of the error in a BCC in-band flux. This error was used to combine all the multipliers, with inverse variance weighting, for a star detected at several wavelengths.

Using the above procedure, I have created calibrated templates for 18 BCC stars, using a given composite to represent any star whose type lies within half a spectral class of the composite's spectral type (a conservative estimate for the uncertainty in spectral classification schemes). Extinctions for all 18 giants are negligible according to the A_V values given by McWilliam (1990), the $E(B-V)$ tabulated by Feast, Whitelock, & Carter (1990; hereafter FWC), or that can be deduced from the $B-V$ in Mermilliod's *UBV* archives (e.g., Mermilliod 1994) so that all their spectra will simply be linearly proportional to the intrinsic spectra derived from the composites. Table 2 summarizes the particulars of the 18 stellar templates, including the formal uncertainty with which each scale factor was determined. This uncertainty constitutes a wavelength-independent "local bias" (see Paper II), which has been root sum squared together with the wavelength-dependent uncertainties inherent in the original composites (hence in the templates, too). I have augmented the DIRBE data by *IRAS* 12 and 25 μm Point-Source Catalog photometry whenever possible (only one star was unobserved by *IRAS*) to lengthen the wavelength region over which the template can be constrained. For *IRAS*, I have used the Point-Source Catalog's relative uncertainty ("RELUNC") to assign

TABLE 2

THE 18 STARS FOR WHICH CALIBRATED TEMPLATES WERE MADE

HR number	Common Name	Spectral Type	Template Used	BCC Bands Used	*IRAS* Bands Used	Scale Factor	Bias (%)
168	α Cas	K0$^-$ III	K0 III	2, 3, 4	1, 2	0.443	0.93
188	β Cet	G9.5 III	K0 III	2, 3, 4	1, 2	0.435	0.80
429	γ Phe	M0$^-$ III	M0 III	4	1, 2	0.251	2.87
587	AR Cet	M3 III	M2.5 III	2, 3, 4	1, 2	0.177	0.69
603	γ^1 And	K3 IIb	K3 III	2, 3, 4	1, 2	0.672	0.66
1003	τ^4 Eri	M3$^+$ III	M2.5 III	2, 3, 4	1, 2	0.363	0.65
1162	π Eri	M2 III	M2.5 III	2, 3, 4	1, 2	0.090	0.91
2878	π Pup	K5 III	K5 III	2	1, 2	0.103	0.96
3803	N Vel	K5 III	K5 III	2, 3, 4	1, 2	0.115	0.96
4057	γ^1 Leo	K1$^-$ III	K1.5 III	2, 3, 4	1, 2	0.114	0.67
4301	α UMa	K0$^-$ III	K0 III	2, 3, 4	1, 2	0.659	0.67
4434	λ Dra	M0 III	M0 III	3, 4	1, 2	0.204	0.94
4630	ϵ Crv	K2.5 III	K3 III	2, 3, 4	1, 2	0.277	0.93
5603	σ Lib	M2.5 III	M2.5 III	2, 3, 4	1, 2	0.445	0.67
5854	α Ser	K2 IIIb	K1.5 III	3, 4	1, 2	0.055	0.99
8502	α Tuc	K3 III	K3 III	2, 3, 4	1, 2	0.407	0.74
8698	λ Aqr	M2.5 III	M2.5 III	2, 3, 4	...	0.219	0.77
9089	YY Psc	M3 III	M2.5 III	2, 3, 4	1, 2	0.189	0.77

errors to each star's measurement in the two bands. I have also included the relevant factors (of order unity) necessary to treat *IRAS* flux densities consistently in our calibration scheme (from Table 3 in Paper I, also confirmed by Table 6 in Paper VII). In practice, the BCC band 1–4 uncertainties are usually smaller than the *IRAS* ones so that DIRBE data still carry greater weight in the normalization of any template. Figure 1 presents an example of a calibrated template (for HR 587 = AR Cet) built from DIRBE and *IRAS* radiometry. This photometry is plotted (*filled squares*) at the correct values for the isophotal wavelength and isophotal flux based on the combination of the actual system passbands and the template shape.

Note that all 18 stars were selected from the "Atlas of Selected Calibrated Stellar Spectra" (Walker & Cohen 1992), whose stars were chosen for their normal K to early M giant character and absence of significant infrared neighbors.

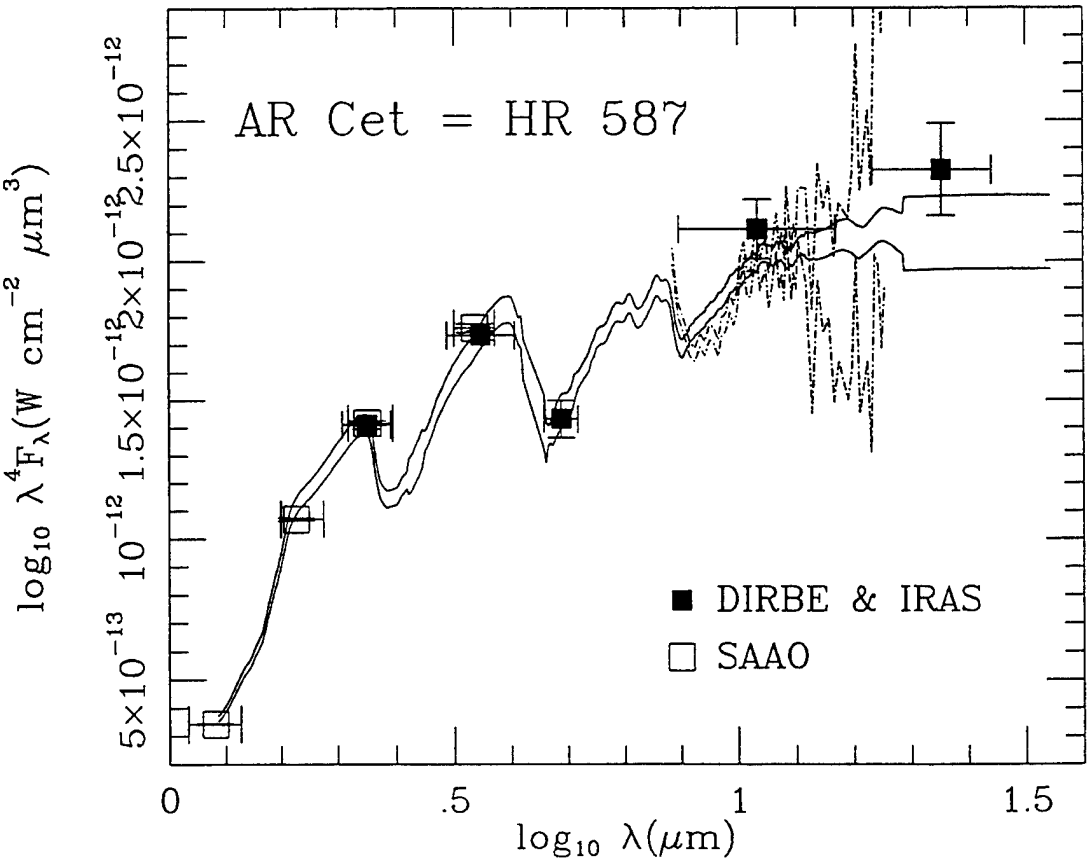

FIG. 1.—Calibrated spectral template for HR 587 = AR Cet, with its normalizing DIRBE and *IRAS* radiometry (*filled squares*), and the validating SAAO ground-based photometry (*open squares*). The two solid lines represent the mean $\pm 1\ \sigma$ bounds on the template. The recalibrated LRS spectrum is shown identically, as the dash-dotted lines. Both spectra are presented in $\lambda^4 F_\lambda$ space, with photometric measurements plotted at the isophotal wavelengths appropriate to the combination of these specific passbands and an M2.5 III spectrum.

To test the reliability of the template technique, I have applied two independent checks to each resulting templated spectrum. The first is to seek well-characterized photometry from the ground for at least a subset of the 18 stars. Those with the latest spectral types were preferentially examined because they will display the most obvious photospheric spectral features. For six of these (HR 587, 1003, 1162, 5603, 8698, 9089), all templatable with the M2.5 III shape, there exist precision South African Astronomical Observatory (SAAO) *JHKL* measurements by FWC. The SAAO "Carter" system has been carefully defined by Glass (1985) and Carter (1990), and the resulting filter profiles, detector radiance response, and mean SAAO atmospheric transmission have been combined and calibrated within our framework (see Paper X for details). The six normalized M2.5 III templates were integrated over the resulting SAAO *HKL* system response curves, and the derived in-band fluxes converted to magnitudes by comparison with the definition of zero-magnitude in-band fluxes defined from the Vega spectrum of Paper I, after applying the zero-point offsets of the SAAO system (these are defined in Paper X; all offsets have modulus less than 0.004 mag.).

For this subset of six stars, the mean differences (with standard deviations) between my synthesized SAAO magnitudes and those measured by FCW are H, -0.007 ± 0.013; K, $+0.020 \pm 0.014$; and L, $+0.020 \pm 0.017$. Therefore, these calibrated templates are validated in the near-IR at the ± 0.03 mag ($2\,\sigma$) level by the independent SAAO photometry. Figure 1 also compares the SAAO observations (*open squares*) with the template for HR 587. Note that the SAAO J point is not formally integrable over our template yet still falls on the curve when plotted at the isophotal wavelength expected for an M2.5 III (based on an appropriate model atmosphere's emergent spectrum).

This check also implies that at least these six stars are insignificantly contaminated by nearby IR sources within the large DIRBE beams, which is a matter of some concern in creating calibrators based on data acquired by, and/or intended for use with, systems with potentially large beam sizes. Likewise, there exist other ground-based, small-aperture near-IR photometric measurements of several of the remaining 12 templated stars that support the isolation of these stars from significant (at the level of $\sim 4\%$) neighbors on a spatial scale of about 10″. Similarly, the fact that *IRAS* 12 and 25 μm flux densities yield scale factors for the intrinsic templates that are entirely consistent with those from DIRBE band 1–4 indicates the absence of contamination of the DIRBE fluxes from midinfrared neighbors on a scale of $\sim 1'$.

The second test involved extracting (and recalibrating according to Paper II) *IRAS* low-resolution spectrometer (hereafter LRS) spectra of as many of the 18 stars as possible, for a direct comparison of spectral shapes. Seventeen (λ Aqr was not observed by *IRAS*) were found with adequate signal-to-noise LRS spectra to afford such checks, at least shortward of 13 μm, and all templates were vindicated within the mutual uncertainties of the LRS and composite spectra. This method provides a complementary mid-infrared constraint (albeit much weaker) on the templates to that offered by the ground-based near-infrared validation described above.

5. CONCLUSIONS

I conclude that DIRBE's context for calibration is statistically identical to that described in Papers I–VII, at about the 2% level for bands 1–4, the 4% level for bands 5–6, and that our current bright K/M giant composite spectra are vindicated by DIRBE at this level of precision. The ramifications of this independent appraisal of our published calibrators are substantial because this accord unifies the basis for near and mid-infrared calibration of each of the DIRBE, *IRTS*, *ISO*, and *MSX* missions. Every aspect of infrared astronomy that depends upon the accurate conversion of raw (e.g., satellite) data or magnitudes (e.g., ground-based) into physical units benefits conspicuously from this uniformity of calibration. More fundamentally, I conclude that the template technique is a valid approach to the creation of faint calibration stars.

DIRBE (BCC) data are suitable for the creation of calibrated stellar templates based upon intrinsic versions of the composites created so far. In the forthcoming Paper X, we will create over 400 calibrated stellar templates using this same technique. At that time, these templates built with DIRBE radiometry will be recreated using additional ground-based data to provide further constraints on a template's average multiplier, rather than to validate it as described in the present paper. All these newly calibrated templates will then be archived along with those based more typically on a combination of ground-based and space-based (*IRAS*) radiometry.

This work was initiated at Jamieson Science and Engineering, Inc. and continued at Vanguard Research, Inc., with funding support from NASA's "ADP" program through contract S-85190-Z. M. C. also thanks NASA Ames for partial support under cooperative agreement NCC 2-142 with UC Berkeley, and Dave Leisawitz and Bill Reach for valuable discussions.

REFERENCES

Carter, B. 1990, MNRAS, 242, 1
COBE Diffuse Infrared Background Experiment (DIRBE) Explanatory Supplement, version 2.3, ed. M. G. Hauser, T. Kelsall, D. Leisawitz, & J. Weiland (*COBE* Ref. Publ. 97-A) (Greenbelt, MD: GSFC)
Cohen, M., & Davies, J. K. 1995, MNRAS, 276, 715
Cohen, M., Walker, R. G., Barlow, M. J., & Deacon, J. R. 1992a, AJ, 104, 1650 (Paper I)
Cohen, M., Walker, R. G., Carter, B. S., Hammersley, P. L., Kidger, M. R., & Noguchi, K. 1998, in preparation (Paper X)
Cohen, M., Walker, R. G., & Witteborn, F. C. 1992b, AJ, 104, 2030 (Paper II)
Cohen, M., Witteborn, F. C., Bregman, J., Wooden, D., Salama, A., Metcalfe, L. 1996a, AJ, 112, 241 (Paper VI)
Cohen, M., Witteborn, F. C., Carbon, D. F., Augason, G. C., Wooden, D., Bregman, J., & Goorvitch, D. 1992c, AJ, 104, 2045 (Paper III)
Cohen, M., Witteborn, F. C., Carbon, D. F., Davies, J. K., Wooden, D. H., & Bregman, J. D. 1996b, AJ, 112, 2274, (Paper VII)
Cohen, M., Witteborn, F. C., Walker, R. G., Bregman, J., & Wooden, D., 1995, AJ, 110, 275 (Paper IV)
Feast, M., Whitelock, P. A., & Carter, B. 1990, MNRAS, 247, 227 (FWC)
Glass, I. 1985, Irish AJ, 17, 1
Jacobsen, L. A. 1990, Comput. Phys., 4, 400
Kessler, M. F., et al. 1996, A&A, 315, L27
McWilliam, A. 1990, ApJS, 74, 1075
Mermilliod, J.-C. 1994, Bull. Inf. CDS, 45, 3
Mill, J., O'Neil, R. R. Price, S. D., Romick, G. J., Uy, O. M., & Gaposchkin, E. M. 1994, J. Spacecraft and Rockets, 31, 900
Mitchell, K. J., et al. 1996, in AIP Conf. Proc. 348, Unveiling the Cosmic Background, ed. E. Dwek (New York: AIP), 301
Murakami, H., et al. 1994, ApJ, 428, 354
———. 1996, PASJ, 48, L41
Walker, R. G., & Cohen, M. 1992, An Atlas of Selected Calibrated Stellar Spectra (NASA Cont. Rep., CR-177604)